DE GRUYTER

REVIEWS in MINERALOGY

(Formerly: "Short Course Notes")

Volume 2

SECOND EDITION

FELDSPAR MINERALOGY

PAUL H. RIBBE, Editor

CONTENTS

MINERALOGICAL SOCIETY OF AMERICA

REVIEWS in MINERALOGY
(Formerly: "Short Course Notes")
Volume 2

SECOND EDITION

FELDSPAR MINERALOGY

P. H. Ribbe, EDITOR and SERIES EDITOR

The Authors

Anne M. Hofmeister & George R. Rossman

Division of Geology and Planetary Science
California Institute of Technology
Pasadena, California 91125

Herbert Kroll

Institut für Mineralogie
Westfälische Wilhelms-Universität
4400 Münster, West Germany

Paul H. Ribbe

Department of Geological Sciences
Virginia Polytechnic Institute & State University
Blacksburg, Virginia 24061

Joseph V. Smith

Department of Geophysical Sciences
University of Chicago
Chicago, Illinois 60637

David B. Stewart

United States Geological Survey
959 National Center
Reston, Virginia 22092

Jan Tullis & Richard A. Yund

Department of Geological Sciences
Brown University
Providence, Rhode Island 02912

MINERALOGICAL SOCIETY OF AMERICA

First edition 1975
Second edition 1983

PRINTED BY

BOOKCRAFTERS, Inc.
Chelsea, Michigan 48118

REVIEWS in MINERALOGY
(Formerly: "Short Course Notes")

ISSN 0275-0279

Volume 2, Second Edition:
FELDSPAR MINERALOGY
ISBN 0-939950-14-6

Aditional copies of this volume as well as those
listed below may be obtained at moderate cost from-

The Mineralogical Society of America
2000 Florida Avenue, NW
Washington, D.C. 20009

Volume		
1	SULFIDE MINERALOGY, P.H. Ribbe, editor (1974)	284 p.
2	FELDSPAR MINERALOGY, P.H. Ribbe, editor (1975; revised 1983)	360 p.
3	OXIDE MINERALS, Douglas Rumble III, editor (1976)	502 p.
4	MINERALOGY and GEOLOGY of NATURAL ZEOLITES, F.A. Mumption, editor (1977)	232 p.
5	ORTHOSILICATES, P.H. Ribbe, editor (1980; revised 1982)	450 p.
6	MARINE MINERALS, R.G. Burns, editor (1979)	380 p.
7	PYROXENES, C.T. Prewitt, editor (1980)	525 p.
8	KINETICS of GEOCHEMICAL PROCESSES, A. C. Lasaga and R.J. Kirkpatrick, editors (1981)	391 p.
9A	AMPHIBOLES and OTHER HYDROUS PYRIBOLES - MINERALOGY, D.R. Veblen, editor (1981)	372 p.
9B	AMPHIBOLES: PETROLOGY and EXPERIMENTAL PHASE RELATIONS, D.R. Veblen and P.H. Ribbe, editors (1982)	390 p.
10	CHARACTERIZATION of METAMORPHISM through MINERAL EQUILIBRIA, J.M. Ferry, editor (1982)	397 p.
11	CARBONATES, R.M. Reeder, editor (1983)	In press

FELDSPAR MINERALOGY

FOREWORD TO THE SECOND EDITION

In October 1975 a Short Course on Feldspar Mineralogy was held at the Hotel Utah, Salt Lake City, in conjunction with the annual meetings of the Mineralogical Society of America. Richard A. Yund, David B. Stewart, Joseph V. Smith and Paul H. Ribbe presented workshops on x-ray single-crystal and powder diffraction methods and electron optical techniques as applied to the study of feldspars and presented eight lectures, the substance of which became the nine chapters of the first edition of *Feldspar Mineralogy*. That book was published by the Mineralogical Society as the second volume of its series entitled "Short Course Notes".

In 1980 the M.S.A. renamed the series "Reviews in Mineralogy" to more accurately reflect the scope and contents of the volumes, some of which -- including Volume 5 (1st and 2nd editions), this volume and a forthcoming one on fluid inclusions -- were written without presentation at a short course. Eleven volumes are now available from the M.S.A. at reasonable cost (see p. ii).

Three years ago it was decided not to reprint *Feldspar Mineralogy* when its second press run sold out. That was a mistake, because as this, the second edition, was slowly taking shape, no volume on feldspars has been available for two years. Unfortunately the present revised volume was advertised and orders were accepted, with resulting dissatisfaction of patrons. The series editor accepts full responsibility for this; hopefully the updating, improvements, and new contributions in this edition will in part compensate for the inconvenience.

It will be noted by readers experienced with feldspars that there are many new ideas appearing in Chapters 3, 4 and 5 that have neither received scrutiny by review (other than ourselves) nor survived practical tests of time in the research community. There is some danger in this, but the editor decided the greater risk was to produce a review volume soon to be outdated.

Inevitably, given the different goals of individual authors in their assigned topics, some repetition of material has occurred, although usually with quite different emphases. Chapters 1, 2, 9 and 10, in which plagioclase structures and diffraction patterns and their Al,Si distributions, phase equilibria and exsolution textures are featured, are notable in this regard. The editor has attempted to cross-reference these and as many other subjects throughout the volume as feasible. This is a luxury not afforded in other books of this series produced with a short course deadline, and it, together with the detailed Table of Contents, compensates to some degree for the lack of an index.

Paul H. Ribbe
Series Editor
Blacksburg, VA
April 30, 1983

ACKNOWLEDGMENTS

Throughout this book repeated references are made to Smith (1974a,b); these are Volumes 1 and 2 of *Feldspar Minerals*, an encyclopedic work written by Joseph V. Smith and published by Springer-Verlag. We are particularly indebted to Drs. Konrad Springer and H. Wiebking for permission to reproduce many figures free of charge. We also thank the editors and publishers of the following journals and books for their permission to reprint figures:

The American Journal of Science	The American Mineralogist
Bulletin de la Société francaise dé Minéralogie et de Cristallographie	
Chemical Geology	Contributions to Mineralogy and Petrology
Geochimica et Cosmochimica Acta	Journal of Geology
Mineralogical Journal, Japan	Philosophical Magazine
Physics and Chemistry of Minerals	Proceedings of the Japan Academy
Schweizerische Mineralogische und Petrographische Mitteilungen	
The Feldspars	Manchester University Press
Geochemical Transport and Kinetics	Carnegie Institution
Rock-Forming Minerals	Longmans
Electron Microscopy in Mineralogy	Springer-Verlag

The editor (and hopefully this volume) benefitted greatly from numerous stimulating discussions with David B. Stewart, some of which reached a high pitch, none of which came to blows, and several of which produced some palpable scientific progress. Stewart read and criticized many of the chapters. The authors are grateful to numerous individual scientists for figures, for data in advance of publication, and for encouragement and correction.

Margie Strickler and Ada Simmons are to be commended for perseverance and great skill in typing the text and Sharon Chiang and her staff for excellent draftsmanship. The editor's colleagues and the secretarial staff of the Department of Geological Sciences at Virginia Polytechnic Institute and State University are thanked for their patience with him during the long process of writing, rewriting, editing and composing. Support of the University in providing facilities (and salary!) is gratefully acknowledged, as are his A.G.U. friends at the M.S.A. office who suffered much abuse over back-orders for this edition of *Feldspar Mineralogy*, nearly two years overdue.

SELECTED REFERENCE WORKS

The following is a list of useful reference works on feldspar mineralogy published in recent years:

Feldspar Minerals, 1. Crystal Structure and Physical Properties.

Feldspar Minerals, 2. Chemical and Textural Properties. By Joseph V. Smith (1974), Springer-Verlag: New York. 627 and 690 pp.

The Feldspars, Proceedings of a NATO Advanced Study Institute, Manchester, England, 1972. Edited by W. S. MacKenzie and J. Zussman (1974), Manchester University Press: Manchester. 717 pp.

Les Solutions Solides en Minéralogie, Colloque International du C.N.R.S. No. 234, Orleans, 1974. Edited by G. Sabatier (1974). *Bull. Soc. franc. Minéral. Cristallogr. 97*, 89-404.

Electron Microscopy in Mineralogy. Edited by H.-R. Wenk and G. Thomas (1976). Springer-Verlag: Berlin. 525 pp.

Thema Feldspäte, 1967. *Schweizerische Mineralogische und Petrographische Mitteilungen 47/1*, 398 pp.

Rock-Forming Minerals, 4. Framework Silicates. By W. A. Deer, R. A. Howie, and J. Zussman. Longmans: London. pp. 1-178.

Proceedings of the NATO Advanced Study Institute of Feldspars, Olso, 1962. Edited by O.H.J. Christie (1962). *Norsk Geologisk Tidsskrift 42/2*, 606 pp.

The Feldspars -- Phase Relations, Optical Properties, and Geological Distribution. By A. S. Marfunin. Translated from the 1962 Russian edition, 1966. Israel Prog. Sci. Translations: Jerusalem. 317 pp.

Proceedings of a NATO Advanced Study Institute on Feldspars and Feldspathoids, Rennes, France, 1983. Edited by W. L. Brown, untitled at press time.

FELDSPAR MINERALOGY

TABLE of CONTENTS

Page

CHAPTER 3, continued

CHAPTER 4. H. KROLL

LATTICE PARAMETERS and DETERMINATIVE METHODS for PLAGIOCLASE and TERNARY FELDSPARS

CHAPTER 5. D.B. STEWART & P.H. RIBBE

OPTICAL PROPERTIES of FELDSPARS

CHAPTER 5, continued

CHAPTER 6. R.A. YUND & J. TULLIS

SUBSOLIDUS PHASE RELATIONS in the ALKALI FELDSPARS with Emphasis on Coherent Phases

CHAPTER 7. R.A. YUND

MICROSTRUCTURE, KINETICS and MECHANISMS of ALKALI FELDSPAR EXSOLUTION

CHAPTER 7, continued

CHAPTER 8. R.A. YUND

DIFFUSION in FELDSPARS

CHAPTER 9. J.V. SMITH

PHASE EQUILIBRIA of PLAGIOCLASE

Page

CHAPTER 12, continued

CHAPTER 13. J. TULLIS

DEFORMATION of FELDSPARS

Page

CHAPTER 13, continued

Chapter 1

CHEMISTRY, STRUCTURE and NOMENCLATURE of FELDSPARS

P. H. Ribbe

INTRODUCTION

The feldspar minerals are aluminosilicates whose structures are composed of corner-sharing AlO_4 and SiO_4 tetrahedra linked in an infinite three-dimensional array; charge-balancing *A* cations with radius greater than 1.0 Å occupy large, irregular cavities in the tetrahedral framework. The general formula AT_4O_8 characterizes their chemistry, where *T* is Al,Si and *A* is divalent Ca or Ba for $Al_2Si_2O_8$ *alkaline-earth feldspars*, and monovalent Na,K for the $AlSi_3O_8$ *alkali feldspar* series of solid solutions and mixed crystals. A complete range of compositions is observed in the *plagioclase feldspar* series, $Na_yCa_{1-y}Al_{2-y}Si_{2+y}O_8$ ($0 \leqslant y \leqslant 1$), and a somewhat analogous K_xBa_{1-x} series (*hyalophanes*).

Minor or trace substituents in the irregular *A* polyhedral site are Sr, Rb, Cs, Pb, Eu, other rare earths, Fe^{2+} and possibly Mg. A boron analogue of feldspar (*reedmergnerite*, $NaBSi_3O_8$) occurs in nature, as does the ammonium feldspar *buddingtonite* ($NH_4AlSi_3O_8$), which may contain some hydronium (H_3O^+) for NH_4^+. Substituents other than boron in the tetrahedral sites are Fe^{3+}, Fe^{2+}, P, and Ti. See Chapter 12.

Stoichiometric feldspars with a wide variety of *A-T* combinations have been synthesized; *cf.* Table 1. Terrestrial feldspars with a few percent excess Al_2O_3 or SiO_2 have been reported (Smith, 1974b, p. 17-18) and defect structures have been synthesized: $A^{2+}_{1-z}\square_zAl_{2-2z}Si_{2+2z}O_8$ with *A* = Sr (Grundy and Ito, 1974) and *A* = Ca (Bruno and Fachinelli, 1974; Longhi and Hays, 1979). This is not surprising in that coesite, $\square_1Si_4O_8$, a high pressure polymorph of SiO_2, has structural similarities to the feldspars (Megaw, 1970). Calcic

Table 1. A listing of compounds with various combinations of *A* large cations and *T* tetrahedral cations that have been synthesized by Pentinghaus and others.

	T^{3+}				
A^{1+}	B	Al	Ga	Fe	T^{4+}
Na	×	×	×		Si_3
		×	×		Ge_3
		×			AlSiP
K	×	×	×	×	Si_3
	×	×	×	×	Ge_3
		×			AlSiP
Rb		×	×	×	Si_3
		×	×	×	Ge_3
NH_4		×			Si_3

	T_2^{3+}		
A^{2+}	Al_2	Ga_2	T_2^{4+}
Ca	×	×	Si_2
	×	×	Ge_2
Sr	×	×	Si_2
	×	×	Ge_2
Ba	×	×	Si_2
	×	×	Ge_2
Pb	×		Si_2

See chapter on *Chemical Properties of Feldspars* for additional compounds.

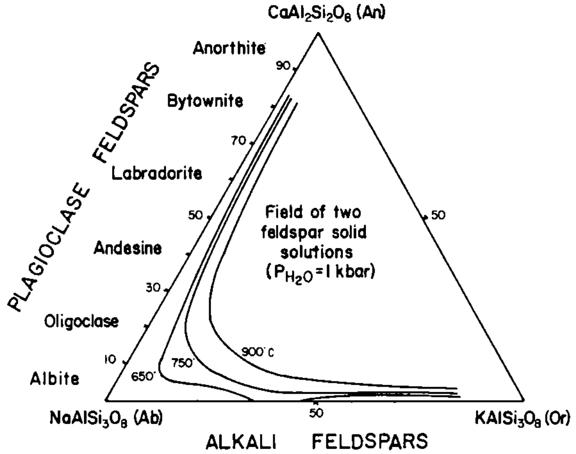

Figure 1. The feldspar An-Ab-Or ternary as determined experimentally by Seck (1971a). Higher pressures P(H_2O) have the effect of moving the solid-solution field boundaries closer to the binary joins. Nomenclature of individual plagioclase feldspars by composition range is indicated.

plagioclases from a lunar basalt have been described with up to 7 mol % $\square Si_4O_8$ (Beaty and Albee, 1980).

This volume will focus on the common natural feldspars with formulas

$$Or_xAb_yAn_{1-(x+y)} \text{ or } K_xNa_yCa_{1-(x+y)}Al_{2-(x+y)}Si_{2+(x+y)}O_8,$$

where $0 \leqslant (x+y) \leqslant 1$ and x is mole fraction K-feldspar (Or), y is mole fraction Na-feldspar (Ab), and 1-(x+y) is mole fraction Ca-feldspar (An). Figure 1 shows the experimentally determined solid-solution fields of these feldspars at one kilobar water pressure and several temperatures.

The nomenclature of feldspars is complex: Smith (1974a, Ch. 9) devotes 45 pages to it! It cannot be properly comprehended apart from a prior knowledge of structural details and phase relationships, including Al,Si order-disorder in the *T* sites, diffusive and displacive polymorphic transformations, antiphase domains, and a bewildering variety of exsolution textures. We will begin our discussion with feldspar topology.

TOPOLOGY OF THE FELDSPAR TETRAHEDRAL FRAMEWORK

Feldspars are aluminosilicates with general formula AT_4O_8 and a three-dimensional framework of corner-sharing AlO_4 and SiO_4 tetrahedra as first recognized by Machatschki (1928). However, a number of minerals and synthetic aluminosilicates also fit this description which are not feldspars; they are listed on the next page.

Monoclinic, $P2_1/a$	Pseudohexagonal	Orthorhombic, *Immm*
Paracelsian, $BaAl_2Si_2O_8$ (Craig *et al.*, 1973)	"Hexacelsian," $BaAl_2Si_2O_8$ -- not a mineral (Müller, 1976)	Metastable $CaAl_2Si_2O_8$ (Takéuchi *et al.*, 1973)
Slawsonite, $SrAl_2Si_2O_8$ (Griffen *et al.*, 1977)	Sr- & Ca-$Al_2Si_2O_8$; $RbAlSi_3O_8$ (See Pentinghaus, 1975)	

Indeed it is the *topology* of the tetrahedral framework which uniquely defines a feldspar, and in describing it we shall borrow heavily from Dr. Helen D. Megaw (1973, 1974a).

The simplest feldspar structure — that of $C2/m$ sanidine, $KAlSi_3O_8$ — was determined by Taylor (1933) who found that its key structural units are four-membered rings of TO_4 tetrahedra which, when corner-shared with similar rings, form double crankshaft-like chains parallel to x or the a-axis. From Figure 2 it is obvious that there are two types of four-membered rings in the chain, one normal to y (the b-axis) and the other approximately normal to x. In developing an understanding of feldspar topology it will be instructive to view the structure first from three projections along mutually perpendicular axes: along a onto $(20\bar{1})$, along c^* onto (001) and along b onto (010). Of course for optimum understanding it is best to refer these to a three-dimensional ball-and-spoke model. See also the stereo-drawings in Figure 4.

The a-axis projection

When viewed down the a-axis (Fig. 3), a four-membered ring consists of two pairs of non-equivalent T_1 and T_2 tetrahedra, one T_1-T_2 pair with apices pointing up (U) and the other with apices pointing down (D). Along the a-

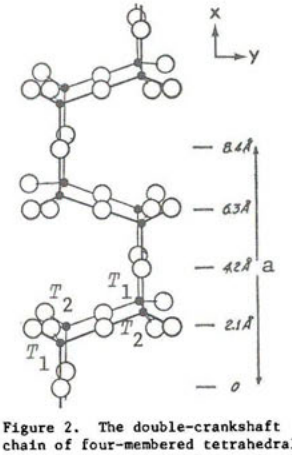

Figure 2. The double-crankshaft chain of four-membered tetrahedral rings that run parallel to a in all feldspars. (After Taylor, 1933.) Compare Figure 4a.

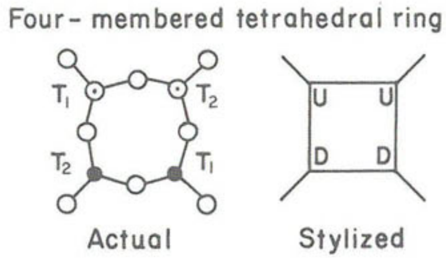

Figure 3. Projection of the four-fold tetrahedral ring on $(20\bar{1})$ (left) and a stylized representation (right): U = upward pointing tetrahedron; D = downward pointing tetrahedron. Compare Figures 2 and 5.

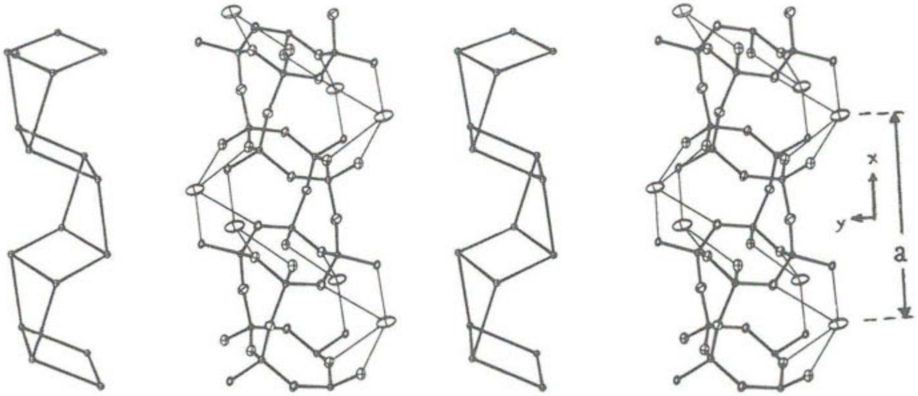

Figure 4a. A stereoscopic pair showing the double crankshaft chain of four-membered tetrahedral rings (on the right) and a stylized representation (on the left) which contains only the tetrahedral (T) modes. The x-axis is vertical; y is normal to x and inclined upwards at ~15° to the plane of the figure.

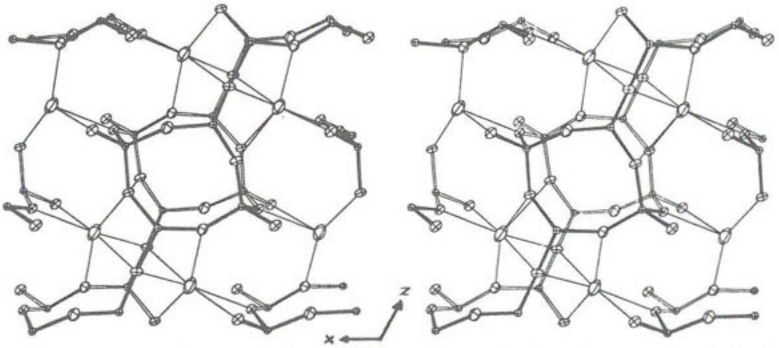

Figure 4b. A stereoscopic pair showing part of a feldspar structure whose fractional atomic coordinates are within the range $y = \pm 0.3$. The largest ellipsoids in both (a) and (b) are the Na atoms, here shown coordinated to seven oxygens (smaller ellipsoids). The smallest ellipsoids are T atoms. Figures 4a and b courtesy of J. Starkey and J.E. Wainwright.

axis U tetrahedra always share vertices with D tetrahedra, and Figure 4a is a stereoscopic view of the resulting structure and its simplified schematic representation in which only T atom positions are indicated. A partial projection onto ($20\bar{1}$) shows how the four-membered rings are linked through shared oxygen atoms (designated O_A2 or A2, for short) on the (010) mirror plane and through the O_A1 oxygens on horizontal two-fold axes parallel to b (Fig. 5a). Smith and Rinaldi (1962) discuss this unique topology in relation to other frameworks (*cf.* Phillips *et al.*, 1974) and these are compared schematically in Figures 5b and c. In one sense, feldspars can be envisaged as composed of these ($20\bar{1}$) sheets joined along the a-axis at vertex-shared O_B atoms, but it is also helpful to visualize the structure from another perspective.

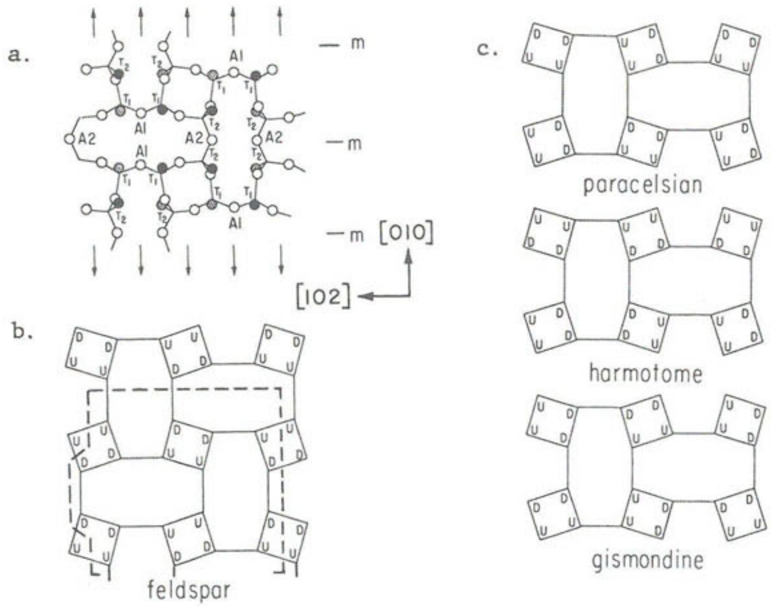

Figure 5. (a) A partial projection of the sanidine structure down the a-axis onto the $(20\bar{1})$ plane, showing how the four-membered tetrahedral rings (see Fig. 3) that make up the double crankshaft chains (Fig. 2) are cross-linked through the O_{A1} oxygens (on 2-fold axes ↑) and O_{A2} oxygens (on mirror planes m) to form a sheet of corner-shared tetrahedra. After Taylor (1933). (b) A stylized sketch of the same projection showing the U (up)- and D (down)-pointing vertices of the corner-shared tetrahedra. Dotted outline is the portion of the structure shown in (a). (c) Comparable tetrahedral sheets that occur in other framework aluminosilicates, paracelsian and two zeolites - harmotome and gismondine. Figures 5b and 5c after Smith and Rinaldi (1962).

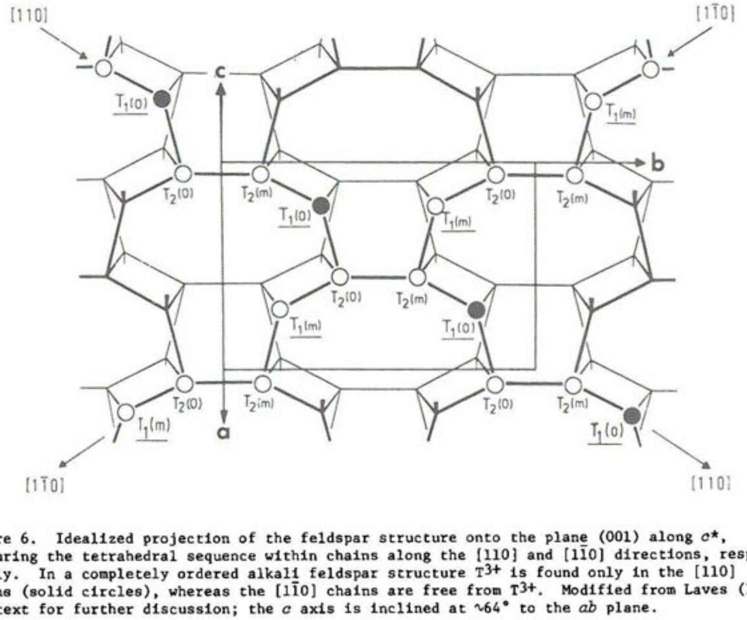

Figure 6. Idealized projection of the feldspar structure onto the plane (001) along c^*, featuring the tetrahedral sequence within chains along the [110] and $[1\bar{1}0]$ directions, respectively. In a completely ordered alkali feldspar structure T^{3+} is found only in the [110] chains (solid circles), whereas the $[1\bar{1}0]$ chains are free from T^{3+}. Modified from Laves (1960). See text for further discussion; the c axis is inclined at ~64° to the ab plane.

The c^*-axis projection

Figure 6 is an idealized projection of the feldspar framework onto (001) -- the "dog face" projection. Only the tetrahedral nodes are shown, and the T-O-T linkages are drawn as straight lines. T sites which are related by mirror planes parallel to (010) in $C2/m$ (pseudo-mirrors in $C\bar{1}$) feldspars are arbitrarily designated $T_1$0,T_1m and $T_2$0,T_2m. In the four-membered rings normal to b, $T_1$0,T_1m and $T_2$0,T_2m are related by two-fold axes in $C2/m$, pseudo-two-folds in $C\bar{1}$. In both monoclinic and triclinic feldspars there are centers of symmetry ($\bar{1}$) on the middle of each of the four-membered tetrahedral rings which appear as rectangles in this drawing.

The c^*-axis projection illustrates how the double crankshaft chains (Fig. 2) are linked through adjacent T_2 vertices -- O_A2 oxygens -- in the b-direction, thereby producing sheets of crankshaft chains. There is one such sheet per c-repeat. The O_A2 atoms are located on (010)(pseudo-)mirror planes. Short heavy and light lines are drawn at the T_1 sites pointing upwards and downwards. They represent those T_1 vertices by which successive sheets of double crankshafts are linked in the c direction. These O_A1 oxygen atoms are situated on two-fold axes or pseudo-two-fold axes. In summary, T_2 tetrahedra only have bonds within the sheets, connecting the crankshafts, whereas T_1 tetrahedra are linking the sheets. Each T_2 tetrahedron is joined by one T_2 and three T_1 tetrahedra, each T_1 tetrahedron is joined by one T_1 and three T_2 tetrahedra.

The b-axis projection

Figure 4b is a stereoscopic view down the b-axis of part of the Na-feldspar structure, showing to particular advantage the coordination of Na to seven oxygens. Megaw (1974a) has constructed a conceptually simple diagram of the structure in this orientation (Fig. 7), which in essence is a stylized projection of one of the crankshafts between y = 0 and $y = \frac{1}{2}$ (*cf.* the stylized representations in the stereo view, Fig. 4a). Figure 7a contains a projection of the unit cell ($a \sim 8$ Å, $b \sim 13$ Å, $c \sim 7$ Å, $\alpha \sim \gamma \sim 90°$, $\beta \sim 116°$) onto the (010) plane. Choosing the origin of coordinates in the lower right-hand corner of the cell, the T_1 sites, whose fractional atomic coordinates are $x \sim 0.00$, $y \sim 0.15$, $z \sim 0.25$, 0.75, are introduced along the z axis at $\sim$0.25 c and $\sim$0.75 c. A square is drawn with z as its diagonal, and the opposite corners are labelled T_2. This nearly coplanar T_1-T_2-T_1-T_2 four-membered ring is at fractional height $\sim$0.15 along the vertical y axis of the projection. (Notice: This is the ring which is *parallel* to the a-axis in Fig. 2; it is not the same ring as that shown in

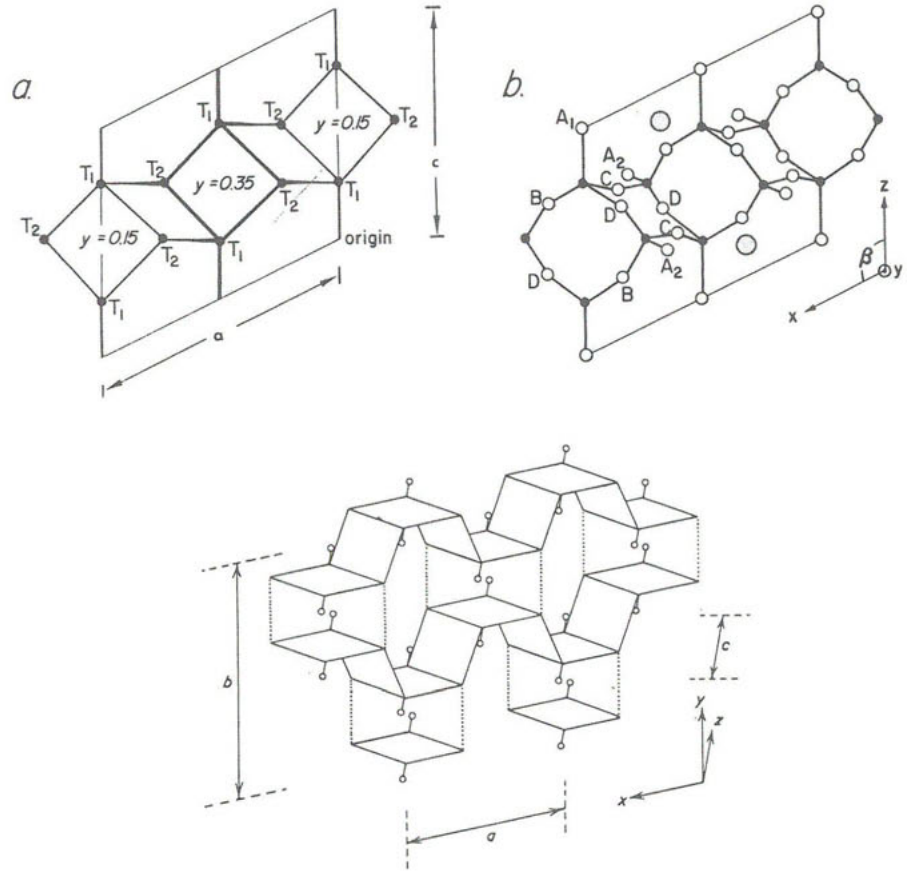

Figure 7. Projections of the feldspar structure on (010). See text for details. (a) Nodes representing the tetrahedral atoms. (b) Oxygen atoms are added to (a) as open circles. *A* atoms at heights $y = 0.0$, 0.5 are shown as large shaded circles. Their location on the *ac* plane is halfway between A1 and A2 on a horizontal line joining those two oxygen atoms. Modified from Megaw (1974a). (c) Schematic perspective diagram showing the "crankshafts" reflected by (010) mirror planes at $y = 0.25$, 0.75. Solid lines join *T* atoms as in (a), the O_{A2} atoms lie on dotted lines joining one crankshaft to its mirror image, and the O_{A1} oxygens are represented by circles. After Megaw (1973, Fig. 11-25).

Fig. 3.) The ring is repeated at the opposite end of the cell by the *a* translation vector. An exactly similar ring can be constructed by adding 0.5 to all the *x* coordinates of the atoms in the first ring; it is related to the other rings by an *a*-glide plane at height $y = 0.25$. Thus the *y* coordinates of all of its *T* atoms are $0.5 - 0.15 = 0.35$. When the oxygen atoms are added (Fig. 7b), the partial projection shows O_B and O_D atoms (B and D for short) within the rings normal to *b*, with O_C connecting these rings and O_A1 connecting the double crankshafts in the *c*-direction. All

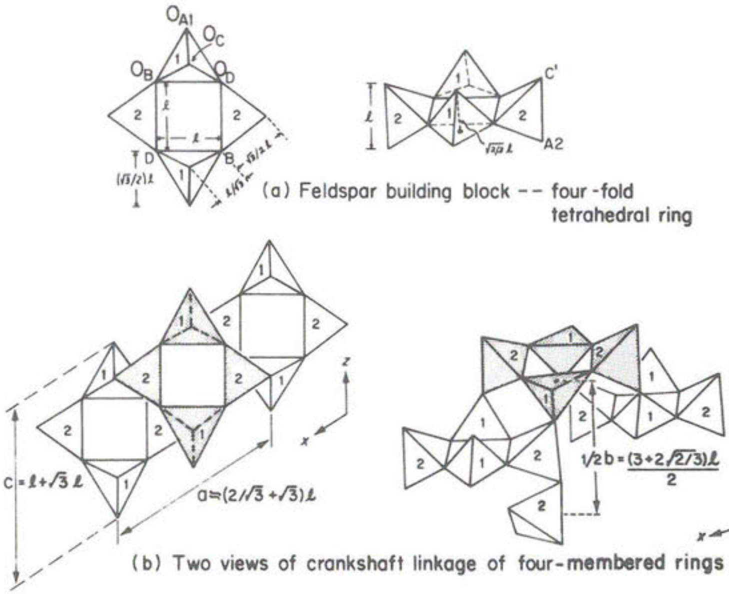

Figure 8. Perspective views of the feldspar tetrahedral framework showing idealized cell edges expressed in terms of the geometry of regular tetrahedra of edge-length ℓ. Modified from Megaw (1974a).

atoms are repeated by a mirror plane located at height $y = \frac{1}{2}$. There is a center of symmetry at $x,y,z = \frac{1}{4}\,\frac{1}{4}\,\frac{1}{2}$ which relates diagonally opposite T sites in the $(20\bar{1})$ ring (Fig. 3) and an axis of two-fold rotation which relates them in the ring nearly parallel to (010). The $C2/m$ space group symmetry elements are shown in a later figure (10a).

It is enlightening to look at the feldspar framework in partial perspective views of ideal tetrahedra (modified from Megaw, 1974a). These drawings are based on the approximation that all tetrahedra are regular and identical in size, and that the unit cell is monoclinic ($\alpha = \gamma = 90°$). Figure 8a illustrates the idealized four-membered ring. In (010) projection the base of the T_1 tetrahedron has its O_A2-O_C edge nearly vertical, i.e., the x and z fractional atomic coordinates of these oxygens are very nearly the same. The T_1 and T_2 tetrahedra are joined so that their O_B-O_D edges are perpendicular, and the rings are linked as shown in Figure 8b, forming the double crankshaft chain parallel to a.

Idealized cell parameters

Megaw has shown on the basis of this simplistic model that idealized feldspar cell parameters may be calculated from the tetrahedral edge length ℓ which ranges from 2.62 Å for Si-rich to 2.88 Å for Al-rich tetrahedra. Reference to Figure 8 will indicate the source of the following equations.

Equation*	Predicted**	Observed (albite)
$a \approx (2/\sqrt{3} + \sqrt{3})\ell$	8.1 Å	8.1 Å
$b = (3 + 2\sqrt{2/3})\ell$	13.0 Å	12.8 Å
$c = (1 + \sqrt{3})\ell$	7.6 Å	7.2 Å
$\beta = \arcsin(1 + \sqrt{2})\ell/a$	123°	117°
$\beta = -\arccos(1 + \sqrt{3}/3)\ell/a$	123°	117°

*The second and fifth equations have been corrected for errors in the original paper (Megaw, 1974a, p. 9) and the equation for a has been added. The term $\sqrt{2/3}\ \ell$ in the second equation is the height of a regular tetrahedron of edge length ℓ.

**Using a tetrahedral edge length ℓ = 2.8 Å.

Differences between predicted and observed values are due in part to tilting of tetrahedra from the assumed idealized positions (Megaw, 1974b) as well as to variations in *A* cation size, the Al/Si ratio, and the degree of Al,Si order-disorder.

Feldspars with Al:Si less than ∿1.8:2.2 have *c* dimensions of ∿7 Å, but those with Al:Si nearer to 2:2 have *c* ∿ 14 Å. The reason for this doubling of the cell becomes obvious when we examine the ordering patterns of Al and Si in the tetrahedral sites.

PATTERNS OF ALUMINUM,SILICON ORDER-DISORDER: NOMENCLATURE BASED ON STRUCTURE AND CHEMISTRY

The following pages are an attempt to describe all observed types of Al,Si distribution and their related topologies and space groups.

Alkali (Na,K) feldspars with Al:Si = 1:3 and *c* ∿ 7 Å

We have seen that in the monoclinic *C*2/*m* feldspars there are only two symmetrically non-equivalent tetrahedral sites, T_1 and T_2 (Fig. 7); but because there are 16 *T* sites per unit cell (*Z* = 4) and 4 Al + 12 Si atoms to fill them, it is not possible to have an ordered Al,Si distribution in these two sites. The bulk chemistry requires that in the average four-membered ring the probability of finding an Al atom is 1.0. Adopting the convention of Kroll (1971), in which t_1 represents (on the average) the Al content of the T_1 site, we may write

$$2t_1 + 2t_2 = 1.0. \quad (1)$$

If the Al,Si distribution is random, the structure is said to be completely disordered and

$$t_1 = t_2 = 0.25 \quad \text{or} \quad 2t_1 = 2t_2 = 0.5 \quad (2)$$

as in *high sanidine*, the rapidly quenched, monoclinic polymorph of $KAlSi_3O_8$, or *monalbite*, the $C2/m$ polymorph of $NaAlSi_3O_8$ which exists only above 980°C. Given somewhat more slow annealing, Al^{3+} is observed to migrate preferentially into the T_1 sites and Si^{4+} into the T_2 sites in order to satisfy local electrostatic charge balance considerations (the oxygens coordinating T_1 are more closely bonded to the large A^+ cation than those surrounding T_2). The boundaries for the terms *high* and *low sanidine* (HS, LS) and *orthoclase* (OR) have been defined only on the basis of optical properties ($2V_x$) -- Figure 2 in Chapter 5, which we use to define the following structural limits:[3,4]

$$\text{HS: } 0.5 < 2t_1 < 0.666; \quad \text{LS: } 0.667 < 2t_1 < 0.74; \quad \text{OR: } 0.74 < 2t_1 < 1.0 \quad (3)$$

Notice that t_1 cannot exceed 0.5, and that if further ordering is to occur, the two T_1 sites (as well as the two T_2 sites) in the four-membered ring must be differentiated. The two-fold axis parallel to b and the (010) mirror are destroyed. This is best illustrated in a schematic of the tetrahedral nodes in Figure 6, expanded portions of which are presented in Figure 9. Sites related by the (010) mirror plane are arbitrarily designated with postscripts 0 and m. The postscript c arbitrarily designates one of a pair of two symmetrically identical T sites related by a center of symmetry (o in the center of the drawing). If

$$t_1o = t_1m \quad \text{and} \quad t_2o = t_2m \quad \text{and} \quad t_1oc = t_1mc \quad \text{and} \quad t_2oc = t_2mc \quad , \quad (4a,b)$$

---

[3] Martin (1974a) used the term *ordered orthoclase* to indicate the most highly ordered monoclinic phase consistent with Equation 3, i.e., $t_1 = 0.5$, $t_2 = 0.0$. He presumed first order transformations from high sanidine to "ordered orthoclase" to low microcline (see Fig. 2b, Chapter 6), although it is highly doubtful whether such a phase exists. See later discussion.

[4] The term *adularia* is mineralogical, describing K-rich feldspar with a distinctive morphological habit. It typically occurs in hydrothermal veins or occasionally in low-grade metamorphic rocks. Structurally, adularia may be classified as sanidine, "orthoclase," or microcline, and it is commonly a metastable mixture of monoclinic and triclinic domains (Bambauer and Laves, 1960).

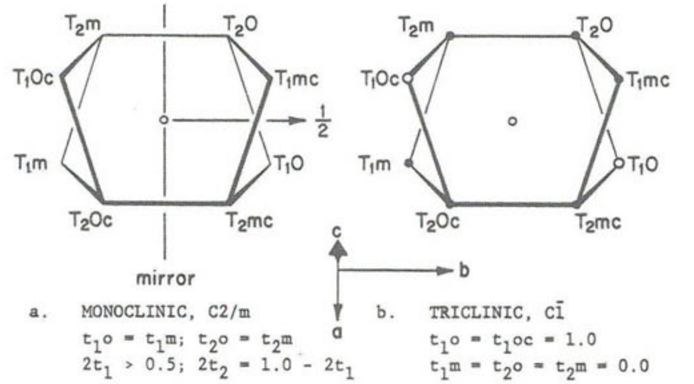

Figure 9. Projections onto (001) of certain portions of the feldspar tetrahedral framework (*cf.* Fig. 6). (a) The site occupancies consistent with $C2/m$ symmetry. (b) The site occupancy of $C\bar{1}$ low albite and maximum microcline. Sites T_1O and T_1Oc are related by the center of symmetry shown as a small o at the center of the structural unit, likewise T_1m and T_1mc, etc.

the structure may, but need not be monoclinic (Fig. 9a). If Al happens to concentrate in T_1O at, say, the expense of T_1m, these sites are no longer equivalent and the symmetry degenerates to $C\bar{1}$ (Fig. 9b), a subgroup of $C2/m$. The centers of symmetry at the previous intersections of the two-folds and the mirrors persist in the average structures of all alkali feldspars.

The Al,Si distribution in Figure 9b is completely ordered with

$$t_1o = 1.0; \quad t_1m = t_2o = t_2m = 0.0, \tag{5}$$

and this is characteristic of *low albite* and *low microcline* (often called *maximum microcline*). Intermediate degrees of Al,Si disorder are evident in triclinic potassium feldspars which are called *intermediate microclines* (Bailey, 1969):

$$t_1o > t_1m > t_2o = t_2m, \tag{6}$$

and in triclinic sodium feldspars which are called *intermediate albites*. In the latter, which have been synthesized directly (Martin, 1969) or formed by heat-treatment of low albite (MacKenzie, 1957),

$$t_1o > t_1m = t_2o = t_2m. \tag{7}$$

Analbite is "metrically triclinic" (i.e., truly triclinic, $C\bar{1}$) at room temperature but has Al,Si distributions resembling those of monoclinic sanidines (*cf.* Eqns. 2 and 3):[5]

$$t_1o = t_1m = t_2o = t_2m = 0.25 \text{ (disordered)} \tag{8}$$

or

$$t_1o = t_1m > t_2o = t_2m \quad \text{(partially ordered)} \tag{9}$$

Analbite is said to be "topochemically monoclinic", i.e., the topology of its Al,Si distribution makes it possible for it to invert -- at elevated temperature -- by a simple *displacive transformation* from $C\bar{1}$ (metrically triclinic) to $C2/m$ (metrically monoclinic): no further diffusion of Al,Si is required. The reason that analbite is triclinic, even though its Al,Si arrangement is consistent with the monoclinic symmetry typical of sanidine, is found in the fact that Na^+ has an effective radius of ∿1.0 Å whereas K^+ has an effective radius of ∿ 1.3 Å. Figure 10 indicates that the tetrahedral framework is "held open" by potassium but collapses around the smaller, highly anisotropic sodium atom. At temperatures greater than ∿ 980°C analbite does become monoclinic because the thermal vibration effectively increases the size of the sodium atom and the framework cavity. Monoclinic Na-feldspar is called *monalbite*. The term *high albite* should be reserved for highly disordered Na-feldspar in which the Al,Si distribution is "topochemically triclinic" (e.g., Eqn. 6 or 7), and which therefore cannot invert to monalbite without a *diffusive transformation* involving the equalizing of Al contents in the two T_1 sites and the two T_2 sites.

The Al,Si distributions portrayed in Figures 9a,b are represented along with their space groups in (010) projections in Figure 11. $C\bar{1}$ is an unconventional triclinic space group which is used to preserve the axial orientations from one feldspar to another. A $P\bar{1}$ cell could be chosen instead (as in Donnay *et al.*, 1963, p. 59), but direct structural comparisons would then become much more difficult.

Ca and Ba feldspars with Al:Si = 2:2 and c ∿ 14 Å

As noted earlier, feldspars with the formulas $A^{2+}Al_2Si_2O_8$ have c ∿ 14 Å. The rationalization for this doubling of the unit cell is found in the *aluminum avoidance principle*, attributed to Loewenstein (1954) but perhaps more clearly stated by Goldsmith and Laves (1955): "An ordered Al-Si array where the Al:Si ratio is 1:1 should be expected to follow Pauling's electrostatic valence principle best if each Al tetrahedron is surrounded by Si tetrahedra and vice versa." In other words, in framework aluminosilicates Al-O-Al linkages tend to be unstable and thus not to occur. Whether this principle is universally applicable or not is moot: in the plagioclases it provides the most consistent rationalization for exolution phenomena, antiphase domain textures, and observed Al,Si order-disorder patterns.

---

[5] Laves (1960) introduced the term *analbite*. *High albite* was used inaccurately for analbite in the first edition of this volume.

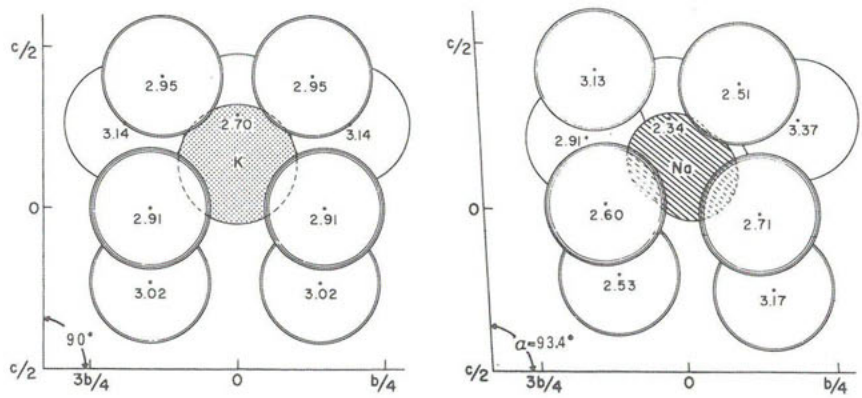

Figure 10. (a) Oxygen coordination around K in *C2/m* high sanidine and (b) around Na in $C\bar{1}$ analbite, both at room temperature. Projection is onto the *bc* plane; the numbers are K-O of Na-O distances in Ångströms.

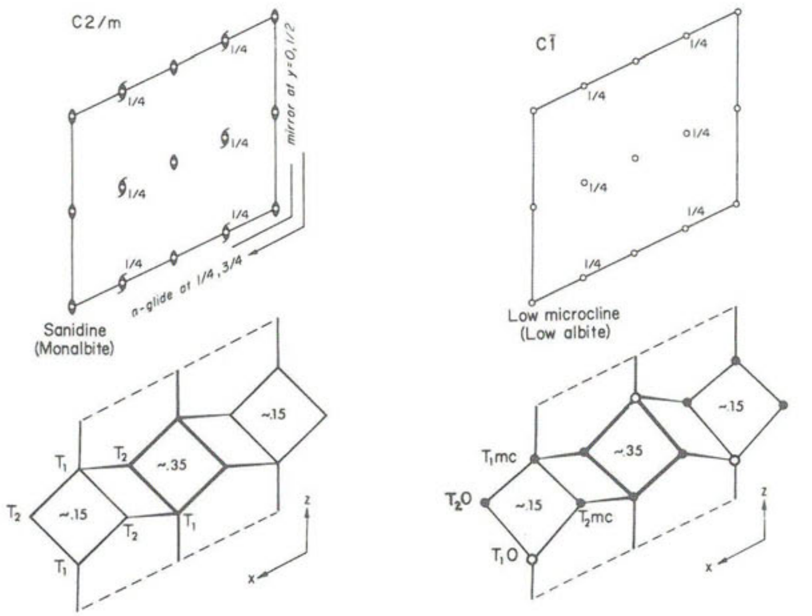

Figure 11. The two drawings on the left are (010) projections of the space group symmetry and topology of monoclinic alkali feldspars, as in Equations 2, 3 and 4. The pair to the right are for triclinic K,Na feldspars with Al (open circles) ordered (or partially ordered) into $T_1$0, as in Equations 5, 6 and 7. *Cf*. Figure 7.

In the particular case of anorthite, perfect •••Al•••Si•••Al•••Si••• alternation is established from the mean T–O bond lengths for each tetrahedron in the structure.[6] Celsian, $BaAl_2Si_2O_8$, is expected to have a similar Al,Si distribution. We will consider the ideally ordered celsian structure first because it is monoclinic due to the expansive effect of the large barium atom (radius ∿ 1.4 Å) on the framework, whereas anorthite is triclinic (radius of calcium ∿ 1.0 Å).

I2/c *celsian*. Celsian crystallizes in the unconventional space group $I2/c$ with $a \sim 8.6$, $b \sim 13.0$, $c \sim 14.4$ Å; $\beta \sim 115°$. Its symmetry elements are shown in Figure 12a and the accompanying distribution of Al and Si in 12b. Notice that the only way to satisfy the aluminum avoidance principle for the case of an Al:Si ratio of 2:2 is to double the c cell dimension (*cf.* with Fig. 11). Adjacent four-membered rings along the z direction are geometrically very similar, but differ in Al,Si arrangement, and the pairs of T sites in the doubled cell which are related by a pseudo-translation along z are given labels $T_1$00-$T_1$0z, $T_2$00-$T_2$0z, etc. Because of the Al,Si ordering pattern, atoms which were related by a mirror plane in $C2/m$ feldspars (Fig. 11) are now related by a pseudo-mirror operation which is, in fact, a c-glide parallel to (010) through the origin. Thus, as perceivable in Figure 12b, $T_1$00 is symmetrically equivalent to T_1mz, $T_2$0z is equivalent to T_2m0, and all four contain Si. Of necessity, then,

$$t_1oz = t_1mo = 1.0 \ \& \ t_2oo = t_2mo = 1.0; \ t_1oo = t_1mz, \ \ t_2oz = t_2mo = 0.0.$$

The a-glides at $y = \frac{1}{4},\frac{3}{4}$ of space group $C2/m$ persist in celsian, although half of the centers of symmetry and half of the two-folds and two-fold screw axes are destroyed. C-face centering of the 7 Å lattice is replaced by I-centering in the 14 Å cell (Fig. 13). The barium atom and O_A2 in celsian are located coincidentally on the c-glide at $y = 0$, and O_A1 is at $x = 0$, $z = 0$ (*cf.* Fig. 7b).[7]

P$\bar{1}$ *anorthite*. The ordering pattern in anorthite is the same as that in celsian, and thus c must be 14Å. But because calcium is smaller than

---

[6] For a silicon-containing tetrahedron these values are close to 1.614 Å, and for an aluminum-containing tetrahedron 1.747 Å (Wainwright and Starkey, 1971). Differences in tetrahedral means and even individual T–O bond lengths from these values can be explained in terms of anion coordination and bond angles (Phillips *et al.*, 1973; Ribbe *et al.*, 1974); but see Chapter 3 for detailed bonding explanation.

[7] This is not the case for Sr, O_A1, and O_A2 in synthetic Sr-feldspar which has the same space group and ordering pattern as celsian (Chiari *et al.*, 1975, Fig. 1, p. 113).

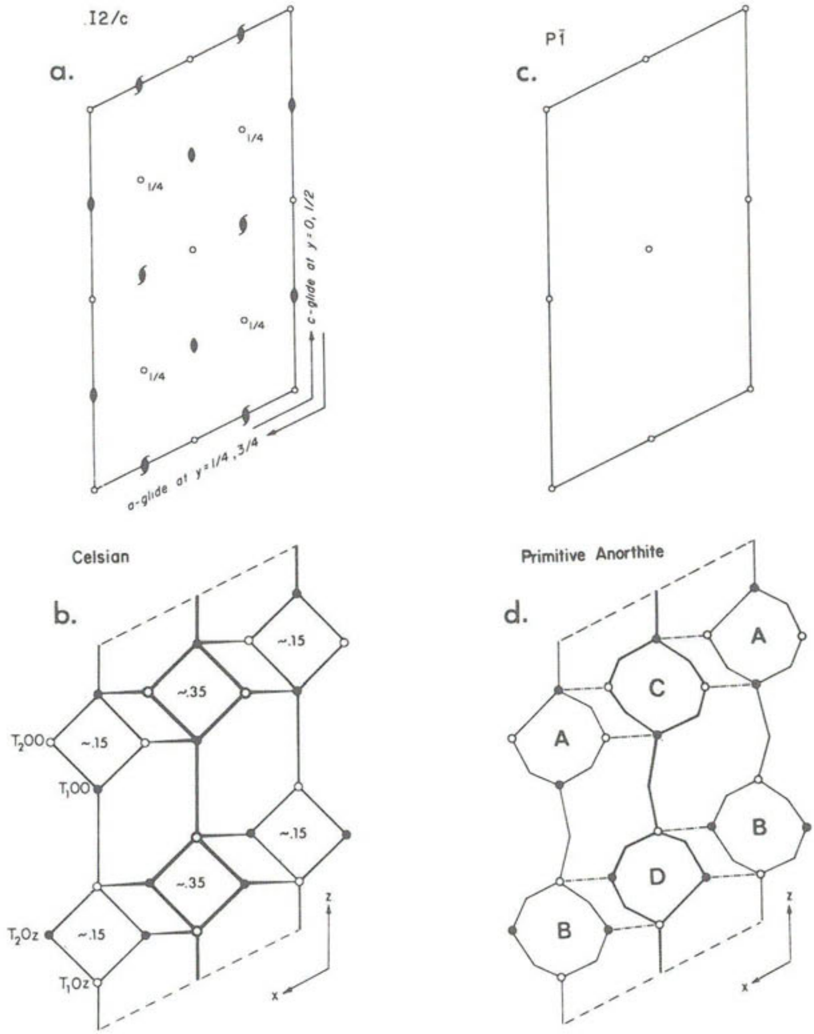

Figure 12. (a) The symmetry elements of $I2/c$, the unconventional space group of celsian. (b) The distribution of Al (open circles) and Si (dots) in celsian; $c \sim 14$ Å, *cf.* Figure 11 (right side). (c) The $P\bar{1}$ space group and (d) The Al,Si distribution in ordered anorthite. The distortion of the four-membered ring is shown to demonstrate their non-equivalence: pairs A,D and C,B are topologically similar but the sequences of Al...Si...Al...Si are different, whereas the reverse is true of pairs A,C and B,C. Modified from Megaw (1974a).

barium, anorthite has a partially collapsed framework and space group $P\bar{1}$, which is a subgroup of $I2/c$. Glide planes, rotational symmetry operators, and one-half of the centers are lost (*cf.* Figs. 12a and 12c). The four-membered rings which in celsian were related by both pseudo-translation

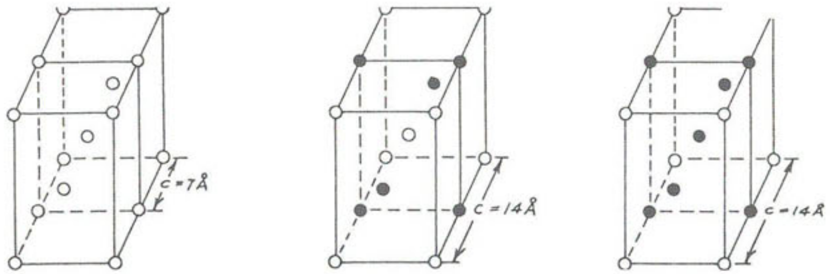

C$\bar{1}$, C2/m
Alkali feldspars
Sodic plagioclases
High plagioclases

I2/c , I$\bar{1}$
Celsian
Bytownite
Anorthite at high T

P$\bar{1}$
Anorthite

Figure 13. Perspective sketches of the feldspar lattices. Open circles are lattice points, filled circles are pseudo-lattice points. Two unit cells of the 7Å *C* lattice are shown for comparison with the 14Å *I* and *P* lattices. See Figure 14.

and pseudo-mirror operations[8] are no longer symmetrically equivalent because of distortions of the ring geometries (Fig. 12d). There are now 16 unique *T* sites, 8 contain Al and 8 Si. There is a high degree of pseudo-symmetry relating these *T* sites, all of it inherited from the topologic similarities uniting all feldspars to what Megaw (1974a) calls the *aristotype*, i.e., *C*2/*m* sanidine. There are pseudo-mirrors (as in $C\bar{1}$ albite and microcline), pseudo-translations (as in celsian), pseudo-centers and pseudo-*C* and *I* centering. The sequence of lattice types C ($c \sim 7$Å) $\rightarrow I$ ($c \sim 14$Å) $\rightarrow$ P ($c \sim 14$Å) is presented in Figure 13. When the Al,Si distribution changes from a disordered to an ordered state, the crystal's space group changes from $C\bar{1}$ to $I\bar{1}$. This may occur during cooling as the plagioclase leaves the $C\bar{1}$ stability field, or isothermally, when the plagioclase -- first metastably crystallized in $C\bar{1}$ -- inverts to $I\bar{1}$. The $I\bar{1} \rightarrow P\bar{1}$ inversion is displacive in nature and occurs during cooling at lower temperatures. These polymorphic phase transitions are possible because of the high degree of pseudosymmetry in the anorthite structure.

I$\bar{1}$ *anorthite*. With heating, anorthites which are primitive at room temperature invert to body-centered structures at temperatures that are dependent on their exact composition and their thermal history (i.e., the degree to which antiphase domains have developed on initial cooling). Using ^{27}Al NMR signals, Staehli and Brinkmann (1974) found that an $An_{99.5}$ (composition corrected by Brinkmann -- see Adlhart *et al.*, 1980a, p. 451)

---

[8] These in combination are equivalent to the *c*-glide operation in space group *I*2/*c*.

sample inverted from $P\bar{1}$ to $I\bar{1}$ at 241±4°C. Using neutron methods Adlhart *et al.* (1980a,b) found that An_{100} inverted at 240±4°C, An_{95-97} below 200°C; the transition is displacive and reversible, and *above* T_c the time-averaged lattice is exactly body-centered, and not just a space-averaged structure as was concluded by earlier authors[9] and as is the case for $I\bar{1}$ bytownite (see below). The Al,Si distribution of the $I\bar{1}$ anorthite is like that in $I2/c$ celsian and presumably unchanged from that in the room-temperature $P\bar{1}$ phase. Compare Figures 12a,b and Figure 16 (see below), which gives the symmetry elements for the $I\bar{1}$ cell.

Summary of feldspar site nomenclature

Figure 14a shows schematically the pseudosymmetrical relationships among selected sites associated with each of the lattice and pseudo-lattice points in the $P\bar{1}$ anorthite cell, which has the lowest symmetry of all feldspars. Specifically, $T_1$000 is related to $T_1$0z0 by a pseudo-z translation $z \sim \frac{1}{2}[001]$, to $T_1$00i by pseudo-body-centering $i \sim \frac{1}{2}[111]$ and to $T_1$0zi by a combination of z and i which is equivalent to pseudo-C-centering, ½[110] (see Fig. 14b). Each of these sites is in turn related by a pseudo-mirror at $y = \frac{1}{2}$ to T_1m00, T_1mz0, T_1m0i, T_1mzi. There is a completely analogous set of T_2 sites, and the Al occupancies in ordered anorthite are summarized below:

Si sites: $t_1$ooo ≅ $t_1$ooi ≅ $t_1$mzo ≅ $t_1$mzi ≅ $t_2$ozo ≅ $t_2$ozi ≅ $t_2$moo ≅ $t_2$moi ≅ 0.0

Al sites: $t_1$ozo ≅ $t_1$ozi ≅ $t_1$moo ≅ $t_1$moi ≅ $t_2$ooo ≅ $t_2$ooi ≅ $t_2$mzo ≅ $t_2$mzi ≅ 1.0

The notation for these sixteen T sites (as well as the 4 calcium and 32 oxygen sites) in P-anorthite was established by Megaw (1956). With reference to the foregoing text and Figure 14, it should be possible to decipher the pseudosymmetrical relationships of chemically similar sites to one another both within a given unit cell type and amongst the five main feldspar space groups. But in my experience, many students of feldspar crystal chemistry are thoroughly confused by the site nomenclature. For that reason a flow-chart connecting pseudosymmetrically related T sites is presented in Figure 15. When a $C\bar{1}$, c = 7 Å "average structure" is discussed, the Al contents of the two or four sites connected by arrows to $T_1$0 are averaged, likewise those connected to T_1m, $T_2$0 and $T_2\bar{0}$ (see Fig. 16 in Ch. 2). Note that the 7 Å average structure both of $I\bar{1}$ and $P\bar{1}$ anorthite has equal Al in all four T sites.

We have not yet considered one of the structure types listed among the 14 Å plagioclases. It is called '*body-centered*' *anorthite* or '*body-centered*' *bytownite* for reasons described below.

----

[9]See Brown *et al.* (1963); Bruno and Gazzoni (1967); Foit and Peacor (1967, 1973); Czank *et al.* (1970); Laves *et al.* (1970).

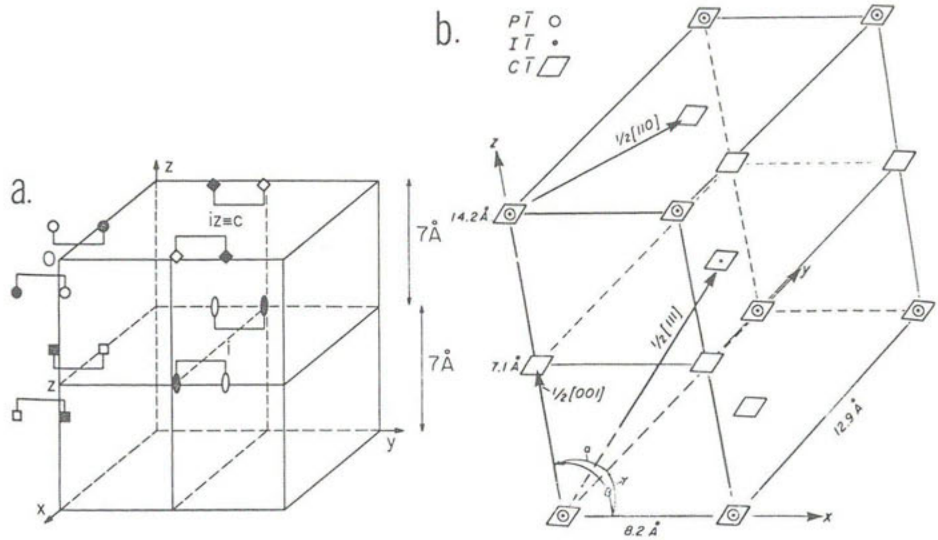

Figure 14. (a) Schematic drawing of the topologic properties of the four subcells in the unit cell of anorthite. The operators i, z and $C = iz$ take the starting positions denoted by O and produce the three further sets. Identical symbols are related by the centers of symmetry in $P\bar{1}$. Open and filled symbols are related by the pseudo-mirror plane perpendicular to the y-axis. In body-centered anorthite, the sets O and i, and z and iz become identical in pairs to yield the potential topologic symmetry of $I2/m$. In albite, all four sets become equal to yield the potential topologic symmetry $C2/m$. After Smith and Ribbe (1969, Fig. 2).

(b) An illustration from Wenk *et al.* (1973) showing the three feldspar lattices of Figure 13 superposed on a $P\bar{1}$, c = 14.2 Å cell. The equivalent lattice points for the $C\bar{1}$, $I\bar{1}$ and $P\bar{1}$ space groups are indicated by the symbols in the key. The body-centering (i) vector is ½[111], the c-translation (z) vector ½[001], and the C-centering (iz) vector ½[110]. The approximate cell dimensions are a = 8.2, b = 12.9, c = 7.1 or 14.2 Å.

Figure 15. A "flow chart" of T-site nomenclature for the feldspars. The sites which contain aluminum in ordered feldspars are in italics. The order of T_1 and T_2 postscripts is not an essential feature of the site designation. For completely labeled figures of the ($P\bar{1}$ anorthite), see Wainwright and Starkey (1971).

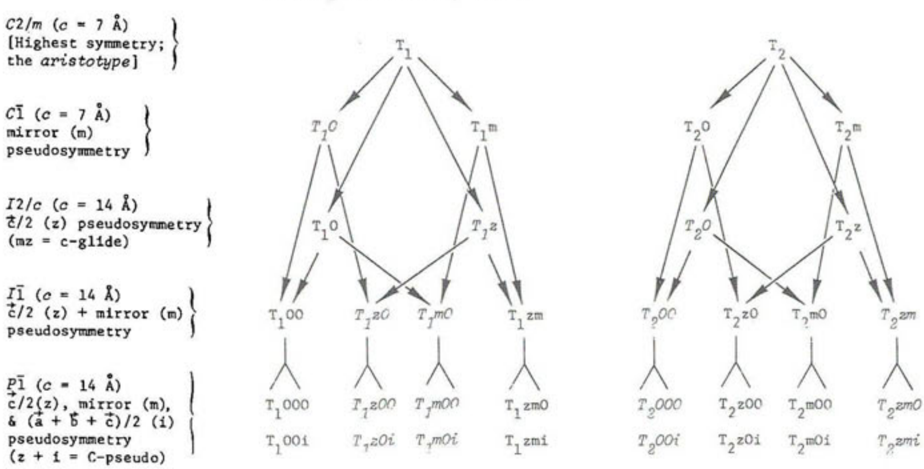

Antiphase domains and the $I\bar{1}$ average structure

Single-crystal diffraction patterns indicate that certain bytownites ($An_{\sim 80}$) and possibly some calcic plagioclases *appear* to be body-centered ($I\bar{1}$) at room temperature (Fleet *et al.*, 1966; see Fig. 16). This phenomenon arises from the high degree of *I*-pseudosymmetry in the primitive $c \sim 14$ Å structure (described above for anorthite) in which there are pairs of subcells so nearly alike that "a mistake is possible which puts them out of step, i.e., *out of phase* by in their Bragg diffraction effects" (Megaw, 1974, p. 17). Megaw (1962) describes this phenomenon in detail, so I will not reiterate except to point out that it is domains of perfect structure ($P\bar{1}$) related to one another by stacking vectors ½[111] (Fig. 14b), producing the so-called average structure which is imaged by x-ray diffraction (Fig. 16). The domains are called 'antiphase' domains because their superposition results in the extinction of a class of Bragg diffraction maxima $h+k+\ell$ odd. More details of this effect are discussed in the following chapter.

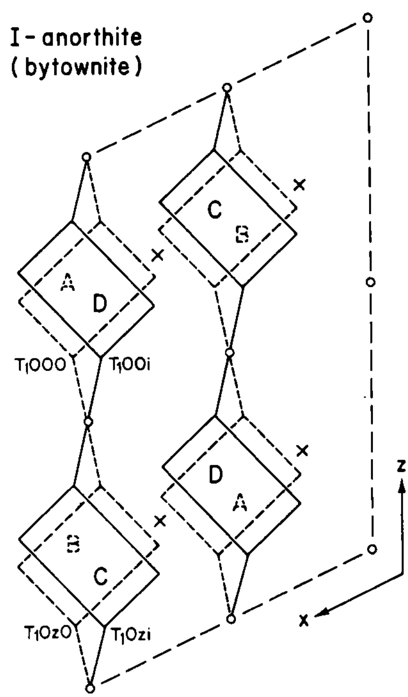

Figure 16. A representation of the effective structural averaging that occurs by the antiphase superposition of domains of primitive anorthite-like structure (stylized rings A,B, C,D - *cf*. Fig. 12) to form $I\bar{1}$ 'body-centered' anorthite or bytownite. Modified from Megaw (1962). Small open circles, as in Figure 12c, represent centers of symmetry found in $P\bar{1}$; small ×'s are centers at y = 1/4,3/4 in $I\bar{1}$. The averaging involves sites in $P\bar{1}$ anorthite which are related by pseudo-body-centering, e.g., T_1000 and T_1001. The 'average atom' is anisotropic in the $T_1000 \leftrightarrow T_1001$ direction, and the contoured electron density near this and other *T*-sites looks like this:

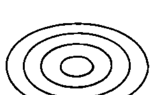

Chapter 2

ALUMINUM-SILICON ORDER in FELDSPARS; DOMAIN TEXTURES and DIFFRACTION PATTERNS

P. H. Ribbe

INTRODUCTION

The intent of this chapter is to summarize, insofar as possible, the phenomena accompanying the ordering of aluminum and silicon in the tetrahedral framework of feldspars of a variety of initial bulk compositions. This is a difficult undertaking, because for the most part our experimentation has involved either (1) synthesis of highly disordered phases which upon annealing do not readily order because of high kinetic barriers to Al,Si diffusion or (2) heating of natural specimens in which Al,Si diffusion often can be shown with certainty to trace a different path to a disordered arrangement than occurred in the reverse direction during annealing in a geologic time framework. Furthermore, exsolution accompanies Al,Si ordering in many alkali and plagioclase feldspars, and in the latter this is of considerable consequence since phase separation involves NaSi $\rightleftarrows$ CaAl substitution and thus diffusion of tetrahedral Al and Si over hundreds or even thousands of Ångströms (see Ch. 10). Twins, antiphase domains and superstructures complicate the scenario. Therefore, ultimately we must rely heavily, though not exclusively, on detailed observations of suites of natural specimens from well characterized geologic environments to construct sensible models of reality. High resolution transmission electron microscopy (HRTEM) has proven epsecially valuable in this endeavor, and when coupled with less resolute methods of observation (crystal structure determinations, unit cell dimensions, optical and other physical properties), there has been a great deal of progress in recent years.

We will consider each feldspar composition range separately, discussing the ordering process and accompanying structural and textural changes, together with diffraction phenomena. Where exsolution occurs, references will be made to appropriate chapters elsewhere in this volume. Inevitably, some of our data have been derived using methods described in later chapters, but detailed explanations are deferred in the interest of simplicity.

SEQUENCES OF Al,Si ORDERING IN ALKALI FELDSPARS

Ordering in K-feldspars involving a monoclinic → triclinic inversion

With the nomenclature of the previous chapter in mind, I will now attempt a simplistic explanation of the ordering mechanisms operative in single-phase K-rich feldspars. Monoclinic high sanidine (Eqn. 2, Ch. 1) is the most disordered K-feldspar polymorph, and it is represented only rarely in rocks quenched near 1000°C (Stewart and Wright, 1974). If this material is annealed for geologic times at lower temperatures, Al migrates preferentially into the T_1 sites from the T_2 sites in an attempt to lower the free energy by balancing the local electrostatic charge distribution. The charge imbalance can be traced to oxygen atoms, O_A1 and O_A2, both of which are bonded to two T atoms.[1] In sanidine O_A1 is bonded to two four-coordinated T_1 atoms and two nine-coordinated monovalent K atoms at ∿2.9 Å, but O_A2 is bonded to two T_2 atoms and only *one* potassium atom at ∿2.7 Å. Thus O_A1 is formally overbonded because the total bond strength[2] reaching it is $\Sigma S = [2 \times \frac{3}{4} \div 4] + [2 \times \frac{1}{9}] = 2.097$, whereas for O_A2 $\Sigma S = [2 \times 3\frac{3}{4} \div 4] + [1 \times \frac{1}{9}] = 1.986$. Since the T_1 atom is bonded to $O_A1 + O_B + O_C + O_D$ and the T_2 atom is bonded to $O_A2 + O_B + O_C + O_D$ (Fig. 7b, Ch. 1), Al will prefer the T_1 site and Si the T_2 site, leading to smaller values of ΣS for O_A1 and larger values for O_A2. Configurational entropy increases and free energy decreases as Al orders into T_1. This is demonstrated in Figure 1 for the known refinements of K-rich feldspar structures. Notice that mean T–O bond lengths have been plotted for each of the symmetrically nonequivalent sites in the structures. This avoids for the moment a direct conversion of these values to Al contents which have in the past been estimated using any one of several linear models relating Al-content of T sites to mean T–O distances (see discussion in Ch. 3). Approximate Al contents may be read from the upper abscissa.

The $\langle T\text{–O}\rangle$ data for K-rich feldspars (Fig. 1) do not represent a *unique* path of Al,Si segregation into nonequivalent T sites as a function of temperature. But the manner in which ordering occurs at the atomic scale is quite straightforward: Al migrates into $T_1$0 and T_1m and the center-of-symmetry related sites, $T_1$0c and T_1mc, with equal probability as long as the structure

---

[1]As are all oxygen in feldspars: the Zoltai (1960) sharing coefficient for tetrahedral frameworks is 2.00.

[2](Pauling, 1929). The formal charge on the average atom $\frac{1}{4}Al^{3+} + \frac{3}{4}Si^{4+}$ which occupies T_1 and T_2 in sanidine is $3(\frac{1}{4}) + 4(\frac{3}{4}) = 3\frac{3}{4}$.

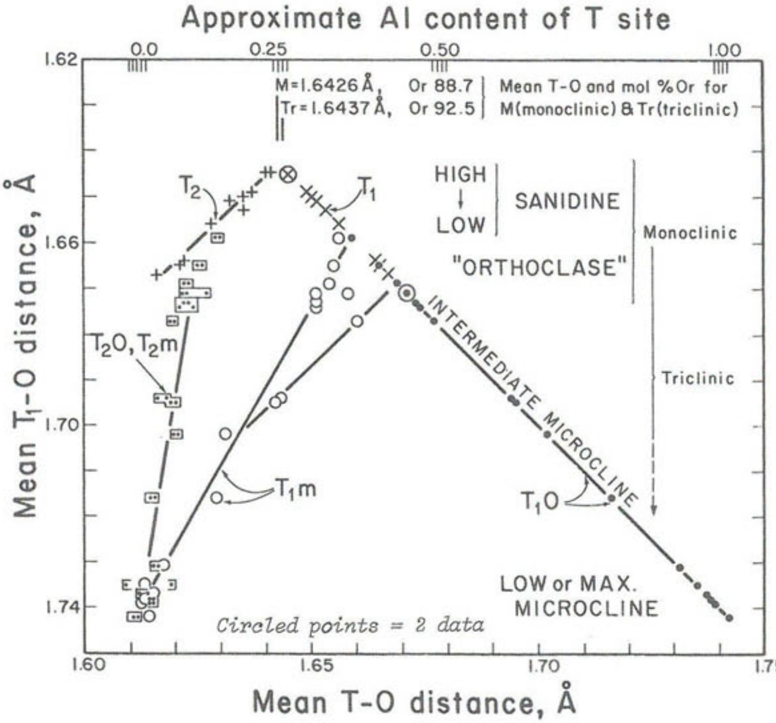

Figure 1. A plot of the mean T-O distances as a function of the mean T_1O-O distance for the individual tetrahedra in K-rich feldspars, as determined by crystal structure analyses (see Tables 2 and 3, Ch. 3; 4 microclines from Blasi, pers. comm.). Presentation of the data in this manner disposes of the necessity of selecting a model -- linear or otherwise -- for relating mean T-O to Al content of the T site, but *approximate* Al contents are indicated on the upper abscissa. The variation of $t_1o - t_1m$ (as represented by the T_1m data points) observed in the more highly disordered intermediate microclines suggests that there are a range of paths from microcline to fully ordered low microcline.

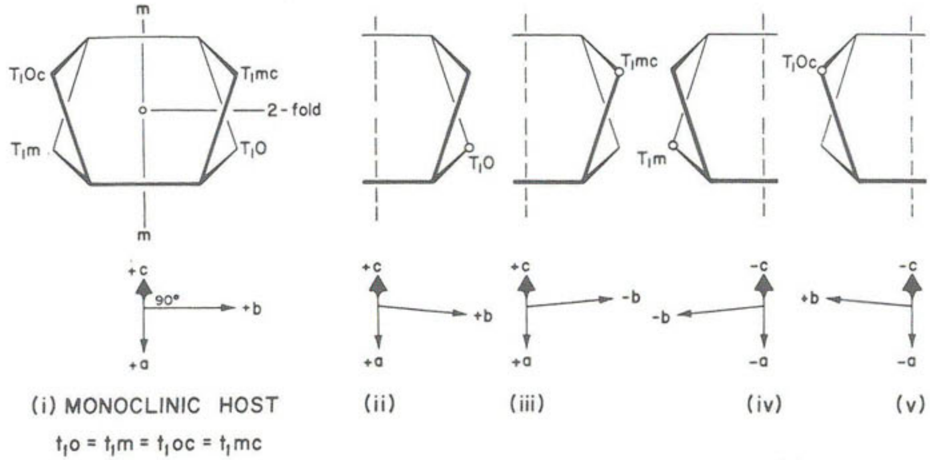

Figure 2. Illustrations based on the (001) projection of the feldspar structure (*cf*. Fig. 9, Ch. 1 and Brown, 1962) showing the sites available for Al occupancy and the geometrical distortion of the stucture which results with each occupancy. (i) The undistorted monoclinic host; $\alpha = \gamma = 90°$. Note that T_1Oc is related to T_1O by a center of symmetry indicated by the small open circle. (ii - iv) The various distortions of the unit cell to triclinic geometry ($\alpha \neq \gamma \neq 90°$) as Al segregates into T_1O, T_1mc, T_1m, T_1Oc, respectively. The axial orientations are all relative to that shown in (i).

remains monoclinic. But complications set in because as unit cell-scale domains nucleate and grow, local stresses are built up due to the tendency of the structure to distort to a triclinic configuration consistent with local segregation of the larger Al atom into one of the available T_1 sites. With reference to Figure 2 it is evident that there are four possible orientations of distorted cells (i.e., triclinic cells), beginning from a monoclinic host feldspar whose axial orientation is chosen as a reference.

Development of polysynthetic twins in microcline.[3] If one of the triclinic domains, illustrated in Figure 2(ii)-(iv), were to nucleate and grow alone with, for example, Al segregating into the site designated $T_1$0, the resulting triclinic microcline would have axial orienation (ii); if Al instead went systematically into T_1m, the axial orientation would be (iii).[4] If any two of these orientations develop simultaneously in proximity to one another, either an Albite twin pair or a Pericline twin pair will result. The Albite twin pair would have (010) as its composition plane and the normal to (010) (i.e., b^*) as its twin axis; the Pericline twin pair would have b as twin axis and a nonrational plane parallel to y (the rhombic section) as its composition plane.[5]

If all four of these orientations develop in the originally monoclinic feldspar as Al orders into $T_1$0, T_1m, $T_1$0c, and T_1mc in different regions of the crystal, a particular texture develops which can be imaged only by transmission electron microscopy (Fig. 3). McConnell (1971) suggested that this texture resulted from a metastable balance between the reduction in free energy resulting from increasing Al,Si order (inversion energy) and the local strain energy produced by structural distortions as Al segregates into the four equivalent T_1 sites. At an early stage of development mutually orthogonal distortion waves are superimposed on the monoclinic lattice of the feldspar (Fig. 4), the amplitude of the "wave" increasing as ordering increases. In single-crystal x-ray diffraction patterns this phenomenon would show up as rows of spots similar to superlattice reflections whose periodicity in reciprocal space is

----

[3]Early ideas were developed by Goldsmith and Laves (1954a,b).

[4]There is some confusing slight-of-hand that occurs in the latter case, because the label on the T_1m site as originally assigned in the drawing of the monoclinic structure (Fig. 2(i)) must be changed to $T_1$0 to conform to conventions for triclinic feldspars, but the axial orientation relative to (i), (ii), (iv), and (v) remains unchanged.

[5]See Smith (1974b, Ch. 18) for an extensive review of feldspar twin geometry and genesis and Chapter 13 for discussion of mechanical twinning.

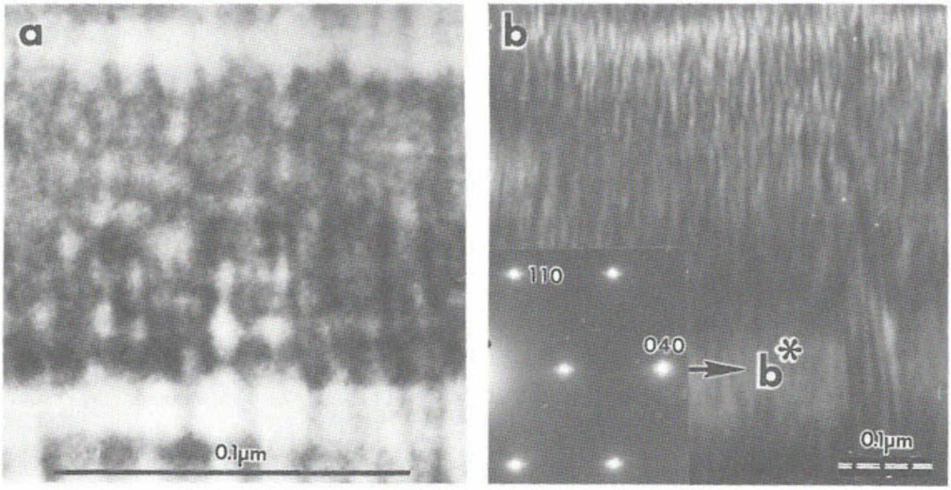

Figure 3. (a) Dark-field TEM photo of an adularia which is structurally classified as low sanidine or orthoclase. The dark and light contrast is caused by superimposed, mutually orthogonal transverse distortion waves (Fig. 4) which in turn result from Al,Si ordering in a monoclinic host. See text and McConnell (1971) for full discussion. From McConnell (1965). (b) "Orthoclase". Photo courtesy of Chr. Krause, Münster.

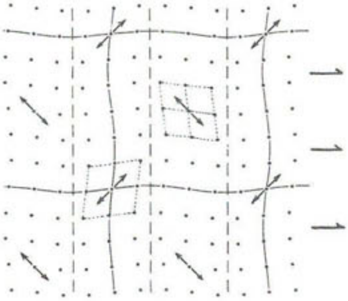

Figure 4. Schematic diagram illustrating the pattern of distortions due to two orthogonal transverse waves in the lattice of a monoclinic adularia. The dots represent the positions of the lattice points, and the two types of distortion are indicated by the system of arrows. After McConnell (1971, Fig. 2). Dashed vertical lines are traces of an a-glide parallel to (010), indicating how weak, diffuse reflections $h+k$ odd may possibly appear in single-crystal diffraction patterns, producing a feldspar with space group $P2_1/a$, such as that discovered by Laves and Goldsmith (1961).

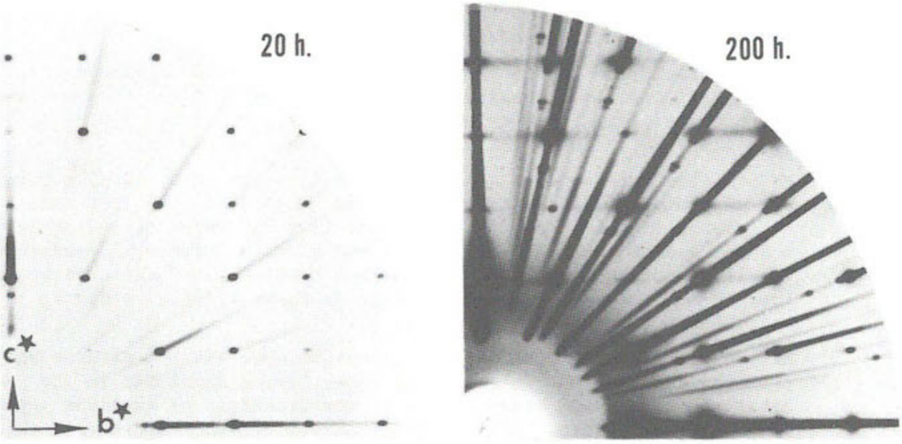

Figure 5. Partial zero-level x-ray precession photographs of an orthoclase (not one those pictured in Fig. 3). The 200 hour exposure shows diffuse streaks resulting from distortion waves (*cf.* electron diffraction pattern in Fig. 3b). Streaking is much more prominently developed parallel to b^* than normal to it, indicating a predominance of Albite twin-like domains (*cf.* Fig. 6). If triclinic domains had developed to larger sizes, splitting into pairs of reflections along b^* would be expected, with streaks between them. Notice that in the 20 hour exposure with CuK_α radiation, streaking is not evident. Use of an oscillating precession camera would speed up observations by a factor of three or more. Photos courtesy of Prof. M. Korekawa.

inversely related to the "wavelength" of the distortion. In nature the periodicity of the waves is not sufficiently regular to produce this type of pattern; in fact, diffuse streaks elongate normal to the crests and troughs of the distortion waves are observed through the Bragg diffraction maxima of the monoclinic lattice (Fig. 5). The structure of such a feldspar (usually low sanidine, orthoclase or adularia) is still formally considered to be monoclinic; at least optically, although x-ray peaks in powder diffraction patterns may show some broadening.

For one of these distorted domains to obtain its own identity as a highly ordered triclinic crystal its size must be sufficient for coherent diffraction (∿500-1000 Å); ultimately, all four Albite and Pericline twin orientations should be present in roughly equal volumes with twin composition planes forming at the boundaries between differently-oriented domains. Powder patterns will now indicate triclinic feldspar, and likewise optical properties, if the twins are large enough to be resolved optically (5000-10,000 Å). Otherwise the light rays will average over the domains and give optical properties still consistent with monoclinic low sanidine or orthoclase, thus accounting for the peculiar mixture of triclinic powder patterns and monoclinic optics observed by Laves and Viswanathan (1967).

The intricacies of one particular monoclinic → triclinic inversion have been strikingly illustrated by Eggleton and Buseck (1980) using HRTEM and conventional x-ray methods, together with an analysis of the strain energy that develops as the triclinic domains are constrained within the basic monoclinic topology of the original crystal. Their electron-petrographic study led them to deduce the following sequence of events.

(1) Highly disordered K-rich feldspar crystallizes from a granodiorite, with Al,Si order progressing until each of the T_1 sites in monoclinic orthoclase ($Or_{\sim 93}$) contains ∿0.40 Al, i.e., $t_1o + t_1m \simeq 0.80$ (value determined using the *b* and *c* cell dimensions; see Ch. 3).

(2) Minute triclinic domains then form with straight (020) lattice planes but sinusoidal ($\bar{2}01$) planes alternately "tipped" to the left and the right (Fig. 6). A "dimpled domain texture" results (see Eggleton and Buseck, 1980, their Figs. 4 and 5) with structural coherency in all directions, the domains continue to widen, and the crystal remains monoclinic to x-rays. Energy released by Al,Si ordering accumulates as strain energy (Fig. 7).

(3) At $t_1o + t_1m \simeq 0.85$ "the energy balance between elastic strains and twinning dictates the formation of some chevron character in the domains, they become mixed, and discrete triclinic reflections appear in the x-ray pattern. At this stage ... the domain texture causes the angles [α,γ or α^*,γ^*; see Ch. 3] to be constrained towards monoclinic values," i.e., the true Al,Si distribution within the individual domains might be $t_1o - t_1m \simeq 0.8$, but because of strain the angles might suggest $t_1o - t_1m \simeq 0.3$. In all of this the relative position

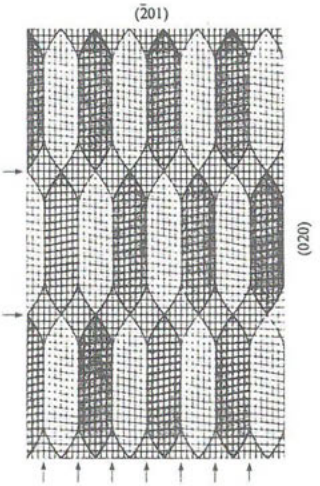

Figure 6. Schematic of the (020) and ($\bar{2}01$) lattice planes in "dimpled terrane" of the Or_{93} discussed in the text. The domains have "part chevron, part sinusoidal variation in obliquity", with the left- and right-oriented triclinic domains tending toward Albite twin configuration and the monoclinic regions (diamond-shaped) serving as domain bounding surfaces (arrows). Half of the ($\bar{2}01$) planes have been omitted. From Eggleton and Buseck (1980, their Fig. 6, p. 128). Compare with Figure 3; streaking like that in Figure 5 might be apparent in x-ray photographs of this material, although if domains are large enough, twinned triclinic patterns might be evident with streaking between twin-related peaks.

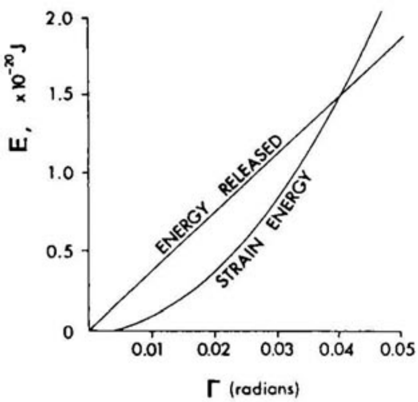

Figure 7. Approximate representation of a linear release of inversion energy, E($\times 10^{-20}$ joules), and a parabolic increase (approximately proportional to Γ^2) of strain energy, plotted against increasing $\Gamma = \pi(90-\gamma)/180$, where γ is the unit cell angle. From Eggleton and Buseck, (1980, their Fig. 9, p. 132).

of cell edges on the *b-c* plot (Fig. 4 in Ch. 3) indicates that $t_1o + t_1m$ remains between 0.85 and 0.9.

(4) Addition of energy (e.g., by tectonic faulting) permits the "accumulated strain to be released by dislocation movement" and larger, Albite-twinned domains of maximum microcline develop. Thus the bimodal distribution of "triclinicites" of K-feldspar megacrysts in the Kameruka granodiorite (Eggleton, 1979) are explained as representing strained intermediate microclines (small values of $t_1o - t_1m$) and unstrained low microclines ($t_1o - t_1m \simeq 1$). The difference between the two values of $t_1o - t_1m$, when converted to inversion energy, "represents the effects of release of strain energy by shear" (Eggleton and Buseck, 1980, p. 132).

From all of this comes the warning that care must be exercised in geological interpretations of average Al,Si distributions determined from cell parameters or optical measurements: K-feldspars may be severely strained (thereby masking their true degree of order) and they probably will not order past the stage at which the release of inversion energy balances the strain energy. "The particular balance reached depends on the situation of the feldspar, and if the strain can be released, whether by shearing, hydrothermal activity, or another process, ordering can proceed unhindered." Thus the Al,Si distribution in a K-feldspar ... "may represent the temperature of the final strain-releasing process" (Eggleton and Buseck, 1980, p. 133).

This explains the persistence of monoclinic orthoclase (which is sometimes strained) and/or severely strained, partly ordered intermediate microcline in rocks containing fully ordered low albite. The two are often intimately intergrown as cryptoperthites (see Chs. 6 and 7). Such a metastable situation is common for K-feldspars in igneous rocks, but when conditions are suitable for inversion (as in some pegmatites and low-grade metamorphic rocks), the microcline which forms is *always* intimately twinned on either or both Pericline and Albite laws, often producing the familiar cross-hatched pattern which in polarized light is much coarser than, but similar in appearance to orthoclase with distortion waves or "dimpled terrane" (Figs. 3 and 6). McLaren (1978) reviewed occurrences of combined Albite-Pericline ("M"-) twinning in microcline, and FitzGerald and McLaren (1982) concluded that the two occur in separate areas of the crystal and that "significant changes subsequently occur which produce microstructure involving essentially Albite twinning only" (McLaren, 1983). In that regard, note the dominance of the Albite-twin component in Figures 3, 5 and 6, and see examples of "M"-twins (Figs. 7 and 8, Ch. 10).

Untwinned or simple-twinned microcline. According to the forgoing, microcline which is simply twinned or is untwinned must have crystallized at moderately low temperatures (<450°C) in the field of triclinic K-feldspar. Authigenic microcline will never be cross-hatch twinned.

One-step or two-step ordering? It is obvious from studying non-authigenic suites of K-rich feldspars that in many if not most terranes they crystallize initially as monoclinic sanidine or orthoclase and subsequently invert to microcline, as described above. This is called an intermediate two-step ordering trend, as defined in the last section of Chapter 3, in which may be found a compendium of recent petrologic studies and a detailed discussion of the various order/disorder trends for K-rich feldspars. A one-step order trend, in which Al migrates into T_1O at an equal rate from T_1m, T_2O, T_2m, seems unlikely for K-feldspar, unless it crystallizes initially as a triclinic phase. But Blasi and De Pol Blasi (1980) reported a series of microclines with $1.0 \leqslant t_1o \leqslant 0.85$, $0.0 \geqslant t_1m \backsim t_2o \backsimeq t_2m \geqslant 0.05$ that plot nearly on the one-step path (Fig. 14 in Ch. 3) and which, because of submicroscopic twinning, they presume crystallized as monoclinic feldspar. Heating low microcline and low albite for various lengths of time generally produces Al,Si distributions along the one-step trend, but heating intermediate microclines and orthoclases produces a variety of disordering paths (see Ch. 3).

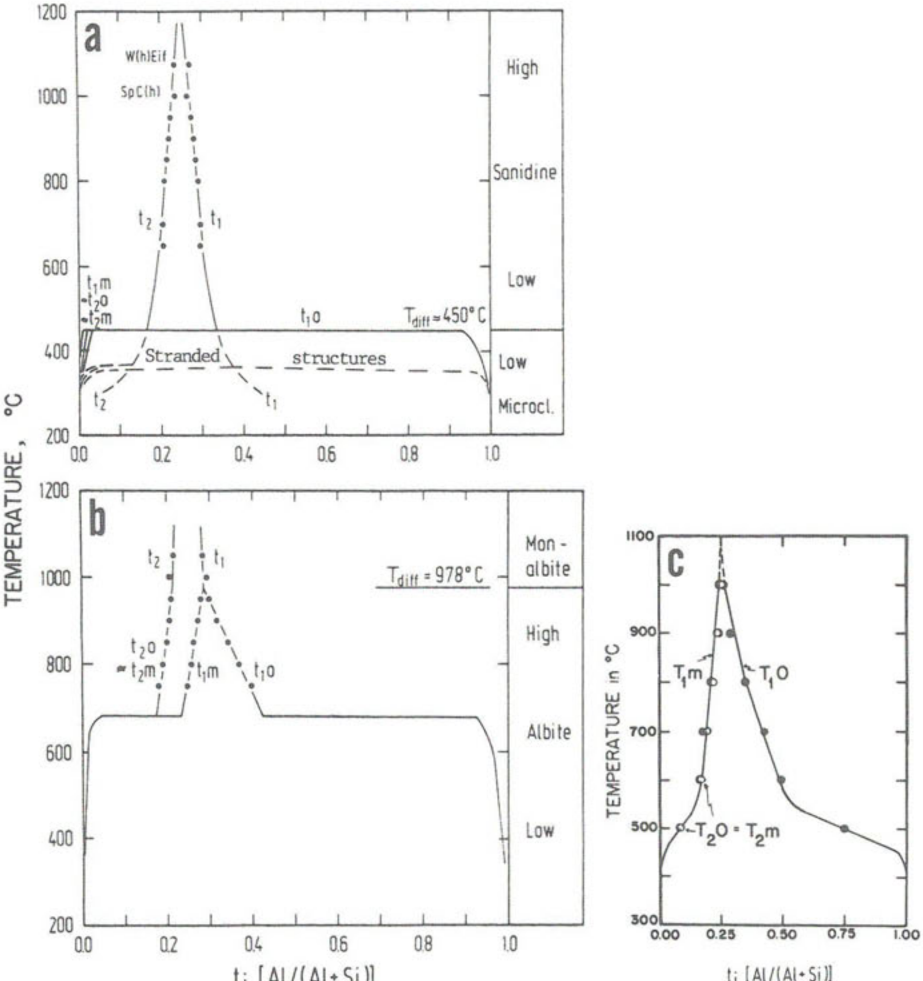

Figure 8.

(a) Approximate variation with temperature of Al site occupancies in K-feldspars. The data points were calculated from Equation (i) in Table 6, Chapter 3, using lattice parameters of synthetic K-feldspars which are thought to be equilibrated at least at $T > 800°C$ (Kroll, 1973). The sanidine-microcline inversion is arbitrarily taken to be a first-order transformation. As a consequence, intermediate microcline has no stability field of its own, but like monoclinic "orthoclase" is regarded as a structure that is stranded kinetically during the sanidine → microcline inversion.

(b) Approximate variation with temperature of Al site occupancies in Na-feldspars. The data points were calculated from Equations (ii) and (iii) in Table 6, Chapter 3, using lattice parameters of synthetic, presumably equilibrated Na-feldspars (Kroll *et al.*, 1980, Table 2a). The high albite → low albite inversion is arbitrarily taken to be a first-order transformation occurring at 680°C (*cf.* Raase, 1971; Senderov, 1980; and Smith, Ch. 9, this volume). From Kroll and Voll (in prep.).

(c) The Al,Si distribution deduced from lattice parameters in the suite of low albites which were annealed for extended times (at the temperatures indicated) by MacKenzie (1957). These data and those of most of the suite of Na-feldspars synthesized by Martin (1970) would fall on the one-step trend (Figs. 12 and 14, Ch. 3), whereas those in (b) above would not. From Stewart and Ribbe (1969, Fig. 6).

Temperature scale for the sanidine → microcline inversion. Stewart and Wright (1974, p. 368 f.) discussed the thermal significance of Al,Si ordering, and were duly cautious in assigning 375 ± 50°C to the upper stability of maximum microcline, ∿625-750°C for the range of crystallization of "orthoclase with $2t_1$ = 0.8 ± 0.1," and 800-900°C for "low sanidine or anorthoclase with $2t_1$ = 0.58 ± 0.05." Kroll and Voll (in preparation) propose a smooth increase of Al in T_1 from disordered high sanidine above 1100°C to $2t_1 \cong 0.65$ at ∿500°C, with a first-order (diffusive) transition to a highly ordered microcline ($t_1o + t_1m > 0.9$) at ∿450°C (Fig. 8a). They assign so-called stranded structures -- the orthoclases and intermediate microclines discussed above -- to metastable states between 450° and ∿350°C. I believe the range of these structures may extend to temperatures above 500°C, but this is difficult to document.

Ordering in triclinic alkali feldspars

Potassium feldspar. In the case of microcline which has inverted from sanidine, both T_1O and T_1m are initially equally enriched in Al relative to T_2O and T_2m. The ordering paths from partly disordered intermediate microcline to completely ordered low microcline are represented in the lower half of Figure 1. The solid lines drawn there are just two possible paths of ordering from high temperatures at which $t_1o \cong t_1m >> t_2o \cong t_2m$. With cooling Al moves most rapidly from T_1m to T_1O and much more slowly from T_2O and T_2m to T_1O. Several natural suites with extensive, but often discontinuous, series of microclines are discussed in the last section of Chapter 3 (see Figs. 12 and 13). Discontinuities are offered as evidence of metastability of intermediate microcline and the possibility of a first order sanidine → microcline inversion.

Sodium feldspar. Because Na-feldspar inverts at a very high temperature, it was formerly assumed that ordering commenced with T_1O already a distinct site. This impression was reinforced by the presumed equilibrium annealing experiments performed on low albite starting materials by MacKenzie (1957), as interpreted by Stewart and Ribbe (1969) in Figure 8c. But it is well documented now that heating experiments, at least for K-feldspars, do not by any means necessarily retrace the ordering paths that occur in nature. Thus we must reinterpret the Na-feldspar ordering sequence.

When pure Na-feldspar first crystallizes, it is monoclinic (monalbite), with $t_1o = t_1m$ and $t_2o = t_2m$. Although complete Al,Si disorder is possible at the highest temperatures, structural evidence and arguments from bonding considerations (see Chs. 3 and 4) indicate that $2t_1 = (t_1o + t_1m)$ may be somewhat greater than $2t_2 = (t_2o + t_2m)$, at least in all the highest structural state specimens investigated to date. This is seen in Figure 8b. At ∿980°C monalbite inverts to triclinic high albite -- the "diffusive transformation" of Laves (1952) -- as T_1m becomes distinct from $T_1$0. The rationale for Al,Si ordering is the same as for K-feldspars, discussed in detail above. Polysynthetic Albite and Pericline twins almost always develop, and without exception periodic A and P twinning on a 50-200 Å scale will develop in Na-feldspar exsolved from K-rich solid solutions (Willaime and Gandais, 1972; Brown and Willaime, 1974). The Na-rich phase in a cryptoperthite will often remain monoclinic to very much lower temperatures than the ∿980°C expected for an equilibrium transformation because there is coherence between the Na- and K-rich phases. Coherence raises havoc with our usual concepts of equilibrium, and the effects of strain on the phase relations of alkali feldspars are discussed in Chapter 6.

No Na-feldspar intermediate between analbite (or high albite) and low albite has been reported in nature, although some containing substantial amounts of Or (and sometimes even An) in solid solution have been called "intermediate albite." However, Thompson and Hovis (1974) report "fossil" evidence in the guise of the rhombic section angle (σ*) which indicates that intermediate albites once had equilibrated at ∿550°C but have since inverted to low albite because "the metamorphic and late-stage plutonic environments in which these intermediate albites would have formed are not conducive to the relatively rapid quenching necessary to preserve [them]." The assumption of Kroll and Voll in Figure 8b is that there is a first-order transformation to low albite at ∿680°C; Smith in Chapter 9 reached the same conclusion, though both acknowledge lack of evidence.[6]

SINGLE-CRYSTAL DIFFRACTION PATTERNS OF PLAGIOCLASES

The diffraction effects observed in plagioclases are many and varied, so before we discuss the sequences of ordering in these complex minerals, it behooves us to have an understanding of the nature and variety of the single-crystal diffraction patterns that have become indispensable to their complete characterization. Wide ranges of submicroscopic exsolution textures, antiphase domain textures (including superstructures), and twins can only be observed using x-ray and electron diffraction techniques. The latter are not readily available and often require a high level of expertise, especially if high-resolution imaging is desired. [Refer to Chapter 10 for details of submicroscopic textures of plagioclases.] But single-crystal x-ray cameras are often accessible, and for

---

[6]There is a first order transformation near 900°C between disordered synthetic $NaAlGe_3O_8$, an analog of albite, and its ordered polymorph (H. Pentinghaus, pers. comm.).

that reason we briefly describe the precession and oscillation techniques.

X-ray techniques

The precession method. The simplest diffraction technique to use and interpret is the x-ray precession method (see Buerger, 1964, or any one of a member of x-ray crystallography textbooks) because it gives undistorted images of the reciprocal lattice. For plagioclases the most informative crystallographic orientation is that normal to [100], although the reciprocal lattice plane normal to [001] is also useful, especially for sodic plagioclases and peristerites. Fortunately these are both available from a single mounting of a feldspar grain. The grain is cemented to a glass fiber with its easily-identified (010) cleavage[7] normal to the fiber. See the inset to the left. The fiber is oriented on a goniometer head so that b^* is parallel to the dial axis of the precession camera, and both the (010) and (001) cleavages, and therefore [100] $\equiv a$-axis, are parallel to the x-ray beam. This orientation yields a [100] precession photo which displays the b^*c^* plane and permits measurement of d_{010}, d_{001}, α^*, and observation of the variety of diffraction effects shown in Figure 9 and summarized for all low plagioclases in Figure 10. From this orientation a hit-or-miss rotation of either $\sim 116°$ (β) or $\sim 64°$ ($180° - \beta$) on the dial axis of the camera brings [001] $\equiv c$-axis parallel to the x-ray beam and the a^*b^* plane into focus so that d_{100}, d_{010}, and γ^* may be measured. The amount of rotation on the dial axis of the precession camera is β or $180° - \beta$. Smith (1974a, Ch. 6) gives standard photographs of both alkali and plagioclase feldspars, and his Figure 6-14 is reproduced here as Figure 9.

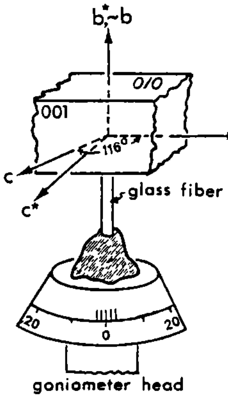

The oscillation method. Before the invention of the precession camera, oscillation techniques were widely used (Henry *et al.*, 1960), especially to study intergrowths and twinning in alkali feldspars. Unfortunately, the excellent oscillation camera built by Unicam, Ltd. is no longer available, although conventional Weissenberg cameras may be used without a layer-line screen and translation of the film cassette. The standard orientation for alkali feldspars

[7]See Chapter 5 or standard optical mineralogy texts for extinction angle methods of distinguishing (010) from (001) cleavage planes.

is exactly that for the [100] precession photograph described above, *if* the crystal is monoclinic. But if the crystal is triclinic, a very slight alignment would be required to bring the b axis parallel to the oscillation (or rotation) axis of the Weissenberg camera. However, for plagioclases the c axis should be mounted parallel to the axis of the camera, and a ±7.5° oscillation photograph centered about a line approximately half way between a^* and b^* (initially parallel to the x-ray beam) should be taken with filtered Cu radiation. Smith (1974a, Ch. 6) summarizes feldspar studies done by oscillation methods, and gives many useful reference photographs.

Summary of plagioclase diffraction patterns

Figure 9 shows selected composites of the $0k\ell$ diffraction patterns observed in the b^*c^* reciprocal lattice planes of plagioclases as they would appear in a [100] precession photograph. These are taken at intervals across the entire composition range.

In single-crystal x-ray patterns there are four classes or types of Bragg diffraction maxima in anorthite, but only one in albite:

ANORTHITE ($c \sim 14$ Å)		ALBITE ($c \sim 7$ Å)	
'a'	$h+k$ even, ℓ even	'a'	$h+k$ even, ℓ even or odd
'b'	$h+k$ odd, ℓ odd		
'c'	$h+k$ even, ℓ odd		
'd'	$h+k$ odd, ℓ even		

By comparison with 'b', 'c', and 'd' reflections, the 'a' reflections are systematically very much more intense. They are characteristic of all feldspars, and their ℓ indices are always even when the x-ray pattern is indexed on a $\sim$14 Å cell, but can be either even or odd when c is $\sim$7 Å (compare the two patterns on the left in Fig. 9). The 'c' and 'd' reflections behave exactly the same in plagioclases, although 'd's are usually very weak. Both are sharp only for anorthite, becoming more diffuse for more sodic compositions. Figure 10 roughly represents the composition ranges over which the various maxima are observed in plagioclases of relatively low-temperature equilibration.

The split line over the range An_2 to $An_{\sim 16}$ indicates that there are two resolvable lattices in the peristerite range. In fact, it is only the peristerite pattern which does not show its two co-existing lattices (Ab and $An_{\sim 25}$) in the b^*c^* orientation of Figure 9. In an a^*b^* photograph (Fig. 11), two a^* directions are clearly resolved, although b^* directions of both lattices are superposed. The 'e' reflections from the $An_{\sim 25}$ phase are generally so diffuse as to be undetectable except in very long x-ray exposures.

In the ranges $An_{\sim 45}$-$An_{\sim 60}$ and $An_{\sim 66}$-$An_{\sim 90}$ exsolution is also commonly

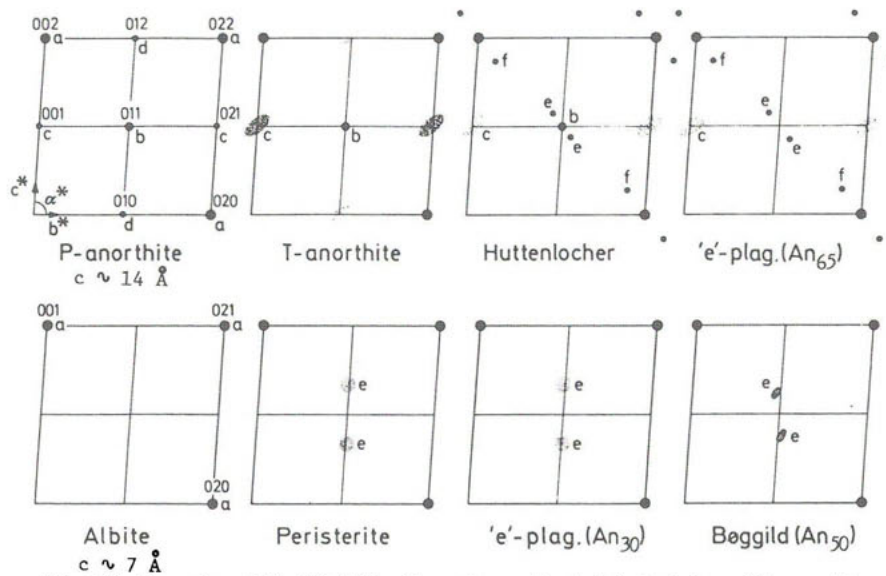

Figure 9. Composites of the $0k\ell$ diffraction patterns of selected plagioclases (the anorthite and albite cells are indexed). When 'c' reflections are diffuse, the 'd' reflections, which are much less intense and usually unobservable. Note the varying positions of the 'e' reflections with composition from An_{70} to An_{50} to An_{30}; *cf.* Equation 2 and Figure 13 below. After Smith (1974a, Fig. 6-14, p. 199).

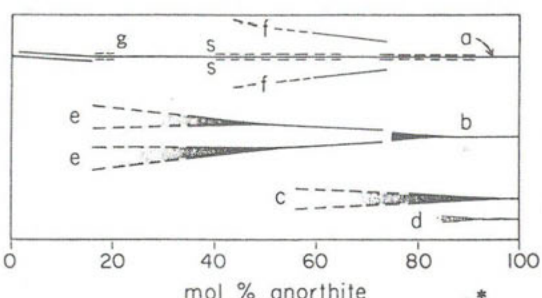

Figure 10. Diffraction phenomena observed in low plagioclases (*cf.* Fig. 9): 'a' reflections are common to all, and there are two sets for the peristerite intergrowths (*cf.* Fig. 11). In each of the ranges $An_{\sim 45}$-$An_{\sim 60}$ and $An_{\sim 66}$-$An_{\sim 90}$ two phases coexist, but the sublattices represented by 'a' reflections are dimensionally indistinguishable by x-rays (but see Chapter 10). Superlattice 's' or 'g' reflections resulting from periodicity of lamellar intergrowths are only visible in intense high-angle or high-resolution x-ray photos. When two phases coexist, their diffraction patterns superpose. Shading on 'e' and 'c' reflections indicates relative degree of diffuseness; weak 'd' reflections behave like 'c's.

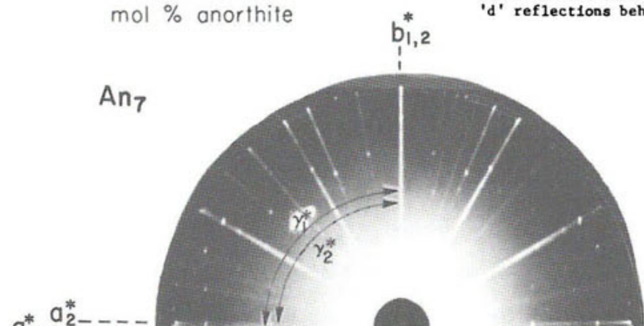

Figure 11. A partial *hk0* precession pattern of a peristerite showing the two reciprocal lattices. The one with $\gamma^* \cong 90.5°$ is low albite, that with $\gamma^* \cong 89°$ is $An_{\sim 25}$. γ^* angles have been used to identify the compositions of the individual phases in peristerites (Ribbe, 1960) employing a curve for that of low plagioclase (see inset on p. 256).

observed (see Ch. 10), but the lattices of the intergrown phases are dimensionally so nearly alike as to be unresolvable in normal photos; 'a' reflections superpose. Lamellar intergrowths of two plagioclases in these three composition ranges, if reasonably periodic, may act as superlattices, giving rise to closely spaced x-ray reflections, usually appearing as faint streaks normal to the plane of the intergrowth. These are the so-called 's' or 'g' reflections which require extraordinary measures to be exsolved in x-ray photographs (Korekawa and Jagodzinski, 1967, Korekawa *et al.*, 1970; Joswig *et al.*, 1977).

Spinodal decomposition and exsolution textures dominate the plagioclase subsolidus (see Ch. 9 and 10), and there are but few regions of what might be called homogeneous structure among natural specimens of lower-temperature origin. Low albite (An_{0-2}) and anorthite (An_{98-100} --discounting antiphase domains) are the only truly ordered phases. Two relatively coarse coexisting phases (normally 500 to 1500 Å, rarely to micron scale) dominate the peristerite

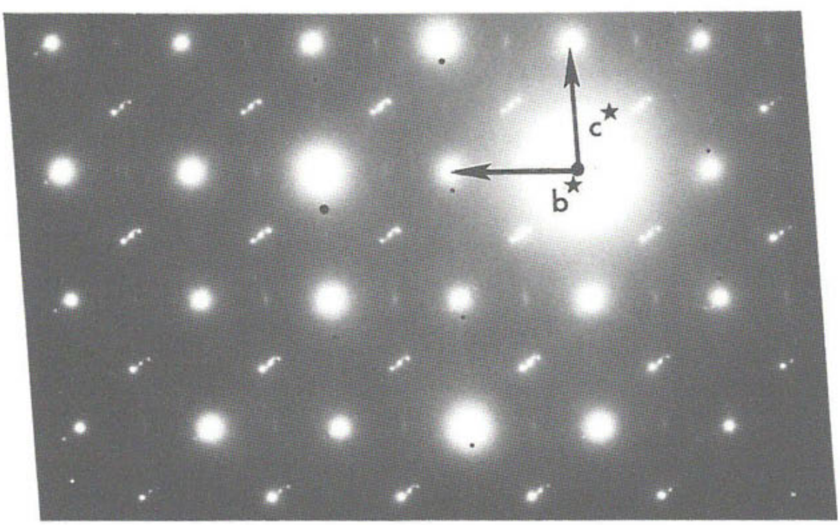

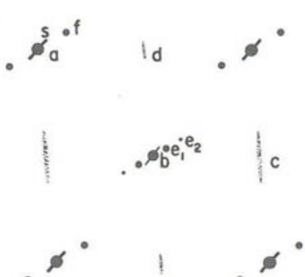

Figure 12. Above: an electron diffraction pattern of An_{72-75} with [100] parallel to the electron beam (*cf.* Fig. 9). This is a Huttenlocher intergrowth of transitional anorthite ($An_{\sim 90}$) and 'e'-plagioclase ($An_{\sim 65}$) like the specimen shown in Figures 14 and 15, Chapter 10. The 'a' reflections from a twin have been blacked out to reduce confusion. Right: reflection types identified.

Courtesy of T.L. Grove.

range, An_{2-16}. Spinodal-like decomposition has been observed on both ends of that range, producing the 100-300 Å scale quasi-periodic superstructure reported by McLaren (1974) for $An_{2.6}$ and by Joswig *et al.* (1977; see Fig. 10, Ch. 10) for $An_{16.5}$, which had resolvable 'g' reflections from the superstructure. Coarse exsolution (500-2000 Å lamellae) is observed in the Bøggild range, $An_{46\pm2}$-$An_{60\pm2}$ (Figs. 18 and 19, Ch. 10). In the Huttenlocher range, $An_{\sim66}$-$An_{\sim90}$, textures range in scale. The Stillwater igneous bytownites have relatively fine-scale quasi-periodic textures ranging from 850 Å at An_{75} to 125 Å at An_{85} (Nord *et al.*, 1974; see Fig. 16, Ch. 10) but micron-scale intergrowths are common in Alpine metamorphics (Fig. 14, Ch. 10). Superstructure 's' or 'g' reflections resulting from these intergrowths require heroic x-ray methods, and they are rarely seen, even in electron diffraction patterns. Figure 12 is an exception.[8]

This diffraction pattern was taken by Grove (1976) of a specimen of bulk composition An_{72-75} which is a Huttenlocher intergrowth consisting of two phases, transitional anorthite and 'e'-plagioclase of composition near An_{65}, as evidenced by comparing sketches of the individual diffraction patterns in Figure 9 with the "composite" in Figure 12. The 'e'-plagioclase superstructure is well developed, leading to multiple orders of 'e' reflections. The thousand-Ångström scale, quasi-periodic intergrowth of $An_{\sim65}$ and $An_{\sim90}$ produces the 's' streaks which are elongate through 'a' and 'b' reflections normal to the exsolution lamellae.

The 'e'- and 'f'-type reflections are observed in what are called "intermediate" plagioclases (vaguely meaning those of composition intermediate between albite and anorthite) or, more specifically, *'e'-plagioclases.* The 'e' and associated, but usually weaker 'f' reflections are the result of periodic antiphase superstructures discussed below. Weak, diffuse 'e's occasionally are seen in x-ray diffraction patterns of peristerites (An_2-An_{16}), but only in association with the $An_{\sim25}$ phase, and stronger, sharp 'e's and 'f's are commonly visible in those of Huttenlocher intergrowths ($An_{\sim66}$-$An_{\sim90}$), but only from the $An_{\sim65}$ phase. Higher order 'e' and 'f' reflections are observed only in electron diffraction patterns; they result from long, highly regular sequences of the antiphase superstructure (see Fig. 13).[8,9]

---

[8] In principle an $0k\ell$ x-ray precession photograph should show the same features, but electron diffraction is much more intense and can record in seconds what may literally take weeks to photograph by x-ray methods (e.g., Fig. 5). Resolution of the details of lattice geometry is also better with TEM because projection distances are greater, wavelengths are much shorter, and a much smaller crystal is used (<1000 Å thick), whereas x-ray diffraction requires crystals 10^5-10^7 times larger by volume.

[9] Mullite (Nakajima and Ribbe, 1981) and sapphirine (Higgins *et al.*, 1982) are two minerals that illustrate similar phenomena.

The superlattice 'f' reflections are "satellites" of the primary lattice nodes ('a' reflections) of the plagioclase $c \sim 7$ Å subcell, whereas 'e' reflections are "satellites" of the lattice nodes resulting from body-centering, i.e., the 'b' reflection positions. With reference to the 14 Å cell, the coordinates of the 'e' reflection pairs are $[h \pm \delta h,\ k \pm \delta k,\ \ell \mp \delta\ell]$, where $(h+k)$ and ℓ are both odd and where $[\delta h,\ \delta k,\ \delta\ell]$ are positive and nonintegral and vary from [0.12, 0.01, 0.34] near An_{30} to [0.02, 0.10, 0.10] at An_{70} (Gay, 1956; Smith, 1974a, p. 151). Second order 'e_2' diffractions (Fig. 12) have δ coordinates twice those of the 'e_1' diffractions. The related 'f' pairs have coordinates $[h \pm 2\delta h,\ k \pm 2\delta k,\ \ell \mp 2\delta\ell]$, where $(h+k)$ and ℓ are both even; they have been observed in x-ray photos in the range $An_{\sim 70}$ to $An_{\sim 50}$ and by TEM in An_{32} (McLaren and Marshall, 1974), whereas 'e's occur between $An_{\sim 70}$ and $An_{\sim 25}$, becoming increasingly diffuse with increasing Ab-content (Figs. 9 and 10).

Smith (1974a, his Ch. 5) summarizes the theory of Korekawa (1967) relating to the type of out-of-step body-centered structure that gives rise to the 'e' and 'f' reflections. See Figure 14. [Compare the theories of Böhm (1975 *et seq.*) and Kitamura and Morimoto (1977). The Al,Si ordering arrangements believed to cause this phenomenon are discussed in the next section.] At the moment it serves our purpose of characterization of plagioclase diffraction patterns to state that the irrational antiphase boundaries vary in both periodicity and orientation with composition of the 'e'-plagioclase phase, but *not* with the bulk composition of a composite crystal in which it may be one of the two exsolved phases. A careful study of Figure 9 reminds us that peristerites contain Ab plus an 'e'-plagioclase, Bøggild intergrowths consist of two 'e'-plagioclases, and Huttenlocher of one 'e'-plagioclase plus transitional anorthite.

Smith (1974a, p. 152f. and p. 488f.) defined a reciprocal lattice vector $\vec{t}$ which may be measured from electron or x-ray diffraction patterns (the latter with considerable difficulty):

$$\vec{t} = 2(\delta h \cdot \vec{a}^* + \delta k \cdot \vec{b}^* - \delta\ell \cdot \vec{c}^*) \qquad (1)$$

This is the vector joining the two 'e_1' reflections or an 'a' and an 'f' reflection in reciprocal space; $\vec{t}$ is twice the magnitude of $\vec{s}$, the vector used by Bown and Gay (1958), and is normal to the lamellar out-of-step domains in 'e'-plagioclase that give rise to the superlattice, whose periodicity $T = 1/|\vec{t}|$ (in Å) gives rise to the 'e' and 'f' reflections. The superlattice can be imaged in selected area electron diffraction photographs of 'e'-plagioclases (Fig. 13a), and high resolution images (13b) show the antiphase nature of the lamellar domains; i.e., the real structure on one side of the boundary (APB) is translated by one-half the translation repeat relative to that on the other side of the APB (*cf.* sketches in Fig. 14). T-spacing varies with composition and $\vec{t}$

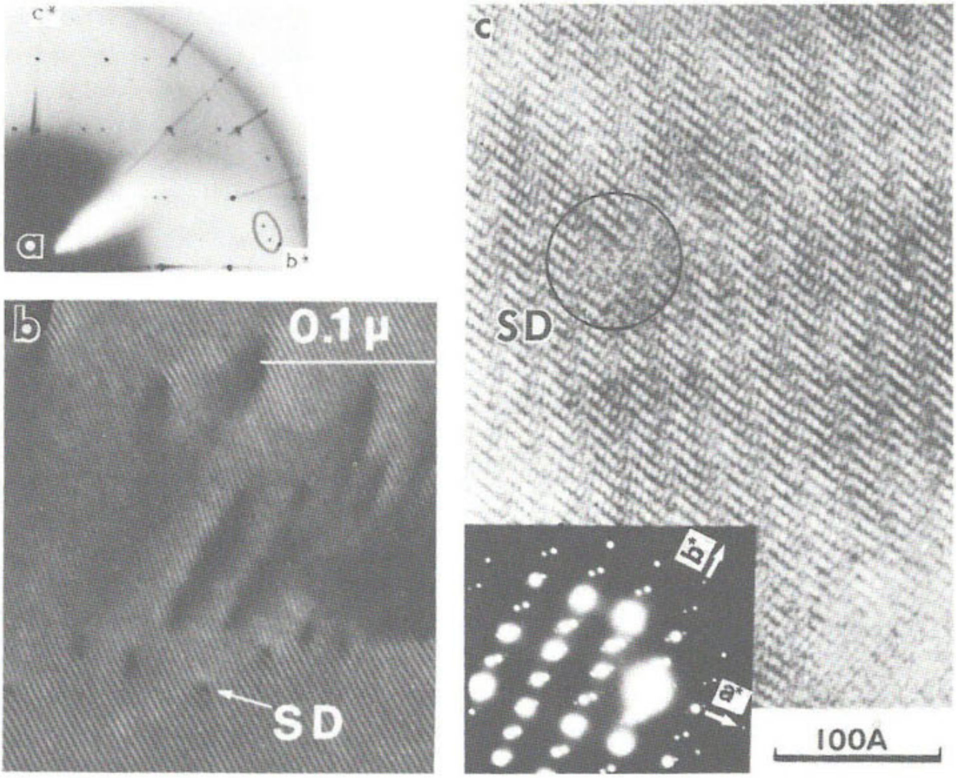

Figure 13. (a) A portion of an $0k\ell$ oscillated precession photograph of albite-twinned An_{45} showing 'e' reflections (circled) for an ~30 Å superstructure. (b) Dark-field TEM image of antiphase superstructure which gives rise to 'e' and 'f' reflections as in Figure 12. From Grove (1976, Fig. 1a, p. 267). The coarser periodicity at top and bottom measures ~37 Å. Superlattice dislocations (SD) appear where the composition fluctuates to a slightly more sodic region across the center of the photo which has periodicity ~32 Å. Note that the fringes are tilted 5° to those of the more calcic regions. (c) High resolution TEM image of the 'e' and 'f' superstructure showing the half-unit translations of the structures relative to one another on either side of the antiphase boundaries (nearly NS). The upper, more sodic portion of this specimen ($An_{\sim 40}$) has a superlattice repeat ~5Å less than the lower portion ($An_{\sim 50}$). A superlattice dislocation (SD) is circled, showing the structural adjustment necessary to accommodate the different periodicities. From Nakajima *et al.* (1977, Fig. 5, p. 221); see Morimoto *et al.* (1975, Fig. 2, p. 731), and compare Figures 15c and 21, Chapter 10.

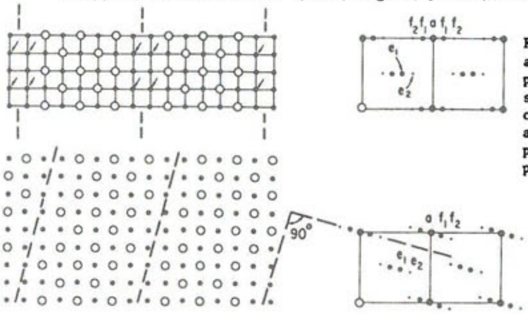

Figure 14. Diffraction patterns (left) for (a) a (body-) centered structure with periodic antiphase boundaries (dashed lines) in rational crystallographic orientation, and (b) a (body-) centered structure with periodic antiphase boundaries in irrational orientations, as in the 'e'-plagioclases. From Smith (1974a, Fig. 5-6d,e, p. 134; complete figure in Ch. 9, Fig. 8).

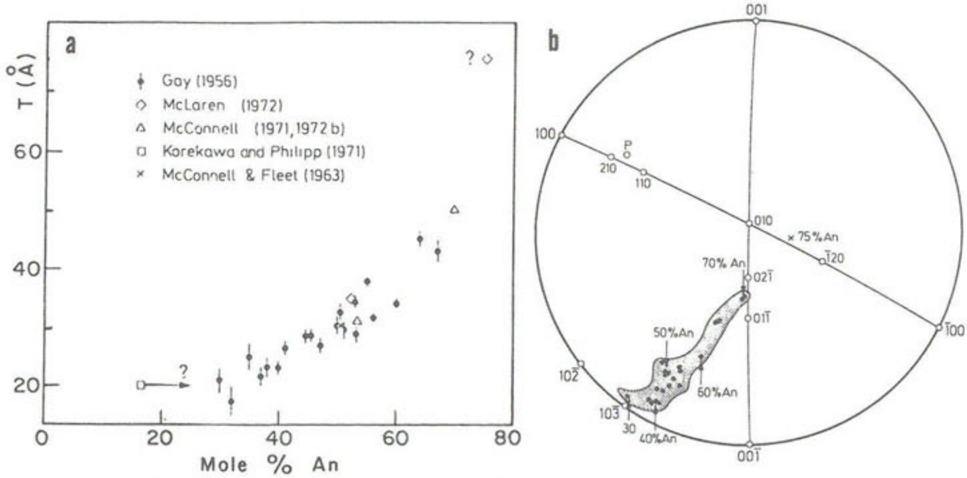

Figure 15. (a) The variation of T-spacing of the 'e'-plagioclase superstructure as a function of An content, and (b) the orientation of $\vec{t}$ vectors shown in stereographic projection. Dots in the stereogram are from Bown and Gay (1958); the × is from McLaren (1972); *P* is the face pole of the great circle which approximates the trend of the data. Contrary to convention, the open circles represent upward or horizontal directions of the face poles; black dots represent projections into the lower hemisphere. Modified from Smith (1974a, Figs. 5-12 and 5-13, p. 153). The data of Slimming (1976) for metamorphic plagioclases, An_{34}-An_{69}, all fit into the shaded area on the stereonet and within the range of values for T in (a).

varies in its orientation, as we casually observed in Figure 13a (and see Figs. 15c and 21, Ch. 10). Details are in Figure 15.

Other plagioclase diffraction phenomena of interest are those associated with the 'b', 'c' and 'd' reflections of primitive, transitional and body-centered anorthite. They are discussed in detail in the following section. All disordered high-temperature feldspars have an albite-like diffraction pattern ($C\bar{1}$, 7 Å) from An_0 to $An_{\sim 80}$, depending on temperature of quenching; but as Al:Si → 2:2, local order develops and a body-centered 14 Å cell is observed from $An_{\sim 80}$ to An_{100}.

SEQUENCES OF Al,Si ORDERING IN PLAGIOCLASES

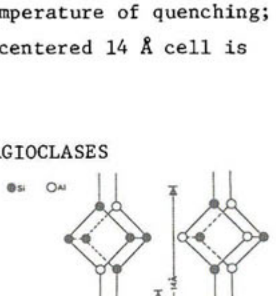

As seen from Figures 11 and 12, Chapter 1 and the inset, there are two basic types of Al,Si order in the plagioclase feldspars, one characteristic of low albite (Al:Si = 1:3; $c \sim 7$ Å) and another characteristic of anorthite (Al:Si = 2:2; $c \sim 14$ Å). Both of these illustrate the aluminum avoidance principle in that there are no Al-O-Al linkages in either structure, although Si-O-Si linkages abound in albite. Inasmuch as the plagioclase feldspar series ostensibly represents chemical mixtures of these end members in infinite variety, one might expect that the Al,Si ordering patterns of chemically intermediate compounds annealed for long times at low temperatures might be some simple mechanical mixture of the low albite and anorthite schemes, or that each composition, representing as it does a unique Al:Si ratio, would have a unique ordering scheme which obeys the aluminum avoidance principle. Neither of these possibilities is observed. In fact there are no truly homogeneous, ordered plagioclases between the end members of compositions An_{0-2} and $An_{\sim 90-100}$! *The ordering patterns of the end members are unique* [DeVore (1956) and Niggli (1967) notwithstanding], and furthermore *they are topologically incompatible* in the sense that it is not possible to mix them in a single, continuous feldspar framework without interposing some special disordered or discontinuous type of boundary between regions with albite- and anorthite-like order (Smith and Ribbe, 1969). This geometrical reality is responsible for development of the astounding variety of exsolution and out-of-step (or antiphase) domain textures observed in the plagioclase subsolidus between $An_{\sim 2}$ and $An_{\sim 90}$. Added to these concepts of the uniqueness and incompatibility of the low albite and anorthite ordering schemes (as consistent with the aluminum avoidance principle) is the fact that *Al and Si diffuse in the solid state only with the greatest difficulty.*[10] [See discussion on p. 214f.]

From this brief introduction we proceed to consider the order-disorder sequences in sodic and calcic plagioclases, after which we will be sufficiently well informed to at least attempt to understand structures of intermediate composition. Later chapters will be devoted to subsolidus phase relations and variation of lattice parameters and optical and other physical properties.

Ordering in sodic plagioclases

Albite. We have already considered the ordering scheme of Al and Si in pure Na-feldspars. Now if we examine the Al,Si distribution in low albite (inset above) we see that it is not possible to add Al to the structure without violating the aluminum avoidance principle unless, of course, Al which is already present in the T_1O site is displaced into one of the adjacent T_2 sites. In other words, chemically homogeneous feldspars with compositions more An-rich than An_{0-2} cannot attain a fully ordered Al,Si distribution like that observed in low albite. In fact, ordering is increased by phase separation or exsolution into two phases.

---

[10]For example, the transformation of low albite to high albite in a dry system involved an activation energy of $\sim$74 kcal/mole (McKie and McConnell, 1963).

Peristerites. Homogeneous plagioclases which crystallize in the bulk composition range $An_{\sim 2}$-$An_{\sim 16}$ begin to order in the same manner as Na-feldspar. After inversion, Al migrates into T_1O from the other three sites. However, as we have just seen, a *completely* ordered pattern is not possible. X-ray and transmission microscope studies of feldspars in this composition range indicate that they are *peristerites*[11] and that they usually consist of two intimately intergrown phases which may or may not be coherent.[12] It is highly significant that one of these exsolved phases is always a fully ordered low albite whose reciprocal cell angle γ^* indicates that its composition is An_{0-2}. The other phase has a composition near An_{25}, although it ranges from $An_{\sim 18}$ to $An_{\sim 30}$ depending to some extent on bulk composition of the peristerite [again the assumption is that γ^* is related to An-content (Ribbe, 1960; see Ch. 10)].

In this composition range ordering is expressed by exsolution into one structurally simple, ordered phase (Ab) and one which is more complex ($An_{\sim 25}$). Phase separation does not occur because of differences in size of the *A* cations (as is the case for Na,K feldspars) but rather because the lowest free energy configuration is one in which Al and Si are the most completely ordered. Low albite inevitably forms and its ordering may be considered to be the driving force of the exsolution. The An-rich phase forms in proper proportion to the initial bulk composition, but never in greater volume than the Ab phase. Its composition is not invariant, and although there may be a particularly low energy configuration at $An_{\sim 25}$, An_{25} (Al:Si = 5:11) does not have a completely ordered Al,Si arrangement and the reason why it forms is enigmatic.

[For a study of the diffusive and displacive transformations in synthetic sodic plagioclases, see Kroll and Bambauer (1981) and Chapter 4. In Chapter 9 Smith reviews details of experiments that attempt to trace the analbite → low albite transformation. For discussion of peristerite phase equilibria, see Chapters 9 and 10.]

---

[11] *Peristerite* comes from the Greek περιστερα, meaning *pigeon*. The term was chosen in reference to the interference colors commonly seen in these feldspars and on the neck feathers of pigeons. See Chapter 10 for further discussion.

[12] For an extended discussion of coherency of intergrown phases, see Chapter 6. There may be some strain as a result of coherency between the Ab- and An-rich phases, but this is not always demonstrable. See discussions in Chapter 10. There are bulk compositions near 2.5 and 16.5 mole % An in which the scale of 'exsolution' is so fine (100-200 Å) as to assure some degree of coherency (McLaren, 1972, and Joswig *et al.*, 1977). Of course at that scale x-ray diffraction peaks from the individual phases are indistinct in any case.

Average structure models of plagioclase

At this stage in our discussion it is necessary to re-introduce the concept of average structure which was used in the description of $I\bar{1}$ bytownite and anorthite in Chapter 1 and will be used again in Chapters 3-5 in connection with determinative methods for Al,Si distribution based on lattice parameters and optical properties. It can be illustrated best by an example.

Consider a peristerite of bulk composition An_8 which is 70% by volume An_2 and 30% An_{25}; the two phases are intergrown on a submicroscopic scale as in Figure 12a, Chapter 10. Single-crystal x-ray patterns of a grain of An_8 contain two reciprocal lattices, one for low albite (An_2) and the other for "low" An_{25} (see Fig. 11). But a powder pattern of the bulk specimen lacks the resolution necessary to discriminate between the reflections from the individual phases because their $d_{hk\ell}$-spacings are so nearly equivalent. If we were to investigate the structure of An_8 using the powder pattern, we could only obtain information about the average structure. Lattice parameters, bond lengths and angles, and optical properties would be 70-30 weighted averages of those of the two phases involved.

In the case of plagioclases $An_{\sim 20-75}$ of relatively low temperature origin, information on average structures is obtained from 'a' reflections while ignoring 'e' and 'f' reflections which contain information about the *true*, complex structure of 'e'-plagioclase. The resulting structure refinements give atomic parameters consistent with an albite-like $C\bar{1}$ cell. This average structure concept is also useful in describing $I\bar{1}$ or $P\bar{1}$ bytownites or anorthites (An_{70-100}) which have $c \sim 14$ Å. In a powder pattern of these minerals only 'a' reflections are regularly observed, and without prior knowledge that the sample was bytownite or anorthite, it is likely that the pattern would be indexed on the 7 Å cell. The effect would be to average or reduce the $P\bar{1}$, 14 Å cell to a $C\bar{1}$, 7 Å cell. Likewise, if a crystal structure analysis of primitive anorthite were undertaken using only 'a' reflections, the result would be average structure with average bond lengths and angles, an albite-like unit cell, and only one type of four-membered ring in the (010) projection instead of four T such rings (*cf.* Figs. 10 and 12d in Ch. 1). Each of four T sites in this cell, corresponding to $T_1$0, T_1m, $T_2$0, T_2m in albite, would be averages of four sites, one from each of the four pseudosymmetrically related rings (A,B,C,D) in anorthite. In other words, the Al occupancy of $T_1$0 would be the average of the Al-contents of the pseudosymetrically related sites (refer back to Fig. 15, p. 18):

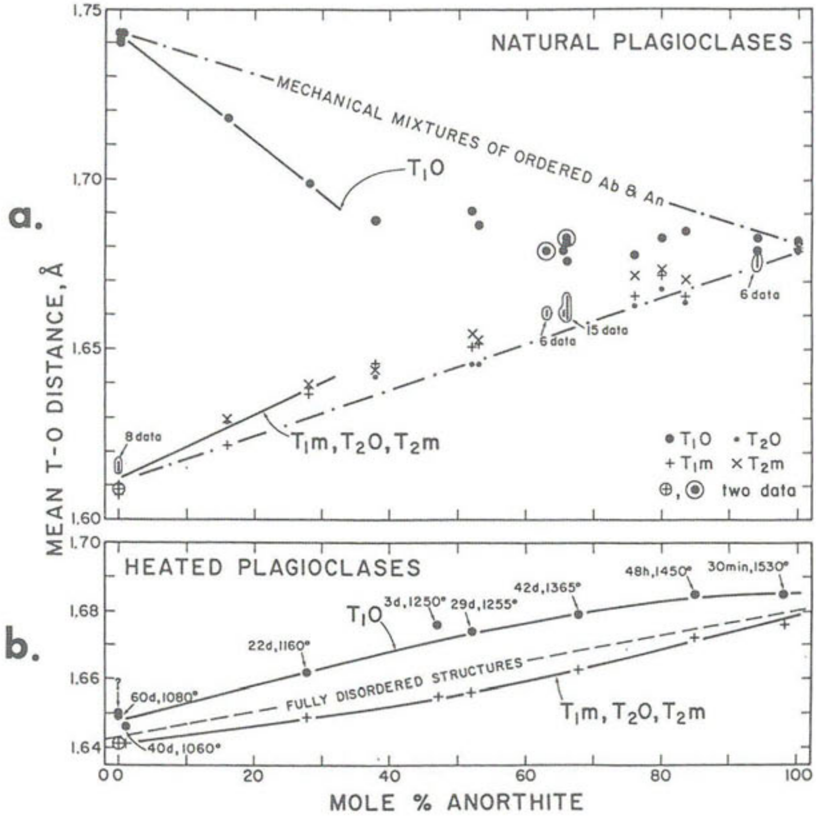

Figure 16. The mean T-O distances of the average structures of natural plagioclases (a) and heated plagioclases (b) are plotted against An/(An + Ab + Or), using data from Table 1, Chapter 3. (a) For structures in which $\langle T_1\text{m-O}\rangle$, $\langle T_2\text{O-O}\rangle$ and $\langle T_2\text{m-O}\rangle$ overlap, only the ranges of values are shown. Dash-dot lines give loci of $\langle T\text{-O}\rangle$ distances which would be expected if compositions intermediate between ordered low-albite and primitive anorthite were mechanical mixtures of those two phases. (b) The grand mean T-O bond length for the three sites, T_1m, T_2O and T_2m sites are shown (+) with the mean T_1O-O bond lengths (•) for heated natural plagioclases. A dashed line joins the overall mean T-O distance for disordered Na-feldspar to that for $P\bar{1}$ anorthite, thereby delineating the values of $\langle T\text{-O}\rangle$ expected if the average structures of high-temperature plagioclases were *completely* disordered. None of the heat-treatments indicated on the graph was sufficient to totally disorder any of these specimens.

$$t_1o = (t_1ooo + t_1zoo + t_1ooi + t_1zoi)/4 = (0.0 + 0.0 + 1.0 + 1.0)/4 = 0.5$$

When thus averaged onto a $C\bar{1}$, 7 Å cell, $P\bar{1}$ (and by analogy $I\bar{1}$) anorthite appears to be disordered:

$$t_1o = t_1m = t_2o = t_2m = 0.5 \tag{2}$$

The nearly equal mean T-O distances for the average structure of anorthite are plotted in Figure 16a. They cluster near $\langle\langle T\text{-O}\rangle\rangle$ = 1.68 Å which defines one end of the dashed line in Figure 16b. The opposite end represents $\langle\langle T\text{-O}\rangle\rangle$

for Na-feldspar, and the line itself is the locus of expected values for *fully* disordered plagioclases.

If it were possible to describe the Al,Si ordering patterns of low-temperature plagioclases of intermediate compositions as mechanical mixtures of ordered primitive anorthite and low albite, An_{50} (for example) would have the following Al,Si distribution in its $C\bar{1}$, 7 Å average structure:

$$t_1o = (1.0 + 0.5)/2 = 0.75; \; t_1m = t_2o = t_2m = (0.0 + 0.5)/2 = 0.25 \quad .$$

[See dash-dot lines in Fig. 16a to obtain <*T*-O> values and use Equation 5 in Ch. 3 to convert them to Al contents.] This is *not* the observed distribution in An_{50}, and no other low plagioclases give indication that they even approach strictly mechanical mixtures. But, as evident from Figure 16, *all* plagioclases have average structures with $t_1o > t_1m \simeq t_2o \simeq t_2m$. The model to explain this fact is complicated, and we will approach it gradually by next examining Al,Si ordering in calcic plagioclases and the much more complex 'e'-plagioclases.

Ordering in calcic plagioclases

Anorthite. Even though its *average* structure appears disordered (Eqn. 2), the actual structure of annealed *pure* anorthite is presumed to be almost completely ordered at room temperature (Fig. 12d, Ch. 1). It has been shown in selected area electron diffraction (SAD) studies, as summarized by Heuer and Nord (1976), that some anorthites with sharp 'a', 'b', 'c', 'd' reflections initially crystallized in space group $C\bar{1}$ (with $c \sim 7$ Å). Even at high temperature it is unlikely that there is a great deal of Al,Si site disorder in this $C\bar{1}$ cell. In fact, one may presume that dynamic positional disorder in this highly pseudosymmetric structure produces the apparently unquenchable $C\bar{1}$ arrangement which quickly inverts to $I\bar{1}$ and subsequently to $P\bar{1}$ as annealing proceeds. Dark-field TEM images of 'b' reflections ($h+k$ odd, ℓ odd) show the antiphase domain boundaries (APB's) which are relics of the $C\bar{1} \rightarrow I\bar{1}$ inversion. These outline the so called *'b'-domains* which are common in anorthite but more abundant in sodic anorthites and bytownites (Fig. 17a,b). They grow with annealing time, and their average sizes may convey useful information (Heuer and Nord, 1976). Kroll and Müller (1980) annealed synthetic An_{100} glass at 1430°C and obtained the following results with TEM.

Annealing time	Types of reflexions $^+$ Diffuse	Size of *b*-domains [Å]	Size of *c*-domains [Å]
5 Min	$a\ b^+\ c^+$	< 100	< 100
45 Min	$a\ b\ c^+\ d^+(?)$	~ 200–500	< 100
1 Day	$a\ b\ c^+\ d^+$	~ 500–1,000	~ 100
4 Days	Not investig.	~ 1,000	Not investig.
8 Days	$a\ b\ c^+\ d^+$	~ 1,000	Not investig.
16 Days	$a\ b\ c\ d$	~ 2,000–10,000	~ 500

From this table it is clear that the $I\bar{1}$ phase, like $C\bar{1}$, is unquenchable for pure An_{100}, because diffuse 'c' reflections appear (along with diffuse 'b's) after only 5 min. annealing. My guess is that Al and Si are ordered even in An_{100} liquid (the mean refractive index of An glass is almost identical to that of crystal) and that the small amount of disorder quenchable at very high temperatures (Chiari *et al.*, 1978) is mainly responsible for the frequency of out-of-step boundaries and thus the mean sizes of the antiphase domains.

The APB's imaged with 'c' reflections ($h + k$ even, ℓ odd) outline *'c'-domains* which on the average are columnar in shape parallel to $[2\bar{3}\bar{1}]$ (see Fig. 17c; and especially McLaren and Marshall, 1974, Fig. 3). All authors agree that structures with coarse-scale 'c' domains only occur when the crystal has a uniform primitive structure. See Heuer *et al.* (1976) for a clarifying discussion of the origin of 'c' domains.

Even if anorthite has both 'b'- and 'c'-domains, it consists of structure

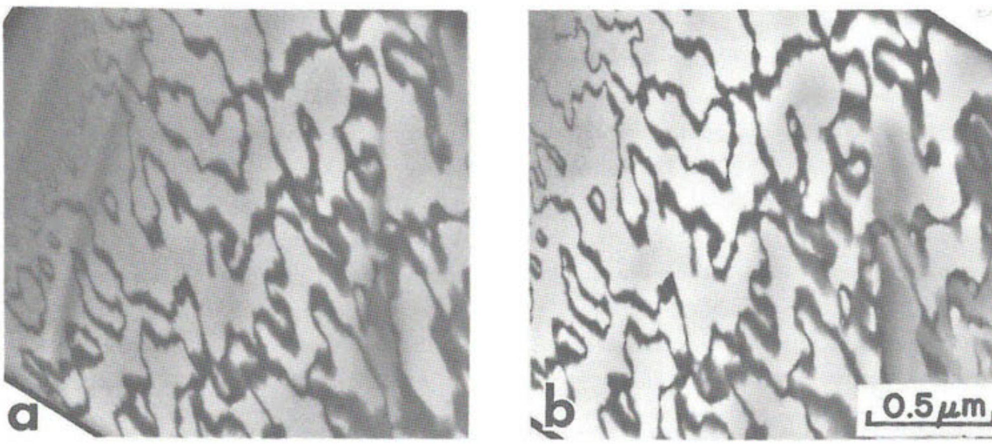

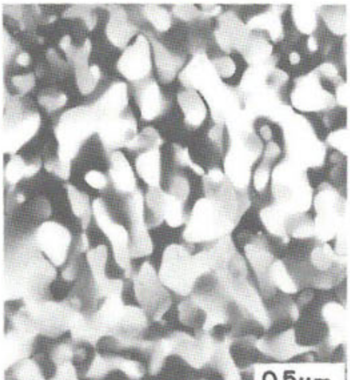

Figure 17. (a,b) Antiphase boundaries between domains related by the vector ½[111] shown here in a TEM stereo pair photographed at 800 kV using only the intensity from the diffracted beam 021, a type 'c' reflection. These 'c'-domains are from a lunar anorthite (An_{97}) in Apollo 15415, a slowly cooled anorthosite. From Heuer and Nord (1976, Fig. 6b, p. 289). (c) Antiphase boundaries between domains related by the vector ½[110] or ½[001] ('b'-domains). The boundaries were photographed at 1000 kV using only the intensity from the diffracted beam $\bar{1}01$, a type 'b' reflection. The domains imaged are from the core (An_{95}) of a zoned synthetic plagioclase crystallized at 1150°C, cooled at 2°C/hr to 865°C, and quenched by G. Lofgren. The 'c' diffractions from this area of the crystal were diffuse and weak. Courtesy of G. L. Nord.

in which Al and Si alternate quite regularly in the tetrahedral framework. Bits of primitive structure, independently nucleated while the dynamically "disordered" structure -- no doubt containing some Al,Si mistakes -- was in a higher space group at high temperature, meet at boundaries on either side of which the structures are out of phase by 180° (see McLaren and Marshall, 1974, Fig. 4). Heuer and Nord (1976) "considered and rejected" the possibility that 'b'- and 'c'-domains are the result of "growth mistakes" rather than the result of a phase transition: I think both mechanisms are operative, especially in more sodic compositions where some residual Al,Si disorder is required by the stoichiometry.

Unfortunately, much of this textural information is not available to the mineralogist or petrologist who lacks TEM expertise in examining his specimens (or a TEM!). What can be done with more readily accessible single-crystal x-ray methods to discern structural details of anorthite?

As we have seen, anorthite with sharp 'a', 'b', 'c', 'd' reflections is highly ordered, but $P\bar{1}$ anorthites have increasingly diffuse 'c' reflections when successively cooled from temperatures higher than ∿600°C (the 'd's are relatively very weak, often invisible). See reviews by Heuer and Nord (1976) and Heuer *et al.* (1976). The degree of diffuseness of these reflections is an indication of the mean size of the 'c' domains. The same is true of 'b' reflections, which are rarely diffuse in nature, although extreme heating and fast quenching may produce diffuseness. Unfortunately, the degree of diffuseness of 'c' reflections cannot be used as a geothermometer, because both temperature *and* annealing time at that temperature are involved in domain size, and there is yet a third very important factor -- the amount of NaSi substituting for CaAl. It would be convenient if the $P\bar{1} \rightarrow I\bar{1}$ inversion temperature (T_c = 240 ± 4° for $An_{99.5}$; see Ch. 1, pp. 16-17) could be used to gain insight into the state of domain texture, but Adlhart *et al.* (1980b) reported complexities regarding the inversion of $An_{97.5}$ and $An_{95.5}$, other studies give conflicting results,[13] and experiments are too involved for routine petrologic investigations in any case. The best that can be attained is to study 'c' reflection diffuseness in either an isocompositional suite of varying degrees of annealing and quench rates or in zoned crystals whose last annealing and quenching could be taken to be the same for all values of An (e.g., the Miyaké, Japan volcanic anorthites; see early study by Laves and Goldsmith, 1954). For further discussion

---

[13]See Foit and Peacor (1967), Czank *et al.* (1970), Brown *et al.* (1963), Müller and Wenk (1973), etc.

see Smith, Chapter 9.

Anorthites and calcic bytownites with diffuse 'c' (and 'd') reflections have been called *transitional*, in the sense that they are in a state transitional between $P\bar{1}$ and $I\bar{1}$. Higher and higher temperatures of heating, and/or heating and quenching, and increasing NaSi for CaAl all have the effect of "moving" $P\bar{1}$ toward $I\bar{1}$. At room temperature the $I\bar{1}$ structure may contain an extremely high frequency of antiphase boundaries, thus earning the designation "average structure" (Fig. 16, p. 19), in which extremely fine scale (< 100 Å ?) domains of $P\bar{1}$ structure are out-of-step along ½[111] vectors relative to one another, although continuity of the aluminosilicate framework is maintained throughout the crystal. Alternatively, *at* elevated temperatures, dynamical atomic positional disorder (but not Al,Si interchange) produces a truly body-centered lattice, as in the case of specimens above T_c.

A structure analysis of anorthite in $I\bar{1}$ using only 'a' and 'b' reflections (whether or not there is residual intensity in diffuse 'c' and 'd' reflections), produces a refinement in which the T sites of the $P\bar{1}$ structure are averaged in pairs, reducing the number of T sites from 16 in $P\bar{1}$ to 8 in $I\bar{1}$ with $T_1$000 ≡ $T_1$00i, $T_1$0zo ≡ $T_1$0zi, etc. Unlike the averaging of $P\bar{1}$ onto $C\bar{1}$, the Al,Si distribution in $I\bar{1}$ is ordered:

$$t_1\text{ooo} \cong t_1\text{mzo} \cong t_2\text{ozo} \cong t_2\text{moo} \cong 0.0;\; t_1\text{ozo} \cong t_1\text{moo} \cong t_2\text{ooo} \cong t_2\text{mzo} \cong 1.0.$$

[See Fig. 15, p. 18 for details of site nomenclature and Al contents.] Crystal structure analyses of "body-centered" anorthite *at* high temperatures (Czank, 1973; Foit and Peacor, 1973) have shown exactly this, but in addition they show that the two symmetrically nonequivalent Ca atom positions, of which there are four in the $P\bar{1}$ structure, must still be described by four "half-atoms" in order to properly satisfy the highly asymmetric electron density distributions appearing in Fourier maps at these sites. The implication is clear: even though the $h+k+\ell$ odd reflections are systematically absent, the anorthite structure that has $I\bar{1}$ diffraction symmetry consists mainly of antiphase domains of primitive structure. Thermal vibration of all atoms is sufficient, even without the introduction of substitutional disorder, to make the atomic nodes pseudo-related by ½[111] at room temperature become exactly I-related at higher temperatures. But the electron densities at the Ca sites are so markedly anisotropic as to convince any investigator that they can only be attributed to *positional disorder*, i.e., space-averages composed of one-half Ca(000) plus one-half Ca (00i) and likewise for the Ca(z00)-Ca(z0i) pair. This is less spectacularly true also of electron densities at T and oxygen atom sites, and it is possible to obtain complete "half-atom" refinements of $I\bar{1}$ average structures which prove conclusively the primitive nature of the domains (see Fleet *et al.*, 1966; Ribbe, 1963; and *cf.* Fig. 16, p. 19 which shows site superposition).

Bytownite. For low plagioclases it is apparent that departure of Al:Si from 2:2 (anorthite) toward, say 1.8:2.2 (bytownite), introduces disorder in the An_{100} scheme. Thus as composition changes, the probability of out-of-step mistakes increases, the frequency of antiphase domains increases, and 'c' and 'd' diffuseness increases, all of which reduce T_c from its value of 240°C for pure anorthite.

As structure determinations have shown (listed in Table 1, Ch. 3, p. 60) Si in excess of 2.00 in the $I\bar{1}$ structure of $An_{\sim 80}$ ($Na_{.2}Ca_{.8}Al_{1.8}Si_{2.2}O_8$), for example, is more or less equally distributed over the Al-rich sites, whereas the Si-rich sites contain little or no aluminum.[14] This sort of substitutional disorder leads to primitive structure in antiphase superposition, as discussed in the preceding paragraphs. The average structure of bytownite, like that of anorthite, when reduced to a $C\bar{1}$, 7 Å unit cell appears to be highly disordered, and the four average *T*-O bond lengths, plotted individually in Figure 16a, could equally well be plotted on the curves in 16b for heated plagioclases. These are near but not on the locus of disordered plagioclases --T_1O is still somewhat Al-rich. Implications of this $C\bar{1}$ average structure will be considered in Kroll's discussion of lattice parameters of plagioclases in Chapter 4.

High plagioclases. When heated for long times near its melting point, especially in the presence of H_2O, the more sodic bytownites can attain complete long-range Al,Si disorder, producing a true $C\bar{1}$, 7 Å cell. Like high albite and other "disordered" plagioclases, it is interpretable in terms of unit-cell scale domains with high degrees of short-range Al,Si order being averaged onto a 7 Å cell with the resultant extinction of both the $h+k+\ell$ odd reflections (as in $I\bar{1}$) *and* the $h+k$ odd, ℓ odd set of 'b' reflections (Ribbe *et al.*, 1969). The $C\bar{1} \rightarrow I\bar{1}$ transformation was delineated by experimentally heating natural specimens to range upwards from ~900°C at $An_{\sim 57}$ to ~1430°C (the solidus) at $An_{\sim 77}$ (Carpenter and McConnell, unpublished ms.). Grove *et al.* (1983) (Figs. 8 and 9) suggest on their hypothetical T-X diagrams that the range is from ~800°C at $An_{\sim 75}$ to ~1200°C at $An_{\sim 90}$ and/or just below the solidus at $An_{\sim 100}$.[15] The $I\bar{1} \rightarrow C\bar{1}$

---

[14]The grand mean *T*-O bond lengths are 1.730 and 1.617 Å, respectively, for the Al- and Si-rich sites (Fleet *et al.*, 1966) as compared with 1.747 Å and 1.614 Å for <Al-O> and <Si-O> in primitive anorthite (An_{100}; Wainwright and Starkey, 1971).

[15]Their recent discussion of the phase transitions and decomposition relations in calcic plagioclase is highly recommended as supplementary reading to this and Smith's Chapter 9 (this volume), but note that their temperature for $I\bar{1} \rightarrow P\bar{1}$ is unrealistic.

transformation has not been carefully investigated *at* high temperatures.

Huttenlocher intergrowths. As was the case for the peristerite composition range, plagioclases between $An_{\sim 66}$ and $An_{\sim 90}$ are intergrowths of two distinct phases, one of which is An-rich ($An_{\sim 95}$) and the other $An_{\sim 65}$. These have been called *Huttenlocher intergrowths* and it is presumed by analogy with the peristerites that it is the low-entropy configuration of the ordered anorthite structure that "drives" the exsolution. The physical aspects of these intergrowths are discussed in Chapter 10 and the phase relations in Chapter 9. Huttenlocher intergrowths are easily recognized in single-crystal x-ray photographs (Fig. 9) or by TEM (Fig. 12), but would be entirely overlooked in a powder diffraction study or in an optical investigation, unless the lamellar structure were coarse enough (>1 μm) to be seen in thin section (where it is sometimes mistaken for fine scale twinning).

An electron diffraction pattern of an exsolved specimen of bulk composition An_{72-75} (Fig. 12) was discussed in the previous section. It is remarkable in that it shows nearly every type of diffraction phenomenon known to occur in the entire plagioclase feldspar series. The sharp 'a' and 'b' and diffuse 'c' and 'd' reflections arise from the transitional anorthite ($An_{\sim 90}$), which undoubtedly has hundred Ångström scale 'c'-domains and coarser 'b' domains (see table above).

The average structure of the more sodic phase, an 'e'-plagioclase of composition $An_{\sim 65}$, has lattice parameters very close to those of $An_{\sim 90}$, thus its 'a' reflections superpose on those from the calcic phase. The antiphase superstructure which produces 'e' and 'f' reflections is imaged in Figure 13b; in this particular specimen the periodicity ranges between ∿32 and ∿37 Å due to compositional inhomogeneity, which may represent a secondary stage of exsolution.

In general, the two exsolved phases coexist as complicated lamellar intergrowths on the scale of a few hundred Ångströms to optically visible (micron-scale). The 's' streaks through the 'a' reflections (Fig. 12) are inclined to b^* and c^* and are approximately normal to $(03\bar{1})$; they result from the imperfectly developed $(03\bar{1})$ quasi-periodic lamellar "superstructure" of alternating slabs of calcic and 'e'-plagioclase, like those illustrated in Figure 14-16 in Chapter 10. A second lamellar set parallel to $(30\bar{1})$ is sometimes observed. X-ray patterns never give clues to the orientation of exsolution lamellae, but if the average total thickness of an $An_{\sim 65}$ + $An_{\sim 95}$ pair is in the range of 1350 to 2400 Å, interference colors may be visible from a plane which is parallel to their interface (see Ch. 10, pp. 266-270).

Ordering in plagioclases of intermediate composition

First we will discuss the structures of two low plagioclases which showed only 'a' reflections in x-ray photographs.

Oligoclase. Average structures of two oligoclases, An_{16} and An_{28}, were reported by Phillips *et al.* (1971). It is assumed from their pegmatitic occurrences that they are as ordered with respect to Al and Si as is possible, and indeed their diffraction patterns, lattice parameters (Chapter 4) and optical properties (Chapter 5) indicate structural states consistent with low-temperature equilibration. However, their Al,Si distributions are far from ordered in either the low albite or $P\bar{1}$ anorthite sense. Data are shown in Figure 16 and recorded in Table 1, Chapter 3.

Because T_1O is Al-rich and the other three T sites are equally Si-rich, it is clear that, just as in albite, Al concentrated in T_1O as these feldspars inverted from their respective disordered arrangements. But t_1o is significantly less than 1.0 in both An_{16} and An_{28}, even though there are 1.16 and 1.28 Al atoms available in these structures to fill T_1O. This is one limiting model for low plagioclase -- we will call it "full T_1O". Another possible model involves mechanical mixtures of the two fully ordered end members of the plagioclase series, low albite [LA; $t_1o = 1.0$, $\langle t_1m \rangle \equiv \frac{1}{3}(t_1m + t_2o + t_2m) = 0.0$] and anorthite [An; $t_1o = t_1m = t_2o = t_2m = 0.5$; Eqn. 2 above]. The Al distributions expected from these are listed below in contrast with the "actual" values determined from crystal structure analyses using Equation 5, Chapter 3.

Model	$n_{An} = 0.16$		$n_{An} = 0.28$	
	t_1o	$\langle t_1m \rangle$	t_1o	$\langle t_1m \rangle$
"full t_1o"	1.00	0.05_3	1.00	0.09_3
mech'l mix	0.92	0.08	0.86	0.14
"actual"	0.81_5	0.11_5	0.68	0.20

Clearly there must be an ordered LA structural "component" to account for the concentration of Al in T_1O, and an anorthite structural "component" to account for the observed composition, and, in order to raise the Al content of T_1m, T_2O, T_2m to the "actual" t_1m, t_2o, t_2m values; one might add a third "component" that consists of disordered albite (call it analbite, AA) which in turn must be subtracted from the LA "component" to keep the formula balanced. If the fraction of anorthite "component" in such a model is given as n_{An}, then the fraction of AA is $4[\langle t_1m \rangle_{obs} - \frac{1}{2}n_{An}]$ and the fraction of LA is $[1 + n_{An} - 4\langle t_1m \rangle_{obs}]$. For low An_{16} and An_{28} the values are 16:14:70 and 28:24:48, respectively.

To explain the observed Al,Si distribution of these and other low plagioclases, Smith and Ribbe (1969) proposed a model similar to this but which involves coherent out-of-step domains, on the scale of ten or more Ångströms, consisting of alternating ordered LA-like and An-like structure in a continuous tetrahedral framework. Between the two types of ordered structure are boundaries in which some degree of Al,Si disorder must exist because of the topologic incompatibility of the 1:3 and 2:2 ordering patterns. The reported Al,Si distributions in the four T sites of the $C\bar{1}$, 7 Å cell represent an average of that which exists in these domains and the disordered boundary regions separating them. This model is discussed in more detail below.

'e'-plagioclase. As we have seen, one of the members of the peristerite exsolution is low albite with its unique Al,Si ordering scheme; the other is an 'e'-plagioclase of somewhat variable composition, averaging near $An_{\sim 25}$ (see Ch. 10). Likewise one of the phases of Huttenlocher intergrowths is transitional anorthite, which is only slightly disordered by the replacement of some Al by Si, and the other phase is an 'e'-plagioclase of $An_{\sim 65}$ composition. Thus, 'e'-plagioclases, which are observed as one of the two phases in these intergrowths and as discrete phases in the range $An_{\sim 20}$ to $An_{\sim 75}$, are ubiquitous among low plagioclases of bulk composition from $An_{\sim 2}$ to $An_{\sim 90}$. We conclude our consideration of Al,Si ordering with a discussion of these structurally complex feldspars. The details of their diffraction patterns were given earlier, and J. V. Smith elaborates on these and the structural model that both he and I favor in Chapter 9. To avoid unnecessary duplication, the reader is referred to pp. 229-233 at this juncture...

... In summary, of the many models for 'e'-plagioclase, all are in agreement that alternating lamellar regions of ordered (or least highly ordered) albite and anorthite, bounded by regions of intermediate composition and degrees of order are involved in the formation of the antiphase structure. The stereographic projection of Figure 15 shows the range of orientation of the antiphase structure with composition, but Grove (1977a) illustrated it more simply by determining that $\vec{t}$ (his $\vec{s}$) ranged, with considerable scatter, from an inclination to (100) of -11° to +11° between An_{30} and An_{75}. For that reason he constructed an idealized model of the 'e'-plagioclase superstructure based on an (100) projection (Fig. 18a; his d_{2s} = our T). Figure 18b gives a helpful 3-D perspective of the orientation of the antiphase superstructure for An_{50} from Kumao *et al.* (1981), who attribute the unique character of the diffraction patterns and HRTEM images of 'e'-plagioclases mainly to Na,Ca segregation. This view does not contradict our model of LA-, An-type segregation which we have assumed is caused by Al,Si ordering. Na and Ca merely "follow" the Al,Si distribution to balance charge.

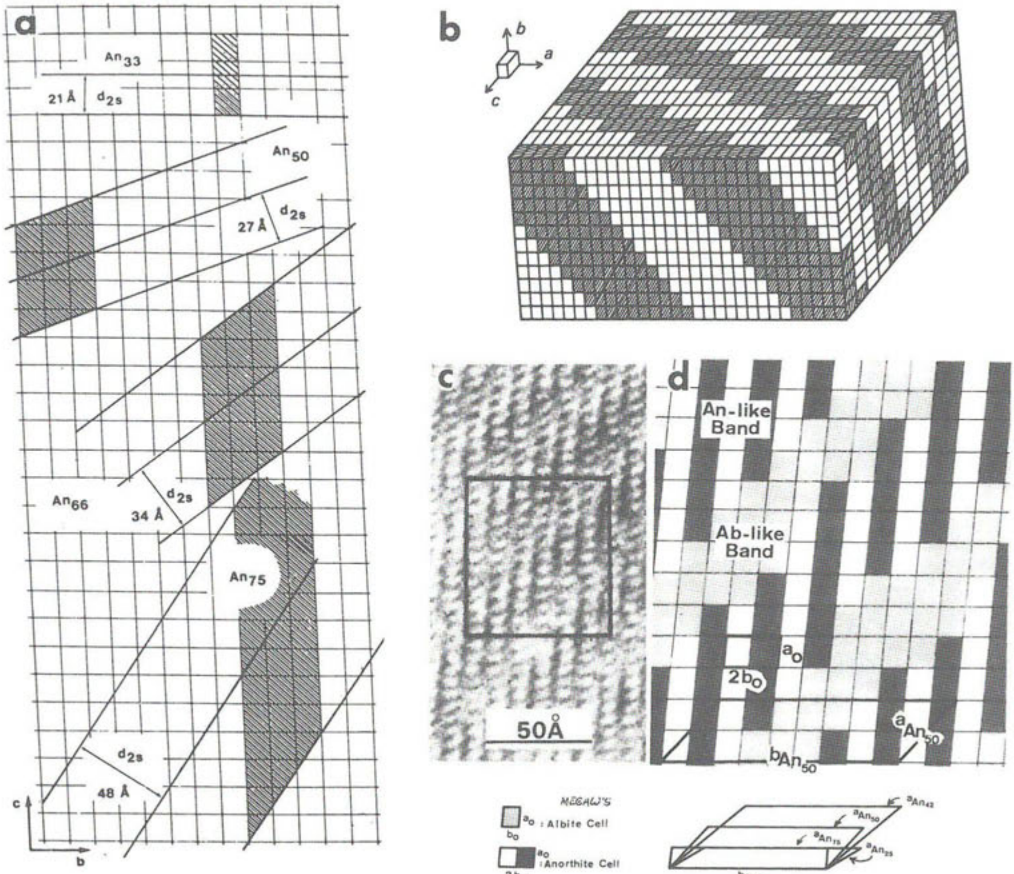

Figure 18. Legend is on the next page.

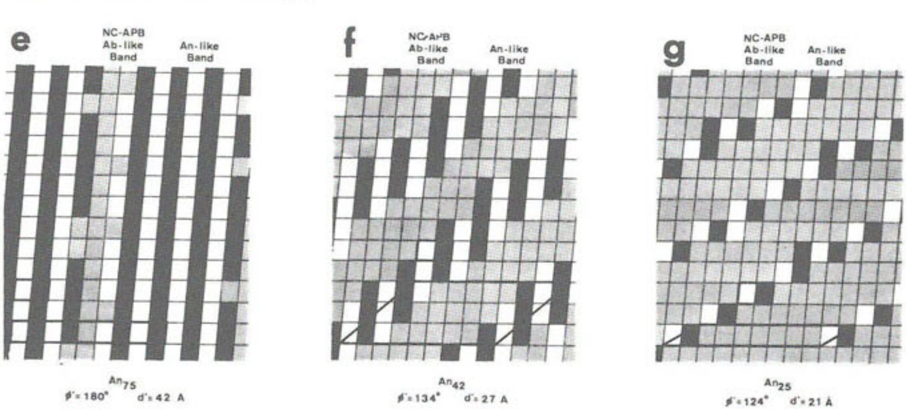

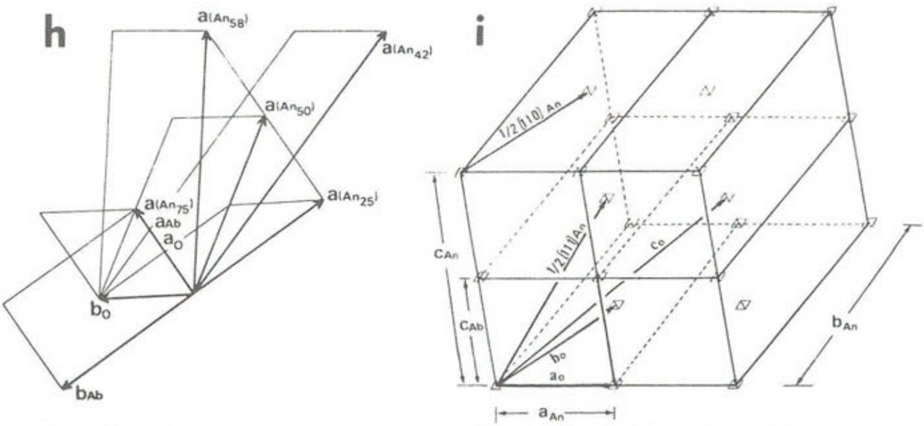

Figure 18. (a) The periodic antiphase model for 'e'-plagioclase of Grove (1977a, his Fig. 4), who found that the "slab orientation for all compositions is nearly perpendicular to (100). Thus the supercells are described by one translation that is nearly normal to (100) and two other translations that lie in (100) and vary in length and orientation." (b) A 3-D schematic representation of the model of Kumao *et al.* (1981, their Fig. 9) for An_{50}: "Ca and Na atom arrangement in white and shaded regions are in antiphase solution." (c,d) HRTEM structure image of An_{52} (as in Fig. 13c) compared to the model of the antiphase An-like bands separated by Ab-like bands in the model of Kitamura and Morimoto (1975, 1977). Their supercell is compared with that of Megaw (1960) -- see insets and (h) and (i). From Nakajima *et al.* (1977, Fig. 6, p. 225). (e,f,g) Similar models for An_{25}, An_{42} and An_{75}, based on other supercells -- see (h) and (i). From Morimoto *et al.* (1975, Fig. 1, p. 730). (h) Schematic diagram showing the unit cell of anorthite (subscript An), the displacement vectors ½[110] and ½[111] based on the anorthite cell (*cf.* Fig. 14b, Ch. 1) and Megaw's (1960) cell (subscript O) used for the 'e'-plagioclases as in (i). From Nakajima *et al.* (1977, Fig. 1, p. 215). (i) The orientation relation between Megaw's axes and the cells defined for (d), (e), (f) and (g). From Kitamura and Morimoto (1977, Fig. 5, p. 210).

The excellent HRTEM work of Nakajima, Morimoto and Kitamura in resolving the structures of 'e'-plagioclases is illustrated in Figures 18c-g. Unfortunately, they chose the Megaw (1960) unit cell as a reference for their supercell orientations. Figure 18(h,i) gives information that may help to unscramble their supercell designations.

That the periodic modulations of 'e'-plagioclase really involve Al,Si ordering is evidenced by dry heating experiments. With increasing and decreasing temperature the 'e' reflections lose and reversibly regain intensity without changes in $\vec{t}$ or T (Foit and Peacor, 1967), indicating dynamic positional disorder at higher temperatures within Ab- and An-rich regions which brings both temporarily to a $C\bar{1}$ configuration. If the sample is heated for long times near the melting point, the 'e' reflections become more and more weak and diffuse, eventually disappearing irreversibly as the NaSi $\rightleftarrows$ CaAl diffusion gradually spreads from the disordered boundaries, permanently "flattening" the Ab-An modulation (see Fig. 7, Ch. 9) and destroying the periodic structure by truly homogenizing it. In fact McConnell (1974a found that the 'e' superlattice was eliminated at ∿600°C in An_{37}, at ∿800°C in An_{53}, and ∿1000°C in An_{65}. The last attained an $I\bar{1}$, 14 Å cell with sharp 'b' reflections, indicating that the anorthite-like basis for the calcic 'e'-plagioclases is indeed a realistic one. The An_{37} and An_{53} homogenized to $C\bar{1}$ disordered arrays analogous to high albite.

In conclusion, two problems require comment.

(1) The models of 'e'-plagioclase we have represented here assume that there is a reasonably consistent relationship between the length and orientation of $\vec{t}$ with composition, even though a considerable spread of data points is evident in Figure 15. Wenk (1979), Wenk *et al.* (1980) and Wenk and Nakajima (1981) reported a major departure from this for the specimen Vz 433 for which they determined the crystal structure and gave the composition An_{63}. But Smith and Wenk (1983) have found that the composition is $An_{38\pm5}$, not An_{63}, so "until proven otherwise, there is no need to assume that the 'e'-vector of metamorphic plagioclase is a simple function of metamorphic grade as stipulated by H. R. Wenk (1979). However, recombination of 'e' APB's in metamorphic plagioclase demonstrates that the 'e' superstructure is less regular than in igneous crystals (Wenk and Nakajima, 1981) which corresponds to observations in annealed metal alloys..." (Smith and Wenk, 1983).

(2) The "modulated structure of a plagioclase An_{52}", published by Horst *et al.* (1981) has two problems. The first is minor: the Al content they report for the eight *T* sites of their specimen totals only 1.38 in contrast to the 1.52 required by the bulk composition. An application of Equation 5 in Chapter 3 solves that. But, the second is much more serious. They used (without TEM investigation) a sample from Labrador which undoubtedly contains not one homogeneous 'e'-plagioclase, but *two* (see following section on Bøggild intergrowths). Even if one accepted their method of structure determination by "deconvolution" according to the satellite theory of Jagodzinski and Korekawa (1978), one must seriously doubt their results for this specimen. The work of Toman and Freuh (1972 *et seq.*) on An_{55} is open to the same criticism.

Bøggild intergrowths. In the range $An_{46\pm2}$ to $An_{60\pm2}$, exsolution of two 'e'-plagioclases occurs, one with a composition of $An_{44\pm4}$ and the other $An_{58\pm6}$, each having its appropriate diffraction pattern. A bulk specimen would thus presumably show distinct 'e' and 'f' reflections, with $\vec{t}$ vectors differing in orientation and T spacing differing by ∿10 Å (*cf.* Fig. 13b with Fig. 21 on p. 265, Ch. 10). As indicated in Figure 9, x-ray reflections probably overlap, but in high magnification TEM, resolution of the coarser (>1500 Å) lamellae is possible by selected area diffraction. Bøggild intergrowths are more commonly recognized from their brilliant interference colors than from their diffraction patterns. In this composition range exsolution is apparently ubiquitous, even though not evidenced visually.

Chapters 9 and 10 contain details of these feldspars.

SUMMARY

The plagioclases are intensely complex, but the principles governing their structures can be traced to the uniqueness of the 1:3 and 2:2 Al,Si ordering schemes, as consistent with the aluminum avoidance principle, and the slow diffusion of Al and Si through the tetrahedral framework. High resolution transmission electron microscopy and careful x-ray and neutron diffraction studies have brought us to a fairly good understanding of the structures, and the "big picture" of plagioclase equilibria is nearly in focus, though some details of both the 'e' structure and the phase diagram remain to be clarified.

Chapter 3

LATTICE PARAMETERS, COMPOSITION and Al,Si ORDER in ALKALI FELDSPARS

H. Kroll & P. H. Ribbe

INTRODUCTION

The unit cell parameters of an alkali feldspar reflect its composition, its Al,Si configuration, and in some cases the effects of strain accumulated during the sanidine → microcline inversion (see Ch. 2) or during exsolution of coherent phases (*cf.* Chs. 6 and 7).[1]

Our first concern will be to characterize homogeneous feldspars and then to examine effects of strain. Lattice parameters are usually obtained by least-squares refinement of x-ray powder diffraction patterns, and the Appendix of this volume contains practical information on indexing them and evaluating results.

However, before we proceed to elaborate on what have become fairly reliable and relatively simple methods of determining K,Na content and Al,Si order-disorder in alkali feldspars using various metric parameters of the direct and reciprocal unit cells, we will discuss the methods of their calibration. Ultimately we rely on crystal structure refinements, together with microprobe or chemical analyses and sometimes TEM investigation of domain textures, to provide the basis of interpretation. Many of the principles elucidated here will be carried over to our discussion of plagioclases in the next chapter.

The notation we use is from Chapter 1. The average Al content of a tetrahedron T_i, also called its Al site occupancy, is denoted by t_i, where $t_i \equiv$ number of Al atoms occupying T_i tetrahedra divided by the number of T_i tetrahedra, so that $0 \leqslant t_i \leqslant 1$; Si content = $1 - t_i$. The symbol for the Al occupancy corresponds to the symbol for the tetrahedral site: t_1, t_2 for monoclinic $C2/m$ feldspars with T_1 and T_2 tetrahedral sites; t_1o, t_1m, t_2o, t_2m for triclinic $C\bar{1}$, $c \sim 7$ Å feldspars with T_1O, T_1m, T_2O and T_2m tetrahedral sites. The number of Al atoms in one feldspar formula unit, $(K,Na)_{1-x}Ca_xAl_{1+x}Si_{3-x}O_8$, is $1+x$, where x is equivalent to n_{An}, the mole fraction Ca-feldspar. One unit cell (with $c \sim 7$ Å) contains four formula units, i.e., $4(1 + n_{An})$ Al atoms.

---

[1]Nonstoichiometry in natural specimens is rare and limited in extent; its effect on cell dimensions has not been documented, and we will ignore it.

There are 16 tetrahedra in one unit cell, eight of each type (T_1,T_2) in monoclinic feldspars, four of each type (T_1O, T_1m, T_2O, T_2m) in triclinic feldspars. Therefore, the average tetrahedral Al content is

$$\langle t \rangle = 0.25(1 + n_{An}) \ , \quad (1)$$

and the sum of individual occupancies corresponding to one formula unit is

$$\Sigma t = 2(t_1 + t_2) = 1 + n_{An} \ , \quad (2)$$

$$\Sigma t = t_1o + t_1m + t_2o + t_2m = 1 + n_{An} \ . \quad (3)$$

The following abbreviations for various alkali feldspars and their compositions are convenient and will be used throughout:

ALKALI FELDSPARS				COMPONENTS	
MA	Monalbite	HS	High sanidine	Ab	Na-feldspar
AA	Analbite	LS	Low sanidine	An	Ca-feldspar
HA	High albite	OR	Orthoclase	Or	K-feldspar
LA	Low albite	LM	Low microcline	Cn	Ba-feldspar

TETRAHEDRAL SIZE AND Al,Si DISTRIBUTION

The linear model

The refinement of a feldspar structure can yield Al site occupancies in two ways:

(1) The Al content may be deduced indirectly from mean T-O bond length, $\langle T\text{-O}\rangle$, because Al is larger than Si.

(2) Al,Si occupancies may be refined directly from the different scattering powers of Al and Si for x-rays and neutrons.[2]

Smith (1954) proposed a linear relationship between grand mean T-O distances, $\langle\langle T\text{-O}\rangle\rangle$, averaged over all tetrahedra in a unit cell, and average Al content of those tetrahedra, and Smith and Bailey (1963) made it specific for feldspars. The latest compilation is in Figure 1. In the past twenty years revisions of the original model have appeared periodically along with equations based on it to calculate the Al content t_i of an *individual* tetrahedron from the mean of its four T-O distances, $\langle T_i\text{-O}\rangle$. Much discussion has ensued, and it is now

----

[2]If x-ray intensities are used, only the highest quality data, thoroughly corrected for absorption and especially extinction, will yield meaningful results because the scattering powers of Al and Si are very similar and scale factors, thermal parameters, site occupancies and extinction correction parameters are highly correlated. The same is true for neutron diffraction, although the scattering factors of Al and Si for neutrons differ much more than those for x-rays. There has been a general tendency to trust neutron refinement more than mean T-O distances as an indicator of Al,Si distribution (Harlow and Brown, 1980), but this has been questioned in one instance (Stewart and Wright, 1974, p. 360).

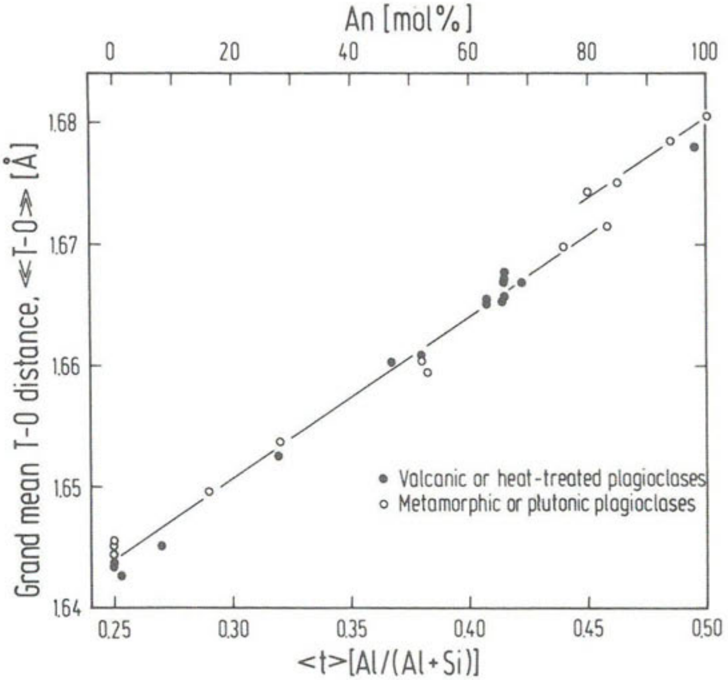

Figure 1. Variation of the grand mean *T*-O distance <<*T*-O>> with mean tetrahedral Al content <t> in plagioclase feldspars (see Table 1).

generally agreed that no simple linear model is adequate.[3] The Al/(Al+Si) ratio for the site is of first importance, because <Al-O> distances are ∿0.13 Å longer than <Si-O>. But, for example, an individual Si-O bond will be ∿0.03 Å longer if the oxgen atom is bonded to another Si than if it is bonded to Al. The coordination of that oxygen to 0, 1 or 2 K, Na and/or Ca atoms has a further effect and the *T*-O-*T* angles are significant as well (Ribbe *et al.*, 1974). Of course all these must be considered and averaged for all four *T*-O distances that constitute the <T_i-O> value from which t_i is to be derived. These effects are manifested in the fact that within (presumedly) fully ordered anorthite (Wainwright and Starkey, 1971), individual Si-O distances range between 1.571 and 1.647 Å, individual Al-O distances between 1.698 and 1.779 Å, and even the mean *T*-O distances vary from 1.608 to 1.617 Å for <Si-O> and 1.742 to 1.755 Å for <Al-O>. Grand mean values are <<Si-O>> = 1.614 Å,

----

[3]See Jones (1968), Ribbe and Gibbs (1969), Phillips and Ribbe (1973a), Smith (1974a, p. 70), Ribbe *et al.* (1974), Ribbe (1975, p. R-22), Harlow and Brown (1980), Kroll (1980), and Ferguson (1980, 1981 -- see Blasi's (1982) critique).

Table 1. Compositions, mean T-O distances for the T_1o, T_1m, T_2o, T_2m sites of the <u>average</u> ($C\bar{1}$-7Å) structure of the plagioclase, site occupancies t_1o and $\langle t_1m\rangle = \frac{1}{3}(t_1m+t_2o+t_2m)$ [Al/(Al+Si)], repeat distances tr110 and tr$1\bar{1}0$ [Å] for 30 structurally analyzed plagioclases selected from the literature. Space group assumed in the structure analysis and type of radiation used (X-ray or neutron) are indicated. Site occupancies were calculated as $t_i = 0.25(1+n_{An}) + (\langle T_i\text{-O}\rangle - \langle\langle T\text{-O}\rangle\rangle)/0.130$.

No.	Feldspar	[*]	(**)	Mol % An	Mol % Ab	Mol % Or	S.G.	Rad.	Mean T-O distances [Å] T_1o	T_1m	T_2o	T_2m	Site occupancy t_1o	$\langle t_1m\rangle$	Repeat dist. tr110	tr$1\bar{1}0$	Comments
1	Low albite	[A]	(1)	0.1	99.3	0.6	$C\bar{1}$	n	1.743	1.607	1.615	1.616	1.000	0.000	7.716	7.438	
2	Low albite	[A]	(1)	0.1	99.3	0.6	$C\bar{1}$	x	1.743	1.609	1.614	1.616	1.000	0.000	7.716	7.438	
3	Low albite	[B]	(2)	0	99.75	0.25	$C\bar{1}$	x	1.740	1.609	1.614	1.615	0.985	0.005	7.710	7.437	
4	Low albite	[C]	(3)	0.1	99.7	0.2	$C\bar{1}$	x	1.741	1.610	1.615	1.617	0.985	0.005	7.714	7.437	
5	High albite	[B]	(4)	0	99.75	0.25	$C\bar{1}$	x	1.650	1.640	1.641	1.643	0.300	0.235	7.605	7.619	htd.
6	High albite	[B]	(5)	0	99.75	0.25	$C\bar{1}$	x	1.649	1.642	1.640	1.642	0.295	0.235	7.600	7.629	htd. 60d, 1080°C
7	High albite	[D]	(6)	1.2	98.3	0.5	$C\bar{1}$	x	1.646	1.641	1.641	1.642	0.280	0.245	7.602	7.633	htd. 40d, 1060°C
8	High albite	[E]	(7)	8	84.5	7.5	$C\bar{1}$	x	1.670	1.637	1.636	1.637	0.465	0.205	7.639	7.615	unheated
9	Oligoclase	[F]	(8)	16	82	2	$C\bar{1}$	x	1.718	1.622	1.629	1.630	0.815	0.115	7.679	7.515	
10	Oligoclase	[G]	(8)	28	70	2	$C\bar{1}$	x	1.699	1.637	1.639	1.640	0.670	0.205	7.646	7.581	
11	Oligoclase	[H]	(9)	27.8	68.1	4.1	$C\bar{1}$	x	1.662	1.649	1.649	1.649	0.395	0.295	7.611	7.645	htd. 22d, 1160°C
12	Andesine	[I]	(10)	47	49	4	$C\bar{1}$	x	1.676	1.653	1.656	1.656	0.490	0.325			htd. 3d, 1250°C
13	Labradorite	[J]	(11)	52	45.5	2.5	$C\bar{1}$	x	1.691	1.651	1.646	1.655	0.610	0.305	7.627	7.617	exhibits schiller
14	Labradorite	[J]	(9)	52	45.5	2.5	$C\bar{1}$	x	1.674	1.655	1.658	1.656	0.485	0.345	7.602	7.649	htd. 29d, 1255°C, no schiller
15	Labradorite	[J]	(12)	53	43	4	$C\bar{1}$	x	1.687	1.652	1.646	1.653	0.600	0.310	7.624	7.618	exhibits schiller
16	Labradorite	[K]	(13)	63			$C\bar{1}$	x	1.679	1.660	1.661	1.662	0.510	0.375	7.596	7.653	
17	Labradorite	[K]	(13)	63			$C\bar{1}$	n	1.679	1.661	1.660	1.661	0.510	0.375	7.596	7.653	
18	Labradorite	[K]	(14)	65.6	33.8	0.6	$C\bar{1}$	n	1.679	1.661	1.660	1.662	0.520	0.380	7.596	7.653	
19	Labradorite	[L]	(13)	66			$C\bar{1}$	x	1.683	1.663	1.659	1.663	0.535	0.375	7.593	7.655	
20	Labradorite	[L]	(13)	66			$C\bar{1}$	n	1.676	1.661	1.660	1.666	0.495	0.390	7.593	7.655	
21	Labradorite	[L]	(3)	66			$I\bar{1}$	x	1.683	1.664	1.660	1.664	0.530	0.375	7.593	7.655	
22	Labradorite	[L]	(15)	66			$I\bar{1}$	n	1.682	1.662	1.661	1.664	0.535	0.380	7.593	7.655	
23	Labradorite	[M]	(9)	68.7	31.1	0.2	$C\bar{1}$	x	1.679	1.663	1.663	1.662	0.515	0.390	7.587	7.659	htd. 42d, 1365°C
24	Bytownite	[N]	(16)	76			$I\bar{1}$	x	1.678	1.666	1.663	1.672	0.505	0.420	7.581	7.662	
25	Bytownite	[O]	(17)	80			$P\bar{1}$	x	1.683	1.672	1.668	1.674	0.515	0.430	7.583	7.663	
26	Bytownite	[P]	(18)	83.4	16.2	0.4	$I\bar{1}$	x	1.685	1.666	1.664	1.671	0.560	0.425	7.588	7.664	
27	Bytownite	[Q]	(19)	85	15	0	$I\bar{1}$	x	1.685	1.672	1.671	1.673	0.535	0.440	7.581	7.680	htd. 48h, 1450°C
28	Anorthite	[R]	(3)	94			$P\bar{1}$	x	1.683	1.675	1.677	1.680	0.520	0.475	7.557	7.694	
29	Anorthite	[S]	(20)	98			$I\bar{1}$	x	1.685	1.670	1.680	1.678	0.550	0.475	7.561	7.696	htd. 30', 1530°C
30	Anorthite	[T]	(21)	100			$P\bar{1}$	x	1.682	1.680	1.679	1.680	0.515	0.495	7.546	7.698	

Table 1 supplement: direct and reciprocal lattice parameters of structures 1-30.

No.	Feldspar	[*]	(**)	Mol % An	Mol % Ab	Mol % Or	a/a* [Å]/[Å^{-1}]	b/b* [Å]/[Å^{-1}]	c/c* [Å]/[Å^{-1}]	α/α* degrees	β/β* degrees	γ/γ* degrees	V/V*·10^5 [Å^3]/[Å^{-3}]
1	Low albite	[A]	(1)	0.1	99.3	0.6	8.142(2) 0.13738	12.785(2) 0.078429	7.159(2) 0.15653	94.19(2) 86.47	116.61(2) 63.48	87.68(2) 90.50	664.5(9) 150.49
2	Low albite	[A]	(1)	0.1	99.3	0.6	8.142(2) 0.13738	12.785(2) 0.078429	7.159(2) 0.15653	94.19(2) 86.47	116.61(2) 63.48	87.68(2) 90.50	664.5(9) 150.49
3	Low albite	[B]	(2)	0	99.75	0.25	8.1333 0.13753	12.7808 0.078462	7.1552 0.15664	94.272 86.36	116.615 63.47	87.725 90.41	663.1 150.81
4	Low albite	[C]	(3)	0.1	99.7	0.2	8.1353(7) 0.13748	12.7852(7) 0.078436	7.1582(7) 0.15655	94.274(6) 86.38	116.600(5) 63.49	87.685(6) 90.45	663.9(1) 150.64
5	High albite	[B]	(4)	0	99.75	0.25	8.152 0.13709	12.858 0.077969	7.108 0.15754	93.589 85.93	116.455 63.48	90.115 88.08	665.4 150.30
6	High albite	[B]	(5)	0	99.75	0.25	8.161(1) 0.13696	12.875(2) 0.077866	7.110(1) 0.15750	93.53(1) 85.94	116.46(1) 63.47	90.24(1) 87.97	669.8(2) 149.30
7	High albite	[D]	(6)	1.2	98.3	0.5	8.1535(4) 0.13708	12.8694(5) 0.077900	7.1070(4) 0.15756	93.521(4) 85.94	116.458(3) 63.47	90.257(3) 87.96	665.95(8) 150.161
8	High albite	[E]	(7)	8	84.5	7.5	8.1838(6) 0.13649	12.8737(8) 0.077836	7.1252(5) 0.15703	93.351(6) 86.36	116.421(5) 63.54	89.801(6) 88.56	670.9(1) 149.05
9	Oligoclase	[F]	(8)	16	82	2	8.1553(3) 0.13699	12.8206(5) 0.078189	7.1397(4) 0.15681	93.965(7) 86.25	116.475(3) 63.55	88.632(5) 89.55	666.59(5) 150.017
10	Oligoclase	[G]	(8)	28	70	2	8.169(3) 0.13670	12.851(4) 0.077989	7.124(2) 0.15706	93.63(3) 86.22	116.40(2) 63.58	89.46(2) 88.80	668.4(2) 149.61
11	Oligoclase	[H]	(9)	27.8	68.1	4.1	8.1733(6) 0.13653	12.8818(5) 0.077804	7.1103(6) 0.15721	93.314(6) 86.17	116.282(4) 63.65	90.275(4) 88.05	669.7(1) 149.32
12	Andesine	[I]	(10)	47	49	4	not known						
13	Labradorite	[J]	(11)	52	45.5	2.5	8.1780(6) 0.13634	12.8649(5) 0.077911	7.1093(6) 0.15714	93.533(4) 86.10	116.205(4) 63.75	89.916(5) 88.35	669.5(1) 149.36
14	Labradorite	[J]	(9)	52	45.5	2.5	8.1739(8) 0.13636	12.8752(10) 0.077859	7.1032(7) 0.15719	93.407(7) 86.01	116.133(5) 63.79	90.394(6) 87.89	669.5(1) 149.37
15	Labradorite	[J]	(12)	53	43	4	8.1764(8) 0.13638	12.8637(7) 0.077916	7.1090(7) 0.15715	93.500(6) 86.12	116.214(5) 63.74	89.948(9) 88.33	669.3(1) 149.42

Table 1 supplement, continued.

No.	Feldspar	[*]	(**)	Mol % An	Mol % Ab	Mol % Or	a/a*	b/b*	c/c*	α/α*	β/β*	γ/γ*	V/V*·10^5
							[Å]/[Å^-1]			degrees			[Å^3]/[Å^-3]
16	Labradorite	[K]	(13)	63			8.1739(5) 0.13628	12.8740(5) 0.077877	7.1024(4) 0.15712	93.470(4) 85.90	116.049(3) 63.87	90.474(4) 87.77	669.73(8) 149.313
17	Labradorite	[K]	(13)	63			8.1739(5) 0.13628	12.8740(5) 0.077877	7.1024(4) 0.15712	93.470(4) 85.90	116.049(3) 63.87	90.474(4) 87.77	669.73(8) 149.313
18	Labradorite	[K]	(14)	65.6	33.8	0.6	8.1739(5) 0.13628	12.8740(5) 0.077877	7.1024(4) 0.15712	93.470(4) 85.90	116.049(3) 63.87	90.474(4) 87.77	669.73(8) 149.313
19	Labradorite	[L]	(13)	66			8.1747(9) 0.13631	12.8708(6) 0.077898	7.1015(6) 0.15719	93.461(5) 85.89	116.086(5) 63.83	90.514(6) 87.73	669.3(1) 149.41
20	Labradorite	[L]	(13)	66			8.1747(9) 0.13631	12.8708(6) 0.077898	7.1015(6) 0.15719	93.461(5) 85.89	116.086(5) 63.83	90.514(6) 87.73	669.3(1) 149.41
21	Labradorite	[L]	(3)	66			8.1747(9) 0.13631	12.8708(6) 0.077898	14.2030(12) 0.078595	93.461(5) 85.89	116.086(5) 63.83	90.514(6) 87.73	1338.6(2) 74.70
22	Labradorite	[L]	(15)	66			8.1747(9) 0.13631	12.8708(6) 0.077898	14.2030(12) 0.078595	93.461(5) 85.89	116.086(5) 63.83	90.514(6) 87.73	1338.6(2) 74.70
23	Labradorite	[M]	(9)	68.7	31.1	0.2	8.1748(6) 0.13620	12.8687(7) 0.077912	7.0964(5) 0.15717	93.428(5) 85.89	115.986(4) 63.92	90.602(5) 87.66	669.3(1) 149.41
24	Bytownite	[N]	(16)	76			8.174 0.13631	12.867 0.077924	14.197 0.078615	93.400 85.89	116.066 63.84	90.670 87.59	1337.8 74.75
25	Bytownite	[O]	(17)	80			8.178(3) 0.13605	12.870(4) 0.077915	14.187(5) 0.078569	93.50(8) 85.79	115.90(8) 64.00	90.65(8) 87.57	1339.5 74.65
26	Bytownite	[P]	(18)	83.4	16.2	0.4	8.180(3) 0.13620	12.874(3) 0.077885	14.196(3) 0.078621	93.45(2) 85.85	116.06(2) 63.85	90.63(2) 87.61	1339.4(5) 74.66
27	Bytownite	[Q]	(19)	85	15	0	8.183(1) 0.13595	12.883(2) 0.077834	14.186(2) 0.078550	93.38(2) 85.84	115.87(2) 64.02	90.82(1) 87.45	1341.9 74.52
28	Anorthite	[R]	(3)	94			8.1784(7) 0.13614	12.8736(8) 0.077893	14.1766(12) 0.078642	93.187(5) 85.90	115.938(5) 63.94	91.142(5) 87.18	1338.5(2) 74.71
29	Anorthite	[S]	(20)	98			8.186(1) 0.13584	12.876(2) 0.077889	14.182(2) 0.078524	93.30(2) 85.79	115.79(1) 64.09	91.12(1) 87.16	1342.0 74.51
30	Anorthite	[T]	(21)	100			8.173(1) 0.13621	12.869(1) 0.077922	14.165(1) 0.078687	93.113(6) 85.92	115.913(6) 63.96	91.261(6) 87.08	1336.4 74.83

* Localities of structures 1-30, Table 1.

[A] Amelia, Virginia, USA
[B] Tiburon, California, USA
[C] Cazadero " "
[D] (synthetic)
[E] Dundee, Scotland
[F] Camedo, Switzerland
[G] Mitchell Co., N.C., USA
[H] Quebec, Canada
[I] Essex Co., New York, USA
[J] Labrador, Canada
[K] Surtsey, Iceland
[L] Lake Co., Oregon, USA
[M] Roneval, S. Harris, Scotland
[N] Crystal Bay, Minnesota, USA
[O] St. Louis Co., Minnesota, USA
[P] Moon, Apollo 12038 72
[Q] Traversella, Switzerland
[R] Grass Valley, California, USA
[S] Vesuvius, Italy
[T] Val Pesmeda, Austria

** References for structures 1-30, Table 1.

(1) Harlow & Brown (1980)
(2) Wainwright & Starkey (1968)
(3) Wenk (in prep.)
(4) Wainwright & Starkey (In: Smith, 1974, v. 1, p. 71)
(5) Winter et al. (1979)
(6) Prewitt et al. (1976)
(7) Kroll & Tobi (to be published)
(8) Phillips et al. (1971)
(9) Kroll (1978)
(10) Hall et al. (In: Smith, 1974, v. 1, p. 76)
(11) Klein & Korekawa (1976)
(12) Krahl (1976)
(13) Wenk et al. (1980)
(14) Joswig et al. (1976)
(15) Tagai et al. (1978)
(16) Wainwright (1969)
(17) Fleet et al. (1966)
(18) Appleman et al. (1971; pers. comm., 1972)
(19) Facchinelli et al. (1979)
(20) Bruno et al. (1976)
(21) Wainwright & Starkey (1971)

Table 2. Or content, mean T-O distances for the T_1 and T_2 sites, site occupancies t_1 and t_2 [Al/(Al+Si)] and repeat distances tr110 for 10 structurally analyzed monoclinic K-feldspars. Or content was calculated from cell volume (Equation 8a: analbite - high sanidine series). Site occupancies were calculated as $t_i = 0.25 + (\langle T_i\text{-}O\rangle - \langle\langle T\text{-}O\rangle\rangle)/0.125$.

No.	Feldspar		[*]	(**)	Mol% Or	<T-O> dist. [Å] T_1	T_2	Site occupancy t_1	t_2	tr110	Comments
1	Sanidine	W(h)-Eif	[A]	(1)	88.8	1.645	1.640	0.270	0.230	7.794	htd. 21d, 1000°C
2	Sanidine	SpC(h)	[B]	(2,3)	90.6	1.645	1.640	0.270	0.230	7.796	htd. 13d, 1075°C
3	Sanidine	7002-Eif	[A]	(4)	84.1	1.650	1.637	0.300	0.200	7.783	
4	Sanidine	BHPS-Eif	[A]	(5)	86.4	1.650	1.635	0.310	0.190	7.786	
5	Sanidine	W-Eif	[A]	(1)	90.0	1.653	1.635	0.320	0.180	7.791	
6	Sanidine	OF-Eif	[A]	(6)	87.0	1.651	1.632	0.325	0.175	7.787	
7	Orthoclase	SpC	[B]	(7)	89.6	1.656	1.629	0.360	0.140	7.781	
8	Adularia	SpB	[C]	(7)	87.9	1.663	1.622	0.415	0.085	7.768	
9	Adularia	7007	[C]	(4)	84.1	1.665	1.621	0.425	0.075	7.765	
10	Orthoclase	Him	[D]	(8)	88.6	1.668	1.617	0.450	0.050	7.768	

Table 2 supplement: direct and reciprocal lattice parameters of structures 1-10.

No.	Feldspar		[*]	(**)	Mol % Or	a/a^*	b/b^*	c/c^*	α/α^*	β/β^*	γ/γ^*	$V/V^* \cdot 10^5$
						[Å]/[Å^{-1}]	[Å]/[Å^{-1}]	[Å]/[Å^{-1}]	degrees	degrees	degrees	[Å^3]/[Å^{-3}]
1	Sanidine	W(h)-Eif	[A]	(1)	88.8	8.546(5)	13.037(5)	7.178(5)	90	115.97(5)	90	719.0
						0.13016	0.076705	0.15496	90	64.03	90	139.09
2	Sanidine	SpC(h)	[B]	(2,3)	90.6	8.5642(2)	13.0300(4)	7.1749(2)	90	115.994(5)	90	719.7
						0.12991	0.076746	0.15506	90	64.01	90	138.95
3	Sanidine	7002-Eif	[A]	(4)	84.1	8.539(4)	13.015(5)	7.179(3)	90	115.99(2)	90	717.2
						0.13029	0.076834	0.15497	90	64.01	90	139.44
4	Sanidine	BHPS-Eif	[A]	(5)	86.4	8.5425(11)	13.0195(11)	7.1829(7)	90	115.994(7)	90	718.1
						0.13024	0.076808	0.15489	90	64.01	90	139.26
5	Sanidine	W-Eif	[A]	(1)	90.0	8.549(5)	13.028(5)	7.188(5)	90	116.02(5)	90	719.4
						0.13017	0.076758	0.15481	90	63.98	90	139.00
6	Sanidine	OF-Eif	[A]	(6)	87.0	8.543(3)	13.021(5)	7.183(1)	90	115.98(3)	90	718.3(3)
						0.13021	0.076799	0.15487	90	64.02	90	139.22
7	Orthoclase	SpC	[B]	(7)	89.6	8.5616(2)	12.9962(4)	7.1934(2)	90	116.015(5)	90	719.3
						0.12997	0.076946	0.15469	90	63.98	90	139.02
8	Adularia	SpB	[C]	(7)	87.9	8.554(2)	12.970(2)	7.207(2)	90	116.007(10)	90	718.7
						0.13008	0.077101	0.15439	90	63.99	90	139.16
9	Adularia	7007	[C]	(4)	84.1	8.545(2)	12.967(5)	7.201(3)	90	116.00(2)	90	717.1
						0.13021	0.077119	0.15451	90	64.00	90	139.44
10	Orthoclase	Him	[D]	(8)	88.6	8.5632(11)	12.9633(14)	7.2099(11)	90	116.073(9)	90	718.9(1)
						0.13001	0.077141	0.15441	90	63.93	90	139.10

* Localities

[A] Volkesfeld, Eifel, W-Germany
[B] Burma
[C] St. Gotthard, Switzerland
[D] Himalaya Mine, Ca., USA

** References

(1) Weitz (1972)
(2) Cole et al. (1949)
(3) Ribbe (1963)
(4) Phillips & Ribbe (1973)
(5) Brown et al. (1974)
(6) Ohashi & Finger (1974)
(7) Colville & Ribbe (1968)
(8) Prince et al. (1973)

Table 3. Or content, mean T-O distances for T_1o, T_1m, T_2o, T_2m sites, site occupancies t_1o, t_1m, $\langle t_2o\rangle = \frac{1}{2}(t_2o + t_2m)$[Al/(Al+Si)] and repeat distances tr110 and tr$1\bar{1}0$ [Å] for 14 structurally analyzed microclines. Or content was calculated from cell volume (Equation 8b: low albite - low microcline series). Site occupancies were calculated as $t_i = 0.25 + (\langle T_i\text{-}O\rangle - \langle\langle T\text{-}O\rangle\rangle)/0.125$.

No.	Feldspar	[*]	(**)	Mol% Or	<T-O> distances [Å] T_1o	T_1m	T_2o	T_2m	Site occupancy t_1o	t_1m	$\langle t_2o\rangle$	Repeat dist. tr110	tr$1\bar{1}0$
1	Interm. Micr. P2B	[1]	(1,2)	98.5	1.659	1.656	1.630	1.629	0.375	0.350	0.150	7.788	7.788
2	Interm. Micr. P2A	[1]	(1,2)	96.7	1.665	1.655	1.625	1.626	0.425	0.350	0.110	7.784	7.784
3	Interm. Micr. CA1A	[1]	(1,2)	92.0	1.671	1.658	1.622	1.622	0.470	0.370	0.080	7.777	7.777
4	Interm. Micr. P17C	[1]	(1,2)	91.7	1.669	1.654	1.623	1.622	0.465	0.345	0.095	7.792	7.761
5	Interm. Micr. A1D	[1]	(1,2)	91.3	1.673	1.651	1.623	1.622	0.500	0.320	0.090	7.808	7.745
6	Interm. Micr. CA1B	[1]	(1,2)	91.5	1.695	1.642	1.620	1.619	0.660	0.240	0.050	7.833	7.711
7	Interm. Micr. P1C	[1]	(1,2)	94.4	1.702	1.631	1.620	1.620	0.720	0.150	0.065	7.850	7.698
8	Interm. Micr. RC20C	[1]	(1,2)	92.6	1.716	1.629	1.615	1.615	0.830	0.130	0.020	7.862	7.673
9	Interm. Micr. CA1E	[1]	(1,2)	91.7	1.731	1.617	1.616	1.615	0.940	0.025	0.015	7.891	7.640
10	Interm. Micr. K235	[2]	(3)	94.5	1.671	1.651	1.622	1.627	0.475	0.320	0.105	7.801	7.751
11	Interm. Micr. SpU	[3]	(4)	93.7	1.694	1.643	1.618	1.616	0.660	0.250	0.045	7.826	7.716
12	Low Micr. Po	[4]	(5)	94.8	1.735	1.613	1.619	1.609	0.975	0.010	0.010	7.909	7.629
13	Low Micr. Pe	[5]	(6)	92.8	1.742	1.614	1.611	1.611	1.020	-.005	-.005	7.910	7.623
14	Low Micr. Pri	[6]	(7)	96.5	1.738	1.613	1.614	1.615	0.995	0.000	0.000	7.917	7.623

* Localities

[1] Adamello Massif, N-Italy
[2] Kûgnât, SW-Greenland
[3] Kodarma, Bihar, India
[4] Pontiskalk-Formation, Switzerland
[5] Pellotsalo, Lake Ladoga, USSR
[6] Prilep, Yugoslavia

** References

(1) Dal Negro et al. (1978)
(2) De Pieri (1979)
(3) Ribbe (1979)
(4) Bailey (1969)
(5) Finney & Bailey (1964)
(6) Brown & Bailey (1964)
(7) Strob (1983)

Table 3 supplement: direct and reciprocal lattice parameters of structures 1-14.

No.	Feldspar	[*]	(**)	Mol % Or	a/a^*	b/b^*	c/c^*	α/α^*	β/β^*	γ/γ^*	$V/V^* \cdot 10^5$
					[Å]/[Å^{-1}]			degrees			[Å^3]/[Å^{-3}]
1	Interm. Micr. P2B	[1]	(2)	98.5	8.589 0.12956	12.995 0.076953	7.198 0.15460	90 90	116.02 63.98	90 90	722.0 138.51
2	Interm. Micr. P2A	[1]	(2)	96.7	8.583 0.12968	12.989 0.076988	7.202 0.15455	90 90	116.05 63.95	90 90	721.3 138.63
3	Interm. Micr. CA1A	[1]	(2)	92.0	8.563 0.12996	12.984 0.077018	7.204 0.15448	90 90	116.03 63.97	90 90	719.7 138.95
4	Interm. Micr. P17C	[1]	(2)	91.7	8.568 0.12989	12.980 0.077042	7.201 0.15455	90.07 90.04	116.03 63.97	89.75 90.24	719.6 138.97
5	Interm. Micr. A1D	[1]	(2)	91.3	8.563 0.12996	12.984 0.077021	7.201 0.15453	90.13 90.10	116.02 63.98	89.50 90.49	719.4 139.00
6	Interm. Micr. CA1B	[1]	(2)	91.5	8.559 0.13004	12.976 0.077077	7.211 0.15433	90.30 90.14	116.03 63.97	89.02 90.94	719.5 138.98
7	Interm. Micr. P1C	[1]	(2)	94.4	8.574 0.12983	12.971 0.077113	7.212 0.15431	90.33 90.23	116.03 63.97	88.78 91.20	720.5 138.78
8	Interm. Micr. RC20C	[1]	(2)	92.6	8.566 0.12993	12.961 0.077183	7.217 0.15417	90.43 90.26	116.00 64.00	88.48 91.48	719.9 138.91
9	Interm. Micr. CA1E	[1]	(2)	91.7	8.558 0.13001	12.963 0.077193	7.217 0.15408	90.52 90.40	115.93 64.07	87.98 91.99	719.6 138.97
10	Interm. Micr. K235	[2]	(3)	94.5	8.643(3) 0.12900	12.929(4) 0.077347	7.190(3) 0.15506	90.13(3) 90.05	116.24(3) 63.76	89.60(3) 90.38	720.6 138.77
11	Interm. Micr. SpU	[3]	(4)	93.7	8.578 0.12968	12.960 0.077170	7.211 0.15425	90.30 90.09	115.97 64.03	89.12 90.83	720.7 138.76
12	Low Micr. Po	[4]	(5)	94.8	8.573 0.12979	12.962 0.077211	7.218 0.15404	90.57 90.46	115.92 64.08	87.75 92.22	720.7 138.73
13	Low Micr. Pe	[5]	(6)	92.8	8.560(4) 0.12989	12.964(7) 0.077201	7.215(3) 0.15399	90.65(8) 90.39	115.83(8) 64.17	87.70(8) 92.24	720.0 138.88
14	Low Micr. Pri	[6]	(7)	96.5	8.5756(8) 0.12978	12.9635(6) 0.077207	7.2211(5) 0.15400	90.678(5) 90.39	115.940(4) 64.07	87.646(5) 92.29	721.3(1) 138.65

<<Al-O>> = 1.747 Å for anorthite, 1.613 and 1.742 Å for low albite (Table 1; average of four refinements), and 1.613 and 1.738 Å for low microcline (Table 3 and Blasi *et al.*, 1983; average of five refinements).

The <<T-O>> versus <t> diagram (Fig. 1) covers the range from 0.25 to 0.5 Al/(Al+Si), and even if the bonding effects just mentioned were insignificant, long extrapolations from 0.25 to 0 and 0.5 to 1.0 would be necessary to represent the full range of t values in individual tetrahedra. This leads to systematic discrepancies, and Smith (1974a, p. 70) "in desperation" suggested using two separate straight lines in the regions of 0 to 0.5 and 0.5 to 1.0 Al/(Al+Si), but with limited success. Direct refinements of site occupancies by neutron diffraction methods are few in number and not without their own difficulties (see footnote 1).

A new model

Ribbe (1975, p. R-22) suggested deriving Al contents of T sites, not from the <T-O> distances themselves, but from differences in mean distances. His method eliminated some uncertainties of the linear models that arose from long extrapolations and from the fact that the mean Al-O and Si-O distances are different in the different ordered structures, namely LA, LM and $P\bar{1}$ anorthite, but did not account for bonding effects. Furthermore, it did not permit an independent determination of Σt apart from a knowledge of n_{An} (see Eqn. 3).

This last problem may be overcome by considering the differences between average individual and grand mean tetrahedral distances, i.e., $\langle T_i\text{-O}\rangle - \langle\langle T\text{-O}\rangle\rangle$, rather than size differences among individual tetrahedra as in Ribbe's model. The procedure for calculating site occupancies may be recast into a single equation if we consider separately the difference Δt between the individual and the average values of t:

$$\Delta t \equiv t_i - \langle t\rangle \quad , \quad \text{or} \quad t_i = \langle t\rangle + \Delta t \ . \tag{4}$$

<t> is found from chemical composition by Equation 1, and Δt is related to $\langle T_i\text{-O}\rangle - \langle\langle T\text{-O}\rangle\rangle$, so that Equation 4 becomes

$$t_i = 0.25(1 + n_{An}) + (\langle T_i\text{-O}\rangle - \langle\langle T\text{-O}\rangle\rangle)/\text{const} \ , \tag{5}$$

where 'const' ≡ <<Al-O>> - <<Si-O>>; it is equal to 0.125 Å for K-rich feldspars and is taken to be 0.13 Å for Na-rich feldspars and plagioclases.

At this stage, the An-content still must be known in order to find t_i. However, we can eliminate this by expressing <t> in terms of <<T-O>>. Figure 1 indicates that the linear model must be modified for this purpose by (1) treating the An-rich plagioclases separately, and (2) considering that the

$\langle\langle T\text{-O}\rangle\rangle$ distances of ordered feldspars -- especially alkali feldspars and sodic plagioclases -- are slightly larger than those of their disordered equivalents.

Since it is desirable to substitute $\langle t\rangle$ by $\langle\langle T\text{-O}\rangle\rangle$ in Equation 5, we chose $\langle t\rangle$ as the dependent variable in a regression analysis of the data listed in Tables 1, 2 and 3 (excluding An-rich plagioclases):

$$\begin{aligned}\langle t\rangle &= 0.25(1 + n_{An}) \\ &= -11.215 + \underset{(\pm.076)}{6.981}\ \langle\langle T\text{-O}\rangle\rangle + \underset{(\pm.017)}{0.124}(\langle T_1\text{O-O}\rangle - \langle T_1\text{m-O}\rangle)\end{aligned} \tag{6}$$

with a correlation coefficient $r^2 = 0.996$. Estimated standard deviations are given in parentheses. The third term on the right accounts for the amount of order present. When T_1O and T_1m tetrahedra are identical in size, Equation 6 reduces to the original linear model. The values of $\langle t\rangle$ expected from chemical composition are reproduced with a standard deviation of $\pm$0.005 Al/(Al+Si), corresponding to $\pm$ 2 mol % An.

An analogous equation for An-rich plagioclases is

$$\langle t\rangle = -12.088 + 7.491\ \langle\langle T\text{-O}\rangle\rangle\ . \tag{7}$$

The reason why $\langle\langle T\text{-O}\rangle\rangle$ distances of An-rich plagioclases are larger than would be expected from sodic and intermediate compositions is open to question. One is tempted to ascribe it to some bonding effect due to Ca, but the substantial discontinuity near An_{80} in Figure 1 is disturbing, as is the fact that An_{98} refined in $P\bar{1}$ by Bruno *et al.* (1976) gave $\langle\langle T\text{-O}\rangle\rangle$ = 1.681 Å, but refinement in $I\bar{1}$ gave 1.678 Å.

Combination of Equation 6 or 7 with Equation 5 allows us to derive site occupancies from $\langle T_i\text{-O}\rangle$ distances without making reference to chemical composition. This procedure is indicated when the total Al content so derived is to be checked against the Al content expected from the chemical formula: they should not differ by more than 2 mol % An. To simplify calculations, it is safe to assume that $t_1m = t_2o = t_2m$ for all natural Na-rich feldspars and plagioclases (Table 1; *cf.* Fig. 16, Ch. 2) and $t_2o = t_2m$ for intermediate microclines (Table 2; *cf.* Fig. 1, Ch. 2). A sample calculation for intermediate microcline A1D (#5, Table 3) follows.

$\langle T\text{-O}\rangle$ for T_1O = 1.673, T_1m = 1.651, T_2O = 1.623, T_2m = 1.622 Å; $\langle\langle T\text{-O}\rangle\rangle$ = 1.642 Å

$$\begin{aligned}\text{and}\qquad t_1o &= 0.25 + (1.673 - 1.642)/0.125 = 0.50 \\ t_1m &= 0.25 + (1.651 - 1.642)/0.125 = 0.32 \\ t_2o = t_2m &= 0.25 + (1.622_5 - 1.642)/0.125 = 0.09\end{aligned}$$

Correction of bonding effects

As mentioned earlier, a statistical study of bond length variation in feldspars by Phillips and Ribbe (1973a) and Ribbe *et al.* (1974) produced three factors, in addition to Al content, which perturb individual T-O bond lengths:

(1)	Linkage	Si-O → Si bonds are ∿0.03 Å longer than Si-O → Al bonds.
(2)	Bonds to Na,K,Ca	The coordination number (2, 3 or 4 in feldspars) of the oxygen atom is related directly to T-O distance.
(3)	T-O-T angle	Longer T-O distances are associated with narrower T-O-T angles.

Strob (1983) has completed an elegant study of alkali feldspars in which he has produced regression equations to correct for these effects. Adjustments to observed <T-O> distances reach ±0.005 Å, about three times the estimated standard deviation in <T-O>. Their importance is that they adjust for what are small, but obviously systematic, errors in our estimation of Al contents of individual tetrahedra. They have less importance in our subsequent discussion of the derivation of t_i values from lattice parameters than they do for modelling the precise details of Al,Si ordering paths, for example, that are shown in Figure 8b in Chapter 2 for Na-feldspar. The effect of these is to slightly decrease the value of <$T_1$0-O> and increase <T_1m-O> and thereby redistribute estimated Al contents, for which Strob has derived a somewhat modified version of Equation 5. Two examples suffice to illustrate the results for Na-feldspars; K-feldspars are generally much less affected.

Sample	Site	Observed <T-O>, Å	Corrected <T-O>, Å	t_i from Equation 5	Corrected value of t_i
Tiburon HA	$T_1$0	1.6490	1.6467	0.296	0.278
#8 in	T_1m	1.6420	1.6458	0.240	0.271
Table 1	$T_2$0	1.6400	1.6393	0.224	0.218
	T_2m	1.6420	1.6413	0.240	0.234
	<<T-O>>	1.6433	1.6433	Σ = 1.000	Σ = 1.001
Average LA	$T_1$0	1.7411	1.7365	0.991	0.998
#1-3 in	T_1m	1.6080	1.6128	-0.033	-0.010
Table 1	$T_2$0	1.6145	1.6151	0.017	0.008
	T_2m	1.6154	1.6146	0.024	0.004
	<<T-O>>	1.6448	1.6448	Σ = 0.999	Σ = 1.000

We have calibrated our feldspar structural data in the form of mean T-O distances with Al occupancies of individual tetrahedral sites as well as we can at the moment. Unfortunately, none of the crystal structures used in this endeavor has had its composition determined on the very grain used for the structure refinement, and we have assumed that each bulk sample analysis is correct and have used them as reported.

LATTICE PARAMETERS OF ALKALI FELDSPARS

Alkali exchange series

For alkali feldspars it is possible to prepare complete Na ⇄ K solid solution series by cation exchange starting from structurally well characterized, single-phase materials. The method of Orville (1967) involves producing Na- and K-end-member compositions by repeated anhydrous alkali exchange of the starting material in molten NaCl and KCl, respectively, followed by analysis. Carefully weighed proportions of these end members are mixed by grinding and then homogenized at ∿900°C for a few days. It has been demonstrated convincingly that if the sample is kept dry, very little if any Al,Si migration occurs. Unmixing of Na and K are prevented by rapid quenching of the specimen. The run products subsequently may be analyzed and their unit cell parameters determined by x-ray powder methods.

Cell dimensions of most of the known complete alkali-exchange series are given in Figure 2, including three LA-LM series (Orville, 1967; Waldbaum and Robie, 1971, redetermined by Hovis and Peckins, 1978; Kroll *et al.*, unpublished), "orthoclase P50-56F" (Wright and Stewart, 1968), and AA-HS (Hovis, 1977; Kroll *et al.*, unpublished). Two HA-HS series prepared by hydrothermal crystallization of glasses have been omitted (Orville, 1967; Donnay and Donnay, 1952 -- cell dimensions refined by Wright and Stewart, 1968), because there are differences in structural state from sample to sample, and based on their *b* and *c* cell edges, it is found that they are not as fully disordered as the Kroll AA-HS series.

The curves in Figure 2 have been drawn through the LA-LM data set of Kroll and coworkers, who used low albite from Cazadero, California (crystal structure by H.-R. Wenk, pers. comm.; specimen #4, Table 1) and low microcline from Prilep, Yugoslavia (structure by Strob, 1983; #14, Table 3) as starting materials. To prepare the disordered series, the Cazadero low albite was converted by long-term heating into monalbite (which on cooling becomes analbite). A single-crystal precession study of this material showed that it attained monoclinic symmetry at ∿980°C. This analbite was K-exchanged to give high sanidine, and the Na- and K-end members were mixed at 5 mol % intervals to produce the AA-HS series through which curves are drawn in Figure 2.

---

[4]Stewart (1975) lists numerous partial series (Wright and Stewart, 1968; Müller, 1969; Waldbaum and Robie, 1971; Hovis, 1974; Thompson *et al.*, 1974), "series ... prepared by prolonged heating to 1050-1130°C" (Spencer, 1937; Hovis, 1974), and other series crystallized from glasses (Parsons, 1968; Luth and Querol-Suñé, 1970; Martin, 1970; Raase, 1971; Kroll, 1973).

Table 4. Cell parameters of alkali feldspar end members.

Parameter (units)	Low albite $t_1o = 1$	Low microcline $t_1o = 1$	Analbite $t_1o = 0.28$	High sanidine $t_1o = 0.28$
a (Å)	8.135	8.592	8.156	8.606
b (Å)	12.785	12.962	12.871	13.031
c (Å)	7.158	7.222	7.108	7.177
α (°)	94.27	90.62	93.52	90.00
α^*(°)	86.39	90.44	85.94	90.00
β (°)	116.60	115.95	116.44	116.03
γ (°)	87.68	87.67	90.26	90.00
γ^*(°)	90.46	92.29	87.96	90.00
V (Å^3)	663.81	722.60	666.44	723.22
tr[110] (Å)	7.7145	7.9190	7.6030	7.8080
tr[1$\bar{1}$0] (Å)	7.4365	7.6285	7.6345	7.8080
Δtr (Å)	0.2780	0.2905	-0.0315	0

$\mathrm{tr}[110] \equiv \frac{1}{2}(a^2 + b^2 + 2ab\cos\gamma)^{\frac{1}{2}}$; $\mathrm{tr}[1\bar{1}0] \equiv \frac{1}{2}(a^2 + b^2 - 2ab\cos\gamma)^{\frac{1}{2}}$;
$\Delta\mathrm{tr} \equiv \mathrm{tr}[110] - \mathrm{tr}[1\bar{1}0]$

°2θ, Cu$K\alpha_1$ radiation:				
$\bar{2}$01	22.06	20.99	22.00	20.95
131 - 1$\bar{3}$1	1.10	-0.81	2.00	0
060	42.51	41.81	42.20	41.55
$\bar{2}$04	51.14	50.52	51.48	50.86

Based on lattice parameters found in the literature and on those determined for the two new exchange series which include new structure refinements, Kroll chose values for the end members of the series (Table 4), some of which differ slightly (0.0025 Å and 0.015°, on the average) from those given by Stewart (1975, Table St-2) and less from those of Smith (1974a, p. 258). The one major difference in all of this is that the AA-HS series is not assumed to be completely disordered (with $t_1o = t_1m = t_2o = t_2m = 0.25$) but rather to have residual Al in t_1, i.e., $t_1o = t_1m = 0.28$, $t_2o = t_2m = 0.22$. This is based in part on an analysis of <*T*-O> distances in the light of bonding considerations, as discussed above, but more so on the arguments detailed below.

> Refinement of a high albite structure by Prewitt *et al.* (1976) resulted in $t_1o = 0.28$ (Table 1), and HA is structurally very close to analbite -- their lattice parameters at room temperature are not distinguishable. The Cazadero LA, which was converted by long-term heating into AA, attained the same lattice parameters and thus was assumed to have $t_1o = 0.28$. High sanidine with $t_1 = 0.28$ was then produced by K-exchange of Cazadero AA. Its a and b cell edges give the same value (tr[1$\bar{1}$0] = 7.808 Å; $t_1 = 0.28$) as independently found from the regression equation given in Figure 9 for monoclinic K-feldspars. In this way the AA-HS site occupancies were "pinned" on both sides. Furthermore, synthetic homogeneous $Or_{58}Ab_{42}$, quenched from

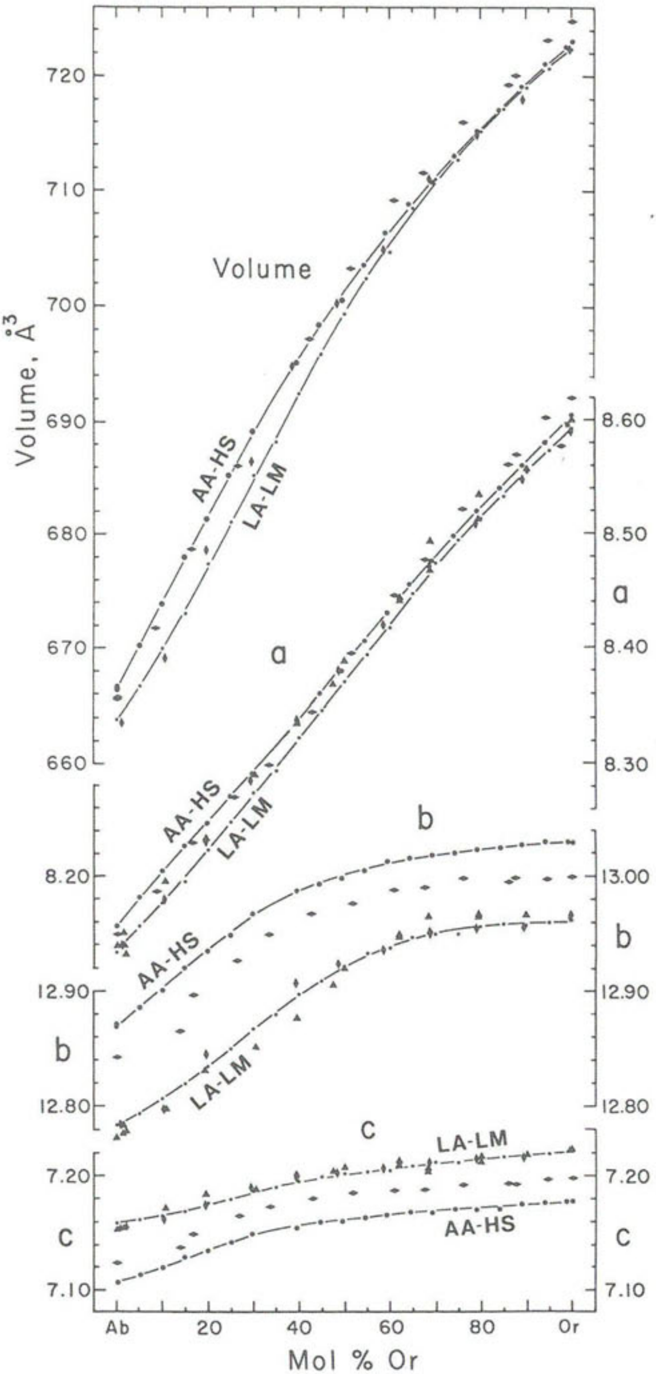
Volume
Volume, Å^3
720
710
700
690
680
670
660
AA-HS
LA-LM
a
8.60
8.50
8.40
8.30
8.20
b
13.00
12.90
12.80
c
7.20
7.10
Ab
20
40
60
80
Or
Mol % Or

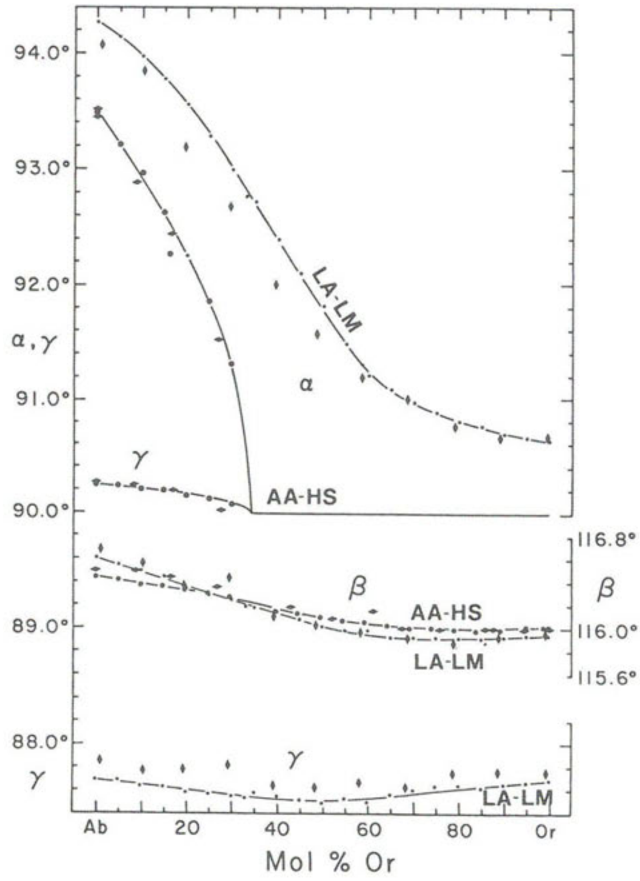

Figure 2. Unit cell parameters for five cation-exchange series of alkali feldspars in each of which (presumably) Al,Si distribution is invariant with composition (mol % Or). The curve for the LA-LM series is arbitrarily drawn through the small dots, representing unpublished data of Kroll and co-workers for the Cazadero low albite-Prilep low microcline series (see Tables 1 and 3 for end members). The LA-LM series are: triangles, Waldbaum and Robie (1971) --*a*, *b*, and *c* only; vertical diamonds, Orville (1967). The curve for the AA-HS series is arbitrarily drawn through the large dots, representing Kroll and co-workers' heat-treated and cation-exchanged series. The horizontal diamonds represent the "orthoclase series structurally equivalent to P50-56F" of Wright and Stewart (1968, Table 7).

750°, P_{H_2O} = 2.5 kbar, was found by Fenn and Brown (1977) to have t_1o = 0.29 and t_1m = 0.28, and the two most disordered sanidine structures (#1 and #2 in Table 2) yield t_1 = 0.27, all values being calculated using Equation 5. If further evidence is needed, the structure of the three triclinic anorthoclases refined by Harlow (1982) average 0.29 Al in T_1O, 0.27 in T_1m and 0.22 in T_2(0,m) and the one refined by De Pieri and Quareni (1973) is nearly identical [values from Eqn. 5, normalized to 0.00 An-content].

As Stewart (1975, p. St-6) commented, "Plots for individual parameters against Or-content of series with the same Al,Si order are not linear [Fig. 2]: there is a change in slope near Or_{40} in a plot of any cell parameter against composition for every series studied, and therefore the cause for the change in slope cannot be the different Al,Si arrangements of these series. The most probable cause is change in oxygen coordination of the alkali atoms" (*cf.* Fig. 10, Ch. 1, and see statistical analysis of nonlinearity by Vogel *et al.*, 1973).

Cell volume and the *a* dimension

Unit cell volume V is highly dependent on K,Na content and is nearly, but not entirely, independent of Al,Si distribution. Polynomials have been derived from the unpublished data of Kroll and coworkers for the AA-HS series:

$$n_{Or} = -584.6683 + 2.58732\ V - 3.83499 \times 10^{-3}V^2 + 1.90428 \times 10^{-6}V^3 \qquad (8a)$$

and for the LA-LM series:

$$n_{Or} = -1227.8023 + 5.35958\ V - 7.81518 \times 10^{-3}V^2 + 3.80771 \times 10^{-6}V^3. \qquad (8b)$$

A curve to use when structural state is intermediate or completely unknown:

$$n_{Or} = -929.1523 + 4.07032\ V - 5.96146 \times 10^{-2}V^2 + 2.91994 \times 10^{-5}V^3. \qquad (8c)$$

Stewart and Ribbe (1969, p. 448) demonstrated that very little change is expected in the *a* cell dimension with ordering because all four *T* sites (T_1O, T_1m, T_2O, T_2m) are encountered in equal numbers in any traverse chosen through the feldspar structure along *a* (see Figs. 2, 6 and 8 in Ch. 1). This means that for all feldspars, including plagioclases (see Fig. 1, Ch. 4), the *amount* of Al (and thus Si) encountered along *a* will be the same, regardless of structural state, and its distribution *among* the sites will not affect the *a* dimension appreciably.

Unit cell angles

For monoclinic alkali feldspars, the direct cell angles α and γ and their reciprocal cell counterparts, α* and γ*, are 90°. The β angles range from about 116.6° to 115.9° with composition, but are essentially unsensitive to

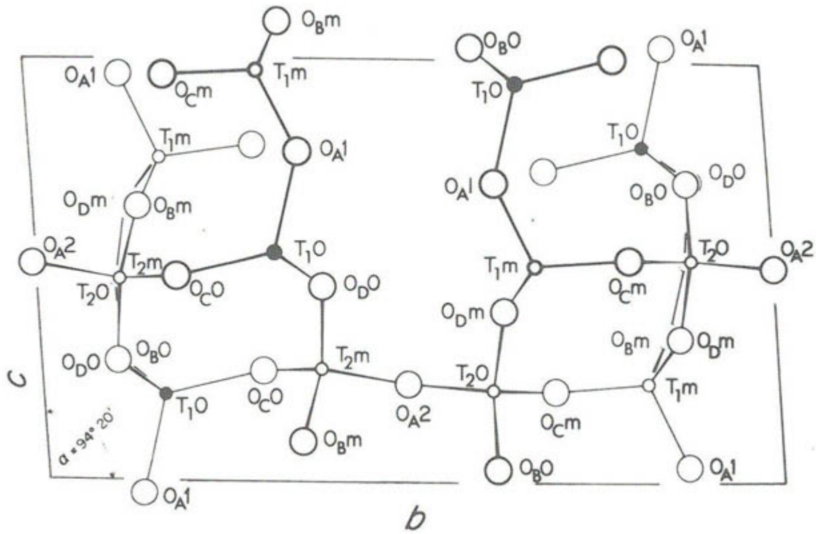

Figure 3. A projection onto (100) of part of the low albite structure. The T sites are the labelled small circles: T_10 contains Al (black dots); the others contain Si. Na is not shown.

Al,Si order (Fig. 2). The angle γ varies little with composition, but is almost uniformly sensitive to Al,Si distribution across the entire range from Or_0Ab_{100} to $Or_{100}Ab_0$. As expected, the related angle γ* (not plotted here -- see Fig. 5 below) has similar properties. The angle α has a lesser and more variable sensitivity to Al,Si order than γ. In the AA-HS series of Kroll and coworkers, a plot of $\cos^2\alpha$ versus n_{Or} is nearly perfectly linear [$\cos^2\alpha(\times 10^4) = 37.13 - 108.01 \cdot n_{Or}$; $R^2 = 0.9996$] and extrapolates to zero ($\alpha = 90°$) at 34.3 mol % Or. The triclinic → monoclinic inversion at room temperature is thus firmly fixed, and it agrees very well with the value of Or_{36} determined in a study of natural and heated anorthoclases by Harlow (1982). For the LA-LM series, α varies by 3.7° from Or_0 to Or_{100}. The determinative value of α,γ and α*,γ* in alkali feldspars will be discussed in a later section.

The *b* and *c* cell dimensions

The *b* and *c* dimensions depend on both composition *and* Al,Si order in alkali feldspar series (Fig. 2) and in plagioclases (Fig. 1, Ch. 4). In order to comprehend the net effect of changes in *T*-O bond lengths due to Al,Si substitution on *b* and *c*, we may examine ···*T*-O-*T*-O··· paths through the structure in these directions. Along *c* there are six sub-parallel paths visible in this partial projection of Figure 3; for example (starting near the origin), O_A1-T_1O-O_DO-T_2m-O_Bm-T_1m-O_A1, and next to it, O_Bm-T_2m-O_DO-T_1O-O_A1-T_1m-O_Bm. All paths along

c contain one T_1O site, one T_1m site, and either one T_2O or one T_2m site. Thus the total Al encountered along c is

$$\Sigma Al_c = t_1o + t_1m + t_2(o \text{ or } m), \quad \text{where } t_2o = t_2m. \tag{9a}$$

Along b several paths may be chosen, e.g., O_A2-T_2m-O_DO-T_1O-O_CO-T_2m-O_A2-T_2O-O_Dm-T_1m-O_Cm-T_2O-O_A2. All paths along b contain one T_1O, one T_1m, and four T_2 sites. Thus the total number of Al atoms encountered along b is

$$\Sigma Al_b = t_1o + t_1m + 4[t_2(o \text{ or } m)], \quad \text{where } t_2o = t_2m. \tag{9b}$$

Stewart and Ribbe (1969, Table 2, p. 450) tabulated the actual changes in individual bond lengths as projected onto the b and c axes which are caused by a redistribution of Al and Si in the T sites in the inversion of analbite (AA) or high albite to low albite (LA). As noted in Table 4, c increases by 0.050 Å, while b decreases by 0.086 Å (values are 0.045 Å and 0.069 Å for HS → LM). Why?

A simplistic explanation is found by applying Equations 9a and 9b to the Al,Si distributions in AA and LA, assuming AA to be completely disordered and LA to be completely ordered.

$$\begin{aligned}
\Sigma Al_c \text{ (LA)} &= 1.00 + 0.00 + 0.00 &&= 1.00\\
\Sigma Al_c \text{ (AA)} &= 0.25 + 0.25 + 0.25 &&= \underline{0.75}\\
&\quad \text{Difference, } \Delta Al_c && +0.25 \text{ Al}\\[1ex]
\Sigma Al_b \text{ (LA)} &= 1.00 + 0.00 + 4(0.00) &&= 1.00\\
\Sigma Al_b \text{ (AA)} &= 0.25 + 0.25 + 4(0.25) &&= \underline{1.50}\\
&\quad \text{Difference, } \Delta Al_b && -0.50 \text{ Al}
\end{aligned}$$

Using these values and the fact that <<Al-O>> = 1.742 Å and <<Si-O>> = 1.613 Å in ordered low albites (Table 1), one might expect a change in c of +0.25(1.742 - 1.613) = +0.032 Å and in b of -0.50(0.129) = -0.065 Å; the actual values are +0.050 Å and -0.086 Å, respectively.

However, the calculated values represent changes expected only if $c \sim 3 \times$ <T-O> and $b \sim 6 \times$ <T-O>, as we assumed in our calculations of ΣAl_c and ΣAl_b (Eqns. 9a and 9b). But c is ~7.13 Å and b is ~12.83 Å, and the grand mean T-O distance for both LA and AA is 1.644 Å. Thus better estimates of expected changes in c and b can be made by multiplying 0.032 Å by $[7.12/(3 \times 1.644)] = 1.45$ and -0.065 Å by $[12.83/(6 \times 1.644)] = -1.30$ to obtain 0.046 Å and -0.085 Å, respectively.[5] These are quite reasonable approximations of the observed changes.

[5]Using values of $t_1o = t_1m = 0.28$ and $t_2o = t_2m = 0.22$, as in Table 4, the results are $\Sigma Al_c = 0.72$, $\Delta Al_c = 0.22$, $\Sigma Al_b = 1.44$, $\Delta Al_b = -0.44$. The argument is unaffected; predicted changes in c and b would be +0.041 Å and -0.074 Å instead of +0.046 Å and -0.085 Å.

Stewart and Ribbe observed that interchange of Al between T_1O and T_1m resulted only in trivial shifts in *b* and *c* (<0.004 Å) because the total Al encountered is unchanged: both paths include one T_1O and one T_1m site. However, when Al moves from T_2 sites into T_1 sites with increasing order (or vice versa), *b* and *c* change significantly. This information led to the deduction that relative position of an alkali feldspar on a *b*-*c* plot like that initially proposed by Wright and Stewart (1968), is a function of total Al in T_1O and T_1m, i.e., $(t_1o + t_1m)$, and is independent of $(t_1o - t_1m)$.

THE *b*-*c* PLOT TO DERIVE $(t_1o + t_1m)$

Wright and Stewart (1968) found that to plot the *b* and *c* cell edges against each other produced more or less linear arrays for alkali feldspars of different composition but equivalent Al,Si order, regardless of the symmetry of the specimen. Thus a particular alkali exchange series would define a line subparallel to (or coincident with) the LA-LM or AA-HS limiting series, depending solely on the Al,Si distribution of the starting material. Stewart and Ribbe (1969) assumed that the LA-LM series was fully ordered, $(t_1o + t_1m) = 1.00$, and the AA-HS series fully disordered, $(t_1o + t_1m) = 0.50$, and contoured the *b*-*c* plot proportionally (see Fig. 1 in Stewart and Wright, 1974). But, as discussed above, there is good reason now to believe the latter value should be 0.56, and that revised values of *b* and *c* for the LA, LM, AA and HS corners of the quadrilateral should be used (Table 4). Furthermore, Strob (1983), employing data for 24 K-rich feldspars (Tables 2 and 3), has determined that although there is only one population of *c* cell edges versus Al content of T_1 sites [$c = 7.1226 + 0.100\ t$, where $t = 2t_1$ or $(t_1o + t_1m)$, from structure analyses], there are separate populations of *b* cell edges versus *t* for monoclinic and triclinic K-feldspars [$b_M = 13.1473 - 0.207(2t_1)$; $b_T = 13.0692 - 0.110(t_1o + t_1m)$].

Thus we have found it useful to give separate *b*-*c* plots (Fig. 4) and new linearized equations for determining $2t_1$ or $(t_1o + t_1m)$, depending on whether the alkali feldspar is topochemically monoclinic --

$$2t_1 = -7.590 - 2.3258 \cdot b + 5.3581 \cdot c\ , \tag{10a}$$

or triclinic --

$$(t_1o + t_1m) = \frac{b - 0.7138 - 1.7505 \cdot c}{-7.7245 + 1.0150 \cdot c}\ . \tag{10b}$$

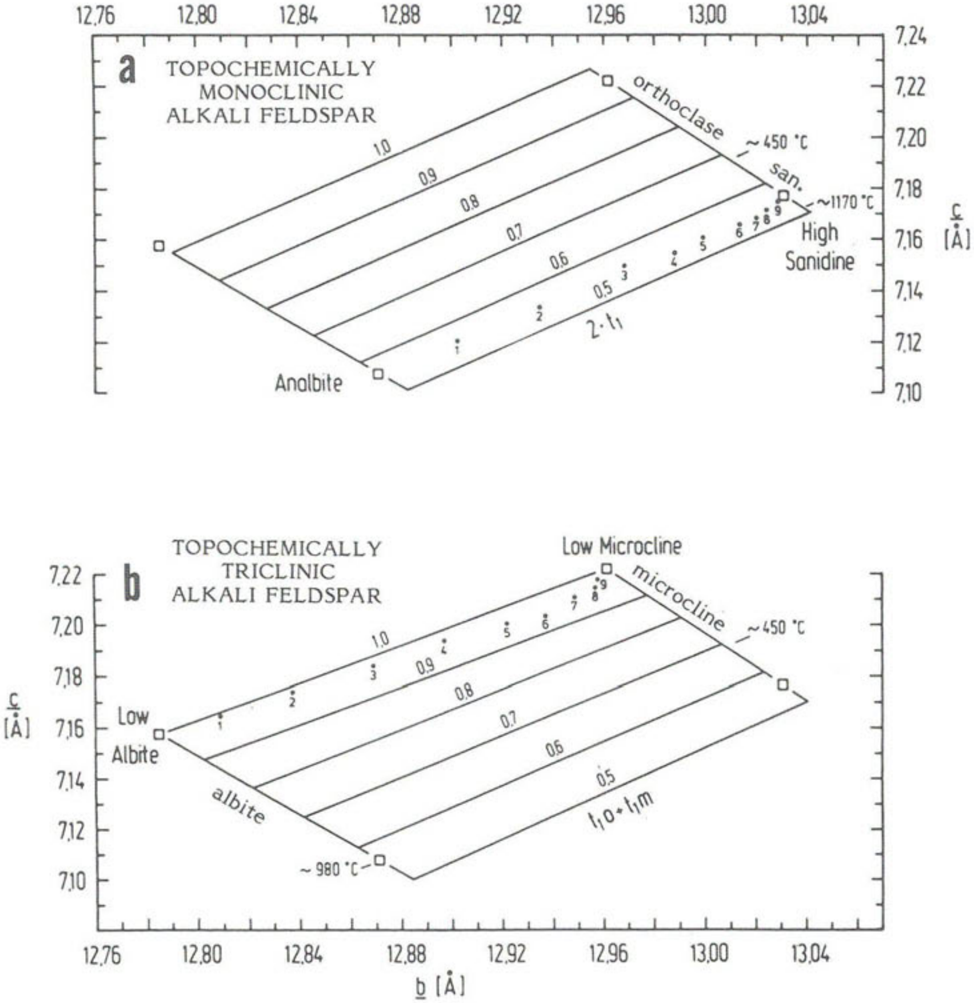

Figure 4. Plots of *b* versus *c* for (a) topochemically monoclinic alkali feldspar and (b) topologically triclinic alkali feldspar. These plots simply represent graphical solutions to Equations 10a and 10b, respectively. The numbered dots represent mol % ($\times 10^{-1}$) Or of the AA-HS and the LA-LM cation exchange series.

If one desires simply to compare relative structural states of members of a suite of alkali feldspars, we suggest plotting them all on one *b*-*c* plot, namely Figure 4b, but if more precise estimates of $2t_1$ (or $(t_1o + t_1m)$) are desired, use Equations 10a (or 10b) or Figure 4a (or 4b).

The primary weakness of this, and all other similar methods for approximating structural state, is the assumption of linearity.[6] To emphasize this, we have plotted data of Kroll and coworkers, with compositions labelled 1 to 9 for Or_{10} to Or_{90}, for the unstrained and nearly linear AA-HS series in Figure 4a and the unstrained but clearly nonlinear LA-LM series in Figure 4b. We did not contour for the *a* cell dimension, for reasons noted later.

THE α^*-γ^* PLOT TO DERIVE $(t_1o - t_1m)$

MacKenzie and Smith (1955) first used plots of the angles α^* versus γ^* as frames of reference to compare and interpret alkali feldspars from a variety of geologic terrains. Figure 5 shows that the α^*-γ^* plot is bounded on one side by LA-LM exchange series, which is not strictly a straight line, as was the case in the *b*-*c* plot. The AA-HS boundary is straight, but all specimens with Or > 34.3 mol % are monoclinic and plot at $\alpha^* = \gamma^* = 90°$. It would be possible to contour this diagram for composition, but the practicality of such a move is questionable since few natural single-phase specimens exist more than a few tenths of a degree from the N-S boundaries, and there are better means of determining composition.

Stewart and Ribbe (1969), using crystal structural data, showed that the α^*-γ^* plot could be used as quantitative measure of the difference in Al-contents of the T_1O and T_1m sites -- symbolically, $(t_1o - t_1m)$. In the ordered LA-LM series, $t_1o = 1.0$, $t_1m = 0$ and $(t_1o - t_1m) = 1.0$. In the AA-HS series and in all topochemically and metrically monoclinic feldspars, $t_1o = t_1m$ and thus $(t_1o - t_1m) = 0.0$. After proportioning the α^*-γ^* quadrilateral by straight lines subparallel to the limiting exchange series and assuming that relative position of points on this plot are directly proportional to the values $(t_1o - t_1m)$, as labelled on the contours, this model was then tested and proven by structure analyses of intermediate microclines (Table 3) and by the fact that alkali exchange series of intermediate structural states always plot on lines which are essentially parallel to the contours. When dealing with highly ordered samples of compositions $Or_{20}Ab_{80}$ to $Or_{70}Ab_{30}$, which are rare if not absent in nature, the curvature of the LA-LM limiting boundary (numbered dots in Fig. 5) should be taken into consideration. Otherwise the linear

---

[6]Blasi (1980) reported that relative position on a b^*-c^* plot contoured for $(t_1o + t_1m)$ in a manner similar to Figure 4 produces data somewhat at variance with $(t_1o + t_1m)$ from a single *b*-*c* plot. We suggest this may be due to the differences in *b* (and thus b^*) for the monoclinic and triclinic populations of K-rich feldspars.

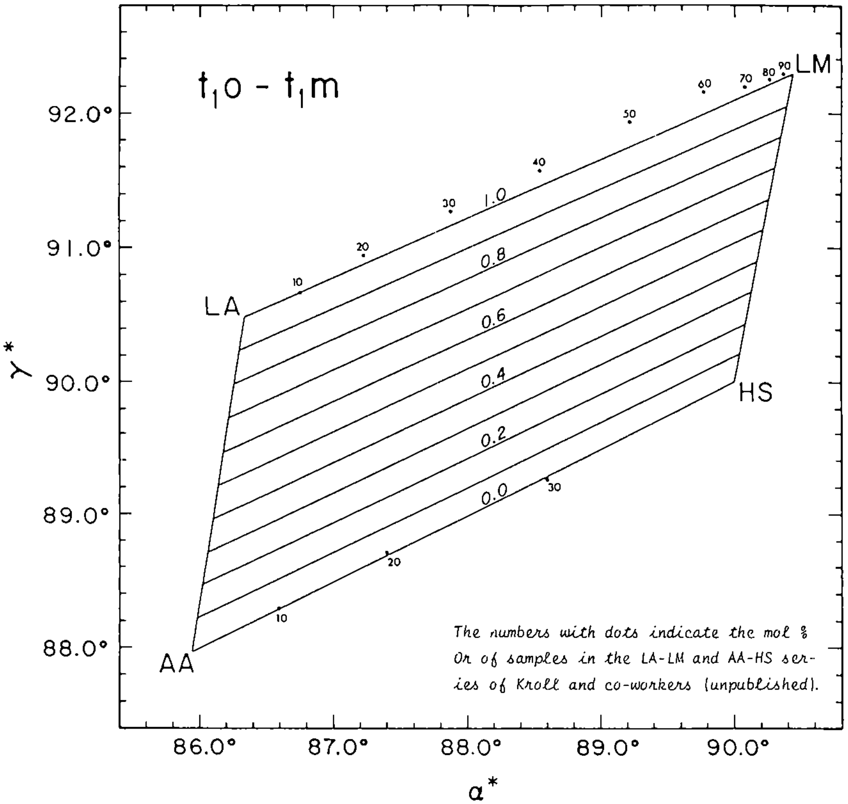

Figure 5. Plot of α^*–γ^* alkali feldspars contoured for $t_1o - t_1m$ with complete order in the low albite–low microcline series. t_1o equals t_1m in analbite and monoclinic feldspars. The estimated error in $t_1o - t_1m$ is 0.05.

model is quite reliable; the estimated error of $(t_1o - t_1m)$ is 0.05 or better. An equation obviates the need for the graph:

$$(t_1o - t_1m) = \frac{\alpha^* + 89.118 - 1.9902\cdot\gamma^*}{-24.691 + 0.2229\cdot\gamma^*} \tag{11}$$

CALCULATION OF Al,Si DISTRIBUTION FROM *b*-*c* AND α^*-γ^*

Stewart and Ribbe (1969)[7] showed that calculation of *T* site occupancies is straightforward: $(t_1o + t_1m)$ and $(t_1o - t_1m)$ can be determined respectively

---

[7]There are typographical errors on p. 455 of Stewart and Ribbe (1969): line 13 should read $\Delta Al = Al_{T_1O} - Al_{T_1m}$, line 34 should read $Al_{T_1O} = \frac{\Delta(bc) + \Delta(\alpha^*\gamma^*)}{2}$, etc. Their $\Delta Al \equiv t_1o - t_1m$, and $Al_{T_1O} = t_1o = \frac{(t_1o + t_1m) + (t_1o - t_1m)}{2}$, etc.

either graphically (Figs. 4a or 4b and 5) or by Equations 10 or 10b and 11. Since $t_2o = t_2m$ and $1 - (t_1o + t_1m) = (t_2o + t_2m)$ for all alkali feldspars, a few simple calculations give the entire Al,Si distribution. Intermediate microcline A1D (#5, Table 3) serves as an example.

According to De Pieri (1979, its lattice parameters are:

$$a = 8.563\ \text{Å};\ b = 12.984\ \text{Å};\ c = 7.201\ \text{Å};\ \alpha = 90.13°;$$

$$\beta = 116.02°;\ \gamma = 89.50°;\ \alpha^* = 90.08°;\ \gamma = 90.48°.$$

The volume is 719.44 Å^3; and the composition is between Or_{90} and Or_{91} (from Eqns. 8a and 8b, respectively). What Al,Si distribution is predicted?

$$\begin{array}{ll} \text{From Equation 10b:} & t_1o + t_1m = 0.81 \\ \text{From Equation 11:} & \underline{t_1o - t_1m = 0.19} \\ & 2t_1o \qquad = 1.00, \text{ thus } t_1o = 0.50 \text{ Al.} \end{array}$$

By substituting into either starting equation, $t_1m = 0.31$ Al. By difference, $1.0 - (t_1o + t_1m) = (t_2o + t_2m)$, and $t_2o = t_2m = (t_2o + t_2m)/2$. Thus for this specimen, $t_2o = t_2m = (1.0 - 0.81)/2 = 0.09_5$ Al. As we have already seen (p. 68), the mean T-O distances give $t_1o = 0.50$, $t_2m = 0.32$, $t_2o = t_2m = 0.09$.

In general, estimates of this sort compared with results of feldspar structure determinations appear to be within 0.02-0.04 Al and are certainly good enough to reveal gross errors in either cell dimensions or structure determination.

STRAINED FELDSPARS

The b-c plot was originally contoured for the a cell dimension by Stewart and Wright (1974) using data from homogeneous feldspars, including data from all the alkali-exchange series available at that time. Although a is highly correlated to Or content, with very little sensitivity to structural state (Fig. 2), a is not a particularly good estimator of composition nor are individual powder diffraction peaks such as $\bar{2}01$ or 400, which are strongly or entirely dependent on a. The reason is that many alkali feldspars are strained.

In most cryptoperthites and some microperthites there is often a degree of structural coherency between adjacent K-rich and Na-rich phases that have exsolved from what was once a single, homogeneous feldspar crystal at some higher temperature. Continuity of the $[AlSi_3O_8]$ tetrahedral framework is preserved as nearly as possible across the interface between the phases as they segregate, but because Na and K are so different in size, considerable strain is experienced in this region. It is manifested in adjustments of bond lengths and bond angles which affect cell dimensions, especially a, up to 5%. Brown and Willaime (1974), Tullis (1975), and Yund and Tullis (1983) give detailed studies; see discussions in Chapters 6 and 7.

But our interest is in characterizing composition and Al,Si distribution from observed cell dimensions; therefore, it is helpful to be able to recognize whether a feldspar is strained or not. Stewart and Wright (1974, p. 362f.) suggested plotting the b and c dimensions and estimating a from their contoured b–c plot. This value is then used to determine $\Delta a \equiv a_{\text{observed}} - a_{\text{estimated}}$. They used $\Delta a = 0.05$ Å as a "threshold value" above which strain is said to be significant. They found that Δa is usually positive for the K-rich and negative for the Na-rich phase of the perthite, and that K-rich phases in dominantly sodic bulk feldspars are usually the most highly strained. Figure 6 illustrates this clearly, but Figure 7, devised by W. Bernotat (Münster), has a further helpful feature.

Bernotat plotted a versus $b \cdot c$ (in Å^2) and found that unstrained alkali feldspars fall in a narrow curved band. Strained K-feldspars fall above the band with Na-feldspars below it. If the two data from a single perthite are connected by a straight line, the slope of that line will be a measure of the degree of coherency. The more nearly vertical the line, the stronger the coherency, the greater the strain and the more nearly alike are the b and c dimensions.[8] A ranking of strain in several pairs is F97 > F99 >> F91. To determine $a_{\text{estimated}}$ from $b \cdot c$, use the following regression equation:

$$a_{\text{est}} = 8.634 - (11.437 - 0.12226\ b \cdot c)^{\frac{1}{2}}\ ;$$

$\Delta a = a_{\text{obs}} - a_{\text{est}}$, as defined by Stewart and Wright.

Stewart (1975) comments, "The effects of certain components sometimes found in alkali feldspars (B, Fe, NH_4^+, and H_3O^+?) may be confused with the effects of coherence, so that if a feldspar is known to be homogeneous and a significant Δa is observed, composition should be carefully checked. The cell volume of a strained feldspar is only a first approximation to the cell volume

----

[8]The plane of intergrowth is close to (100). Thus in the potassic phase b and c will be smaller than "normal," a will be larger, and vice versa in the sodic phase.

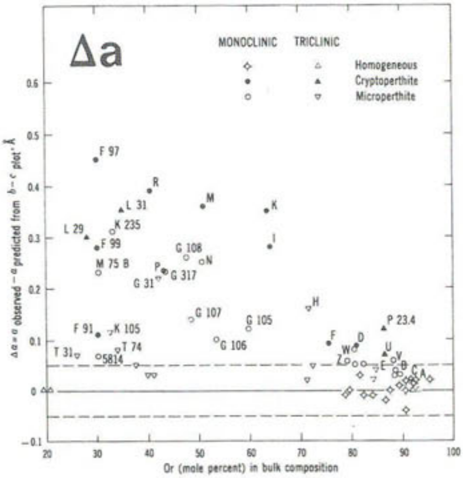

Figure 6. Values of Δa for the potassic phases of chemically analyzed bulk compositions of perthites. See Stewart and Wright (1974, Fig. 9, p. 374) for data sources. Dashed lines at ±0.05 Å are arbitrary limits for "strained" feldspars. Cryptoperthites have greatest strain, the more so if they are monoclinic. Compare with Figure 7.

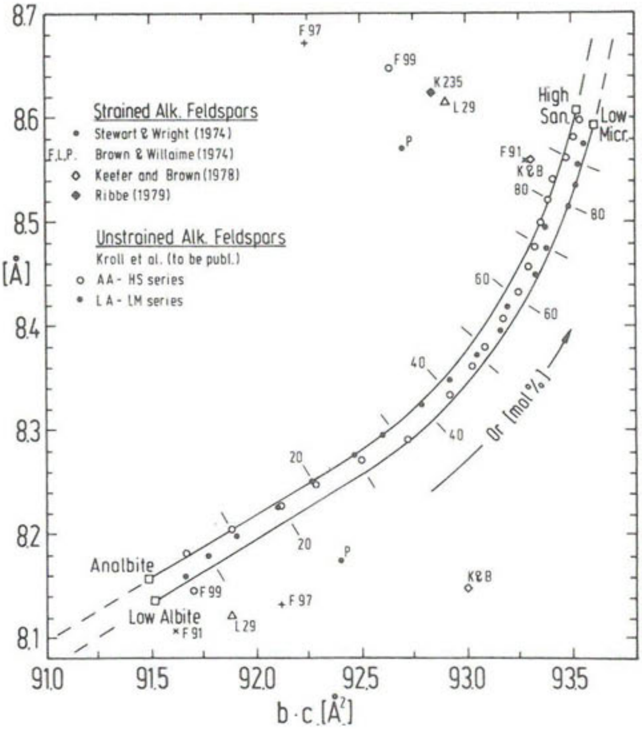

Figure 7. Variation of a with $b \cdot c$ in alkali feldspars. 'Normal' alkali feldspars all plot in a narrow curved band. Samples with strained lattice parameters plot outside this band. The horizontal and vertical distances between such a data point and the band are a measure of strain. The diagram was suggested by W. Bernotat, Münster. See Bernotat (1982).

of a homogeneous feldspar with the same composition and degree of Al,Si order. As the difference in cell volumes between the two perthite phases increases, the failure of the approximation also increases." Although Crosby (1971) found good agreement between composition estimated from the cell volume and that determined by electron probe microanalysis, errors up to 10-15 mol % Or may be encountered. Robin (1974b) and Tullis (1975) have established procedures to correct apparent compositions to "true" composition; Tullis' method is presented in Chapter 6. Keefer and Brown (1978) found that none of these adequately described their strained sanidine-high albite pair, but they failed to question their own assignments of compositions which are based rather tenuously on K,Na site refinements of x-ray intensity data.

Three structural refinements of strained alkali feldspars have been completed: high sanidine (HS) intergrown with high albite (HA) (Keefer and Brown, 1978) and K-235 intermediate microcline (IM) (Ribbe, 1979). All three are plotted in Figure 7. The site occupancies derived from <T-O> bond lengths using Equation 5, from cell parameters using Equations 10 and 11 and from repeat distances along [110] and [1$\bar{1}$0] (Kroll, 1980; see later sections) are listed below.

	HS, Δa= +0.10	HA, Δa= -0.23		IM, Δa= +0.28	
	$t_1o = t_1m$	t_1o	t_1m	t_1o	t_1m
From Eqn. 5	0.30	0.31	0.32	0.50	0.33
From Eqns. 10 and 11	0.32	0.27	0.29	0.51	0.36
From tr[110],tr[1$\bar{1}$0]	0.33	0.25	0.27	0.51	0.34

The agreement among the sets of site occupancies is considered to be reasonably good, especially in view of the peculiar features which the HA phase has with respect to lattice parameters and T-O bond lengths. Thus strain apparently has only a minor effect on our determinative methods for Al and Si among the T sites.

THE [110] METHOD FOR DETERMINING Al,Si DISTRIBUTIONS

The methods described above are basically limited to alkali feldspars; none can be applied to the full composition range of (K,Na,Ca)-feldspars. Kroll (1971, 1973, 1980) has developed methods to exploit an order-sensitive parameter involving the translation distances in the [110] and [1$\bar{1}$0] directions (Fig. 8). These are designated tr[110] and tr[1$\bar{1}$0] and are calculated from a, b and γ as follows:

$$\mathrm{tr}[110] \equiv \tfrac{1}{2}(a^2 + b^2 + 2ab\ \cos\gamma)^{\frac{1}{2}}\ ,\ \mathrm{tr}[1\bar{1}0] \equiv \tfrac{1}{2}(a^2 + b^2 - 2ab\ \cos\gamma)^{\frac{1}{2}}\ .$$

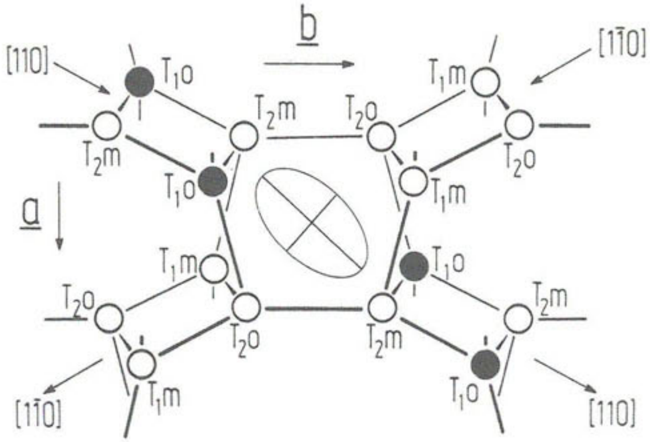

Figure 8. Idealized projection of the feldspar framework along c^* onto (001). Only tetrahedral nodes, no oxygen atoms are shown (after Laves, 1960; *cf.* Fig. 6, Ch. 1). The Al atoms in ordered alkali feldspars are seen to be concentrated in four-fold rings extending along [110]. In the center of the figure a deformation ellipse is drawn, the position of which was calculated from analbite and low albite lattice parameters at room temperature (data from Winter *et al.*, 1979). It indicates those directions along which the triclinic feldspar structure most strongly expands and contracts during the ordering process. These directions nearly coincide with [110] and [1$\bar{1}$0], respectively.

Basis of the [110] method

Changes in temperature, composition, and Al,Si distribution all produce changes in the size and shape of the unit cell, as we have seen. The effects of all of these may be accounted for by calculating the position of strain ellipsoids, thereby specifying directions of greatest expansion or contraction (Ohashi and Finger, 1973). For example, during Al,Si ordering *triclinic* feldspars expand along [110] and contract along [1$\bar{1}$0], and these directions turn out to be subparallel to the major and minor axes of the strain ellipsoid calculated using the lattice parameters of analbite and low albite at room temperature (see Fig. 8). By contrast, in *monoclinic* feldspars one principal axis of the deformation ellipsoid coincides for symmetry reasons with the b axis, and thus [110] and [1$\bar{1}$0] can no longer be the directions of maximum change. In fact, most of the contradiction during ordering is along the b axis direction (see Fig. 2). The contraction in [110] amounts to only ~70% of the contraction in b.

The sequence of tetrahedral sites in the [110] and [1$\bar{1}$0] directions are $T_1\mathrm{O}{\rightarrow}T_2\mathrm{O}{\rightarrow}T_2\mathrm{m}$ and $T_1\mathrm{m}{\rightarrow}T_2\mathrm{O}{\rightarrow}T_2\mathrm{m}$, respectively (Fig. 8). During ordering Al finally concentrates in the T_1O tetrahedral sites. By this process those four-fold tetrahedral rings which extend along [110] "absorb" all Al, whereas the four-fold rings arranged along [1$\bar{1}$0] simultaneously become depleted in Al.

Since Al- and Si-tetrahedra differ in size by ∿0.13 Å, tr[110] and tr[1$\bar{1}$0] change lengths by 0.1-0.2 Å with Al,Si order. Since their standard errors generally do not exceed 0.003 Å, they are capable of sensitively tracing the variations of the Al,Si distribution.[9]

Properties of known feldspar structures permit the introduction of some simplifications that are necessary in quantifying the [110] method.
(1) For all feldspars, $\langle T_2\text{o-O}\rangle$ and $\langle T_2\text{m-O}\rangle$ bond lengths are nearly identical (Tables 1 and 3), allowing us to assume $t_2o = t_2m$. Thus we define

$$\langle t_2o\rangle \equiv (t_2o + t_2m)/2 \ . \tag{12}$$

(2) Although bonding considerations [above] somewhat contradict it (especially for highly disordered specimens, we assume that -- because their sizes are so similar -- the T_1m, T_2O, and T_2m tetrahedra contain the same amount of Al in all Na-rich feldspars and plagioclases. Thus $t_1m \cong t_2o \cong t_2m$, and we define

$$\langle t_1m\rangle \equiv (t_1m + t_2o + t_2m)/3 \ . \tag{13}$$

These averagings reduce the number of parameters in our calculations of Al,Si site occupancies from lattice parameters. Equation 3 may now be written

$$t_1o + t_1m + 2\langle t_2o\rangle = 1 + n_{An} \tag{14}$$

for K-rich $C\bar{1}$ feldspars and

$$t_1o + 3\langle t_1m\rangle = 1 + n_{An} \tag{15}$$

for Na-rich feldspars and plagioclases.

Considering these simplifications and the sites encountered along paths in Figure 8, we may expect tr[110] to be a function of $t_1o + 2\langle t_2o\rangle$ and tr[1$\bar{1}$0] a function of $t_1m + 2\langle t_2o\rangle$. Properly calibrated these parameters, like b-c and α^*,γ^*, will give Al site occupancies for average structures.

Within the plagioclase series, the space group changes with increasing n_{An} from $C\bar{1}$ with $c \sim 7$ Å to $I\bar{1}$ and $P\bar{1}$ with $c \sim 14$ Å (see Chs. 1 and 2), not taking account of the 'e'-plagioclase complexities. It is the regular alternation of Al- and Si-rich tetrahedra that causes c to double, and every Al-rich tetrahedron at $z = 0$ is matched by an Si-rich one at $z = \frac{1}{2}$. Since tr[110] and tr[1$\bar{1}$0] contain no c component, they actually register only the

---

[9]During the ordering process T-O bond lengths vary and O-T-O and T-O-T bond angles are affected. Kroll (1973) investigated their contribution to the total changes of tr[110] and tr[1$\bar{1}$0]. It may suffice here to state that both bond length and bond angle variations are additive in their effects on the two repeat distances.

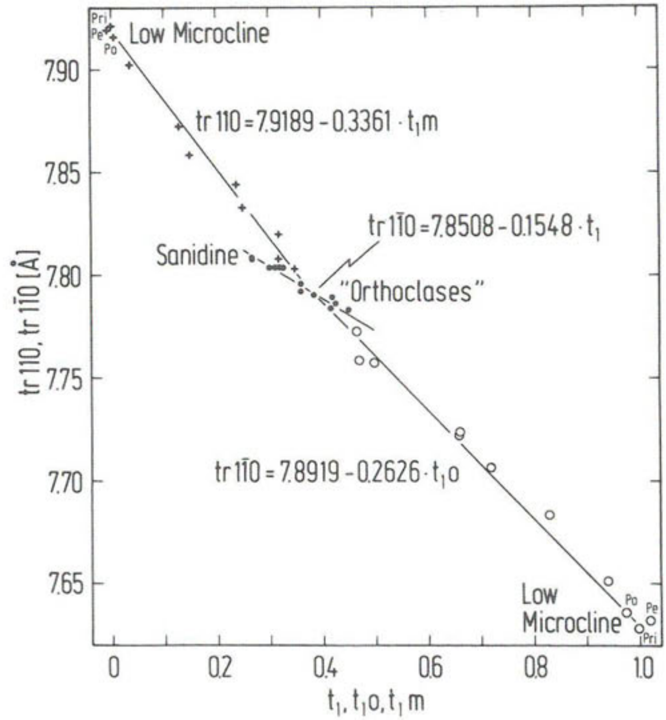

Figure 9. Variation of tr[110] and tr[$1\bar{1}0$] with Al,Si order in monoclinic and triclinic K-feldspars (see Tables 2 and 3). tr[110] and tr[$1\bar{1}0$] were corrected to correspond to Or_{100}: $tr[1\bar{1}0]_{cor} = tr[1\bar{1}0]_{obs} + a_2 \cdot (V_{Or_{100}} - V_{obs})$ and $(tr[110] - tr[1\bar{1}0])_{cor} = (tr[110] - tr[1\bar{1}0])_{obs} + b_2 \cdot (V_{Or_{100}} - V_{obs})$, where $V_{Or_{100}} = 723.22 Å^3$, $a_2 = 0.32747 \cdot 10^{-2}$, $b_2 = 0$ for monoclinic K-rich feldspars and $V_{Or_{100}} = 722.60 Å^3$, $a_2 = 0.36213 \cdot 10^{-2}$, $b_2 = -0.04902 \cdot 10^{-2}$ for triclinic K-rich feldspars (compare Tables 4 and 5).

average site occupancies from subparallel chains separated by $z = \frac{1}{2}$ in the doubled cells. In other words, site occupancies characteristic of a $C\bar{1}$; $c \sim 7$ Å subcell are determined for $I\bar{1}$ and $P\bar{1}$ feldspars. Thus

$$\text{in } I\bar{1},\quad t_1o = (t_1oo + t_1zo)/2, \quad \text{and}$$

$$\text{in } P\bar{1},\quad t_1o = (t_1ooo + t_1ozo + t_1ooi + t_1ozi)/4$$

(see pp. 17-19). The same sorts of averages are applicable for t_1m, t_2o and t_2m. This is the principal limitation of *all* determinative methods for Al,Si distribution dependent on lattice parameters or optical methods. Only *average* t_1 values are accessible.

The [110] method for alkali feldspars

In order to establish a quantitative relation between metrical variation and Al,Si distribution we will rely on two sources of reference data: the analbite-high sanidine and low albite-low microcline solid solution series of Kroll and coworkers (discussed above; see Fig. 2 and Table 4 for cell dimensions of end members) and numerous crystal structure refinements by x-ray and neutron diffraction.

In Figure 9 data for tr[110] and tr[$1\bar{1}0$] of K-rich feldspars are plotted versus their Al occupancies as determined from structure refinements using Equation 5 (all data are in Tables 2 and 3). Since the Ab content varies in these feldspars, tr[110] and tr[$1\bar{1}0$] were corrected to correspond to Or_{100} (see caption of Fig. 9). Least-squares lines were drawn through the data points and by heavy weighting were made to pass through the low microcline reference data. The equations are given on the figure. As expected, tr[110] and tr[$1\bar{1}0$] change as a function of the Al,Si distribution. Within the monoclinic region extending from high sanidine to (theoretical) low sanidine tr[110] = tr[$1\bar{1}0$] decrease, because the sum of Al contents (ΣAl) in the three tetrahedra comprising one repeat distance drops from 0.75 to 0.5 (note parallels to the arguments for variations in *b* and *c*):

	tr[110] =	f(t_1 +	t_2 +	t_2) =	f(ΣAl)
HS	7.812	0.25	0.25	0.25	0.75
LS	7.773	0.50	0	0	0.50

Within the microcline region tr[110] increases because ΣAl increases from ∿0.6 to 1, whereas tr[$1\bar{1}0$] decreases because ΣAl decreases from ∿0.6 to 0:

	tr[110] =	f(t_1o +	t_2o +	t_2m) =	f(ΣAl)
IM	7.792	≈0.4	≈0.1	≈0.1	≈0.6
LM	7.919	1	0	0	1

	tr[$1\bar{1}0$] =	f(t_1m +	t_2o +	t_2m) =	f(ΣAl)
IM	7.792	≈0.4	≈0.1	≈0.1	≈0.6
LM	7.629	0	0	0	0

It is seen from the slopes of the regression lines that the [110] and [$1\bar{1}0$] repeat distances react more sensitively to site occupancy changes in triclinic than in monoclinic K-feldspars.[10] The monoclinic/triclinic change in Figure 9

---

[10] A qualitative explanation is that after inversion from monoclinic to triclinic symmetry, Al migrates from T_1m into $T_1$0 tetrahedra, which then become underbonded relative to T_1m. For compensation the K-0 → $T_1$0 bonds shorten, whereas the K-0 → T_1m distances increase. K-0_C bonds are most strongly affected: K-0_Cm − K-0_C0 = 0.4 Å. Since the shortened K-0_C bonds are parallel [$1\bar{1}0$] and the lengthened K-0_Cm bonds are parallel [110], their combined effects operate in the same direction as do site occupancy changes, and therefore the regression lines have a steeper slope in the triclinic region.

appears as a point on the "monoclinic line", from which two "triclinic lines" diverge. Ideally, at thermal equilibrium this point would represent the Al,Si distribution at the sanidine-microcline inversion. However, when cooled below the temperature of the diffusive transformation sanidine first changes to orthoclase rather than triclinic microcline (see the discussion in Chapter 2, p. 22f.). Thus the point of separation is moved to a value larger than would correspond to the equilibrium inversion, namely $t_1 \cong 0.38$. The point of separation is *not* unique, and it is probable that each pair of microcline data points has its own t_1 starting point. Thus, the "triclinic lines" represent an *average* ordering path.[11]

Diagrams to estimate t_1o and $(t_1o - t_1m)$

As a measure of the Al content in T_1O, tr[1$\bar{1}$0] is the parameter more sensitive to site occupancy changes (Fig. 9). Thus tr[1$\bar{1}$0] is plotted in Figure 10 versus cell volume, and contours for t_1 and t_1o are drawn. The fully ordered LA-LM series forms the lower limit of the diagram. The variation of tr[1$\bar{1}$0] in this series is approximated by two straight lines intersecting at $V = 692$ Å^3, the equations of which are given in Table 5. The upper limit of the diagram is formed by the AA-HS series, which also may be described by two straight lines. The kink at $V = 695$ Å^3 ($Or_{\sim 35}$) is due to the triclinic/monoclinic symmetry change. The T_1O site occupancy of the AA-HS series is taken as 0.28 Al/(Al+Si), as discussed earlier in this chapter.

Figure 10 was contoured by dividing the AA-LA side proportionately between 0.28 and 1.00 Al/(Al+Si); the HS-LM side was calibrated using the equations of Figure 9 for monoclinic and triclinic K-feldspars. Straight lines tr[1$\bar{1}$0] = f(V) were then calculated for the triclinic K-rich feldspars ($V >$ 692 Å^3) with various values t_1o. The equation to start with was that for K-rich low alkali feldspars (Table 5), the slope and intercept of which was changed with t_1o such that the straight line representing $t_1o = 0.38$ was parallel to the Na-sanidine line. Thus, the equation for the contours takes the form:

$$\mathrm{tr}[1\bar{1}0] = b_o + b_1 V \text{ where } b_o = a_1 + a_2(t_1o) \text{ and } b_1 = a_3 + a_4(t_1o)\ .$$

Thus $$\mathrm{tr}[1\bar{1}0] = a_1 + a_2(t_1o) + a_3 V + a_4(t_1o)V\ . \qquad (16)$$

----

[11]Triclinic adularias, grown within the microcline stability field, may deviate from this line. The equilibrium t_1 value of the sanidine → microcline inversion, which cannot be directly observed, can at least be approximated: sanidine from Volkesfeld, Eifel, has $t_1 = 0.315$, according to four structure refinements (Table 2); 'Spencer C' orthoclase has $t_1 = 0.36$. The equilibrium value can thus be assumed to be $t_1 = 0.34 \pm 0.02$.

Table 5. Variation of tr[1$\bar{1}$0] and tr[1$\bar{1}$0] - tr[110] with cell volume V in the limiting series analbite-high sanidine (AA-HS) and low albite-low microcline (LA-LM) (Figs. 10 and 11):

$$tr[1\bar{1}0] = a_1 + a_2V \text{ and } tr[110] - tr[1\bar{1}0] = b_1 + b_2V.$$

Coefficients	a_1	$a_2 \cdot 10^2$	b_1	$b_2 \cdot 10^2$
AA-HS series: V < 692 $Å^3$	5.6103	0.30373	-.8393	0.12128
V > 692 $Å^3$	5.4396	0.32747	0	0
LA-LM series: V < 692 $Å^3$	5.5129	0.28978	-.3813	0.09933
V > 692 $Å^3$	5.0123	0.36213	0.6452	-.04902

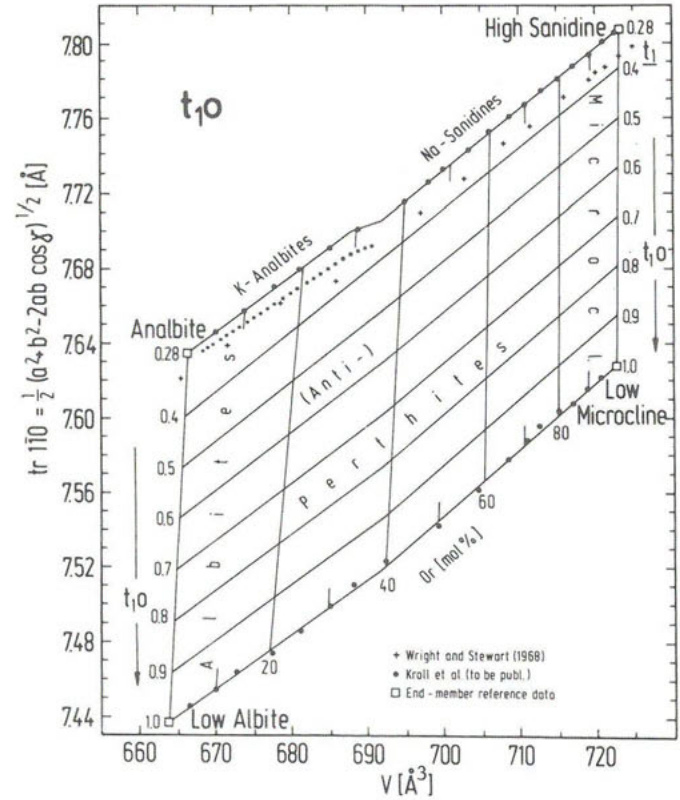

Figure 10. Diagram to determine t_1 and t_1o from tr[1$\bar{1}$0] and cell volume of alkali feldspars. The dotted line separates topochemically monoclinic (K-) analbites from topochemically triclinic (K-) high albites. Equations for the contours are given in Table 6.

The contours were then produced from $V = 692$ Å^3 to the AA-LA side. It turned out that all contours have a kink point at $V = 692$ Å^3, but the contour at $t_1o \doteq 0.4$ is a single straight line. In addition, lines drawn perpendicular to this contour bisect the angles between the left and right parts of the other contours.

In this case, it is not necessary to have separate equations 16 for Na- and K-rich alkali feldspars. By expanding the a_4-term, a single equation suffices:

$$tr[1\bar{1}0] = a_1 + a_2(t_1o) + a_3V + a_4|c_1-V|[c_2-(t_1o)] \ , \tag{17}$$

where $c_1 = 692$ Å^3 and $c_2 = 0.4$. When $V = c_1$ and/or $t_1o = c_2$, the equation reduces to that of a plane, the t_1o contours of which would be parallel lines. If now a term like $a_4|c_1-V|$ is added, a kink in the contours is produced at $V = c_1$. Addition of $[c_2-(t_1o)]$ transforms the parallel contours to the left and right of c_1 into two fans of contours. The coefficients of Equation 17 are given in Table 6. In the topochemically monoclinic region no indication was found for the contours to change slope as a function of t_1. Thus, the equation of a plane

$$t_1 = a_1 + a_2(tr[1\bar{1}0]) + a_3V \tag{18}$$

is assumed to adequately represent the contours. Two such equations would be necessary for K- and Na-rich alkali feldspars. However, when the K-analbite line is produced to the K-feldspar side it happens that the high sanidine data point plots on that line. Then once again we can use a single equation when we account for the different slopes of the K-analbite and Na-sanidine lines. This can be done by adding a correction term to the a_2-term, $a_2(tr[1\bar{1}0] + c\Delta V)$, where $\Delta V \equiv 723.22 - V$. (The cell volume of high sanidine is 723.22 Å^3.) Above $\sim$690.5 Å^3 the correction would be zero, and thus ΔV is set equal to zero when $690.5 < V < 723.22$. The coefficients of Equation 18 are also listed in Table 6.

The change from monoclinic to triclinic topochemistry in K-rich feldspars is documented by a change of symmetry, whereas at room temperature Na-rich feldspars are always triclinic, regardless of their topochemistry. The regions of monoclinic and triclinic topochemistry are separated in Figure 10 by a dotted line, the position of which was estimated from Wright and Stewart's (1968) "orthoclase" K-exchange series and from synthetic Na-rich alkali feldspars of Kroll *et al.* (1980). Wright and Stewart's data plot below that line, because K-analbites invert to high albites at smaller t_1 values than the K-exchange series has inherited from its orthoclase end member.

Table 6. Equations and coefficients to calculate from tr[110],[1$\bar{1}$0] (Å) and cell volume V (Å^3) the Al site occupancies t_1, t_1o and ($t_1o - t_1m$).

(i) $t_1 = a_1 + a_2(\mathrm{tr}[1\bar{1}0] - 0.00022\cdot\Delta V) + a_3 V$

(ii) $t_1o = \dfrac{\mathrm{tr}[1\bar{1}0] - a_1 - a_2 V - 0.4a_4|V-692|}{a_3 - a_4|V-692|}$

(iii) $t_1o - t_1m = \dfrac{(\mathrm{tr}[110] - \mathrm{tr}[1\bar{1}0]) - a_1 - a_2 V}{a_3 - a_4 V}$

$2(t_1 + t_2) = 1 + n_{An}$ and $t_1o + t_1m + 2\langle t_2o\rangle = 1 + n_{An}$,

where n_{An} = mole fraction An ($0 \le n_{An} \le 1$)

COEFFICIENTS (alkali feldspars)

	a_1	a_2	a_3	a_4
(i)	35.758	-6.5241	0.02138	0
(ii)	5.545	0.003255	-0.2793	$-0.0604\cdot10^{-2}$
(iii)	-0.839	0.001213	0.4579	$0.0220\cdot10^{-2}$, if V < 692 Å^3
	0	0	0.6452	$0.0490\cdot10^{-2}$, if V > 692 Å^3

(i) $\Delta V = 0$, if V > 690.5 Å^3; $\Delta V = (723.22 - V)$, if V < 690.5 Å^3.

Equation (i) applies to topochemically monoclinic alkali feldspars. If these are metrically triclinic (K-) analbites, we have $t_1 = t_1o = t_1m$ and $t_2 = t_2o = t_2m$. Equations (ii) and (iii) apply to topochemically triclinic alkali feldspars.

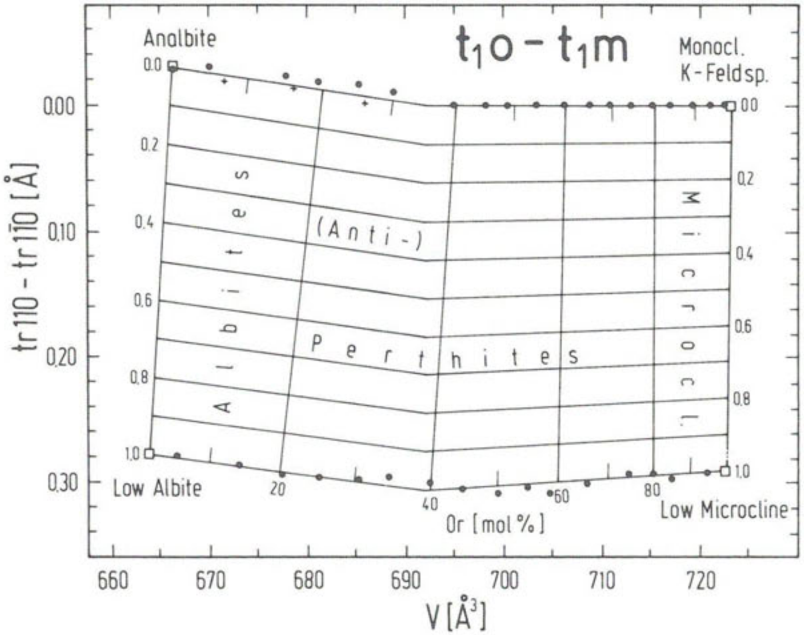

Figure 11. Diagram to determine $t_1o - t_1m$ from tr[110] - tr[1$\bar{1}$0] and cell volume of alkali feldspars. Equations for the contours are given in Table 6.

To fully describe the Al,Si distribution of triclinic alkali feldspars it is necessary to refer to a second diagram (Fig. 11). Since tr[110] estimates $t_1o + t_2o + t_2m$ and tr[1$\bar{1}$0] estimates $t_1m + t_2o + t_2m$, the difference tr[110] - tr[1$\bar{1}$0] is a measure of $t_1o - t_1m$ just as $\alpha^*-\gamma^*$ is. Therefore Figure 11 has been subdivided proportionately by contour lines for $t_1o - t_1m$. As in the diagram for t_1o, the lower limit of the data is formed by the LA-LM series, where $t_1o - t_1m = 1$. The upper limit is formed by topochemically monoclinic alkali feldspars with $t_1o - t_1m = 0$. The K-rich members of this group all have tr[110] - tr[1$\bar{1}$0] = 0, whereas the Na-rich ones are triclinic with values tr[110] - tr[1$\bar{1}$0] > 0. Only samples prepared by K-exchange and thus known to be topochemically monoclinic may plot slightly below that contour, as do the Na-rich members of Wright and Stewart's (1968) exchange series. The contours on the Na- and K-rich sides of the diagram can be described by two equations of the type of Equation (16). The coefficients are given in Table 6: they have been derived from end-member data (Table 4) and from the equations given in Table 5 and Figure 9.

ESTIMATION OF ERRORS

Various sources of random and systematic errors affect the estimation of site occupancies from determinative diagrams and equations. Random errors result from erroneous lattice parameters. Their effect can be estimated from the error progation law, which for a function $F(x_i)$ takes the form

$$\text{var } F(x_i) = \sum_{i=1}^{n} (\delta F/\delta x_i)^2 \cdot \text{var } x_i \ , \tag{19}$$

if covariance terms are neglected. By way of example, in the case of the [110] method, $F(x_i) = t_i(\text{tr}[1\bar{1}0], V)$. Because tr[1$\bar{1}$0] itself depends on a, b and γ, propagation of error has to be calculated. If we assume $\sigma(a) = \sigma(b) = 0.002$ Å and $\sigma(\gamma) = 0.02°$, then it turns out that $\sigma(\text{tr}[110]) \approx \sigma(\text{tr}[1\bar{1}0]) \approx 0.002$ Å, i.e., the error in the [110],[1$\bar{1}$0] repeat distances is virtually the same as in cell edges. The error in t_1, t_1o and $(t_1o - t_1m)$ can then be calculated from Equations (i) to (iii) in Table 6. For $\sigma(\text{tr}[110]) = \sigma(\text{tr}[1\bar{1}0]) = 0.002$ Å and $\sigma(V) = 0.3$ Å^3 we find $\sigma(t_1) = 0.015$, $\sigma(t_1o) = 0.01$ and $\sigma(t_1o - t_1m) = 0.005$. This means that errors due to lattice parameter refinement are relatively insignificant.

However, systematic errors are probably much more important and certainly more difficult to evaluate. The primary ones are:

(1) incorrect determination of T-O distances, lattice parameters and chemical composition of the structurally analyzed feldspars and solid solution series used to construct the determinative diagrams,

(2) incorrect transformation of <T-O> distances into site occupancies due to incorrect assumptions (e.g., that LA, LM and $P\bar{1}$ anorthite are fully ordered and HA, AA and/or HS are fully disordered) and to unknown or unaccounted bonding effects, and

(3) deviation from assumed linear or other relationships among site occupancies, volume, repeat distances (*b*, *c*, tr[110], tr[$1\bar{1}0$]) and angles (α^*,γ^*).

If values of t calculated from tr[110] and tr[$1\bar{1}0$] are compared with observed ones (Tables 2 and 3), we obtain the following standard deviations: $\sigma(t_1)$ = 0.015, $\sigma(t_1o)$ = 0.02 and $\sigma(t_1m)$ = 0.015; these are encouraging, but should not be taken as indicators of accuracy.

OTHER DETERMINATIVE METHODS

Optical methods for determining structural states of K-rich and Na-rich alkali feldspars have become fairly well defined recently, but for the intermediate compositions (Or_{10} to Or_{75}) there are only scattered and poorly understood data. These are discussed by Stewart and Ribbe in Chapter 5. Other determinative methods based on various parameters of the unit cell have been proposed, and they are summarized with minimum comment below.

In addition to the *b*-*c* and tr[110],[$1\bar{1}0$] methods discussed earlier, one may contour b^*-c^* (Luth, 1974; Smith, 1968; 1974a, Fig. 7-18a) and combinations of *b*, *c*, b^* and c^* for ($t_1o + t_1m$). Blasi (1980) commented on the relative utility of *b*-*c* and b^*-c^*, but see footnote 6 above. Wright (1968) used 2θ values of the 060 and $\bar{2}04$ peaks to delineate relative structural state: this approach merits further study. Ferguson (1980, 1981) proposed new determinative curves for K-rich feldspars (>Or_{85}), but these are highly model-dependent, and we agree with Blasi (1982) that they produce systematically "erroneous" results. In addition to α^*-γ^* and tr[110],[$1\bar{1}0$], procedures for deriving ($t_1o - t_1m$) are numerous and include:

(1) α-γ (Blasi, 1978), α^*-γ (Thompson and Hovis, 1978), and various trigonometric functions thereof.

(2) Other measures of "obliquity" or "triclinicity," such as ϕ, σ, σ^* (Thompson and Hovis, 1978), and $\Delta 2\theta(131) \equiv 2\theta(131) - 2\theta(1\bar{3}1)$, or $[d(1\bar{3}1) - d(131)]$ (Goldsmith and Laves, 1954; McConnell and McKie, 1960, etc.). Jiránek's (1982) use of the height/width ratio of the 131 peak as a "method of assessing the structural state of monoclinic K-feldspars" may give insight to the range of fairly disordered *triclinic* or mixtures of triclinic *and* monoclinic feldspars

Table 7. Listing by rock type, authors and locality of geological studies that have involved determining structural states of alkali feldspars by methods described in Chapter 3. For studies prior to 1973, see Smith (1974a,b) and Stewart and Wright (1974). Note: References added in proof are marked * and listed in the footnote.

ANATEXITES	Blasi & DePol Blasi (1980) Mt. Pélago, Maritime Alps, France Blasi et al. (1981) Mt. Caval, Maritime Alps, France Blasi et al. (1982) Haut Boréon, Italy
DOLERITE	Patchett et al. (1979) Sweden, various localities
GNEISSES	Bambauer & Bernotat (1976*, 1982) Aar and Gotthard Bernotat & Bambauer (1980, 1982) Massifs, Switzerland Bernotat & Morteani (1982) Tauern Window, Austria Collerson (1976) Musgrave Ranges, Amata, central Australia Grew (1979) Kilbourne Hole, New Mexico, USA Hiss (1979)* Central Alps, Switzerland Raase & Morteani (1976) Western Hohe Tauern, eastern Alps
GRANITES & GRANITOIDS (some overlap with gneisses)	Blasi et al. (1980) Gilgit area, northwestern Pakistan Bychkov et al. (1977)* Raumd Massif, Rushanski Range, Pamir Cherry & Trembath (1978, 1979a) St. George Pluton, N.B., Canada Godinho & Jaleco (1975) Castro-Daire, Portugal Hafner & Loida (1980)* Central Alps, Switzerland Iball & Hubbard (1982) Varberg, Sweden Jiránek (1982) Karlovy Vary, Czechoslovakia Martin (1977) Andrew's Point, Cape Ann, Massachusetts, USA
GRANODIORITE	Eggleton (1979) Kameruka Pluton, Bega Batholith, SE Australia
GRANULITE	Hörmann et al. (1980)* Iralojoki - Inarijaervi, Finland
PEGMATITE	Shmakin (1979) USA, various localities
QUARTZITE	Kroll (1980) Scotland Siematkowska & Martin (1975) Sudbury region, Ontario, Canada
Miscellaneous	Bonin & Martin (1974) Cauro-Bastelica ring complex, Corsica DalNegro et al. (1978) Pegmatite, vaplite and tonolite DePieri (1979) dikes of the Adamello Massif, N. Italy

Bambauer, H.-U. and W.H. Bernotat (1976) Fortschr. Mineral. 54, 6.
Bychkov, A.M., V.N. Volkov & R.D. Gavrilin (1977) Geokhim. 3, 394.
Grew, E.S. (1979) Am. Mineral. 64, 912.
Hafner, St. & A. Loida (1980) Eclogae Geol. Helv. 73, 563.
Hiss, B. (1979) Schweiz. Mineral. Petrogr. Mitt. 58, 243.
Hörmann, P.K., M. Raith, P. Raase, D. Ackermand & F. Seifert (1980) Geol. Surv. Finland Bull. 308, 95 p.

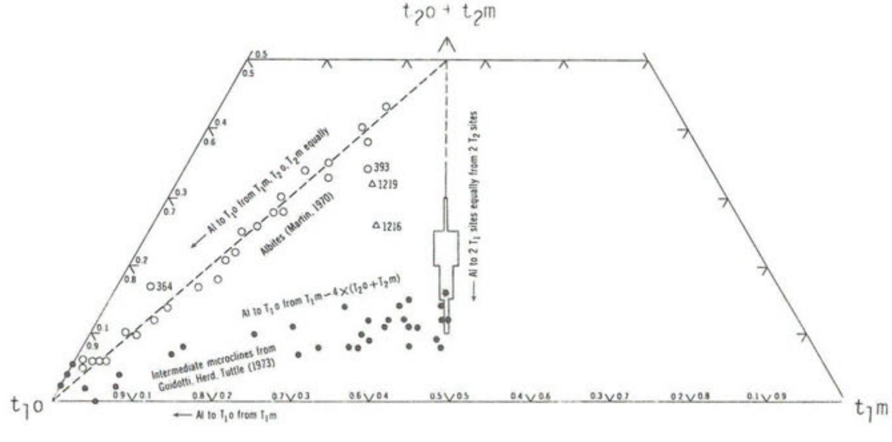

Figure 12. Triangular plot of Al content in tetrahedral sites (calculated from b-c and $\alpha^*-\gamma^*$) in alkali feldspars with ΣAl = 1.0. Data for albites from Martin (1970, Table 1) are shown by circles, most of which fall on the *one-step* ordering path, and triangles, which do not. Na-feldspar samples 393, 1219 and 1216 (formed at 200-250°C) apparently have Al-enriched T_1m sites. It is possible these samples partially ordered metastably with monoclinic symmetry before becoming triclinic (see Ch. 2, Fig. 8).

Intermediate microclines (solid dots) studied by Guidotti, Herd, and Tuttle (1973) order along a path where Al moves to T_1O from T_1m approximately 4 times faster than from T_2O and T_2m combined. The shaded area with $t_1o = t_1m$ diagrammatically represents the relative abundance of the monoclinic feldspars from the same region. Monoclinic feldspars from this area ordered further with monoclinic symmetry on cooling before becoming triclinic. From Stewart and Wright (1974, Fig. 7, p. 371).

present in a powder sample, but does not accomplish his stated objective.

(3) (tr[011] - tr[0$\bar{1}$1]) versus (tr[110] - tr[1$\bar{1}$0]) or Δ011 *vs* Δ110 (Blasi and Blasi De Pol, 1977).

Each of these has its merits and some are of restricted value, but all are based on interrelated metrical parameters of the unit cell and, if properly calibrated, should produce similar values of ($t_1o - t_1m$).

Jowhar's (1981) procedure for "calculating lattice parameters and distribution of aluminium in tetrahedral sites of alkali feldspars" is unworkable and should be ignored (Blasi, 1983).

PETROLOGIC APPLICATIONS

The relative ease of application of the *b-c*,α*-γ* and the tr[110],[1$\bar{1}$0] methods and the many occurrences of alkali feldspars have led to an ever-increasing number of petrologic studies whose interpretations are based on the structural states of these feldspars. Smith (1974a, p. 255f.) and Stewart and Wright (1974, p. 368f.) summarized earlier studies, and we have compiled references to a number of them published since 1974 (Table 7). It is beyond the scope of this volume to discuss the details, but we present several examples as guides to future work, with suggestions as to the best way to display data from suites of alkali feldspars.

Ordering paths

The suite described by Guidotti *et al.* (1973) from a K-feldspar-sillimanite grade metamorphic terrane was interpreted by Stewart and Wright (1974), who displayed the Al,Si distribution of individual specimens on the triangular diagram in Figure 12. The apices of the triangle are t_1o, t_1m and ($t_2o + t_2m$) or $2t_2$. All monoclinic specimens and the triclinic ones with $t_1o = t_1m$ plot on the central vertical line. Fully disordered specimens plot at $t_1o = t_1m = 0.25$, $t_2o + t_2m = 0.5$; hypothetical "ordered orthoclase" plots at $t_1o = t_1m = 0.5$, $t_2o = t_2m = 0$.

There are two extreme types of paths of Al,Si migration between fully ordered ($t_1o = 1.0$) and fully disordered Al,Si distributions.

(1) *One-step path.* If Al moves to or from the *T*1O site equally from or to *T*1m, *T*2O, *T*2m, the feldspar is said to be ordering or disordering along a one-step trend. Most of Martin's (1970) synthetic Na-feldspars plot on that trend (Fig. 12), as do the annealed specimens of MacKenzie (1957) and Müller (1969, 1970). [See Chapter 2 for a discussion of ordering of natural Na-feldspar.] Müller (1970) and Blasi *et al.* (1983) have documented an almost straight, one-step disordering of K-feldspar from low microcline ($t_1o = 1.0$) to monoclinic sanidine. In Müller's sanidine, $t_1o = t_1m = 0.285$ after 8

days dry heating at 1100°C. After one more day of heating ($t_1o - t_1m$) remained at 0.0, but ($t_1o + t_1m$) decreased by 0.01.

(2) *Ideal two-step path.* Starting from high sanidine at high temperatures *all* the Al could order into T_1 equally from T_2, producing what Laves (1960) called "(theoretical) low sanidine", but which Martin (1974a) called "ordered orthoclase" (see footnote 3, p. 10). From that point ordering would proceed by migration of Al from T_1m into T_1O.

A third type of ordering path appears most likely in nature, as discussed earlier for K-rich and Na-rich feldspars (Ch. 2, see especially Figs. 1 and 8).

(3) *Intermediate two-step trend.* If the relatively disordered phase stable at highest temperatures is topochemically monoclinic, i.e., $t_1o = t_1m$ and $t_2o = t_2m$, ordering normally appears to progress along the first limb of the two-step path, branching off toward the $t_1o = 1.0$ apex of the triangle when ($t_1o + t_1m$) $\geqslant 0.75$, $2t \leqslant 0.25$, but not necessarily with strict structural continuity. In other words, there may be a first-order phase transition at lower temperature. The reverse process attained by dry-heating natural specimens is complex: see Müller (1970), Cherry and Trembath (1979a,b) and Blasi *et al.* (1983).

The feldspar suite of Guidotti *et al.* (1973) is a case in point (Fig. 12). It was deduced that the highest temperature of formation of K-rich feldspar was 655±20°C, and Stewart and Wright (1974) suggested that all of the monoclinic specimens with $2t_1 > 0.8$ and all the triclinic ones "ordered during cooling after the thermal maximum, different degrees of order and inversion reflecting kinetic factors such as deformation, presence of alkali-rich solutions, etc. The triclinic samples plot as a band of points extending from monoclinic samples with $2t_2 < 0.15$ toward maximum microcline. This suggests that a single ordering event occurred within the band: Al migrated to T_1O from T_1m at approximately four times the combined rate from T_2O and T_2m. However, the band does not originate at the place where most monoclinic feldspars occur. An additional amount of ordering of approximately $2t_1 \sim 0.07$ took place with monoclinic symmetry before the inversion to triclinic symmetry occurred, but little, if any change in $t_1o + t_1m$ (<0.05) accompanied the symmetry change. Details of the peak splitting suggest that ordering may have become discontinuous after an initial continuous stage. Very few of the triclinic samples are maximum microclines, so that even the cooling of hundreds of cubic miles of metamorphic rocks (10^7 years?) was too rapid for equilibrium Al/Si distributions to be attained.

"Stewart and Wright (1974) summarized data for the ordering and disordering of alkali feldspar suites formed by heating or cooling of igneous and metamorphic rocks and concluded these data are best interpreted by

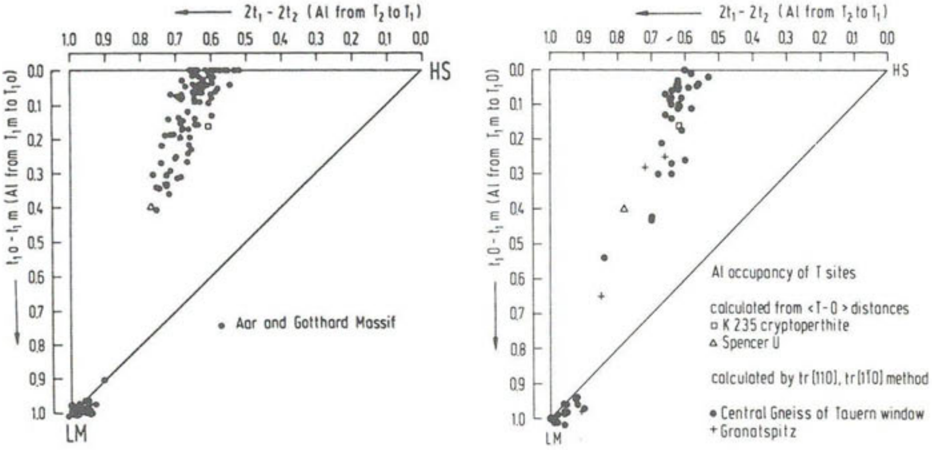

Figure 13. (a) Plot of the Al,Si distributions in K-feldspars of perthites from the Aar and Gotthard Massifs (Bambauer and Bernotat, 1982, Fig. 10). (b) Plot of data from gneisses of the Tauern Window, Eastern Alps (Bernotat and Morteani, 1982, Fig. 5). Al,Si values were calculated by the tr[110],[1$\bar{1}$0] method.

hypothesizing a discontinuous transformation between orthoclase and microcline. They could not suggest what the stability field for intermediate microcline might be, if indeed there is one" (Stewart, 1975, p. St-21f.).

Certain other suites of alkali feldspars also suggest a sort of "discontinuity" for this particular monoclinic → triclinic inversion (e.g., Eggleton, 1979, interpreted by Eggleton and Buseck, 1980), and discontinuities between fairly disordered intermediate microclines and fully-ordered low microclines are often observed (Iball and Hubbard, 1982; Bambauer and Bernotat, 1982; Bernotat and Morteani, 1982). See Figure 13. It seems likely that intermediate microclines are metastable stages between monoclinic K-feldspars with $2t_1 \approx 0.8$ and low microcline. However, Kroll (1980) reported a continuous series of microclines from rocks that reached maximum metamorphic temperatures well above the microcline-sanidine transformation temperature (450°C-500°C) and then very slowly cooled through the temperature stage between 500°C and 300°C, where triclinic ordering proceeded (Kroll and Voll, in prep.).

Suggested convention for plotting Al,Si distribution data

As is often the case after years of experience, a recommendation for a conventional method of plotting data runs counter to any methods used to date. After considering the triangular plot of Stewart and Wright (1974, see Fig.

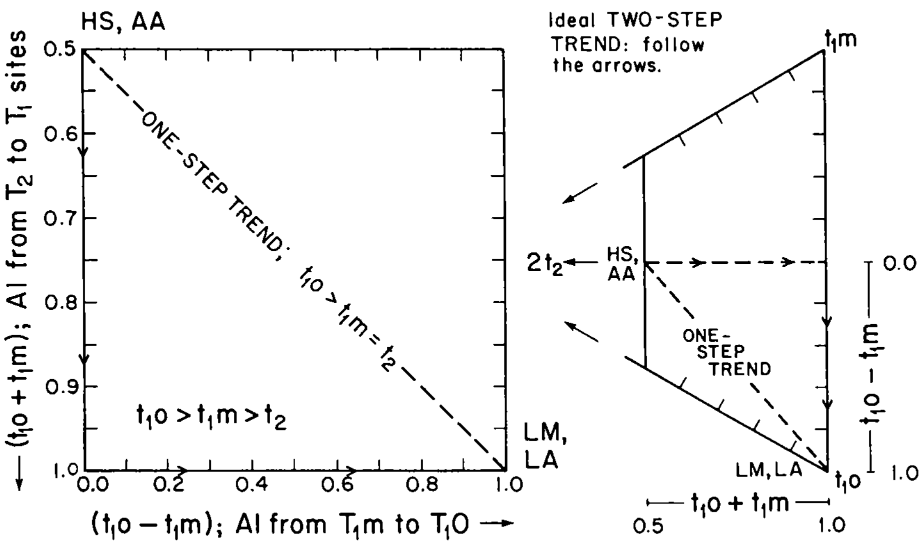

Figure 14. To the right is shown the triangular plot of Stewart and Wright (1974; *cf.* Fig. 12) tilted to simulate the topology of the graph to the left which is modified in orientation from Smith's (1974a) Figure 7-19 and those in Figure 13. It is suggested that the format on the left be adopted as the conventional representation of Al,Si distributions in suites of alkali feldspars; $t_2o = t_2m$ is assumed. Compare this to Blasi and Blasi De Pol (1977, Fig. 4) and see the text.

12), and the different orthogonal plots of Bernotat and coworkers (see Fig. 13) and Smith (1974a, Fig. 7-19), we suggest a modification of Smith's method. It is shown in Figure 14 with a triangular plot to illustrate their relationship. This method has the advantage of recording exactly what one may calculate from lattice parameters or from optical data (see Ch. 5), namely (t_1o + t_1m) and (t_1o - t_1m). The first-formed, higher-temperature phases plot in the upper left, the last-formed, lowest-temperature phases plot in the lower right.

Chapter 4

LATTICE PARAMETERS and DETERMINATIVE METHODS for PLAGIOCLASE and TERNARY FELDSPARS

H. Kroll

INTRODUCTION

When a homogeneous alkali feldspar is cooled from elevated temperatures, the unmixing of Na and K and the ordering of Al and Si may develop independently of each other, in the sense that local electrostatic neutrality does not require these processes to be coupled. In plagioclases, by contrast, the *A* and *T* cations do not migrate independently of each other: there must be a linkage between Na-Si and Ca-Al to preserve charge balance. Since Al and Si diffuse very sluggishly within the tetrahedral framework, metastable microstructures develop as exsolution and ordering proceed. These microstructures are usually of such a fine scale that X-ray powder methods cannot resolve the various "phases". As a consequence, the lattice parameters represent averages over regions or domains within the bulk crystal that may have distinctly different structures and chemical compositions. Furthermore, as pointed out in Chapter 3, it is not possible to determine from lattice parameters the true Al,Si distribution in a calcic plagioclase with a c = 14 Å cell and space group $I\bar{1}$ (or $P\bar{1}$). This is possible only when the unit cell has c = 7 Å and space group $C\bar{1}$, i.e., when there are only four rather than 8 (or 16) non-equivalent tetrahedral sites. Therefore, we will speak only of the 7 Å *average structures* in relation to cell parameters and Al,Si distributions. Although parameters which represent average structures provide only limited information, we shall see that it is possible to use simple X-ray powder techniques to obtain a measure of the relative degree of average Al,Si order. Specifically, we will discuss the lattice parameter variation of plagioclases and ternary feldspars with respect to composition, structural state and temperature. And we will adapt the [110] method, previously used for deriving Al site-occupancies in alkali feldspars (Chapter 3), for use with plagioclases.

Unlike the alkali feldspars, there exists no established method to obtain both composition *and* Al,Si distribution of a plagioclase from any combination of lattice parameters because the two are structurally interrelated, and Na and Ca are similar in size. Ideally, compositions should be determined by electron microprobe. Otherwise, the An-content may be determined from Viswanathan's (1971) K-exchange method, or from the refractive indices α or α', because these are essentially independent of structural state and Or-content

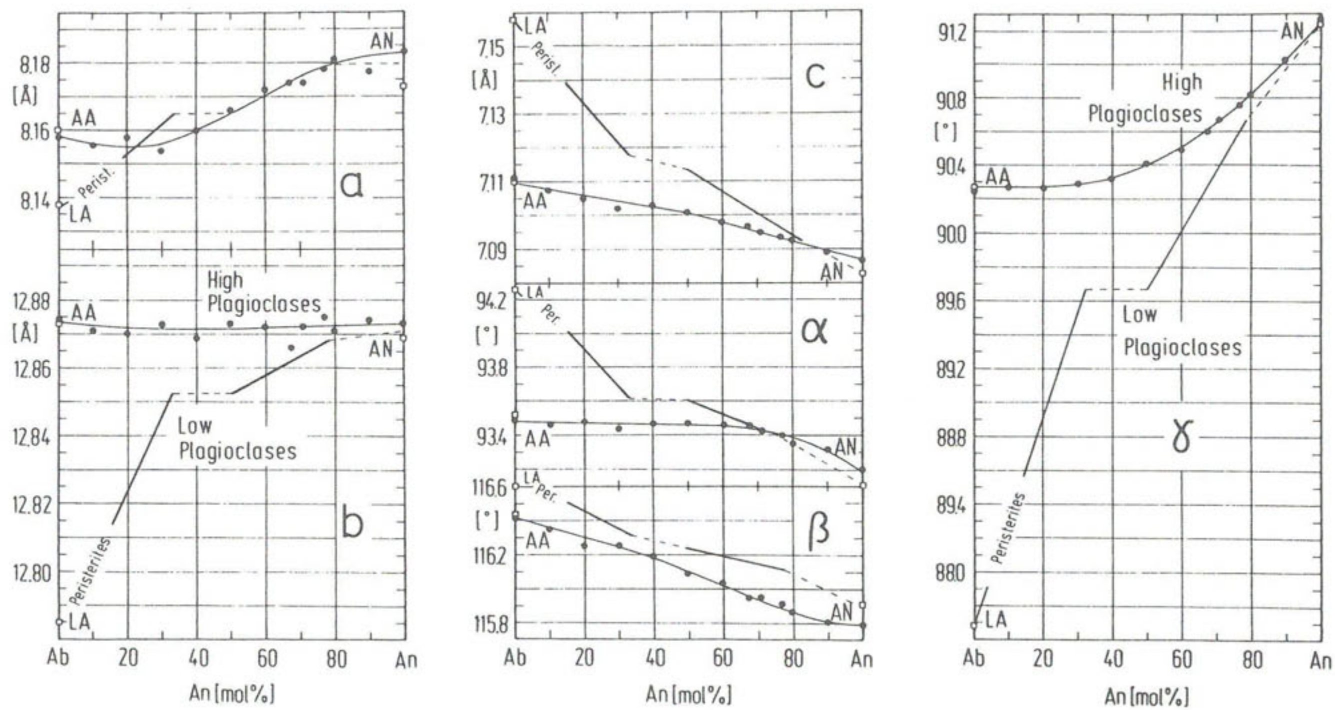

Figure 1. Lattice parameters of high and low plagioclases. Curves for the low series are drawn from the original data of Bambauer *et al.* (1967). Curves for the high series are based on synthetic samples prepared by dry devitrification of glasses at temperatures between 30°C and 120°C below solidus temperature. AA = analbite, LA = low albite, AN = anorthite. From Kroll and Müller (1980).

(Chapter 5). The significant effect that Or-content has on certain lattice parameters can be accounted for from a combination of the repeat distances tr[110] and tr[1$\bar{1}$0], as shown later on.

LATTICE PARAMETER VARIATION

<u>High plagioclases</u>

Lattice parameters of high plagioclases are plotted in Figure 1. The samples were prepared at 30°C below solidus temperatures and have conventionally been assumed to represent the highest state of disorder attainable in plagioclases. However, members of the series are neither fully disordered nor are they homogeneous with respect to degree of disorder. Plagioclases between An_0 and $An_{\sim15}$ are topochemically monoclinic (Na,Ca)-analbites, that is, their *Al,Si distributions* are balanced equally between $T_1$0 and T_1m and between $T_2$0 and T_2m, consistent with $C2/m$ symmetry (although they are metrically triclinic); see Figure 2. Those between $An_{\sim15}$ and An_{60-70} adopt the high albite-type structure, i.e., their topochemistry is triclinic; and those above $\sim An_{70}$ are body-centered ($I\bar{1}$), characteristic of anorthite with its regular Al,Si alternation. It is seen from Figure 9b, Chapter 2, that only the end members analbite and anorthite -- when averaged onto a $C\bar{1}$-7 Å cell -- are disordered. High plagioclases of intermediate composition are not completely disordered. This is in contrast to previous assumptions made in the literature which were discovered to be in error by Kroll (1978; see also Kroll and Ribbe, 1980).

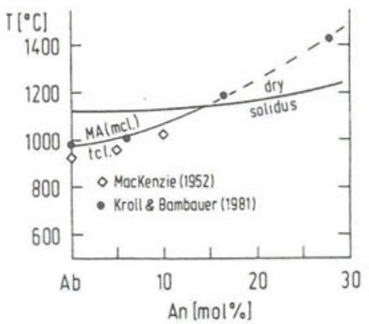

Figure 2. Variation of the temperatures T_{displ} and T_{diff} of the displacive and diffusive transformations in sodic plagioclases. There is strong evidence that T_{displ} and T_{diff} coincide in the plagioclase series. Thus, for rapid cooling, the monoclinic/triclinic transition curve corresponds to the displacive transformation, whereas for slow (equilibrium) cooling it corresponds to the diffusive transformation. MA = monalbite. After Kroll and Bambauer (1981). (1981).

The nature of the $C\bar{1}$ to $I\bar{1}$ transformation and the composition at which it occurs are still controversial. Kroll and Müller (1980) placed it at An_{60-70} based on TEM observation of 'b' reflections in samples prepared synthetically at 30°C below solidus. Using a Weissenberg camera and monochromatized radiation, Tagai and Korekawa (1981) reported that 'b' reflections disappeared in a body-centered An_{66} plagioclase from Lake County, Oregon, when heated for a long time at 1180°C (190°C below the solidus), but they reappeared on slow cooling to 900°C. H. Schäfer (pers. comm.)

investigated a sample of composition An_{70} which had been dry heated for a long time at 30°C below the solidus, and he found that 'b' reflections were lacking in long-exposure, filtered precession photographs, but did show up as sharp spots in electron diffraction patterns. Further investigation of the high-temperature phase relations is under way.

As pointed out, variation of the plagioclase cell parameters only reflect changes in the *average* structure. There are two types of structural variations between analbite and anorthite which are relevant to lattice parameters: those related to the NaSi → CaAl substitution and those related to the varying degrees of Al,Si disorder within the series. Comparing NaSi- with CaAl-feldspars we find:

(1) The <Al-O> bond is 0.13 Å longer than the <Si-O> bond.

(2) The <Ca-O> bond is 0.16 Å shorter than the <Na-O> bond, assuming seven-fold coordination.

(3) Due to decreasing <*A*-O> and increasing <<*T*-O>> bond lengths, the ratio <*A*-O>/<<*T*-O>> is smaller in anorthite than in analbite. Related to this ratio is the average *T*-O-*T* angle, which decreases by 4° from analbite to anorthite.

(4) Edges shared tetween an *A*-polyhedron and a *T*-tetrahedron become shorter as Ca is substituted for Na; unshared edges become longer.

These affect the unit cell parameters in various ways; however, changes in <<*T*-O>> and <*A*-O> bond distances tend to balance one another, and thus only small variations of the cell edges are observed.

The variation of the degree of Al,Si disorder within the high plagioclase series is not clearly reflected in the cell edges, but it is more evident in the α and γ angles. We will discuss the variation of α and γ within the context of three questions, following Kroll and Müller (1980):

(1) Why are both α and γ in analbite and anorthite larger than 90° (or smaller, if the crystallographic orientation is reversed)?

(2) Why is the change of α small (0.3°) compared to γ (1°)?

(3) Why does the variation of γ follow a curve falling *below* a straight line connecting analbite with anorthite?

The answer to (1) is suggested by considering Figure 3, which shows curves of equal volumes calculated for anorthite by keeping a, b, $c/2$ and β constant and varying α and γ. When a feldspar is topochemically monoclinic and observed at a temperature above its displacive transformation (which is ∿980°C for analbite, but for anorthite is projected to be far above its melting point), both angles are 90°. On collapse of the structure around the A cation, one would expect α and γ to deviate from 90° in such a way as to achieve a decrease in volume with as small a variation of angles as possible because this

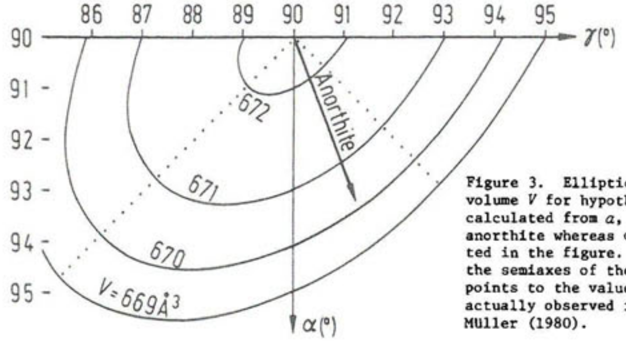

Figure 3. Elliptical curves of constant cell volume V for hypothetical anorthites. V was calculated from a, b, $c/2$ and β as observed in anorthite whereas α and γ were varied as indicated in the figure. The dotted lines represent the semiaxes of the ellipses. The heavy line points to the values of α, γ and V that are actually observed in anorthite. From Kroll and Müller (1980).

minimizes concomitant strain. In other words, α and γ should be found to follow closely the short semiaxes of the ellipses, just as observed.

To answer the second question we refer to Megaw (1974) and Bruno and Faccinelli (1974), who have shown that α is closely related to the shape of the oxygen "parallelogram" surrounding the *A* atom in the *bc* plane (Fig. 4), such that α increases with increasing difference in length of the parallelogram diagonals: $[(A\text{-}O_D m) + (A\text{-}O_B m)] - [(A\text{-}O_D 0) + (A\text{-}O_B 0)]$. As Ca substitutes for Na, all *A*-O distances shorten, such that the difference of the diagonals is nearly constant. Thus the concomitant change in α is small.

The variation of γ is best considered in terms of the tetrahedral chains along the [110] and [1$\bar{1}$0] diagonals in the *ab* plane (Figs. 2 and 8, Chapter 3). The longer tr[110] becomes relative to tr[1$\bar{1}$0], the smaller γ must be. From an-albite to anorthite, the *T*-O-*T* angles decrease in both chains by about the same amount (3.4°), but the O-*T*-O angles behave differently. In the [110] chain two of three angles become narrower, the third one widens, but in [1$\bar{1}$0] two of them widen and the third one narrows. The net effect is an increase of tr[1$\bar{1}$0] relative to tr[110] by 0.15 Å. This roughly corresponds to a widening of γ by 1°.

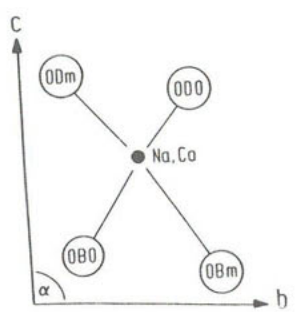

Figure 4. Projection onto the *bc* plane of the oxygen atoms coordinating Na,Ca in this plane.

Question (3) may be answered from the results of structure refinements of high plagioclases. In fully disordered plagioclases the variation of γ would be expected to follow a straight line joining analbite (AA) and anorthite (AN) in Figure 1. However, high plagioclases show a considerable degree of residual order (Kroll and Ribbe, 1980; *cf.* Fig. 9b, Chapter 2). Due to the preference of Al for the $T_1 0$ tetrahedron, tr[110] increases and tr[1$\bar{1}$0] decreases relative to fully disordered plagioclases. The γ angles thus become smaller due to ordering and plot below the hypothetical straight line. Similar arguments apply to the variation of α. However, α is less sensitive than γ to changes in the degree of order, and the effect is less pronounced.

Low plagioclases

The lattice parameters in Figure 1 were taken from Bambauer *et al.* (1967, Figs. 2 and 3 and Table 1), whose investigation of natural specimens is the most extensive yet undertaken. Straight lines with sharp kinks were drawn by them for simplicity; they are not intended to indicate the range of existence of a particular structural state. The data points of the original diagrams were omitted; they show considerable scatter, probably due in part to variable structural states. It should be emphasized that in low plagioclases there is no series comparable to the low alkali feldspar series (which has a unique set of lattice parameters), because low plagioclases for the most part consist of complex "stranded" structures or mixtures of structures. Thus, the scatter in these diagrams does not come as a surprise. In any case, the lines were drawn for each parameter emphasizing the data points of plagioclases which were found to be "low" and "well behaving" with respect to all other lattice parameters. Bambauer *et al.* (1967) assume a straight line variation between An_{16} and An_{33}, and between An_{50} and An_{76}, but the situation between An_{33} and An_{50} is uncertain. See also Doman *et al.* (1965), Speer and Ribbe (1973) and Wolfe (1976) for discussions of possible discontinuities in this region.

Whereas in high plagioclases the effect of the varying degree of Al,Si order-disorder is small relative to the effect of the NaSi $\rightarrow$ CaAl substitution, just the opposite is true for low plagioclases. Low albite is fully ordered, but anorthite in its *average* structure is fully disordered. Between An_0 and An_{33} the variation of all lattice parameters indicates a stronger increase in disorder than would correspond to a mechanical mixture of end members (see Chapter 1). The analogy to a mechanical mixture is more closely followed from An_{50} to An_{100}. The change in behavior occurs between An_{33} and An_{50}.

K-exchanged plagioclases

When plagioclases are heated for short times in molten KCl, their Na content is replaced by K (Viswanathan, 1971; 1972). This K-exchange serves two purposes: (1) The structural state of the original plagioclase can be characterized from the lattice parameters of its K-equivalent.

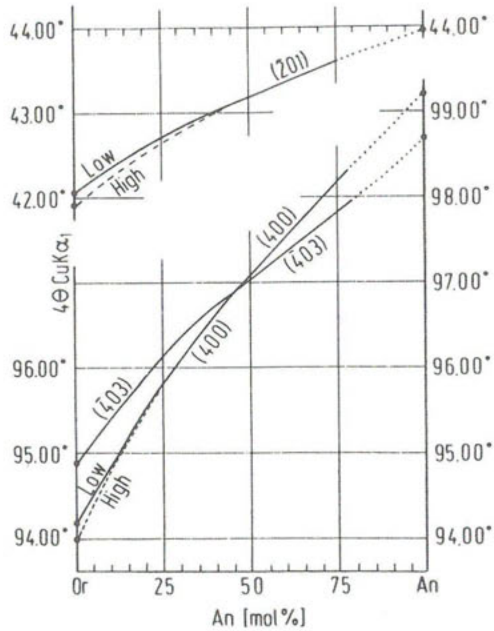

Figure 5. Variation in 4θ values of various lines in X-ray powder patterns of K-plagioclases (i.e., plagioclases whose Na content was K-exchanged). From Viswanathan (1971). The ($\bar{2}01$) curve for high K-plagioclases was kindly provided by W. Johannes, Hannover. See also Johannes (1979).

Viswanathan (1972) used the *c* parameter to estimate Al occupancies. Kroll and Bambauer (1981) K-exchanged sodic plagioclases to test their topochemistry: topochemically monoclinic plagioclases would be transformed into metrically monoclinic Ca-sanidines; topochemically triclinic ones would remain metrically triclinic. (2) The K-exchange produces (K,Ca)-plagioclases. The large size difference between K and Ca atoms provides the opportunity to determine An content from *V*, *a* or some diffraction peak depending on *a*, using Figure 5, just as Or content is determined in alkali feldspars. This method is especially useful when the plagioclases occur in fine-grained rocks or synthetic products where other methods are difficult to apply. Viswanathan (1972) claims an accuracy of $\pm$ 1% An.

Thermal expansion

Figure 6 shows the variation with temperature of cell angles α and γ in various Na-feldspars. In analbite, the deviation of α and γ from 90° is due to purely displacive structural changes (light arrows in Fig. 6). When the temperature is raised at rates rapid enough to avoid Al,Si interchange, the displacive changes decrease to become zero at ∼980°C, where analbite inverts to monalbite (the "displacive transformation" of Laves, 1952).

In high albites which were equilibrated with respect to their Al,Si distribution and X-rayed *at* their temperatures of equilibration, α and γ vary due to displacive as well as diffusive structural changes. The extent to which partial Al,Si order causes α to increase and γ to decrease is shown by the heavy arrows at 700°C. It is seen from the differing lengths of the light and heavy arrows that γ almost completely depends on diffusive changes, whereas α is dominated by displacive changes. Both angles reach 90° at 978°C, where high albite inverts to monalbite (the "diffusive transformation" of Laves, 1952).

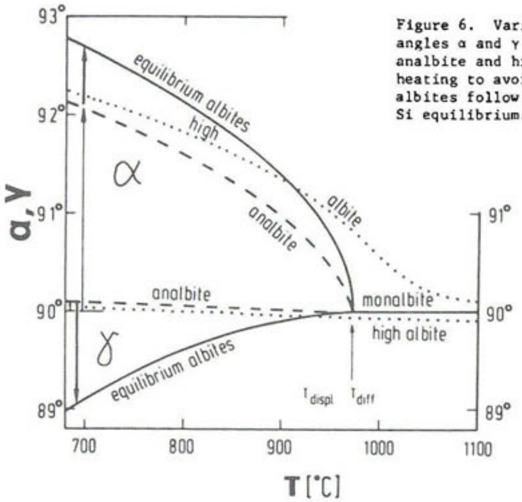

Figure 6. Variation with temperature of lattice angles α and γ in Na-feldspars. The curves for analbite and high albite correspond to rapid heating to avoid Al,Si interchange. Equilibrium albites follow a path representing states of Al, Si equilibrium. After Kroll *et al.* (1980).

When high albite is rapidly heated, only the displacive part of its "triclinicity" is removed. The remaining diffusive portion prevents α and γ from reaching 90°. Considering that the diffusive structural changes raise α, but decrease γ, we are not surprised to find α being larger than 90° at any temperature, but γ finally being smaller than 90° at high temperatures at which the displacive changes are no longer operative. High albite at high temperature is analogous to high microcline at room temperature, with the vibrating Na atom "substituting" for the large K atom.

The curves for the α angles of analbite and equilibrated albites are drawn such that they reach the abscissa with infinite slope. This is a consequence of the suggestion made by Thompson *et al.* (1974) to linearize α versus T by plotting $\cos^2\alpha$ versus T. Assuming that this suggestion is valid also at temperatures immediately below the transformation, we write the linear equation

$$\cos^2\alpha = A + B(T). \tag{1}$$

At the temperature T_c of the transformation, $\cos^2\alpha = 0$ and $B = -A/T_c$. Substituting into Equation 1, we obtain

$$\cos\,\alpha = a[(T_c - T)/T_c]^{\frac{1}{2}} \qquad (a \equiv A^{\frac{1}{2}}). \tag{2}$$

This notation is similar to the critical exponent notation of order parameters for second-order phase transformations. cos α approximates $\alpha - \pi/2$ when α approaches $\pi/2$, so that we may write

$$\alpha - \pi/2 = a[(T_c - T)/T_c]^{\frac{1}{2}}\ .$$

Differentiating α with respect to T gives $d\alpha/dT \to \infty$ for $\alpha \to \pi/2$, in other

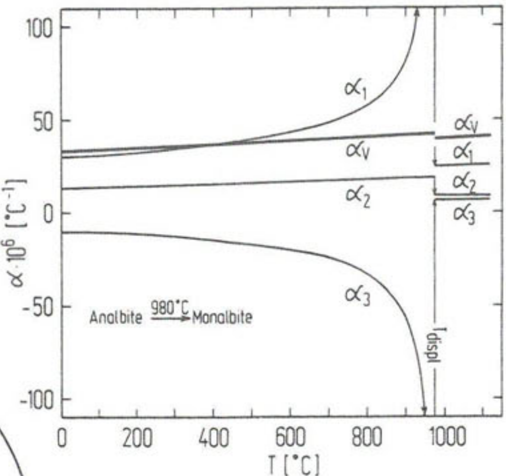

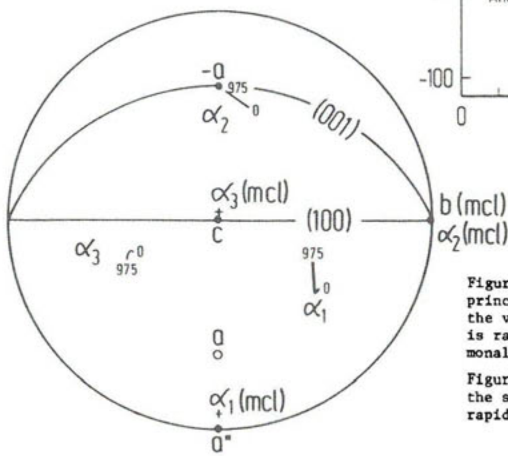

Figure 7 (above). Temperature variation of the principal expansion coefficients α_1, α_2, α_3 and the volume expansion coefficient α_V when analbite is rapidly heated and displacively inverts to monalbite.

Figure 8 (to the left). Positional variation of the strain ellipsoid axes of analbite when it is rapidly heated to displacively invert to monalbite.

words, α approaches 90° with infinite slope, as is shown in Figure 6. Equation 1 has two further consequences for the thermal expansion behavior. First, the volume expansion coefficient $\alpha_v \equiv (1/V)\cdot(dV/dT)$ changes discontinuously at T_c. This becomes apparent when $V = V(a,b,c,\alpha,\beta,\gamma(T))$ is differentiated with respect to T, making due reference to Equation 1. Secondly, the principal strain components α_1 and α_3 of the strain ellipsoid approach infinity at T_c. This is shown in Figure 7, which was calculated for the analbite/monalbite inversion using the STRAIN-program of Ohashi and Finger (1973). A topologically similar diagram results for the *equilibrium* high albite/monalbite inversion. To calculate Figure 7 the variations between room temperature and melting point of the lattice parameters *a*, *b*, *c* and β were approximated by polynomials. The variation of γ up to the critical temperature was also described by a polynomial, whereas α was treated according to Equation 1. The variation of α_1 and α_3 may be rationalized as follows: among the three lattice angles α shows the strongest variation with temperature, and we expect that the position of the α_1,α_3-plane of the expansion ellipsoid will be close to the *bc* plane of the unit cell. Since α approaches 90° with infinite slope "to make the *bc* plane rectangular", the [011] and [0$\bar{1}$1] diagonals also must change drastically in the same manner as α_1 and α_3, which are related to the expansion along [011] and the contraction along [0$\bar{1}$1], respectively (compare Fig. 4).

The temperature variation of the position of the strain ellipsoid calculated for the analbite/monalbite inversion is shown in Figure 8.

THE [110] METHOD FOR PLAGIOCLASE FELDSPARS

Diagrams to estimate t_1o and $t_1o-\langle t_1m\rangle$

In deriving diagrams to estimate site occupancies of alkali feldspars (Chapter 3), Na,K solid solution series with constant Al,Si distribution were used, as well as data from structure refinements. For plagioclases no such series exist. The Al,Si distribution necessarily changes within the low plagioclase series and also varies in the high series. However, this is not a disadvantage, because (in contrast to the alkali feldspars) there are a number of refinements of chemically intermediate plagioclases available (Table 1, Chapter 3), permitting us to construct determinative diagrams and to derive equations based entirely on structure refinements.

As mentioned in Chapter 3, in the plagioclase series we will average Al-contents over the T_1m, T_20 and T_2m sites, such that $t_1o + 3\langle t_1m\rangle = 1 + n_{An}$. To prevent confusion, it should be noted at this point that as a consequence of this convention the $t_1o - \langle t_1m\rangle$ diagram (Fig. 10) will *not* show $t_1o - \langle t_1m\rangle = 0$ for analbite -- in contrast to Figure 11 in Chapter 3, because in analbite we have $t_1o = t_1m > t_2o = t_2m$, such that $t_1o - t_1m = 0$, but $(t_1o - \langle t_1m\rangle) > 0$.

To mathematically describe the variation of t_1o in a plot of tr[1$\bar{1}$0] versus n_{An} (Fig. 9), an assumption was made by analogy to alkali feldspars: when t_1o is given, tr[1$\bar{1}$0] is a linear function of n_{An}, but intercepts and slopes of the straight lines are themselves linearly dependent on t_1o:

$$\mathrm{tr}[1\bar{1}0] = a_1 + a_2(n_{An}) + a_3(t_1o) + a_4(t_1o)(n_{An}) \ . \tag{3}$$

Regression analysis of the data listed in Table 1 of Chapter 3 suggests that two such equations -- one for sodic, one for calcic plagioclases -- are necessary for a satisfactory fit. They can be unified to a single equation by expanding the a_4 term as in the alkali feldspars:[1]

----

[1]It should be mentioned that the coefficients of the tr[110] and tr[1$\bar{1}$0] equations were refined using the "Harmonic Least-Squares" (HLS) procedure of Kroll and Stöckelmann (1979), rather than usual regression analysis (*cf.* Kroll and Ribbe, 1980). The analysis was performed under the constraint $t_1o + 3\langle t_1m\rangle = 1 + n_{An}$, and the "variable metric methods" of Fletcher and Powell (1963) were used in reaching the HLS objective. I am greatly indebted to my colleague Dipl. Math. D. Stöckelmann, Münster, for mathematically solving and programming this problem.

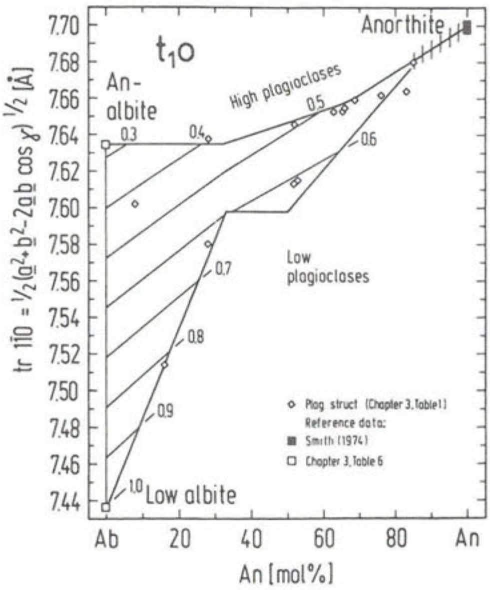

Figure 9. Diagram to determine t_1o from tr[1$\bar{1}$0] and the An content of a plagioclase. The influence of Or content on tr[1$\bar{1}$0] may be corrected with the aid of Equations 6-8. The equation for the contours is given in Table 1.

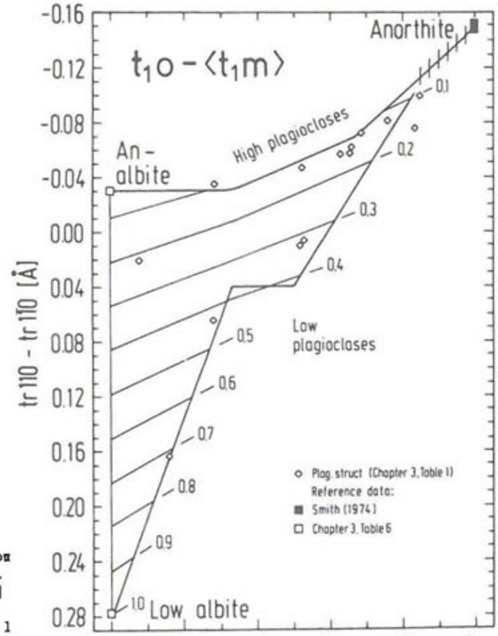

Figure 10. Diagram to determine t_1o - $<t_1m>$ from tr[110] - tr[1$\bar{1}$0] and An content of plagioclase. The influence of Or content on tr[110] - tr[1$\bar{1}$0] may be corrected with the aid of Equations 6-8. The equation for the contours is given in Table 1

Table 1. Equations and coefficients to calculate the Al site occupancies t_1o, $<t_1m>$ and $t_1o - <t_1m>$ of plagioclase feldspars from tr[110], tr[1$\bar{1}$0] (in Angströms), or Δ131 or γ (in degrees), and mole fraction An (≡ n_{An}).

Eqn.

(i) $$t_1o = \frac{tr[1\bar{1}0] - a_1 - a_2 \cdot n_{An} - 0.42 \cdot a_4 |n_{An} - 0.33|}{a_3 - a_4 |n_{An} - 0.33|}$$

(ii) $$<t_1m> = \frac{tr[110] - a_1 - a_2 \cdot n_{An}}{a_3 + a_4 \cdot n_{An}}$$

(iii) $$t_1o - <t_1m> = \frac{(tr[110] - tr[1\bar{1}0]) - a_1 - a_2 \cdot n_{An} - 0.31 \cdot a_4 |n_{An} - 0.33|}{a_3 - a_4 |n_{An} - 0.33|}$$

(iv) $$t_1o - <t_1m> = \frac{\Delta 131 - a_1 - a_2 \cdot n_{An} - 0.35 \cdot a_4 |n_{An} - 0.33|}{a_3 - a_4 |n_{An} - 0.33|}$$

(v) $$t_1o - <t_1m> = \frac{\gamma - a_1 - a_2 \cdot n_{An} - 0.35 \cdot a_4 |n_{An} - 0.33|}{a_3 - a_4 |n_{An} - 0.33|}$$

$t_1o + 3<t_1m> = 1 + n_{An}$; $t_1o = 0.25(1 + n_{An}) + 0.75(t_1o - <t_1m>)$

$\Delta 131 \equiv 2\theta(131) - 2\theta(1\bar{3}1)$[°2θ], CuK$\alpha_1$ radiation

COEFFICIENTS*

Eqn.	a_1	a_2	a_3	a_4
(i)	7.695 (7)	0.1327 (31)	-0.2377(153)	0.1090(470)
(ii)	7.715 (2)	0.1319(105)	-0.4687(114)	-0.1340(217)
(iii)	-0.031 (2)	-0.1018 (21)	0.2815 (83)	-0.1240(251)
(iv)	2.011(11)	0.2471(187)	-0.8600(283)	0.2012(980)
(v)	90.252(24)	0.816 (41)	-2.362 (64)	1.030 (212)

**Errors are in parentheses and refer to the last decimal places.*

$$tr[1\bar{1}0] = a_1 + a_2(n_{An}) + a_3(t_1o) + a_4|c_1 - n_{An}| \cdot (c_2 - t_1o) \ . \qquad (4)$$

Unlike the t_1o diagram it was found that the variation of $<t_1m>$ in a tr[110] versus n_{An} plot could be described by a single equation similar to Equation 3. The coefficients of the tr[1$\bar{1}$0] and tr[110] equations are listed with Equations (i) and (ii) in Table 1. The c_1 and c_2 coefficients in Equation 4 were refined during the first steps, but were kept constant in the final calculations. Thus they are listed without error estimates.

Only Equation (i) of Table 1 is given in diagram form to determine t_1o (Fig. 9). By analogy to the alkali feldspars, the $<t_1m>$ plot is substituted by a $t_1o - <t_1m>$ diagram, where (tr[110] - tr[1$\bar{1}$0]) is plotted versus n_{An} (Fig. 10). In principle, it is sufficient to know An content and t_1o to characterize the entire Al,Si distribution, because $<t_1m>$ follows from $t_1o + 3<t_1m> = 1 + n_{An}$. However, if the plagioclase investigated contains Or (or some other impurities), it may significantly affect the estimation of t_1o and $<t_1m>$, because the lengths of the *a* and *b* cell edges are affected. The influences on tr[110] and tr[1$\bar{1}$0] nearly cancel each other when the difference (tr[110] - tr[1$\bar{1}$0]) is taken, and thus estimation of t_1o - <t_1m> is very little affected. Contouring of Figure 10 for t_1o - <t_1m> was also done by an HLS procedure (see footnote 1) and resulted in coefficients given in Equation (iii) in Table 1.

In the section on ternary feldspars, it will be shown how tr[110] and tr[1$\bar{1}$0] may be corrected for the influence of any Or content, even without knowledge of the amount of Or present. To estimate t_1o and <t_1m>, I would suggest first to apply the correction procedure, if necessary, and then to use Equations (i) and (iii) of Table 1. The values of t_1o independently derived from these two equations should agree fairly well, say within 0.03 Al/(Al+Si), as also should the values of 3<t_1m>. Otherwise lattice parameters and An content should be checked for possible errors. To a first approximation this can be done with the aid of Figure 1. The relative position of all lattice parameters with respect to the limiting high and low series should be consistent with the same state of order, i.e., some of the parameters must not plot near the low curve when others are close to the high curve.

Estimation of errors

Applying the error propagation law (Eqn. 19, Chapter 3) to the coefficients of the determinative equations (Table 1), it is found that the standard deviation of t_1o clusters near 0.05 Al, whereas $\sigma(t_1o - \langle t_1m \rangle) \simeq 0.02$. Random errors of 2 mol % An in chemical composition and 0.002 Å in tr[110] and tr[1$\bar{1}$0] result in standard deviations of 0.015 Al for t_1o and t_1o - <t_1m>. If t_1o and <t_1m> as calculated from Equations (i) and (iii) in Table 1 are compared with the values derived from <T-O> distances (Table 1, Chapter 3), it is seen that the residuals have a standard deviation of $\sigma(t_1o)$ = 0.02 Al and $\sigma(\langle t_1m \rangle)$ = 0.01 Al.

THE [110] METHOD FOR TERNARY FELDSPARS

Natural feldspars are often neither pure plagioclases nor pure alkali feldspars. To properly characterize their Al,Si distribution with the aid of the proposed diagrams and equations, it is useful to account for the deviations from the ideal chemistry, if possible, without knowing in advance the exact extent of the deviation. We will consider only feldspars within the Or-Ab-An system, and for simplicity will refer to all An-containing alkali feldspars and Or-containing plagioclases as "ternary feldspars" regardless of their exact position in the ternary.

Figure 11 is a plot of tr[1$\bar{1}$0] versus tr[110] for several binary and ternary feldspar series. It will be shown from this diagram that ternary feldspars

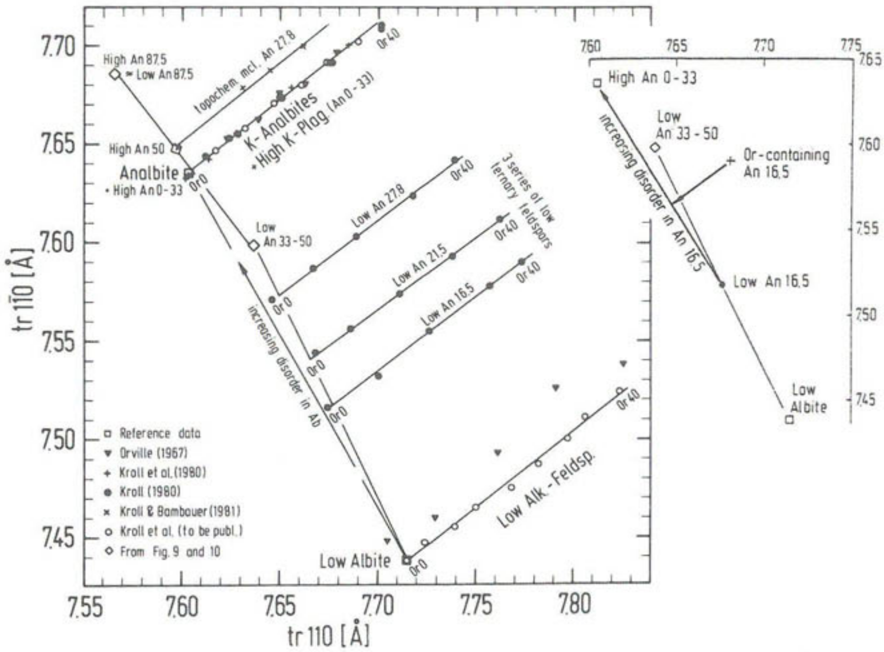

Figure 11. Variation of tr[110] and tr[1$\bar{1}$0] with Al,Si order and composition in various series of binary and ternary feldspars, as listed below.

(1) Two low albite - low microcline series: Orville (1967) and Kroll *et al.* (to be published).

(2) Three sets of analbite-high sanidine data: Orville (1967), Kroll *et al.* (1980, Table 2a) and Kroll *et al.* (to be published).

(3) Three series of low ternary feldspars: Three low plagioclases, $An_{16.5}$, $An_{21.5}$, and $An_{27.8}$, were ion-exchanged in molten KCl to give K-plagioclases. Ternary series were then prepared from the Na- and K-end members (Kroll, 1980).

(4) Two series of high ternary feldspars: Two low plagioclases, $An_{16.5}$ and $An_{27.8}$, were converted into high plagioclases by long term heating (60 days at 1100°C and 31 days at 1120°C, respectively). After K-exchange two ternary series were prepared. The structure of the heated $An_{27.8}$ sample has been refined by Kroll (1978). The topochemically triclinic structural state of both series is discussed by Kroll and Ribbe (1980). Lattice parameters are given by Kroll (1980).

(5) One series of topochemically monoclinic ternary feldspars: A low plagioclase $An_{27.8}$ was first K-exchanged, then heat-treated (10 days at 1100°C) to give a metrically and topochemically monoclinic K-plagioclase, and finally Na-back-exchanged. A ternary series was prepared from the end members (Kroll and Bambauer, 1981).

(6) The straight line connecting low albite with low An_{33} in the figureis drawn according to the low plagioclase lattice parameters of Bambauer *et al.* (1967).

(7) The straight line extending from about low An_{33-50} to $An_{87.5}$ approximates the data points of low and high plagioclases in the range An_{33} to $An_{87.5}$. It was drawn according to the lattice parameters of Bambauer *et al.* (1967) and Kroll and Müller (1980).

INSET, upper right. Use this sketch to follow the example of how to use this diagram, as detailed in the text.

are treated most usefully as Or-containing plagioclases, from which the influence of the Or content on tr[110] and tr[$1\bar{1}0$] has to be removed to yield the repeat distances of a *pure* plagioclase.

We now discuss Figure 11, using data described in the legend. The low alkali feldspar series constitutes the lower boundary line. Only compositions between Or_0 and Or_{40} have been plotted, because in this range tr[$1\bar{1}0$] varies linearly with tr[110]. When heated near the melting point, low alkali feldspars undergo changes in their lattice parameters due to increasing Al,Si disorder until finally they reach the K-analbite line in the upper part of the diagram. Like heat treatment, any calcium entering low alkali feldspars causes the lower boundary line to move upwards as is seen with the three ternary series $An_{16.5}$, $An_{21.5}$, and $An_{27.8}$. This behavior is expected (*cf.* Figs. 9 and 10) as a consequence of increasing disorder due to substitution of NaSi by CaAl in sodic low plagioclases. The nearly disordered equivalents of the three low ternary series coincide with the K-analbite line. As seen with the $An_{27.8}$ series, further disordering to monoclinic topochemistry causes a further shift beyond that line. Within the compositional range $0 < n_{An} < 0.33$ this line separates topochemically monoclinic from topochemically triclinic feldspars: the former do not fall below it, the latter do not plot above it. The data points of all binary and ternary series in Figure 11 follow nearly parallel straight lines, the equation of which is

$$\mathrm{tr}[1\bar{1}0] = \text{constant} + 0.773(\mathrm{tr}[110]) \ . \tag{5}$$

There are no ternary series known in the literature with $n_{An} > 0.50$. However, from Viswanathan's (1972) K-exchange experiments it may be deduced that calcic plagioclases, like sodic plagioclases, follow Equation 5.

Based on the observation that Or-containing plagioclases plot on straight lines parallel to the low alkali feldspar line we may use Figure 11 to correct the influence of the Or content on the [110] and [$1\bar{1}0$] repeat distances. By way of an example, assume an Or-containing plagioclase $An_{16.5}$ has repeat distances tr[110] = 7.680 Å and tr[$1\bar{1}0$] = 7.590 Å (see inset in Fig. 11). First draw a straight line according to Equation 5 through this data point, and then find the point of intersection with a second straight line drawn through the data points of the *pure* low and high plagioclases of the same An content (16.5 mol %). Corrected values of tr[110] and tr[$1\bar{1}0$] are determined thereby and may be used to find t_1o and $\langle t_1m \rangle$ on Figures 9 and 10. Thus it is not necessary to know the Or content of the plagioclase, but its An content must be known.

To develop equations for the correction procedure the plagioclases have been subdivided into two groups: An_0-An_{33} and An_{33}-$An_{87.5}$. Low plagioclases of the first group plot on a straight line connecting "low albite" with "low An_{33}"; their disordered equivalents coincide with the analbite point. Low *and* high plagioclases of the second group can be closely approximated by a single straight line representing the data points between "low An_{33-50}" and "high $An_{87.5}$ = low $An_{87.5}$" (Fig. 11). Within the first group the slope of the lines connecting low with high plagioclases depends on the An content, whereas it is constant within the second group. The point of intersection of a particular "ternary feldspar line" (Eqn. 5) with such an "order → disorder" line represents [110] and [1$\bar{1}$0] repeat distances of a pure plagioclase, which is equivalent to the ternary feldspar with respect to An content and state of order. The values of $tr[110]_c$ and $tr[1\bar{1}0]_c$ corrected for Or content (subscript c) are found from the observed values (subscript o) by means of the following equations:

$$An_0\text{-}An_{33}: \qquad tr[110]_c = \frac{tr[1\bar{1}0]_o - 0.773(tr[110]_o) - 7.6345 + 7.6030(A)}{A - 0.773}$$

$$\text{where } A = \frac{-0.1980 + 0.4894(n_{An})}{0.1115 - 0.2348(n_{An})} \qquad (6)$$

$$An_{33}\text{-}An_{87.5}: \quad tr[110]_c = 8.4569 - 0.4848(tr[1\bar{1}0]_o) + 0.3747(tr[110]_o) \qquad (7)$$

$$An_0\text{-}An_{87.5}: \quad tr[1\bar{1}0]_c = tr[1\bar{1}0]_o + 0.773(tr[110]_c - tr[110]_o)\ . \qquad (8)$$

To complete the example given above, we calculate from Equations 6 and 8 corrected repeat distances $tr[110]_c$ = 7.647 Å and $tr[1\bar{1}0]_c$ = 7.564 Å and can now estimate t_1o and $\langle t_1m \rangle$ from Figures 9 and 10: t_1o = 0.63, $\langle t_1m \rangle$ = 0.18.

Figures 9 and 10 and corresponding equations only account for topochemically triclinic plagioclases. If a ternary feldspar is topochemically monoclinic, this can be recognized from Figure 11: its data point should plot *above* the K-analbite line. As is seen from the $An_{27.8}$ line, even an appreciable An content in the ternary feldspar causes a relatively small shift in tr[110] and tr[1$\bar{1}$0]. For the time being it is recommended that a topochemically monoclinic feldspar with less than 5% to 10% An be treated as an alkali feldspar (Figs. 10 and 11 in Ch. 3). If the An content exceeds 5 to 10 mol % the correction procedure should be followed as outlined and $t_1o = t_1m = t_1$ determined from Figure 9. The difference $t_1o - \langle t_1m \rangle$ would have to be interpreted in this case as $t_1 - \frac{1}{3}(t_1 + 2t_2)$.

THE Δ131 METHOD AND THE γ METHOD

Determination of the Al,Si distribution from tr[110] and tr[1$\bar{1}$0] requires refinement of lattice parameters. A much simpler, though less accurate method is to use the (131) line separation, $\Delta 131 \equiv 2\theta(131) - 2\theta(1\bar{3}1)$, from an x-ray powder pattern using $CuK\alpha_1$ radiation. Smith and Yoder (1956) introduced this method, Ribbe (1972, 1975) gave a quantitative interpretation, and Kroll and Ribbe (1980) produced the determinative diagram in Figure 12. Δ131 is a measure of $t_1o - \langle t_1m \rangle$, but because it is closely related to the γ* angle it has an unfortunately strong dependence on the Or content of the plagioclase. This is seen from the equation given by McKie and McConnell (1963):

$$\Delta 131 \equiv 4 \sin^{-1} [\Phi(c^*\cos\alpha^* + a^*\cos\gamma^*)], \quad \text{where}$$

$$\Phi = 3\lambda b^*/(d^*_{131} + d^*_{1\bar{3}1}) \cos \tfrac{1}{2}(\theta_{131} + \theta_{1\bar{3}1}) \ .$$

"The quantities Φ, $c^*\cos\alpha^*$ and a^* vary by 0.45%, 7.0% and 0.27% between low and high albite, while $\cos\gamma^*$ varies through zero by a factor of more than 9." Diagrams to correct for the Or influence were prepared by Kroll and Ribbe (1980); see Figure 13. Applying the HLS method (Kroll and Stöckelmann, 1979), they calculated contours of $t_1o - \langle t_1m \rangle$ for the Δ131 versus An plot (Fig. 12). The corresponding equation is given as Equation (iv) in Table 1.

The correction for Or content is only approximate, and the reader should be careful not to overestimate the precision of $t_1o - \langle t_1m \rangle$ determined from Δ131. Kroll and Ribbe (1980) gave the following example of the influence of Or: ". . . for high albite γ* = 87.95°, cosγ* = 0.0358, and Δ131 = 2.0°; for high $Ab_{90}Or_{10}$ γ* = 88.23°, cosγ* = 0.0309, and Δ131 = 1.7°. If one were ignorant of the Or content in the latter, the Δ131 plot would give $t_1o - \langle t_1m \rangle$ = 0.35 Al instead of the correct value of 0.04 Al." In contrast, without correction for the Or content one would find from tr[110] – tr[1$\bar{1}$0] that $t_1o - \langle t_1m \rangle$ equals 0.05 Al, i.e., an error of only 0.01 Al would have been introduced, compared to an error of 0.31 Al when the uncorrected value of Δ131 is used.

Diagrams similar to that for Δ131 versus mol % An could be constructed for γ*, $\Delta\bar{2}41 \equiv 2\theta(\bar{2}41) - 2\theta(24\bar{1})$, $\Gamma \equiv 2\theta(131) + 2\theta(220) - 4\theta(1\bar{3}1)$ or σ (for the rhombic section). All are strongly related to γ* and thus to Or content, and all would have weaknesses similar to the Δ131 diagram. But the γ angle is nearly insensitive to Or content (VanSchmus and Ribbe, 1968), and Kroll and Ribbe (1980) prepared Figure 14 and Equation (v) in Table 1 as an alternative to Δ131, to be used if the cell parameters have been refined. An example of its value is illustrated with reference to Figures 12 and 14. The observed

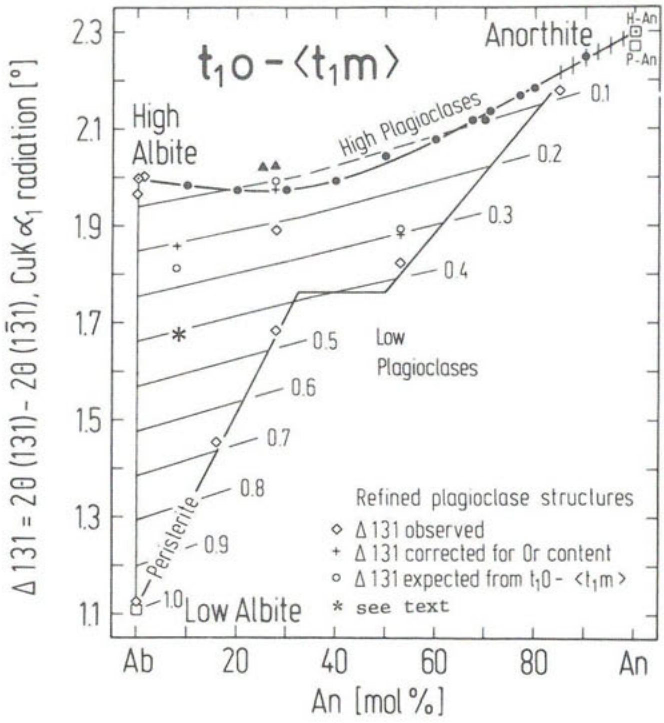

Figure 12. Diagram to determine $t_1o - \langle t_1m \rangle$ from Δ131 and An content of plagioclases. Δ131 ≡ 2θ(131) - 2θ(1$\bar{3}$1) measured in °2θ using CuKα_1 radiation. The equation for the contours is given in Table 1. From Kroll and Ribbe (1980).

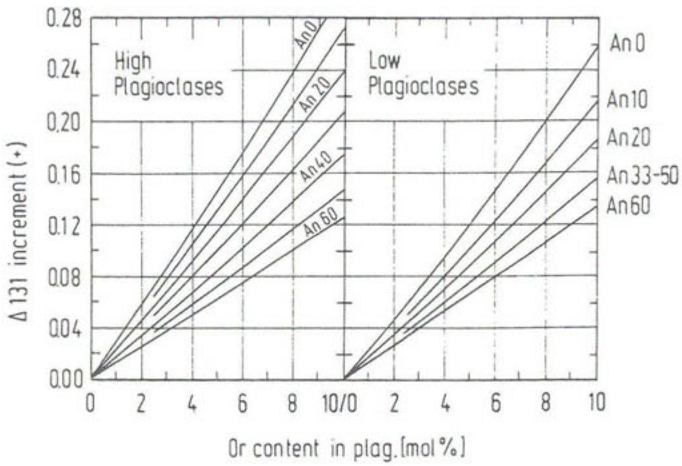

Figure 13. Graphs to aid in correction of Δ131 values for mole percent $KAlSi_3O_8$ (Or) in high and low plagioclases. From Kroll and Ribbe (1980).

Δ131 value for $An_8Or_{7.5}Ab_{84.5}$ is 1.68° (plotted as * in these figures. Using Figure 13 to "correct" this value for the effect of Or content gives an increment of +0.18° and thus an estimated (t_1o - <t_1m>) value of 0.20_5. This is not very close to the value determined from bond lengths: (t_1o - <t_1m>) = 0.465 - 0.205 = 0.26 Al. Notice however that the lattice angle γ is 89.80°, predicting 0.23 Al (Fig. 14).

To simultaneously estimate An content and structural state of a plagioclase, Su and Ye (1981) introduced the line difference 2θ($\bar{2}04$) - 2θ(400) to contour their Δ131 diagram. The dependence of this function on Or content and the precision of this method require further study; initial calculations show the influence of Or content may be three times as large as that of An content.

A GUIDE TO INDEXING PLAGIOCLASE POWDER PATTERNS -- see Appendix

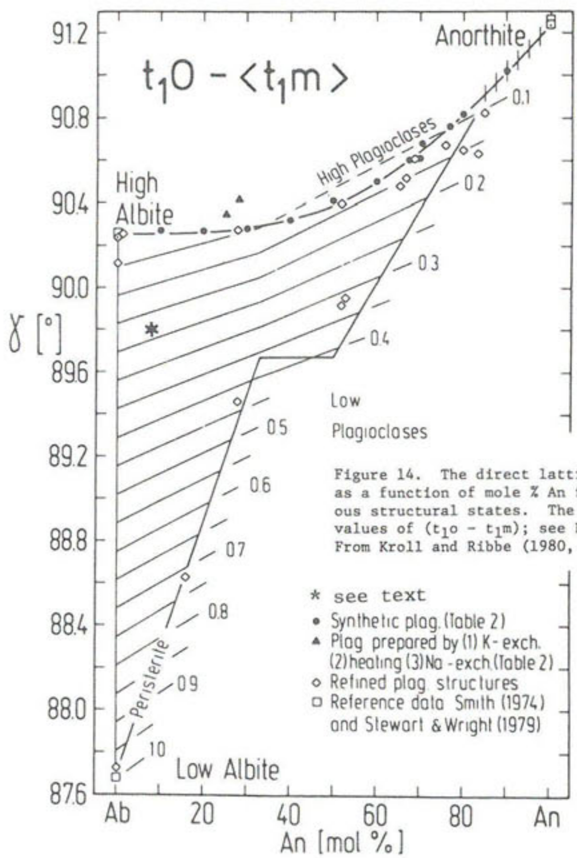

Figure 14. The direct lattice angle γ (in degrees) as a function of mole % An for plagioclases of various structural states. The plot is contoured for values of (t_1o - t_1m); see Equation (v) in Table 1. From Kroll and Ribbe (1980, Fig. 2).

Chapter 5

OPTICAL PROPERTIES of FELDSPARS

D. B. Stewart & P. H. Ribbe

INTRODUCTION

Prior to 1950 optical methods were the principal basis for description of feldspars. In fact, most classification and nomenclature of feldspars are still based on early optical observations, many of which are of excellent quality. The widely available petrographic microscope can be used to examine smaller quantities of feldspar than is required for most x-ray methods, and it can be used with samples almost as small as those examined in electron microprobes and microscopes. Using an optical microscope the mineralogist can quickly and cheaply gather important determinative data for both plagioclases and alkali feldspars, and make valuable observations concerning twin laws, sample homogeneity and the selection of representative samples for more detailed study by other methods.

Since 1950 advances in understanding feldspars have been based on other than optical measurements, requiring substantial reinterpretations of optical data, particularly for the alkali feldspars. Primary amongst them are the now more clearly defined polymorphic and cation-exchanged series of alkali feldspars, the effects of heterogeneity due to exsolution, twinning and antiphase domains, and the effects of coherency strain. Many of these problems have been explored in detail by Smith (1974a, Chapters 8 and 9), by Stewart (1974), and by De Pieri (1979).

Most feldspars are best described as structurally composite crystals, and thus their optical properties are averages of the optical properties of the individual members of the composite. Electron-microscopic studies have revealed that, apart from a few end members and some high-temperature samples, most feldspars consist of two or more types of domains that differ either in orientation or composition, or both, on a scale of 30 to 1000 Å. Because wavelengths of visible light are considerably greater than this, the refractive indices, optic axial angle (2V), and extinction angles of any feldspar grain are -- to a first approximation -- volume-weighted averages of the respective properties of the submicroscopic domains, as Hauser and Wenk (1976) demonstrated. Thus, properly calibrated, optical properties are useful in determining *bulk* composition and *average* structural state.

In this chapter we will summarize the current utility of the optical properties of feldspars, and appraise insofar as possible, their correlation with other structurally and chemically sensitive parameters such as cell dimensions. We will not describe feldspars with extensive ternary solid solution, or with

Table 1. Representative optical properties of alkali feldspars and Al contents of T_1 sites as determined by the method of Chapter 3, or from Figure 2.

	Sym.	$2t_1$ or t_1o+t_1m	Refractive indices α	β	γ	°$2V_x$	γ-α	Ext'n X′ to (001) on (010)	Dispersion
HIGH SANIDINE* Spencer A, heated	M	0.52	1.5192	1.5230	1.5240	54 $\parallel$	0.0048	5.2°	r<v
LOW SANIDINE Spencer G	M	0.68	1.5202	1.5247	1.5249	24 $\perp$	0.0047	5.8°	r>v
ORTHOCLASE Spencer C	M	0.74	1.5188	1.5230	1.5236	44 $\perp$	0.0048	5.3°	r>v
LOW MICROCLINE Pellatsalo	T	1.00	1.5178	1.5217	1.5247	82$\sim\perp$	0.0069	5.0°	r>v
ANALBITE Ramona, heated	T	0.56	1.5273	1.5344	1.5357	47$\sim\perp$	0.0084	7.7°	r>v
LOW ALBITE Ramona	T	1.00	1.5286	1.5326	1.5388	103$\sim\perp$	0.0102	20.5°	r>v

*Data used for the HS reference points on Figures 1-3, corresponding to the "standard" cell parameters for HS given in Table 4, Chapter 3, are $2t_1 = 0.56$; $\alpha = n_a = 1.5175$; $\beta = n_b = 1.5228$; $\gamma = n_c = 1.5237$; $2V_x = 46.5°$, O.A.P. $\parallel$ (010).

REFERENCES: Spencer (1937) for A, G, C; Brown and Bailey (1964) for LM; J.R. Smith (1958) for AA and LA.

extensive substitutions of Ba or Sr for Ca, Fe or B for Al, etc. The effects on certain optical properties of even small amounts of other components can be quite significant, especially compared to the range of variation caused by differences in Na→K substitutions or Al,Si order in alkali feldspars.

ALKALI FELDSPARS

Optical properties are of varying usefulness in determining composition and/or Al,Si order, and Table 1 contains selected properties of representative alkali feldspars. The range of variation of each refractive index with composition for an alkali feldspar series with constant Al,Si order is small, being only 0.011-0.014, so that with a measurement capability of ±0.001, resolution of composition is limited. With special care, refractive indices can be measured to ±0.0002, but determinative curves of such precision are not available, and the effects of minor constituents are expected to be a hindrance. Changes of refractive indices caused by Al,Si ordering in an isochemical series are almost one-third those caused by varying Na,K content.

The birefringence of any alkali feldspar is low (<0.01), and although it does vary with Na,K composition and Al,Si order (Raase and Morteani, 1976, p. 428-429; Hewlett, 1959, p. 520f.), birefringence, like refractive indices, has until now afforded insufficient resolution as a determinative method. Partial birefringences are, however, easily and precisely measurable, and they are highly correlated to optic axial angles. The latter, together with extinction angles, are potentially the most useful optical properties. These will be discussed separately.

<u>Optic axial angle, $2V_x$, an indicator of $(t_1o + t_1m)$</u>

Data for samples for which optic axial angle and cell parameters were known were used by Stewart (1974) to contour the *b*-*c* plot for $2V_x$ with straight lines. Numerous data sets have become available since then, including an extraordinary suite of three monoclinic and five triclinic K-feldspars for which the crystal structure, the unit cell parameters and 2V were all determined on each of the grains by Dal Negro *et al.* and De Pieri (1979). Cell parameters (by powder methods) and optic axial angles were determined by Priess (1981) and Zeipert and Wondratschek (1981) for more disordered (monoclinic) K-feldspars and, although not used here, by Bernotat and Morteani (1982) and Bambauer and Bernotat (1982) for mostly triclinic K-feldspars ($53° < 2V_x < 88°$). These, together with earlier data and revised interpretations of the *b*-*c* plot (see Chapter 3), have been considered in constructing Figures 1, 2 and 3.

$2V_x$ for the low microcline → high sanidine series. Following ideas by Hewlett (1959), the refractive index for light vibrating nearest *a* has been designated n_a, that nearest *b*, n_b and that nearest *c*, n_c. Thus, for low microcline (LM) $n_a = \alpha$, $n_b = \gamma$ and $n_c = \beta$, but for high sanidine (HS), $n_a = \alpha$, $n_b = \beta$ and $n_c = \gamma$. F.D. Bloss suggested a linear plot of n_a, n_b, n_c, which simply connects LM data to indices for HS, and thereby immediately explains the change in optic orientation of K-rich feldspars with Al,Si order. See Figure 1. When relative changes in the *a*, *b* and *c* cell dimensions are added to such a plot, it is obvious that n_b increases and n_c decreases with Al,Si order in almost exact proportion to the decrease of *b* and increase of *c* from HS to LM. The abscissa is scaled in terms of $(t_1o + t_1m)$, which was shown in Chapter 3 to be nearly linearly related to changes in *b* and *c* for all natural alkali feldspars. Note that the *a* cell dimension varies only trivially with Al,Si order, as does n_a (Hewlett, 1959).

Calculating the optic axial angle for this simplistic linear plot of refractive indices, S.-C. Su, F.D. Bloss, and the authors (see Su *et al.*, 1983) showed that 2V must vary sigmoidally with $(t_1o + t_1m)$. To substantiate the relationship, more than 50 data were chosen from the literature without regard to whether the specimens were natural or heated, monoclinic or triclinic, homogeneous or exsolved, strained or unstrained, twinned or untwinned, and these were plotted against $(t_1o + t_1m)$ determined by the tr[110],[$1\bar{1}0$] method of Chapter 3. Bulk compositions range from Or_{75} (Spencer F) to Or_{98} (a microcline),

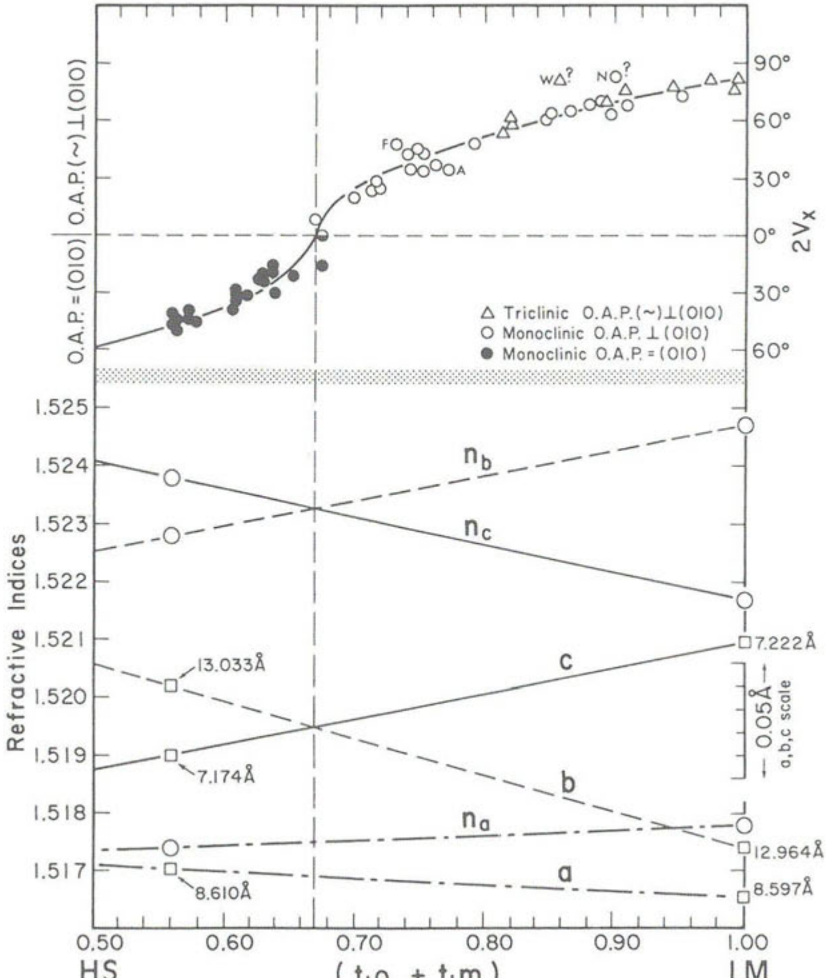

Figure 1. In the center of this figure at ($t_1o + t_1m$) = 0.56 are plotted the refractive indices for high sanidine (HS) [as determined by extrapolation of the "sanidine series" plus "heated" K-feldspars in Fig. 8-9 of Smith (1974a] and at ($t_1o + t_1m$) = 1.0 are those for low microcline (LM) [data are in Table 1]. The refractive index vibrating most nearly parallel to the *a* crystallographic axis is labelled n_a, those nearest *b* and *c*, n_b and n_c: n_b = β for HS, γ for LM; n_c = γ for HS, β for LM; n_a = α for both. The assumed linear variation of n_b and n_c, in particular, when used with n_a to calculate $2V_x$ (sigmoidal curve at top) explains the change in orientation of the optic axial plane (O.A.P.) at ($t_1o + t_1m$) ≈ 0.67, 2V = 0°. Notice however that the proportional changes in cell dimensions are almost perfectly matched, inversely, by changes in n_a, n_b and n_c. The *b* and *c* plots were arbritrarily caused to cross at the same spot as n_b and n_c to emphasize that fact. The scale for cell dimension variation is given on the lower right. The ($t_1o + t_1m$) values for specimens plotted on the $2V_x$ curve were determined by the tr[110],[110] method (Chapter 3; the *b-c*, α*-γ* method gives similar results). Using 2V values reported in the literature, only four specimens exceed an estimation error of ±0.02 Al in T_1O and T_1m. See footnote 2, and see text for discussion of the wide variety of compositions and composite crystals used in this plot. Compare with Figure 2 which contains the same 2V data in a linearized plot. From Su *et al.* (1983).

and in spite of this, the data fit remarkably well.[1] This curve will predict $(t_1o + t_1m)$ to within about 0.02 Al for most natural K-rich alkali feldspars.[2]

Su (pers. comm.) has quantified the $2V_x$ versus $(t_1o + t_1m)$ relation with two equations:

$$\text{O.A.P. } (\sim) \perp (010)\text{: } (t_1o + t_1m) = 0.666 + 0.709 \sin^2 V_x$$

$$\text{O.A.P. } \parallel (010)\text{: } (t_1o + t_1m) = 0.666 - 0.709 \sin^2 V_x$$

Estimated standard deviations are 0.019 Al, excluding the four specimens listed in footnote 2. Figure 2 provides the means to graphically solve for $(t_1o + t_1m)$ using a measured value of $2V_x$. The nearly perfect correlation of 2V with several partial birefringences of this series of specimens suggests that the latter (easily measured with a Berek compensator) may be of occasional value in determining $(t_1o + t_1m)$ if $2V_x$ is not readily determined. Hewlett (1959, p. 530) made such a proposal, noting that composition did not significantly effect the birefringence $n_b - \alpha$. The curves of Figures 1 and 2 were used to determine contour reference points on the LM-HS side of the *b-c* plot in Figure 3.

$2V_x$ for the low albite → analbite series. To contour the LA-AA side of the *b-c* plot, we used refractive indices determined by J.R. Smith (1958; see Table 1) for the Ramona low albite, for which it is assumed that $(t_1o + t_1m)$ = 1.0, and for a heated analbite from the same specimen, assuming $(t_1o + t_1m)$ = 0.56. Given the linear variation of *b* and *c* with $(t_1o + t_1m)$ implicit in Equations 10a and 10b, Chapter 3, values of *b* and *c* corresponding to $2V_x$ = 40, 50, ... 100° were calculated -- based on a linear variation of refractive indices with $(t_1o + t_1m)$ between LA and AA -- and were plotted on Figure 3. The $2\theta(131) - 2\theta(1\bar{3}1)$ data of Raase and Kern (1969) were used with Equation (iv) in Table 1, Chapter 4, to obtain $(t_1o + t_1m)$ for a series of intermediate albites on which they measured 2V. These and several low and high albites are found to plot in reasonable agreement with the contours on this side of the diagram. The sodic equivalents of potassic starting materials, which may have been either triclinic microclines or monoclinic orthoclases or sanidines before Na-exchange was undertaken, also fit well within the 2V contouring scheme. This further substantiates the fact that 2V is not affected by differences in Al,Si distribution

---

[1]We did not adjust the 2V values to remove the effect of the Na-feldspar component (see Smith, 1974a, Fig. 8-5, p. 380), but if we had, the 2V values would have shifted by up to 10°.

[2]Exceptions in Figure 1 include four of Spencer's (1937) specimens whose $(t_1o + t_1m)$ values -- along with many of the Spencer specimens -- were determined from cell parameters of the K-rich phase only (Stewart and Wright, 1974, Table II). They are labelled in Figure 2.

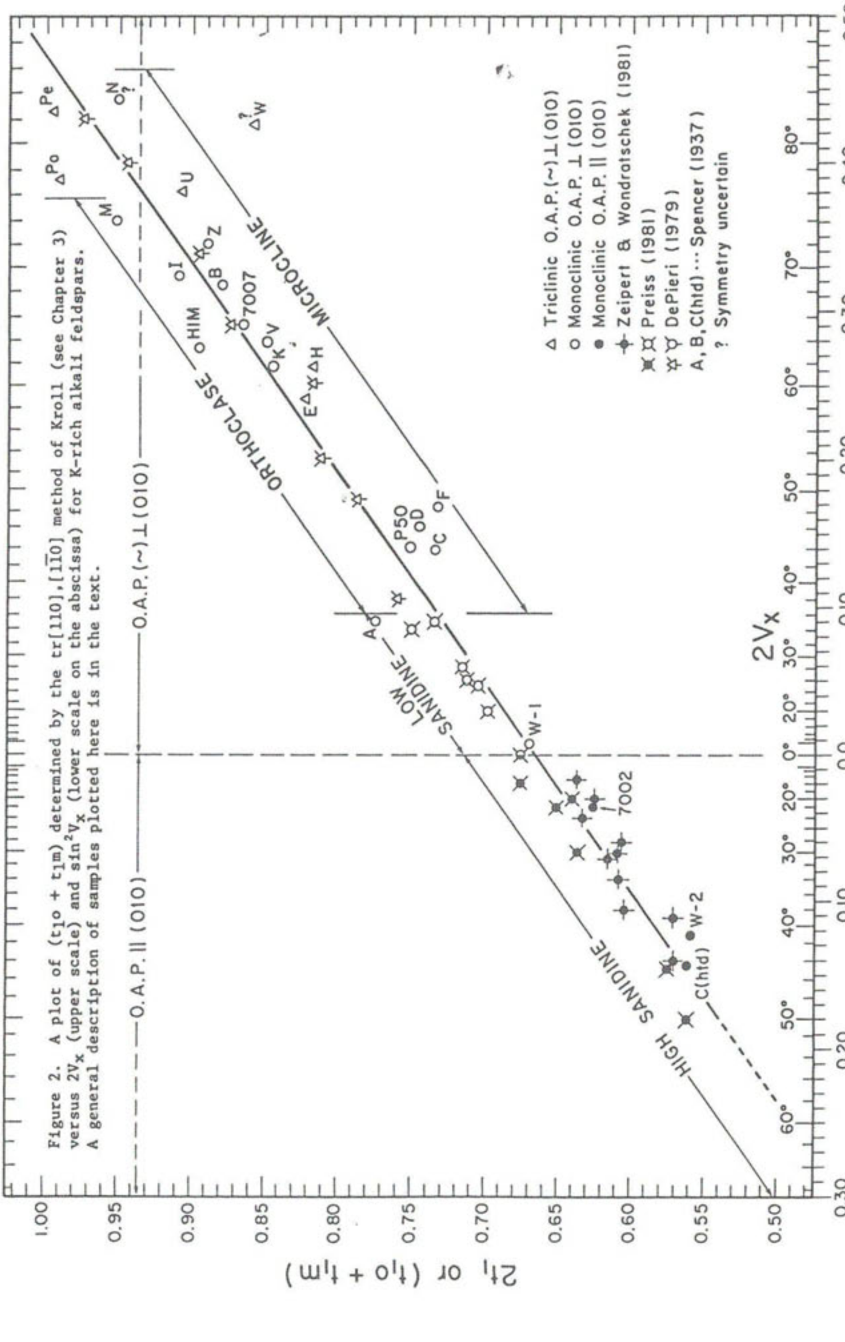

Figure 2. A plot of ($t_1o + t_1m$) determined by the tr[110],[$1\overline{1}0$] method of Kroll (see Chapter 3) versus $2V_x$ (upper scale) and $\sin^2 V_x$ (lower scale on the abscissa) for K-rich alkali feldspars. A general description of samples plotted here is in the text.

between the T_1O and T_1m sites, but that (apart from compositional effects) it is dependent on the *total* Al in these sites, i.e., (t_1o + t_1m).

$2V_x$ for the low albite → low microcline series. Except for LA and LM, there are no refractive indices available for this isostructural series. However, Rankin's (1967) attempt to obtain optic axial angles for the tiny fragments of Orville's (1967) LA-LM alkali-exchange series suggests (with considerable scatter) that $2V_x$ varies linearly with composition. His data are plotted on Figure 3; they are the closest to the LA-LM edge. We did not use these values to contour the LA-LM side of the *b-c* plot, but instead relied on an extrapolation of the 2V versus (t_1o + t_1m) and *b*,*c* curves of Figures 1 and 2 to obtain limiting values for 2V = 90° and 100°. This is expedient, but clearly requires further refinement.

$2V_x$ for the high albite (or analbite) → high sanidine series. This side of the *b-c* plot contains a change in orientation of the optic axial plane with composition, just as the O.A.P. changed with (t_1o + t_1m) for LM-HS. But in this case the variations in structural state are nil and cell dimensions change nonlinearly with Na → K substitution (Fig. 2 in Chapter 3). For the time being, we assume that refractive indices vary linearly; n_b (= β for HS, γ for AA) and n_c (= γ for HS, β for AA) cross over at a bulk composition near Or_{55}, (2V = 0°), in a manner similar to the behavior of indices for LM-HS. The values of 2V were calculated as functions of mol % Or, and the Or content was used with the AA-HS curves in Figure 2, Chapter 3 to get corresponding *b* and *c* values for plotting in Figure 3.

The b-c *plot contoured for $2V_x$.* The 2V values calculated as described above for the boundaries of the *b-c* plot were used to contour it (Fig. 3). One discrepancy of the model resulted in the 2V = 40° contour being drawn with some ambiguity. Other contours are subject to revision as well, especially those in the exclusively monoclinic corner of the quadrilateral near HS.

There is considerable scatter among the data on Figure 3 for both the size and orientation of the optic axial angle. Little of the scatter is caused by measurement errors, which typically amount to less than 0.005Å in *b* and *c* and about ±1° in 2V, but may reach ±4° at low 2V. Some scatter results from zoning of major and minor components which cause each refractive index to vary slightly. [Note that a 0.0003 change in refractive index β can cause 2V to change by ∿8°!] Twinning, strain between unmixed feldspar phases, and differences in the Al,Si ordering schemes could each affect 2V and the cell dimensions, producing additional scatter. Submicroscopic twinning causes 2V to

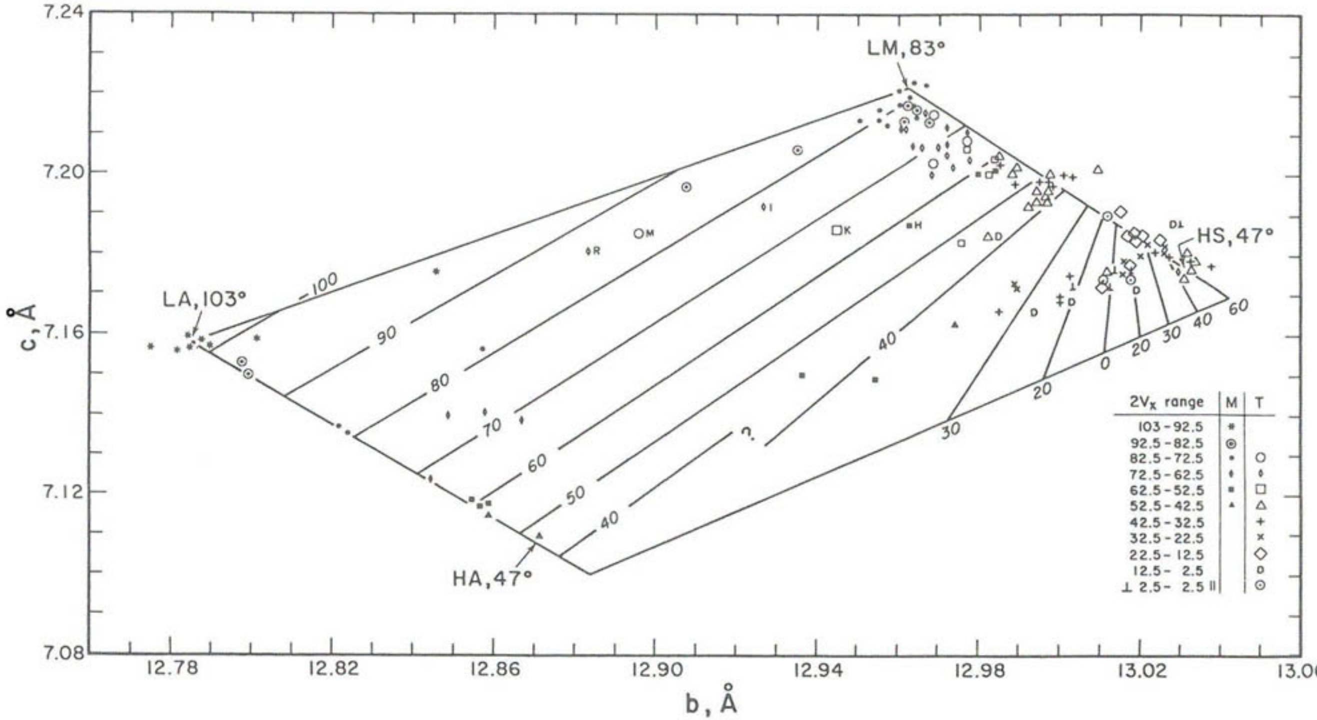

Figure 3. Contoured plot of optic axial angle (2V) against cell edges *b* and *c*. Data plotted are from Stewart (1974) with additional data from De Pieri (1979), Priess (1981), Zeipert and Wondratschek (1981), Wones *et al.* (1967), De Pieri and Quareni (1973), and R.C. Erd (pers. comm. to DBS, 1975). The method of contouring is discussed in the text. Cryptoperthitic samples from Spencer (1937) with large amounts of lattice strain are marked with letters. Potassic feldspars with intermediate to highly ordered structural states may be either monoclinic or triclinic.

decrease by 3-8°, and inasmuch as most alkali feldspars are twinned, this effect is to some degree incorporated into the contours. Strain between unmixed phases has a marked effect on the cell dimensions of both phases, as discussed in detail below and in Chapter 3.

No doubt the most significant cause of scatter is that fewer than 8% of the 2V data plotted in Figure 3 were measured on the very crystal for which *b* and *c* are reported and *none* have had their composition determined on the same grain that was studied optically. In summary, the following features of Figure 3 are significant:

(1) Despite the scatter, of points, ($t_1o + t_1m$) is clearly the dominant structural feature affecting 2V for a given composition.

(2) Symmetry has no directly discernible effect on 2V (*cf.* Figs. 1 and 2).

(3) In general, 2V increases with decreasing Or content in cation-exchange series of alkali feldspars with the same degree of Al, Si order. Although this is not true for exchange series whose K-rich end members have O.A.P. || (010), even they behave quite predictably, based on a model similar to that expounded for the HS-LM series (Fig. 1).

(4) The point at which the $2V_x = 90°$ contour intersects the LA-LM boundary is predicted to be near Or_{65}, assuming a linear variation of refractive indices between the end members (Table 1 contains data). However, because *b* versus *c* is *not* a straight line for the LA-LM series (*cf.* Fig. 2, Chapter 3), and the few refractive indices available seem not to vary with strict linearity (Smith, 1974a, Fig. 8-9), it is likely that the 2V = 100°, 90°, and even 80° contours may have considerable curvature toward lower *c*, higher *b* values.

(5) Most alkali feldspars are optically negative, although highly ordered Na-rich specimens are optically positive. Optically positive microcline ("iso-microcline") has been mentioned frequently in the literature, and Blasi (1972) has carefully described four small areas of this material ($2V_x$ = 90-98°) found within a highly ordered and highly potassic microcline perthite macrocrystal ∿2 cm x ∿1 cm. Five other sets of measurements from other parts of the same crystal yielded four normal sets of low microcline values and a single set that may correspond to values for an unbalanced arrangement of twins. Blasi called optically positive microclines "out-of-scheme" variants; possibly they are rare products of composite optics or have unusually highly ordered Al,Si arrangements.

It is clear that much improvement is possible in determining the relationship of $2V_x$, ($t_1o + t_1m$) and Na,K content. Many experiments in which complete optical properties, cell dimensions and composition are all determined on the same grain must be performed in order to calibrate the system. But once this is accomplished, estimates of ($t_1o + t_1m$) will become easily accessible, for example, to petrographers who might have compositions available from microprobe analyses of grains in a polished thin section. Spindle- and universal-stage techniques may yet be revived.

Effects of exsolution and strained composites on $2V_x$

The optic axial angles for each exsolved phase in a perthitic intergrowth can sometimes be measured separately with extra care (Marfunin, 1966, p. 80-82; Wright, 1964). However, as the exsolution can occur on any scale down to a few hundred Ångstroms (see Chapters 6 and 7), and because the wavelengths of visible light are at least an order of magnitude greater than that, composite optics will normally be observed. Spencer (1930, 1937) showed that heating specimens for the short times necessary to homogenize Na and K usually caused 2V to change by less than 5° (both directions observed), so it can be assumed that the effect of exsolution on 2V will be small (see also MacKenzie and Smith, 1956, p. 419-421, and Hewlett, 1959, Table 10).

As discussed in detail in Chapters 3 and 6, strained feldspars have *a* much expanded for potassic phases, and much contracted for sodic phases. The *b* and *c* dimensions are also drastically changed, being contracted for the potassic phase (see Spencer H, I, K, M, N, P, R on Fig. 6 and/or Fig. 7 on p. 83, Ch. 3) and expanded for the sodic phase. As strain increases in the potassic phase, the corresponding point on the *b-c* plot moves further away from the LM-HS side of the quadrilateral, even though the Or content of the potassic phase may be steadily *increasing*, as judged from the cell volume. The effect may yield low 2V values relative to the contours of Figure 3. The 2V angle observed for a perthite with potassic bulk composition, however, is approximately that which would be found on following the contour of equal Al,Si order for the plotted point back to the LM-HS sideline and reading the 2V contour on Figure 3. Thus a measurement of 2V by itself apparently does not indicate whether or not a potassic feldspar sample consists of cryptoperthitically unmixed, strained phases, but it does indicate approximate structural state. It is interesting that the 2V angle reported by Spencer (1930, 1937) for strained specimen M (Δa = +0.36) predicts the same ($t_1o + t_1m$) value as the *b-c* or tr[110], [110] method, but for specimen N (Δa = +0.25), whose cell volume is identical, the discrepancy is significant (∿0.10 Al; see Fig. 2). No doubt other components must be accounted for in any such scrutiny.

$2V_x$ as evidence of highest structural state

Structural evidence that the AA and HS specimens chosen as reference points for the *b-c* plot are not completely disordered was elaborated in Chapter 3. Determinative methods for structural state such as *b-c*, $\alpha^*-\gamma^*$ and tr[110],[$1\bar{1}0$] are thus based on the assumption that AA, HS and other natural and cation-exchanged members of the series have ($t_1o + t_1m$) ≅ 0.56, rather than 0.50 as previously understood. The $2V_x$ values corresponding to these are $2V_{AA}$ = 47° (O.A.P. ∿ ⊥ (010) and

$2V_{HS}$ = 46.5° (O.A.P. || (010); see Table 1). But heated Amelia albites produced 2V as low as 40° (Laves and Chaisson, 1950). Spencer A ($Or_{\sim 94}$) gave 2V = 54° after 300 hours heating at 1075°C, and 2V = 58° after an additional 24 hours at 1120-1130°C (Spencer, 1937; composition from Smith and Ribbe, 1966). A 2V of 58° corresponds to ($t_1o + t_1m$) = 0.50 on Figures 1, 2 and 3. Furthermore, Tuttle (1952) synthesized a K-feldspar with 2V = 63°, the highest value ever reported, and which may indicate the true end-member value for completely disordered Or_{100}.

EXTINCTION ANGLES

Extinction angle on (001)

In potassic feldspars the extinction angle on (001), or more specifically, X' or α' to the trace of (010) on (001), may be linearly related to the difference ($t_1o - t_1m$), but the evidence is meager. Balanced amounts of submicroscopic, polysynthetic twinning after twin laws with composition planes other than (010) may cause the average extinction angle to become zero. The (010) plane is the symmetry plane of monoclinic crystals so that their extinction on (001) must be zero, and the extinction angles on (001) of the monoclinic potassic feldspars whose structures have been determined are in fact zero.

The extinction angles on (001) of some triclinic potassic feldspars are plotted against γ* in Figure 4. If γ* is linearly dependent on ($t_1o - t_1m$) at constant composition, which seems to follow from data for analyzed potassic feldspar structures plotted on an α*-γ* plot (Chapter 3), there seems to be a simple dependence between extinction on (001) and ($t_1o - t_1m$), although the data are few indeed, and the relationship need not be linear. However, if the extinction angle on (001) of a potassic feldspar exceeds more than a few

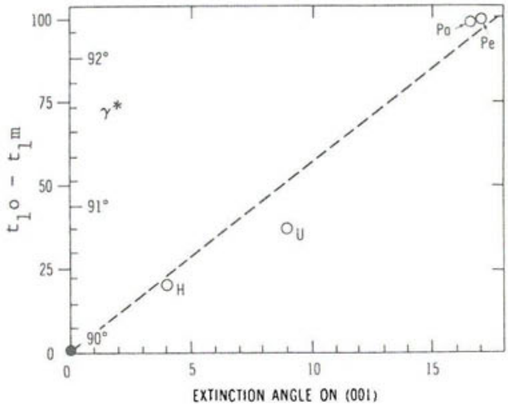

Figure 4. Extinction angle on (001) versus γ* for potassic feldspars. The difference in the Al contents of the T_1 sites, ($t_1o - t_1m$), assumes a linear dependence on γ* at constant composition (see Chapter 3 for details). Samples with $t_1o = t_1m$ plot at the solid dot. H and U are Spencer (1937) samples, Po = Pontiskalk and Pe = Pellotsalo microclines. The dashed line joining the origin and a point at γ* = 92°16.5', extinction angle = 18°, is for reference only and may not specify the nature of the variation. After Stewart (1974, Fig. 2, p. 158).

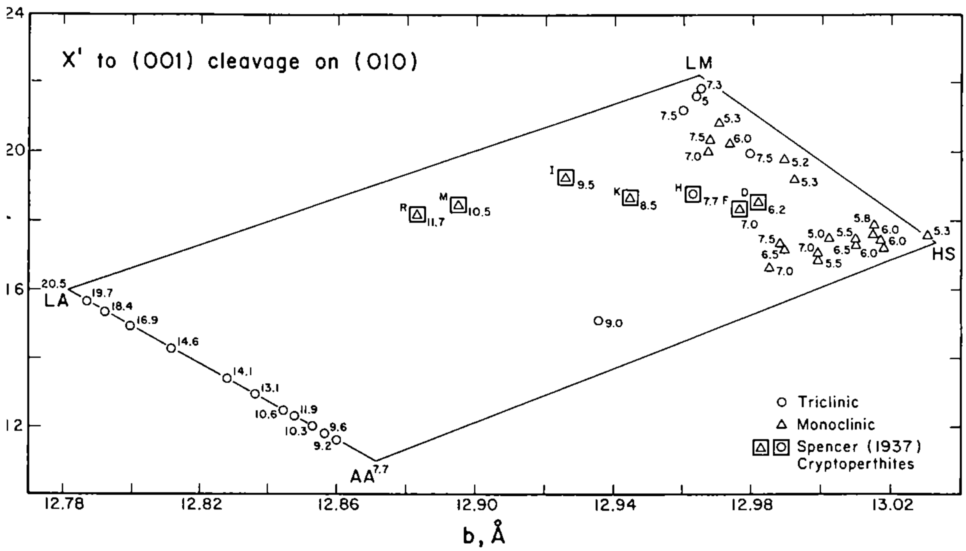

Figure 5. Extinction angles on (010) plotted on the *b*-*c* plot. Data are from sources cited by Stewart (1974), with additional data from Raase (1978) [assuming linear dependence of 2θ(131) - 2θ($1\bar{3}1$) and (t_1o + t_1m) for intermediate albites], and from Blasi (1972) and R.C. Erd (pers. comm. to DBS, 1975).

degrees (the maximum effect of assuming composite optics with exsolved sodic feldspar and a small measurement error) t_1o cannot equal t_1m, and thus t_1o is greater than t_1m.

The extinction angle of low albite on (001) is ∿3° (2.8±0.9°, Raase, 1978). Raase found the extinction angle of intermediate albites varies linearly with decreasing Al,Si order, reaching 8.1±0.9° for high albite. This variation of extinction angle on (001) is too small to provide detailed resolution of Al,Si order unless done at spindle- or universal-stage, and it seldom has been measured.

The α^*-γ^* plot cannot be contoured for extinction on (001) because there are data only for the potassic and sodic end members and these vary in opposite directions with increasing (t_1o - t_1m).

Extinction on (010)

Sufficient data for the extinction angle on (010), or more specifically, X' or α' to the trace of (001) on (010), are known for some generalizations to be made based on Figure 5. The lowest value for the extinction angle on (010) is the same (+5° to +6°) for all the usual homogeneous potassic feldspars regardless of Al,Si ordering or twinning; Blasi (1972) reported +1° to +3° for "iso-microcline". Data for intermediate albites were given by Raase (1978), who found a linear variation between low albite and high albite. No reliable data are available for series of alkali-exchanged feldspars with the same

Al,Si order.

That exsolved alkali feldspars show composite extinction angles on (010) seems to have been adequately described by Spencer (1930, pp. 304 and 341). The extinction angle is a simple additive property in proportion to the volume abundance of end members and their extinction angles. Spencer showed that high extinction angles on (010) decreased to near-normal values upon heating to homogenize alkalis. Spencer's model applies to submicroscopic cryptoperthites as well as microperthite. The strained potassic phase of cryptoperthites is shown by a different symbol in Figure 5. The extinction angle on (010) of strained feldspars increases from about 7° as they become more strained (while still highly coherent) until a value of almost 12° is attained. These more highly strained cryptoperthites also tend to have more sodic bulk compositions (Fig. 6, Chapter 3), and presumably the proportion of sodic phase is greater the higher the Ab-content of the bulk crystal. An extinction angle on (010) larger than 7° in K-rich alkali feldspar is a sensitive indicator of exsolved sodic feldspar and may also be an indicator of the magnitude of coherence between the exsolved phases in cryptoperthites. More data are needed to distinguish the effects of greater coherence or more sodic bulk composition in samples with similar proportions and size of exsolved phases.

Conclusions

The few available data allow only partial interpretation of 2V and extinction angles of alkali feldspars, and several carefully measured series of alkali exchanged feldspars would be especially valuable. However, these data do demonstrate the dependence of optic axial angle on *total* Al in T_1 sites and Or content, and the independence of 2V from the manner in which Al,Si are distributed *between* the two T_1 sites. In fact, for K-rich feldspars 2V is a fairly precise indicator of ($t_1o + t_1m$), if Figure 2 is to be believed.

The effects of twinning, exsolution, and strain on 2V are small, so that the wide range in 2V values observed in natural samples with nearly the same compositions represents a wide range of Al,Si order. Geologic evidence is abundant for a range in 2V of tens of degrees within one feldspar crystal, and of 50° or more among the crystals in a single hand specimen. This makes it unlikely that an equilibrium Al,Si distribution was attained in such materials so that a unique temperature cannot be assigned nor can a simple geologic thermal history necessarily be interpreted.

The extinction angle on (001) in potassic feldspar depends on the difference between t_1o and t_1m, but twinning effects and the small inherent range of the angle restrict application to those samples which are comparatively free of twinning. The extinction angle on (010) has value in suggesting the presence of exsolution in cryptoperthites. In pure sodium feldspar the extinction angles on both (001) and (010) vary linearly with Al,Si order.

PLAGIOCLASE

Other than direct analysis by electron microprobe techniques, refractive index measurement remains the single best method for determining the bulk composition of small plagioclase grains. However, most determinative curves in the literature have not been established under the best of experimental conditions. Ideally, individual grains should be carefully analyzed by electron microprobe after both single-crystal x-ray examination and optical property measurements have been completed. Only in this manner will it be possible to produce multiple regression curves to account for minor element concentrations and Al,Si order. Thus, although the accumulated mass of data is impressive and modern optical techniques are capable of giving 2V to a tenth of a degree and refractive indices to a few parts in the fourth decimal place, the reader is cautioned against overly zealous efforts to extract highly precise compositional or structural state information from optical measurements alone.

Graphical compilations of recent optical data of plagioclases are presented which are likely to be of greatest utility in determining bulk compositions and structural states (i.e., some relative measure of Al,Si order-disorder).

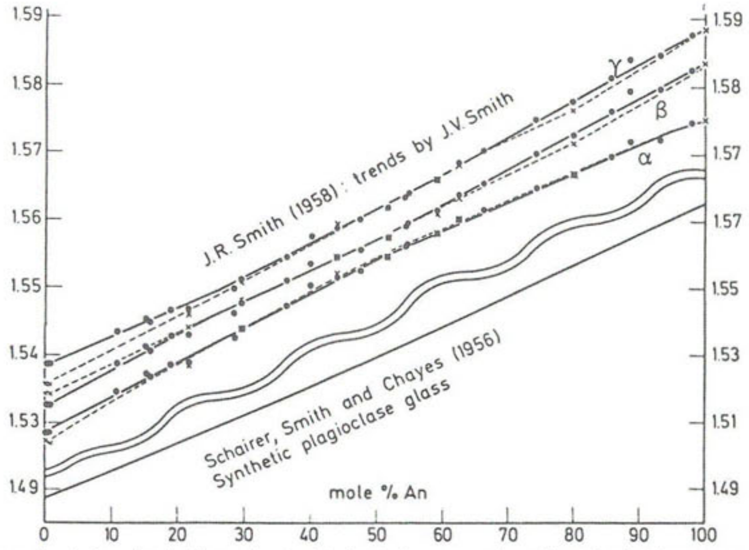

Figure 6. Refractive indices of natural plagioclase crystals and synthetic glasses as a function of composition. Solid lines are the durves for highly ordered plagioclases; dashed lines are the curves for highly disordered plagioclases. Data are represented by dots for natural and by ×'s for heated plagioclases. Note that the refractive index scale for the glasses is half that of the crystals (Emmons *et al.*, 1960). Adapted from Smith (1974a, Fig. 8-14, p. 397).

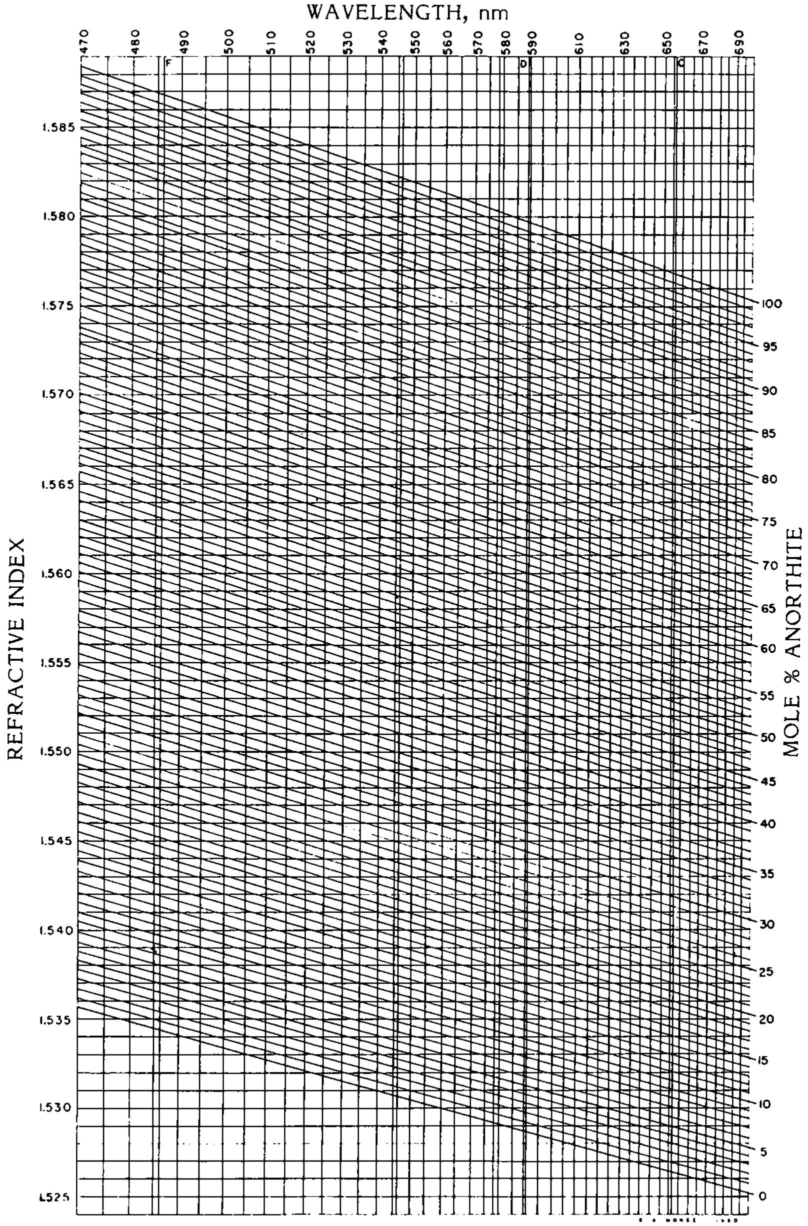

Figure 7. Low plagioclase dispersion chart for the refractive index α' on (001) cleavage flakes. Tsuboi (1934) curves modified by Morse (1968, Fig. 3, p. 110), using data from J.R. Smith (in Hess, 1960), and tested by Morse (1978).

We forego an historical review in deference to that by Smith (1974a, pp. 391-405), and refer the reader for details to Marfunin (1966)[3] and especially the exhaustive treatise on plagioclase optics by Burri *et al.* (1967).

Refractive indices

The simplest methods for determining plagioclase composition are those based on refractive indices, and in particular, on the α or α' index. It was shown by J.R. Smith (1958) that α varies insignificantly with structural state, although in the range An_0 to An_{15} there may be a small effect of Al,Si order-disorder leading to a maximum error of 2% An (see Fig. 6). This error is within the range of anticipated accumulated errors due to minor chemical components (K, Sr, Ba, Fe, Ti, P, etc.), microscopic or submicroscopic textural features (if any), zoning, and measurement. For routine composition determination, refractive index precision of ±0.001 (the equivalent of ±2% An) is in line with the present determinative curves.

To attain precision of ±2% An in composition, one may forego the spindle- or universal-stage and use the Tsuboi (1934; revised by Tsuboi *et al.*, 1977) method of measuring the lower value of the α' index directly on (001) or (010) cleavage fragments. Morse (1968, 1978) refined Tsuboi's technique, and Figure 7 contains calibration curves for α' measured on (001) cleavage fragments. This method takes advantage of the dispersion of Cargille index oils with wavelength of the incident light, and thus it requires a monochromator or interference filter as well as temperature control. The following regression equations are useful to determine plagioclase compositions using α' measured on (001) [$\equiv n$]:

RANGE, mol % An	EQUATION (Morse, 1978, p. 769)
0-24	$An = 1936(n - 1.5287)$
24-31	$An = 1790(n - 1.5277)$
31-84	$An = 1944(n - 1.5290)$
84-100	$An = 2133(n - 1.5328)$

Ultimately the spindle stage may be the easiest and most useful method for measurement of the optical properties of individual plagioclase grains, especially if, in addition to an estimate of composition, 2V, dispersion of birefringence and optic axes, and Euler angles are desired [see Bloss (1981), in which measurements of certain feldspar optical properties -- some at elevated temperatures -- are described in detail].

----

[3]Corrections to Marfunin's optical orientation diagram are in Macek (1975).

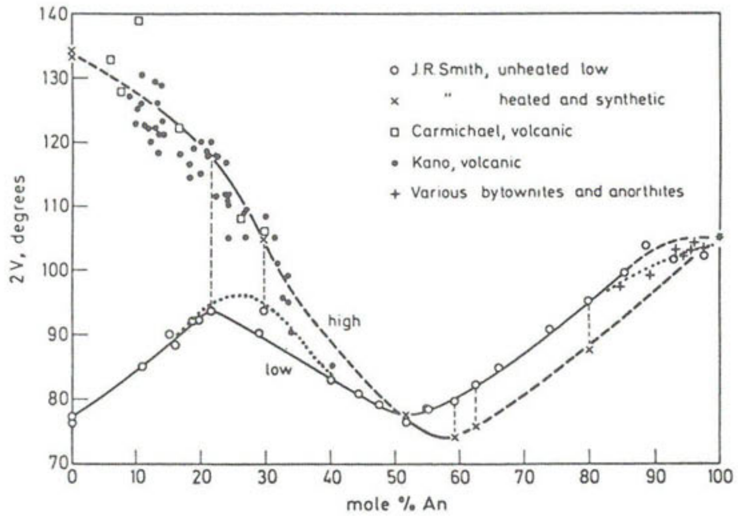

Figure 8. Optic axial angle 2V as a function of plagioclase composition for high (dashed line) and low (solid line) structural states. Data compiled by Smith (1974a, Fig. 8-13, p. 395); dotted line fits 2V data by Wolfe (1976) based on microprobe analyses of the same grains by Ribbe (unpublished).

Optic axial angle, $2V_x$

Selected 2V curves for low and high structural states of plagioclases are shown in Figure 8. There is a clear distinction between 2V for ordered and disordered plagioclases in the range An_0-An_{25}. The curves cross near An_{50} and then are separated by ∿8° in the range An_{69}-An_{85}, becoming essentially indistinguishable for anorthite. For the LA-AA series, 2V is almost linearly related to the angular separation of the 131 and $1\bar{3}1$ peaks in an x-ray powder pattern (Raase and Kern, 1969), and $\Delta 2\theta$ ($\equiv 2\theta_{131} - 2\theta_{1\bar{3}1}$) is linearly related to ($t_1o - t_1m$) (see Chapter 4). Thus there is a nearly linear relationship between 2V and the difference in Al contents of T_1O and T_1m. This relationship apparently does not carry over into the more calcic plagioclases.

Optic axial angles measured on feldspars consisting of submicroscopically exsolved phases, be they plagioclases (peristerite, Bøggild or Huttenlocher intergrowths -- see Chapter 10) or cryptoperthitic alkali feldspars, are volume-weighted averages of the 2V values of the individual phases present, with some as yet unquantified effects due to coherency strain. Refractive indices of such composite materials are also average values and are thus useful for determining *bulk* compositions.

Optic orientation and extinction angles

A skilled microscopist can determine rather precisely the orientation of the optic axes relative to the crystallographic axes of plagioclase using spindle- or universal-stage methods. Migration curves are available over the entire composition range for both low and high structural states (Burri *et al.*, 1967, Plate VI). However, the precision of determining composition and structural state is no better than that achieved by the simpler methods described above. Of course, this technique is particularly useful with feldspars in thin section. Extinction angles are even more easily measured, but they yield less precise information.

Extinction angles may be measured to (010) and (001) cleavages, to a wide variety of twin composition planes, or rarely to crystal faces. The primary uncertainties in determining composition are (1) the positive identification of the cleavage, twin or face, (2) the deviation of these planes from vertical in the thin section, (3) zoning, (4) effects of structural state for a given composition, and (5) errors in the determinative diagrams themselves. More than one morphological feature is commonly visible in a grain, and this reduces the chances of misidentification of the plane; the other problems may be considered to be relatively minor, but precision of the composition determination probably will not exceed ±5 mol % An. Universal-stage methods can simultaneously yield twin laws, structural state and composition, but the precision will probably not exceed ±2 mol % An.

In the Michel-Lévy (1877) method the extinction angle between the fast ray and the trace of vertical (010) cleavage or twin planes is measured in thin section (Fig. 9). Only the maximum value is used to determine plagioclase composition, and Glazner (1980, p. 1051) found that "ten measurements give a high probability of being within 5 mol % of the true composition, and [that] the bias in the calculated composition is small." Heinrich (1965, Fig. 12.38, p. 364) presented a frequently useful curve for the variation in the extinction of microlite elongation with plagioclase composition. Other extinction angle curves are available in many standard references (Winchell and Winchell, 1951; Burri *et al.*, 1967; Bambauer *et al.*, 1979; Phillips and Griffen, 1981); the two reproduced in Figure 10 are from Deer *et al.* (1963, Vol. IV).

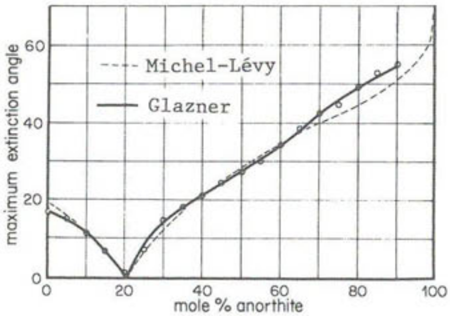

Figure 9. Comparison of the curve plotting maximum extinction angle versus composition determined by Glazner (1980, Fig. 2) with the Michel-Lévy curve taken from Heinrich (1965, p. 364).

Figure 10. (a) Extinction angles to α' on plagioclase cleavage fragments parallel to (001) and (010); specific gravity, D, shown in lower half. (b) Extinction angles with respect to α' in the so-called "symmetrical zone" and in sections normal to [100]. After Deer *et al.* (1963, Vol. IV, pp. 137-8; by permission of Longmans).

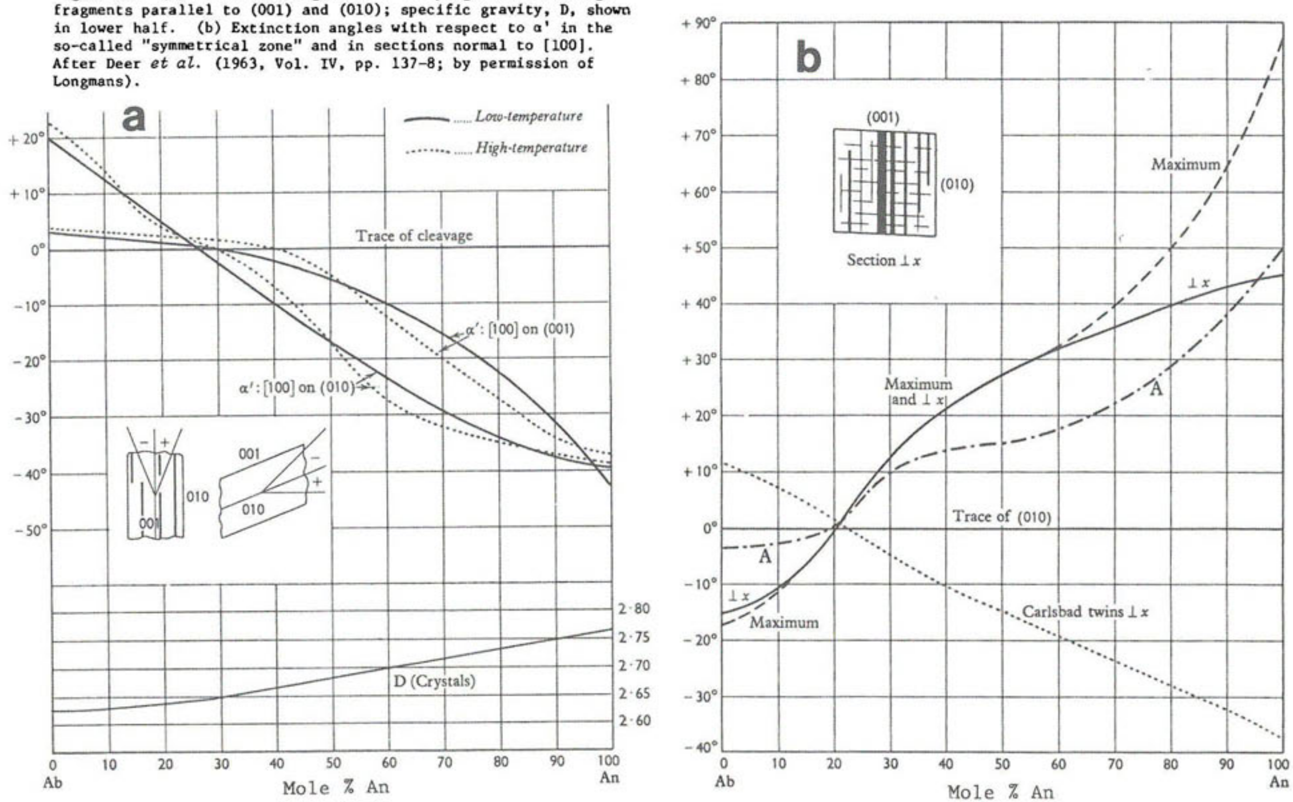

Chapter 6

SUBSOLIDUS PHASE RELATIONS in the ALKALI FELDSPARS with EMPHASIS on COHERENT PHASES

R. A. Yund & J. Tullis

INTRODUCTION

The subsolidus transformations in the alkali feldspars can be divided into (1) a displacive transformation between analbite and monalbite, (2) Al/Si order-disorder relations in both the sodic and potassic phases, and (3) exsolution or phase separation within the miscibility gap. The structural changes associated with the first two transformations have been described in the previous chapters. The emphasis in this chapter is on the compositional relations of the coexisting phases within the miscibility gap. These relations depend on how the two-phase intergrowth forms and on the nature of its interface, i.e., whether the phases are structurally coherent or not. The concept and results of coherency are treated in some detail, and because of the importance of crystal elasticity to an understanding of coherency, an Appendix is included which briefly reviews the concepts of crystal eleasticity and discusses the elastic constants for feldspars and their relation to the feldspar crystal structure. The chapter can be read independently of the Appendix, but readers unfamiliar with crystal elasticity will gain a much better appreciation and understanding of coherent phase relations by reading it.

DISPLACIVE AND ORDER-DISORDER RELATIONS

Determination of the subsolidus phase relations in the alkali feldspars is severely limited by the kinetics of most of the transformations. Diffusion of Al and Si is extremely slow (see Chapters 1 and 2) and demonstration of the stable distribution of these ions in the tetrahedral sites under experimental conditions has been mostly unsuccessful. The alkali ions diffuse more rapidly, but the migration of even these ions is slow on the scale of microns and determination of the strain-free solvus is difficult. Thus any attempt to construct a phase diagram must be based partially on naturally occurring phases, unproven assumptions, and educated guesses. Nevertheless, there is qualitative agreement on several points, and certain quantitative agreement is emerging.

Recently, Kroll *et al.* (1980) summarized the results and the remaining problems about the displacive and diffusive transformations of Na-rich

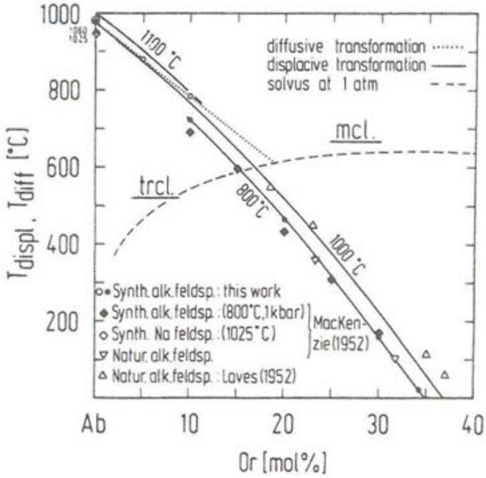

Figure 1. Stable phase boundary of the diffusive transformation high albite ⇄ monalbite (········) and metastable phase boundaries of the displacive transformation analbite ⇄ monalbite (————) drawn for three equilibration temperatures (800°, 1000°, 1100°C). The temperatures of the displacive transformation are given by the regression equation

$$T_{displ} = 715 - 18.9 \cdot Or - 0.221 \cdot Or^2 + 0.269 \cdot T_{equil},$$

where Or is mol % K-feldspar. The temperature of the diffusive transformation follows a straight line (see equation in text), which meets the one atmosphere solvus of Thompson and Waldbaum (1969) at ~600°C and $Or_{\sim 20}$. From Kroll *et al.* (1980).

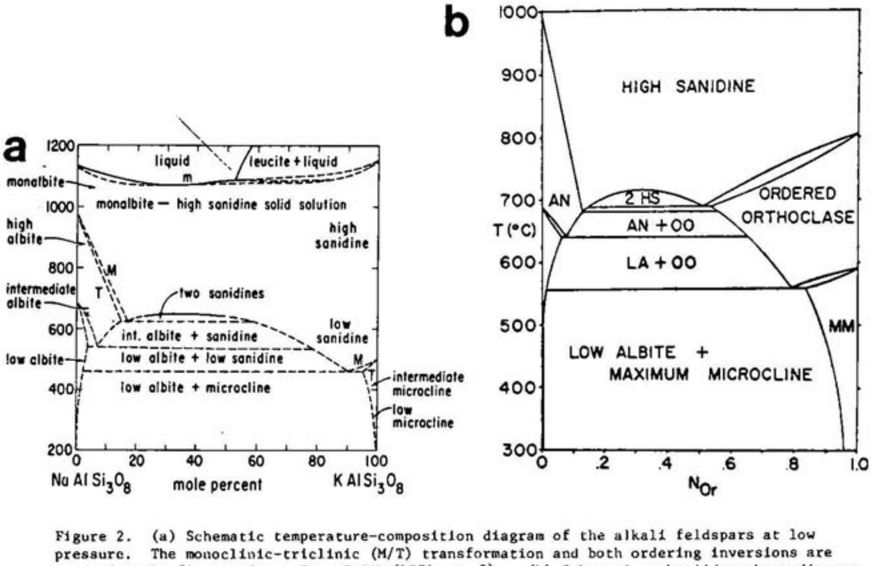

Figure 2. (a) Schematic temperature-composition diagram of the alkali feldspars at low pressure. The monoclinic-triclinic (M/T) transformation and both ordering inversions are assumed to be first order. From Smith (1974a, p. 2). (b) Schematic subsolidus phase diagram for alkali feldspars at approximately 5 kbar. AN is for *anorthoclase*; high albite is considered a special case of anorthoclase. From Martin (1974a).

alkali feldspars. Their partial subsolidus phase diagram and the hypothetical diagrams of Smith (1974a, p. 2) and Martin (1974a) are presented in Figures 1, 2a and 2b. These show some of the major features of agreement and disagreement. The relations shown in these diagrams are briefly summarized below.

Monalbite - analbite

Just below the melting temperature the stable Na-feldspar is monalbite. It is isostructural with high sanidine. Its Al,Si distribution is nearly disordered ($t_1 \gtrsim t_2$), and the topochemical and actual symmetry are monoclinic (*C2/m*). When monalbite is rapidly quenched, it undergoes a displacive transformation to triclinic analbite ($C\bar{1}$), caused by the puckering of the tetrahedral framework around the Na ions when their thermal vibration can no longer expand the structure to be monoclinic. Because analbite is topochemically monoclinic, but metrically triclinic, it is unstable at any temperature. The structural changes accompanying the transformation involve only slight changes in bond lengths and angles.

The temperature of the displacive transformation T_{displ} is strongly dependent on the Or content. Increasing substitution of K for Na lowers T_{displ}, such that at approximately Or_{35} the transformation occurs at room temperature. To some extent T_{displ} also depends on the temperature of equilibration T_{equil}, i.e., on the degree of Al,Si order attained at T_{equil} and measured by the difference $t_1 - t_2$ (Hovis, 1980; Kroll *et al.*, 1980). It is seen from Figure 1 that the higher T_{equil}, the higher T_{displ} and the more K-rich the inversion composition (Or_{displ}) at room temperature. Kroll *et al.* (1980) give the following equations which relate T_{displ} to T_{equil} and Or content, and Or_{displ} to T_{equil}:

$$T_{displ}[°C] = 715 - 18.9 \cdot Or - 0.221 \cdot Or^2 + 0.269 \cdot T_{equil},$$

$$Or_{displ}[mol\ \%] = 27.5 + 0.00842 \cdot T_{equil}\ .$$

The most interesting application of these equations to natural feldspars would be to determine Or_{displ} and/or T_{displ} and then to find T_{equil}. It should be kept in mind, however, that "T_{equil}" determined in this way often represents some uncharacteristic temperature at which Al/Si ordering froze in during the cooling process of the host rock. Nevertheless, applying equations similar to those given above yielded reasonable temperatures T_{equil} for three Na-K exchange series.

On slow cooling monalbite inverts to albite by a diffusive transformation at T_{diff} = 978°C (Kroll *et al.*, 1980). Albite is topochemically and metrically triclinic, i.e., $t_1O \neq t_1m$ in space group $C\bar{1}$. It is stable at temperatures below $T_{diff.}$ The nearly or fully ordered form of albite ($t_1O \approx 1$, $t_1m \approx t_2O \approx t_2m \approx 0$) is termed low albite, and less ordered forms ($0.28 < t_1O < 1$, see Figure 8 in Chapter 2) are termed high or intermediate albite. With increasing substitution of K for Na the temperature of the diffusive transformation is lowered according to the equation (Kroll *et al.*, 1980):

$$T_{diff}[°C] = 978 - 19.2\ Or[mol\ \%]$$

as shown by the dotted line in Figure 1.

Stability of ordered phases

Slightly below solidus temperatures, the stable alkali feldspar structure is monoclinic with Al and Si almost randomly distributed over the tetrahedral sites. At lower temperature an ordered or partially ordered arrangement is formed. The evidence for a completely ordered state is clear from natural specimens. The problems lie in determining the exact nature of the ordering scheme, the stability of partially ordered states, the stability of monoclinic potassic feldspar with all the aluminum in T_1 ("ordered" orthoclase?), and the temperature-composition relations of the stable states (see Chapter 2).

The diagrams shown in Figures 2a and 2b are superseded by Figure 1 with respect to the position of the diffusive transformation (K-) monalbite-(K-) high albite. Figures 2a and 2b both assume that there is a single, first-order transformation between partially ordered high or intermediate albite (labeled anorthoclase, AN, on Fig. 2b) and ordered low albite. The temperature of this transformation in pure Na-feldspar (~680°C) is based on experimental data (Raase, 1971; Mason, 1979); the transformation temperature on the solvus is largely speculative, as is the choice of its order. Senderov (1980) discusses this point in detail on the basis of quasi-chemical theories of order/disorder transformations.

On the potassic side the diagrams show two different possibilities. Figure 2a shows a single transformation analogous to that for the sodic phases, but at lower temperature. Figure 2b assumes that an 'ordered' orthoclase is stable at intermediate temperatures, but the stability and even the existence of this structure is questionable (see Chapter 1). The original sources for these diagrams should be consulted for a discussion of the data and inferences on which these relations are based.

STRAIN-FREE SOLVUS

The compositional relations of the sodic and potassic phases in perthites depend on whether the phases are coherent or not. If the perthitic phases are non-coherent, or if the rock consists of separate grains of sodic and potassic feldspar, their equilibrium compositions are given by the *strain-free* or *equilibrium solvus*. This is the solvus which has been studied extensively in the past. Whenever the term *solvus* is used alone, it is understood to mean the strain-free solvus. The compositional relations between coherent phases are discussed in a later section and the concept of a coherent solvus for these phases will be presented.

Sanidine - high albite

Experimental data for the sanidine-high albite solvus are available from a number of studies including those of Orville (1963), Luth and Tuttle (1966), Morse (1970), Seck (1972), Luth *et al.* (1974), Goldsmith and Newton (1974), and Smith and Parsons (1974). Thompson (1967) and Thompson and Waldbaum (1969a,b) have developed a useful technique for smoothing the experimental data as well as for extrapolating the data to other temperatures and pressures.

There are several major problems concerning the location of the strain-free solvus for sanidine-high albite. In addition to the major problem of achieving and demonstrating equilibrium in the experiments, other errors and sources of uncertainty include differences in the x-ray determinative curves, the effect of Al-Si ordering, and possible nonstoichiometry of the phases.

Luth and Tuttle (1966) first proposed different solvi depending on whether the starting material for the experiments is synthesized from bulk compositions on the $NaAlSi_3O_8$-$KAlSi_3O_8$ join, with excess alkali silicate (*peralkaline*), or with excess alumina (*peraluminous*). Luth and Fenn (1973) corrected Luth and Tuttle's original compositions, and concluded that the differences between these solvi are real and significant. Figure 3a shows the differences between the peralkaline (curve 1), the peraluminous (curve 2),

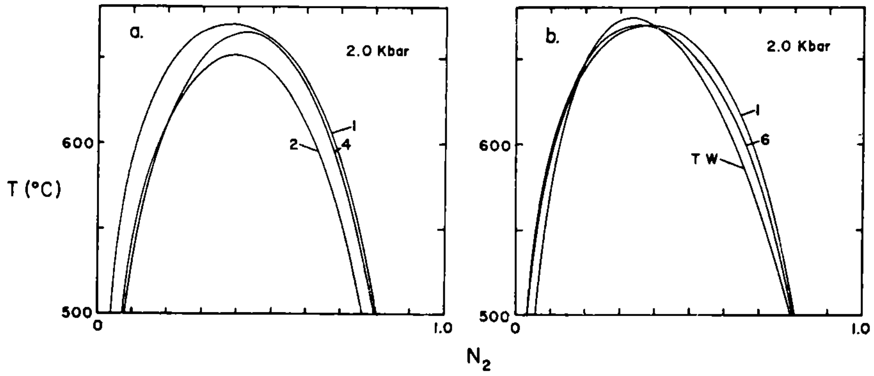

Figure 3. (a) Comparison of solvi for peralkaline (1), peraluminous (2), and stoichiometric (4) starting materials. (b) Comparison of (1) above with Orville's (1963) data (6) as selected by Thompson and Waldbaum (1969b) and their original solvus (TW) based in part on Luth and Tuttle's (1966) uncorrected data. From Luth and Fenn (1974).

and the stoichiometric (curve 4) solvi. All three are based on Orville's (1967) x-ray determinative curve. (See Luth and Fenn (1973) for the positions of these solvi using different determinative curves.) In contrast, Goldsmith and Newton (1974) and Smith and Parsons (1974) have concluded that compositional factors do not noticeably affect the equilibrium position of the solvus, although they do affect the rate of attainment of equilibrium. Equilibrium is achieved faster with peralkaline than with peraluminous starting materials.

Luth *et al.* (1974) and Martin (1974b) have reported a discontinuity in the solvus between 475° and 525°C at 2.5 kbar. The position of this break as a function of pressure is shown on Figure 4. They attribute this break to a first-order phase change in the potassic phase. Martin interprets this as a metastable manifestation of the first-order transformation between "ordered orthoclase" and maximum microcline (Fig. 2). However, Goldsmith and Newton (1974) and Smith and Parsons (1974) have not observed a discontinuity in the solvus in their experiments. Goldsmith and Newton's data at 15 kbar are shown in Figure 5. The arrows indicate the direction of the reaction, and the open circles define a calculated solvus based largely on Orville's (1963) data with selected points from Luth and Tuttle's (1966) corrected data for peralkaline starting material.

Smith and Parsons (1974) have recently completed a study of the alkali feldspar solvus at 1 kbar. They gave particular attention to approaching the solvus from both directions. Their preferred solvus is shown by the solid line in Figure 6, along with the data from previous studies.

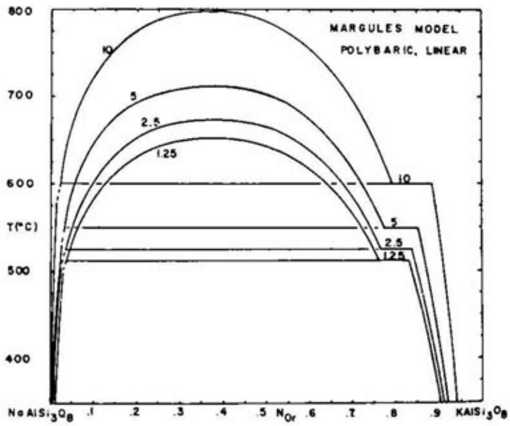

Figure 4. Polybaric solvi based on preferred high- and low-temperature data sets. Pressure in kilobars is shown on each curve. Data from Luth *et al.* (1974) and figure from Luth (1974).

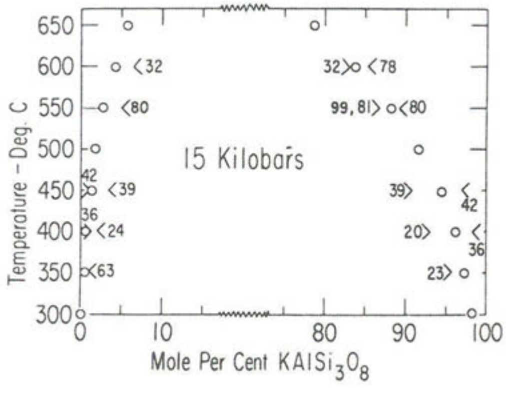

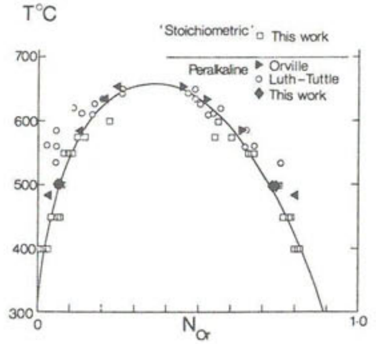

Figure 5 [left]. The strain-free solvus for sanidine-high albite at 15 kbar. The direction of the arrows indicates the direction of the reaction and brackets the solvus. Open circles are calculated points based on Orville's (1963) data and selected data from Luth and Fenn (1974). From Goldsmith and Newton (1974).

Figure 6 [right]. The smoothed solvus (solid curve) at one kilobar based on Smith and Parson's (1974) data which are indicated by "this work." Data from previous studies are indicated by the symbols. All two kilobar data have been adjusted down by 16°C/kbar. Apices of triangles show change in solid composition with time in Orville's (1963) experiments. From Smith and Parsons (1974).

Thompson and Waldbaum (1969b) used selected data from Orville (1963) and the peralkaline data from Luth and Tuttle (1966) to calculate a solvus and the effect of pressure on this solvus. They included the effects of the displacive monoclinic-triclinic transformation. Their solvus has been widely used, but it should be recognized that it is based partially on Luth and Tuttle's original data.

The Thompson-Waldbaum solvus (TW) is shown in Figure 3b together with the solvus based on selected data from Orville (curve 6) and the one based on Luth and Tuttle's corrected peralkaline data (curve 1). Note that curves (1) and (6) both lie outside the Thompson-Waldbaum solvus on the potassic limb. Although the Thompson-Waldbaum solvus is not shown in Figure 6, Smith and Parsons' solvus agrees with it to within two mole percent except below 600°C on the potassic limb. At 400°C, the Smith-Parsons solvus lies about 10 mole percent *inside* the Thompson-Waldbaum solvus.

The bewildering number of solvi is disconcerting; however, the agreement on the position of the solvus is improving, and the principal uncertainty is in the lower temperature portion of the potassic limb. For the purpose of later discussions we will assume that these solvi approximate a stable equilibrium solvus which is applicable to naturally occurring, disordered alkali feldspars. The original Thompson-Waldbaum solvus or the new solvus of Smith and Parsons will be used for comparison with the coherent solvus for high sanidine-high albite in later discussions.

Low or maximum microcline - low albite

The position of the alkali feldspar solvus is dependent on the structural state of the phases. Although the maximum microcline-low albite solvus is only stable below approximately 500° to 600°C (Figs. 1 and 2), the disordering rate is so very slow that the higher temperature metastable extension of this solvus can be determined experimentally. This was done independently, but reported on jointly, by Bachinski and Müller (1971). They used alkali-exchanged maximum microcline and low albite as starting materials. Their calculated solvi are based on experiments only above 650°C, i.e., presumably in the temperature range where this solvus is metastable.

Luth *et al.* (1974) used gels as starting materials and their experiments were done between 295° and 500°C and 1.25 to 10 kbar. The potassic phase in their experiments did not have a low structural state, but the agreement with Bachinski and Müller's data is surprisingly good.

The strain-free maximum microcline-low albite solvus which will be used in later discussions is based on Bachinski's 22 data points at one atmosphere. The coordinates of this solvus are listed in Table 9 of Bachinski and Müller (1971), and this solvus is shown in a later figure (Fig. 14).

COHERENT EXSOLUTION

Introduction

Subsolidus exsolution in the alkali feldspars produces perthites, which may occur with a number of different textures and on a wide range of scales. Lamellar exsolution is one of the common textures, and the width of exsolution lamellae varies from submicroscopic to several millimeters. The most useful classification scheme for perthites was proposed by Laves and Soldatos (1963). They suggest the term *cryptoperthite* for any perthite with submicroscopic lamellae, and *micro-* or *macroperthite* for optically visible perthites. The distinction between submicroscopic and coarser perthites is especially important because it roughly corresponds to the difference between *coherent* or *semicoherent* and *noncoherent* perthites, respectively. Further classification of perthites can be made on the basis of bulk composition, structural state or crystallography of the phases, or their microstructure. The reader should consult Smith (1974b, pp. 399-519) for a comprehensive review of perthite nomenclature and its significance.

The existence of coherent exsolution in the feldspars was first recognized by Laves (1952), who observed the structural relations between the potassic and sodic lamellae in cryptoperthites and demonstrated that their structures were continuous across the lamellar interface. In this section we will examine the nature of this coherency, describe how coherency can be recognized, and then consider the implications of this coherency for the orientation and compositions of the exsolved lamellae.

Coherent exsolution involves elastic stresses and strains in the phases, and thus an understanding of coherency and its effects requires an understanding of crystal elasticity. An Appendix to this chapter briefly reviews the concepts of crystal elasticity, as well as the elastic constants for feldspars and their relation to the feldspar crystal structure. The Appendix should be consulted for a more detailed understanding of the quantitative aspects of coherency.

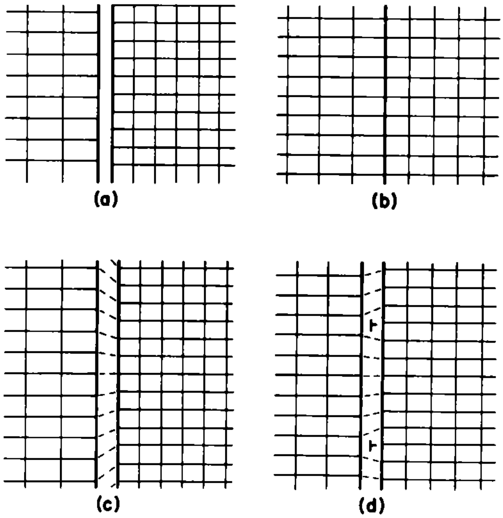

Figure 7. Schematic illustration of noncoherent, coherent, and semicoherent boundaries. (a) Two lattices of different spacing because of compositional difference. If pushed together they would form a *noncoherent* boundary. (b) Same lattices (phases) as in (a) but joined with perfect *coherency* and homogeneous strain. (c) Impossible way to achieve coherency. (d) *Semicoherent* boundary with dislocations: the strain is inhomogeneous in the interface region.

Coherent exsolution lamellae

Exsolution involving phases of like or similar structures often occurs by a mechanism which leaves the structure unchanged and continuous across a lamellar interface. In the alkali feldspars, the $AlSi_3O_8$ tetrahedral framework remains unchanged except for a slight adjustment of bond lengths and angles due to the redistribution of the alkali ions.

The compositional difference between the sodic and potassic phases causes a difference in the spacing of their lattice planes. This situation is shown schematically in Figure 7a. If the two halves of the diagram are brought together there results a two-dimensional analog of a grain boundary. (In this diagram the relations along a direction normal to the page are similar to those along the vertical direction.) A few of the lattice planes may match across the boundary, but for the most part there is no continuity of lattice planes from one grain to another. (For a normal grain boundary, it is unnecessary and unlikely for the vertical planes to be parallel on either side.) The situation shown in Figure 7a may be described as a *noncoherent* boundary or interface.

In contrast, a perfectly *coherent* boundary between two phases is shown in Figure 7b. Here the horizontal lattice planes are continuous across the interface. All other lattice planes would also be continuous and those not normal or parallel to the boundary are bent at the interface. Cryptoperthites commonly occur as lamellae whose thicknesses are small compared to their other dimensions. The condition of coherency at the lamellar boundaries requires an adjustment of the lattice spacings in the two phases. The horizontal lattice planes on the left of the interface in Figure 7b must be elastically compressed somewhat, and those on the right stretched, to achieve this condition of perfect coherency. The spacing of the horizontal planes will be a compromise between those for the two phases in their unstrained state (Fig. 7a). This matching of the lattice spacings imposes elastic strain within the coherency planes, but the spacings of all other lattice planes, including those parallel to the lamellar boundaries, will also be different from their unstrained values. They will adjust so as to minimize the elastic strain energy, in a way that can be determined exactly from a knowledge of the coherency strains and the elastic constants (see discussion below).

Is this the only way of achieving coherency between the lamellae? Is it possible, for example, for the horizontal planes to maintain their unstrained spacings in most of the volume of the lamellae but to achieve continuity by bending in the interface region? Figure 7c shows that the amount of tilting (or warping) becomes progressively greater on either side of a perfectly matching horizontal plane, such as that at the center, and the amount of distortion becomes very large until planes nearly in line with one another are not connected. It does not matter whether this distortion is shown as tilting or warping of the planes, or whether the width of the interface region accommodating the distortion is increased. The situation shown in this drawing is untenable unless the lamellae partially lose coherency or all dimensions of the exsolved phase are small. The latter situation does not exist in most cryptoperthites because the exsolved phase has a lamellar shape. Thus, perfectly coherent lamellae of the same symmetry must have homogeneous strain and the lattice spacings in each phase must be constant. This condition is relaxed somewhat if the lamellae are only partially coherent, if one phase is monoclinic and the other triclinic and twinned (e.g., Tatekawa, 1975), or for very small and more equi-dimensional particles.

The situation for partial coherency is shown in Figure 7d. There are more horizontal planes on the right-hand side of the interface than on the left. Each of these additional planes is equivalent to an edge dislocation as indicated by the symbols. With the addition of dislocations, some bending of other planes will occur, and this situation is generally referred to as a *semicoherent* boundary. The strain is inhomogeneous compared to the homogeneous strain for the perfectly coherent boundary shown in Figure 7b. Brown and Willaime (1974) discuss coherency strain and use a model based on edge dislocations to calculate how the strain decreases away from a boundary. They use the results to discuss the situation for "total coherency" and mention that "the strain will extend further (from the boundary) than if coherency is partial" (pp. 448-449). However, as noted above, total coherency of untwinned lamellae of the same symmetry *requires* homogeneous strain.

Identification of coherent lamellae

Cryptoperthites with coherent lamellae can be recognized by observing the spacings of lattice planes normal to the lamellae. Figure 8 is a schematic illustration of the situation for alkali feldspar. For simplicity we will assume that the lamellae are parallel to (100); i.e., parallel to b and c and normal to a^*. If the lamellae are coherent, $(0k0)$ planes (horizontal on Fig. 8b) and (00ℓ) planes will have the same spacing in both phases. On an $hk0$ level x-ray precession photograph, the $0k0$ reflections will be single and sharp since the spacing and orientation of these planes is the same in both the potassic and sodic lamellae. This is shown in Figure 9, which is a sketch of a portion of such a diffraction pattern for a cryptoperthite. Any plane normal to the interface will give a single sharp reflection. Reflections for the two phases from planes not normal to the interface show some separation, and this separation will be greatest for planes approximately parallel to the interface. Thus, the $h00$ reflections on Figure 9 are doubled and the direction of the doubling is approximately normal to (100). For a pair of $h00$ reflections, the one with the largest reciprocal lattice spacing (smallest direct lattice spacing) corresponds to the sodic phase and the other one corresponds to the potassic phase. The reader should correlate the features shown in Figure 8b with the diffraction pattern in Figure 9, realizing that a 90° rotation of one of the figures will bring the two into proper crystallographic orientation.

X-ray or electron diffraction patterns of single crystals provides a direct method for determining whether the lamellae are coherent. However, coherency is also indicated by 'anomalous' cell dimensions (see Chapter 3), and perhaps the most sensitive measure of the degree of coherency is to determine the bulk composition and homogenization temperature of a cryptoperthite. We will return to these questions in subsequent sections.

Orientation of the lamellae

It should be clear from the above discussion that not only can the condition of coherency be recognized, but the orientation of the lamellae can be determined from several photographs which represent different sections through the reciprocal lattice. Laves (1952) used this method to determine that the lamellae in cryptoperthites are approximately parallel to ($\bar{6}01$). This agrees with the orientation reported for coarser perthites whose orientation can be determined optically. Transmission electron microscopy (TEM) also provides a convenient method for determining the orientation of very fine lamellae. Recent TEM results report orientations near ($\bar{8}01$) and ($\overline{10}\cdot 0\cdot 1$). The latter plane makes an angle of six degrees with (100); thus, the approximation shown in Figure 8 is reasonable.

Why do the lamellae have this particular orientation? The answer lies in the elastic strain energy associated with the coherency. In order for the total free energy of a crystal to be minimized both the Gibbs (or chemical) energy and the elastic strain energy must be a minimum, and the magnitude of the strain energy term depends on the orientation of the lamellae.

The expression for the elastic strain energy (see Appendix) involves two terms, both of which vary with crystal direction: the elastic compliances, and the elastic coherency strains. The latter term is squared, and thus is dominant. The elastic coherency strains arise from the change in lattice dimensions as a function of composition. For example, the change in b or c is about one percent between pure $KAlSi_3O_8$ and $NaAlSi_3O_8$, but the change in a^* is about five percent. If the lamellae are parallel to (100), which includes b and c (Fig. 8), the amount of strain required for coherency will be less than if the lamellae are parallel to (010) or any plane approximately parallel to a^*. Thus the lamellae will tend to seek out that orientation which results in the minimum elastic strains within the coherency plane. It should be remembered that lattice planes parallel to the interface, in this case approximately (100), will also adjust their spacing to minimize the strain energy associated with the coherency. In the section below, we will consider the consequences of this for determining the compositions of the lamellae.

In the above example, the prediction of the approximate orientation of the lamellae was simple because of the large difference in the compositional strain between a^* and the mutually perpendicular directions of b and c. However, some other orientation near (100) may actually provide a better

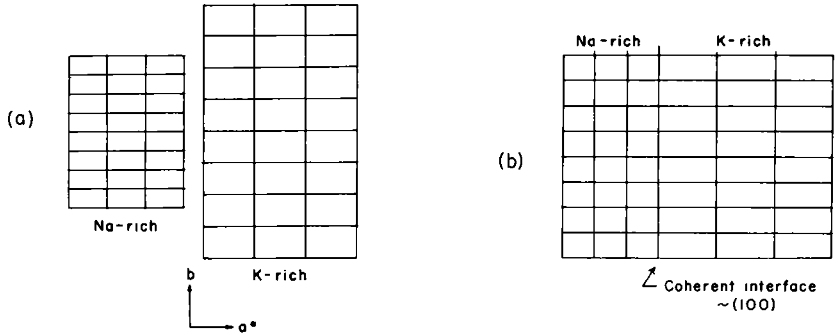

Figure 8. (a) Schematic representation of the lattices for unstressed sodic and potassic-rich lamellae. (b) Same for coherent lamellae assumed parallel to (100). From Yund (1974).

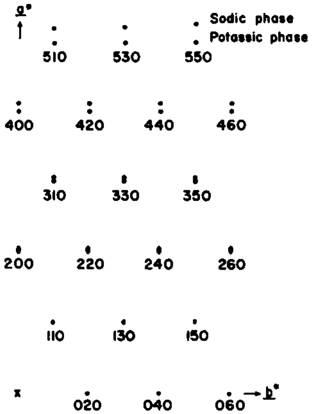

Figure 9. Schematic representation of a portion of an *hk*0 level x-ray precession photograph of a coherent cryptoperthite as shown in Figure 8b. The vertical separation of the reflections is due to the compositional difference of the lamellae and the direction of separation is normal to the trace of the lamellar interface. The precession photo should be rotated 90° relative to Figure 8b to bring it into proper crystallographic orientation. The symmetry of both phases is *C*2/*m*.

fit and hence a lower strain (and strain energy). Also, the difficulty of predicting even the approximate orientation of coherent lamellae becomes more complex if the strains parallel to three nearly perpendicular lattice directions are approximately equal. In order to determine the plane of minimum compositional strain exactly, one must calculate the compositional strain ellipsoid for the crystal. A coherent interface parallel to the minor and intermediate axes of the strain ellipsoid will produce the minimum elastic strain in the crystal. Brown and Willaime (1974), Willaime and Brown (1974), and Ohashi and Finger (1973) have made this calculation for alkali feldspars. The orientation of the plane of least strain depends somewhat on the compositions of the lamellae; it is near ($\bar{6}01$) when the potassic phase is monoclinic, and ($\overline{66}1$) when it is triclinic. Willaime and

and Brown (1974) have made similar calculations for the plagioclases in an attempt to predict the orientations of peristerite, Bøggild, and Huttenlocher lamellae. Olsen (1979) has extended their calculations to include the effects of K substitution, and Fleet (1981) has used similar considerations to predict the orientations of the modulations responsible for '*e*' reflections in plagioclase (see Chapters 2 and 9).

The second term in the expression for elastic strain energy is the elastic anisotropy of the crystal which is expressed in terms of its elastic constants. The force necessary to elastically compress or stretch a crystal varies with direction (see Appendix). If the plane of minimum compositional strain should happen to be parallel to the most compliant directions of the crystal, this would be optimum for minimizing the elastic strain energy. If, on the other hand, it were parallel to the stiffest directions in the crystal, some adjustment in the orientation of the lamellae might result, in order to minimize the elastic strain energy. However, the elastic anisotropy of most silicates is not large and the role of the elastic constants is usually secondary in determining the orientation of the lamellae. This is true for the alkali feldspars. However, for other minerals in which there are two nearly perpendicular planes giving rise to essentially equal compositional strain, the elastic anisotropy may be important. Also, in order to calculate the magnitude of the elastic strain energy, the elastic anisotropy must be considered.

The above discussion illustrates that the orientation of coherent lamellae can usually be well approximated by using a criterion of minimum *strain*, because this is the dominant term in the strain energy expression. This is equivalent to selecting the orientation of the potassic and sodic lamellae which gives the best 'fit' of planes across the interface. This was recognized by Bollman and Nissen (1968) and used to formulate the theory of optimal phase boundaries. However, a more exact determination of the coherency plane can be obtained by considering the elastic anisotropy, and using a criterion of minimum elastic *strain energy*. Furthermore, a consideration of the elastic anisotropy allows the compositions of the coherent phases to be determined from their strained lattice spacings.

Compositions of the coherent lamellae

The lamellae in a cryptoperthite are obviously too small to be analyzed by standard electron probe techniques, and their compositions must be determined indirectly from x-ray determinative curves.

These relations have been described in previous chapters, but a complication arises if the lamellae are coherent. Examination of Figure 8b indicates that lattice planes will not have the same spacing as they would if the lamellae were noncoherent. X-ray determinative curves are based on homogeneous, unstrained phases and, consequently, measured spacings for cryptoperthites will yield an apparent composition. Smith (1961) recognized this problem and suggested an approximate correction method based on the assumption that each phase would have the same unit cell volume as it would if unstrained. Others (e.g., Stewart and Wright, 1974) have used the same method, taking the measured *b* and *c* spacings as correct and using the constant volume assumption to derive the 'correct' *a* spacings. There are three problems with this approach: (1) The *b* and *c* spacings are themselves strained, and so one uses the wrong constant volume; (2) elastically strained crystals do not maintain constant volume (this can be seen immediately from an examination of the elastic constants; see Appendix); and (3) the structural state of the feldspars is a non-negligible parameter in the volume-compositional relation (Ribbe, 1979).

An accurate correction of 'anomalous' compositions uses the known compositional strains within the coherency plane plus the elastic compliances to calculate the strain (change in lattice spacing) in any other crystal direction. These strains can be subtracted to yield the spacings which would be characteristic of the strain-free (non-coherent) material, and thus to determine the correct compositions. This approach requires that one know (1) the degree of coherency, (2) the symmetry of the two coherent phases, together with presence or absence of twinning, (3) the volume proportions of the two phases, and (4) the orientation of the coherency plane.

Robin (1974b) and Tullis (1975) have independently devised methods for correcting the compositions of monoclinic alkali feldspars. Tullis makes the correction based on apparent compositions determined from a^*, which is easily measured on an $hk0$ precession photograph such as that shown in Figure 9. The amount of the correction depends on the bulk composition of the cryptoperthite. Her diagrams for three bulk compositions are shown in Figure 10. The true compositions of the sodic and potassic phases show less compositional difference than the apparent compositions, which are often negative (e.g., Smith, 1961; Stewart and Wright, 1974). It should be noted that corrections based on the constant volume assumption are too great by a factor of about two.

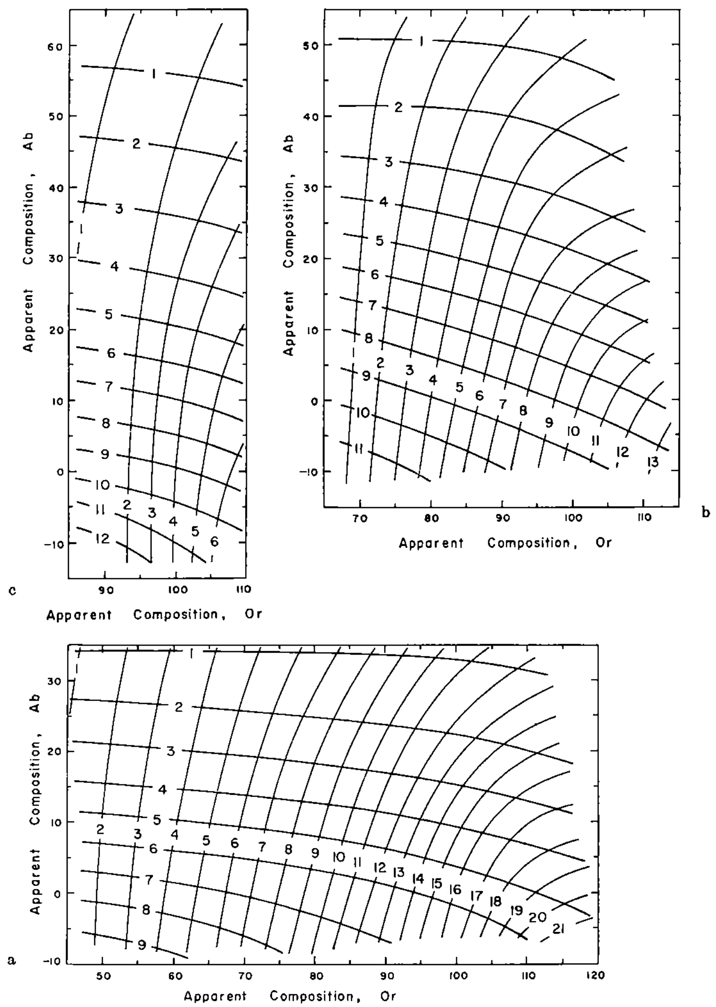

Figure 10. Diagrams to correct apparent compositions of coherent cryptoperthites, as determined from a^*, to true compositions for bulk compositions of Or_{40} (a), Or_{60} (b), and Or_{80} (c). The approximately horizontal contours indicate the number of mole percent Or which must be added to the apparent composition of the sodic phase and the nearly vertical lines show the number of mole percent Or which must be subtracted from the apparent composition of the potassic phase. From Tullis (1975).

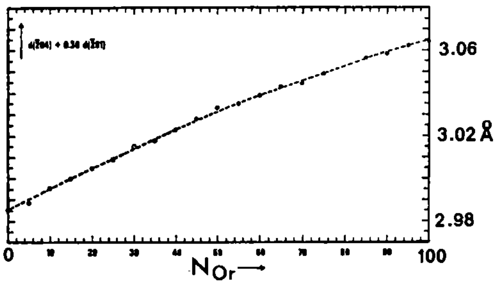

Figure 11. X-ray determinative durve of $d_{\bar{2}04} + 0.30\ d_{\bar{2}01}$ versus weight percent orthoclase for coherent alkali perthites. The linear combination of these two lattice spacings is not affected by the elastic strain due to coherency. From Robin (1974b).

An alternative method for correcting anomalous compositions of coherent monoclinic alkali feldspars has been proposed by Robin (1974b). Because some lattice spacings of coherent lamellae are stretched and some are compressed, there will be linear combinations of these which should remain unaffected. Robin (1974b) found that given the simplifying assumption that compositional strains vary linearly with composition, the function $d_{\bar{2}04} + 0.3d_{\bar{2}01}$ is independent of the elastic coherency strain. This allows correct compositions to be determined directly from x-ray powder data (see Fig. 11).

The authors are preparing a paper (1982) which presents a slight modification of Tullis' correction method, and a comparison of this with Robin's correction method for a number of cryptoperthites, as well as a discussion of the paper by Keefer and Brown (1978) who have performed a structure refinement of the potassic phase of a partially coherent cryptoperthite and report a compositional correction much larger than that given by either Tullis' or Robin's methods. The points they intend to make are briefly outlined here. (1) Tullis' method has been modified to consider only reasonable pairs of coherent compositions (those close to the experimental solvus), and to eliminate the need to extrapolate a^* to negative compositions. The results are mostly within a few mole percent of the values determined from Tullis' original diagrams (Fig. 10). (2) New data are presented allowing $d_{\bar{2}01}$, such as determined from x-ray powder diffraction, to be used to determine true compositions. (3) A comparison of Tullis' and Robin's correction methods for several natural cryptoperthites shows that the methods agree very well for the potassic-rich phases, but less well for the sodic-rich phases. This may be due to Robin's estimate of the elastic strain and because $d_{\bar{2}04}$ is not resolved for the two phases. (4) Keefer and Brown's (1978) results imply compositional corrections so large that they would place the experimentally determined coherent solvus of Sipling and Yund (1976) (see section below) well within the region in which coherent exsolution is observed by TEM, which is physically impossible.

The calculation of elastic strains provides an exact method for the solution of problems involving coherency. Further improvements in the values of the cell parameters and elastic constants would provide refinement of the results. The method of constant volume is wrong in principle unless Poisson's ratio is 0.5, which it is not for most crystalline materials. There is also a need to make calculations of the strains, and thus the compositional corrections, for coherency between triclinic phases, and between a monoclinic potassic phase and a twinned, triclinic sodic phase. In a related problem, Willaime and Gandais (1972) have used elastic strain energy considerations to explain the observed relation between the thickness of triclinic sodic exsolution lamellae and the periodicity of their twinning.

THE COHERENT SOLVUS

One of the principal consequences of the coherency of cryptoperthitic lamellae is the restriction on the compositions of the lamellae compared to noncoherent phases. We refer here to the true compositions, which we assume can be determined by one of the methods described above. The compositional relations for the coherent phases and the coherent solvus can be contrasted to the compositional relations of noncoherent phases and the strain-free solvus which were summarized in the first part of this chapter. The coherent solvus will be developed using a hypothetical example; then the data for the alkali feldspars will be discussed.

General relations

Equilibrium between phases consisting of discrete grains with noncoherent boundaries is expressed by the usual formulation for the free energy of the system. The compositional relations for such phases are commonly shown on a free energy versus composition diagram, at constant pressure and temperature, such as curve (g) on Figure 12. A common tangent, x-x', to the free energy curve defines the compositions of the coexisting phases for that pressure and temperature. The relation shown by curve (g) is applicable to coarse perthites or coexisting grains in a two-feldspar rock.

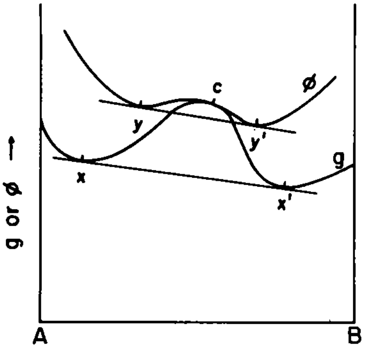

Figure 12. The Gibbs free energy (g) and a new energy function (ϕ) for a hypothetical system A-B. The function ϕ is drawn for bulk composition C and includes the coherency strain energy. For the temperature and pressure of this diagram, x-x' are points on the strain-free solvus and y-y' are points on the coherent solvus.

Cahn (1962) showed that it is possible to define a new free energy function (ϕ), which is obtained by adding a strain energy term due to the coherency to the usual Gibbs or chemical energy term. The addition of this new term and the new energy function is only necessary for coherent phases. Exsolution mechanisms which can produce these coherent phases are discussed in the following chapter. For now it is sufficient to recognize that coherent exsolution lamellae do exist in the form of cryptoperthites; they are also common in pyroxenes.

This new energy function for bulk composition C is represented schematically on Figure 12 by curve (ϕ). A common tangent to this curve gives the compositions of the coherent phases. These compositions must lie inside the equilibrium or strain-free solvus because the change in the Gibbs energy, which is always negative, must be larger than the strain energy term which is positive. Thus the curve for the new function must lie above the curve for the Gibbs energy function, and the points on the common tangent to this new curve define compositions which must lie inside those for the strain-free solvus. Thus the strain energy associated with the coherency of the phases prevents their compositions from reaching the strain-free solvus. The locus of points such as y and y' as a function of temperature defines the coherent solvus as shown on Figure 13.

The free energy function for coherent phases was formulated by Cahn (1962) on the assumption of isotropic elasticity and isotropic compositional strain. This has been extended to the more general case of anisotropic relations by Robin (1974a,b). These excellent articles should be consulted for the mathematical treatment of coherent phase relations.

Several additional general comments about the relations shown on Figure 13 may be helpful. The coherent phase relations are only applicable

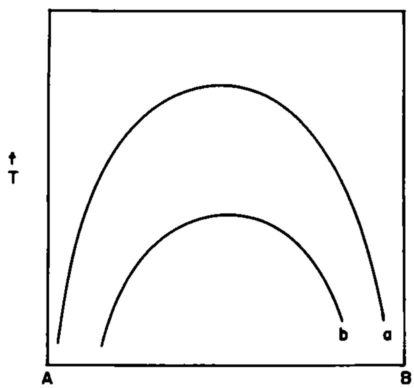

Figure 13. Schematic temperature-composition diagram showing the relation between the strain-free solvus (a) and the coherent solvus (b).

to exsolution processes which produce coherent phases. The compositions of noncoherent phases, regardless of how they form, are independent of curve (b) and are represented by curve (a). Between the coherent solvus (b) and the strain-free solvus (a), the strain energy term is greater than the change in the Gibbs free energy. Therefore, coherent phases of different compositions cannot exist in this region of T-X space, although they are beneath the strain-free solvus.

Exsolution may produce coherent lamellae which slowly become noncoherent with time due to climb or glide of dislocations to the interface. The compositional relations during this loss of coherency shift from (b) to (a). However, as long as coherency is retained, the relations given by curve (b) are reversible. For example, a sample whose bulk composition lies within the miscibility gap at some temperature will consist of coherent lmaellae whose compositions are given by (b). If the temperature is raised or lowered, the compositions of these coherent phases will change along curve (b). If the temperature is raised above the intersection of the bulk composition and the coherent solvus, the sample will homogenize and remain so unless some process can operate which will produce noncoherent exsolution. Thus the coherent phase relations can be determined by reversals in experimental studies.

The separation between the coherent solvus and the strain-free solvus depends on the magnitude of the strain energy. This may be large for some mineral solid solutions such as the alkali feldspars which are discussed below, and less for other systems. Some of the confusion concerning the "solvus" for pyroxene systems may be due to comparison of data which are partially based on true exsolution experiments and give rise to coherent phases whose compositions are given by the coherent solvus, and partially based on other experiments which produce noncoherent phases whose compositions are given by the strain-free solvus. The compositional difference between the coherent solvus and the strain-free solvus for the pyroxenes is probably less than that for the alkali feldspars because the compositional strain is less.

The reader may wonder which solvus in Figure 13 is the equilibrium solvus. Other factors being equal, the lowest energy state for a system of two phases is attained when it consists of discrete grains. Grains containing coherent lamellae are in a higher energy state than unstrained grains. Thus curve (a) represents equilibrium for unstrained solids (Robin, 1974a). This is not to say that the coherent solvus relations are a brief transitory state on the way to equilibrium. Cryptoperthites with coherent lamellae remain unchanged at or near the earth's surface for millions of years. The loss of coherency will be discussed later.

Application to alkali feldspars

From the above discussion it may appear surprising that the importance of coherency strain was not recognized earlier and the coherent solvus determined and distinguished from the strain-free solvus for alkali feldspars as well as for other minerals. However, the experimental determination of subsolidus phase relations usually has not included true exsolution experiments. Commonly, a gel or a glass is annealed below the miscibility gap and crystalline phases of varying compositions produced. Equilibrium between these discrete grains is governed by the strain-free solvus. The phases produced in Orville's (1963) alkali exchange experiments were also noncoherent. Sometimes experiments were done which were implied to be exsolution experiments, but in actuality were not. For example, Müller's (Bachinski and Müller, 1971) "unmixing" experiments used mechanical two-phase mixtures.

It also appears that true exsolution experiments may have been considered slower than other types of experiments. Experimentalists may have considered that exsolution required a greater change in composition than solution experiments which start with phases whose compositions are close to the equilibrium composition. In fact, the coherent solvus is easier to determine than the strain-free solvus. The scale of the exsolution produced experimentally in alkali feldspars is typically on the order of a few hundred Ångstrøms, and diffusion of the alkalis over these distances clearly is faster than over micron distances which are typical of the grain size used to determine the strain-free solvus. In addition, the diffusion paths are continuous as opposed to diffusion in dry experiments which can only occur where grains touch their neighbors. In hydrothermal experiments, the fluid phase can offer a high diffusion path between grains, or it may afford a nonsolid-state mechanism for reaction such as dissolution and reprecipitation.

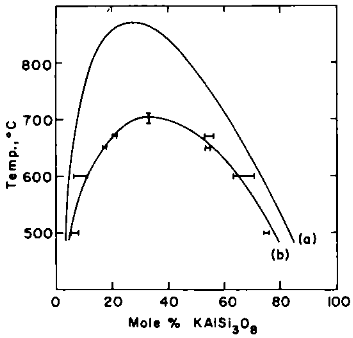

Figure 14. **Approximate location of** the coherent solvus (b) **for the maximum microcline**-low albite series. The compositional data (horizontal bars) are uncorrected for coherency strain. The strain-free solvus (a) is from Bachinski and Müller (1971). From Yund (1974).

The higher solubility of feldspar in a peralkaline solution may be one reason for the faster attainment of equilibrium with these starting materials.

When true exsolution experiments were performed and compositions of exsolved phases were determined which did not agree with the expected position of the strain-free solvus, the results were discounted and the significance of the results was not realized. Robin (1974b) and Yund (1974) independently recognized the existence of a coherent solvus for the alkali feldspars, and their results together with more recent data are discussed below.

Maximum microcline - low albite coherent solvus. The coherent solvus for the ordered alkali feldspars was reported by Yund (1974) who exchanged a maximum microcline in molten alkali chlorides to produce homogeneous samples of Or_{33} and Or_{45} mole percent. These were then annealed at atmospheric pressure for various times at temperatures between 750° and 500°C. Below about 700°C exsolution could be detected by the elongation of $h00$ reflections normal to $(\bar{6}01)$. At lower temperatures these reflections become distinct doublets similar to those shown in Figure 9. The original albite twinning in the microcline sample also gave rise to doubling of $h00$ reflections, but in this case the separation was parallel to b^* (see Yund, 1974, Fig. 4).

The x-ray precession photographs indicated that the two phases were coherent and that the orientation of the lamellae was approximately $(\bar{6}01)$. The apparent compositions of the phases were determined from a^*. These apparent compositions were not corrected for coherency strain because an accurate method is not available for triclinic crystals. The approximate position of the coherent solvus is shown in Figure 14. Assuming that Tullis'

(1975) corrections for monoclinic feldspars are approximately correct for these triclinic phases, the corrections are from two to six mole percent. The corrected compositions for the coexisting phases are closer together than the apparent compositions shown on the figure.

The time necessary to reach steady state compositions in these experiments is not more than 24 hours at and above 600°C. The best measure of the degree to which coherency is maintained is indicated by the reversal experiments. A grain exsolved at lower temperature was subsequently annealed at a higher temperature and a^* was redetermined. Apparent compositions measured from these crystals agreed with those determined from crystals which were first annealed at the higher temperature.

The critical point of the coherent solvus is about Or_{33} and 710°C. Crystals first exsolved at lower temperature would rehomogenize when annealed above the coherent solvus, although they were well below the strain-free solvus. The strain-free solvus shown in Figure 14 is from Bachinski's data (Bachinski and Müller, 1971) calculated for one atmosphere. The distinction between the coherent and strain-free solvi for the ordered feldspars is clear. Because the compositions shown on Figure 14 are uncorrected for coherency strain, no attempt was made to analyze this coherent solvus using Margules or other parameters.

The results clearly demonstrate that a coherent solvus exists in the alkali feldspars, that it can be experimentally determined, and that its position can be defined by compositional reversals. However, the equivalent coherent solvus for the sanidine-high albite series is of more interest because most potassic feldspars probably start to exsolve when they are monoclinic (Figs. 1 and 2).

Sanidine - high albite coherent solvus. Preliminary experimental data for this solvus were reported by Yund (1974) and Sipling and Yund (1974), and the details were given by Sipling and Yund (1976). Robin (1974b) calculated the solvus by evaluating the elastic strain energy due to the lamellar coherency, and his method was slightly modified and the results expanded by Tullis and Yund (1979). The following discussion will first consider the experimental determination of the coherent solvus, and conclude with a summary of the calculated solvus curves.

The coherent solvus reported by Sipling and Yund (1976) is shown in Figure 15 along with the strain-free solvus from Thompson and Waldbaum (1969b) for comparison. (The strain-free solvus of Smith and Parsons,

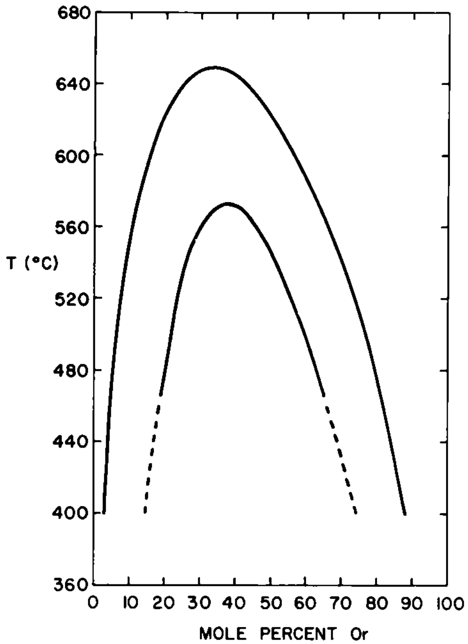

Figure 15. **Comparison of the strain-free solvus (upper curve) and the coherent solvus (lower curve) for the sanidine-high albite series at 1 atm. The strain-free solvus is from Thompson and Waldbaum (1969b) and the coherent solvus is the smoothed experimental data of Sipling and Yund (1976).**

1974, is shown in a later figure.) The starting material was an adularia crystal which had been heated at 1110°C to produce a completely disordered feldspar as indicated by its unit cell parameters. This material was then used to prepare homogeneous crystals of intermediate K/Na ratios. The annealing and x-ray analysis were similar to those described by Yund (1974) for the maximum microcline - low albite series. Thirty-two pairs of coexisting lamellae were determined between 540° and 450°C including several reversals to demonstrate that steady state conditions had been attained. These compositions were corrected using the method of Tullis (1975) and then smoothed using the r-s method of Thompson and Waldbaum (1969a). The critical point of this coherent solvus is 573°C and $Or_{37.4}$.

The accuracy of this solvus is determined by several factors. The combined exsolution and homogenization experiments show that steady-state compositions were closely approximated, at least above 470°C. The value of a^* can be reproducibly measured with a precision corresponding to ±2 mole percent Or. These compositions have to be corrected because of the elastic strain of the lamellae which affects a^*. The corrections are only about 2 mole percent at 450°C, and about 4-6 mole percent at 450°C. Thus even if there is a large percentage error in the corrections, the absolute values for the coherent solvus would only be in error by a few mole percent.

Independent and confirming data on the position of the coherent solvus are provided by the TEM observations of Sipling and Yund on synthetic samples of eight compositions which were annealed at various temperatures. In this way, they determined the temperature-composition region in which coherent exsolution was observed. The boundary of this region is the coherent spinodal (see Fig. 8 in the following chapter), and the coherent spindoal must coincide with the coherent solvus at their common critical point. The TEM data agree very well with the experimental data in Figure 15 for the upper portion of the coherent solvus, and place a minimum temperature limit on the coherent solvus at lower temperature. Owen and McConnell (1974) observed exsolution at a slightly higher temperature (see Fig. 5 in the following chapter), but this is consistent with the greater Al,Si order in their sample. One area of further study would be to evaluate the effect of Ca on the position of the coherent solvus.

The concept of a coherent solvus is new, but previous studies have indicated that cryptoperthites define a solvus which is different from and at lower temperature than the strain-free or equilibrium solvus. Tuttle and Bowen (1958) and Smith and MacKenzie (1958) determined the approximate compositional relations of the coexisting phases in natural cryptoperthites, and the relation of their results to Sipling and Yund's coherent solvus will be briefly considered.

Three specimens from Tuttle and Bowen's work can be used to define approximately the critical point of the coherent solvus. Luth (1974) has fitted Margules parameters to these data which consist of only three coexisting compositions for each sample. The Spencer Sparling Gulch sample gave a critical point of 537°C and Or_{43}. Spencer P and Mitchell Mesa rhyolite yield nearly identical values for the critical point of 576-577°C and Or_{35-37}. This is remarkably close to the critical point determined by Sipling and Yund. Unfortunately, Tuttle and Bowen's lower temperature data are not very useful because they used $d_{\bar{2}01}$ to determine the compositions. The strain in $d_{\bar{2}01}$ becomes large for sodic and potassic-rich compositions, hence their values for these compositions have larger errors than their higher temperature data.

Smith and MacKenzie (1958) recognized the problem of determining compositions of cryptoperthites from $d_{\bar{2}01}$, and they used the reciprocal lattice angles α^* and γ^* to determine the compositions of the sodic-rich phase in Spencer P. These parameters may be less sensitive to coherency strain, but it has not been determined exactly how much compositions determined from these parameters are in error. The position of the sodic limb of their solvus is consistently about seven mole percent inside the coherent solvus of Sipling and Yund. Smith and MacKenzie determined the potassic limb by identification of homogeneous versus unmixed states of cryptoperthites of known compositions (MacKenzie and Smith, 1956). The location of this

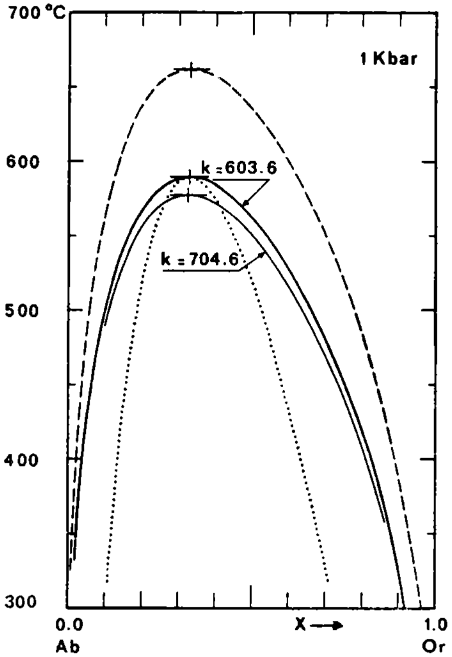

Figure 16. Comparison of the calculated coherent solvi for two sets of elastic constants (solid curves) with the strain-free solvus of Waldbaum and Thompson (1969b) (dashed curve). The calculated coherent spinodal for one set of the elastic constants is shown by the dotted line. From Robin (1974b).

boundary is probably less exact and should be compared to the coherent spinodal rather than the coherent solvus (see the following chapter). The critical temperature of their solvus is 570°C.

Robin (1974b) calculated the position of the coherent solvus by evaluating the elastic strain energy of the coherent lamellae. The elastic strain energy, for a given orientation and compositions of the lamellae, is determined by the difference in the cell parameters of the phases and the values of their elastic compliances (see Appendix to this chapter). Robin used the following equation as an approximation for the elastic strain energy (E):

$$E = k(X-X_o)^2 \qquad (1)$$

where X is the composition of a lamella in a cryptoperthite of average composition X^o, and k is the molar "strain energy coefficient." Robin then used the new function ϕ, which is given by

$$\phi = \bar{G} + E \qquad (2)$$

where $\bar{G}$ is the molar Gibbs energy and ϕ is sometimes called the Cahn energy (see Cahn, 1962). He then showed that a Margules expansion of ϕ is formally identical to Thompson's (1967) equation (81) for $\bar{G}$, except that the Margules parameters W_1 and W_2 are replaced by $(W_1 - k)$ and $(W_2 - k)$. He assumed a linear variation of lattice parameters with composition and assumed that k is independent of temperature and bulk composition. He calculated two coherent solvi for two different sets of elastic compliances (see Appendix), and his results are shown by the solid lines in Figure 16.

Tullis and Yund (1979) have modified Robin's elegant formulation to calculate the compositional strains exactly rather than using a linear

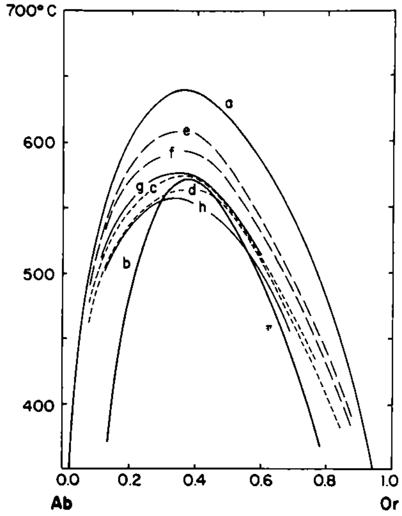

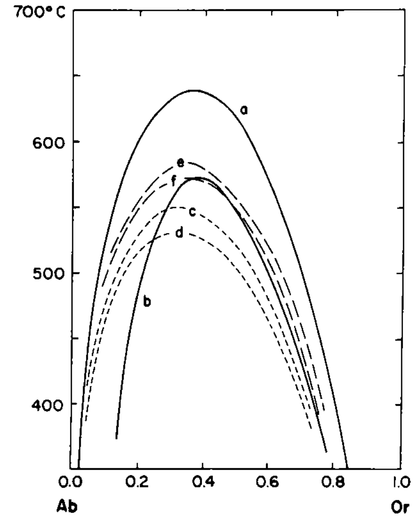

Figure 17 [left]. Temperature-composition diagram for alkali feldspar, showing calculations based on the **strain-free** solvus of Thompson and Waldbaum (1969), which is shown for 1 bar by curve a. Curve b is the coherent solvus experimentally determined by Sipling and Yund (1976). Curves g and h are the coherent solvi calculated by Robin (1974b) for the less stiff (g) and stiffer (h) set of elastic constants. Curves c and d are the coherent solvi we have calculated using the same room-temperature cell parameters and the same elastic constants, but calculating the compositional strains more accurately. Curves e and f are the coherent solvi we have calculated using the estimated high-temperature cell parameters and the same elastic constants. From Tullis and Yund (1979).

Figure 18 [right]. Temperature composition diagram for alkali feldspars, showing calculations based on the **strain-free** solvus of Smith and Parsons (1974), which is shown for 1 bar by curve a. Curve b is the coherent solvus experimentally determined by Sipling and Yund (1976). Curves c and d are the coherent solvi we have calculated using the room-temperature cell parameters; c represents the less stiff elastic constants, and d the stiffer set. Curves e and f are the coherent solvi we have calculated using the estimated high-temperature cell parameters and the same elastic constants. From Tullis and Yund (1979).

approximation. The term $(X - X_o)$ in equation (1) was taken to be half the compositional difference between the lamellae; thus, there would be a slightly different bulk composition at each temperature because the hydrostatic solvus is asymmetrical. They establish an iterative method to calculate the elastic strain, the lamellar orientation, and the coherent compositions until the compositions do not change by more than 0.01 mole percent. Thus there is a slightly different value for the lamellar orientation and k for each temperature. They use this method to evaluate the effect of different sets of elastic constants and of room and high-temperature cell parameters. The calculations are compared with Robin's solvi and the experimental coherent solvus in Figure 17. All of the coherent solvi in this figure were calculated using Thompson and Waldbaum's (1969) strain-free solvus. A similar set of solvi based on Smith and Parson's (1974) strain-free solvus is shown in Figure 18.

The principle sources of error or uncertainty in these calculations, in the order of probable significance, are: (1) the choice of *strain-free* cell parameters of the lamellae at a given temperature, especially for the sodic-rich compositions; (2) the position of the strain-free solvus; (3) the values for the elastic constants; and (4) the assumption which Robin makes that the elastic strain energy at a given temperature is independent of the bulk composition of the cryptoperthite. Given these uncertainties and the different possible solvi which can be calculated using the best data available, the coherent solvus for sanidine - high albite appears to be best defined by the experimental results.

A direct measure of the compositions of coherent cryptoperthite lamellae would be desirable. Clearly, the widths of coherent lamellae are too small for compositions to be measured directly with the electron microprobe. At present, the necessary accuracy is difficult or impossible to obtain with the analytical electron microscope or ion microprobe. For depth-profiling with the ion microprobe the lamellae would have to be of uniform thickness and very accurately oriented parallel to the sample surface. The results from point analyses give variable results (Miüra and Rucklidge, 1979, Fig. 5), and samples with low An must be chosen for comparison with the experimental and calculated solvi.

It is clear that natural cryptoperthites have remained at least partially coherent, and the compositions of the coherent lamellae define the coherent solvus. The following chapter considers the mechanism and kinetics of cryptoperthite exsolution.

APPENDIX

CRYSTAL ELEASTICITY AND ELASTIC CONSTANTS FOR FELDSPARS

There have probably been more applications of crystal elasticity to the feldspars than to any other mineral group. These applications come mostly in consideration of the effects of coherent exsolution, as discussed in this chapter. There has been some slight confusion in the literature about these applications of crystal elasticity, and yet it represents an elegant, straightforward, and very powerful concept.

Elastic strain is totally and instantaneously recoverable when the differential stress is removed. For a given stress applied to a given orientation of a crystal, the elastic strain (in all crystal directions) is completely specified by a set of elastic compliances. Similarly, if the strain is given, the stress in all directions is completely specified by the set of elastic stiffnesses. Because of the growing awareness of the usefulness of this concept, the sections below present a brief review of crystal elasticity, as well as a discussion of the elastic compliances and stiffnesses which have been determined for feldspars and their relations to the feldspar crystal structure. The bulk elastic properties of polycrystalline aggregates will not be treated here.

CRYSTAL ELASTICITY

For small stresses on crystalline materials, the strain is linearly proportional to the stress (Hooke's Law) and it returns to zero when the stress is removed. This can be easily understood qualitatively in terms of the atomic structure of crystals. In an unstrained crystal the atoms are maintained in their equilibrium positions by interatomic forces; if a stress (either a compression or a tension) is applied to the crystal, the atoms are displaced by an amount which depends on the strength of the interatomic forces. Obviously, the atoms return to their equilibrium positions when the stress is removed, as long as no bonds have been broken.

For an elastic deformation in which the stress is given, the strain is uniquely determined from the measurable constant of proportionality, known as the elastic constant. If we write (ε) in terms of stress (σ), $\varepsilon = S\sigma$, then the constant S is known as the elastic compliance and has units of reciprocal stress (because strain has no units). If we write stress in terms of strain, $\sigma = C\varepsilon$, then the constant C is known as the elastic stiffness and has units of stress. In fact, stress and strain are symmetrical second rank tensors, denoted σ_{ij} and ε_{ij}, respectively, and for elasticity every component of the stress tensor is a linear function of all the components of the strain tensor. Using the Einstein summation convention (Nye, 1957, p. 7), this may be written succinctly as:

$$\varepsilon_{ij} = S_{ijkl}\sigma_{kl} \,. \tag{A1}$$

This equation actually stands for nine equations, each with nine terms on the right side; thus, there are 81 S_{ijkl} compliance coefficients (and 81 C_{ijkl} stiffness coefficients). These each form a fourth rank tensor; they may be written in the shorthand matrix notation as S_{ij} and C_{ij}, respectively, in which case one is the reciprocal of the other.

Because the stress and strain tensors are symmetric, the number of independent elastic constants is reduced from 81 to 36, and because the S_{ij} and C_{ij} matrices are symmetric, this number is still further reduced to 21 (Nye, 1957, pp. 136-137). This number may be still further reduced, depending on the symmetry of the crystal under consideration; triclinic feldspars have the full 21 independent coefficients, whereas monoclinic feldspars have just 13. In fact, no one has ever measured the 21 coefficients for a triclinic mineral, and all feldspars measured have been treated as monoclinic.

It is worth considering some of the non-intuitive aspects of elastic deformation. First, equation (1) implies that if one applies a single component of stress to a crystal, *all* strain components may be non-zero. That is, an axial compressive stress may produce an axial shortening, a transverse lengthening, and probably shear strains as well. Similarly, coherent exsolution lamellae will generally experience a strain in all their lattice spacings. Second, elastic deformations do not necessarily involve constant volume. Again, considering the case of cryptoperthites, the potassic phase has its *b* and *c* parameters compressed by the coherency, but its a^* parameter, though free to expand by any amount, expands by only half that required to maintain constant volume (Tullis, 1975). The important point is that the elastic constants allow one to calculate *exactly* what strains will result from any given applied stress (or strain); see the example below.

Two special cases should be mentioned. The volume compressibility, which gives the change in volume when a crystal is subjected to a hydrostatic pressure, is given by S_{iikk}. (The reciprocal of the volume compressibility is the bulk modulus.) The linear compressibility is the relative decrease in the length of a line when a crystal is subjected to hydrostatic pressure; this is given by $S_{ijkk}\ell_i\ell_j$, where ℓ is a unit vector in the given direction.

The elastic behavior of a crystal cannot be represented completely by a single diagram, but a useful surface is the one that shows the variation of $1/S_{11}$ (known as Young's modulus) with crystal direction; this shows the amount of longitudinal strain in a given crystal direction for an applied stress in that same direction. Even in the isometric system this surface is not spherical, and for a monoclinic or triclinic crystal it is a very complex function (given by Nye, 1957, p. 144).

Elastic strain energy is stored in elastically strained atomic bonds, and can be fully recovered from the body as mechanical work (no heat) when the applied force is removed. If the deformation process is isothermal and reversible, the work done (dW) is equal to the increase in the Helmholz free energy (dΨ), and we can write (per unit volume):

$$d\Psi = dW = \sigma_{ij} d\varepsilon_{ij} \quad . \tag{A2}$$

If Hooke's Law is obeyed, then this becomes:

$$W = \tfrac{1}{2}\sigma_{ij}\varepsilon_{ij} = \tfrac{1}{2}S_{ijkl}\varepsilon_{ij}\varepsilon_{kl} \ . \tag{A3}$$

The normal range of elastic strain in crystals rarely exceeds 0.5%, but the stress necessary to produce this strain may be large; the stresses within the coherency plane of cryptoperthites are several kilobars (Tullis, 1975). This is because the applied stress is opposed by the restoring forces of atomic bonds. Before the stresses can get large enough to produce larger elastic strains, most natural materials will undergo plastic strain such as fracture, slip, or mechanical twinning. The magnitude of the elastic strain energy involved in coherent exsolution is generally small; that for cryptoperthites is on the order of 10 to 100 cal/mole (Tullis, 1975).

As an example of how crystal elasticity can be used, consider the case of a cryptoperthite consisting of lamellae of Or_{20} and Or_{65} (each monoclinic) which are coherent on ($\bar{6}01$); the problem is to determine the strain in the $d_{\bar{2}01}$ spacing of each phase. First, set up a coordinate system with 2 = *b*, 3 = [$\bar{1}06$], and 1 normal to the lmaellar boundaries, and transform the elastic compliances into this system.

The normal forces within the coherency plane must be equal and opposite for the two phases, so given the volume fraction $x = V_{Or}/V_{Ab}$, we can write (taking compression to be negative and using matrix notation):

$$\sigma_2^{Ab} = -x\sigma_2^{Or} \ , \quad \sigma_3^{Ab} = -x\sigma_3^{Or} \ . \tag{A4}$$

In fact, many of the stress and strain terms are zero, which considerably simplifies the calculations. If the coherency plane contains the *b* axis of both phases, then symmetry requires that there be no shear stresses or strains across the planes that contain *b*. In addition, if the lamellae have a large aspect ratio, then there can be no shear stresses across the coherency plane, and because the lamellae are 'free' to shrink or expand in the direction perpendicular to the lamellar boundaries, there can be no normal stresses across the coherency plane. Thus, the only non-zero stresses are σ_2 and σ_3, and the only non-zero strains are ε_2, ε_3, ε_1, and ε_5.

The strains ε_2 and ε_3 within the coherency plane can be obtained from the stress-free lattice parameters; ε_2 results from the mismatch in *b*, and ε_3 results from the mismatch in [$\bar{1}06$]. The total strain in each of these two directions is the sum of the strains in the two phases (a negative compression in one phase and a positive expansion in the other):

$$\varepsilon_2 = \varepsilon_2^{Ab} - \varepsilon_2^{Or} \ ; \tag{A5}$$

thus;

$$\varepsilon_2^{Or} = \varepsilon_2^{Ab} - \varepsilon_2 \ . \tag{A6}$$

An alternate way to write ε_2^{Or} is in terms of the unknown stresses in the coherency plane and the known elastic constants. For this we use the general relationship $\varepsilon_i = S_{ij}\sigma_j$, but because σ_2 and σ_3 are the only non-zero stresses, we only need consider two terms (instead of 13 corresponding to the 13 non-zero elastic constants):

$$\varepsilon_2^{Or} = S_{22}^{Or}\sigma_2^{Or} + S_{23}^{Or}\sigma_3^{Or} \ . \tag{A7}$$

We can write similar expressions for the other stress and strain components in the coherency plane, making up four equations in four unknowns (the two stresses and two strains for one of the phases). When these are solved, it is simple to get the same quantities for the other phase.

A knowledge of the two stresses for each phase now allows one to solve for the other two non-zero strain components, the shear strain ε_5 and the normal strain in the 'free' direction ε_1. Using the same general relation and again with only two terms to be considered:

$$\varepsilon_5^{Or} = S_{52}^{Or}\sigma_2^{Or} + S_{53}^{Or}\sigma_3^{Or} \tag{A8}$$

$$\varepsilon_1^{Or} = S_{12}^{Or}\sigma_2^{Or} + S_{13}^{Or}\sigma_3^{Or} \ . \tag{A9}$$

Finally, from the known values of the four non-zero strains, one can calculate the strain in any other crystal direction, such as the $d_{\bar{2}01}$ spacing. If ϕ is the angle between the 1 axis and the direction normal to the ($\bar{2}01$) planes, then

$$\varepsilon_{d(\bar{2}01)}^{Or} = \varepsilon_1^{Or}\cos^2\phi + \varepsilon_3^{Or}\cos^2(\tfrac{\pi}{2}-\phi) + 2\varepsilon_5^{Or}\cos\phi\sin\phi \ . \tag{A10}$$

ELASTIC CONSTANTS FOR FELDSPARS

There have not been many measurements of elastic constants for feldspars; the available data are summarized in Table 1. All measurements have been made at room temperature and pressure. The elastic constants were calculated from the velocities of propagation of elastic compressional and shear waves in six different crystal directions: [100], [010], [001], [110], [101], and [011]. The wave velocities were measured by means of ultrasonic pulse apparatus (Aleksandrov, 1958).

The samples utilized were crystals 9 to 17 mm on a side, which unfortunately contained cracks, pores, inclusions, twins, and/or exsolution features; these flaws are believed responsible for most of the three to 12% error estimated for the elastic constants (Alexandrov and Ryzhova, 1962). Simmons (1964) and Christensen (1966) have measured compressional elastic wave velocities in feldspar single crystals as a function of pressure and find that cracks close by a pressure of 2 kbar, so that extrapolation of the higher pressure velocities should give a better measure of the room pressure elastic properties of the material. The extrapolated velocities compare reasonably well with those listed by Alexandrov and Ryzhova (1962), Ryzhova (1964), and Ryzhova and Alexandrov (1965), but the stiffnesses in Table 1 should probably be considered as minimum values. For the alkali feldspars (which seem to show no trend with composition), the 'best' values to use may be those for $Or_{64.9}$, which has a relatively high value for all its stiffnesses and thus may contain few flaws.

Table 1. Elastic Stiffnesses for Feldspars[1]

Sample	C_{1111}	C_{2222}	C_{3333}	C_{2323}	C_{1313}	C_{1212}	C_{1122}	C_{1133}	C_{2233}	C_{1113}	C_{2213}	C_{3313}	C_{2312}	Ref.[2]
$Or_{53.5}Ab_{34.6}An_{9.2}$	0.630	1.522	1.179	1.101	0.268	0.356	0.359	0.490	0.361	-0.129	-0.018	-0.181	-0.026	1
$Or_{60.7}Ab_{35.6}An_{1.6}$	0.596	1.568	1.195	0.136	0.226	0.342	0.344	0.280	0.216	-0.170	-0.059	-0.129	-0.018	1
$Or_{64.9}Ab_{26.6}An_{3.6}$	0.596	1.581	1.049	0.139	0.203	0.370	0.362	0.360	0.285	-0.118	-0.057	-0.129	-0.026	1
$Or_{66.6}Ab_{28.6}An_{0.0}$	0.584	1.468	0.988	0.124	0.185	0.343	0.333	0.340	0.216	-0.107	-0.043	-0.130	-0.030	1
$Or_{74.0}Ab_{18.9}An_{1.9}$	0.619	1.583	1.002	0.141	0.203	0.360	0.434	0.368	0.218	-0.100	-0.018	-0.121	-0.023	1
$Or_{75.0}Ab_{22.0}An_{0.0}$	0.572	1.483	1.026	0.137	0.180	0.323	0.328	0.333	0.193	-0.124	-0.061	-0.112	-0.025	1
$Or_{78.5}Ab_{19.4}An_{2.1}$	0.625	1.720	1.244	0.143	0.223	0.374	0.428	0.358	0.241	-0.154	-0.143	-0.115	-0.028	2
An_9	0.749	1.375	1.289	0.172	0.303	0.311	0.363	0.376	0.326	-0.091	-0.104	-0.191	-0.013	3
An_{15-16}	0.806	1.630	1.242	0.177	0.274	0.362	0.417	0.538	0.374	0.161	0.171	-0.074	0.010	2
An_{24}	0.818	1.449	1.328	0.177	0.312	0.333	0.393	0.407	0.341	-0.090	-0.079	-0.185	-0.008	3
An_{29}	0.845	1.505	1.325	0.185	0.314	0.343	0.417	0.409	0.330	-0.087	-0.069	-0.185	-0.011	3
An_{53}	0.970	1.629	1.410	0.196	0.330	0.370	0.507	0.442	0.370	-0.096	-0.051	-0.150	-0.016	3
An_{56}	0.989	1.730	1.414	0.199	0.341	0.376	0.521	0.441	0.366	-0.081	-0.051	-0.191	-0.019	3
An_{57-60}	1.010	1.582	1.510	0.214	0.335	0.370	0.617	0.480	0.260	-0.003	-0.080	-0.096	-0.056	2

1. Units are Mbar (10^{11} dyne/cm^2) Subscripts refer to a coordinate system in which 1 is parallel to [100], 2 is parallel to [010], and 3 is parallel to c*.

2. References: 1. Ryzhova and Aleksandrov, 1965
2. Ryzhova, 1964
3. Alexandrov and Ryzhova, 1962

Alternatively, one might choose the highest absolute value for each stiffness from among the group of seven alkali feldspars measured (Robin, 1974b).

All measurements have been made assuming monoclinic symmetry, which is in part justified because twinning makes the crystals pseudomonoclinic. In any event, the errors introduced by this assumption are not large compared to those in the coefficients themselves. All measurements have been made using a Cartesian coordinate system with the 1 axis parallel to [100], the 2 axis parallel to [010], and the 3 axis parallel to c^*. Thus, S_{1111} relates a stress applied parallel to [100] to the resulting strain in the [100] direction, whereas S_{1122} relates a stress applied parallel to [010] to the resulting strain in the [100] direction. If one wants to know the values of the elastic constants in some other coordinate system, such as that including a plane of exsolution, the given constants can be easily transformed, using the standard methods for transformation of fourth rank tensors (see Nye, 1957, p. 133).

In general, the stiffness of a crystal in a given direction will depend on the compressibility of the various polyhedra in the structure and on the flexibility of the linkages between them (Hazen and Prewitt, 1977a; Hazen and Finger, 1979). The T-O tetrahedra are relatively incompressible, whereas the higher coordination alkali polyhedra are more compressible (Hazen and Prewitt, 1977b). The data in Table 1 show that the stiffnesses for plagioclase vary systematically with composition, with samples of higher An content being stiffer. The mean Ca-O bond in anorthite is 0.16 Å shorter than the mean Na-O bond in high albite (Ribbe, Chapter 1, this volume), and shorter cation-oxygen bonds are less compressible. There are no clear systematic compositional variations in the stiffnesses of the alkali feldspars. Although the K ion is larger than Na, the fact that they both have the same charge and coordination gives the alkali polyhedra the same compressibility (Hazen and Prewitt, 1977a). Thus, the alkali feldspars all have about the same elastic constants, eliminating effects due to twinning, exsolution, etc.

The data in Table 1 also show that the feldspars are elastically quite anisotropic; this is a direct consequence of their crystal structure. For all feldspars the direction of greatest compliance (least stiffness) is [100], the direction of the double crankshaft chains of tetrahedra (see Chapter 1). This arrangement of the tetrahedra allows them to easily rotate at their shared corners, without distortion of the tetrahedra themselves, with a concomitant (relatively easy) distortion of the alkali polyhedra. (This crystal direction also shows the greatest change in cell edge with substitution of Na for K.) For all feldspars the direction of greatest stiffness is parallel to [010]. In this direction the tetrahedra form a very rigid framework, with Si-O-Si angles close to 180°, so that very little rotation of the rigid tetrahedra is possible. In the [001] direction the stiffness of feldspars is also high. It appears that somewhat more rotation of the tetrahedra is possible in this direction than parallel to [010], but much less than parallel to [100]. Also, compression parallel to [001] tends to push the cations very close together. The anisotropy of feldspar elasticity described above means that the linear compressibility is highest parallel to [100] (Hazen and Prewitt, 1977b); that is, when a hydrostatic pressure is applied, the volume change occurs mostly by a decrease in length parallel to [100].

In addition to the full determination of the elastic constants listed in Table 1, both Simmons (1964) and Christensen (1966) have determined the compressional elastic wave velocities in feldspar single crystals at room temperature as a function of pressure. Simmons (1964) made his determinations on a microcline, in three directions, [100], [010], and [001]; Christensen (1966) made his determinations on an albite and a microcline perthite in the same six directions as used by Alexandrov and Ryzhova (1962). Also, linear compressibilities have been determined for a low albite (Hazen and Prewitt, 1977b). Determinations of bulk elastic properties for anorthite aggregates have been made as a function of pressure by Liebermann and Ringwood (1976).

Chapter 7
MICROSTRUCTURE, KINETICS and MECHANISMS of ALKALI FELDSPAR EXSOLUTION

R. A. Yund

INTRODUCTION

The study of exsolution microstructures in minerals has been expanded in recent years to include transmission electron microscope (TEM) observations and the application of solid state theories of exsolution mechanisms and kinetics. This approach offers considerable potential for understanding the development of exsolution microstructures, and for the interpretation of thermal histories and possibly other parameters from the preserved microstructures. Although this chapter will concentrate on the development of exsolution microstructures in the alkali feldspars, the principles are applicable to the ternary and plagioclase feldspars (Chapter 10) as well as to other minerals.

The possible exsolution mechanisms in alkali feldspars will be reviewed first, then the exsolution microstructure in alkali feldspar will be briefly considered, and the experimental data concerned with the mechanism and kinetics of exsolution will be summarized. The chapter will conclude with a brief discussion of how the experimental results can be used to estimate the thermal histories of cryptoperthites and place constraints on the evolution of coarser perthites.

EXSOLUTION MECHANISMS

Nucleation

The unmixing or exsolution of a homogeneous solid solution below its strain-free solvus may involve the formation of nuclei of a new phase which are different in composition and may be different in structure from the host or parent phase. The formation of a nucleus requires an increase in the free energy of the crystal, and this is referred to as the energy barrier for nucleation.

The change in the free energy (ΔG) for forming a nucleus can be divided into several terms. The change in the Gibbs or chemical energy is negative; whereas, the surface or interfacial energy and strain energy terms are positive. When the nucleus is small, the interfacial and strain terms dominate and so ΔG is initially positive. With increasing size the change in the

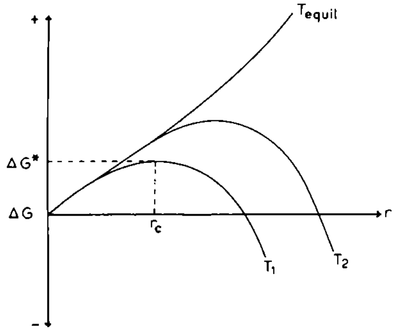

Figure 1. The change in free energy (ΔG) for forming a spherical nucleus as a function of its radius (r) at different temperatures below the strain-free solvus. r_c is the critical radius and ΔG^* the energy barrier at T_1. $T_1 < T_2 < T_{equil}$. From Yund and McCallister (1970).

Gibbs energy becomes dominant and ΔG decreases. The change in ΔG as a function of the radius of a spherical nucleus is shown schematically in Figure 1. ΔG^* is the energy barrier for nucleation, and r_c is the critical radius for the nucleus. For $r > r_c$ the nucleus is stable and further growth by exchange of material with the surrounding host lowers the free energy. Atomic migration of all the constituent ions is implied by a nucleation mechanism.

The values of ΔG^* and r_c depend on the degree of undercooling below the strain-free solvus which increases the supersaturation of the crystal. At the strain-free solvus (T_{equil}), the nucleation barrier is infinite and it decreases rapidly with decreasing temperature (T_1 is less than T_2 in Fig. 1). However, if migration of any of the ions is very slow, this may limit or prevent nucleation regardless of the magnitude of ΔG^*.

Spinodal decomposition

An alternative mechanism to classical nucleation and growth is spinodal decomposition, which has received considerable attention in recent years. The early applications were largely to alloy systems, but the alkali feldspars were one of the first mineral systems for which experimental evidence of spinodal decomposition was reported. Especially useful reviews of the spinodal decomposition theory are those by Cahn (1968) and Hillard (1970), and more recent theoretical developments are discussed by Langer (1973). Further discussion of spinodal behavior in silicates can be found in various sources including those by Champness and Lorimer (1976) and Putnis and McConnell (1980).

The theory of spinodal decomposition was first developed for fluids, and it is useful to consider this as a starting point for crystalline solids. The free energy of a hypothetical binary system at constant temperature and pressure is shown in Figure 2. The relation shown is for conditions below

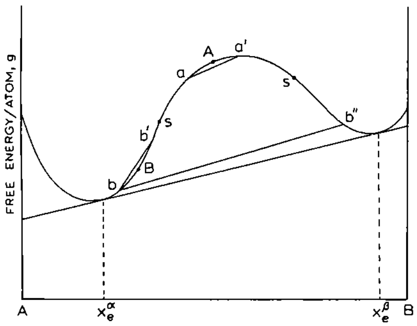

Figure 2. Free energy per atom (g) as a function of composition for a hypothetical binary A-B. Temperature and pressure are constant and below the critical point of the miscibility gap. S are the inflection points or spinodes. See text for explanation. From Yund and McCallister (1970).

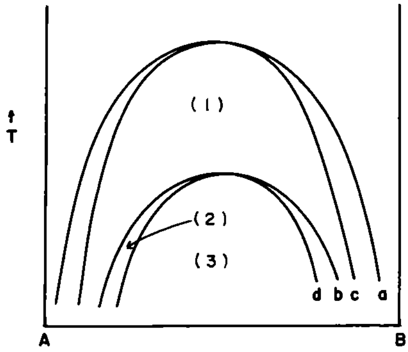

Figure 3. Schematic T-X diagram showing the relations between the strain-free solvus (a), the coherent solvus (b), the chemical spinodal (c), and the coherent spinodal (d). Ignoring the chemical spinodal (c), the miscibility gap can be divided into the three areas shown. See text for explanation.

the critical point of the miscibility gap. The common tangent to this curve gives the equilibrium compositions of the coexisting phases (X_e^α and X_e^β). The inflection points on this curve, $\partial^2 g/\partial X^2 = 0$, are spinodes (s) and the locus of these points on a temperature-composition diagram is the chemical spinodal. The relations are shown on Figure 3, where (a) is the strain-free solvus, (b) is the coherent solvus for a solid, and (c) is the chemical spinodal.

Even a "homogeneous" solid solution such as composition A on Figure 2 will have numerous random compositional fluctuations on an atomic scale (Christian, 1965, p. 219). These compositional perturbations can grow if the bulk composition of the sample is situated between the spinodes. Composition A can lower its free energy by growth of these fluctuations because this lowers the free energy of the crystal as shown by line a-a'. (Initially, of course, the difference in these compositional fluctuations would be too small to illustrate on the scale of this diagram.) This process does not involve a nucleation event because the compositional perturbations change continuously from their initial state to that in which the phases have a maximum compositional difference. It is easiest to imagine this process of spinodal decomposition as the change in amplitude (composition) of a sinusoidal wave where the wavelength is a distance parameter in the crystal. These A- and B-rich regions may be in the form of coherent lamellae, but regardless of their shape, the compositions cannot exceed the coherent solvus unless coherency is lost. In this way the final result is not different from a coherent nucleation mechanism.

Between the spinodal and the strain-free solvus (s-X_e^α and s-X_e^β on Fig. 2) an increase in the compositional difference between the original fluctuation and the surrounding host would raise the free energy of the system as shown by the line b-b' for composition B. Exsolution in bulk compositions between the chemical spinodal and the strain-free solvus requires the formation of a nucleus of some composition such as b". After the crystal has exsolved to a mixture of b and b", it will have a lower Gibbs energy as shown on Figure 2. However, this figure does not take into account the increase in free energy of initially forming nuclei of composition b". This increase is due to interfacial and strain energy terms as discussed above.

The above argument must be modified for spinodal decomposition in crystalline solids. The growth of the compositional perturbations implies that their lattice is continuous and the A- and B-rich regions are coherent. This means that the elastic strain energy associated with the compositional differences must be considered, and the treatment is similar to that described in the previous chapter for the coherent solvus. Figure 2 is similar to Figure 12 in that chapter. The latter shows the energy function (ϕ) which is analogous to the Gibbs function but includes the elastic strain energy due to coherency. The same argument advanced above can now be applied to curve ϕ (Fig. 12). The inflection points on this curve lie inside those of the curve for the Gibbs free energy (g). The inflection points on curve ϕ might be called the *coherent spinodes* and define the limit of spinodal decomposition when the elastic strain energy is included. The locus of the coherent spinodes on a T-X diagram defines a *coherent spinodal* as shown by curve (d) on Figure 3. The coherent spinodal bears the same relation to the coherent solvus as the chemical spinodal does to the strain-free solvus.

The chemical spinodal is not meaningful for exsolution mechanisms or kinetics and should not be used for this purpose. It is unnecessary to refer to the chemical spinodal when developing the concept of spinodal decomposition in solids. However, this development may help the reader to better appreciate the difference between the chemical and coherent spinodal curves and to recognize the source of confusion regarding spinodal decomposition which exists even in recent mineralogical literature.

The orientation of the exsolved phase is independent of the mechanism by which it forms. As disucssed in the previous chapter, the exsolved phase commonly forms as lamellae with the interface approximately parallel to directions of least compositional strain. The compositional fluctuations are subject to the same control; hence, a modulated structure is produced by spinodal decomposition. Therefore, when a coherent solvus or spinodal is shown on a T-X diagram, it should be labeled with the orientation of the lamellae. Usually this is unnecessary because there is one orientation of lamellae or modulated structure which has a much lower strain energy than any other. However, it may occasionally happen that two dissimilar orientations have similar strain energies associated with them; then there may be two sets of curves (b) and (d) in Figure 3 which are close to each other. This situation arises in the pyroxenes (see Volume 7 in this series).

The phase diagram shown in Figure 3 can be divided into various regions characterized by the possible exsolution mechanisms. Area (1), between curves (a) and (b), is often referred to as the region of heterogeneous nucleation because it is the *only* mechanism possible in this region. The nucleus must become at least partially noncoherent before it can reach a critical size in this region, and this often limits nucleation to dislocations or grain boundaries. Heterogeneous nucleation can also occur in areas (2) and (3), but it is not the only possible mechanism in these areas. Area (2) lies between curves (b) and (d), and area (3) is below curve (d). In areas (2) and (3), a coherent nucleus can reach critical size; hence, nucleation is more likely to occur randomly and at many places, giving rise to homogeneous nucleation. Area (3) is the upper limit for spinodal decomposition. Because there is no nucleation barrier to overcome by this process, area (3) is often referred to as the unstable region of the diagram. The rate of exsolution is only limited by the diffusivities of the ions. By contrast, exsolution in areas (1) and (2) must overcome the nucleation barrier, and these areas comprise the metastable region. In this region a solid solution should exsolve, but the nucleation barrier must be overcome, and this may retard or even prevent exsolution from occurring.

In alloys, spinodal decomposition and homogeneous nucleation are recognized as competing mechanism in area (3), and the distinction between these mechanisms is very difficult to make experimentally. Most of the experimental verification of spinodal decomposition in alloys has come from low-angle x-ray scattering which reveals how compositional fluctuations change with time. The expected behavior is that a dominant or preferred wavelength will be selected from the broad spectrum of compositional fluctuations, and this wavelength will receive maximum amplification (Hillard, 1970; Langer, 1973). This preferred wavelength is characteristic of the annealing temperature below the coherent spinodal (undercooling). The wavelength is infinite at the coherent spinodal and decreases rapidly with increasing undercooling. For a typical alloy the dominant wavelength for 10°C undercooling is about three times what it is for several hundred degrees undercooling (Cahn, 1968).

Unmixing in alloys involves the migration of all atoms and hence nucleation and spinodal decomposition may be competing mechanisms in area (3) on Figure 3. Unmixing in silicates may be viewed somewhat differently (Aaronson *et al.*, 1974). Many silicates have a fixed substructure consisting of Si, Al, and O. Judging by the rate of tetrahedral ordering and disordering, Si and Al migration essentially ceases at subsolvus temperatures (see Chapter 8). In alkali feldspar, unmixing by a spinodal mechanism requires diffusion of only the alkalis through the relatively immobile silicate substructure. Thus, spinodal decomposition may be expected to be relatively fast, limited only by the diffusivities of the alkalis; whereas, nucleation requires the migration of all ions in the structure. Even though the barrier to nucleation may become small at high supersaturation (Fig. 3), the kinetics of nucleation may be limited by the slowest diffusing ions. The diffusivities of Si and Al may be so slow that nucleation does not occur even in many geologic environments. This is an important question to which we will return shortly.

EXSOLUTION MICROSTRUCTURE

The exsolution microstructure which is produced experimentally in alkali feldspar is similar to that observed in many natural cryptoperthites. Figure 4 shows a typical bright field TEM image of exsolution lamellae produced by annealing a sanidine-high albite crystal of Or_{41} (mol %) in air at 500°C for 14 days. The plane of the micrograph is approximately (010) which is normal to the lamellae. The lamellae are clearly visible along the bright bend contour because of the diffraction contrast between the lamellae. (Diffraction contrast is due to the difference in the spacing or orientation of equivalent lattice planes in different parts of a crystal. The difference in the composition of the lamellae, structure factor contrast, contributes very little to the contrast between the lamellae.)

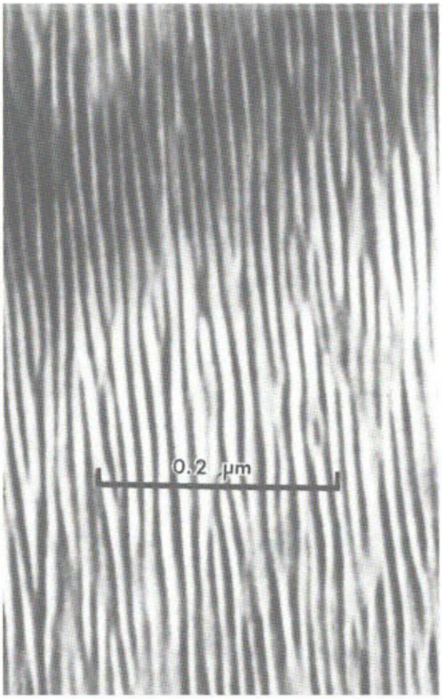

Figure 4. Bright-field TEM image of exsolution lamellae in annealed Or_{41} crystal. The lamellar periodicity is ~145 Å.

Several aspects of the microstructure in Figure 4 should be noted. In general, individual lamellae are long compared to their width and the same would be observed on a micrograph taken parallel to (001). Thus the lamellae have a large aspect ratio. They are parallel to $(\overline{10}\cdot0\cdot1)$.

The lamellae are not perfectly straight although they tend to be uniform in width and a lamellar spacing is easy to measure. The lamellae occasionally bifurcate and their ends are pointed. Most importantly, these lamellae are developed uniformly throughout the grain, and there is no significant variation in lamellar width throughout a grain.

The electron diffraction pattern of this grain is essentially identical to one which is shown in a later figure (Fig. 8). The reflections normal to the lamellae interface are sharp; whereas $h00$ reflections are doublets indicating a major compositional difference between the lamellae. Each principal reflection in a doublet has side bands normal to $(\overline{10}\cdot0\cdot1)$. The separation of the side bands from the principal reflection indicates a periodicity which agrees with the lamellar spacing measured on the micrographs. This spacing is approximately 145 Å.

Although the microstructure shown in these figures is clearly due to exsolution, it has no characteristics which permits one to say whether it formed by coherent and homogeneous nucleation beneath the coherent solvus, or by spinodal decomposition beneath the coherent spinodal. The fact that the lamellae are coherent indicates that the exsolution did not occur outside the coherent solvus. Because the microstructure is uniformly developed throughout the crystal and the lamellae are on a much smaller scale than the spacing of dislocations (none of which are visible in Fig. 4), it is clear that if classical nucleation was involved it was not heterogeneous.

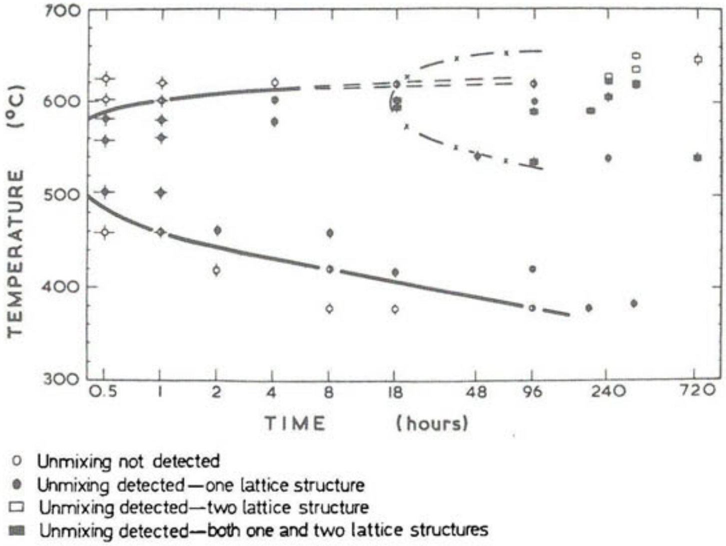

Figure 5. Time-temperature-transformation diagram for exsolution in an alkali feldspar of 37 wt % Or. From Owen and McConnell (1974).

The assumption is commonly made that such a microstructure formed by spinodal decomposition, but proof of the mechanism requires additional evidence which is discussed in the next section.

EXPERIMENTAL STUDY OF ALKALI FELDSPAR EXSOLUTION

This discussion will be divided into two parts; the first concerns the initial development of a lamellar microstructure and the identification of the exsolution mechanism. The second part will consider coarsening of the lamellar microstructure during additional annealing. The latter process is independent of the mechanism by which the initial microstructure formed.

Development of the initial microstructure

Owen and McConnell (1974) have published details of an experimental study of the kinetics and mechanism of alkali feldspar exsolution. They started with a natural cryptoperthite with a lamellar spacing of approximately 100 Å and a mean composition of $Or_{37}Ab_{63}$ weight percent. This sample was homogenized by heating at 750°C, and its unit cell parameters (a = 8.305 Å, b = 12.973 Å, c = 7.165 Å, and β = 116.45°) indicate that it is partially ordered (see Fig. 4 in Chapter 3). The homogenized sample was subsequently annealed hydrothermally at one kilobar and various temperatures. The exsolution microstructure produced in these samples was observed by TEM. The results of their experiments are shown in Figure 5.

Diagrams of the type shown in this figure are commonly used in alloy studies. They show the time required at various temperatures for a specified volume fraction of the sample to transform, in this case to exsolve. These time-temperature-transformation or TTT diagrams normally specify the percent transformation (Yund and McCallister, 1970; McConnell, 1975). In this sense the diagram shown in Figure 5 is somewhat different because it shows the type of microstructure, if any, observed in the annealed samples.

No exsolution was observed at conditions either above or below the solid curve in this diagram. Between the solid curves and in the area of the solid dots a fine-scale microstructure similar to that shown in Figure 4 was observed. The lamellar spacing in this microstructure was typically 90 to several hundred Ångstrøms. In the area of the unshaded rectangles a similar microstructure was observed except that it had a larger spacing, typically 600 Å. The electron diffraction pattern of the latter showed doubling of the principal reflections; whereas; only side bands were observed about a single principal reflection from the finer scale microstructure. They refer to these as one- and two-phase structures, respectively. Both microstructures were observed at the conditions shown by the solid rectangles.

Owen and McConnell interpreted the difference in the microstructure as due to different mechanisms. The wavelength of spacing of the fine-scale (one-phase) microstructure appeared to be characteristic of the annealing temperature and larger at the higher temperature. This agrees with predictions of spinodal theory, and this is the principal evidence to support this mechanism in alkali feldspar exsolution.

They also studied the variation of the modulation wavelength (lamellar spacing) as a function of annealing time. The wavelength was determined from the side band spacing on single-crystal x-ray oscillation photographs. The crystal was heated in air on the camera. The results are shown in Figure 6. They conclude from these experiments that coarsening of the lamellar microstructure does not occur.

The coarse microstructure shows doubling of principal reflections which they attribute to nucleation and growth. The data in Figure 5 suggest that this is a random event, more probable at the higher temperatures and longer annealing times. They also observe Albite twinning in the lamellae of the sodic phase which they attribute to the displacive inversion from monoclinic

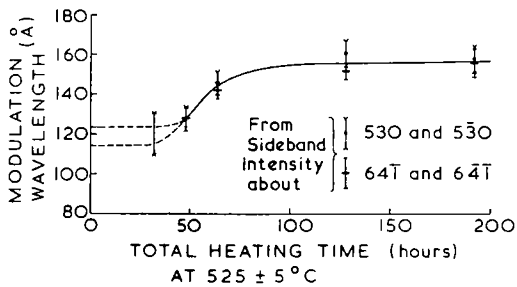

Figure 6. The modulation wavelength of maximum amplitude as a function of annealing time at 525°C. The wavelength was determined from the side band spacing on single-crystal x-ray oscillation photographs. From Owen and McConnell (1974).

to triclinic symmetry. The sodic lamellae in the fine-scale microstructures do not invert to triclinic symmetry because they are perfectly coherent and the strain is homogeneous.

In a later study, Yund *et al.* (1974) examined the microstructure of samples used to determine the coherent solvus for the maximum microcline-low albite series (Yund, 1974), which was discussed in Chapter 5. The principal points of contrast with Owen and McConnell's results are the observation of a single exsolution microstructure and the coarsening of this microstructure with further annealing. Because the coherent solvus and coherent spinodal are at a higher temperature for the ordered alkali feldspars, the annealing can be done at a higher temperature and changes in the microstructure are more readily detectable because of the faster kinetics.

A series of TEM micrographs and details of the electron diffraction patterns from Yund *et al.* are shown in Figure 7. After short annealing times at 600°C, a lamellar microstructure is observed (a) and its diffraction pattern (b) consists of single $h00$ reflections with side bands. This is in agreement with Owen and McConnell's results. However, with increasing annealing time, the $h00$ reflections become elongated and finally two distinct reflections are observed in addition to side bands (d). This indicates that the compositional difference between the lamellae has increased and the lamellar compositions are approaching the coherent solvus. The lamellar spacing also becomes larger with increasing annealing time (compare a and c), but this coarsening is relatively slow compared to the compositional change. As the lamellae become larger the sidebands become unresolved, but the lamellae remain perfectly coherent. The continuous change in the composition and coarsening of the lamellae is not inconsistent with spinodal unmixing as Owen and McConnell suggest. Coarsening occurs regardless of the exsolution mechanism and is

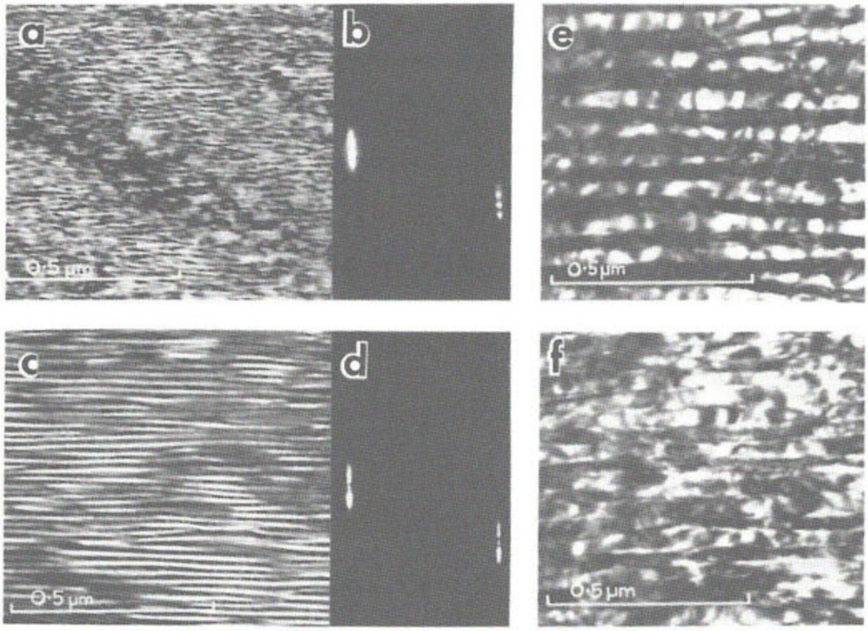

Figure 7. Dark-field images of exsolution lamellae and details of diffraction patterns. (a) Sample annealed at 600°C for 4 hours, $\bar{g}$ = 400. (b) Diffraction pattern of (a). (c) Sample annealed at 600°C for 28 days, $\bar{g}$ = 200. (d) Diffraction pattern of sample annealed at 600°C for 7 days. (e) Sample annealed at 700°C for 28 days, $\bar{g}$ = 200. (f) Same area as (e) except imaged with $\bar{g}$ = 002. From Yund et al. (1974).

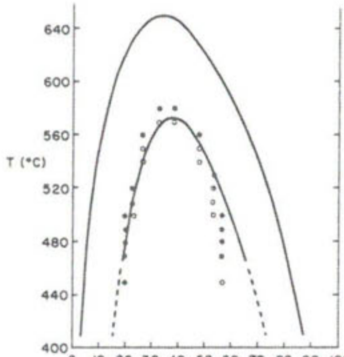

Figure 8. TEM observations of samples with exsolution (open circles) and samples in which no exsolution was observed (solid dots). Observations are shown relative to the coherent solvus for sanidine-high albite and these data approximately outline the coherent spinodal. Upper curve is the strain-free solvus. From Sipling and Yund (1976).

unrelated to the selection of a dominant wavelength during spinodal unmixing. The sharpness of the double principal reflections suggests that by the time the exsolution has reached this stage a compositional profile across the lamellae would be nearly a square wave. Although coarsening is continuous with spinodal unmixing, it is a late stage process and the two processes have different driving forces (see next section).

Sipling and Yund (1976) have reported on the exsolution microstructure observed in samples of the high albite-high sanidine series. The preparation of these materials was described in the previous chapter. The micrograph shown in Figure 4 is characteristic of these samples, and the change in the microstructure with time is essentially the same as that described above for the maximum microcline-low albite series. The important results of the TEM examination of the disordered feldspars are given in Figure 8. All experiments were done at one atmosphere. The smoothed curve for the coherent solvus in this system is shown by the lower of the two curves. The upper curve is the approximate strain-free solvus at one atmosphere (Thompson and Waldbaum, 1969).

The TEM data in Figure 8 are superimposed on the coherent solvus and indicate whether an exsolution microstructure was observed by TEM. Samples represented by a solid dot did not show any evidence of exsolution, even though experiments were done for over six months above the coherent solvus. Samples represented by open circles developed an exsolution microstructure in 24 hours or less. These results agree well with the position of the coherent solvus at the higher temperature. At lower temperature on the potassic limb the TEM microstructural data indicate that exsolution does not occur except well inside the coherent solvus. Sipling and Yund interpret this as indicating spinodal unmixing inside the coherent spinodal. Only well below the critical point are the coherent spinodal and coherent solvus sufficiently separated for this distinction to be made (*cf*. Fig. 8).

The available experimental results demonstrate that alkali feldspar exsolution probably does occur by a spinodal mechanism. The principal question is whether nucleation outside the coherent spinodal does occur, and if so, under what conditions.

Owen and McConnell have interpreted the coarse scale microstructure in their experiments as due to nucleation and growth between the coherent spinodal and the coherent solvus. They place this interval between 630° and 650°C. The higher overall temperature compared to Sipling and Yund's results is easily accounted for by the slightly lower structural state of Owen and McConnell's sample. However, it is surprising that for the composition of their sample, which is near the critical composition, they would have detected the difference between these curves. Sipling and Yund have observed only one microstructure which they attribute to spinodal unmixing. The late stage coarsening of this microstructure is similar to the coarser microstructure of Owen and McConnell.

Sipling and Yund's experiments were done dry; whereas, Owen and McConnell's were done hydrothermally at one atmosphere. The presence of water could promote nucleation through a dissolution and reprecipitation mechanism, but this would not account for the homogeneous distribution of the nuclei throughout the grains. Unpublished data by the author indicate that the microstructural observations shown in Figure 8 can be reproduced (at slightly higher temperature) using starting materials synthesized from gels and annealed hydrothermally at two kilobars.

Exsolution in the alkali feldspars can be contrasted to that in plagioclase. In order for plagioclase feldspars ($NaAlSi_3O_8$-$CaAl_2Si_2O_8$) to unmix, Al and Si as well as Na and Ca migration are required. Consequently, even spinodal unmixing is slow and the low-temperature miscibility gap in the plagioclase feldspars is uncertain and not amenable to conventional experimental study for the most part.

Coarsening of the lamellar microstructures

The experimental study by Yund *et al.* (1974) established that coarsening of the lamellar microstructure does occur in the ordered alkali feldspars, and a more detailed study of the kinetics of lamellar coarsening in the sanidine-high albite series was reported by Yund and Davidson (1978). Their coarsening data are shown in Figure 9. The lamellar spacing (λ) is proportional to the cube root of the annealing time (t) at constant temperature, and it is given by the relation:

$$\lambda = \lambda_o + kt^{1/3} \qquad (1)$$

where λ_o is the spacing at zero time and k is a rate constant for each temperature. According to the Arrhenius relation, the log of k should vary linearly as a function of 1/T, and this is shown in Figure 10. The data define a straight line within experimental uncertainty, and the equation of this line is:

$$k(\text{Å}/\text{day}^{1/3}) = (1.78 \pm 2.20) \times 10^8 \exp[(-25{,}000 \pm 1200)/RT] \qquad (2)$$

where R is the gas constant and T is °K. These data were obtained for samples annealed in the air, but no difference was observed in the coarsening rate at 2 kbar water pressure and 530°C.

Coarsening of small precipitates occurs because the interfacial energy can be lowered by reducing the surface area. This applies to coherent or noncoherent particles. The slight difference in the thickness and regularity of the lamellar microstructure is sufficient for certain of the lamellae to grow at the expense of others. A $t^{1/3}$ dependence has been empirically observed for coarsening of other lamellar microstructures including SnO_2-TiO_2

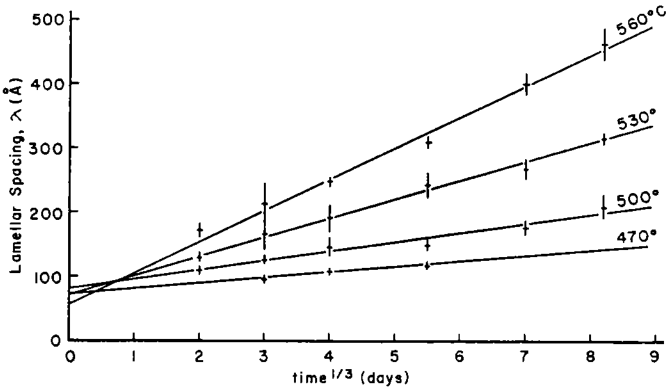

Figure 9. Change in the lamellar spacing for sanidine-high albite samples annealed in the air at the temperatures shown. Lines are least-squares fits to the data. From Yund and Davidson (1978).

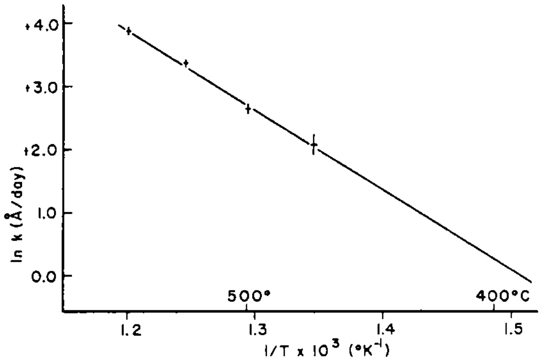

Figure 10. An Arrhenius plot of the rate constant k for lamellar coarsening versus temperature. The equation for the line is given in the text. From Yund and Davidson (1978).

(Park *et al.*, 1976) and iron-free clinopyroxenes (McCallister, 1978). The theory of lamellar coarsening kinetics predicts a $t^{1/3}$ dependence for the growth of spherical precipitates (Lifshitz and Slyozov, 1961; Wagner, 1961; Langer, 1971), but the time dependence for the growth of lamellae has not been worked out. On the strength of the empirical data, the experimental results can be extrapolated to longer times to predict thermal histories for cryptoperthites as described in the next section.

MINERALOGICAL APPLICATIONS

The nearly ubiquitous occurrence of perthites in granitic rocks has prompted extensive study of their microstructures over many years. It is impossible to mention more than a few of the observations and ideas of the many researchers who have contributed to our understanding of perthites. These studies are summarized by Smith (1974b, pp. 399-519), and the reader is strongly advised to consult this review for the many important references and ideas not mentioned in this section.

Although there are still many questions to be answered, the material presented in this and the previous chapter can be used to demonstrate several potential ways of interpreting the thermal histories of crypto- and coarser perthites. The emphasis in this section reflects the author's interests and prejudices, but hopefully, it will encourage the reader to consider other ways in which perthites can be used to help understand geological processes. The reader is referred to the paper by McConnell (1975) in order to see another potential, and somewhat different, approach to this problem.

Cryptoperthites

Lamellar cryptoperthites. Cryptoperthites are easier to interpret than coarser perthites because their microstructures are similar to those produced experimentally. We will consider first those cryptoperthites with more or less regular lamellae parallel to approximately ($\bar{6}01$) and at least partially coherent.

Coherent cryptoperthites can only have formed by exsolution when the originally homogeneous phase intersected the coherent solvus or the coherent spinodal. Exsolution above the coherent solvus, or any origin other than exsolution, would result in noncoherent phases. Spinodal unmixing is probably the operative mechanism unless cooling between the coherent solvus and coherent spinodal is very slow. Consequently, there is some uncertainty in whether to use the intersection of the bulk composition with the coherent solvus or the coherent spinodal to determine the temperature at which exsolution commences. For bulk compositions near the critical composition, the difference in the temperatures of the coherent solvus and the coherent spinodal is small and of little significance for estimating the temperature at which exsolution began. The distinction between spinodal unmixing and coherent nucleation is more important for sodic or potassic bulk compositions.

If the lamellae are coherent, the temperature at which they homogenize will indicate the coherent solvus and give a maximum temperature for the

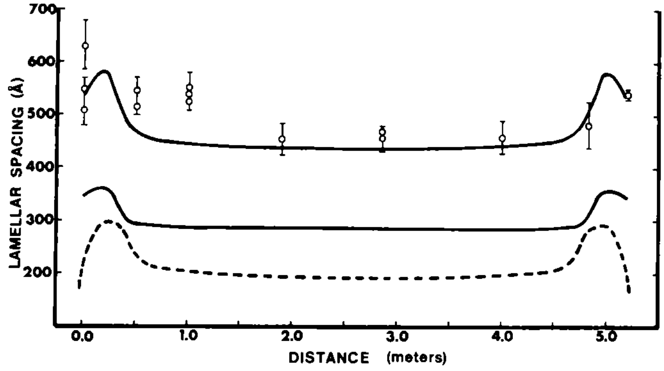

Figure 11. Comparison of observed (circles with bars) and calculated lamellar spacings (smooth curves) across a 5.2 m wide dike. The solid and dashed curves are for different heat flow calculations. The two solid curves show the difference for a coarsening activation energy of 24,000 cal/mole (upper curve) versus 25,000 cal/mole. From Christoffersen and Schedl (1980).

initiation of exsolution. This independent determination of the coherent solvus is especially useful if the cryptoperthite contains more than 1-2 mole percent anorthite. Isothermal annealing and examination by x-ray diffraction can be used to determine the homogenization temperature, although TEM examination would be more accurate.

The compositions of the lamellae, determined by x-ray diffraction and corrected by one of the methods described, will indicate whether the cooling rate was very fast or occurred more slowly. If the lamellar compositions are near Or_0 and Or_{90}, the exchange of alkalis between the lamellae must have continued to very low temperature. If the compositions are more similar, then the coherent solvus can be used to estimate a "quenching-in" temperature. However, except for cryptoperthites which cooled essentially at the earth's surface, the compositions of the lamellae will probably be so near the end-members that this information is not very useful.

One method for estimating thermal histories is based on the coarsening of coherent lamellae in a cryptoperthite during relatively slow cooling. The experimental data summarized by equation (2) have been used to estimate the thermal histories of cryptoperthites from a dike 5.2 meters wide (Christoffersen and Schedl, 1980) and from two lava flows, one overlying the other (Yund and Chapple, 1980). The control on the thermal histories for both of these situations is based on heat flow calculations. There is good agreement between the observed lamellar spacings and those predicted from heat flow calculations and equation (2) for the dike. Some of the results are shown in Figure 11.

The observed lamellar spacings in the lower flow increase slightly as one goes upward from the base, then decrease, but increase again near the top of the flow. This pattern is predicted from the heat flow calculation, assuming that the top of the lower flow was heated by the upper flow. However, the quantitative agreement between the observed and calculated lamellar spacings is not as good for these flows as it is for the dike. The observed spacings in the flows are larger than those predicted from the heat flow calculations and equation (2). Uncertainties or unknown factors include the value for λ_o, how accurate the $t^{1/3}$ is for extrapolation to long times, the parameters used in the heat flow calculation, uncertainties in the original thickness of the flows and their age relations, and the effect of other parameters on the coarsening kinetics. For example, an increase in the Ca content compared to the experimental samples would result in a higher temperature for the top of the coherent solvus/spinodal (Smith, 1978). This would raise the exsolution temperature, which would cause significantly more coarsening. However, Mardon and Yund (1981) report that several mole percent An reduce the exsolution rate, perhaps because of the effect of Ca on the alkali interdiffusion rate. Clearly, more work is needed to evaluate these and other factors and to further test the use of lamellar spacings for estimating the thermal histories in other cryptoperthites.

Nonlamellar cryptoperthites. Cryptoperthites which have cooled slowly may undergo changes in addition to simple coarsening of the lamellar microstructure. Fleet and Ribbe (1963), Bollman and Nissen (1968), Brown *et al.* (1972), Brown and Willaime (1974), McLaren (1974), Lorimer and Champness (1973), and others have reported on microstructures observed in cryptoperthites. Initially, the sodic phase is constrained by its coherency with the potassic phase to have monoclinic symmetry. However, in most natural cryptoperthites the sodic phase is triclinic and has closely spaced Albite twins. Laves (1952) suggested that the twinning increases the effective symmetry of the triclinic sodic lamellae and this reduces the elastic strain energy. This change in symmetry and twinning occurs with little loss of coherency, but the wedge-shaped volumes along the twins are no longer homogeneously elastically strained. Willaime and Gandais (1972) and McLaren (1974) have developed models to explain why the Albite-twin period is a function of the thickness of the sodic lamellae.

The electron micrograph in Figure 12 shows the Albite-twinned sodic lamellae in Spencer M. From the high homogenization temperature reported by Tuttle and Bowen (1958), we can conclude that Spencer M is not perfectly

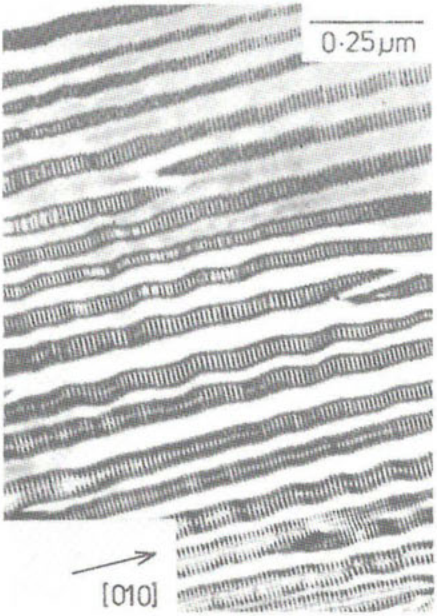

Figure 12. Bright-field electron micrograph of an (001) section of Spencer M. The sodic phase is Albite-twinned. Note the zig-zag nature of the lamellae. From Lorimer and Champness (1973). (1973).

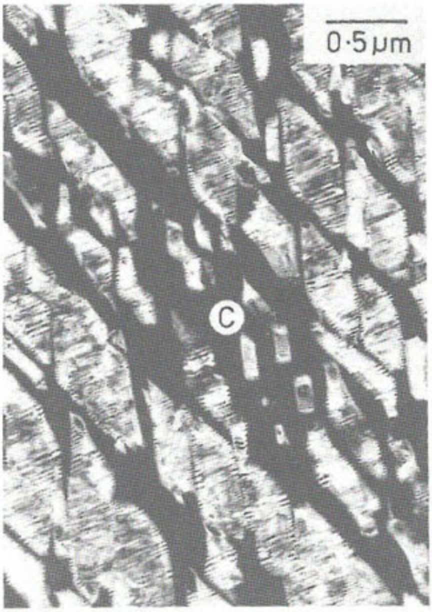

Figure 13. Bright-field micrograph of an (001) section of Spencer N. The discrete sodic particles are mostly rhombic in section and are Albite-twinned. The remnants of an earlier zig-zag pattern can be seen at C. From Lorimer and Champness (1973).

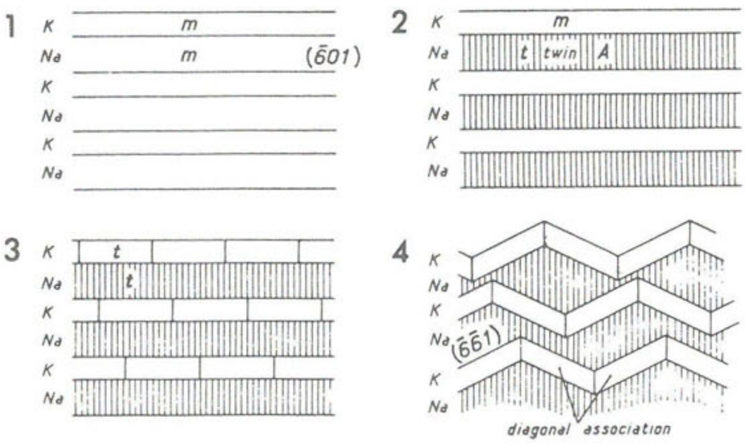

Figure 14. Suggested scheme for the formation of microstructure in cryptoperthite. Symbols m and t are monoclinic and triclinic respectively. See text for discussion of the sequence (1) through (4). From Brown and Willaime (1974).

coherent; however, Δa is 0.36 (Stewart and Wright, 1974), which indicates that the lamellae are at least partially coherent (see Chapter 3). MacKenzie and Smith (1962) report that Pericline twins are present when the sodic phase is highly disordered; whereas, Albite twins predominate if the sodic phase is at least partially ordered.

The exsolution lamellae commonly develop a zig-zag pattern as shown in Figure 12 when the sodic phase is Albite-twinned. Other specimens show rhomb-shaped particles of the sodic phase as illustrated in Figure 13. The interfaces of these rhombs are near $(6\bar{6}1)$ and $(\bar{6}\bar{6}1)$ of the potassic phase. Brown *et al.* (1972) originally suggested that this might be due to two orientations of exsolution lamellae, but more recently Brown and Willaime (1974) and Willaime *et al.* (1976) have suggested that this microstructure is formed from lamellae initially parallel to $(\bar{6}01)$. They suggest the scheme shown in Figure 14 to explain the origin of this microstructure. Exsolution occurs initially on $(\bar{6}01)$ as shown in (1), and this is followed by inversion of the sodic phase and formation of Albite twins as shown in (2). The boundary remains parallel to $(\bar{6}01)$ until the potassic phase becomes triclinic and twinning occurs to minimize the strain due to the inversion (3). The interface changes to $(\bar{6}\bar{6}1)$ because this orientation has a lower elastic strain energy when both phases are triclinic (4).

Lorimer and Champness (1973) emphasize another mechanism to account for the final microstructure shown in Figure 13. Their scheme is illustrated in Figure 15. Initial spinodal unmixing on $(\bar{6}01)$ is followed by coarsening and development of low-energy interfaces which creates a zig-zag pattern. Twinning before or after this stage would result in a microstructure similar to Spencer M (Fig. 12). Further coarsening produces rhombs bounded by $(6\bar{6}1)$ and $(\bar{6}\bar{6}1)$ as the particles tend towards an equilibrium shape. Final alignment or "rafting" of the rhombs is due to interaction of the strain fields in the particles which have different elastic compliances from those of the matrix. Champness and Lorimer (1976) agree that the change in the interphase boundary from $(\bar{6}01)$ to $(\bar{6}\bar{6}1)$ probably occurs as a result of the transformation of the K-feldspar phase to triclinic symmetry.

Coarse perthites

Lamellar perthites which are coarser than a few microns are almost always noncoherent, and this raises a question of whether they passed through a coherent cryptoperthitic stage. The continual gradation in size of some lamellae and the regularity of lamellae in some coarse perthites suggest that they could have been coherent initially, and lost coherency during coarsening.

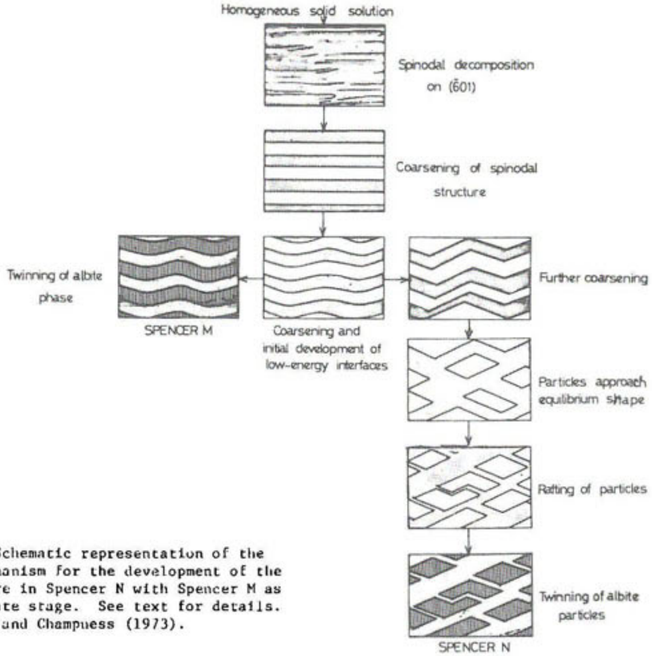

Figure 15. Schematic representation of the proposed mechanism for the development of the microstructure in Spencer N with Spencer M as an intermediate stage. See text for details. From Lorimer and Champness (1973).

However, this is a very subjective interpretation, and certainly many perthites are less regular and their microstructures are not suggestive of a cryptoperthite origin. The real problem is that very slow cooling in plutonic rocks might favor nucleation and growth of noncoherent, irregular perthites above the coherent solvus/spinodal, and this would be indistinguishable from late-stage coarsening and shape changes following a cryptoperthitic origin.

Even if a coarse lamellar perthite has developed by coarsening and loss of coherency from a cryptoperthite, the coarsening rate might be expected to change with time. Once coherency is lost, the nature of the lamellar boundary changes and this would probably change the rate of diffusion along it. Lattice diffusion of the alkali ions does not appear to be dependent on the presence of water (see chapter on diffusion), and this is consistent with the experimental observation that the coarsening rate for coherent lamellae is independent of whether water is present (see earlier section). The coarsening rate for noncoherent lamellae would presumably depend on the nature of the boundary, and this includes the presence of water. Although there are no measurements which allow us to compare grain boundary diffusivities along a dry and a "wet" grain boundary in feldspar, it is generally assumed that the "wet" boundary will allow faster migration of ions along it. Water may also

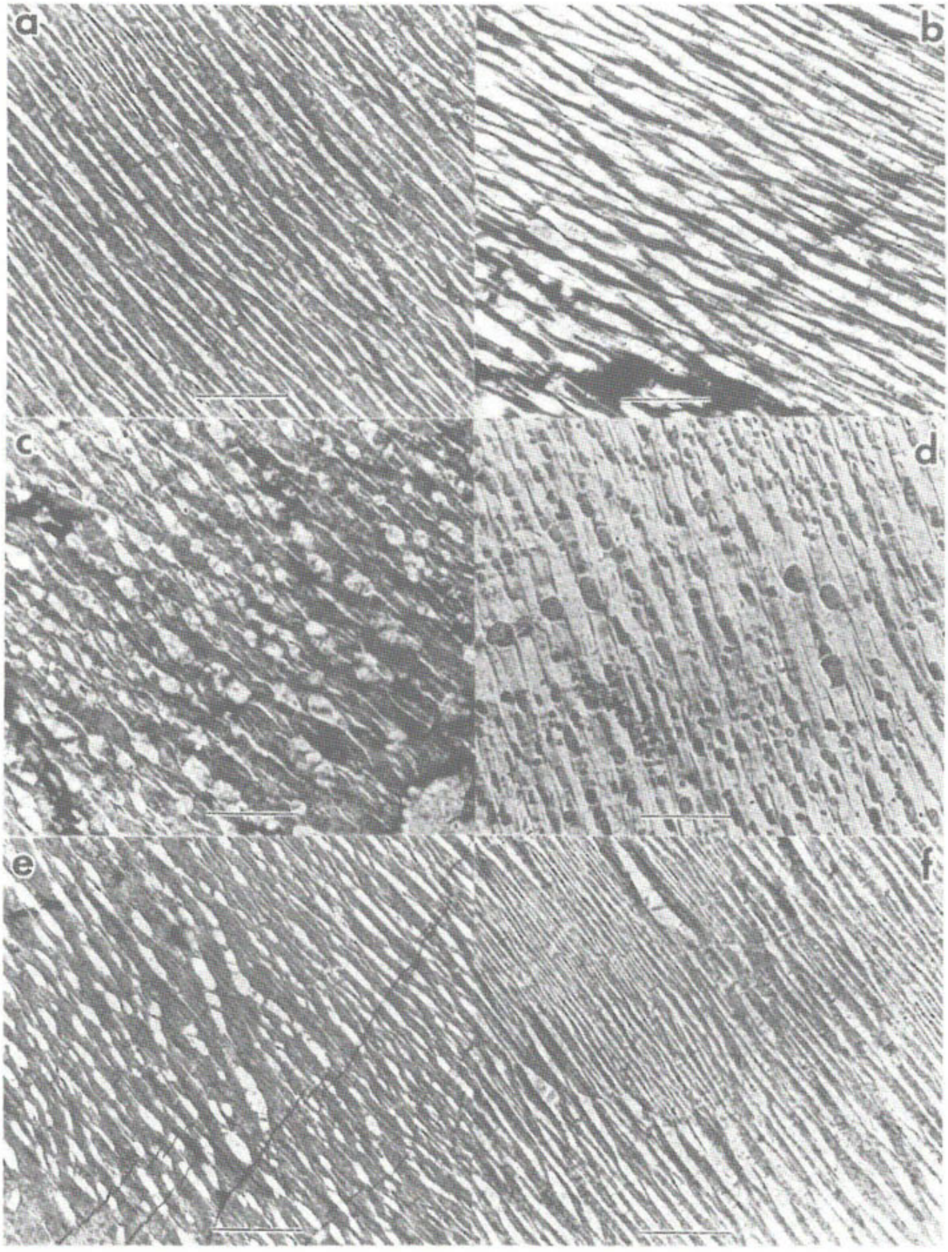

Figure 16. Optical micrographs of coarse perthites from the Storm King Granite (New York). The bar on each photo is 100 μm. See text for description and discussion. From Yund and Ackermand (1979).

influence the development of the microstructure by local dissolution and re-precipitation in coarse, noncoherent perthites.

Although the available evidence indicates that water does not affect coarsening of coherent feldspar lamellae, Parsons (1978) and others have argued that coarse perthites from the same rock mass often show a variability in their microstructures, and he emphasizes that water is likely to have played a dominant role in the development of these microstructures. The importance of water in the development of coarse perthites in many granitic rocks seems very likely, and water may be the dominant factor in many instances. However, the presence and concentration (or activity) of water at the time that the microstructure developed is not easy to determine. Before assuming that water is the only factor, other factors should be evaluated, especially in situations where the water content was either very low or fairly uniform over the sample area. The following examples indicate some of the additional factors which should be considered, and how it may be possible to identify these factors in selected geological situations.

The first four micrographs (a-d) in Figure 16 show the continuous variation in perthite microstructures in the Storm King Granite (New York) from regular lamellae to isolated and roughly equant blebs (Yund and Ackermand, 1979). The potassic phase has a nearly constant composition ($\sim Or_{97}Ab_3$), but the sodic phase ranges from $An_{3.8}$ (lamellae) to An_{21} (blebs). The authors suggested that this correlation of the microstructures with composition was due to a higher exsolution temperature for the Ca-rich grains because of the effect of Ca on the strain-free solvus (Smith, 1978) and/or on the coherent solvus/spinodal. A higher temperature for the initial exsolution involves the effect of Ca on the phase relations as opposed to the effect of Ca on coherent exsolution which may be related to its effect on alkali lattice diffusion (Mardon and Yund, 1981). The variability of the microstructure within individual grains is shown in micrographs (e) and (f) of Figure 16. This variability and lack of a perfect correlation between the Ca content and the microstructure may represent the effect of water on the coarsening kinetics of these microstructures.

Perthites from the granulite complex of Finland (Yund *et al.*, 1980) contain a variety of microstructures (Fig. 17). Many grains contain coherent lamellae (some faintly visible in optical micrograph b) and a third feldspar which is coarser, noncoherent, Ca-rich, and occurs in the form of blebs (micrographs b-d). The suggestion was made that the Ca-rich blebs formed at high temperature by heterogeneous nucleation where it is easier to

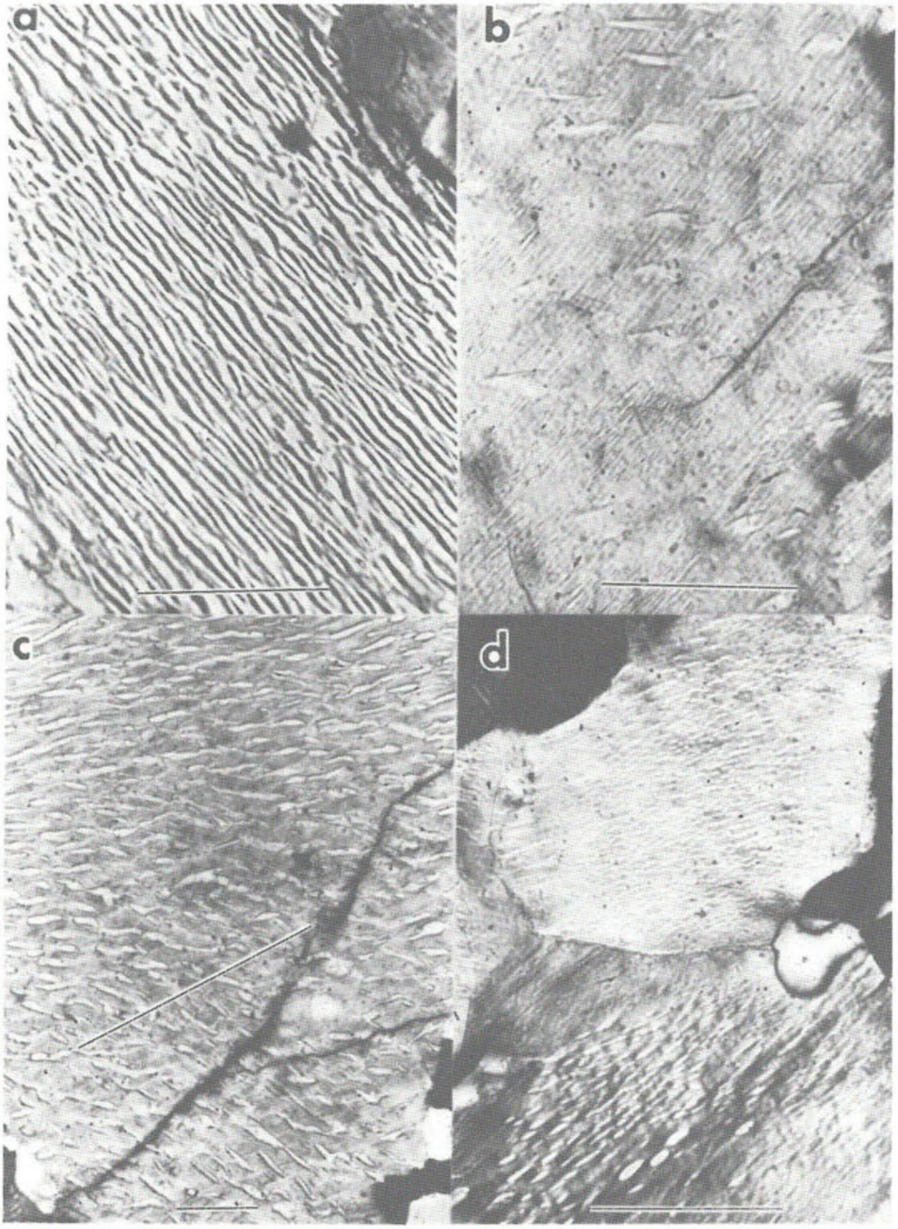

Figure 17. Optical micrographs of perthites from the Finnish granulite complex. The horizontal bar on each photo is 100 µm. (a) A mesoperthite. (b) Microperthite with faintly visible lamellae and coarser blebs. (c) Cryptoperthite (orientation of lamellae shown by diagonal bar) and coarser blebs. (d) Grains showing a large variation in the size of the coarse blebs. From Yund *et al.* (1980).

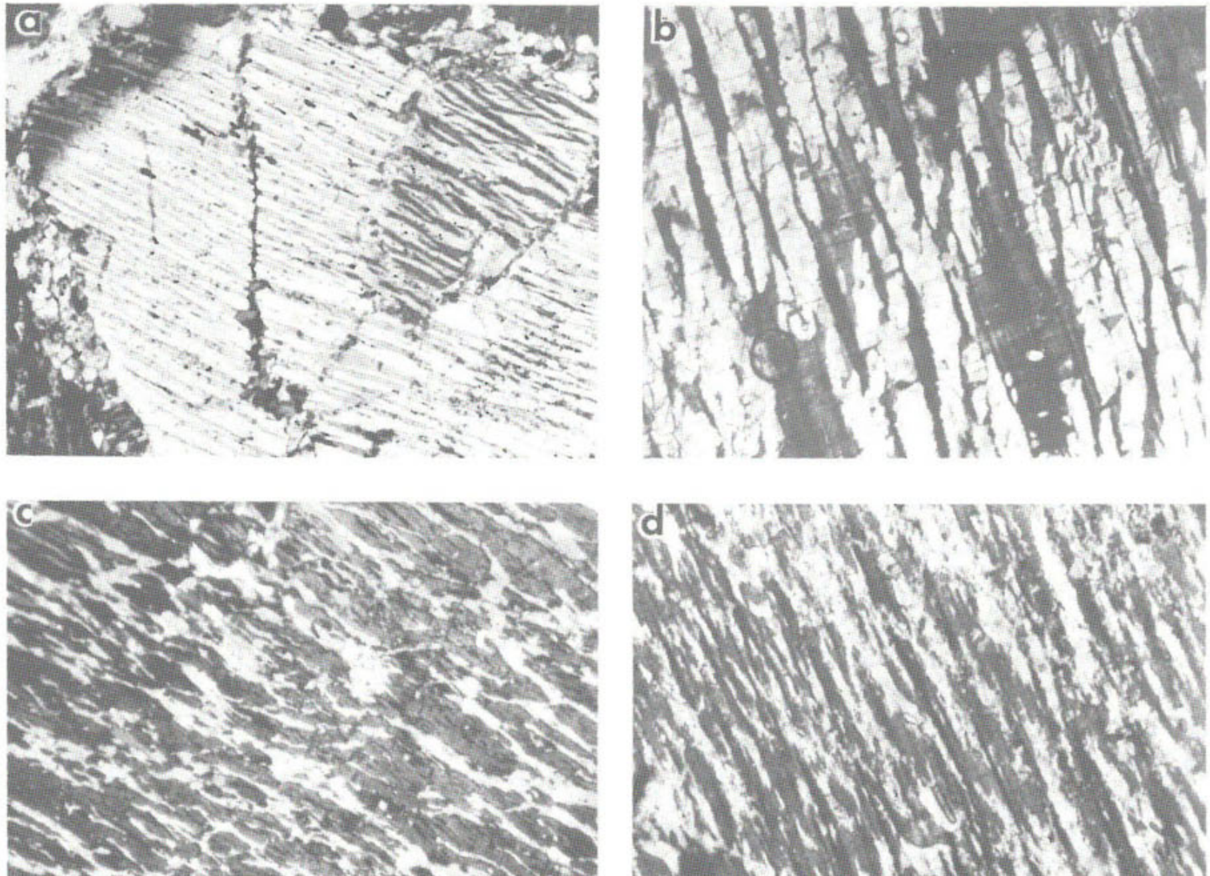

Figure 18. Perthites from the Scituate Granite (Rhode Island). Short **dimension of each** optical micrograph is 2 mm. (a) **Regular vein perthite.** (b) Extremely coarse regular to irregular vein perthite. **(c) and (d) Irregular** vein perthites.

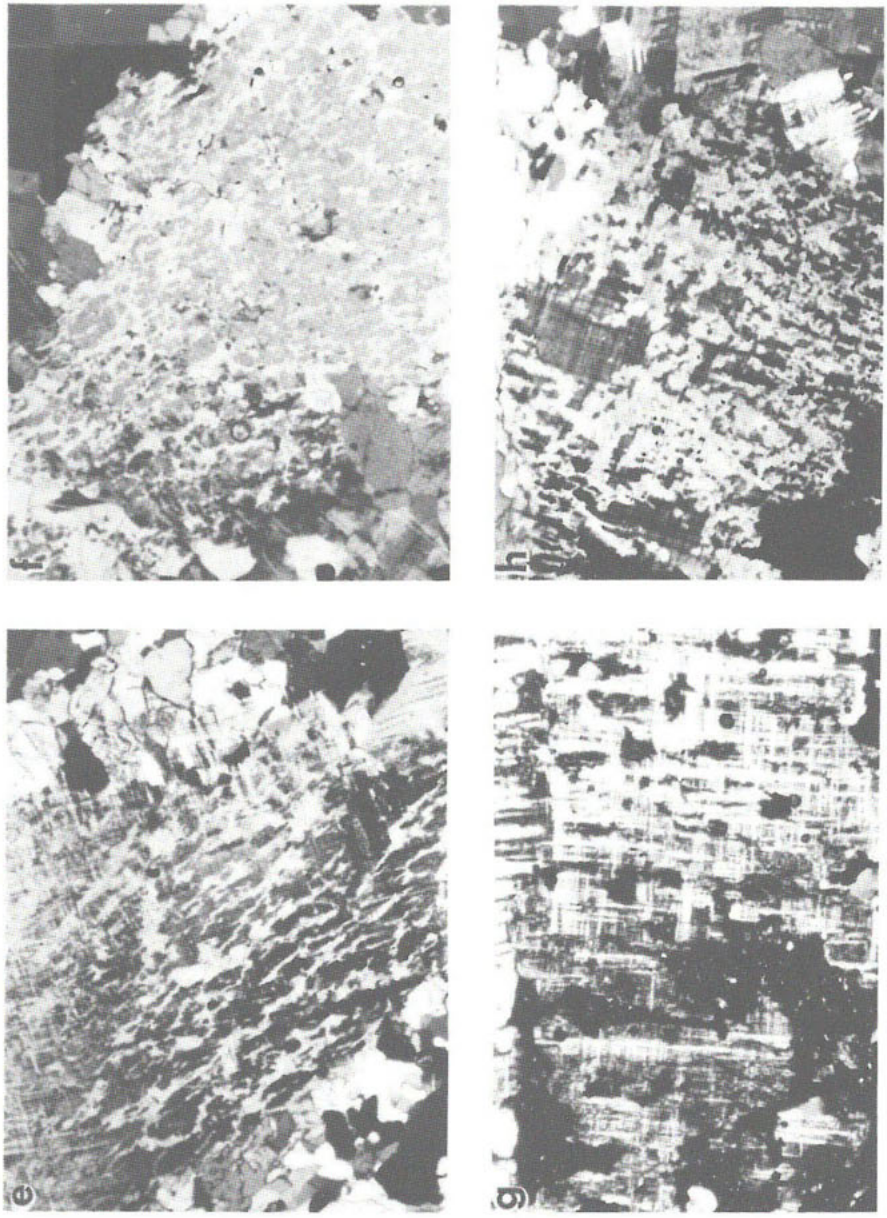

Figure 18 [continued]. (e) Irregular vein perthite with incipient patches. (f) Patch perthite with remnant irregular veins. (g) and (h) Patch perthites. From Day and Brown (1980).

overcome the nucleation barrier. The Ca-poor lamellae formed by spinodal decomposition at lower temperature. Perhaps these microstructures are preserved because of the low water content of these granulite grade rocks.

Day and Brown (1980) report that the irregular vein and patch perthites from the Scituate Granite (Rhode Island) show a geographic variation as illustrated in Figure 18. They have correlated this systematic change with the maximum temperature achieved during prograde metamorphism. Again, water may have played an important role in the development of these perthites, but the water content or pressure could have been sufficiently uniform that it did not mask the effect of the thermal gradient.

Although coarse perthites are difficult to interpret, the progress in our understanding of exsolution mechanisms and kinetics of alkali feldspars has provided some constraints on these problems. The kinetics of late-stage coarsening and shape changes in perthite microstructures are much too slow to be directly investigated experimentally. Hence, most of the progress in understanding these microstructures is likely to come from careful studies of natural samples where the microstructures can be correlated with water content, chemical composition, thermal gradients, etc.

Chapter 8
DIFFUSION in FELDSPARS
R. A. Yund

INTRODUCTION

The kinetics of many mineralogical processes and reactions depend on the migration of ions within essentially perfect crystals. Some of the important processes which depend on this lattice or volume diffusion are exsolution, cation ordering, the exchange of ions or isotopes between minerals or between a mineral and a fluid during subsolidus cooling, and ductile deformation by dislocation creep. Lattice diffusion is generally slower than transport along grain boundaries which in turn is slower than transport by fluid flow. Thus the long range transport of ions during metamorphism must occur primarily by grain boundary diffusion or by fluid flow, but the exchange of ions between adjacent phases may be controlled by lattice diffusion. This chapter will be concerned primarily with lattice diffusion of various ions in feldspars.

Accurate diffusion measurements are often difficult under the best of conditions, but this is especially true for silicates because the diffusion rates of most ions are very slow. There has been considerable interest during the last decade concerning diffusion rates in minerals, and feldspars have been intensively studied. Fortunately, to know the value of a diffusion coefficient to within an order of magnitude is sufficient for many mineralogical applications, and that level of understanding has been achieved for some ions in feldspar.

In the first section below, the meaning and use of diffusion coefficients will be briefly outlined, in the second section the determination of diffusion coefficients for feldspars will be considered, in the third section the data for feldspars will be summarized and critically evaluated, and in the last section several applications will be discussed.

DIFFUSION COEFFICIENTS

The diffusion coefficient, D, relates the flux of ions, J, to the concentration gradient ($\partial c/\partial X$); it is given by Fick's first law,

$$J = -D\left[\frac{\partial c}{\partial X}\right]_t \; , \qquad (1)$$

for transport in one dimension at a fixed pressure and temperature. The common units for D are $cm^2 sec^{-1}$. This relation is only applicable to a steady state, i.e., when there is no change in the concentration gradient with time, t. For most experimental designs and in most mineralogical processes the gradient does change with time, and then the appropriate relation is given by Fick's second law:

$$\frac{\partial c}{\partial t} = \frac{\partial}{\partial X}[D\frac{\partial c}{\partial X}] \quad . \tag{2}$$

The solution of this equation can take many different forms depending on whether or not D is assumed to be independent of composition and on the boundary conditions for a particular situation. Solutions for equation 2 at different conditions are given by Crank (1975).

Diffusion in a crystal is somewhat more complicated than the above equations indicate because ionic diffusion may not be equal for different directions in nonisometric crystals. Volume diffusion coefficients are expressed by a second-rank tensor, and for a triclinic feldspar crystal there are six independent D_{ij}'s. However, at our present level of understanding and application of the data, it is often sufficient to treat the diffusion as approximately isotropic, or to determine the difference between the fastest and the slowest directions in a crystal.

The dependence of D on temperature and pressure is given by the relation (Lazarus and Nachtrieb, 1963)

$$D = D_o \exp[-\frac{Q}{RT}] \exp[-\frac{P\Delta V^*}{RT}] \quad , \tag{3}$$

where Q is the activation energy (commonly given in kcal mole^{-1} or eV; 1 eV equals 23.06 kcal mole^{-1}), R is the gas constant, T is in °K, P is pressure, and ΔV^* is the activation volume. The term in the last parentheses is often much less than one, and hence for conditions within the crust the effect of pressure on lattice diffusion can often be ignored. (An exception to this is the rather special situation with regard to oxygen diffusion in feldspar which will be discussed in a later section.) The first part of equation 3 is the Arrhenius relation, and it is very useful for extrapolating experimental data to lower or higher temperatures. In fact, failure of experimental data to fit closely to the Arrhenius relation generally raises a question as to the validity of the data.

Lattice or volume diffusion coefficients (D_ℓ, D_V, or just D unless the meaning is not clear) are often determined by measuring the diffusion of an isotope in the absence of a chemical gradient. These so-called tracer or self-diffusion coefficients, D*, do vary with the composition of a binary solid solution series; e.g., D^*_{Na} varies as a function of the Ab-Or composition.

Although D* values can be determined for any composition, they have only been determined for end-member or near end-member compositions for the alkali feldspars. On the other hand, the rate of chemical exchange, e.g., between an albite crystal in contact with an orthoclase crystal, is determined by the so-called chemical or interdiffusion coefficient, $\bar{D}$. The interdiffusion coefficient also depends on composition, and its value will be a function of position along the concentration profile (Wagner, 1969).

The relation between $\bar{D}$ and D* has caused some confusion in the literature because a different relation is valid for ionic compounds than for metals (Manning, 1968; Brady, 1975). This difference is due to a fixed anion lattice and the need to maintain charge neutrality in an ionic crystal. For the $NaAlSi_3O_8$ - $KAlSi_3O_8$ binary, this relation is given by

$$\bar{D}(N_{Ab}) = \left[\frac{D^*_{Na} D^*_{K}}{N_{Ab} D^*_{Na} + N_{Or} D^*_{K}}\right]\left[1 + \frac{\partial ln\gamma_{Ab}}{\partial ln N_{Ab}}\right]_{P,T} \tag{4}$$

where D^*_{Na} and D^*_{K} are the tracer diffusion coefficients for a particular mole fraction of albite (N_{Ab}), γ_{Ab} is the activity coefficient, and the last term in brackets corrects for the nonideal mixing of the system. At low temperature, where the alkali feldspar series departs significantly from ideality, the term in brackets becomes very significant (Brady and Yund, in press).

Diffusion coefficients can also be defined for non-lattice diffusion in and through a crystal, e.g., D_{gb} related to diffusion along a grain boundary. These coefficients are discussed at the end of the next section and in the last section where high diffusivity paths in feldspars are considered.

DETERMINATION OF DIFFUSION COEFFICIENTS

Various methods have been used to determine diffusion coefficients for feldspars. Some methods have an inherently higher precision than others, and the scatter of the data on an Arrhenius plot indicates the internal consistency of the data. However, the absolute accuracy of a diffusion coefficient is usually difficult to evaluate. The different experimental methods commonly involve different assumptions or approximations, and the inherent errors are often very different. Furthermore, some methods are applicable only when the D values are within a certain range. Thus the real significance of a comparison of different methods and their results is that it provides the best indication of the ultimate accuracy of the data.

Tracer diffusion coefficients have been determined in various ways. A planar crystal surface of known orientation can be coated with the desired radioactive isotope (Bailey, 1971) or the isotope can be implanted near the surface (Misra and Venkatasubramanian, 1977). A sectioning technique is commonly used to remove a layer of known thickness, in order to determine the isotopic profile in the crystal after annealing. One of the principal limitations of this method is depth resolution, and it gives the best results when the diffusion coefficient is relatively large ($\gtrsim 10^{-12} cm^2 sec^{-1}$). Much smaller D values can be determined ($>10^{-18} cm^2 sec^{-1}$) if the isotopic profile is determined with an ion microprobe (e.g., Giletti *et al.*, 1978). The primary beam in the ion probe is used to sputter a hole in the crystal and the ions emitted from the bottom of the hole are simultaneously analyzed. The depth of the hole is subsequently measured, and by assuming a constant sputtering rate a concentration profile can be determined.

In recent years, a hydrothermal technique has been used to study diffusion in feldspars and other silicates (Hofmann, 1969). The first application to feldspar was by Mérigoux (1968) who studied oxygen diffusion. Carefully sized crystals of feldspars are sealed in noble metal tubes with an aqueous fluid which has an isotopic ratio of alkalis or oxygen significantly different from that in the feldspar grains. After annealing at the desired pressure and temperature, the isotopic ratio in the grains is determined by conventional mass spectrometry (e.g., Foland, 1974a; Yund and Anderson, 1974), or by radioactive counting methods (Lin and Yund, 1972). The diffusion coefficient can be calculated from the rate of uptake of the isotope by the grains from the fluid reservoir. The calculation is outlined in several papers (e.g., Foland, 1974a), and the method is referred to as the bulk isotopic or integrative method. With the integrative method one must assume either isotropic diffusion (spherical model), or some simple anisotropy such as diffusion in a plane but not normal to the plane (cylindrical model). D values calculated using the cylindrical model are about 2.2 times larger than those for the spherical model. Another source of error is that the grains tend to be parallelepipeds rather than spheres or cylinders. However, the assumption of spherical grains gives a D which is only about 0.25 times greater than that for the true parallelepiped shape (Kasper, 1975). This is comparable with the analytical uncertainty of most measurements.

An alternative method is to determine the isotopic profile in a specific crystal direction using the ion microprobe (e.g., Giletti *et al.*, 1978). This technique enables the diffusional anisotropy in the crystal to be determined, as well as providing a completely different method for determining diffusion coefficients.

An important question with regard to the hydrothermal technique concerns how the isotopic exchange occurs. In the original study (Mérigoux, 1968), it was assumed that only lattice diffusion contributed to the isotopic exchange unless the grains and fluid were out of chemical equilibrium. When the Na/K ratio of the feldspar and the fluid is far from equilibrium, the grains are reconstituted by a fine-scale dissolution and reprecipitation process (O'Neill and Taylor, 1967). At high temperature, and probably at high pressure where solubility is greater, the grains may be modified by dissolution and reprecipitation even if they are in chemical equilibrium with the fluid. The amount of dissolution and reprecipitation is temperature-pressure-time dependent, and the window for lattice diffusion measurements of ions in any mineral must be determined. Untwinned and disordered overgrowths on grains of a maximum microcline were used to demonstrate that only lattice diffusion contributes to the isotopic exchange below about 800°C and 2 kbar water pressure (Lin and Yund, 1972).

Additional proof that the rate of isotopic exchange between feldspar and fluid is controlled by lattice diffusion is provided by the different isotopic exchange rates for potassium and oxygen in the same feldspar at the same temperature and pressure (Yund and Anderson, 1974). A difference in the rates would not be observed if the exchange was due to a mechanism other than lattice diffusion. Finally, there is very good agreement between the results determined by the integrative and ion microprobe methods for potassium diffusion in low albite (Kasper, 1975; Giletti *et al.*, 1974), and for oxygen diffusion in adularia (Yund and Anderson, 1974; Giletti *et al.*, 1978). If dissolution and reprecipitation significantly contributed to the exchange, the results from the two methods would not agree and the isotopic gradient would not be a diffusion profile.

Inter-diffusion coefficients are commonly determined by bicrystal experiments in which two crystals of different compositions are polished and held together during the anneal (e.g., Christoffersen *et al.*, 1981). The resulting concentration profile is measured with the electron probe. Diffusion anisotropy can be determined by this method, and the principal limitation is that it is difficult to accurately determine D values less than about 10^{-14} cm^2 sec^{-1}. [An ion microprobe could be used to determine smaller $\bar{D}$ values.] Petrović (1972) used a variation of this technique which involved the partial exchange of alkalis between a crystal and molten chloride.

A recent technique for determining an average interdiffusion coefficient for a compositional interval is based on the rate of homogenization of exsolution lamellae of known composition and thickness (Brady and McCallister, 1980; Brady and Yund, in press).

Electrical conductivity is related to ionic transport in silicates, and these data can be used to estimate diffusion coefficients (Maury, 1968). The possibility of multiple charge carriers and the actual identification of which one(s) is (are) functional appear to limit the usefulness of this method.

Grain boundary diffusion measurements involve the determination of diffusion profiles in a sample across a grain boundary, and a mathematical treatment is used to extract the grain boundary diffusion coefficient D_{gb} when D_{ℓ} is known. The quantity determined is actually D_{gb} times the grain boundary width, and the evaluation of the grain boundary width is rather subjective. Commonly, an effective diffusion coefficient is used which is the product of D_{gb} and the width.

EXPERIMENTAL RESULTS

The feldspar samples used in most of the earlier cation diffusion studies were perthitic or otherwise not single crystals (Rosenquist, 1949; Jensen, 1952; Sippel, 1963). It is difficult to evaluate the validity of these studies for volume diffusion. Some of the results (Sippel, 1963) are in reasonably good agreement with more recent data, whereas others are clearly a composite measurement of grain boundary and volume diffusion. The samples in these studies were not characterized in detail, and the effect of the different types of diffusion cannot be evaluated. These studies will not be considered any further here.

In the following discussion the experimental results are arranged by topic because this permits a more meaningful evaluation of the data as well as identification of remaining questions and problems. Some of the data are presented in tables, and these should be consulted for information about how particular diffusion coefficients were determined. However, the data for some of the topics are presented only in the text where they are discussed. The figures provide a convenient comparison of the data and show the temperature interval over which the data were determined.

Anisotropy of diffusion in feldspar

The anisotropy of sodium diffusion in an albite at 595°C and one atmosphere was investigated by Bailey (1971). He observed that the diffusion coefficient normal to (010) was 0.1 to 0.6 as large as that for diffusion normal to (001), but within his experimental error these diffusivities could be equal.

Petrović (1972) observed that alkali interdiffusion in an albite is slower normal to (010) than normal to (001), but he ascribed this difference to fractures and spallation of the crystal. He also reported that the alkali diffusion rates normal to (001) and (110) of adularia were about equal, but diffusion normal to (120) was somewhat slower. In reference to unpublished data, he reported that interdiffusion normal to (010) was about one hundredth of that normal to (110) at 890° and 1000°C (Petrović, 1974). The details of these experiments have not been published.

Giletti *et al.* (1974) reported that potassium profiles determined by the ion microprobe in low albite indicate that the diffusion coefficient normal to (010) was one tenth that normal to (001) at 800°C. Preliminary results by Christoffersen *et al.* (1981) for alkali interdiffusion between adularia and albite at 1000°C and 15 kbars also indicate that alkali interdiffusion normal to (010) is one tenth that normal to (001), with diffusion parallel to [011] being intermediate. Preliminary results (Christoffersen, pers. comm.) indicate that interdiffusion parallel to [100] is about equal to that parallel to [011]. Nevertheless, we will use a cylindrical model as the simplest approximation for alkali diffusion in the following sections.

The data for Sr diffusion (Misra and Venkatasubramanian, 1977) indicate that at 800-870°C the diffusion coefficient normal to (010) in a microcline is only about half of that normal to (001) in an orthoclase. The anisotropy of Sr and alkali diffusion need not be numerically equal, but it is reasonable to expect that the relative anisotropy would be the same for these ions.

The anisotropy of oxygen diffusion has been investigated in two albites at 800°C and 1-2 kbar (Giletti *et al.*, 1978). The diffusion coefficients normal to (001), (010), (111), and (130) are approximately consistent with an isotropic (spherical) model.

Effect of hydrostatic pressure and water on alkali diffusion

The early studies of alkali diffusion were either done at one atmosphere or a water pressure of 1-2 kbar. None of these studies observed any effect of hydrostatic pressure within experimental error, but other factors were not constant and the pressure range was small. A more recent study of alkali interdiffusion at 1000°C (Christoffersen *et al.*, 1981) found no difference in the diffusion coefficient normal to (001) between five and 15 kbar. Thus, it appears that the activation volume for alkali diffusion is small (see equation 3), and that the effect of hydrostatic pressure on alkali diffusion in feldspar can be disregarded in most mineralogical applications.

The effect of water is somewhat more problematical. Alkali diffusion coefficients determined in molten salt (Petrović, 1972, 1974; Lin and Yund, 1972) appear to be consistent with those done at 1-2 kbar water pressure when other factors are taken into account. The rate of growth of coherent exsolution lamellae in alkali feldspar at 560°C appears to be the same whether the samples are annealed in air or at 2 kbar water pressure (Yund and Davidson, 1978). Goldsmith and Newton (1974) report that water greatly enhances the attainment of chemical equilibrium at 10 kbar in reversal experiments on the alkali feldspar strain-free solvus, although this reaction rate may not be controlled by lattice diffusion.

In spite of the apparent lack of effect of water on alkali diffusion in most experiments, the question should probably not be considered completely answered. It is known that even a trace amount of water greatly affects the Al/Si disordering rate of alkali feldspar, greatly enhances oxygen diffusion, and extends the field of dislocation creep to lower temperatures (see later section). The possibility must be considered that the molten salt experiments contained traces of water, or that a trace of water is only effective when the confining pressure is above several kilobars. Alkali interdiffusion experiments have been done at 15 kbar with a bicrystal which was vacuum dried at 800°C for several hours before sealing the Pt tube (Christoffersen, pers. comm.). The preliminary results agree with those for an undried sample, indicating that the trace of water ($\sim$0.02 wt %) in the undried sample did not affect the alkali diffusion at 15 kbar.

Alkali diffusion coefficients

The self-diffusion coefficients for Na and K, which are summarized in Table 1 and plotted on Figure 1, show good agreement in some respects and poor agreement in others. The greatest disagreement is between some of the high temperature results (curves 2, 4 and 8 in Fig. 1) and the lower temperature data. The high-temperature data were calculated from alkali diffusion profiles in adularia and albite which were partially exchanged with molten alkali chlorides. These results have a lower precision (up to an order of magnitude) than most of the lower temperature data, and include assumptions of ideality and independence of the self-diffusion coefficient on composition.

Data for high temperature Na diffusion in adularia (curve 8) are in fair agreement with those for Na diffusion in orthoclase shown by curve 9. Similarly, the high-temperature K diffusion for adularia (curve 2) is in fair agreement with that for K diffusion in orthoclase as given by curve 3 in the 600-800°C interval. However, the activation energies for these two sets of data

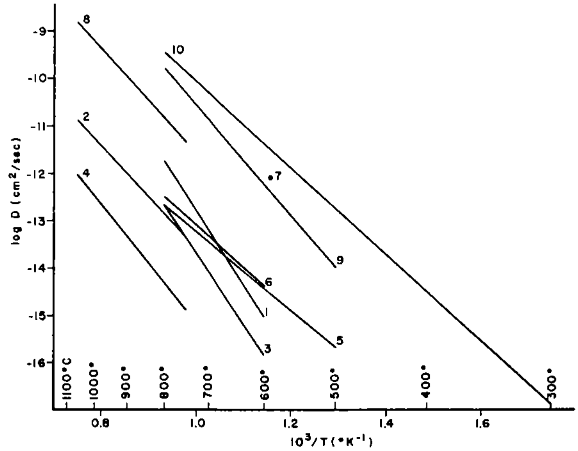

Figure 1. Alkali self-diffusion in feldspar. (1) K in microcline (Lin and Yund, 1972), (2) K in adularia (Petrović, 1972), (3) K in orthoclase (Foland, 1974a), (4) K in low albite (Petrović, 1972), (5) K in low albite (Giletti *et al.*, 1974), (6) K in low albite (Kasper, 1975), (7) Na in low albite (Bailey, 1971), (8) Na in adularia (Petrović, 1972), (9) Na in orthoclase (Foland, 1974a), and (10) Na in low albite (Kasper, 1975). See Table 1 for additional information.

Table 1. Alkali Diffusion in Feldspars.

Ion	Sample & Composition	Temperature °C	Pressure bars	D_o cm^2/sec	Q kcal/mole	Note
K	max. microcline Or_{100}	600–800	500–2000	3×10^2	70 ± 2	1
K	adularia	750–1060	1	$2 \times 10^{-3 \pm 2}$	50 ± 7	2
K	orthoclase $Or_{94}Ab_6$	600–800	2000	$16.1 \begin{smallmatrix}+8.9 \\ -5.7\end{smallmatrix}$	68.2 ± 0.9	3
K	low albite	750–1060	1	$3 \times 10^{-3 \pm 2}$	58 ± 5	4
K	low albite $Ab_{98}Or_{1.4}An_{0.6}$	500–800	2000	1.1×10^{-5}	38	5
K	low albite $Ab_{98}Or_{1.4}An_{0.6}$	600–800	2000	$7.5 \pm 8.8 \times 10^{-5}$	41 ± 6	6
Na	low albite	595	1	$D = 8 \pm 5 \times 10^{-13}$	cm^2/sec	7
Na	adularia	750–1060	1	$3.5 \times 10^{-1 \pm 2}$	51 ± 8	2
Na	orthoclase $Or_{94}Ab_6$	500–800	2000	$8.92 \begin{smallmatrix}+6.68 \\ -3.83\end{smallmatrix}$	57.7 ± 1.1	3
Na	low albite $Ab_{98}Or_{1.4}An_{0.6}$	300–800	2000	.125 ± 0.69	42 ± 2	6

1. Lin and Yund (1972). Hydrothermal-intergrative method. Fine scale cross-hatched twinning. Data are for cylindrical model (original data were for isotropic diffusion).
2. Petrović (1972). Calculation from interdiffusion coefficients (crystal in molten chloride) determined with electrom microprobe. Compositional range Or_{86}-Or_{100}.
3. Foland (1974b). Hydrothermal-integrative method. Data for cylindrical model.
4. Same as (2) except composition range is $Or_2Ab_{96}An_2$-$Or_{10}Ab_{88}An_2$.
5. Giletti et al. (1974). Hydrothermal-ion microprobe. Data for diffusion normal to (001).
6. Kasper (1975). Hydrothermal-integrative method. Data for cylindrical model (original data were for isotropic diffusion).
7. Bailey (1971). Radioactive tracer and sectioning method. Average for diffusion normal to (001) and (010).

are rather different (Table 1); hence, the difference in their D values at lower temperatures will be large. The high-temperature curve for K diffusion in low albite (curve 4) is much lower than that given by curves 5 and 6, and curve 4 is probably less reliable. (The values for D_o and Q given in Kasper, 1975, for K and Na diffusion supercede those given in Kasper, 1974.)

At the level of uncertainty in these data, K diffusion appears to be independent of the Al/Si order in the K-rich phase. The difference between K diffusion in microcline (curve 1) and orthoclase (curve 3) may be due in part to more rapid diffusion along the twin boundaries in the closely spaced albite and pericline twins in microcline.

Considering just the lower temperature data, Na appears to diffuse more slowly in the K-rich end member (curve 9) than it does in albite (curve 10), and K also diffuses more slowly in the K-rich phase (curve 3, and ignoring curve 1 as noted above) than in albite (curves 5 and 6). The Na diffusion data for microcline exchanged to albite (Lin and Yund, 1972) should be disregarded because the grain size was greatly reduced during the alkali exchange and resulted in the calculated D being too large, as noted by Petrović (1974).

Two recent studies of alkali interdiffusion have provided partial experimental confirmation of equation 4 and are reasonably consistent with the lower temperature data shown on Figure 1. Christoffersen *et al.* (1981) measured interdiffusion coefficients for different crystal directions at 1000°C, at 5-15 kbar, for crystals dried at 60°C. The experimental $\bar{D}$ values for diffusion normal to (001) are only about an order of magnitude lower than those calculated from equation 4 using Foland's (1974a) and Kasper's (1975) self-diffusion data, and assuming that D^*_{Na} and D^*_K vary linearly with composition. [Waldbaum and Thompson's (1969) data were used for the activity coefficient as a function of composition.] Interdiffusion coefficients calculated from the homogenization rate of coherent cryptoperthite lamellae at 600°C (Brady and Yund, in press) also show fair agreement with these self-diffusion data. This study also demonstrates the importance of the thermodynamic factor (last term in equation 4) at low temperature. An asymmetrical Margules expression obtained from the coherent solvus of Sipling and Yund (1976) was used to evaluate the thermodynamic factor for the coherent cryptoperthites, and at 600°C this term reduces the interdiffusion coefficient by as much as two orders of magnitude near the coherent solvus.

On the basis of these results it appears that for mineralogical applications the diffusion coefficients shown by curves 3, 5, 6, 9, and 10 give results which are the most internally consistent. It would be useful to have Na

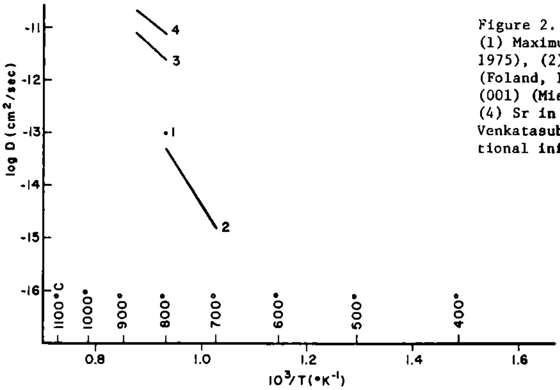

Figure 2. Rb and Sr self-diffusion in feldspar. (1) Maximum value for Rb in low albite (Kasper, 1975), (2) Rb in orthoclase (cylindrical model) (Foland, 1974a), (3) Sr in orthoclase normal to (001) (Misra and Venkatasubramanian, 1977), and (4) Sr in microcline normal to (010) (Misra and Venkatasubramanian, 1977). See text for additional information.

and K self-diffusion coefficients determined for one or more intermediate compositions along the Or-Ab binary.

Rb, Sr, and Ca diffusion

The diffusivities of these cations are not as well known as those for K and Na. In hydrothermal experiments there is difficulty in achieving equilibrium partitioning of Rb between the fluid and the crystal (Foland, 1974a), and a major portion of the Rb, Ca, and Sr may be present as a second phase (Kasper, 1975). Both of these studies used the hydrothermal and integrative method to determine diffusion coefficients. Kasper (1975) reports that in low albite the maximum value for Rb diffusion is approximately 10^{-13} $cm^2 sec^{-1}$ at 800°C (see Fig. 2). [The values given for Rb and Ca in Kasper (1974) should be ignored.] Foland's (1974a) data for Rb diffusion in orthoclase at 700-800°C using a cylindrical model yield an activation energy Q of 73±5 kcal $mole^{-1}$ and a D_o of 38 (+589, -35.7) $cm^2 sec^{-1}$ and are shown on Figure 2.

Misra and Venkatasubramanian (1977) used ion implantation of ^{90}Sr and a sectioning technique. They measured Sr diffusion in orthoclase (Or_{94}) normal to (001) between 800° and 870°C at one atmosphere (Q = 41.2 kcal $mole^{-1}$ and $D_o = 6 \times 10^{-4}$ $cm^2 sec^{-1}$). Their data are shown on Figure 2.

The data for Rb show the same pattern as do those for Na and K; i.e., each ion diffuses faster in low albite than in the K-rich phase, and the smaller Sr ion appears to diffuse faster than the larger Rb ion. The anisotropy of Sr diffusion appears similar to that for the alkalis. Additional determinations of Rb, Sr, and Ca diffusion coefficients, especially at lower temperatures, are needed to better define these diffusivities.

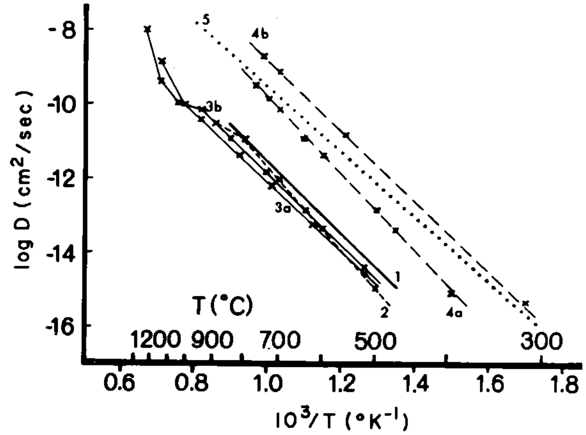

Figure 3. Selected argon diffusion data for feldspar. (1) Foland (1974b), (2) Baadsgaard *et al.* (1961), (3a and 3b) Newland (1963), (4a and 4b) Frechen and Lippolt (1965), and (5) Fechtig *et al.* (1961). Reprinted from Foland (1974b).

Argon diffusion

Because of its interest for K-Ar age dating of minerals, there have been numerous studies of Ar diffusion in feldspar. Many of the earlier studies used perthitic samples, or the experiments were done at conditions where the feldspar was not stable. The results for Ar diffusion in feldspars have been summarized and discussed by Foland (1974b) and will only be briefly outlined here. Figure 3, which is from Foland (1974b), shows the most reliable data for volume diffusion of Ar. Curves 4a, 4b, and 5 (Frechen and Lippolt, 1965; Fechtig *et al.*, 1961) are significantly above the other curves, and it is not known if these samples were inhomogeneous or if the effective diffusion radius was equivalent to the particle size used to calculate the D values.

The four lower curves on Figure 3 show very good agreement below 1000°C and have almost identical activation energies. [Curve 1 is from Foland (1974b); curve 2 is from Baadsgaard *et al.* (1961); and curves 3a and 3b are from Newland (1963).] Recent studies of ^{39}Ar release during heating of microclines (Harrison and McDougall, in press) indicate that the activation energy for argon diffusion may also be a function of the structural state of the feldspars.

Silicon and Aluminum Diffusion

The diffusivities of Al and Si in feldspar are much slower than those for the alkalis. This is indicated by the difficulty of experimentally determining the phase relations of the plagioclases which require Al/Si migration. There have been no direct determinations of these diffusivities using tracer techniques. The available information comes from kinetic studies of tetrahedral order/disorder relations, and from limited kinetic data for homogenization of a lamellar microstructure in bytownite.

A wide range of activation energies (74-94 kcal mole^{-1}) have been reported for disordering of albite in air (McKie and McConnell, 1963). The activation energy for disordering of two albites of the same grain size and water content was about 86 kcal mole^{-1} in air, but at 10 kbar water pressure the value was about 67 kcal mole^{-1} (Yund and Tullis, 1980). At 1000°C and 10 kbar the disordering rate is about twenty times faster than that for samples heated in the atmosphere. Thus the presence of water, at least at high pressure, affects the kinetics of Al/Si interchange in feldspar.

An estimate of NaSi-CaAl interdiffusion is provided by the homogenization data for Huttenlocher lamellae. Grove and Speer (1981) used Nord's *et al.* (1974) homogenization data for a bytownite heated in air to estimate a value of 10^{-17} cm^2/sec for 1300-1240°C. The interdiffusion coefficient at 800°C would be about 5 x 10^{-23} or 10^{-21} cm^2/sec for an assumed activation energy of 85 or 65 kcal/mole, respectively. Clearly, either of these values is much less than those for the alkalis or oxygen which is discussed below.

Oxygen diffusion

There is a significant difference in the rate of oxygen exchange between feldspar and dry air on the one hand, and that between feldspar and water or water vapor on the other hand. As shown in Figure 4, the exchange with air is

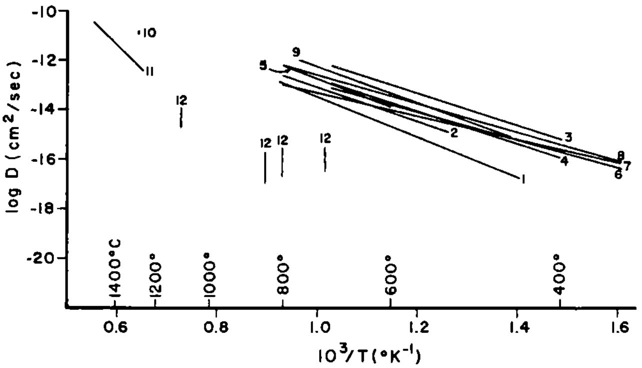

Figure 4. Oxygen diffusion in feldspar. (1) low albite (Mérigoux, 1968), (2) adularia (Mérigoux, 1968), (3) maximum microcline (Yund and Anderson, 1974), (4) adularia (Yund and Anderson, 1974), (5) low albite (Anderson and Kasper, 1975), (6) adularia (Giletti *et al.*, (7) low albite (Giletti *et al.*, 1978), (8) anorthite (Giletti *et al.*, 1978), (9) low albite (Yund *et al.*, 1981), (10) plagioclase (Muehlenbachs and Kushiro, 1974), (11) anorthite (Muehlenbachs and Kushiro, 1974), and (12) approximate values for adularia and microcline (Yund and Anderson, 1974). All data for hydrothermal exchange except (10), (11), and (12) which are dry exchange. See Table 2 for additional information.

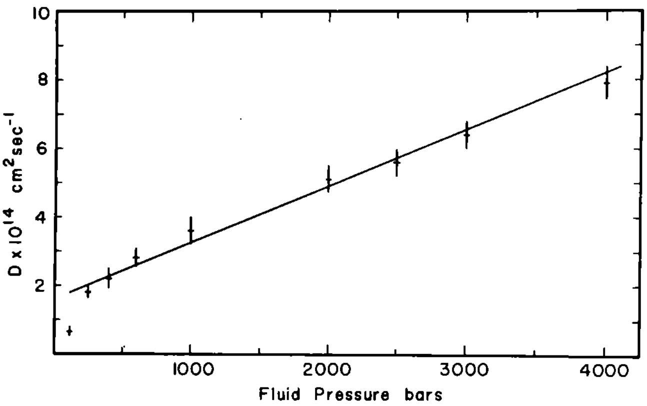

Figure 5. Variation in the measured D value for oxygen in adularia at 650°C as a function of fluid pressure. The least-squares line does not include the 125 bar point. Reprinted from Yund and Anderson (1978).

Table 2. Oxygen Diffusion in Feldspars.

Sample & Composition	Temperature °C	Pressure bars	D_0 cm^2/sec	Q kcal/mole	Ref.[1]
low albite $Ab_{99}Or_1$	440-805	250-600	4.5×10^{-5}	37	2
low albite $Ab_{98}Or_{1.4}An_{0.6}$	600-800	2000	$2.5 \pm 1.4 \times 10^{-5}$	37 ± 2	3
low albite Ab_{97} and Ab_{99}	350-800	1000-2000	$2.3 \pm 0.1 \times 10^{-9}$	21.3 ± 1.2	4
low albite $Ab_{96}Or_1An_3$	450-750	2000	$9.8 \pm 6.9 \times 10^{-6}$	33.4 ± 0.6	5
adularia $Or_{86.5}Ab_{13.5}$	520-800	325-600	9×10^{-7}	32	2
adularia Or_{100}	400-700	2000	$5.3 \pm 1.0 \times 10^{-7}$	29.6 ± 1.1	6
adularia Or_{98}	350-700	1000	4.51×10^{-8}	25.6	7
max. microcline Or_{100}	400-700	2000	$2.8 \pm 4.7 \times 10^{-6}$	29.6 ± 0.9	6
anorthite $An_{95.3}Ab_{4.3}Or_{0.4}$	350-800	1000	$1.39 \pm 0.07 \times 10^{-7}$	26.2 ± 1.1	4
anorthite	1250-1525	1	3.3	90	8
plagioclase	1280	1	$D = 1.4 \times 10^{-11}$	cm^2/sec	8

1. All entries except for the last two (8) were determined using the hydrothermal technique. Of these all were done using the integrative method and assuming isotropic diffusion, except (5) which was determined using ion microprobe. (8) are for exchange with air and using the intergrative method. (2) Merigoux (1968), (3) Anderson and Kasper (1975), (4) Giletti et al. (1978), (5) Yund et al. (In Press), (6) Yund and Anderson (1974), (7) data from (4) and (6) combined, (8) Muehlenbachs and Kushiro (1974).

much slower than that with water. This might reflect the rate-limiting transfer of oxygen across the air-feldspar interface, although this transfer is not rate-limiting for the exchange of oxygen with forsterite (Reddy *et al.*, 1980) or with most oxides (Evenson and Decker, 1978).

As previously noted, water enhances the disordering rate of Al/Si in alkali feldspar, as well as extends the dislocation creep field of feldspar to lower temperature (Tullis and Yund, 1980). Oxygen exchange between water and feldspar increases with increasing water pressure, especially at low pressures (Yund and Anderson, 1978), as shown in Figure 5. Exactly how these different effects are related is not known, but the evidence indicates that water, or one of its components, is responsible for the faster migration of oxygen in feldspar. The effect is on the diffusive migration of oxygen in the solid state, as discussed in a previous section, and is not due to dissolution-reprecipitation or any reconstitution of the feldspar. The mechanism of this enhancement is not known, nor has the diffusing species been identified. For simplicity, we will continue to refer to this as oxygen diffusion, but H^+, OH^-, or other species may be involved.

The rate of oxygen diffusion in the absence or near absence of water vapor is not well known because the D values are so low. The best data are for high temperatures (Muehlenbachs and Kushiro, 1974); only approximate values for D are known at lower temperatures (Yund and Anderson, 1974). The activation energy from the high temperature data is 90 kcal mole^{-1} (Table 2), and below 800°C the difference in the D values for dry versus wet samples is many orders of magnitude (Fig. 4).

The results from hydrothermal experiments by both the integrative and ion microprobe methods are consistent. The data are listed in Table 2 and shown in Figure 4. Most of these data are for 1-2 kbar, but the lower pressure data, curves 1 and 2, would be raised somewhat if adjusted for pressure according to Figure 5. The highest curve 3 in Figure 4 is for microcline, and again there may be some enhancement of the diffusion along twin boundaries as noted for K. All of the hydrothermal experiments for albite, with the exception of curve 7, give activation energies of 33.4 kcal mole^{-1}. The lower value (21.3 kcal mole^{-1}) for the albite determined with the ion microprobe (Giletti *et al.*, 1978) may be real, but this seems somewhat unlikely. In addition to the data shown in Figure 4 and listed in Table 2, there are data for an oligoclase and a labradorite (Giletti *et al.*, 1978) and for the phases in a perthite (Nagy, 1981). Separate D_o and Q were not calculated for these data, but their D values plot near curves 6 and 8.

The available data indicate that oxygen diffusion in feldspar under hydrothermal conditions shows little anisotropy (see earlier section), and the diffusion rate is nearly the same in all feldspars studied. Future studies need to determine the role of water in the migration of oxygen, and to compare this with its effect on the migration of the alkali ions.

Mechanism of ionic diffusion in feldspars

The atomic mechanism of alkali migration in feldspar has been discussed by Petrović (1974). He points out that possible interstitial sites and large cation vacancies are directly connected only in the (010) plane. This observation is in qualitative agreement with the experimental observation of faster alkali diffusion in this plane, but it seems one might expect even a slower diffusivity than is observed normal to (010).

Petrović (1974) argues that alkali diffusion must occur by a vacancy mechanism (i.e., jump of an ion from a large cation site to a neighboring large cation vacancy) because an indirect interstitial mechanism would be possible only approximately in the [001] direction, and he was not aware of any evidence that diffusion was faster in this direction than for other directions in the (010) plane. These arguments are mostly qualitative, and they may have to be reexamined when new and more complete diffusion data are available. The linearity of the diffusion data on an Arrhenius plot indicates that there is probably not a significant change in the atomic mechanism over the temperature interval of the individual measurements.

The crystal-chemical factors affecting the mobility of ions in minerals have been discussed by Dowty (1980). On the basis of (1) anion porosity, (2) electrostatic site energy, and (3) size of the ion, he relates the relative mobilities of ions to their observed diffusivities. He also concludes that under hydrous conditions the mobility of oxygen should be about that of a large univalent cation, whereas under anhydrous conditions the mobility would be about equal to that for a large divalent cation. [Compare Figure 2 and Figure 4.] He also argues that the presence of water should have little effect on cation mobility; this is in accord with the available data for alkalis, but it appears that Si and Al migration may be dependent on water if disordering rates and dislocation creep rates are any indication.

High diffusivity paths in feldspar

Both grain boundary and dislocation-assisted diffusion have been studied in alkali feldspar. Grain boundary transport of oxygen along a lamellar boundary in a perthite has been studied by Nagy (1981) and Giletti and

Nagy (1981). A hydrothermal technique was used to exchange ^{18}O between a perthitic feldspar and a fluid at 500 to 700°C and 1 kbar. The ion microprobe was used to determine lattice and grain boundary diffusion coefficients. The lattice diffusion coefficients were consistent with those previously determined (see earlier section), and $D_{gb} = 0.18\ cm^2sec^{-1}\ exp(-37\ kcal\ mole^{-1}/RT)$, assuming that the effective grain boundary width was 100 Å. [The values in Giletti and Nagy (1981) supercede those given in Nagy and Giletti (1980) and Nagy (1981).] At a given temperature, D_{gb} is about three to four orders of magnitude larger than D_{ℓ} in adularia. This result is somewhat surprising because the activation energy for grain boundary diffusion in oxides is normally less than that for lattice diffusion. As the authors point out, this perthite has a rather special type of grain boundary with a small crystallographic misorientation across it, and the reported value may be a minimum value for D_{gb} of oxygen in feldspar.

The effect of a high, static dislocation density on volume diffusion of oxygen in albite has been evaluated (Yund *et al.*, 1981). Again the hydrothermal and integrative methods were used to evaluate the diffusion coefficients. Measurements were made on undeformed material ($<10^6$ dislocations per cm^2) and on samples which were plastically deformed (5% strain at 1000°C and 15 kbar) to produce a dislocation density of $5 \times 10^9\ cm^{-2}$. The Arrhenius relation for the undeformed albite is given in Table 2 and shown in Figure 4 as curve 9. The effect of the increased dislocation density on volume diffusion for the deformed grains, which is referred to as dislocation-assisted diffusion, D_a, is shown in Figure 6 and is given by $D_a = 7.6 \pm 4.0\ cm^2sec^{-1}\ exp(-30.9 \pm 1.0\ kcal\ mole^{-1}/RT)$. D_a is only about 0.5 to 0.7 orders of magnitude larger than D at 700° and 450°C, respectively. Thus even a moderately high, static dislocation density does not greatly enhance the overall rate of diffusion of oxygen in albite.

From the above data, a value can be estimated for the diffusion coefficient along a dislocation core, so-called pipe diffusion, D_p, if one knows the effective diffusion radius for a dislocation core. Assuming a 3 or 4 Å radius, which is about half the typical Burgers vector for a dislocation in feldspar (see Chapter 13), D_p is about five orders of magnitude larger than D or D_a as shown in Figure 6. The reason for the large difference between D_p and D_a is not surprising when one considers that even for a dislocation density of $5 \times 10^9\ cm^{-2}$, the average separation of uniformly distributed dislocations is about 160 unit cells.

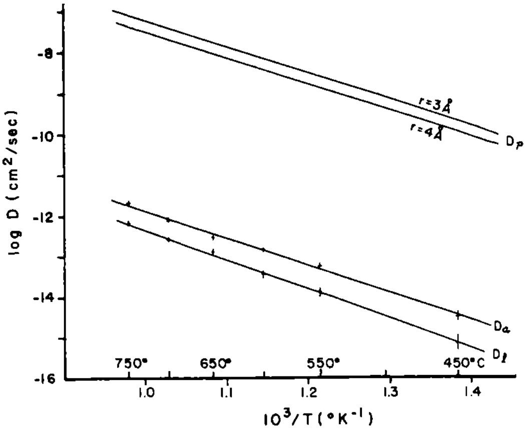

Figure 6. Oxygen diffusion in albite. D_ℓ is lattice diffusion, D_a is dislocation-assisted diffusion for a dislocation density of 5×10^9 cm^{-2}, and D_p is pipe diffusion along the core of a dislocation which a radius (r) as shown. Reprinted from Yund *et al.* (1981).

The above study involved a static dislocation density, i.e., it is equivalent to a ductile deformation preceding the diffusion event. During metamorphism, deformation and diffusion may be simultaneous, and this so-called strain enhanced diffusion, D_s, would be faster because of the motion of the dislocations while diffusion is occurring. However, for a mobile dislocation density of 10^9 cm^{-2} and a typical geological strain rate of 10^{-14} sec^{-1}, D_s would not be significantly larger than D_a.

These results are for oxygen in albite, and it is reasonable that other feldspars would show a similar behavior. It is not clear, however, whether the diffusion rate of cations along dislocations would show a similar enhancement relative to their lattice diffusion coefficients. This together with cation diffusion rates along grain boundaries needs to be evaluated for feldspars.

APPLICATION OF THE DIFFUSION DATA

Lattice diffusion in feldspars, as well as in most minerals, is only significant for transporting ions on the scale of individual grains, but these diffusivities are rate limiting for many mineralogical and geochemical processes. Alkali diffusion is relatively fast compared to ionic diffusion in some silicates, but Al,Si diffusion is very slow in feldspars and most other silicates. Oxygen diffusion is also relatively fast when water is present, but its diffusivity is significantly slower if water or its components have a very low concentration or activity in the feldspar. The general significance of the diffusion data for feldspar are briefly outlined below.

Depending on the mechanism of exsolution, the development of the microstructure may include kinetic factors of nucleation as well as diffusion of the components. However, the formation of alkali feldspar cryptoperthites occurs by a spinodal mechanism (see Chapter 6), and this mechanism does not include the formation of a nucleus. Hence, the exsolution rate is controlled by the diffusivities of the alkali ions. The experimentally observed rate of the reverse process, the homogenization of the lamellae, can be adequately accounted for by the known alkali diffusion data. This is shown by the fact that the average value for the alkali interdiffusion coefficient determined from homogenization experiments agrees well with the diffusion data determined independently (see p. 212).

The rate of alkali interdiffusion not only controls the initial exsolution rate of cryptoperthites, but it also controls the coarsening (change in size) of the lamellar microstructure (see Chapter 7). A quantitative model for this lamellar coarsening has not been developed, but it must include information about the diffusion path. Both the experimental coarsening rate as well as the diffusion data are available, and it should be possible to model this process and then compare the results with the experimental data. If indeed the lamellae are noncoherent, then the coarsening rate is expected to also involve grain boundary diffusion, and evaluation of these kinetics requires additional experimental data for grain boundary diffusion.

Because the interdiffusion of the alkali ions is relatively rapid, pronounced K/Na compositional gradients are not common in alkali feldspar phenocrysts or porphyroblasts. In fact, coexisting alkali feldspars in plutonic and metamorphic rocks continue to exchange alkalis as they cool, and their final compositions commonly correspond to solvus temperatures on the order of several hundred °C. However, if Al and Si are involved in the equilibrium, as in coexisting plagioclases, the (K,Na)-Ca exchange rate is much slower because of the slow diffusivity of Al and Si. Many of the complex microstructures in the plagioclases (see Chapters 9 and 10) are probably a result of the very slow rate of tetrahedral ordering and/or NaSi-CaAl exsolution. In order to use these microstructures to estimate thermal history, we need a better understanding of their formation and better diffusion data for Si and Al.

Tetrahedral ordering obviously requires shorter atomic migrations than does the formation of 10-1000 Å wide exsolution microstructures. However, the slow rates of Al,Si migration severely limit the attainment of ordered states in potassic-rich feldspars and most plagioclases. It now appears, at least for the alkali feldspars, that the degree of tetrahedral ordering may reflect more the presence of water in the feldspar structure than the thermal history of a specimen. Clearly, a better knowledge of the mechanism(s) of atomic migration is needed to help us understand the role of water in Al,Si and oxygen diffusion as opposed to alkali diffusion.

Oxygen diffusion in all feldspars is considerably faster under hydrothermal conditions than one might have predicted based on the concept of a rigid Si-O framework. Significant exchange of oxygen isotopes between a hydrothermal fluid and 1 mm diameter grains will occur by diffusion in less than a thousand years at 400°C (Giletti *et al.*, 1978). The ^{18}O depleted zones around epizonal igneous intrusions are believed to involve hydrothermal convection of ground water, and this in turn plays an important role in the development of geothermal systems, hydrothermal alteration, and the formation of ore deposits (Taylor, 1974). One of the possible mechanisms for this oxygen isotopic exchange is oxygen diffusion in feldspar. The existing diffusion data can be used to model the ^{18}O depletion in and around igneous intrusions (e.g., Parmentier, 1981). In spite of the relatively rapid lattice and grain boundary diffusion of oxygen in feldspar, the transport of oxygen (or other feldspar components) over distances $\geqslant$ meter requires diffusion through an intergranular and connected fluid phase or fluid transport (Nagy and Parmentier, 1981).

The various radiometric methods for determining the age of a feldspar in a rock are based on the assumption that the mineral has retained its radioactive isotopes and radiogenic products since the time of the event that one is trying to date. Whether a feldspar grain has remained a closed system or not will depend on its subsequent geologic history (deformation, recrystallization, cooling rate, etc.), and on the diffusivities of the isotopes being used to determine its age. Thus, one very important application of diffusion data is in geochronological studies. Hart (1981) has used the concept of the "compensation effect" which is based on the observation that the diffusion rates of different species tend to converge at a particular temperature, suggesting a correlation between D_o and Q. He used this relation to help understand the closure temperature at which natural diffusion processes are frozen in. He estimates that this temperature for feldspar is in the range of 400-600°C for a cooling rate between 10 and 10^5 °C/myr. The interpretation of radiometric ages also depends on the effective diffusion distance in the grains, and this has been correlated with the size of perthite lamellae and the microstructure of plagioclase (e.g., Harrison and McDougall, 1981).

Chapter 9

PHASE EQUILIBRIA of PLAGIOCLASE

J. V. Smith

INTRODUCTION

This chapter on the phase equilibria of plagioclase has been revised, though not extensively, over that first published in 1975. It concentrates rather dogmatically on the highlights, giving short change to some of the ideas that have been advanced. Figure 1 summarizes the chemical and diffraction properties of plagioclase as discussed in some detail in Chapter 1, while Figure 2 is a hypothetical phase diagram. For true thermodynamic equilibrium, a solid-solution series should move towards a mechanical mixture (or mixtures) of two (or more) ordered phases as the temperature falls towards absolute zero. In plagioclase, the only observed ordered phases are low albite and anorthite, and all the *micrometer intergrowths* and *'e' superstructures* can be interpreted as nonequilibrium assemblages of coherent or near-coherent structures. Absolutely crucial to the following interpretation is the concept that all sub-solidus plagioclases are moving towards the stable assemblage of low albite and *P*-anorthite, and that they are stranded at intermediate structural states controlled by kinetic factors. The present treatment is based largely on Smith and Ribbe (1969), Smith (1972), and Smith (Vols. I and II, 1974a and b). Careful readers will note that some of the earlier ideas have been modified or discarded: in particular, the phase diagram in Smith (1972, Fig. 9) has been replaced by Figure 2 (Smith, 1974a, Fig. S-2a). Much of the present material is abstracted from Smith (1974a,b), and I am greatly indebted to Drs. Konrad Springer and H. Wiebking of Springer-Verlag for generously giving permission to reproduce so much material.

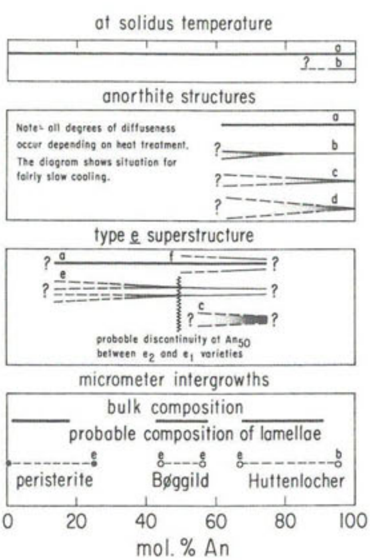

Figure 1. Summary of the chemical and diffraction properties of plagioclase. From Smith (1974a, Fig. S-2b, p. 7).

MELTING RELATIONS

Bowen (1913) determined the dry melting relations at one atmosphere, and interpreted them as the result of ideal solid solutions of plagioclase and

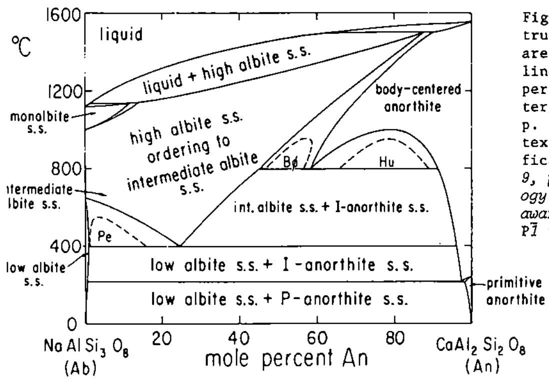

Figure 2. Hypothetical phase diagram for true equilibrium in which all relations are idealized to first order. Dashed lines show metastable curves which govern peristerite, Bøggild and Huttenlocher intergrowths. From Smith (1974a, Fig. S-2a p. 6). See the following chapter, the text, and Smith (1983) for suggested modifications. *(Cf. Grove* et al. *1983, Fig. 9, p. 51 for a possible alternative topology of the An_{35}-An_{100} subsolidus -- but be aware that their temperature for the $I\bar{1} \rightarrow P\bar{1}$ transition is too high by 600°.* Ed.*)*

liquid, or equal deviations for both. Current structural knowledge requires that the solidus is intersected by two transitions from monalbite to high albite solid solution to body-centered (*I*) anorthite. First-order thermodynamic relations are used in Figure 2, but non-first-order relations are likely. The monalbite-high albite transition occurs near An_{15} (Kroll and Bambauer, 1981), and the transition to *I*-anorthite at the solidus should be moved to An_{60-70} in Figure 2 (Kroll and Müller, 1980). With increasing An-content, the high albite solid solution must show increasing local order.

Lindsley (1968) determined the dry melting relations at 10 and 20 kbar, and Yoder, Stewart and Smith (1956) determined the relations for 5 kbar of excess water. Innumerable studies involve plagioclase with other components (e.g., diopside): The distribution of Ca and Na between plagioclase and the liquid can be used as a geothermometer (Kudo and Weill, 1970; Mathez, 1973). In the earth, plagioclase is transformed into other minerals including pyroxene, amphibole, spinel, and garnet at a few tens of kilometers depth, but the complex phase relations are beyond the scope of this chapter.

ANORTHITE

Detailed justification for the following statements is given by Smith (1974a, Chs. 5, 7 and 10). Anorthite has alternating Al and Si atoms which cause the *c*-axis to become doubled from ∿7 to ∿14 Å and to attain a body-centered lattice (see Chapter 1, p. 13f.). Specimens annealed below 1000°C have indistinguishable cell dimensions and sharp 'b' diffractions requiring essentially complete Al,Si ordering. Those annealed above 1000°C have properties indicating some Al,Si disorder, especially ones examined after quenching from near the melting point (Chiari *et al.*, 1978). Substitution of the albite "molecule" mathematically requires some degree of Al,Si disorder.

Therefore, the field of body-centered anorthite in Figure 2 could be contoured by an order function.

Anorthites cooled below 250°C show long-range order of the Ca atoms. Crudely speaking, the aluminosilicate framework is too large for the Ca atoms and it twists and collapses, thereby dropping the symmetry from $C\bar{1}$ to $P\bar{1}$ (*cf.* Ch. 1, Figs. 12-13). Complex domain textures develop whose coarseness depends on previous heat treatment and the extent of chemical substitution, especially of the NaSi for CaAl. Each domain has long-range order in which the Ca atoms are displaced the same way, and each domain boundary involves a switch-over to the other direction of displacement. The smaller the domains the more diffuse are the 'c' diffractions which characterize *P*-anorthite. As the temperature rises, increasing thermal vibration blurs out the domain texture, and near 250°C long-range order is lost.

Above 250°C, both the time- and space-averaged structures have body-centered symmetry (Frey *et al.*, 1977; Adlhart *et al.*, 1980a). The Ca atoms and the framework still show locally the features of *P*-anorthite (as shown in electron density maps: Fig. 16, Chapter 1), but *long-range* correlations have disappeared. As NaSi replaces CaAl, the sharp reversible transition for An_{100} becomes blurred out and shifted to lower temperature (Adlhart *et al.*, 1980b). Probably the NaSi-rich units or regions have a significant control on the orientation, shape and spacing of the boundaries between domains (Adlhart *et al.*, 1981). Electron-optical micrographs show that the domain texture becomes finer as the Ab-content increases, and as the Al,Si order decreases at constant Ab-content (papers in Wenk (1976)). Phase relations at high pressure and temperature are given by Goldsmith (1980, 1981).

ALBITE

The phase relations of albite at low temperature are uncertain because of metastable crystallization of high albite followed by a sluggish approach to the equilibrium state. After earlier complications caused by ion-exchange of albite with K-rich vapors from furnace linings, it is now certain that *at equilibrium*, triclinic analbite transforms reversibly to monoclinic monalbite at 978°C (e.g., Kroll *et al.*, 1980). Monalbite has strong Al,Si disorder, and any significant ordering towards the low albite structure *forces* the albite to remain triclinic at all temperatures. Between 980°C and about 680°C equilibrium under hydrothermal conditions has probably been obtained, and the careful results of MacKenzie (1957) have been confirmed by later workers (Smith, 1972, Fig. 2). At constant temperature, the $2\theta_{131} - 2\theta_{1\bar{3}1}$ ($\equiv \Delta 2\theta_{131}$) indicator (see Chapter 4) moves asymptotically to a value characteristic of

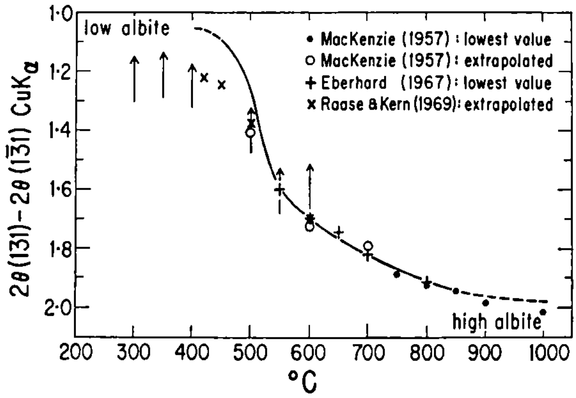

Figure 3. The $\Delta 2\theta_{131}$ indicator of annealed albites plotted against synthesis temperature. Arrows show the lowest value obtained by Martin (1969), and the curve shows the interpreta- of MacKenzie's (1957) data by McConnell and McKie (1960). From Smith (1972, Fig. 2).

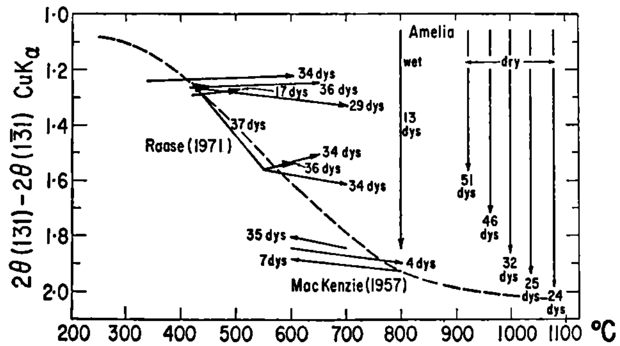

Figure 4. Change of the $\Delta 2\theta_{131}$ indicator produced by prolonged annealing of (a) synthetic albite at a temperature (arrow head) different from the synthesis temperature (arrow tail), and (b) low albite from Amelia, Virginia. From Smith (1972, Fig. 4).

the temperature; this value for the supposed "equilibrium albite" moves from the value for maximum high albite towards the value for maximum low albite. Therefore, "equilibrium albite" shows a continuous increase of Al,Si order as the temperature falls to 700°C (Chapter 2, Fig. 8). Below 700°C, the situation is quite uncertain. Prior to the studies of Martin (1969) and Raase (1971), all the data could be accommodated by the assumption that $\Delta 2\theta_{131}$ (and hence the Al,Si ordering) changes in a sigmoid fashion with temperature (Fig. 3): This of course implies that the inversion from low albite to high albite is non-first order. The data of Raase (1971), shown in Figure 4, are inconsistent with the sigmoid curve, and further unpublished data (pers. comm.) have confirmed the original data. Three of the arrows point upwards to the right implying that the equilibrium albite is close to low albite at temperatures below ∿675°C, and that there is a rapid change, perhaps discontinuous, between low and high albite between 650 and 700°C. This conclusion was confirmed by increasing ordering of intermediate albite heated at 650°C (Senderov and Shchekina, 1976). From a rate analysis of the data of MacKenzie (1957), a discontinuity between 550 and 700°C was invoked by McConnell and McKie (1960), but Smith (1974b, Ch. 16) queried the proposal for a smeared transformation. The natural occurrences of albite are difficult to interpret, but Orville (1974) suggests that low albite inverts to high albite at 575°C on the basis of its relation to oligoclase in metamorphic rocks together with a thermodynamic model based on the thermochemical data of Holm and Kleppa (1968). Probably the sum total of the evidence favors a sharp transition at ∿680°C in *pure* albite (*cf.* Senderov, 1980; and see discussion in Chapter 2).

For simplicity, I assume that a first-order inversion from low to high albite occurs near 680°C, and that both types of albite show a continuous variation of ordering. This assumption is inconsistent with Figure 6 in Stewart and Ribbe (1969), which would be modified by a sudden change of ordering near 680°C, as suggested by Figure 8b in Chapter 2. Of course the one-step type of ordering can occur whatever the type and position of the inversion.

FIELDS OF HOMOGENEOUS PLAGIOCLASE

Eberhard (1967) hydrothermally annealed synthetic plagioclase for long periods at one kilobar. The $\Delta 2\theta_{131}$ indicator (Fig. 5) decreased with annealing temperature from the reference curve for high plagioclase. No single crystal data were taken, and it is not known whether any specimens developed complex structures. Figure 6 summarizes the effect of heating natural plagioclases either dry (Gay, 1954; Gay and Bown, 1956; Nord *et al.*, 1974) or hydrothermally (McConnell, 1974a). The hydrothermal experiments indicate that 'e'-plagioclase transforms to high albite solid solution (s.s.) for sodic compositions and to *I*-anorthite s.s. for calcic compositions. Most dry experiments probably did not achieve equilibrium, but are not inconsistent with the general relations proposed in Figure 2 when account is taken of metastability. Data on natural volcanic and plutonic plagioclases also are not inconsistent.

Key features of Figure 2 are: (1) with falling temperature and increasing An-content, high albite s.s. becomes more ordered, but the order is merely of the short-range type; (2) *I*-anorthite s.s. extends to about $Ab_{40}An_{60}$; (3) the inversion between high albite and *I*-anorthite is first order and moves to lower temperature as the Ab content increases--this is believed to occur because Ab substitution reduces the order and allows the inversion to the

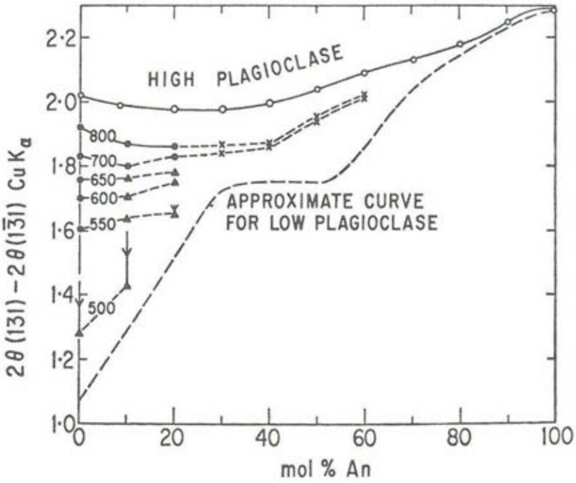

Figure 5. Relation between $\Delta 2\theta_{131}$ indicator and synthesis temperature of plagioclase (Eberhard, 1967). Dots represent syntheses for which equilibrium was claimed, triangles represent extrapolations to infinite annealing time, and crosses may represent equilibrium. Arrows show the extent of extrapolation for three triangles. From Smith (1972, Fig. 6). See Kroll and Ribbe (1980, Fig. 3) for revised high and low boundary curves.

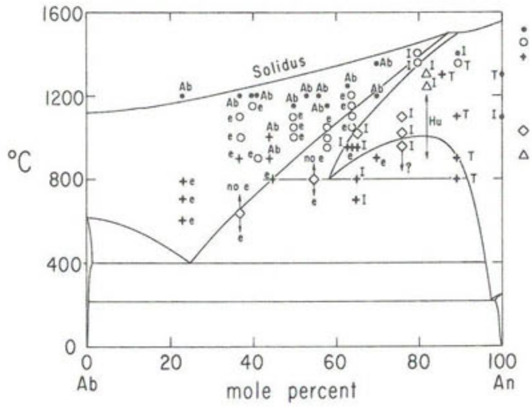

Figure 6. Summary of the crystal structures of heated plagioclases after quenching to room temperature. Each symbol is plotted at the heating temperature and labelled with the observed structure type. From Smith (1974a, Fig. 5-10, p. 148). See Wenk (1978) for heating of An_{66} plagioclase and Tagai and Korekawa (1981) for heating of Huttenlocher intergrowths.

disordered phase to occur at lower temperature; and (4) the homogeneous fields are cut off at lower temperature by a solvus intersected by three inversion loops.

Unfortunately, there are only reconnaissance heating studies for the range An_{40} to An_{90} and from 700°C to solidus temperatures, and the proposed phase relations are based on very few data. X-ray and electron-optical studies of feldspars held in this range for long periods of time would go far towards proving or disproving the relations suggested in Figure 2. It cannot be emphasized too strongly that the underlying data are fragmentary, and the interpretation highly subjective. In particular, note that Eberhard's data for pure albite are inconsistent with the suggestion that there is a sharp transition at ∿680°C. Note also that the transition from intermediate albite to *I*-anorthite in Figure 6 must be shifted to higher Ab content at the solidus.

'e'-PLAGIOCLASE

(See also Chapter 2)

All natural plagioclases of composition from about An_{20} to An_{70} which have been annealed under plutonic conditions have the 'e'-structure type. Complications from the micrometer intergrowths will be described later. A detailed account of the diffraction phenomena, and of the structural models (especially those of Toman and Frueh and Korekawa and Jagodzinski) is given in Smith (1974a, Ch. 5), and only the key features and my preferred interpretation are given here.

I believe that only low albite and *P*-anorthite are stable at low temperature, and that the equilibrium situation involves a single solvus intersected by inversion loops (Fig. 2). The 'e'-structure type is merely a coherent small-scale intergrowth of domains[1] which locally have structures like those of low albite and anorthite. The complexities arise because (1) the texture varies with bulk composition and (2) the domains interfere with each other. Thus, Smith and Ribbe (1969) modified the Chao and Taylor (1940) model of alternating slabs of albite and anorthite by the concept of albite- and anorthite-like "domains" separated by hybrid boundary regions. Figure 7 shows cross-sections through the domains which are thin, near-planar slabs lying in an irrational crystallographic direction. For An_{70}, the albite-like slabs repeat every 50 Å on a statistical basis, and the anorthite-like slabs are thick enough to approximate the structure of *P*-anorthite in

---

[1]For a discussion of coherency between intergrown phases, see Chapter 6. *Ed.*

the middle. For An_{30}, the albite-like slabs repeat every 20 Å and the anorthite-like slabs are too thin to develop the structure of *P*-anorthite. Indeed, the unique structural unit of feldspar is only slightly less than 10 Å across, and the concept of albite-like and anorthite-like slabs is rather artificial. A more sophisticated approach is to use the concept of modulation in which statistically $CaAl_2Si_2O_8$ concentrates in planes at atomic positions resembling those for anorthite, and $NaAlSi_3O_8$ concentrates in planes at atomic positions resembling those of low albite.

The crystallographic details are highly complex but the key features are as follows: (1) The ordering pattern is classifiable as "antiphase irrational centered." Figure 8 shows in two dimensions how the three features combine to give the irrational 'e' (and 'f') diffractions which characterize 'e'-plagioclase. In three dimensions, the centering feature (as shown by the 'e' diffractions lying in pairs about the positions for 'b' diffractions ($h+k$ odd, ℓ odd) in anorthite) results from the contrast between the *I*-centered 14 Å cell of *I*-anorthite and the *C*-centered 7 Å cell of albite. (2) The orientation of the 'e' diffractions changes with An-content (Chapter 10, Fig. 21), and there is a probable discontinuity at An_{50} documented by Doman *et al.* (1965). (3) The 'e' diffractions move further apart and become more diffuse as the An-content decreases, thereby requiring the texture to become finer as in Figure 7 (see also Chapter 2, Fig. 13). Type 'f' diffractions are either very weak or absent for sodic compositions. Type 'c' diffractions ($h+k$ even, ℓ odd) occur as very weak diffuse diffractions in some calcic specimens, and indicate that the calcic domains resemble *P*-anorthite. (4) The structural interpretation of diffraction intensities by Toman and Frueh (1972) shows that the major atomic displacements are near the *b*-axis (as confirmed by Kitamura and Morimoto, 1975). This is consistent with the model because the atomic coordinates of atoms in low albite and anorthite differ mainly in the *b* direction. (5) Furthermore, the detailed interpretation by Toman and Frueh (1973) indicates that the atoms are displaced by a modulation wave which distorts the framework and displaces the cations, while Kitamura and Morimoto (1975) have been able to satisfy the diffraction intensities for an An_{73} specimen using a modulation model (Fig. 9) of alternating albite- and anorthite-like regions separated by transitional regions (*cf.* Fig. 7). The original papers should be consulted for details. (6) Detection of Al,Si ordering by crystal structure analysis is very difficult, but the plot of mean *T*-O distance versus An-content for 'e'-plagioclase (Chapter 2, Fig. 16) shows that aluminum favors the T_1O site as in low albite, and the diffraction relation of 'e'-plagioclase to *I*-anorthite shows that some of the structure must have regularly alternating Al and Si atoms in the

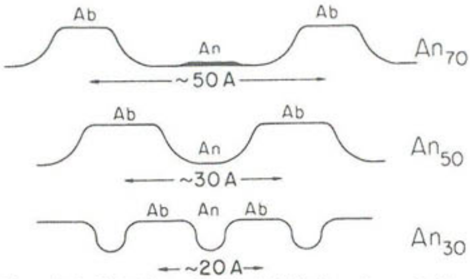

Figure 7. The model of Smith and Ribbe (1969) for the periodic structure of 'e'-plagioclase as a function of composition. By contrast with the standing square waves of Na and Ca modulation (Korekawa and Jagodzinski, 1967) it assumes gradual modulations between low albite-like (and therefore NaSi-rich) and anorthite-like structure. Sloping boundaries indicate the presumed disordered volumes in which Al,Si arrangements and ratios accommodate the incompatibility of the 1:3 and 2:2 ordering schemes. The variation of T-spacing with composition is consistent with the diffraction data; the migration of $\vec{t}$ is discussed by Korekawa (1967) and Toman and Frueh (1971 *et seq.*), Kitamura and Morimoto (1975), Grove (1977a), Kumao *et al.* (1981) and others (see text). Modified from Figure 10 of Smith and Ribbe (1969).

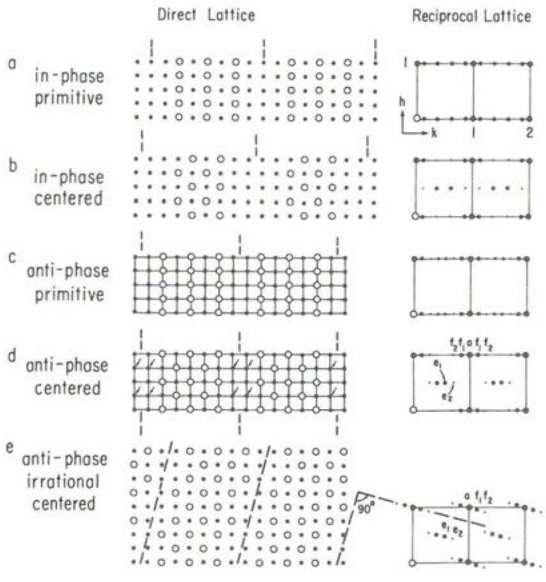

Figure 8. Diffraction patterns for ordered structures with different symmetries and phase characteristics. From Smith (1974a, Fig. 5-6, p. 134).

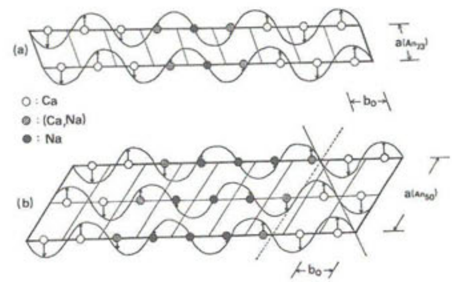

Figure 9. Model for modulation of Ca and Na positions in 'e'-plagioclase for (a) An_{73} and (b) An_{50}. The b_o axis is for the Megaw cell; it is the half-diagonal of the *ab* face of the usual albite cell. The *a*-axis is not the usual one: it was chosen to lie in the plane of modulation. From Kitamura and Morimoto (1975, Fig. 4, p. 422).

tetrahedral framework. Thus the data are consistent with an intergrowth of regions resembling low albite and *I*-anorthite. In addition, the thermal transformations in 'e'-plagioclase are so sluggish that migration of Al and Si must be the controlling factor. (7) Hybrid regions must occur to accommodate the topochemical differences between the ordering patterns of low albite and anorthite (Smith, 1974a, Fig. 5-17).

From the viewpoint of phase equilibria, I therefore regard 'e'-plagioclase as a coherent intergrowth which develops inside the theoretical solvus between albite and anorthite. Note that 'e'-plagioclase develops only for compositions between about An_{70} and An_{20} which correspond to the middle region of the proposed solvus and which may represent the coherent spinodal. Detailed diffraction data by Gay, Bown and others show that the greater the extent of geologic annealing (e.g., in plutonic as opposed to near-surface rocks), the sharper are the 'e' diffractions for a given An content and hence the better developed the modulation. Also, the data indicate that 'e'-plagioclase develops more easily in bulk compositions which are more calcic (e.g., x-ray powder data in Smith, 1974a, Fig. 7-42), but the controlling factors are unclear.

I deliberately left the preceding material unchanged from the first edition, and now list the important results of research since 1975. Slimming (1976) confirmed the discontinuity at An_{50}, and Slimming (1976) and Wenk (1978) gave evidence that the antiphase vector t is not a unique function of An-content. Wenk *et al.* (1980) found that the averaged structures of labradorites (An_{62-66}) from volcanic and metamorphic rocks are essentially identical, and concluded that all are based on periodic stacking of similar basic units probably like *I*-anorthite. Because the intensity of subsidiary diffractions is the same for x-ray and neutron techniques, they concluded that these intensities result more from atomic displacements than from changes of site occupancy. Perhaps the most direct evidence on the structure of 'e'-plagioclase comes from the beautiful direct electron-optical images (Morimoto *et al.*, 1975a,b; Kumao *et al.*, 1981; see Fig. 13, Chapter 2) which clearly demonstrate the zig-zag nature of the antiphase domain intergrowths, and show a slightly blurred distinction between the positions of Na and Ca atoms. The Kitamura-Morimoto model (Fig. 9) was developed further by Kitamura and Morimoto (1977) and Nakajima *et al.* (1977) using coherent slabs of composition near An_5 and An_{80}. Grove (1977a) produced idealized models for 33, 50, 66 and 75% An, and Fleet (1981) proposed that the orientation of the interfaces in the Kitamura-Morimoto model is controlled by minimization of interface energy during spinodal-like unmixing of high plagioclase (but what is the relation to the

Bøggild intergrowth?). Another approach uses the concept of structural resonances (McConnell, 1978). Finally, all the electron-optical data on natural and heated 'e'-plagioclases (e.g., Grove, 1977; Wenk, 1979a; Wenk and Nakajima, 1980) are consistent with metastable coherent intergrowths controlled by local diffusion and strain factors (e.g., Grove and Spear, 1981).

PERISTERITE

(See also Chapters 2 and 10)

Some, but not all, plagioclases with bulk composition from An_2 to An_{16} occur as intergrowths of low albite ($\sim An_0$) and a plagioclase, probably near An_{25}. Some intergrowths are planar and of thickness near the range of optical wavelengths giving interference colors (Chapter 8), while others are narrower and can be detected by superstructure diffractions in single crystal x-ray patterns (Korekawa *et al.*, 1970). At least many intergrowths are coherent (Viswanathan, 1973) resulting in lattice distortion (as seen in plots of $\alpha^*\gamma^*$ reciprocal lattice angles), and composition estimates from angles are not always definitive. The calcic component gives weak 'e' diffractions in some peristerites, but it is not known whether this is universal. There are two orientations of the peristerite intergrowth, and these have been explained by coherency strain (Smith, 1974b, Chapter 19). See Chapter 10 for further data.

Addition of extra aluminum to fully ordered low albite mathematically requires that some oxygen atoms would be bonded to two aluminums, but this need not occur for high albite solid solution which is disordered. Dissociation of a high albite s.s. into a peristerite intergrowth must involve complex atomic effects, and the simple concepts of either an unmixing solvus or a binary loop must be too simple.

I tend to prefer a binary loop between low albite and high albite solid solutions (Fig. 2), because it allows simple depiction on a phase diagram (an unworthy reason, admittedly!), and because it allows a first-order inversion in albite. Tuttle and Bowen (1950) first proposed a binary loop, and Orville (1974) carefully re-evaluated the geological and thermochemical evidence. In favor of a solvus were Laves (1960), Ribbe (1962), Crawford (1966), Christie (1968) and Viswanathan and Eberhard (1968). The apparent conflict between the range of bulk compositions (An_2-An_{16}) and the probable composition of the exsolved phases (An_0 and $An_{20\to33?}$) is easily reconciled by either a binary loop or an asymmetric solvus. In the former (Fig. 2), the peristerite would be produced inside the dashed region for coherent intergrowths, and more calcic bulk compositions would remain in a stranded state. A similarly-shaped

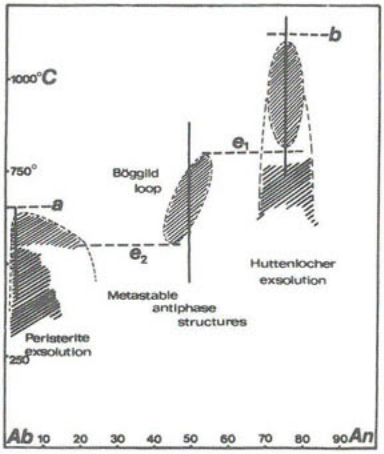

Figure 10. Temperature-composition plot for plagioclases showing regions of spinodal behavior (light shading) and of possible true exsolution (heavier shading in the lower temperature regions of the peristerite and Huttenlocher compositions). From McConnell (1974a, Fig. 5).

spindoal region would occur for an asymmetric solvus. McConnell (1974a) proposed that true exsolution occurred at a lower temperature than spinodal decomposition (Fig. 10).[2]

All peristerites occur in regionally metamorphosed rocks or in pegmatites. These environments are consistent with prolonged annealing at low temperature of a high albite s.s. which crystallized either stably or metastably.

The petrologic data of Crawford (1966) are particularly interesting. She found that in two suites of regionally metamorphosed semipelitic schists, oligoclase grains appeared at the margins of albite grains at low grade, and that as the grade went above the almandine isograd the oligoclase began to surround the albite and to occur as separate grains. The albite composition was near An_{2-3} but the oligoclase composition appeared to outline the asymmetric flank of a peristerite solvus with a crest near An_5 and a temperature near 450-500°C. Many other petrologic data indicate the existence of a composition gap in the peristerite region for sodic plagioclases in metamorphic rocks, as detailed in a review article written by J.R. Goldsmith (1982a). Particularly interesting are the data of Maruyama *et al.* (1981), which taken together with the data of Crawford (1966), Nord *et al.* (1978), Spear (1980), and other workers, lead to the conclusion that the peak of an inferred peristerite solvus shifts toward albite composition and higher temperature with increasing pressure. The temperatures estimated from metamorphic mineral assemblages (∿400°C at low pressure to ∿600°C for several kilobars) are lower than the estimated temperature of 680°C for the high-low transition in pure albite. In order to reconcile an unmixing solvus with a discontinuous inversion in pure albite, either a discontinuity is needed in the solvus, or a discontinuous inversion changes into a continuous one, or both (*cf.* Carpenter, 1981).

Finally, the following papers provide further information on peristerite intergrowths: Miúra and Rucklidge (1979), ion microprobe analyses of alternating lamellae of An_2Or_1 and $An_{19-23}Or_3$ compositions; Olsen (1975, 1979),

---

[2]See Chapter 6 for a discussion of spinodal decomposition. *Ed.*

TEM observations and estimates of coherent lattice energies; Lorimer *et al.* (1974), reinterpretation of apparently coarse peristerite as a sub-grain texture; Joswig *et al.* (1977), superstructure: details are in Chapter 10.

HUTTENLOCHER INTERGROWTH

(See also Chapters 2 and 10)

This intergrowth is common in non-volcanic plagioclases with bulk compositions from $An_{\sim 66}$-$An_{\sim 90}$. The calcic component is an anorthite s.s. and the sodic component is an 'e'-plagioclase. Detailed studies were reported by Nissen (1974), McConnell (1974a) and Nord *et al.* (1974). A general review is given by Smith (1974b, Chapter 19, pp. 540-544). Various data for lunar plagioclases are to be found in the *Proceedings of the Lunar Science Conferences*.

Crucial to the interpretation of the Huttenlocher intergrowth is the evidence from heating experiments that it transforms to *I*-anorthite s.s. at high temperature. The hydrothermal experiments by McConnell (1974a) on an An_{76} bytownite from the Stillwater Complex showed conversion to *I*-anorthite s.s. above 960°C, and inversion at even lower temperatures might occur. Dry experiments by Nord *et al.* (1974) on an An_{82} bytownite, also from the Stillwater Complex, showed conversion beginning in one week at 1215°C. The proposed solvus in Figure 6 was fitted to the hydrothermal experiments, and the dry experiments were assumed not to have reached equilibrium. Of course, many more data are needed to test the proposed solvus, and considerable adjustment may prove necessary. Nord *et al.* noted that antiphase boundaries remained in the *I*-anorthite s.s. produced by heating, and this indicates that the *I*-anorthite nucleated in a matrix of $C\bar{1}$ symmetry (i.e., high albite s.s.). Thus the Huttenlocher intergrowth can be interpreted as the result of the following sequence of reactions: (1) growth of high albite s.s.; (2) inversion to *I*-anorthite s.s.; (3) coherent dissociation into calcic and sodic components perhaps governed by a coherent spinodal inside a solvus: these components form a lamellar intergrowth with orientation(s) governed by strain relations (Nissen, 1974); (4) ultimate transformation of the calcic and sodic components to *P*-anorthite s.s. and 'e'-plagioclase. Undoubtedly, the details are extremely complex, and depend on the thermal history as well as the bulk composition. Figure 10 shows McConnell's (1974a) interpretation in terms of spinodal behavior and possible true exsolution. Nord *et al.* (1974, Fig. 10) proposed that the Huttenlocher intergrowth results from a solvus with asymptotes at An_{65} and An_{90}: This implies than an ordered compound exists at An_{65}, an assumption which is contradicted by the occurrence of 'e'-plagioclase at that composition.

Nissen (1974) described Huttenlocher intergrowths from 25 localities. All the specimens came from environments where prolonged annealing at fairly high temperatures could be expected (e.g., layered igneous complexes) and none came from simple volcanic environments. Most of the specimens fall into the granulite and/or amphibolite metamorphic facies though the ultimate origin may have been igneous (e.g., anorthosites). It is difficult to predict the temperature-time history of most of the specimens since they derive from deep-seated environments in which poly-metamorphism is probable.

The following new data extend the above discussion. Grove (1977b) observed complex textural varieties in specimens from Warwick (high-grade metamorphic), Nain (anorthosite), Ardnamurchan (eucrite) and Mariana Islands (andesite), and outlined a region of decreasing coarseness of intergrowths on a plot of increasing cooling rate versus An content. Above the temperature range for Huttenlocher intergrowths, the inversion from $C\bar{1}$ to $I\bar{1}$ plagioclase was placed at An_{75}. Tagai and Korekawa (1981) reviewed the literature, and made diffraction studies of plagioclases An_{66-70}, of which the Lake County specimen was heated to 1300°C. Types 'a' and 'e' diffractions were found after quenching from 1180°C, but not the 'b' type, while only the 'a' type was found after quenching from 1300°C. This indicates that the $C\bar{1}$ structure type is stable at An_{66} and 1300°C. Comparison with the near-solidus data by Kroll and Müller (1980) suggests that the phase relations are quite uncertain in the region An_{50-100} from above the presumed solvus to the solidus. See later for Kotelnikov *et al.* (1981).

BØGGILD INTERGROWTH

(See also Chapters 2 and 10)

Experimental data on Bøggild intergrowths $An_{46\pm1}$ to $An_{60\pm1}$, are difficult to interpret, and further study is needed (see Smith, 1974b, pp. 532-540, for summary). There has not been a detailed survey, but it appears that all iridescent Bøggild intergrowths derive from high-grade metamorphic environments typically of Precambrian age. Non-iridescent Bøggild intergrowths may be common but can only be recognized using electron microscopy. Just as for the Huttenlocher intergrowth, it appears that extensive annealing at high temperature is needed. The simplest model is that Bøggild intergrowths develop at fairly high temperature by spinodal decomposition and that one or both of the components develop the 'e'-structure at lower temperatures. Figure 10 is McConnell's kinetic interpretation: I have suggested that the Bøggild intergrowth results from spinodal behavior related to the inversion between high albite s.s. and *I*-anorthite s.s. (Fig. 2; see also Grove et al., 1983).

In the following chapter Ribbe gives detailed descriptions of Bøggild intergrowths, but in summary it may be stated that (1) the two phases differ in composition by 12 to 16 mol % An; (2) both are probably 'e'-plagioclases (see Fig. 21, Chapter 10), although x-ray diffraction data have revealed only a single set of 'e' reflections, and Hashimoto *et al.* (1976) found in one specimen ($An_{53.6}Or_{0.8}$) that 'f' superlattice fringes pass right across major and minor exsolution lamellae without change of width or orientation;[3] and (3) the Bøggild intergrowth develops only in specimens with more than about 2 wt % Or in the bulk composition, although there is no satisfactory explanation of this and the specimen of Hashimoto *et al.* (1976) is an exception. A new idea about (3) is the possibility that all plagioclases from high-grade meta-igneous complexes of Precambrian age crystallized from the melt with substantial Or-content, and that the correlation between Or-content and Bøggild intergrowth is merely a secondary one.

Although not a Bøggild intergrowth, it is convenient to list here the intergrowth of $An_{69.5}Or_{1.0}$ with $An_{61}Or_{0.7}$ from a gneiss at Broken Hill, NSW, Australia (Phillips *et al.*, 1977) -- this is a puzzle.

OTHER ASSEMBLAGES IN METAMORPHIC ROCKS

In principle, one might hope that (1) some micrometer-scale intergrowths might recrystallize into separate grains, perhaps under the influence of shear (by analogy with perthite) and (2) some plagioclases might crystallize directly as separate grains that straddle an equilibrium solvus. Unfortunately, the occurrence of plagioclases in metamorphic rocks is complicated by complex phase relations in which the anorthite component breaks down at low temperature in the presence of H_2O, or CO_2, or both (Goldsmith, 1982a,b and in preparation).

Unfortunately, Voll (1971) has not amplified his abstract on the exsolution of An_{50-55} into An_{18} and An_{93} at grain boundaries in plagioclase from metamorphic rocks in north Bavaria, and some one should follow up this tantalising teaser. Spear (1977) found an immiscibility gap between An_{39} and An_{88} for plagioclases coexisting with hornblendes in Post Pond Volcanics, New Hampshire and Vermont, and further study is again needed. The clearest evidence of the stable coexistence of low albite and *P*-anorthite was found in amphibole schists near the Bergell granite (Wenk, 1979b). Transmission electron

---

[3]They surmised that the composition of the lamellae may be symmetrical about An_{50} with an interchange of Al,Si configuration. Regions without 'f' fringes were interpreted to be structurally disordered.

microscopy revealed large andesine crystals with 'e'-type antiphase domain boundaries changing over 0.1 μm into pure albite and anorthite (An_{95}). Wenk *et al.* (1975) observed coarse intergrowths of An_{34} and An_{66} in calcsilicate rocks of amphibolite facies in the Central Alps. The coarse lamellar texture was attributed to epitaxial nucleation of andesine on the ($1\bar{1}0$), (110), (100) and (130) faces of the labradorite. It is not clear why the labradorite host is dusty and the andesine guest is clear. The observation of only one superstructure is also puzzling. Finally, Wenk and Wenk (1977) described a bewildering set of complications involving microscopic and submicroscopic intergrowths from banded metamorphic rocks from Val Carecchio, and presented a hypothetical temperature-composition diagram (idealized in Wenk (1979)) showing the following gaps: peristerite ($\sim An_{5-15}$), An_{26-32}, overlapping An_{35-63}, and Huttenlocher (An_{72-86}). Goldsmith (1982a) raises an important question in his review of metamorphic plagioclases about the relative roles of crystal-structural parameters and inter-mineral distribution factors in determining the chemical compositions. I take an agnostic view at this time about the *details* of coexisting plagioclases, but tentatively believe that certain compositions yield coherent partly-ordered intergrowths so close in stability to mechanical mixtures of Na-rich and Ca-rich plagioclases that they tend to persist indefinitely.

EXPERIMENTAL SUB-SOLIDUS PHASE EQUILIBRIA

There are few data on direct synthesis of plagioclases in the subsolidus region, as distinct from heating experiments on natural plagioclases. The syntheses by Eberhard (1967) produced no evidence for unmixing. Kotelnikov *et al.* (1981) reported an exsolution gap between An_{67} and An_{92} (i.e., the Huttenlocher gap) for plagioclase equilibrated with one-molar $CaCl_2$ and NaCl aqueous solution at 700°C and 1000 atmospheres (see also Kravchuk (1981) for discussion of the plagioclase phase relations). This conclusion differs from that of Orville (1972) whose data obtained at 700°C and 2000 bars (note the higher pressure) were interpreted in terms of an ideal solution of disordered high albite structure for An_0-An_{50-55} with constant activity coefficients $\gamma_{Ab} = 1.00$ and $\gamma_{An} = 1.28$; an ideal solution of ordered anorthite structure for An_{85-90}-An_{100} with constant $\gamma_{Ab} = 1.89$ and $\gamma_{An} = 1.00$; and a nonideal solution for An_{50-55}-An_{85-90}. Nevertheless, both interpretations are indicative of strong non-ideality, and the former is consistent with the occurrence of Huttenlocher intergrowths.

According to Goldsmith (1982b), at 8-10 kbar in the system Ab-An-H_2O, all plagioclase compositions from $\sim An_{40}$ to An_{100} break down to zoisite, kyanite, quartz and sodic plagioclase (plus vapor) along the same P-T curve. This behavior is consistent with an exsolution gap between An_{40} and An_{100} such that the An component acts like independent crystals of anorthite. The breakdown temperatures are 615°C at 8 kbar and 715°C at 10 kbar. The composition range of An_{40} to An_{100} encompasses the Huttenlocher and Bøggild regions, and provides evidence confirming the conclusion from X-ray diffraction data that An_{67} is not a *truly* stable ordered compound.

Goldsmith also discusses the effect of bulk composition and physical factors of a rock on the occurrence (or not) of the peristerite gap -- see also Orville (1974).

SUMMARY

The fragmentary nature of the evidence on sub-solidus phase relations of plagioclase cannot be emphasized too strongly. Further progress will depend on sympathetic coordination of data from both natural and synthetic plagioclases using the complete range of physical, chemical, mineralogical and petrological tools. Figure 2 cannot be correct in detail, and may not even be correct in general. However, the evidence strongly favors the absence of ordered compounds between albite and anorthite, and I believe that metastable solvi occur within a truly stable single solvus intersected by inversion loops. Although the concept of a peristerite solvus is supported by several studies, it still seems wise to retain the possibility of some kind of combined first-order inversion in *pure* albite and a partly non-first-order inversion in adjacent plagioclase. Another region of uncertainty involves the inversion between high-albite solid solution and body-centered anorthite solid solution. Much more work is needed in the region An_{40-90} and 800-1200°C.

Chapter 10
EXSOLUTION TEXTURES in TERNARY and PLAGIOCLASE FELDSPARS; INTERFERENCE COLORS

P. H. Ribbe

INTRODUCTION

In this chapter we will describe in further detail those two-phase intergrowths which already have received comment in previous chapters. As background for this, it is advisable to review sections in Chapter 2 which deal with the sequences of Al,Si ordering in plagioclase feldspars, including peristerites and Bøggild and Huttenlocher intergrowths, and those in Chapter 9 , which treat the phase relations of these regions of the plagioclase subsolidus. The concepts of the coherent solvus, as contrasted with the strainfree or equilibrium solvus, is expounded in Chapter 6, where spinodal decomposition also is discussed in some detail. The exsolution mechanisms detailed there are illustrated in Chapter 7, and that documentation of the textures of two-phase intergrowths from the 100 Å scale in cryptoperthites to visually observable perthites more than adequately characterizes the alkali feldspars.

The principles of decomposition as described for Na-K feldspars, in which tetrahedral atoms need not migrate during exsolution, may be different in some details from those required to explain the two-phase textures observed in plagioclases. But probably the greatest difference is in the rate factor. For example, phase separation of a disordered homogeneous solid-solution of An_8 ($Na_{.92}Ca_{.08}Al_{1.08}Si_{2.92}O_8$) into a peristerite consisting of two parts ordered low albite ($NaAlSi_3O_8$) and one part by volume $An_{\sim 25}$ ($Na_{.75}Ca_{.25}Al_{1.25}Si_{2.75}O_8$) involves diffusion of Al,Si (see Chapter 8) over several thousand Ångströms. At the temperatures of low-grade metamorphism or pegmatite formation (<600°C) in which this peristeritic exsolution typically occurs, many millions of years may be necessary for an equilibrium assemblage to be established (if indeed it ever is!). By contrast, in alkali feldspars some of the two-phase textures found in nature have been duplicated in the laboratory.

There is much to learn in principle about plagioclase exsolution by analogy with alkali feldspars, but one must continually bear in mind the fact that the driving force for phase separation in plagioclases primarily involves ordering of the larger trivalent Al and the smaller tetravalent Si atoms within the tetrahedral framework, according to patterns apparently governed by the aluminum avoidance principle (Chapter 1, p. 13). Na^+ and

Ca^{2+}, which are nearly equal in size, simply follow Si^{4+} and Al^{3+} to maintain local electrostatic charge balance. The extreme sluggishness of Al,Si diffusion greatly inhibits decomposition, in marked contrast to that observed in alkali feldspars where Na and K have both radically different sizes and high diffusivities within the $AlSi_3O_8$ framework. Plagioclase intergrowths are generally submicroscopic, although they are occasionally observed at the 1-2 μm scale. Smith (Chapter 9) discusses two-plagioclase assemblages in which the feldspars occur as discreet grains. Coexisting phases may be coherent, partially coherent, or non-coherent (Laves, 1974, Figs. 3-5), just as in alkali feldspars (Fig. 7 in Chapter 6). Apart from observation by TEM or single-crystal x-ray methods, the most obvious evidences of intergrowths in plagioclases are interference colors which may vary from pale white to brilliant reds and blues.

For reviews of exsolution textures in feldspars which parallel this one, see McLaren (1974) and especially Champness and Lorimer (1976). Alkali feldspars are discussed in Chapter 7; this chapter is concerned with ternary and plagioclase feldspars.

EXSOLUTION IN TERNARY FELDSPARS

Johannes (1979) presents the most recent phase equilibria studies of the *ternary feldspars*, i.e., those which contain >5 mol % Ab, Or *and* An. The proposed nomenclature of Smith (1974a) is reproduced in Figure 1.

In this section we briefly examine two distinct regions of the ternary, one in which the plagioclase coexisting with $Or_{\sim 90}Ab_{\sim 10}$ generally has compositions in the range An_{15}-An_{18} and another in which the plagioclase is An_{30-32}. For the former, bulk compositions lie in Smith's "Ca-K high albite" field, forming *mesoperthites*; the latter is nearer to his "K-oligoclase" field, forming *antiperthites*.

Mesoperthites

Often exhibiting bright interference colors, mixed crystals -- mesoperthites -- from larvikites (*cf*. Smith and Muir, 1958) and from the last crystallized fraction of the Kiglapait layered igneous intrusion (Speer and Ribbe, 1973) have formed by exsolution from homogeneous monoclinic crystals of bulk composition $Ab_{60-70}An_{8-18}Or_{20-30}$ (see Fig. 1). Using single-crystal a^*b^* precession photographs (see Chapter 2 and Smith, 1974a, pp. 179-203), the plagioclases of our specimens were found to be twinned on both the

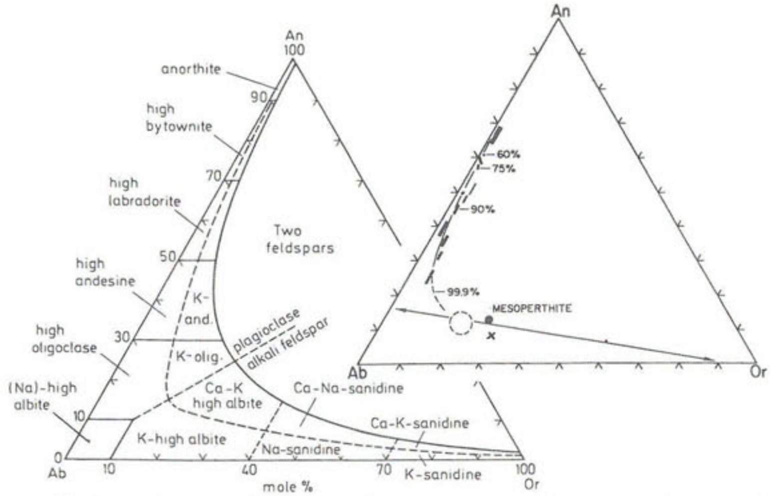

Figure 1. The lower triangular diagram gives the nomenclature for homogeneous feldspars in high structural states proposed by Smith (1974a, Fig. 9-16, p. 447). His "K-high albite" is frequently called *anorthoclase* in the petrographic literature. The smaller diagram to the right shows the compositional relationships of the plagioclases [the bars indicate composition ranges in polished thick sections] and the bulk compositions of the ternary feldspars [called *mesoperthites*] in feldspars of the Kiglapait intrusion, Labrador. Arrow points indicate compositions of oligoclase (An_{15-18}) and orthoclase ($Or_{\sim 90}$) which have unmixed from a "Ca-K high albite." The numbers represent the percent of the intrusion which was solidified when these feldspars crystallized. Modified from Speer and Ribbe (1973, Fig. 3, p. 473). The solid circle and × represent bulk compositions of feldspars from larvikites studied by Muir and Smith (1956) and Smith and Muir (1958), and pictured in Figure 2 below.

Albite and Pericline laws, the Albite twins sharing b^* with the untwinned monoclinic K-feldspar. With reference to a determinative diagram like that shown later (p. 256), the readily measured γ^* angle for the triclinic plagioclase yields an approximate composition of An_{15-18}. From the same photograph a^* [= $1/d(100)$] can be measured with fair precision for the K-rich phase and compared to a^* values from alkali feldspars of known composition (Wright and Stewart, 1968) to arrive at an approximate composition of $Or_{90}Ab_{10}$ for the monoclinic member of the exsolved pair.

Some textural relationships are shown in Figures 2 and 3a: in 2a the monoclinic K-feldspar lamellae are *in contrast* (bright) and the oligoclase lamellae are *out of contrast* (dark). This dark-field image was formed by isolating with an aperture reflection from the K-feldspar reciprocal lattice in the diffraction pattern (inset to the right).[1] This pattern has two lattices, one for $Or_{\sim 90}$ and one for An_{15-18}. Reflection pairs are joined by faint streaks, most likely indicating a degree of structural coherency between adjacent phases. Figure 2c is a dark-field image of an (001) cleavage flake with c^* nearly parallel to the electron beam. The K-feldspar lamellae are

[1] See discussion of electron microscopy by Yund and Tullis in Chapter 6 and more detailed treatments by McLaren (1974) and Van der Biest and Thomas (1976). The latter give an excellent general bibliography for transmission electron microscopy.

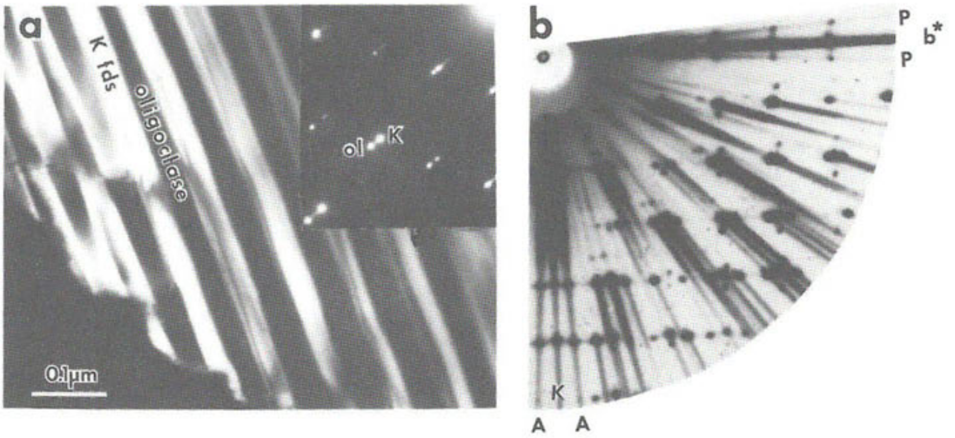

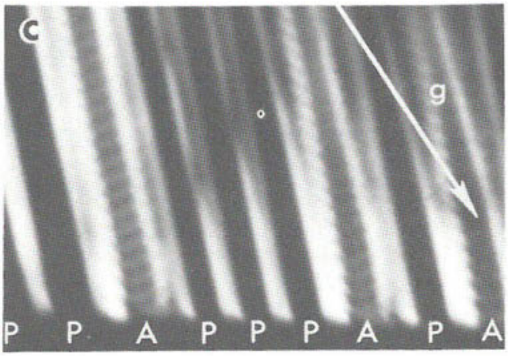

Figure 2. (a) TEM photo of a ternary feldspar from Larvik, Norway. (b) Part of an b^*c^* x-ray precession photograph of this mesoperthite, showing the reciprocal lattice of untwinned K-feldspar and of plagioclase twinned on both Pericline (P) and Albite (A) laws. To interpret this photo, refer to the electron diffraction pattern and the accompanying stereographic projection below (Fig. 7b,c). (c) TEM image showing Albite twins; see text for discussion. Scale as in (a). (d) Optical micrograph of feldspars from the last liquid (99.99%) to crystallize in the Kiglapait intrusion, Labrador (see inset in Fig. 1). The coarser intergrowth (top) appears to be a later stage crystallization than the mesoperthite with the fine lamellar exsolution texture, shown at higher magnification in (e).

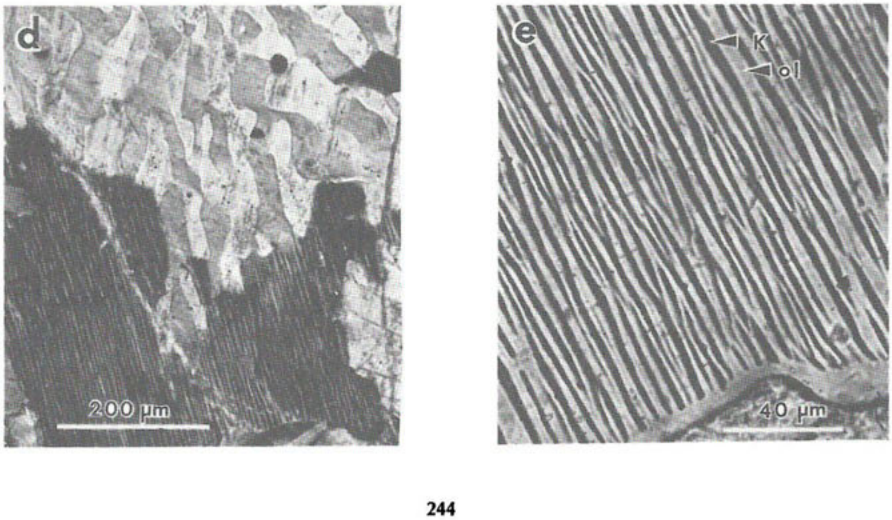

again in contrast and some oligoclase lamellae are Albite-twinned (A) with a fuzzy, but periodic repeat visible (*cf.* Fig. 3a); others are Pericline-twinned (P), although their composition planes are not oriented properly to be seen in this photograph (but compare Fig. 8 below). Mesoperthites with two distinct, microscopically coarse textures are pictured in Figures 2d and e. See legend for details.

Polysynthetic Albite twinning with periodic repeats ranging from ∿155 to ∿175 Å in the b^* direction (E-W in Fig. 3a) is shown in another mesoperthite from Larvik (*cf.* Fig. 12, Chapter 7 and accompanying comments by Yund). As first suggested by Laves (1952), this fine-scale twinning on (010) of the triclinic plagioclase effectively increases its symmetry to monoclinic, thereby reducing the strain energy at its boundaries with the enveloping monoclinic orthoclase. Careful measurements indicate that the twin periodicity decreases with decreasing thickness of the oligoclase lamella. Willaime and Gandais (1972) gave a detailed theoretical treatment of this observation in terms of elastic properties of feldspar and showed that $t = k\omega^2$, where t is the lamellar thickness and ω is the thickness of a left- and right-oriented twin pair (Fig. 3b). The specimens used in their study were also feldspars from Larvik, and they obtained a value of 0.42 erg/cm^2 for the surface energy in albite twinning for the particular bulk composition with I presume is near $Or_{30}Ab_{60}An_{10}$ (as are those of feldspar from the same locality specified by • and × in Fig. 1). McLaren (1974, p. 417) states that k is supposedly "...a function of the elastic constants, the magnitudes of the shear angles and the twin-boundary energy only." But his observations show that, enigmatically, k also varies with bulk composition in cryptoperthites (Fig. 4).

If twin periodicities are perfectly regular, superlattice reflections with spacings inversely proportional to ω will appear in diffraction patterns in place of reflection pairs expected from a simple twin; but if periodicities have a range of values within a "single crystal," the superlattice spots will be smeared out into paired streaks whose centers will be located in the expected positions for simple twins, be they Albite or Pericline twins.

Quite apart from twinning, it appears that the mechanisms of exsolution in these ternary feldspars are very similar to those in alkali feldspars (Chapters 6 and 7), except that calcium and the aluminum in excess of the 1:3 Al:Si ratio end up in a (homogeneous?) plagioclase phase whose composition is on the Ca-rich side of the peristerite solvus or binary loop. It is no doubt significant that this single phase is somewhat more An-rich than

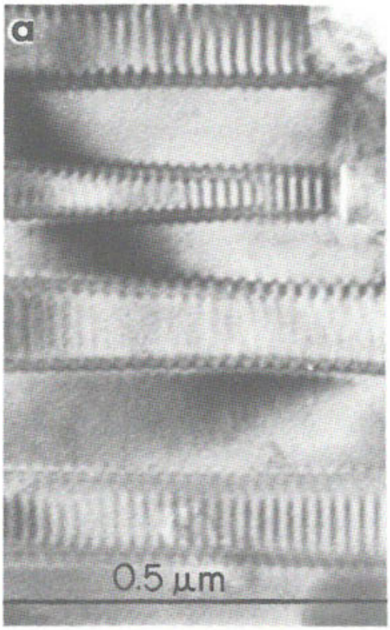

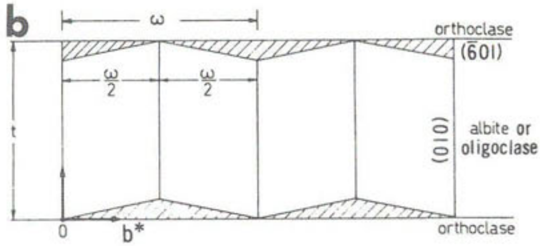

Figure 3. (a) Mesoperthite from Larvik, Norway with coexisting Albite-twinned An_{15-18} and monoclinic K-feldspar; periodicities range from 155-175 Å. Courtesy of H.-U. Nissen. Compare with a later figure (8a). (b) An idealized model, modified from McLaren (1974, Fig. 26), defining the periodicity ω of a twin pair and the thickness *t* of a twinned plagioclase lamella exsolved from a monoclinic precursor on ($\bar{6}01$), and applicable to mesoperthites, antiperthites and alkali feldspars alike. See Figure 4.

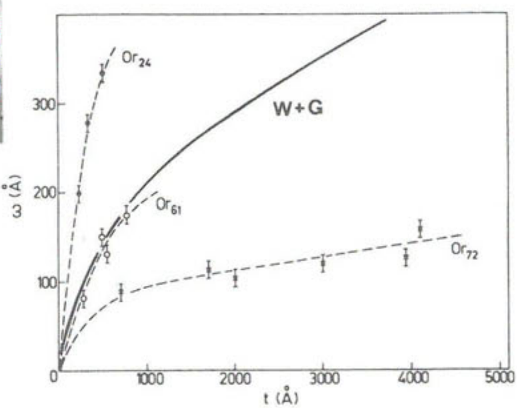

Figure 4. Curves showing the variation of Albite twin periodicity ω with thickness, *t*, of the albite lamellae in cryptoperthites of bulk compositions Or_{24}, Or_{61} and Or_{72}. See Figure 3. After McLaren (1974, Fig. 27). Solid curve from Willaime and Gandais (1972, Fig. 5) for a feldspar of approximate bulk composition $Or_{30}Ab_{60}An_{10}$.

the most calcic peristerite yet observed with two coherently diffracting phases (i.e., $An_{\sim 13}$, see discussion below).

As annealing progresses, coarser textures develop, as seen optically in a thin section from the Kiglapait intrusion (Fig. 2d). However, it is the submicroscopic texture of alternating, roughly planar lamellae of $Or_{\sim 90}$ and An_{15-18} (500-1000 Å thick; Fig. 2a,b) which gives rise to the iridescent colors often seen in larvikites. We shall discuss these interference phenomena in a later section, because they are observed in plagioclase intergrowths as well.

Antiperthites

Whether produced by spinodal decomposition, nucleation and growth, or metasomatic processes, K feldspar intergrowths with (Ab+An) > Or are

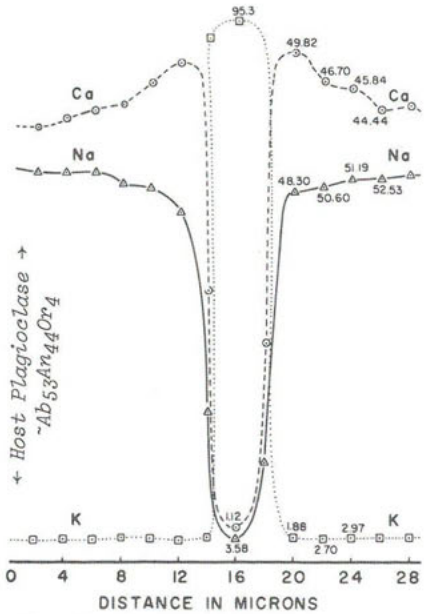

Figure 5. Electron microprobe traverses across a K-feldspar bleb in a plagioclase host from a Laramie Range gabbroic anorthosite, showing higher An-content near the boundaries. Numbers are mole percent An on Ca line, Ab on Na line and Or on K line. After Kay (1977, Fig. 2).

technically called *antiperthites*. Most plagioclase crystals from igneous rocks and many from high-grade metamorphic rocks contain K-feldspar inclusions, which may be spectacularly prominent or so small as to be overlooked or even unobservable by light microscopy. We confine our discussion to antiperthites formed by exsolution mechanisms, but Smith (1974b, p. 426ff.) has catalogued a wide variety of occurrences and textures.

The most sophisticated study to date is that by Kay (1977, 1978; *cf.* also Carstens, 1967). She examined relatively coarse antiperthites from anorthosites and conclusively demonstrated their exsolution origin with the following evidence: (1) "The An-content of the host plagioclase increases near the K-feldspar bleb, indicating slow diffusional transport" of Ca + Al exchanged for Na,K + Si away from the bleb, as illustrated in Figure 5. Here 4-5 μm bleb of composition $\sim Or_{95}Ab_4An_1$ has exsolved from a homogeneous ternary feldspar $\sim Ab_{50}An_{44}Or_6$ (composition calculated from many potassium x-ray distribution photographs taken using an electron microprobe). The matrix plagioclase is $\sim Ab_{53}An_{44}Or_3$. (2) "The flattened sides of the bleb are oriented ... subparallel to planes with minimal elastic strain" in peristerites. (3) "The crystallographic axes of the noncoherent blebs [of "variable" structural state] and the [low structural state e-] plagioclase host are subparallel." (4) Numerous heating experiments suggest that, "at high enough temperatures over long periods of time, diffusion rates of Al and Si are adequate to produce antiperthites by exsolution." Apparent equilibrium of plagioclase host and K-feldspar inclusions near 1060°C (the melting point of the blebs) suggests that "the chemical solvus lies above this temperature and that exsolution probably occurred at a coherent or semicoherent solvus" (Kay, 1977, p. 905 and 910; see also Kay, 1978). Two examples of antiperthite are illustrated below.

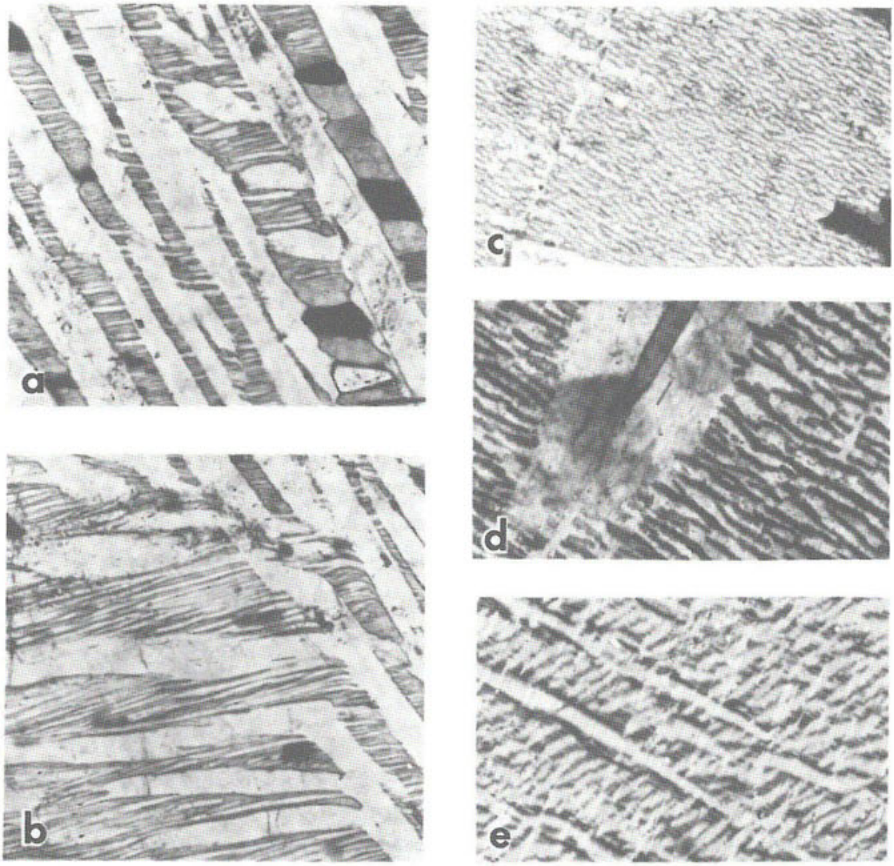

Figure 6. Five views in polarized light of antiperthitic megacrysts in the Montpelier, Virginia metamorphosed anorthosite. (a) and (b) Sections cut parallel to (010), scale: 1 cm = 133 μm. K-feldspar (darker) has formed in (001)-bounded platelets stacked along a in discontinuous lamellae approximately parallel to ($\bar{6}01$). Plagioclase is in optical continuity from one lamella to the next; thin rutile needles near the top are exactly parallel to a in (001). Numerous quartz grains are simultaneously in optical extinction. (c,d,e) Sections cut parallel to (001). In (c) and (e), scale is 1 cm = 333 μm; in (d) 1 cm = 133 μm.

Andesine antiperthite from a metamorphosed anorthosite. Clement and Bice (1982) and Bice and Clement (1982) describe the occurrence of this specimen in a "highly metamorphosed saprolitic andesine anorthosite" at Montpelier, Virginia. The latter describe at least two stages of perthite development, but we are concerned here only with the first in which K-feldspar of composition $\sim Or_{86}Ab_{11}An_2Cn_1$ coexists with an andesine, $\sim Ab_{67}An_{32}Or_1$ (Fig. 6), in large subhedral crystals up to 10 cm. in dimension. X-ray precession photographs indicate that the K-feldspar is untwinned microcline, and this plagioclase is twinned only on the Albite law, evidence that "exsolution" probably occurred at temperatures below $\sim 600°C$.

The textures of these intergrowths, with microcline as the darker phase, are illustrated in thin sections cut approximately parallel to (010) -- Figures 6a,b -- and (001) -- 6c,d,e. In the last of these, fine Albite twins are discernible in the plagioclase: some have apparent continuity from one area to another, but many do not. The orientation of the coarse lamellar texture of microcline and andesine is $\sim$ ($\bar{6}$01), but in Figure 6a the K-feldspar is seen to have been separated into platelets with dominant (001) faces which are S-shaped, as though they formed under a NW-SE shear stress. Quartz grains are grouped into several crystallographic orientations in the microcline lamellae. The plagioclase phase has optical continuity throughout the megacryst.

The details of the crystallization and metamorphic history of this anorthosite are currently in the preliminary stages of investigation, but the following is presented as an excellent example of what can be accomplished by careful crystallographic and textural studies.

"Moonstone" from Labrador. In a large crystal (No. 28 of the Corlett and Eberhard, 1967, collection) Reid and Korekawa (1978) found an extremely complex assemblage of plagioclase and exsolved alkali feldspars in close structural orientation, ranging from coarse (50 μm) granular to fine lamellar textures with complex twinning. Using the transmission electron microscope, they first investigated twinning in regions of the crystal containing only plagioclase (part A ≃ $Ab_{69}An_{27}Or_4$). The Albite and Pericline twins vary in thickness by three orders of magnitude from 10 μm to 100 Å. Figure 7 shows two distinct types of twin boundaries. They are sharp and distinct along (010) in Figure 7a, but they are poorly defined in 7d, with A and P twin individuals partly penetrating each other. The latter is a good example of what is called "M-twinning," which is commonly seen in microclines that have inverted from monoclinic sanidines (Chapter 2) and is presumed to indicate here that the plagioclase initially crystallized as a monoclinic phase.

By means of electron petrography and single-crystal x-ray diffractometry the authors have reconstructed the crystallization history of this material. (1) A homogeneous ternary feldspar first crystallizes with monoclinic symmetry. (2) "Replacement of Na (and Ca) by K in some parts of this crystal [source unspecified] leads to a monoclinic, homogeneous part B with composition $Ab_{50}An_{20}Or_{30}$." (3) Part A, depleted in K from step (1) [by loss to part B in step (2)?] inverts to M-twinned triclinic plagioclase (Fig. 7d). (4) Nucleation of exsolved K-feldspar grains ($Or_{88}Ab_{10}An_2$) "seems to occur

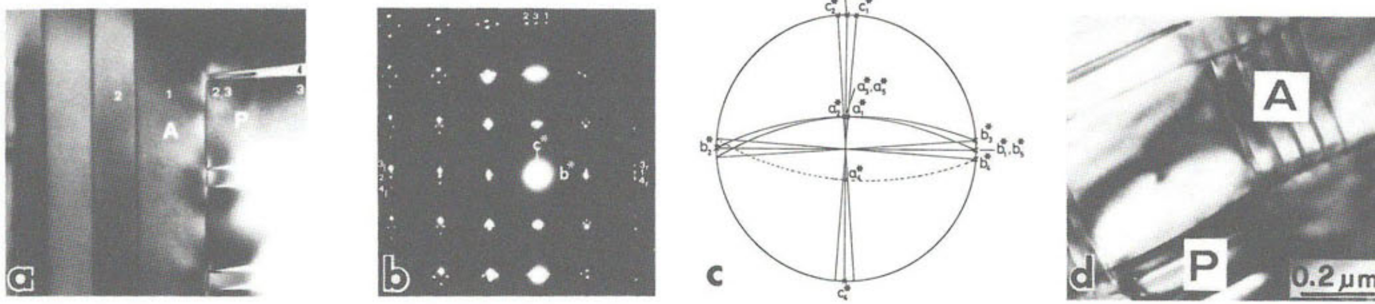

Figure 7 (above). Twinned plagioclase phase ($Ab_{69}An_{27}Or_4$) of part A of sample No. 28 of Corlett and Eberhard (1967): (a) Bright-field image of Albite (A) and Pericline (P) twins with an (010) boundary plane (vertical). (b) Diffraction pattern corresponding to (a) with twin members identified by small numbers which correspond to 1, 2, 3, 4 in (c). (c) Stereographic projection showing twin individuals 1 and 2 related by the Albite law, (010), and 3 and 4 related by the Pericline law, [010]: 5 represents the monoclinic K-feldspar seen in part B of the sample (Fig. 8). (d) An example of A- and P-twins with poorly defined, interpenetrating boundaries -- an excellent example of "M-twinning." (a) and (b) from Ried (pers. comm.), (c) and (d) from Ried and Korekawa (1978, Figs. 1 and 2d, respectively).

Figure 8 (below). Part B: dominant plagioclase ($\sim Ab_{71}An_{28}Or_1$) and exsolved K-feldspar ($\sim Or_{75}Ab_{20}An_5$). (a) Broad albite twins (A) split more finely near "K," the K-feldspar lamella. Pericline twins (P) are not in contrast in this orientation. (b) Extremely fine twinning on the Albite law (40 Å lamellae) and the Pericline law (70 Å lamellae), giving rise to satellite reflections indicative of the respective superstructures (see enlarged inset labelled 026). (c) In this region A- and P-twin lamellae are ~300 Å thick, with K-feldspar coherently exsolved. Maxima labelled I on the 008 reflection is the "intermediate" phase discussed in the text. From Ried and Korekawa (1978, Fig. 3).

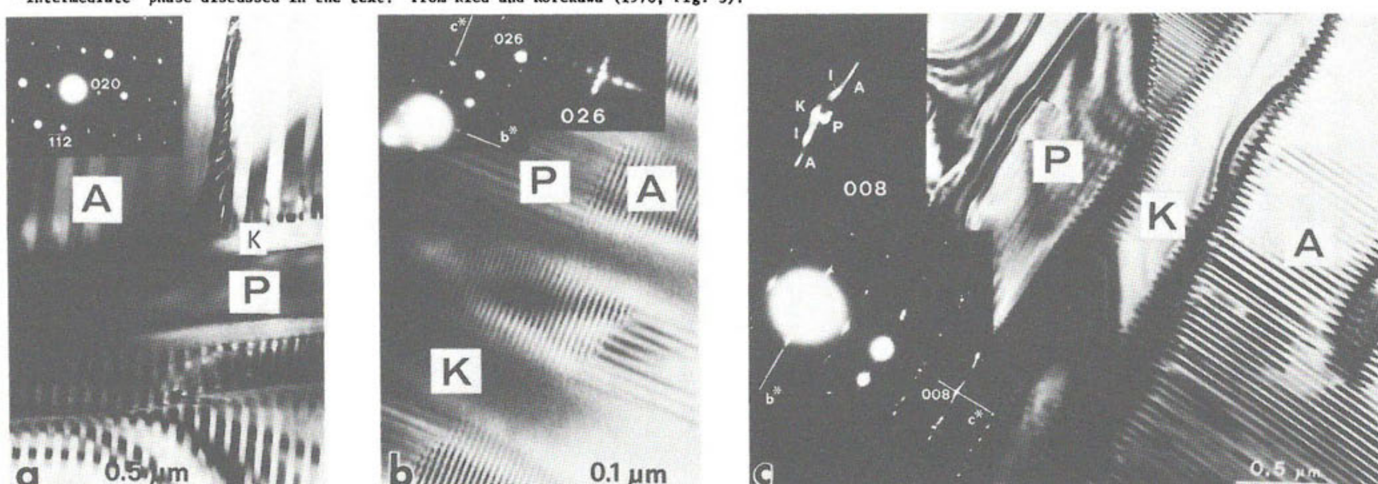

at twin boundaries in part A." The composition of the Albite- and Pericline-twinned plagioclase host is now $\sim Ab_{69}An_{27}Or_4$. (5) Concurrent exsolution of K-feldspar in part B (Fig. 8) leads to "lamellae with compositions $Or_{75}Ab_{20}An_5$ and $Ab_{71}An_{28}Or_1$ ... Nearly simultaneous or subsequent transition of the [latter] lamellae from monoclinic to triclinic symmetry leads to polysynthetic twinning" on a fine scale (Fig. 8b), reducing strain and preserving coherency with the monoclinic K-feldspar whose lamellae are parallel to $(\bar{8}01)$. The diffraction pattern in Figure 8c indicates that there is an "intermediate" phase I which is Albite twinned and both closer to monoclinic symmetry and more K-rich than the M-twinned plagioclase. It could not be imaged by selected area diffraction but is presumed to be located along the strained interfaces of this complex antiperthite.

EXSOLUTION IN PLAGIOCLASE FELDSPARS
(See also Chapter 9)

Inasmuch as the phase equilibria of plagioclase feldspars were discussed in the previous chapter, this section is devoted primarily to illustrations of the textures observed in each of the three regions where exsolution is a predominant feature in the subsolidus, namely the sodium-rich *peristerites* ($An_{\sim 2}$-$An_{\sim 16}$), the calcium-rich *Huttenlocher intergrowths* ($An_{\sim 68}$-$An_{\sim 88}$), and the *Bøggild intergrowths* whose bulk compositions are intermediate in range ($An_{\sim 45}$-$An_{\sim 62}$). Evidence of two-phase intergrowths in other regions of the subsolidus (e.g., An_{30}) is beginning to accumulate, further complicating attempts to draw a definitive equilibrium diagram for plagioclases.

Peristerites

Phase relations. The models for phase separation in the region $An_{\sim 2}$ to $An_{\sim 16}$ are summarized in Figure 9. The reason that this composition range is more restricted than the compositions of the two phases that are reported as "end-members" of the exsolution, i.e., An_{0-2} and $An_{20\pm 5}$, has to do with the kinetic problems discussed in the introduction of this chapter: temperatures are simply too low for large-distance diffusion of NaSi and CaAl when the bulk composition of the plagioclase solid solution is greater than about An_{16}. It seems certain that the driving force for phase separation is the low free energy configuration of ordered low albite, which is universally present as one member of the peristerite exsolution.

Textures. A specimen of bulk composition $An_{16.5}$ (Fig. 10a) illustrates a texture suggestive of early stages of spinodal decomposition with two intersecting, predominantly transverse modulations. The more prominent,

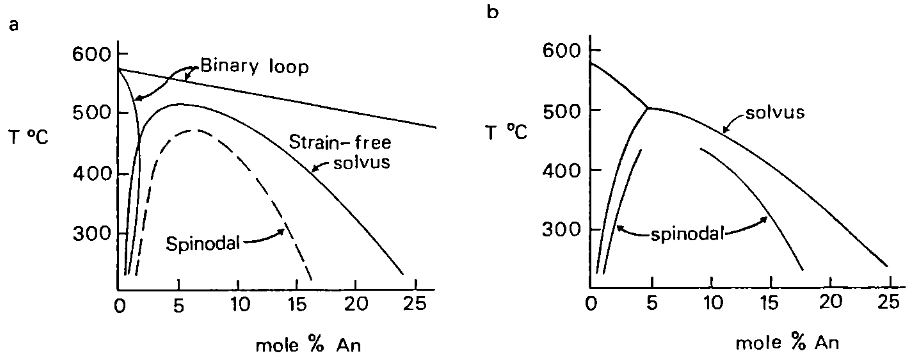

Figure 9. (a) Three possible models for peristerite exsolution: *binary loop* (Orville, 1974; adopted by Smith, 1974a), *strain-free solvus* (Crawford, 1966), *coherent solvus* (spinodal) inside the strain free solvus (Christie, 1968, 1969; Nord, 1978). (b) The model of Carpenter (1981; modified from his Fig. 3, p. 558). Carpenter (p. 554) describes this as a "conditional solvus containing a 'conditional spinodal.' The implications are that the miscibility gap exists only after some degree of order has been achieved and that the order/disorder reaction is other than first order in character." Figures from Jenkins (1980).

trending NW-SE, is near $(0\bar{8}1)$ [albite cell indexing][2]; the SW-NE modulation is approximately parallel to (100). Smith (1974b, Ch. 19) explained the two orientations of peristerite intergrowths in terms of coherency strain, and Olsen (1979) produced estimates of coherent elastic energies. The latter (1974, 1975, 1979) showed that the peristerite miscibility gap extends into the Or-Ab-An ternary and that the orientation of the "exsolution lamellae varies from $(0\bar{8}1)_{Ab}$ to about $(\bar{1},21,2)_{Ab}$ with increasing potassium content."

McLaren (1974, Fig. 21) described a specimen on the albite-side of the "peristerite gap" ($An_{2.6}$) and Lorimer *et al.* (1974) a specimen near An_{12}, both of which showed only single modulations parallel to $(0\bar{4}1)_{An}$ with periodicities of $\sim$200 Å. "It is probable that these two samples represent a later stage in the exsolution process than those containing 'tweed' structures [Fig. 10a] and that peristerites resemble the pyroxenes in producing two initial spinodal modulations, only one of which [usually] coarsens [see Fig. 11b]" (Champness and Lorimer, 1976, p. 195). A specimen described by Miúra (1977) has a similar texture (Fig. 10b), but its high K-content ($Ab_{94}An_3Or_3$) may disqualify it for direct comparison with the peristerites. Clearly each of the above formed by solid-state coherent dissociation of a single-phase solid solution crystal. The extent to which Al,Si order had

[2] In recent years the Miller indices of planes of least strain in exsolved plagioclases have been determined using the anorthite (c = 14 Å) unit cell, but the literature prior to 1970 almost exclusively gives Miller indices based on the albite (c = 7 Å) cell. We will adopt the convention of a subscript to avoid confusion, although we, too, are sometimes unsure of the designation. Example: $(0\bar{8}1)_{Ab} = (0\bar{8}2)_{An} \equiv (0\bar{4}1)_{An}$.

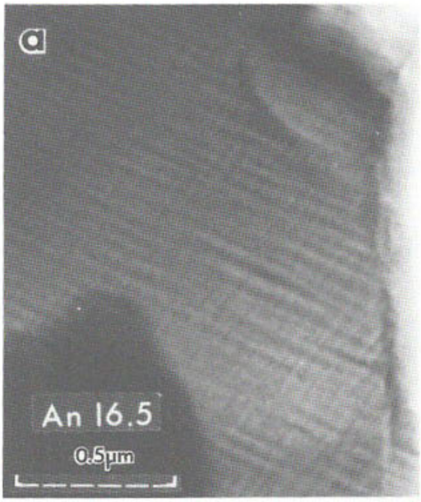

See Joswig et al. (1977) for details of $An_{16.5}$ superstructure.

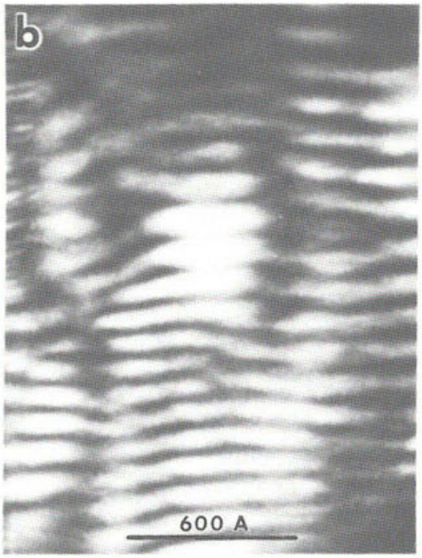

Figure 10. (a) Bright-field TEM photograph of an (001) cleavage fragment of the Sultan Hamud peristerite ($An_{16.5}$). The more prominent $(0\bar{8}1)$ compositional modulation trends approximately NW-SE; the weaker one is approximately parallel to (100). From Korekawa *et al.* (1970), who detected only one reciprocal lattice in this specimen, but observed superlattice spots from the 120-150 Å modulation normal to $(0\bar{8}1)$ [$\equiv$ $(0\bar{4}1)$ indexed on the anorthite unit cell]. No diffraction was seen from the (100) modulation. (b) Compositional modulations in $Ab_{94}An_3Or_3$. Note fine-scale (~40 Å) periodicity in upper left. From Miúra (1977).

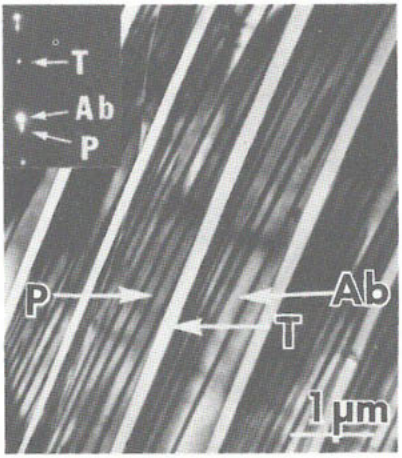

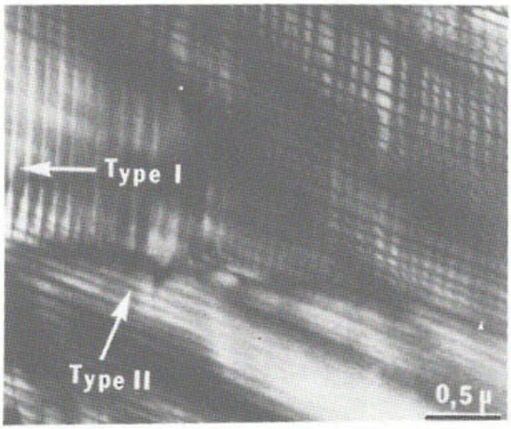

Figure 11. (a) Bright-field TEM image of microtexture in an Albite-twinned peristerite from Seiland, Norway. Three types of lamellae are present: low albite (*Ab*), low albite (*T*) in a twinned orientation with *Ab*, and an untwinned third phase (*P*) which is $An_{\sim 25}$. The inset is part of the electron diffraction pattern. (b) Bright-field image of a peristerite from the same locality showing two well-developed sets lf lamellar "precipitates": Type I has an orientation nearly parallel to $(0\bar{8}1)_{Ab}$, Type II near $(\bar{7}12)_{Ab}$. Interference colors are observed from the Type I lamellae only. From Olsen (1974, Figs. 1 and 3, p. 143).

progressed in the initial phase and subsequent thermal history must be accounted for in any attempt to model the phase relations (see Fig. 9a and b, Carpenter, 1981, and discussion by Smith, Ch. 9).

The textures of peristeritic intergrowths in the range An_5-An_{13} are commonly coarse enough to produce optical interference colors, but these are not always observed because bulk specimens are usually inhomogeneous to some degree, both in composition and in texture (see the last section in this chapter). Figures 11 and 12 illustrate lamellar textures on the 500-1500 Å scale as imaged by transmission and scanning electron microscopy and by photo-emission electron microscopy. As originally deduced by Bøggild (1924) from optical studies of iridescence, the prominent lamellae are parallel to $(0\bar{8}1)_{Ab}$ (*cf*. Fleet and Ribbe, 1965). Interference colors usually are visible in only one direction -- from the $(08\bar{1})_{Ab}$ plane, but the rare coarsening of a second set of lamellae -- which probably is a remnant of the 'tweed' texture of early spinodal decomposition (Fig. 10a) -- potentially leads to a second direction of iridescence or "schiller". Olsen (1974) reported that a specimen from Seiland, Norway ($Ab_{91}An_4Or_5$) contained two directions of lamellar "precipitates" (Fig. 11b). The prominent one, ranging from $(0\bar{8}1)_{Ab}$ to $(\bar{1},21,2)_{Ab}$ with increasing K-content, had periodicities of 1500-2300 Å and visible interference colors in the range 4500-6900 Å. The second, near $(\bar{7}12)$, had a lamellar-pair repeat of ~750 Å, which would produce interference in the 2300 Å (ultraviolet) range (see later section).

Occasionally textures *too coarse* to cause iridescence are observed microscopically. One such specimen was reported by Brown (1962) from an Amelia, Virginia pegmatite, and another by Raith (1969) from a gneiss in the Zillerthaller Alps, Austria. Under certain low-grade metamorphic conditions two plagioclases may grow entirely separately with compositions straddling the "strain-free solvus," thus defining the so-called peristerite gap. See comments by Smith in the previous chapter.

Comparisons of coexisting phases. It is often possible to estimate compositions of the exsolved or coexisting phases of the coarser peristerites using the reciprocal lattice angles γ^*, as measured on an [001] x-ray precession photograph, together with an An-curve like that shown on the next page. In the cases in which structural coherence between coexisting phases is evidenced by streaks connecting pairs of reflections in x-ray or electron diffraction patterns or by additional reflections which may arise from a third phase, incomplete decomposition, a superstructure, or all of these (Viswanathan and Eberhard, 1968), caution is advised in deducing com-

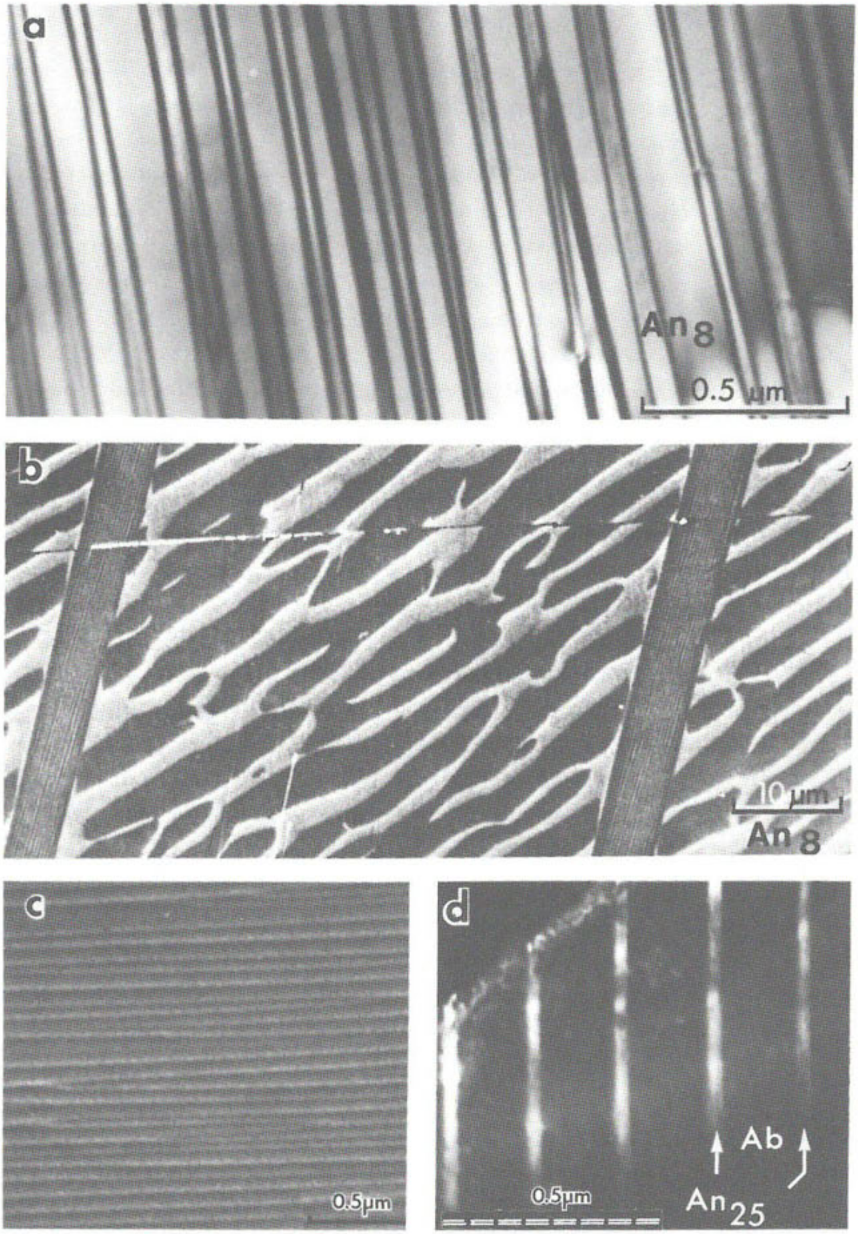

Figure 12. (a) Bright-field TEM photograph of a peristerite ($An_{7.6}$) from Bancroft, Ontario. The alternate set of coarser lamellae is $An_{\sim 0}$; the finer set $An_{\sim 25}$. The electron beam is approximately normal to (001). The diffraction contrast fringes show that the lamellar boundaries are inclined to the beam. Courtesy of A.C. McLaren. (b) Photo-emission electron microscope (PEEM) photograph of an Albite-twinned peristerite ($An_{8.4}$) cut and polished at $\sim 2°$ to the plane of the exsolution lamellae (except in the two narrow twin bands, where the intersection is more nearly vertical). Dark regions are $An_{\sim 0}$ and light regions $An_{\sim 25}$. This photo is discussed by Laves (1974, pp. 545-546) and Weber (1972). (c) A scanning electron microscope (SEM) photograph of the (001) cleavage surface of a peristerite. Courtesy of H.-U. Nissen.

(d) Dark-field TEM photo of a red iridescent peristerite (An_3) from Hybla, Ontario.

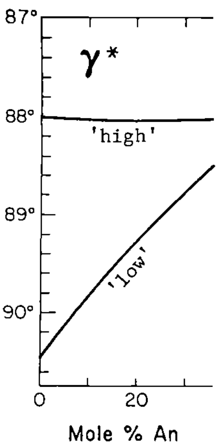

Modified from Speer & Ribbe (1973, Fig.5)

positions from lattice angles which are likely to be somewhat distorted. But for the most part, especially when iridescent colors are observed (indicating lamellar textures in the 500-1000 Å range), the γ^* method is reliable (see inset). This has been confirmed by proportioning the two γ^*-derived compositions according to relative intensity ratios of one or more pairs of x-ray reflections to obtain a bulk composition for the grain (Ribbe, 1960).[3]

Far better, though not generally available, is the method of ion microprobe analysis employed by Miúra and Rucklidge (1979). They report directly measured compositions of $An_{2\pm2}Or_{1\pm1}$ and $An_{19\pm2}Or_{1\pm1}$ for lamellae 1030 Å and 260 Å thick, respectively, in a peristerite of bulk composition $Ab_{94}An_5Or_1$. Values of $An_{2\pm2}Or_{1\pm1}$ and$_{23\pm2}Or_{3\pm1}$ for lamellae of 1310 Å and 310 Å thickness were determined for a specimen of bulk composition $Ab_{92}An_7Or_1$.

Transmission electron microscopy combined with energy dispersive x-ray analysis has been less successful due to difficulties of resolution and calibration (Cliff *et al.*, 1976), although Olsen (1975) used the method to study a series of K-rich peristerites from Seiland, Norway. These specimens, twinned on the Albite law, are remarkable in that every other (010) twin lamella is exsolved into Ab and $An_{\sim25}$, but intervening ones are homogeneous (Fig. 11a). For specimens with bulk compositions near the Na-rich limb of the peristerite solvus, the twin lamellae which are exsolved are slightly more calcic (~2% An) than their homogeneous neighbors (Fig. 13a); the opposite is true near the Ca-rich limb (Fig. 13b), but the difference in An-content may be as large as 6 mol %.

[3] A low structural state is always observed in the Ab-rich phase (Ribbe, 1960; Brown, 1962) and is assumed for the oligoclase phase. The $An_{20\pm5}$ occasionally has been observed to exhibit very diffuse 'e' reflections in single crystal photographs. These are characteristic of 'e'-plagioclase that has at least partly "ordered" into albite and anorthite-like domains on a very fine scale (~30 Å or less). In this connection it is worth noting that Orville (1974) proposed that the "peristerite gap" represents an equilibrium between ordered albite and *disordered* plagioclase solid solution. This may be the case at the time of phase separation, but the disorder does not persist and has not been observed in any natural occurrences at room temperature.

Smith (1974a, Fig. 19-58, p. 526) summarized all γ^* data in the peristerite literature, and found that no intergrowths coarse enough to exhibit distinct lattices have been found with *bulk* An-contents exceeding An_{13}.

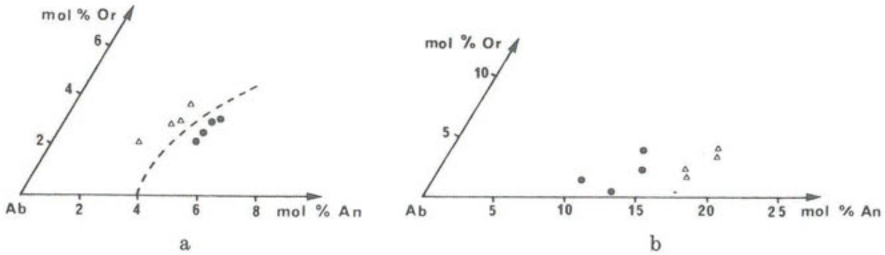

Figure 13. X-ray analysis of pairs of adjacent (010) Albite twin lamellae in peristerites from Seiland, Norway (like that shown in Figure 11a). (a) Specimens with bulk compositions near the Na-rich limb of the solvus. (b) Specimens with bulk compositions near the An-rich limb of the peristerite solvus. Compositions of individual lamellae showing no exsolution are indicated by triangles, those which are exsolved by dots. From Olsen (1975, Figs. 2a,b, p. 300).

Huttenlocher intergrowths

In a petrographic study of plagioclase amphibolites from the northern Italian Alps, Huttenlocher (1942) first reported optically visible exsolution lamellae parallel to $(0\bar{3}1)_{An}$ in bytownites, like those shown in Figures 14a and 14b. Since then many two-plagioclase intergrowths in the composition range $An_{\sim 66}$ to An_{90-95} have been observed (Figs. 14-16). In 1968 Nissen presented x-ray diffraction evidence that the two phases in Huttenlocher's bytownites were transitional or *I*-anorthite (with 'b' reflections) and 'e'-plagioclase (with both 'e' and 'f' reflections), and his results have been verified frequently, especially in electron diffraction studies (see Fig. 12, Ch. 2 for an excellent example). Cliff *et al.* (1976) used an analytical electron microscope equipped with an energy-dispersive x-ray detector to determine that, in a coarsely exsolved bytownite of bulk composition $An_{71\pm 3}$ from the Roneval, Scotland anorthosite, the approximate compositions of the major (8000 Å) and minor (4000 Å) lamellar phases were $An_{69\pm 4}$ and $An_{88\pm 4}$, respectively. These compositions do not represent the two stable end members of the Huttenlocher exsolution for two reasons: (1) other specimens of bulk compositions as low as An_{66} have been observed to contain both transitional (or *I*-centered) anorthite *and* an 'e'-plagioclase (the composition of the latter must certainly be less than An_{66}!); and (2) igneous plagioclases with compositions as high as An_{94} have been observed with fine tweed textures like that pictured in Figure 16, indicating that exsolution or spinodal decomposition may occur very close to the An_{100} end member. Nord *et al.* (1974) studied igneous bytownites from Stillwater and found that "the average 'wavelength' of the exsolution lamellae increases slightly toward the more albitic bulk compositions: An_{85} -- 125 Å, An_{82} -- 200 Å (Fig. 16), An_{81} -- 400 Å, An_{79-76} -- 600 Å, An_{74-76} -- 850 Å." This trend is reminiscent of that seen in peristerites, but at a finer scale.

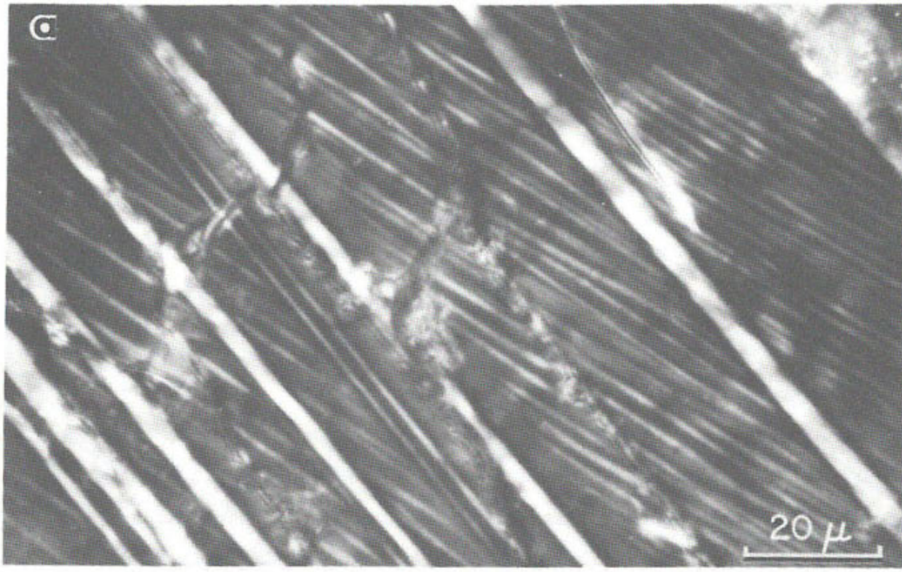

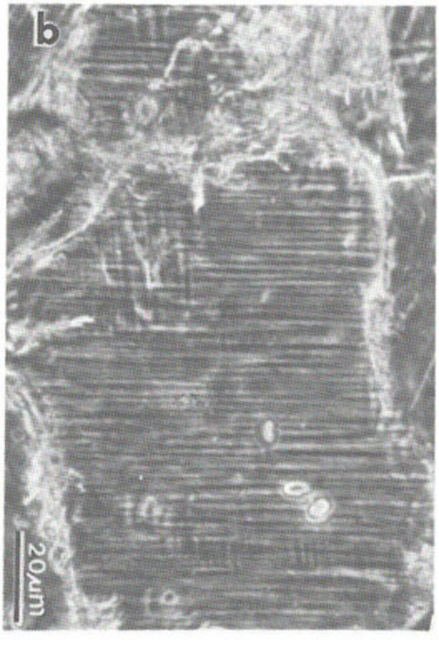

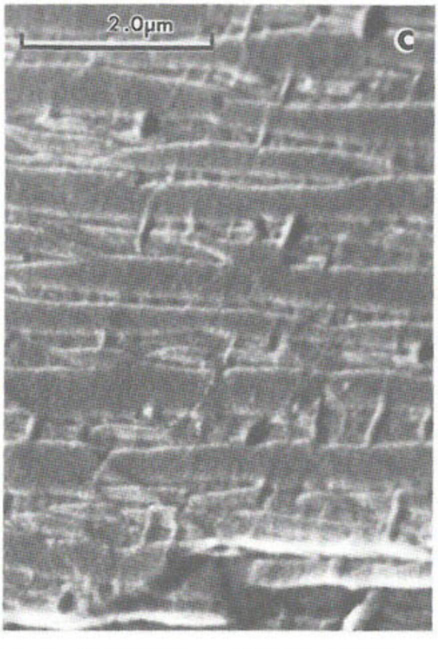

Figure 14. High magnification phase-contrast optical micrographs of (a) An$\sim$73 and (b) An$\sim$67 from a plagioclase amphibolite in Valle d'Ossola, Italy. The major NW-SE lamellae in (a) are Albite twins. The exsolved phases in the broader twin bands are inclined at $\sim$16-20° to (010) and parallel to $(0\bar{3}1)_{An}$. (c) An$\sim$75 (same locality). Scanning electron micrograph of an (001) cleavage surface, etched 30 seconds with 0.4% HF. Note the secondary exsolution of smaller, lenticular, Na-rich phases in the calcic lamellae between the continuous, subparallel sodic lamellae. From Nissen (1974, Fig. 4c, p. 500).

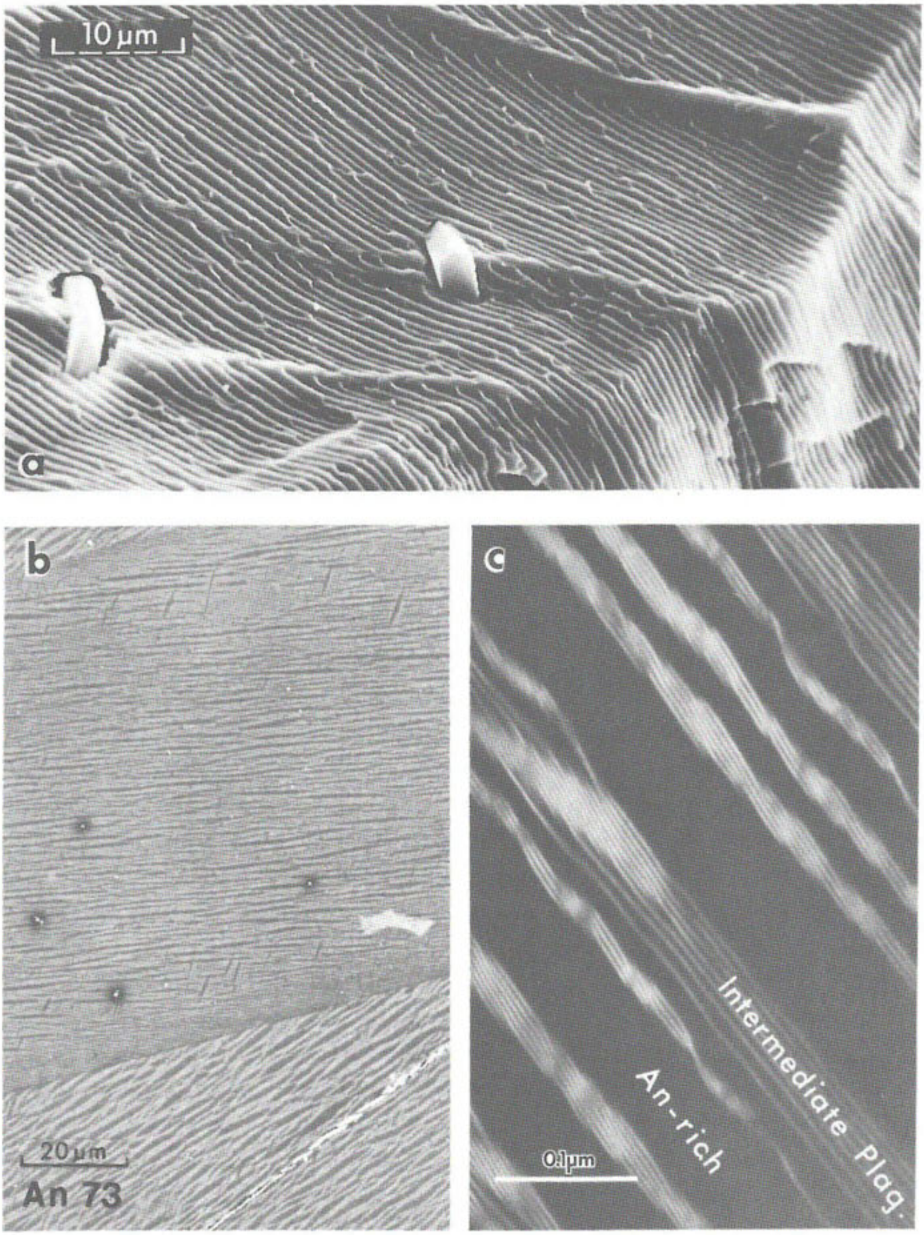

Figure 15. Scanning electron micrographs of a twinned specimen ($An_{\sim 69}$) from the Narødal, Norway, anorthosite. (a) Fracture surface etched 30 seconds in 40% HF. Courtesy of H.-U. Nissen. (b) [below] Photo-emission electron microscope (PEEM) photo of the (100) polished surface of $An_{\sim 73}$ from the same locality. This section shows broad Albite-twinned bands, and remnants of a secondary planar decomposition cutting across the primary lamellar exsolution which is inclined at low angles to the twin boundaries. Courtesy of F. Laves (see Laves, 1974, pp. 546-548).

(c) Dark-field image of a $(30\bar{1})$ calcic lamella exsolved on an optically visible scale from a bytownite (An_{72-75}). The 'e'-plagioclase parallel to $(30\bar{1})$ lamellae represent a secondary stage of exsolution. Courtesy of T.L. Grove (see Grove, 1976, Fig. 2).

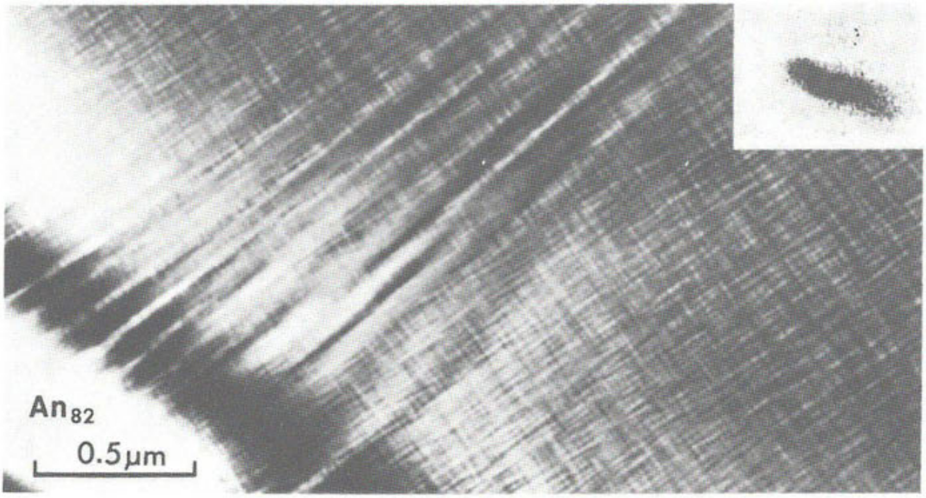

Figure 16. Dark-field micrograph (1000 kV) showing the tweed structure in An_{82}. The modulations are oriented parallel to (010) NW-SE and ($\bar{1}01$) NE-SW. Courtesy of G.L. Nord. Cf. Nord *et al.* (1974, Fig. 9).

Tagai and Korekawa (1981, Fig. 5, p. 80), using all available data and their own careful single-crystal diffraction studies of natural and heated specimens, have proposed a "schematical phase diagram of Huttenlocher exsolution" that has a nearly vertical limb sloping upward from $An_{\sim 65}$ to $An_{\sim 68}$ at 1300°C and a limb sloping gently downward from $An_{\sim 70}$ to $An_{\sim 87}$ at an unspecified lower temperature. Their work is a valuable summary of experimental observations, but Grove's (1977b) wide-ranging TEM investigation of calcic plagioclases (An_{65}-An_{85}) from volcanic, plutonic and metamorphic environments is by far the most comprehensive investigation of Huttenlocher exsolution and related $C\bar{1} \rightarrow I\bar{1} \rightarrow P\bar{1}$ structural transformation sequences. He has arranged these phenomena according to "time-integrated cooling rates" (see his Fig. 13 and Chapter 9).

The most commonly observed orientations of exsolution lamellae are $(0\bar{3}1)_{An}$, $(\bar{2}01)_{An}$ or $(\bar{3}01)_{An}$ and -- in crystals showing the fine tweed textures characteristic of intersecting transverse modulations -- $(\bar{1}01)_{An}$ and (010) (Fig. 16). Cliff *et al.* (1976) and Grove (1976; see Fig. 15c) have reported several occurrences of *secondary* exsolution of an 'e'-plagioclase within the calcic lamellae of a coarser primary Huttenlocher intergrowth. Garrison (1978, p. 148) suggested that both Huttenlocher and Bøggild intergrowths may be present in the same zoned plagioclase grain, Spear (1977; *cf.* 1980) found a low-grade metamorphic assemblage containing An_{39} and An_{88}, the latter most certainly containing submicroscopic exsolution lamellae, and Wenk (1977) reported crystallographically intergrown metamorphic plagioclases with compositions of An_{35-45}, An_{65-70}, and An_{85-92}.

Figure 17. Stereographic projections showing calculated elastic energies (contoured in units of 10^3 J/m^2) of exsolution lamellae as a function of the orientation of the boundary between them. The lattice constants (modified slightly from Olsen, 1977) of the two phases are given for a specimen from Åna-Sira, Norway, $An_{50.6}Ab_{46.6}Or_{2.8}$ [boundary ($\bar{1}$,6,0.72), symbol ▲] and a specimen from Labrador, $An_{53.4}Ab_{44.9}Or_{1.7}$ [boundary ($\bar{4}$,24,3), symbol Δ]. Their boundaries plus those from two other specimens, both of which show 'tweed' textures and thus have two boundary orientations, are shown near calculated minima. Modified from Olsen (1979, Figs. 7d and b, p. 125).

The petrologic implications of these and other assemblages of coexisting plagioclases (see summary by Smith, Ch. 9) are far from being understood, and there are abundant opportunities for creative research. In fact, as this book was going to press, a paper by Grove *et al.* (1983) appeared with a well-reasoned suggestion for the topology of the subsolidus in the range An_{35}-An_{100}.

Bøggild intergrowths

Brilliant interference colors initially attracted the attention of Lord Rayleigh (1923) to the plagioclases of intermediate composition. But it was Bøggild (1924) who undertook the first really systematic study; he determined optically the orientation of the planes from which the colors were originating, listing many in the range from near ($\bar{1}$,12,1) to ($\bar{9}$,33,4), some near (0$\bar{4}$1) and ($\bar{1}$,$\overline{22}$,7) and a few scattered around (30$\bar{1}$). Using TEM methods, Olsen (1979) presented more data and added an analysis of strain energies to explain these observations. Olsen (1977) had used the splitting of Kikuchi lines in TEM diffraction patterns of An_{51} and An_{53} to determine the differences in lattice parameters of the two phases in each of these labradorites. Modifying the cell edges by no more than 0.003 Å the angles < 0.05° (well within the limits of error) and using the coherent model of Willaime and Brown (1974), Olsen (1979) calculated the elastic strain energies as a function of the orientation of the lamellar boundary between these phases. The resulting stereonets (Fig. 17) show minima very close to most of the known lamellar orientations, including specimens which have 'tweed' textures resulting from two transverse modulations intersecting at ∿90° (*cf.* Christie and Olsen, 1974).

Plagioclases in the composition range $An_{46\pm2}$ to $An_{60\pm2}$ exhibiting exsolution textures are called Bøggild intergrowths. See Figures 18 and 19 for examples.

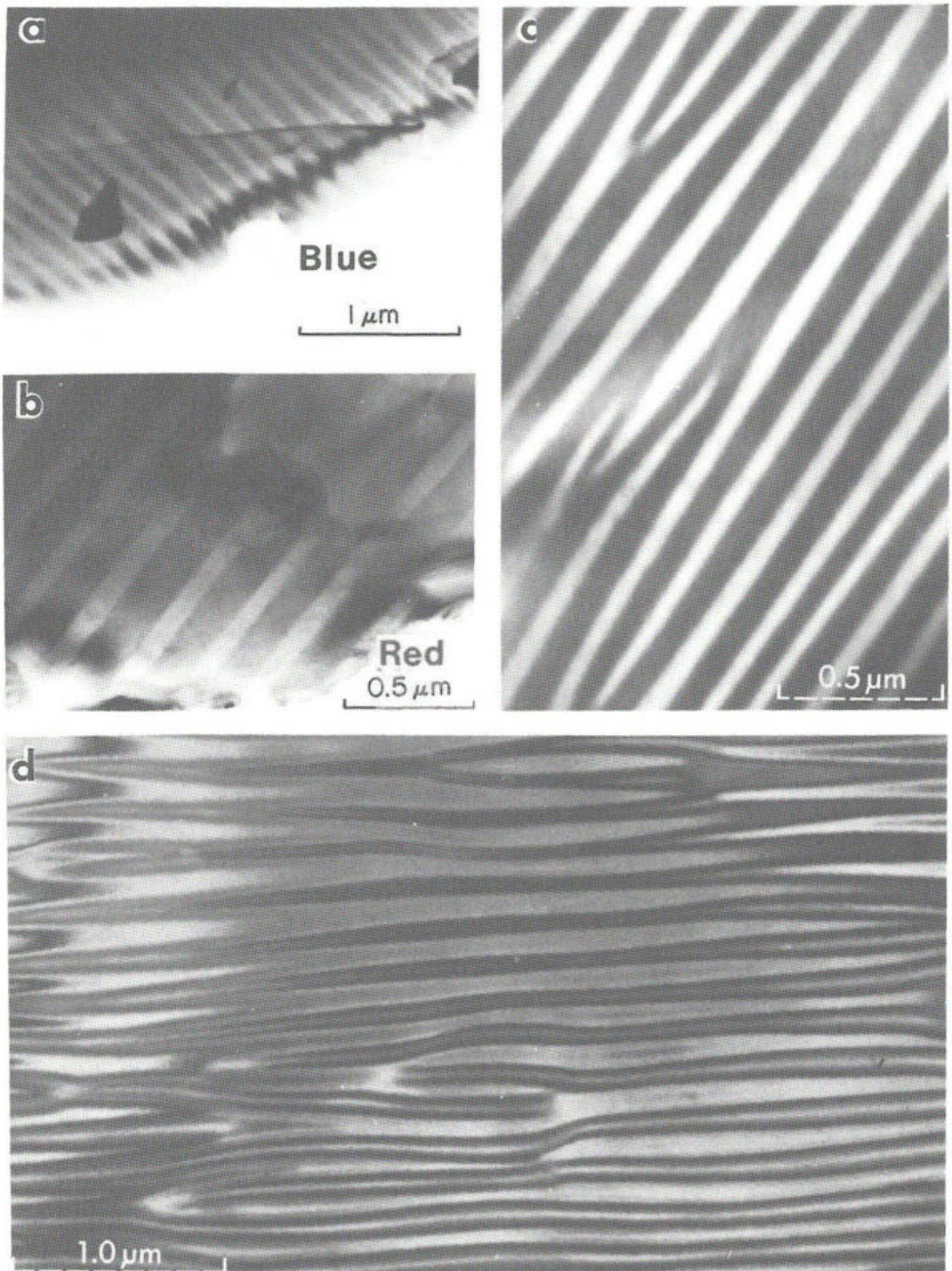

Figure 18. (a) Bright-field TEM photograph (100 kV) of a thin fragment of a Bøggild intergrowth with blue iridescence and (b) another specimen with red iridescence. The wider lamellar set is An-rich, the narrower set is Ab-rich. After Bolton *et al.* (1966; compositions not reported). Dark-field TEM photograph (100 kV) of an ion-thinned specimen of $An_{52}Ab_{45}Or_3$ composition. Courtesy of A.C. McLaren. (d) Bright-field TEM photograph (1000 kV) of a thinned labradorite showing details of inter-lamellar boundaries. Courtesy of H.-U. Nissen.

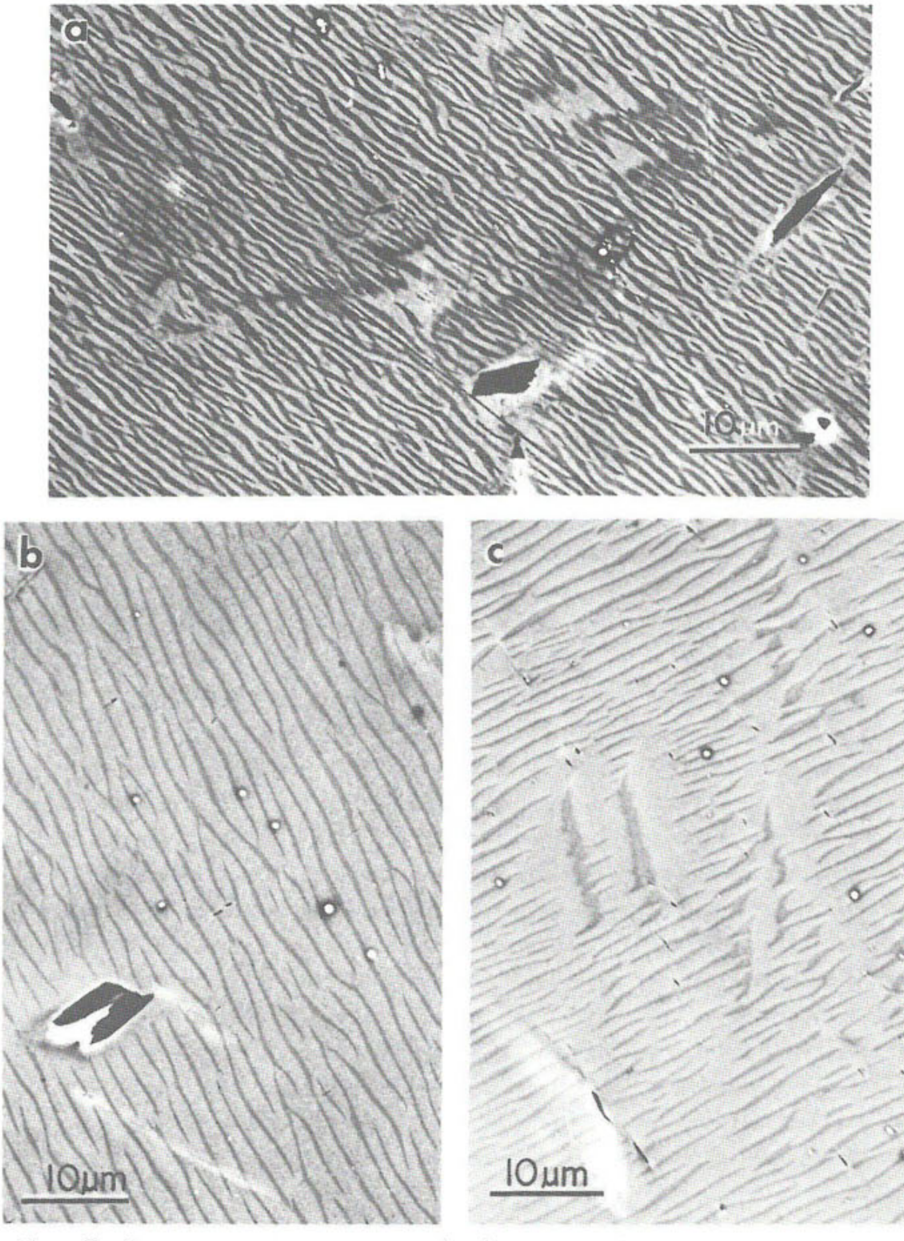

Figure 19. Photo-emission electron microscope (PEEM) photographs of Bøggild intergrowths in labradorite from Finland: the specimens are cut and mechanically polished at a very low angle to (010) and at $\sim 10°$ to the plane of iridescence, producing a magnifying effect, greatly exaggerating the non-planarity of the intergrowths (*cf.* Fig. 18 b). (a) Blue area, $An_{\sim 55}$ and (b) red area, $An_{\sim 57}$ are from the same large crystal (*cf.* Fig. 19 a, b). (c) A green iridescent region from another crystal ($An_{\sim 52}$?). Metioscope photos from Firma Balzers, A.G., courtesy of the late Prof. F. Laves (see Laves, 1974, pp. 542-545).

Compositions of the coexisting phases evaded analysis for many years because their diffraction patterns are essentially overlapping and their lamellar thicknesses are generally less than 2000 Å. Nissen *et al.* (1973) and Cliff *et al.* (1976) demonstrated differences in composition of ∿12 mol % An by semiquantitative x-ray analysis in electron microscopes, but the definitive experiments were those by Miúra and Tomisaka (1978). They used an ion microprobe mass analyzer to sputter through the lamellae in orientations nearly normal to the $^{16}O_2^+$ ion beam (see Fig. 20), and they measured the $^{23}Na^+/^{27}Al^+$ and $^{39}K^+/^{27}Al^+$ isotope ratios to determine compositions of successive lamellae. Typical analyses are given below (estimated errors in parentheses, average lamellar thicknesses (Å) in square brackets):

	An	Or		An	Or		An	Or	
Bulk composition	51	3		53	3		58	3	
Minor lamellae	44(2)	3(0)	[770]	43(6)	4(0)	[710]	46(4)	4(1)	[550]
Major lamellae	57(1)	2(0)	[830]	58(8)	3(1)	[1030]	61(4)	3(1)	[1900]

The average of all measurements came to $An_{44\pm4}Or_{3\pm1}$ and $An_{58\pm6}Or_{2\pm1}$ for minor lamellae, respectively, and as expected, both of these compositions represent 'e'-plagioclases (*contra* McLaren and Marshall, 1977; see Ch. 2, p. 50 and Ch. 9, p. 236).

Figure 21 contains a dark-field image obtained from a Bøggild intergrowth using a pair of intense 'e' reflections in the electron diffraction pattern. It is similar to that examined by McConnell (1974b) in which he traced a sinusoidal variation in both the orientation of the vector $\vec{t}$ (which is normal to the 'e' superlattice fringes -- arrow in Fig. 21b) and the T spacing of the fringes from one exsolution lamella to the next (Fig. 21a). For this reason McConnell postulated spinodal decomposition as a mechanism for phase separation (see Fig. 10, Ch. 9). There are dislocations of 'e' fringes at occasional points of misfit between exsolution lamellae, but for the most part the two phases appear to be coherently intergrown, perhaps accounting for their similarity in lattice parameters (*cf.* Fig. 17). Incidentally, the ∿10 Å difference in T spacing of the fringes between adjacent lamellae corresponds to ∿15 mol % difference in An-content as determined from Figure 15 in Chapter 2; this is in good agreement with most of Miúra and Tomisaka's (1978) ion probe analyses.

It is the average *total* thickness of the An-poor (minor) and An-rich (major) exsolution lamellae that controls the interference color that is observed in any region of an iridescent plagioclase intergrowth. Bulk composition is thus related to color as shown in Figure 22 and discussed in the following section.

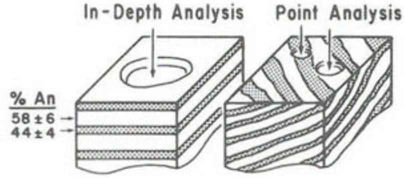

Figure 20. Schematic diagrams of "in-depth" (left) and "point" analysis methods used by Miúra and Tomisaka (1978) for labradorites and by Miúra and Rucklidge (1979) for peristerites (see above). In the former a 50μm beam was used, in the latter a 5μm beam. The large variability of thicknesses and irregularities of lamellar boundaries (*cf.* Figs. 11, 12, 18, 19) account for rather large standard errors in composition determination.

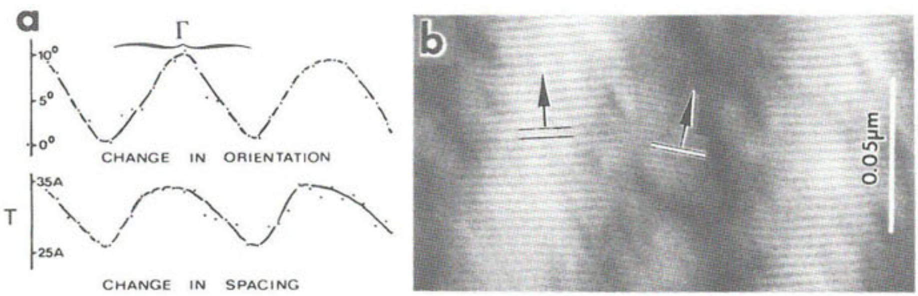

Figure 21. (a) Diagram illustrating the variation in orientation of $\vec{t}$ and T-spacing of the 'e' fringes determined by McConnell (1974b) from a Bøggild intergrowth similar to that shown in (b). Γ corresponds to the coarse intergrowth periodicity. (b) High magnification dark-field image of An_{52} obtained with an anti-phase pair of 'e' reflections in a TEM diffraction pattern. Lines have been added to emphasize differences in T width and $\vec{t}$ orientation. Photo courtesy of Wolfgang Müller.

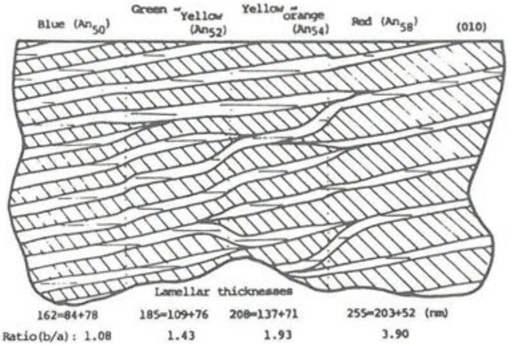

Figure 22. Schematic drawing of color zoning in a section of labradorite normal to (010), illustrating changes in relative thickness of An-poor (thinner) and An-rich (thicker) lamellae, and resulting changes in bulk composition. From Miúra (1978, Fig. 7, p. 102). Compare Figure 19 in which the same effect is illustrated by three different specimens.

INTERFERENCE COLORS

Unlike the Huttenlocher intergrowths in which iridescence is rarely obsrved and the peristerite, ternary and alkali feldspar composition ranges in which it is occasionally observed, low-temperature labradorites in the Bøggild range (An_{46} to An_{60}) nearly all exhibit visible interference colors, variously called "schiller" or "labradorescence".[4] Those without visible iridescence often have spectral peaks in the ultraviolet or infrared. Laves *et al.* (1965) first confirmed that the wavelength λ of observed iridescence followed the Bragg equation

$$N\lambda = 2\,n\,d_{a+b}\sin\theta \tag{1}$$

where N is the order of the reflection (1,2,3,...), n is the mean refractive index, d_{a+b} is the mean thickness of the lamellar pairs (a true repeat is $d_a + d_b$), and θ is the angle of incidence of the light on the sub-planar lamellae.[5]

Bolton *et al.* (1966) expressed the interference relationship for stacks of optically-transparent thin lamellae of alternating refractive indices n_a and n_b and thicknesses d_a and d_b as

$$N\lambda = 2(n_a d_a \sin\theta_a + n_b d_b \sin\theta_b) \ . \tag{2}$$

Because for differences in composition of 12-20% An between lamella a and lamella b, n_a and n_b differ by $\sim$1 % (<0.020) and θ_a and θ_b by correspondingly negligible amounts, either equation is adequate to roughly estimate the wavelength of the interference color, if thicknesses are reliably known. Figure 23 illustrates refraction and first-order interference phenomena in two exceedingly simplified examples.

However, as we have seen from electron micrographs, no intergrowths in alkali, ternary or plagioclase feldspars are sufficiently regular in periodicity or totally flat enough to produce sharp, truly monochromatic reflections from incident white light. Interference colors are impure, containing a range of wavelengths and first- and second-order peak intensities in optical spectra

---

[4]"Schiller" may be used to refer to diffuse, often silvery reflections from mutually oriented, platy inclusions, especially common in labradorite parallel to (010) (Rayleigh, 1923). See Chapter 11 on other causes of color in feldspars.

[5]Baier and Pense (1957) recognized this previously, but had an incorrect twinning model for the plagioclase intergrowths. Also see Pazyuk (1957). Bøggild (1924) suggested interference phenomena for colors in peristerites and labradorites but postulated no structural model for the source of iridescence. Pedagocically I have found the thin-film analogy of an oil slick on water a useful illustration (see Ribbe, 1972, or 1975, p. R-92).

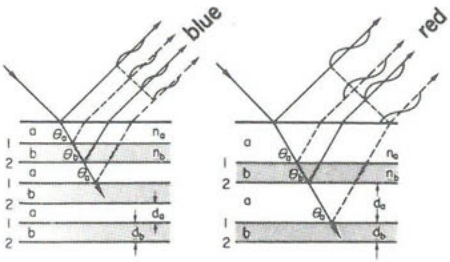

Figure 23. Schematic drawing of interference phenomena in hypothetical blue- and red-schillered specimens. (*cf.* Fig. 18a,b and see Fig. 26 below). The a and b lamellar sets have mean refractive indices n_a and n_b and thicknesses d_a and d_b. Glancing angles of the beam at interfaces 1 and 2 are θ_a and θ_b. When d_a is not equal to d_b (as on the right), the beams from the boundary interfaces 2 are retarded relative to those from interface set 1, although the wavelengths are the same. The two sets of waves shown by solid and dashed lines then interfere to produce a coherent, monochromatic beam . Interference colors are governed by Equation 2: for the blue and red specimens, $d_a + d_b$ = ∿1600 Å and ∿2400 Å, respectively. From Ribbe (1972, Fig. 7, p. 21).

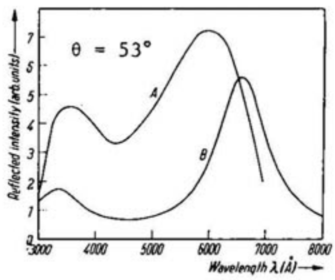

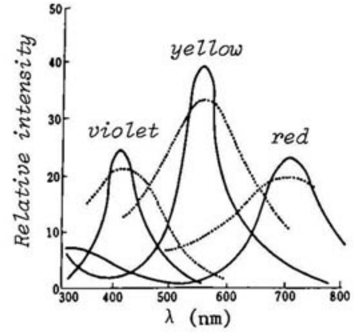

Figure 24 (to the left). Spectral distribution of the intensity of light reflected from a "red" labradorite: Curve A, experimentally observed at θ = 53°; Curve B, calculated by Bolton *et al.* (1966; reprinted from their Fig. e, p. 223).

Figure 25 (to the right). Spectral distributions of the intensity of light reflected from violet, yellow and red iridescent labradorites for θ = 70° (dotted lines). Intensity distributions calculated by Miúra *et al.* (1975, Fig. 2, p. 529) from their Equation 1, using thicknesses d_a and d_b of 776 & 545 Å (violet), 739 & 1228 Å (yellow) and 711 & 1372 Å (red), are shown as solid lines.

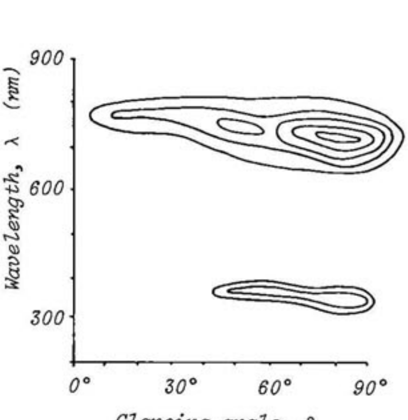

Figure 26. Reflected intensity map of red iridescent labradorite, $An_{58\pm1}$, calculated by Miúra *et al.* (1975) assuming thicknesses d_a = 520 Å, d_b = 2030 Å and refractive indices n_a = 1.55, n_b = 1.57. Modified from Miúra (1976, Fig. 13b, p. 82).

near the λ values which are expected from the mean value of d_{a+b} for the specimen. A sample spectral distribution is shown in Figure 24 (Curve A) for a labradorite (Fig. 18b) of unknown bulk composition which shows red iridescence at normal light incidence. Bolton *et al.* (1966) measured 106 lamellar thicknesses and their standard deviations σ, and obtained the following: mean d_a = 1766 Å (σ = 349 Å); mean d_b = 874 (σ = 261 Å). Applying Equation 1, $\lambda = 2(1.56)(1766 + 874)\sin 53° = 6580$ Å, a value which exceeds the 6000 Å observed peak maximum. Agreement is reasonable, considering the extremely small TEM sample. If there were no regularity in lamellar thickness, a white iridescence would be observed. White peristerite has been incorrectly called *moonstone*.

The angular broadening or diffuseness of interference colors from the lamellar surfaces is dependent not only on irregularities in periodicity of d_a and d_b but also on the planarity of the lamellae. Figures 12, 15, 18, 19 and 22 illustrate the variety of textures which cause diffuse reflections, even from highly collimated light sources. Intensities of interference colors will obviously be dependent on the extent of long-range order in lamellar thicknesses, on planarity and on the primary color and impurity content of the feldspar (see Ch. 11). Bolton *et al.* (1966) calculated an intensity distribution for the red labradorite based on a model derived from the kinematical theory of diffraction. Their result is reasonable (Curve B, Fig. 24), but Miúra *et al.* (1975) seem to have had better predictions for the θ = 70° spectra of three specimens based on a and b lamellar thicknesses listed in Figure 25. They also devised a computer method to calculate contoured intensity maps, a sample of which is shown in Figure 26.

In specimens in which the reflecting lamellae are extremely wavy or rhombic or lenticular in shape (Figs. 13-15, Ch. 7), interference colors may not be evident. In fact, if the exsolved blebs are laterally smaller than the wavelength of light, Tyndall scattering will occur, yielding the diffuse milky-white to pale-blue colors typical of some cryptoperthitic alkali feldspars with the gem name *moonstone*. This phenomenon is much less directional than that observed in most ternary and plagioclase feldspars, and it approaches the light-scattering seen in milky opals (Sanders and Darragh, 1971).

At least in peristerite and Bøggild intergrowths color zoning is composition-related, as illustrated schematically in Figure 22 and by the sketches of crystals in Figure 27. All observations indicate higher An-content for longer wavelength colors. Within zoned labradorite crystals I have observed, the blue region often contains only ∿3 % less An than the red, and the same interference

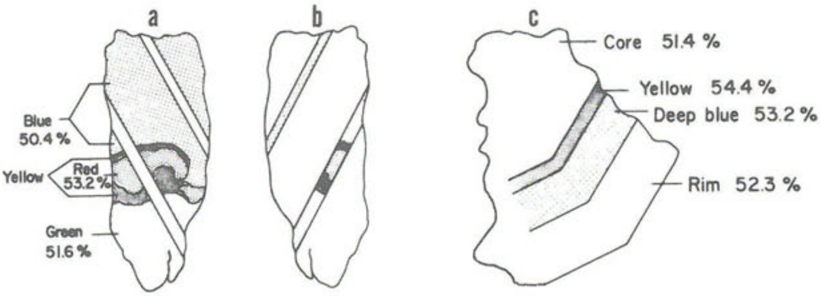

Figure 27. (a) Sketch of the relation between interference color and composition in a thin section of labradorite from the Isle of Paul, Labrador. Notice that every other albite twin lamella (diagonal stripes) does not exhibit schiller in this orientation. (b) Maintaining the same orientation of light source and observation point, the reverse side of the thin section exhibits interference colors in the thin twin lamellae. (c) Blue and yellow schiller in a zoned labradorite crystal from Tevalainen, Finland. The core and rim of this specimen do not exhibit interference colors in the visible range. Compare these compositions with those in Figure 28. From Ribbe (1972).

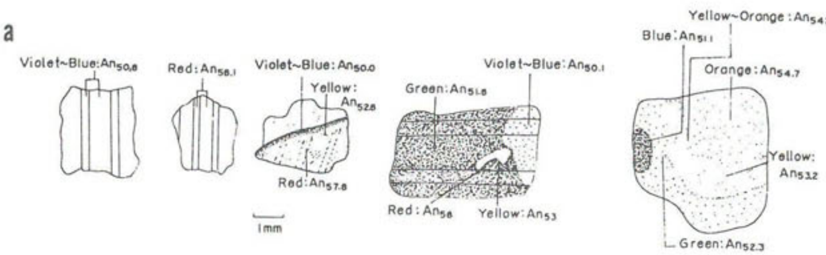

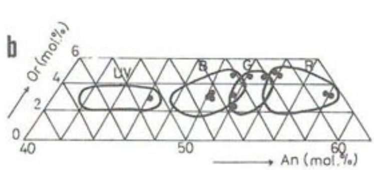

Figure 28. (a) Sketches of the relationships between observed interference colors and compositions determined by microprobe for iridescent labradorites from Labrador, Canada. From Miúra *et al.* (1974, Fig. 15, p. 151). Compare with Figures 22 and 27. (b) A section of the Or-Ab-An ternary showing four composition-color regions; UV = ultraviolet, B = blue, G = green, R = red. After Nissen *et al.* (1967).

color does not signify the same composition, at least not from one locality to another. The results of Miúra *et al.* (1974) differ considerably in that they show much larger differences in bulk composition with color (Figs. 22 and 28) and strong composition-color link from specimen to specimen. They have "derived" these equations (1975, p. 533):

$$\text{An (mol \%)} = 0.009(d_a + d_b) + 36.083 \qquad (\sigma = 0.945),$$

$$100\ d_a(d_a + d_b) = 3.440\ (\text{mol \% An}) - 119.891 \qquad (\sigma = 0.844).$$

I remain skeptical that the Bøggild intergrowths perform so predictably, particularly since Miúra and Tomisaka's (1978) ion probe analyses show such a range in composition of both minor (An-poor) and major (An-rich) lamellae. Of course their equation for the wavelength of interference color at which maximum intensity occurs is less controversial: "$\lambda_{max} = 3.128(d_a + d_b) - 47.798$ (standard deviation [sic]: $\sigma = 0.999$)."

For iridescent peristerites it is always the albite lamellar set that is the thicker -- the Ab:An$_{\sim 25}$ ratio never goes below 1:1. Similarly in Huttenlocher intergrowths it is the more sodic 'e'-plagioclase lamellae that predominate. In fact, coarser exsolution textures are observed in sodic bytownites (Nord *et al.*, 1974, discussed above), just as in sodic peristerites (see Fleet and Ribbe, 1965). Miúra *et al.* (1974, their Fig. 27, p. 161) give what I consider to be an over idealized and unrealistic model of the behavior of d_a and d_b with bulk composition in Bøggild intergrowths in the (theoretical) range An_{35}-An_{65}. The compilation of data by Miúra (1976) is excellent, showing the mean thickness d_b (of the An-rich lamellae) increasing from ∿600 to ∿1900 Å as a function of bulk An content between An_{48} and An_{58} and d_a scattered within the range 500-750 Å. Of course values of $d_a + d_b$ less than ∿1300 Å and greater than ∿2500 Å produce interference in the ultraviolet and infrared, phenomena not much investigated as yet.

SUMMARY

In general it would appear that spinodal decomposition in the solid state of an initially homogeneous feldspar is the most likely mechanism for phase separation in feldspars, although only for alkali feldspars has this been convincingly demonstrated. The sluggish kinetics of Al,Si diffusion over hundreds of Ångströms have prevented the type of experimentation with the plagioclases that might illustrate a similar phenomenon in peristerites and in the Bøggild and Huttenlocher intergrowths. Textural evidences from each of these composition ranges are strikingly similar and suggest similar mechanisms for all. Among others, additional time-temperature-transformation studies are needed to complete a woefully inadequate view of the plagioclase subsolidus.

Chapter 11
COLOR in FELDSPARS
A. M. Hofmeister & G. R. Rossman

INTRODUCTION

Pure feldspar, free of exsolution, is colorless. However, minor chemical substituents, inclusions, interference effects from exsolution lamellae, and radiation damage can produce color in the mineral. Chemical impurities produce the yellow color of sanidine, orthoclase and calcic plagioclase, the blue to green colors of amazonite, and the blue-green color of sodic plagioclase. Inclusions create a wide variety of colors: pink, brick-red, and grays are common; orange, tan and green may also occur. Aventurine and shiller effects also result from inclusions. Radiation produces gray or smoky colors. Exsolution phenomena and oriented intergrowths produce interference colors, schiller and chatoyancy.

This chapter describes the colored varieties of feldspar and their absorption spectra and coloration mechanisms. Labradorescence and moonstone effects, which are produced by interference phenomena and scattering phenomena, were discussed in Chapter 10.

COLORLESS FELDSPAR

When free of minor substituents, inclusions and exsolution phenomena, feldspar does not absorb light in the visible portion of the spectrum and is, therefore, colorless. The onset of absorption in the ultraviolet region is at ∿320 nm, caused by oxygen to cation charge-transfer, most likely due to trace amounts of Fe^{3+} in feldspar. Absorption in the infrared is frequently observed in the 3600-3300 cm^{-1} (3000 nm) region as a result of minor amounts of structural water in the feldspar (Solomon and Rossman, in prep.). Absorption from vibrational motions of the aluminosilicate framework occurs at longer wavelengths.

YELLOW FELDSPAR

Iron substitution produces yellow color in sanidine, orthoclase and calcic plagioclase. In the potassium feldspars substitution is accompanied by a reduction of the aluminum content indicating that iron enters the tetrahedral sites as Fe^{3+}. Yellow sanidine from Leucite Hills, Wyoming, contains up to 18% of the $KFeSi_3O_8$ molecule (Carmichael, 1967); synthetic $KFeSi_3O_8$ is also yellow (Faust, 1936).

Mössbauer spectroscopy confirms that the majority of iron in orthoclase exists as Fe^{3+} in distorted tetrahedral sites. Ferrous iron is also present, but at concentrations too low for standard detection methods (Brown and Pritchard, 1969). Faye (1969) and Veremechik *et al.* (1975) published absorption spectra of orthoclase from Itrongay, Madagascar, attributing the yellow color to absorption bands at 417 and 442 nm (Fig. 1), due to tetrahedrally coordinated Fe^{3+}.

About 0.5 wt % Fe^{3+} is required to cause pale yellow colors in millimeter-thick crystals of bytownite and labradorite. Unlike potassium feldspars, plagioclases should accommodate Fe^{2+} in the large-cation sites, as well as incorporating Fe^{3+} in tetrahedral sites. Mössbauer data on terrestrial plagioclases confirm that iron enters both sites (Schürmann and Hafner, 1972). The optical spectra of Figures 2 and 3 show that both ferric and ferrous iron exist in yellow labradorite from Lake County, Oregon, with ∿0.4 wt % FeO (*cf.* the spectra of lunar anorthitic plagioclases in Bell and Mao, 1973, Fig. 1, p. 756).

AMAZONITE

According to Hintze (1897), the name *amazonstone* was originally applied to nephrite and green feldspar found near the Amazon River. Emmerling (1793, as quoted in Hintze) restricted the definition to include only feldspar. Breithaupt (1847, p. 505) shortened the name to *amazonite* and confirmed the potassic composition. Since then the name has evolved to imply exclusively triclinic potassium feldspars. However, Rudenko and Vokhmentsev (1969) showed that blue-green oligoclase has amazonite properties. Similarly, Cech *et al.* (1971) described the chemistry and structure of green orthoclase from Broken Hill, New South Wales: they proposed that the name amazonite should include not only blue to green microcline, but also green orthoclase and "other feldspars whose color is similar." General usage, however, has not changed.

Blue to green potassium feldspar

Cech *et al.* (1971) and Smith (1974a, p. 556) provide excellent reviews of previous investigations of amazonite; only the most important work and current studies are highlighted here.

Relationships between amazonite coloration and physical properties have been elucidated by a few critical experiments. Oftedal (1957) suggested that the decolorization of amazonite with heating is a diffusion or decomposition process. Noting that the color is stable below 270°C, he concluded

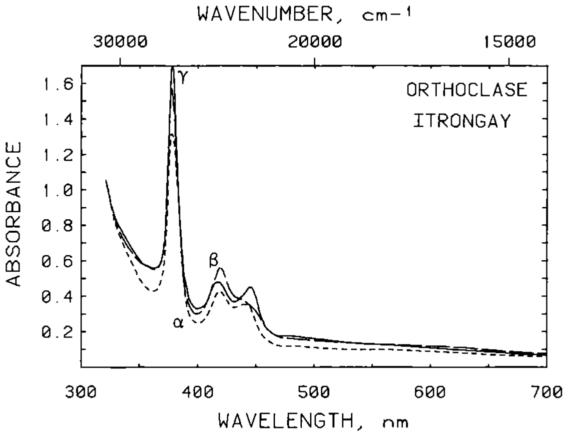

Figure 1. Polarized absorption spectra of yellow, gemmy orthoclase from Itrongay, Madagascar. Thickness is 2.00 cm. Yellow color is due to the absorption bands at 418 and 445 nm. All absorption bands are due to tetrahedral Fe^{3+}; Fe_2O_3 content is 0.42 wt %. The absorption rise towards the ultraviolet is due to Fe-O charge-transfer.

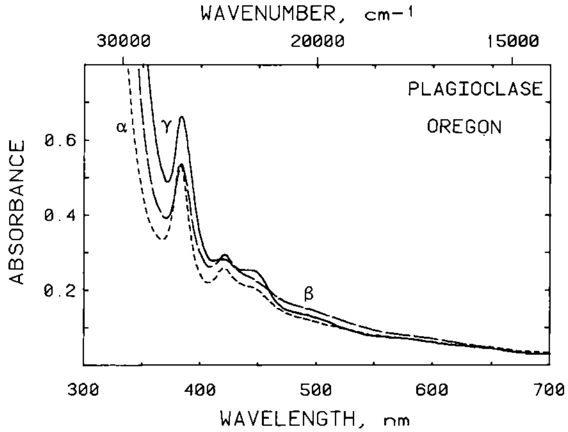

Figure 2. Absorption spectra of yellow, gemmy labradorite from Rabbit Hills, Lake County, Oregon. Thickness is 1.00 cm. The yellow color is caused by the absorption bands at 425 and 450 nm. All bands shown are due to tetrahedral Fe^{3+}. The absorption rise towards the ultraviolet is due to Fe-O charge-transfer. Fe_2O_3 is ∿0.1 wt %; total iron (as FeO) is ∿0.4 wt %.

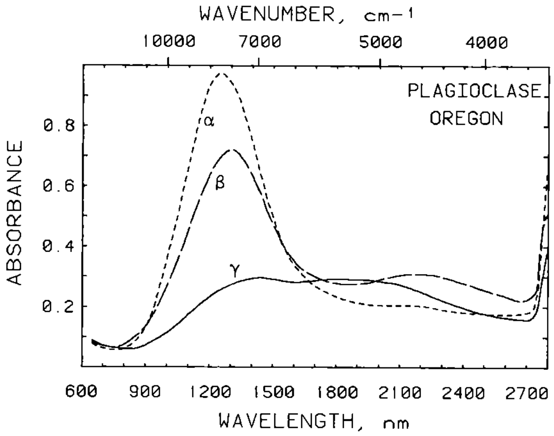

Figure 3. Infrared absorption spectra of the same gemmy, yellow labradorite from Rabbit Hills, Oregon as in Figure 2. Thickness 1.00 cm. All bands shown are due to Fe^{2+} in the large-cation (*A*) site. FeO content is about 0.3 wt %. The bands in the infrared region do not influence the color.

that this is the maximum temperature of formation; and hence that color forms in an "already crystallized and cooled feldspar." Przibram (1956, p. 253) showed that heat-bleached samples can be recolored by X-rays, suggesting that the color of amazonite could be radiation-induced.

The chemistry of amazonites has been widely investigated. Taylor *et al.* (1960) used emission spectroscopy to determine concentrations of seventeen elements in feldspars from a Norwegian pegmatite and concluded there was no chemical difference between the colored and colorless crystals. Shmakin (1968) detected high Pb, Rb, Cs, and Tl contents in Russian amazonites. Nunes (1979) found elevated amounts of Pb, Rb, and Cs in colored feldspars from Mozambique, noting that green amazonites have more Pb than blue ones. Zhirov and Stishov (1965) measured Pb, Rb, and Tl contents of feldspars and found that color is better correlated with Pb than with Rb or Tl, although several samples did not fit the correlation with lead. Foord and Martin (1979) found that color-zoned crystals from Colorado show "an excellent correlation between Pb content and amount of color" (to the eye). They noted enrichment of Rb and Cs, but stated that these "reach a maximum in the growing crystal before the lead" does, and are not correlated with the color.

Although there are many indications that color may be correlated with lead, some lead-containing feldspars are not colored. Furthermore, the usual oxidation state (Pb^{2+}) cannot produce color, because its electronic transitions occur in the ultraviolet region. Data from recent studies provide partial answers. Using electron spin resonance techniques, Marfunin and Bershov (1970) concluded that Pb^{1+} centers are present in amazonites, but not in other feldspars, and Plyusnin (1969) discovered a correlation between the color and the amount of water in ten amazonites.

Foord, Martin, Cocklin, and Simmons (in prep.) have studied the chemistry, structural state, and occurrence of approximately a hundred different amazonites throughout the world. Their investigation embraces a wide range of color, and shows that amazonites with less than 1000 ppm Pb are blue, while the color shifts to green with increasing lead content. No other element correlates with color. Foord *et al.* also note that the apparent intensity usually increases as lead concentration increases. One significant exception is an Amelia, Virginia, sample (Foord and Martin, 1979) in which the lead content is 1000 ppm in both green and white portions of the same crystal. A few other samples are either much more or much less intensely colored than would be expected from the lead content alone. We have studied the spectroscopy of a variety of amazonites, including the "anomalous" ones of Foord *et al.*, and the following is a synopsis of our results (Hofmeister and Rossman, in prep.).

Amazonite color is intrinsic, since it comes from gemmy, unaltered portions of the crystal. Spectroscopic results show that color is controlled by an absorption minima between an oxygen-metal charge-transfer band in the ultraviolet and the amazonite band in the red (Fig. 4). This broad band is polarized, dominating the β spectrum; its location determines the color. The blue color of microcline results from a single absorption band at 620 nm, whereas the green color or orthoclase results from a similar band at 730 nm. Blue-green to green colors arise when both absorptions are present (Fig. 5).

All amazonite color is related to radiation. Heat removes it, and irradiation by X-rays or gamma rays returns it, unless the sample is heated so strongly that the small amounts of structurally bound water present in all

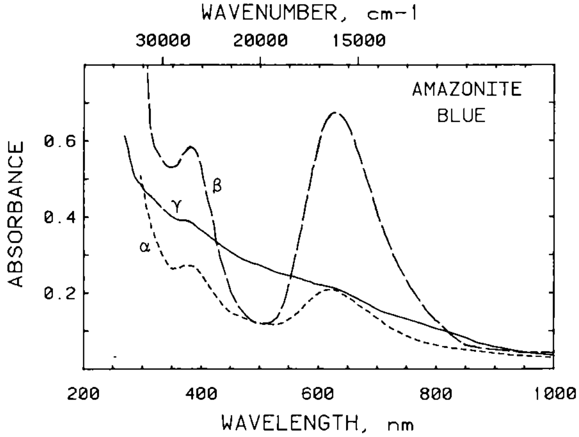

Figure 4. Absorption spectra of gemmy, blue amazonite from Lake George, Colorado. Thickness 0.50 mm. Blue color is due to an absorption minimum (transmission maximum) between the broad, intense, polarized band at 630 nm and the tail of an oxygen-cation charge-transfer band in the ultraviolet. The smaller band at 380 nm is associated with the 630 nm band. The intensity of the 630 band depends on the amount of lead and structural water. This sample has 700 ppm Pb and 20 ppm structural H_2O. The rise in the γ spectrum towards the ultraviolet is due to scattering from turbidity, a common feature of amazonite.

Figure 5. Absorption spectra of the three spectral types of amazonite. Gemmy blue microcline (labeled "620") from Lake George, Colorado with 700 ppm Pb; gemmy green orthoclase (labeled "730") from Broken Hill, Australia with 1800 ppm Pb; turbid blue-green microcline from the New York Mountains, California with 2000 ppm Pb. Thickness 0.50 mm, β orientation. The hue is related to the position of the large absorption band(s). Blue amazonites have a band at 620 nm, the position varying with lead content. High-lead orthoclases have only the 730 nm band and are green. Microclines of intermediate lead content have both bands and are blue-green.

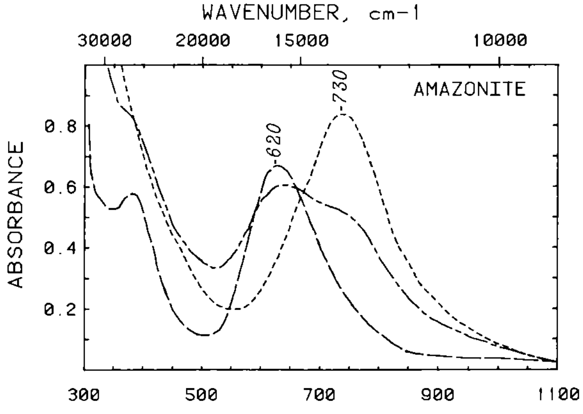

amazonites are removed through dehydration. For individual samples whose structural water content is reduced by dehydration, the intensity of color which can be regenerated by radiation depends linearly on the amount of structural water remaining. The color of natural samples depends on the concentration of both structural water and lead. The intensity of color depends linearly on the component present in the smaller molar quantity, and the intensity of color is the same regardless of whether lead or structural water is the limiting agent. This result implies that lead and structural water in a 1:1 ratio produce color centers in amazonite. Several lines of evidence suggest that the two absorptions are caused by the same mechanism. Blue samples have only the 630 nm band and are triclinic. Monoclinic samples contain only the 720 nm band and are green. Samples with both bands are less well ordered than the blue samples. The structural differences and the color transition from blue to green are induced by increased incorporation of lead and water into the structure.

Based on kinetic studies of the formation of amazonite color by irradiation, and the observation that water is not consumed in the process, Hofmeister and Rossman (1981) proposed a mechanism which involved the reduction of Pb^{2+} to Pb^{1+} by the products of the radiation-induced dissociation of water, followed by the regeneration of the water molecule with concurrent formation of a hole center on an oxygen. The assignment of Pb^{1+} as the chromophore is consistent with Marfunin's ESR experiments and also with the observed intensity of the optical absorption bands. The requirement that color is produced only when lead and structural water are in structural proximity explains why not all the lead is active in high-lead, low-water feldspars. This irradiation-activated color center could be produced in nature either by decay of external elements, such as U or Th, or by decay of ^{40}K within the feldspar.

Blue plagioclase

A pale blue cleavelandite variety of albite (Ab_{94-99}) occurs in the gem pegmatites of Pala (Jahns and Wright, 1951), Mesa Grande, California (Foord, 1977), and elsewhere. Its color has not been studied. Taylor *et al.* (1960) described a pegmatite in which blue cleavelandite with a higher lead content than other uncolored cleavelandite in the pegmatite was associated with amazonite. Rudenko and Vokmentsev (1969) measured the reflection spectra of two blue-green oligoclases, and compared them to that of amazonite. The only difference is a shift of the reflection minima (which is related to the absorption maxima) 30 to 60 nm towards the red relative to amazonite minima. Rudenko and Vokmentsev heated and irradiated their samples and noted that the microcline regained its color, but the oligoclase did not. A spectrum we measured on a blue albite from Mozambique with ∿500 ppm Pb is the same as that of blue microcline except that the peak is shifted 15 nm towards the red. This suggests that the color arises from the same mechanism as in amazonite. Plagioclases are less commonly and more weakly colored because they accept lead into the large-cation site in the structure less readily than potassium feldspar (Smith, 1974b, p. 103).

SMOKY FELDSPAR

Speit and Lehman (1976) investigated smoky color in large transparent crystals of sanidine from Volkesfeld bei Kempenich, Eifel. Their optical, electron paramagnetic resonance, and thermoluminescence data demonstrate that the color is produced by ionizing radiation in a manner similar to that of smoky quartz. Speit and Lehman concluded that coloration is produced by a hole center on an oxygen (O^-) in a cluster of Al ions. The hole's presence was indicated by migration of color towards the cathode in an applied electric field. A spectrum is shown in Figure 6. Sunlight bleaches the color and ionizing radiation regenerates it.

COLORS FROM INCLUSIONS

Feldspar can take on almost any color when it contains colored inclusions. Strictly speaking, these are not feldspar colors, but rather colors of a second, associated phase. White, non-transparent feldspar results from scattering of light from microcracks or from inclusions of alteration products such as clays, and from fluid inclusions. Red color in potassium feldspar is so common that it is frequently a useful diagnostic property for field identification.

Red shiller and red-clouded feldspars

Except for the unique sunstones from Lake County, Oregon (discussed in the next section), the occurrence of red colors in feldspar was comprehensively reviewed by Smith (1974b, pp. 614-623). For completeness, they are summarized here.

Red color in feldspar results from inclusions of hematite flakes. If the flakes are oriented, light is preferentially scattered producing irridescence. This play of light and color is known either as schiller, or

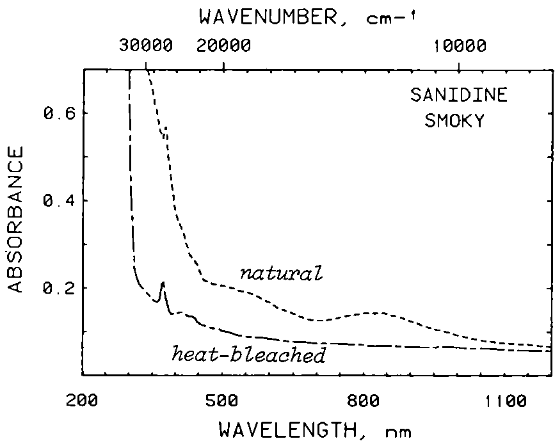

Figure 6. Absorption spectra of smoky sanidine from the Volkesfeld area of the Eifel region. Thickness 3.50 mm, α orientation. β and γ (not shown) are similar. The smoky color results primarily from the broad band at ~550 nm along with the tail of an oxygen-cation charge-transfer band centered in the ultraviolet. The bands between 380 and 450 nm arise from tetrahedral Fe^{3+}.

aventurescence, and when it is exceptionally well-developed, the feldspar may be called *sunstone* (Smith, 1974b, p. 614). Those feldspars having smaller, more dispersed, and unoriented flakes lack shiller but possess a pink to brick-red cloudy color. [See Copley and Gay (1982). *Ed.*]

Andersen (1915) reviewed previous work on aventurine feldspars and presented a thorough study of the optical properties and effect of heating on red shillers in albites, oligoclases, labradorites and perthites from Norway and the United States. From the hexagonal morphology, absorption colors, and presence of iron, he concluded that the lamellae were hematite. Iron hydroxides were ruled out because temperatures greater than 1235°C are needed for feldspars to resorb the flakes. The lamellae are always oriented on (112), $(1\bar{1}2)$, (150) and $(1\bar{5}0)$ planes; the forms (001), (010), (110) and $(1\bar{1}0)$ are rare. From the lack of lamellae on growth faces, Andersen disallowed simultaneous crystallization as the formation mechanism. Later studies have confirmed Andersen's results. Kraeft and Saafeld (1967) showed that the lamellae have the hematite structure. These authors and Neumann and Christie (1962) showed that elements other than Fe^{3+} are present in the inclusions. Divljan (1960) and Neumann and Christie (1962) showed that there is no correlation between the amount of iron in the crystal and the shiller present. Thus Divljan (1960) argued that iron is externally derived, rather than internally derived from exsolution.

Red-clouded feldspars contain ferric oxides, mostly as hematite (Isshiki, 1958; Boone, 1969; Smith, 1974b, p. 618). Boone (1969) made a major contribution to understanding formation of red-clouded feldspar. He observed a gradation of a gray porphyry in the Gaspé peninsula from potassic oligoclase-andesine and weakly altered biotite into a red porphyry consisting of hematiferous albite with muscovite inclusions and chloritized biotite. He showed that the red feldspars formed from reaction of ternary feldspars with an Fe-bearing vapor phase which was released during decomposition and oxidation of biotite. Similar iron metasomatism certainly produced red-clouded potassium feldspars, but whether aventurine results from the same mechanism is not clear. Smith (1974b, p. 623) suggests that more than one mechanism is involved.

Black-clouded feldspars

A brief summary of Smith's (1974b, p. 624-629) extensive review of the literature on black inclusions in feldspar is presented here. The identity of the dark inclusions is not clear, although iron bearing minerals are partially involved. No spectroscopic or magnetic data are available, but oxides of Fe in mixed valence states, possibly with Ti, would produce a dark color, even in tiny amounts. Andersen's (1915) heating experiments show that dark inclusions may be produced from red hematite flakes. Like the red-clouded feldspars, black-cloudiness is independent of iron content. Smith points out that chemical data suggests involvement of water in the formation of the dark inclusions and that chemical migration and/or other minerals are involved. This mechanism is similar to that producing red-cloudiness.

SUNSTONES FROM LAKE COUNTY, OREGON

Labradorite phenocrysts in a basalt flow near the Rabbit Hills in Lake County, Oregon, are noted for their transparent gemmy quality (Stewart *et al.*, 1966; Peterson, 1972). Specimens commonly are uniformly colorless or straw-yellow, but some rare crystals have localized areas of red and/or green coloration. The red or green colorations vary from pale to intense, but whereas the red is weakly pleochroic, the green is strongly anisotropic. Single crystals may contain zones of red or green or shiller, or may have any combination of the three. The schiller consists of round, thin, extremely reflective platelets on (001) and (010). They are isotropic and in transmitted light are opaque to dark brown. The platelets are about 0.2 μm thick up to 30 μm in diameter; inside the crystal they appear pink but near the surface have a white metallic reflection. Andersen (1917) thought that platelets in a similar material from nearby Modoc County, California were metallic copper.

Spectra of the red and green regions, shown in Figures 7 and 8, have no hematite or other iron oxide features. Red color is caused by a weakly polarized absorption band centered at 560 nm. Green color is caused primarily

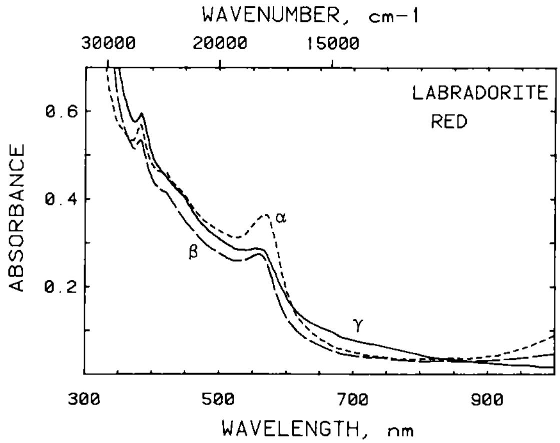

Figure 7. Absorption spectra of red, gemmy labradorite from Rabbit Hills, Lake County, Oregon. Thickness 2.00 mm. The red color is due to a band at 570 nm. The bands between 570 and 450 nm arise from tetrahedral Fe^{3+}. Total iron content as FeO is 0.42 wt %.

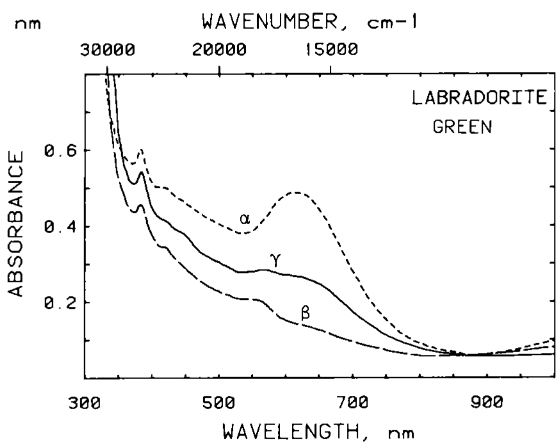

Figure 8. Absorption spectra of gemmy green labradorite from Rabbit Hills, Lake County, Oregon. Thickness 1.00 mm. The green color is due to an absorption minimum between a broad, intense, polarized band at 630 nm and the tail of an oxygen-cation charge-transfer band in the ultraviolet. The bands between 380 and 450 nm are due to tetrahedral Fe^{3+}. The band at 560 nm is the red color (see Fig. 7), which is present to a slight extent in all green samples. Total iron content as FeO is 0.42 wt %.

by a broad, polarized band at 670 nm, which produces an absorption minimum in the green. Other bands in the spectra are from Fe^{3+}. Comparison of the iron spectra among the red, green, and yellow zones of the same crystal give no indication differences in iron environment. It is unlikely that iron causes the color. The colors may be associated with colloids. Particles about 100 Å could produce an unpolarized red color, according to Mie scattering theory. Furthermore, Stookey *et al.* (1978) showed that sub-colloidal silver impregnated glass can have a variety of polarized colors, depending on the size and aspect ratio of the anisotropically shaped particles. The color may be associated with colloids and subcolloids, but more work is needed to test this hypothesis.

Chapter 12

SOME CHEMICAL PROPERTIES of FELDSPARS

J. V. Smith

INTRODUCTION

This chapter considers some chemical features of feldspars which show promise for interpretation of their genesis in terms of rock-forming processes. Of course, the volume percentage and major element content of feldspars are used for petrographic classification of many rocks in the crust of the Earth. Furthermore, the major element content of feldspars has petrogenetic significance, especially with regard to the overall trend of crystal-liquid differentiation from calcic to sodi-potassic compositions: thus, the plagioclase thermometer (Kudo and Weill, 1970; Mathez, 1973) and the phase relations involving alkali feldspars (e.g., Carmichael *et al.*, 1974) are useful, expecially when taken in conjunction with other indices of differentiation. Here we shall look mainly at minor and trace elements.

A chemical composition can be carefully controlled in the laboratory, whereas in Nature one must accept whatever combination of the 92 elements happens to be available in response to differentiation processes. A useful reference is provided by the systematic syntheses of feldspars from as many elements as possible. Reviews are given by Bambauer *et al.* (1974), Smith (1976, Sec. 14.2), and Pentinghaus (in preparation).

In conformity with the ionic model, the *T* sites can be occupied substantially or completely by B, Al, Si, Ga, Ge, Fe^{2+}, Fe^{3+}, and Mg; small amounts of Ti and P in natural feldspars almost certainly enter *T* sites. The *A* (or *M*) sites can be occupied by Na, K, Rb, NH_4, Cs, Ca, Sr, Pb, Ba, Eu and La. Recent syntheses not included in Table 1 of Chapter 1 (this volume) are $CaFe^{2+}Si_3O_8$ (Sclar and Kastelic, 1979), $CaMgSi_3O_8$ (Sclar and Benimoff, 1980), $EuAl_2Si_2O_8$ (Iwasaki and Kimizuka, 1978), and $LaNaAl_4Si_4O_{16}$ (Bettermann and Liebau, 1976).

Interpretation of resonance techniques for iron is not easy because the neighboring oxygens also must change positions in response to ionic substitution, thereby affecting calculations of the crystal field (see Iiyama, 1974a, for discussion of the effect of local lattice deformation on entropy).

Analytical methods; precision

Electron paramagnetic resonance and Mössbauer resonance studies have been widely applied to feldspars; they are summarized by Smith (1974a, Ch. 11). It appears that in the alkali feldspars Fe occurs mostly as Fe^{3+} substituting in *T* sites (Annersten, 1976), whereas in calcic plagioclases it occurs as both Fe^{2+} and Fe^{3+}, the ratio depending on the oxidation state of the host rock (Bell and Mao, 1973a,b; Lesnov *et al.*, 1980; Longhi *et al.*, 1976; see chapter on *Color in Feldspars*, this volume). From electron paramagnetic resonance studies, Morris (1975) concluded that in synthetic anorthite Eu^{2+} enters an *A* ($\equiv M$) site but Gd^{3+} enters a "glass" site. The "glass" site may be an *A* site in which there is strong disorder caused by distortion from the Gd^{3+} ion.

A second problem for interpretation of trace and minor elements involves the reliability and the meaning of chemical analyses of bulk specimens. Mechanical impurities such as apatite obviously cause problems which can be bypassed by microprobe methods (but note the danger of secondary fluorescence in the electron microprobe). It is unfortunate that most published analyses with the electron microprobe are not even assigned an error estimate. Although careful techniques can yield detection levels of 50-100 ppmw (2σ) of elements from Na-Zn, it is quite obvious that some published analyses are not accurate even at the 0.05-0.10 wt % level. Particularly deplorable is the listing of energy-dispersive analyses to the second decimal without a statement that the detection level is at best 0.1 wt % and perhaps even 0.2-0.3 wt %.

Ion microprobe analyses

On the positive side, the ion microprobe has now become established as a reliable instrument for certain elements, but a major problem of absolute calibration remains; still lacking is a truly fundamental theory of secondary ion emission, and all reliable calibrations are empirical. A paper on ion-probe techniques (Steele *et al.*, 1980a) is now being extended to cover further elements and more extensive calibrations (Steele *et al.*, 1982, in preparation). Isotopic ratios for Mg in plagioclase from the Allende meteorite are reported in Hutcheon *et al.* (1978). Electron and ion microprobe analyses of lunar plagioclases in Hansen *et al.* (1979) and Steele *et al.* (1980b, 1981) demonstrated that lunar rocks were not derived from just one reservoir, and that the ferroan anorthosites came from a source more barren in the large-ion lithophile elements than the norites and troctolites. Recent analyses (Steele *et al.*, 1981; Steele and Smith, 1982) of trace elements in plagioclases from the Stillwater Complex have shown that the McCallum-Raedeke trace-element model based on cumulate minerals plus trapped liquid is approximately correct but that some modification is needed (replenishment with fresh magma?; or filter-pressing?). Ion microprobe analyses (Mason, 1982) have revealed the distribution coefficients between coexisting K-feldspar and albite phases of perthites from several pegmatites (Li 1-780; Mg 0.2-1.1; P 0.1-17; Ca 0.02-1.6; Cs 32-820; Ba 24-284; Pb 1.6-30; Fe 0.3-0.7; Rb 60-5500; Sr 1.3-5.1; wt % Kf over albite). There is a wide range of coefficients for each element. Particularly important are complex zoning profiles which can be explained by cross coefficients in the diffusion matrix. Combined electron and ion probe analyses of anorthoclase megacrysts with glass inclusions (Mason *et al.*, 1982) have yielded the following crystal/liquid partition coefficients: Mg 0.008; P 0.04; Ti 0.08; Fe 0.04; Ba 5.2; Sr 8; Rb 0.27. Trace elements in plagioclases from achondritic meteorites provide a test of common parentage (e.g., eucrites and howardites: Steele and Smith, 1982). Zoning in plagioclase phenocrysts was studied by Shimizu (1978).

Summary

In spite of these successful applications of the ion microprobe to determinations of trace elements in plagioclase, many elements including the REE occur either at too low a level or present problems of spectral overlap. Hence, bulk techniques, including neutron activation analysis, will retain their value. Bulk analyses are important anyway for samples in which the mechanical impurities have exsolved from the original feldspar structure. Lead presents a difficult problem because of evidence of high mobility from leaching experiments (Oversby, 1975), and oxygen isotopes (Taylor, 1977) demonstrate extensive subsolidus exchange over huge bodies of feldspar-bearing rocks.

From a geochemical viewpoint, interpretation of the chemical composition of feldspars is extremely difficult. Early use of such indicators as the K/Rb ratio involved lumping together a host of contributing factors. It is now obvious that one must consider many factors including bulk composition of the host rock, pressure, temperature, amount and composition of volatiles, time and degree of approach to equilibrium, etc. The size of the reservoir from which crystallization occurs, the extent of chemical zoning, and the nature of the competing minerals all provide complications.

DEFECT STRUCTURES

The extent of deviation from the AT_4O_8 ideal formula has become somewhat clearer since the review by Smith (1974b, p. 16). Here are further data: Kim and Burley (1971) reported about 5% excess SiO_2 in albite synthesized at 5 kilobars and 670°C; Chatterjee (1972) and Chatterjee and Johannes (1974) found that sanidine synthesized near 700°C hydrothermally in the presence of quartz had a smaller a cell dimension than sanidine synthesized in a quartz-free system; Bhatty, Gard and Glasser (1970) synthesized unusual anorthites below 1150°C from glasses with 5 to 10% excess Al_2O_3, while Bruno and Facchinelli (1974) synthesized anorthites with excess silica from Si-rich gels treated hydrothermally at 500-650°C or dry at 1300°C--for both Al-rich and Al-poor anorthites: annealing at high temperature resulted in approach to normal anorthite. Grundy and Ito (1974) refined the crystal structure of a Sr feldspar with 13% of the Sr sites empty. Goldsmith (1980) synthesized Al-deficient anorthite and corundum at pressures over 10 kbar.

Crystallization of Si-rich alkali feldspars followed by exsolution of quartz which forms a grain boundary precipitate with sodic feldspar is the traditional and easiest explanation of myrmekite (Smith, 1974b, Ch. 20). Wenk and Wilde (1973) discussed the anomalies in the composition of lunar anorthites, while Smith and Steele (1974) suggested that intergrowths of pyroxene and quartz in lunar plagioclase might result from exsolution. This idea could account for only a small amount of pyroxene, and in many lunar anorthosites at least most of the pyroxene must be primary. Some terrestrial plagioclase megacrysts from high-grade metamorphic rocks contain amphibole needles, but whether these result from exsolution (plus hydration) is controversial. Bryan (1974) concluded from detailed electron microprobe analyses of sector-zoned plagioclase from submarine basalts that the formula unit $Ca(Fe,Mg)Si_3O_8$ was involved; this, of course, does not involve defects. Whereas some plagioclases from lunar basalts contain up to 7% Si_4O_8, all terrestrial plagioclases studied by Beaty and Albee (1980) had an AT_4O_8 formula within the accuracy of electron probe analysis.

RARE EARTHS, Sr, Ba, AND THE EUROPIUM ANOMALY IN PLAGIOCLASE

The rare earths, of course, have very similar chemical properties and are useful as geochemical indicators, especially in relation to the alkaline earths Sr and Ba together with Y which tends to act as a super-heavy rare earth element (REE).

In the range of oxidation conditions of natural plagioclase, rare earths occur as trivalent ions except for cerium which can exist as quadrivalent or trivalent and europium which can occur as trivalent or divalent. The divalent Eu ion is rather similar to Sr^{2+} and partitions into plagioclase from basaltic liquid much more efficiently than the trivalent REE. Smith (1974b, Section 14.3.4) reviewed the experimental work by Drake and Weill on the distribution of rare earths between plagioclase and dry silicate liquids of "basaltic" composition. The equilibrium between the Eu ions and oxygen is given by

$$4\ \mathrm{Eu^{III}O_{1.5}(soln.)} = 4\ \mathrm{Eu^{II}O(soln.)} + \mathrm{O_2(gas)}; \quad K = \frac{[\mathrm{EuO}]^4 f(\mathrm{O_2})}{[\mathrm{EuO_{1.5}}]^4}$$

where square brackets denote activities and f denotes fugacity. Under reducing conditions, Eu tends to act like Sr^{2+} and has a greater preference for the large cation site of plagioclase than under oxidizing conditions. Normalization of the REE contents to the mean geochemical abundance (normally assumed to be that measured in *C1* meteorites) results in a positive anomaly for plagioclase and a negative anomaly for the liquid.

At the simplest level, one can test whether two rocks are related by plagioclase separation merely from the Eu anomalies. Thus Haskin *et al.* (1974) interpreted lunar rock 76535, a controversial troctolitic granulite, as a plagioclase cumulate because it has a positive Eu anomaly. Duchesne *et al.* (1974) found no Eu anomaly in monzonoritic rocks from the South Rogaland anorthositic complex of Norway and concluded that these rocks could represent the *original* parent magma for cumulate anorthositic rocks; see also Demaiffe and Hertogen (1981). Barberi *et al.* (1975) used the trend of the Eu anomaly to suggest that the oxygen fugacity increased during differentiation of a basalt-pantellerite sequence in Ethiopia. Paster *et al.* (1974) used the Eu anomaly and other trace elements to conclude that the size of the hidden zone of the Skaergaard intrusion was smaller than for the original model of Wager. Plagioclase accumulation is indicated by the strong positive anomaly in the Samail ophiolite (Pallister and Knight, 1981), and differentiation in the McMurdo volcanic rocks was inferred from the Eu anomaly (Kyle and Rankin, 1976; Sun and Hanson, 1976). The significance of the large positive Eu anomaly in plagioclase from the Allende meteorite (Nagasawa *et al.*, 1977) is unclear since there is no unequivocal evidence of crystal-liquid differentiation in the *present* texture.

Unfortunately, quantitative interpretations of the europium anomaly are not easy. The best approach is to look at Sr, Ba, REE, and Y simultaneously.

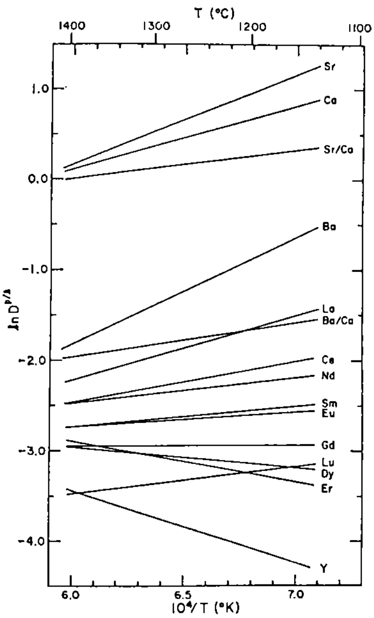

Figure 1. Regression curves on an Arrhenius plot of *ln*D (weight distribution coefficient of plagioclase over liquid) *vs* 1/T (°K). From Drake and Weill (1975, Fig. 2, p. 701).

Drake and Weill (1975) made a detailed study of the partition of these elements between plagioclase feldspar and natural and synthetic melts of basaltic and andesitic compositions. Coexisting plagioclase (An_{35-85}) and melt produced dry at one atmosphere and 1150-1400°C were analyzed with an electron microprobe. The minor elements were doped at a sufficiently high level to permit accurate analysis. These levels were much higher than in natural plagioclase, but the observed partition coefficients did not vary significantly with change of concentration. Strontium and barium tended to act like calcium rather than sodium in the plagioclase structure. The effect of bulk composition on the partition coefficients was not clearly distinguishable from the effect of temperature because the more calcic compositions tended to crystallize at higher temperature. For simplicity, all data were fitted to an Arrhenius plot of *ln*D vs 1/T(°K) where D is the weight coefficient. Figure 1 shows the regression curves. At all geologically-attained temperatures strontium favors plagioclase with D ranging from near unity at very high temperature to ∿3 at 1150°C. Barium favors the liquid at all temperatures with D ranging from ∿8 at high temperatures to ∿2 at 1150°C. The trends for the REE move smoothly from La to Er and are not strongly dependent on temperature. The heavy REE favor the liquid more strongly than do the light REE. Yttrium acts as a super-heavy rare earth and barium as a super-light REE. Sun *et al.* (1974) determined experimentally the distribution coefficients of Eu and Sr for plagioclase versus oceanic ridge basalt. Drake (1974) determined the effect of oxidation state on the distribution of Eu between plagioclase and liquid. Figure 2 shows data for 1290-1300°C. Under atmospheric conditions, the anomaly is trivial, but for $f(O_2) = 10^{-12.5}$ (similar to conditions for lunar basalts) the anomaly is about 15-fold with respect to neighboring REE. Note the steady and weak slope of D from La to Y. This contrasts with different slopes for clinopyroxene, garnet, and other silicates, and is very

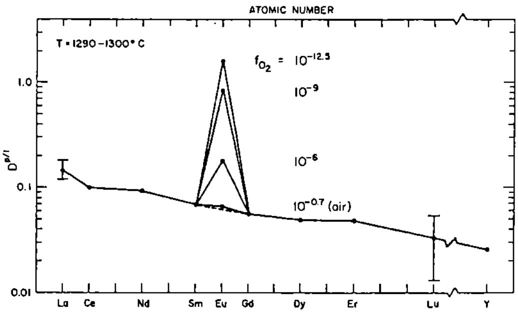

Figure 2. Plot of D versus atomic number for Y and REE using data for Eu at several oxygen fugacities as given by Drake (1974). From Drake and Weill (1975, Fig. 6, p. 708).

useful in petrogenitic models. Morris *et al.* (1974) used electron paramagnetic resonance to show how the ratio of Eu^{2+}/Eu^{3+} in anorthite *glass* changes from 2 at 1570°C and $log P(O_2)$ = -8.0 atm to 0.08 at 1600°C and -0.7 atm.

Drake and Weill (1975) interpreted existing data on the partition of the above elements between natural plagioclase megacrysts and the host rock. For Sr and Ba, there was a general tendency for the temperatures read off Figure 1 to fit semi-quantitatively with values expected from other evidence, but the deviations between the estimates for Ba and Sr in the same specimen ranged from -150°C to +340°C with half of the values below 100°C. They emphasized the difficulties of interpreting natural data. Chemical zoning is a severe problem, but combined electron and ion microprobe analyses may permit progress to be made. Drake (1975) estimated the following oxygen fugacities: 10^{-7} to 10^{-9} atm; lunar ferrobasalts 10^{-13} atm; achondrites perhaps 10^{-15} to 10^{-18}. Griffin *et al.* (1974) used the above elements plus alkali metals to test ideas on the origin of anorthosites.

Experimental data for distribution of Sm and Tm between plagioclase and haplobasaltic liquid indicate different site occupancy for the two REE (Hoover, 1978).

The presence or absence of hydroxylated minerals appears to be important for plagioclase-liquid distribution, as demonstrated for the Peru calcalkaline suite (Liotard *et al.*, 1979). It is obvious that there is a great scope for extension of the pioneering studies discussed above. A general illustration of the value of trace elements in plagioclase is given by (a) the data for five groups of anorthosites (Griffin *et al.*, 1974); see also Henderson *et al.* (1976) for data on the Fiskenaesset anorthositic complex, (b) the distribution coefficients between plagioclase and glass from Sardinian ignimbrites (Vernières *et al.*, 1977), and (c) data for the Colima volcanic complex (Luhr and Carmichael, 1980).

DISTRIBUTION COEFFICIENTS FOR ALKALI FELDSPARS

The following papers illustrate research on the distribution coefficients of trace elements between alkali feldspars and other phases. Carron and Lagache (1980) used radioactive tracers to follow the fractionation of Rb, Cs, Sr and Ba between hydrothermal solution, silicate melt and alkali feldspar in the system Qz-Ab-Or-H_2O at 2 kbar and 700-800°C. Whereas partition coefficients (D) between melt and solution are near unity, those between feldspar and solution deviate strongly from unity and depend considerably on the feldspar composition. Alkali earths prefer the feldspar and alkalis remain in solution: ranges of D are Rb 0.5-0.05, Cs 0.05-0.004, Sr 100-12 and Ba 100-10.

Delbove (1978) determined the following partition coefficients between crystalline or molten albite and hydrothermal NaCl-rich solution at 800-890°C and 1.5 kbar: Rb 0.014, Cs 0.08, Ca 3.8, Sr 11, Ba 4.

Long (1978) determined the partition of Rb, Sr and Ba between K-rich feldspar and a synthetic granitic melt at 8 kbar and 720-780°C. Henry's law is obeyed by Rb up to ∿0.8 wt % Rb_2O in both liquid and feldspar with D ranging close to unity. For Ba, Henry's law is obeyed up to ∿0.6 wt % BaO in the liquid and ∿5 wt % BaO in the alkali feldspar with D ranging from 6 to 14. The relations for Sr are complex, and probably depend on the extent of Ba substitution, and D values range from 1.2 to 5.

Leeman and Phelps (1981) determined the partitioning of many elements, including the REE with a big positive Eu anomaly, between sanidine crystals and glass in eight Yellowstone rhyolites.

Volfinger (1976) studied the partition of Na, Rb and Cs between sanidine, muscovite, phlogopite and a hydrothermal solution at 400-800°C and 1 kbar. Although there is general qualitative agreement with measurements by earlier workers, there is considerable disagreement about details (Bernotat *et al.*, 1976) and it does not appear safe to interpret observed distributions for natural feldspars and coexisting micas in terms of an equilibration temperature. In addition, there is evidence (Neiva, 1977a) for metasomatic growth of albite.

It is certain that the distribution coefficients for trace elements between alkali feldspars, other minerals and fluids involve many complex chemical and physical factors, and that qualitative or semiquantitative interpretation is the best that can be achieved now in spite of the careful experimental studies that have been made.

GENERAL REVIEW OF SOME TRACE AND MINOR ELEMENTS IN FELDSPARS

This section picks out some of the highlights from Smith (1974a, Ch. 14) and deliberately points out uncertainties and opportunities for further study. It is impossible to give a compreshensive account in the available space. Since Chapter 14 was written in 1973 about 700 new references have been noticed. These will be given in a revised edition of *"Feldspar Minerals"* now in active preparation. A few selected references are given here to illustrate the new data on selected trace elements. Papers with routine electron microprobe analyses are omitted.

Boron ranges mostly between 100 ppm with perhaps a weak tendency to increase with An-content in igneous plagioclase. Highest concentrations are in reedmergnerite $NaBSi_3O_8$, a very rare mineral, and in some authigenic K-feldspars with up to 1% B_2O_3 (latest data by Desborough, 1975). These high concentrations result from concentration by aqueous processes following leaching, weathering, and low-temperature crystallization of volcanic ash. Preliminary ion probe analyses (Steele *et al.*, 1980a) showed high sensitivity, but a thorough calibration is still needed (Mason *et al.*, 1982).

Gallium ranges mostly between 10 and 100 ppm with highest values for albites and K-feldspars from pegmatites. In general, Ga is weakly fractionated between feldspar and magma, is weakly correlated with Na, and tends to be lower in meteoritic than in terrestrial plagioclase probably because of fractionation into meteoritic metal.

Germanium ranges mostly from 1 to 10 ppm, with poor indications of geochemical correlation.

Titanium. Bulk analyses of Ti are suspect because of the possibility of mechanical impurities such as ilmenite. Numerous routine electron probe analyses report 0.0*n* wt % TiO_2, but the accuracy is often 0.0*m* wt %, and secondary fluorescence is a problem in fine-grained rocks. Special electron microprobe analyses of 157 plagioclases and 64 alkali feldspars by Ribbe and Smith (1966) and Corlett and Ribbe (1967) showed no detectable TiO_2 in most alkali feldspars and in all Na-rich and Ca-rich plagioclases, but up to 0.06 wt % in some labradorites and bytownites, and up to 0.07 wt % in some alkali feldspars. The simplest interpretations are that Ti^{4+} enters *T* sites, that the Ti substitution depends partly on the Ti content of the parent magma, and that Ti tends to exsolve out of the feldspar as Fe,Ti oxides during metamorphism (e.g., Anderson, 1966). Ion probe analyses of lunar plagioclases

(Steele *et al.*, 1980b) have shown a weak positive correlation between Na and Ti, plus a positive correlation between Ti in plagioclase and Ti in coexisting olivine. It appears that the Ti content of the plagioclase is an indication of the Ti content of the parent magma, and that the spread of Ti values probably is another piece of evidence that there is more than one chemical system on the moon. A thorough study is needed of synthetic plagioclase-liquid pairs and of terrestrial magmatic series. Ion probe analyses of anorthoclases (Mason *et al.*, 1982) revealed 30-60 ppm Ti in most crystals, but 480 and 322 ppm in Mt. Erebus and Kilimanjaro specimens.

<u>Phosphorus</u>. This element is very interesting because it belongs to the infamous KREEP group of "incompatible" elements which tend to stay in magmatic liquid rather than entering olivine, pyroxene, and garnet. Electron microprobe analyses of 168 plagioclases by Corlett and Ribbe (1967) showed 40% with P above the detection level of 0.003 wt % and a general tendency for the mean to increase from 0.002 for calcic plagioclase to 0.02 wt % for albites (highest value 0.33). Phosphorus was detected in only a few alkali feldspars, mostly microperthites with a maximum of 0.10 (Smith and Ribbe, 1966). These and other data reported in Smith (1974b, pp. 63-64) suggest that plagioclase phenocrysts are low in P which tends to stay with magmatic liquids. The partition of P between silicates and metal may have important effects on the P content of meteoritic plagioclase, but present data are inadequate to test this. Phosphorus has relatively low sensitivity for ion microprobe analysis (Steele *et al.*, 1980a); values of 6-74 ppm were found for anorthoclases (Mason *et al.*, 1982) and 6-2030 ppm in K-feldspar and albite lamellae of microcline perthites (Mason, 1982).

<u>Beryllium</u> is found mostly at the level of a few ppm except in Be-rich pegmatites. Kosals *et al.* (1973) report 300 determinations in plagioclases and host granitoids. Ion probe analyses are highly sensitive (0.01 ppm) and preliminary analyses (Steele *et al.*, 1980a) showed a strong positive correlation between Be and Na in plagioclases. Additional data are given by Neiva (1974, 1975, 1977b, 1980), Foord and Martin (1979) and Luecke (1981).

<u>Tin</u> is observed at the ppm level, except for feldspars from greisens.

<u>Iron</u>. The complex iron data for K-feldspars are summarized in Smith (1974b, pp. 58-61). Probably most of the iron is Fe^{3+} replacing aluminum. Whereas pure $KFeSi_3O_8$ can be synthesized in both the sanidine and microcline varieties, natural K-feldspars reach a maximum of 4 wt % Fe in sanidines from highly-differentiated volcanic rocks. In granitic and pegmatitic K-feldspars,

the Fe-content can go down to the ppm level, though the common range is 0.01-0.1 wt %. These data are consistent with a model in which the Fe-content of the feldspar depends largely on the Fe-content of the parent magma and the temperature of crystallization. Metamorphism and alteration reactions result in loss of iron. Because Fe^{3+} should enter K-feldspar much more easily than Fe^{2+}, the oxidation state of the parent magma must also be important.

In plagioclase, the situation is complicated by the tendency for Fe^{2+} to enter the feldspar as well as Fe^{3+} as the oxygen fugacity decreases. The preliminary data from resonance and optical absorption techniques and the somewhat questionable data from bulk gravimetric analyses show that in terrestrial plagioclase the Fe^{2+}/Fe^{3+} ratio varies considerably about a mean value in the region of unity; whereas, in lunar plagioclase (low oxygen fugacity) the ratio tends to be greater than unity. Electron microprobe analyses are rapidly increasing in number, and confirm the known tendency for total iron to increase with An-content from An_0 to An_{90} and to increase with estimated crystallization or recrystallization temperature (i.e., higher for volcanic than for plutonic and regionally-metamorphosed environments). For anorthite, data for both lunar and terrestrial specimens show a tendency for the Fe-content to decrease from An_{90} to An_{100}. The highest values of Fe are $\sim$1 wt % in volcanic bytownites and the lowest values are below 0.01% for pegmatitic albites. Iron-bearing impurities are common in plagioclases, and solid-state expulsion is probable for many of them (e.g., clouded plagioclase -- Armbrustmacher and Banks, 1974), although incorporation at the time of crystallization is also possible. Aventurine and some iridescent labradorites carry oriented plates of Fe-oxides. Braun (1974) found only 0.04 wt % Fe in Na-rich plagioclase produced by saussuritization.

Longhi *et al.* (1976) determined experimentally the distribution coefficients for Fe and Mg (see next section) between plagioclase and basaltic liquids for lunar, terrestrial and synthetic systems. The compositions are consistent with a $Ca(Fe^{2+},Mg)Si_3O_8$ component, and Mg is incorporated into plagioclase twice as readily as Fe^{2+} with respect to reduced lunar basalts and synthetic analogs. With increase of oxygen fugacity, ferric iron becomes important and Fe^{3+} is preferentially incorporated into plagioclase with respect to Mg compared to coexisting oxidized terrestrial basaltic liquids. These data were used to show that lunar anorthosites crystallized from iron-rich liquids; this is important because these liquids can be shown from other evidence to be low in large-ion-lithophile elements and hence not simply related to rocks with low contents of iron and high contents of LIL elements.

Magnesium. Existing data are very hard to interpret because of the possibility of mechanical impurities in bulk specimens, and because most electron microprobe analyses are probably uncertain to ±0.05 wt % MgO (absolute). Many recent analyses confirm the suggestions in (Smith, 1974b, pp. 106-108) that the Mg-content depends mainly on the Mg-content of the host magma, the temperature of crystallization and the degree of recrystallization. Probably magnesium tends to correlate with calcium in plagioclase. The range of Mg is from 0.3 wt % in calcic plagioclases from volcanic rocks (e.g., Ewart *et al.*, 1973) to 10 to 100 ppm in pegmatitic K-feldspars. Ion probe analysis for Mg is straightforward and highly sensitive (1 ppm). Systematic analyses of anorthoclases (2-52 ppm; Mason *et al.*, 1982) should be extended to other feldspars. Lunar plagioclases (see preceding section) contain 100-3000 ppm Mg (Steele *et al.*, 1980b) with the highest values for basalts.

Manganese. Existing data fall mostly in the range of 10 to 100 ppm when inaccurate electron microprobe data are excluded. A systematic study by ion microprobe techniques is needed.

Lithium. Many analyses show up to several tens of ppm in feldspars with the higher concentrations in those crystallized from late solutions. In coexisting feldspars, Li tends to be concentrated in the plagioclase. Recent papers include: Antipin *et al.* (1975), Kravchuk *et al.* (1980), Liotard *et al.* (1979), Luecke (1981), and Mason (1982). Ion microprobe analyses are highly sensitive (∿10 ppb), and Steele *et al.* (1980b, 1981) have found a strong positive correlation between Li and Na from plagioclases of a particular lunar rock, and wide differences from one lunar rock to another one (<8 ppm for anorthosites; up to 35 ppm for other rock types), and from one achondrite to another (Steele and Smith, 1982).

Sodium. Brown and Parsons (1981) demonstrated that the distribution of Na between coexisting plagioclase and alkali feldspar cannot be correctly modeled by any of the thermometers developed after the original simple formulation by Barth. A complex general formulation was developed by Brown and Parsons, but further experimental data are needed to provide a reliable calibration.

Potassium. The content of K in plagioclase deserves detailed study. Existing data suggest that both the bulk composition of the parent magma and the physical conditions of crystallization are important.

Rubidium. The detailed review by Smith (1974b, pp. 68-76) shows that the Rb-content ranges from less than 1 ppm in anorthite to about 100 ppm in oligoclases from granites to 1000 ppm in K-feldspars from granites. In granitic pegmatites the Rb-content may reach several percent in K-feldspars, whereas in albites it is much smaller at 1 to 100 ppm. The old favorite of geochemists, the K/Rb ratio, is not constant for feldspar and ranges over an order of magnitude for igneous rocks. Thus, rubidium must be treated as an individual element and not as an element "camouflaged" by potassium.

Afonina *et al.* (1979) reaffirm earlier data that Rb and Cs (next section) retard the ordering process in K-feldspar. Shmakin (1979) determined Rb, Sr, Cs and Ba in K-feldspars from U. S. pegmatites and found the highest Rb (0.2 wt %) and Cs (>100 ppm) for rare-metal pegmatites. In complex pegmatites, Rb and Cs increase and Ba and Sr (later sections) decrease from the earliest to latest generations; see also Neiva (1977b) and Foord and Martin (1979). Although most of the K-feldspars with high Ba, Rb and Cs are not fully ordered, a few are strongly ordered, perhaps because of late-stage processes. Shmakin suggested that high pressure inhibits the substitution of Rb and Cs and enhances that of Ba and Sr in K-feldspar; this should be tested experimentally. Contents of Rb in meteoritic plagioclases (Curtis and Schmitt, 1979; Mason and Graham, 1970) are similar to those for terrestrial plagioclases of similar composition.

Lipman *et al.* (1978) found much higher Rb in K-feldspar (80-281 ppm) than in plagioclase (0.5-56) from the San Juan volcanic field. The Rb contents reported by Ewart *et al.* (1977) for feldspars from Queensland lavas, and by Gijbels *et al.* (1976) for ones in the Rhum complex, also fit the general pattern given in Smith (1974, Fig. 14-8). Morse (1981) used K/Rb ratios to model differentiation in the Kiglapait complex.

Cesium. Most data for Cs are of low accuracy and those from pegmatitic feldspars are especially prone to error from mica impurities. In general, Cs resembles Rb except that its larger ionic radius makes it less likely to enter feldspar (especially anorthite and albite) and more likely to enter mica.

Thallium. Data for thallium are poor, but its distribution resembles that of cesium. New analyses are given in Antipin *et al.* (1975) for alkali feldspars from granites (1 to 23 ppm), and in Heinrichs *et al.* (1980) for plagioclases in basalts (0.03-0.05 ppm).

Calcium. Many K-feldspars have very low concentrations of Ca at the 0.0*n* wt % level, and Ba concentrations can be higher. Authigenic albites and K-feldspars are almost free of calcium. Because divalent elements must be balanced by Al^{3+}, their substitution involves Al,Si disorder in alkali feldspars. Perhaps the kinetics of ordering K-feldspars are affected by the content of divalent elements. Detailed study of the divalent elements in coexisting low sanidine ("orthoclase") and microcline might be instructive. Note that several Russian authors suggested that substitution of Ba inhibits Al,Si ordering in pegmatitic feldspars (Smith, 1974b, p. 92), but that data for "orthoclases" and microclines from Australian granites did not support extension to these rocks.

Strontium. This element gives very complex results because its size is about halfway between those of K and of Na or Ca and its charge is like that of calcium. The Sr-contents of pegmatitic K-feldspars and albite mostly fall between 10 and 100 ppm whereas those of all other feldspars range from about 100 to 5000 ppm. The details are too complicated to consider here, but there is a fairly good tendency for the partitioning of Sr between coexisting feldspar and liquid, and between coexisting feldspars, to be explainable in terms of laboratory syntheses (*loc. cit.* and Iiyama, 1972; 1974b). The unusually high Sr- and Ba-contents of megacrysts of anorthoclase (e.g., Mason *et al.*, 1982), sanidine and anorthite are particularly striking, and an investigation should be made whether this has any relation to the depth at which crystallization occurred; see also Cundari (1979) for high Sr and Ba in feldspars from lavas in the Roman region. Particularly interesting are the correlations between Sr and Na in lunar and meteoritic plagioclases (Steele *et al.*, 1980b; Steele and Smith, 1982b). Data for the Stillwater complex (Steele and Smith, 1982a) indicate that there should be a strong correlation between Sr and Na for comagmatic plagioclases. All but one lunar specimen fall close to a single trend, but plagioclase from a lunar lherzolite falls well off the trend, and presumably indicates a quite different magmatic reservoir. Reconniassance data for eucrites and howardites provide promise for sorting out which are comagmatic.

Barium. In general, Ba tends to favor K- rather than Na and Ca-feldspars. Feldspar phenocrysts range from $\sim$100 ppm for anorthite to 1 wt % in K-rich sanidines, but there is a wide spread for any particular Or- and An-content. Again the megacrysts from basalts (e.g., Mason *et al.*, 1982) have unusually high Ba-contents, suggesting a correlation with depth of crystallization just as for Sr. Barium tends to be very high, of course, in hyalophane and celsian, which typically occur in late veins. In pegmatitic K-feldspars, Ba is very variable and decreases in the later phases. The partition of Ba favors K-feldspar over plagioclase by two to 40 times, but there is no explanation of the wide range. The importance of Ba as an indicator for granitic feldspars is demonstrated by the data of Mehnert and Büsch (1981) who found that K-feldspar megacrysts in granites have Ba-rich cores surrounded by zoned shells and Ba-absent rims; late veins brought in K-feldspar with a very high content of Ba.

Lead. The geochemistry of lead in feldspars is complex (Smith, 1974, pp. 99-106), and it is not clear how much remobilization (e.g., Ludwig and Silver, 1977) occurs after crystallization. The highest concentrations (100-10,000 ppm) are found in K-feldspars from some pegmatites (e.g., Plimer, 1976), while both K-feldspars and plagioclases may contain less than 10 ppm. Leeman (1979) found that Pb favors basaltic melt about 10-fold over plagioclase, with the preference dropping to unity as the melt changes to rhyolite and the plagioclase to sanidine.

The blue to green color of amazonites tends to correlate in degree with the Pb content (Foord and Martin, 1979), but exceptions occur. An explanation based on a coupled interaction between Pb and H_2O is given in Chapter 11.

Copper. Ewart *et al.* (1973) report 0 to 30 ppm Cu in bytownites from Tonga volcanics, and a strong correlation with An-content, and Foord and Martin (1979) recorded 300 and 7 ppm Cu in the white and green parts of microcline from Amelia.

Ammonium. Honma and Itihara (1981) found ranges of 6-196 ppm NH_4 in K-feldspars and 2-58 ppm for plagioclases in various rocks mostly of granitic nature. Buddingtonite (Erd *et al.*, 1964) occurs only in a special environment in which hydrothermal alteration occurs in the presence of ammonia.

Halogens. Jovanovic and Reed (1979) found that leaching with H_2O followed by nitrate reduced the Cl content of plagioclase from a lunar basalt first to 1.1 ppm and then to 0.04 ppm; Br was reduced to 4 ppb and then to <0.5 ppb. Preliminary ion probe analyses by Steele *et al.* (1980a) have shown a signal for ^{19}F in feldspars, but further study is needed to delineate the ranges. Tentatively, it appears that the Cl and Br contents of feldspar may be very low indeed when mechanical contamination is reduced, whereas there is a definite substitution of F (replacing oxygen?).

Uranium. This is another element affected by mechanical impurities (Smith, 1974, pp. 105-106). Using fission-track mapping, Mitchell and Aumento (1977) found 7-13 ppb in plagioclase from oceanic basalts and gabbros. Higher values of 19-43 ppb were found for feldspars from the Bushveld Complex using neutron activation analysis (Gijbels *et al.*, 1974).

CONCLUSIONS

To meet limitations of space and time, this survey has been selective and succinct. Some additional references may be located by perusal of the element lists given in square brackets at the end of selected references in the bibliography. It is hoped that the geological value of trace elements in plagioclases has become evident even from this abbreviated synopsis, and that some readers will be encouraged to develop research programs to take advantage of the many possibilities opened up by new analytical instruments.

Chapter 13

DEFORMATION of FELDSPARS

J. Tullis

INTRODUCTION

There are several grain-scale deformation mechanisms which are capable of producing plastic strain (permanent shape changes) in crystals. These include microcracking, mechanical twinning, dislocation creep, diffusion creep, pressure solution, and grain boundary sliding. Different mechanisms are dominant at different conditions of temperature, strain rate, pressure, fluid pressure and grain size. Because feldspars are the major mineral constituent of the crust, a knowledge of their deformation behavior is often crucial to an understanding of crustal deformation. But because of their complex structure and refractory nature, there have been few experimental studies and relatively few detailed and unambiguous observations of naturally deformed feldspars. However, there presently is a substantial interest in the deformation of feldspars, and hopefully this review of the existing knowledge will prove useful.

Intracrystalline slip and mechanical twinning are among the more important deformation mechanisms for feldspars and other minerals, and we will examine them in detail, presenting general concepts, a consideration of how they are related to the crystal structure of feldspar, and a review of evidence from experimentally and naturally deformed samples as to the nature and extent of the mechanisms. We will also briefly consider other mechanisms of deformation and the conditions at which the various mechanisms are operative or dominant in nature.

INTRACRYSTALLINE SLIP

Intracrystalline slip is believed to be an important deformation mechanism for most minerals at moderate to high metamorphic grade, but until recently, little work had been done to systematically determine the slip systems active in the structurally complex feldspars. However, some experiments have now been done on both potassic feldspars and plagioclases, and more detailed observations, including transmission electron microscopy (TEM), have been reported on naturally deformed feldspars. The sections below briefly review the process of intracrystalline slip (dislocation glide and climb), and summarize the slip systems identified from these deformed feldspars.

Dislocation glide and climb

Intracrystalline slip involves shear on certain lattice planes in certain lattice directions; it is the macroscopic expression of the passage of dislocations through the crystal. Dislocations are line defects which separate the slipped and unslipped portions of a crystal (Fig. 1). It is easiest to visualize an edge dislocation, which consists of an extra half plane of material (Fig. 2). The Burgers vector is the closure error in circuiting the lattice around the dislocation, or the "thickness" of the extra half plane. In a unit or perfect dislocation the half plane is one unit cell thick, but sometimes it may dissociate into two partial dislocations separated by a stacking fault. In general, dislocations will consist of both edge and screw components (Fig. 3). Additional discussion of dislocations can be found in Nicolas and Poirier (1976).

Glide of a dislocation involves the propagation of the extra half plane through the crystal, leaving perfect crystal structure behind it (Fig. 2). Dislocation glide requires only a few atomic bonds to be broken at a time so that cohesion is never lost; the yield strength for this mechanism is thus much less than that for fracture. The lattice planes on which glide is easiest are those within which the bonds are numerous and/or strong, and across which they are fewer and/or weaker. The crystal directions in which slip is easiest are the close-packed ones of short repeat distance (short Burgers vector), because the energy of a dislocation increases as the square of the magnitude of its Burgers vector. Together a slip plane and its associated slip direction are referred to as a slip system, represented as (hkl) [uvw]. In a crystal subjected to a deviatoric stress, the slip systems activated will be those on which there is a high resolved shear stress.

Compared to metals, dislocations in silicates are more complex and dislocation glide is more difficult. Silicates tend to have larger unit cells and thus larger Burgers vectors, as well as lower symmetry and greater anisotropy; this means that they have fewer easy slip systems than metals. In addition, the ionic-covalent bonds of silicates result in a high Peierls force or intrinsic lattice resistance to dislocation glide. This resistance can be offset by thermal vibrations, so that glide becomes easier at higher temperatures.

Dislocation glide is also inhibited by impurities, and by "tangling" resulting from the intersection of dislocations gliding on different planes. This pinning results in a macroscopic work-hardening behavior, and steady-state deformation by glide requires an accompanying recovery process which allows dislocations to by-pass obstacles and keep gliding. The combination of glide

Figure 1 (to the right). A crystal which has undergone slip on a portion of the slip plane under the applied shear stress shown by the arrows. A dislocation line separates slipped and unslipped portions of the crystal; dislocation has edge character where the solid line appears, screw character where the dashed line appears.

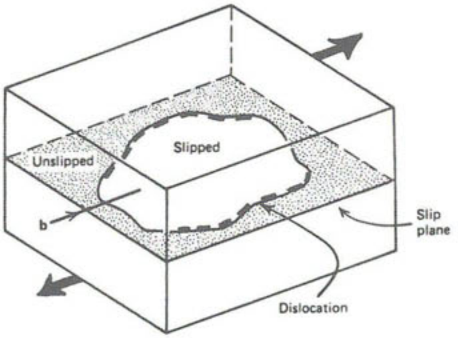

Figure 2 (below). Propagation of an edge dislocation through a crystal under an applied shear stress as shown in (ii). The black circles indicate the extra half-plane of material.

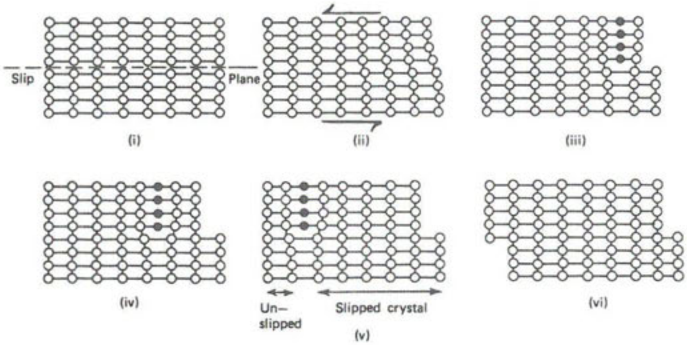

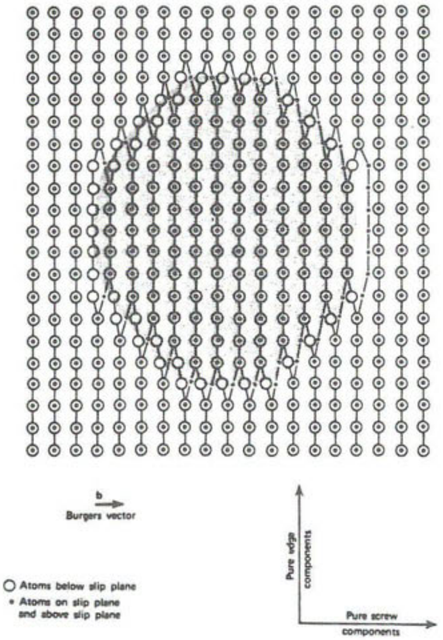

Figure 3. The atomic arrangement around a dislocation loop which separates the slipped (shaded) and unslipped (unshaded) portions of a crystal.

Figures 1-3 are from Hobbs *et al.* (1976, their Figs. 2.1b, 2.2a and 2.1c).

plus recovery constitutes the deformation mechanism known as dislocation creep.

Recovery is thermally activated; it involves a reduction in the dislocation density through annihilation, and a rearrangement of the dislocations into arrays which are of lower energy and allow continued glide. This occurs by cross slip and/or climb of the dislocations. Cross slip involves the gliding of a screw dislocation off one crystal plane onto another intersecting plane, but in the same crystal direction. Climb involves a change in the length of the extra half plane of an edge dislocation by volume diffusion of material toward or away from it. Climb and cross slip allow dislocations to become arranged in stable walls, producing subgrains (which differ in orientation by 1 - 10° and may be optically visible). Recovery is also more difficult in silicates than metals; there are many more atoms per unit cell of the extra half plane which must be removed by diffusion (52 for feldspar), and diffusion itself is much slower (see Ch. 8).

Another optically visible process for reducing the internal strain energy is recrystallization. If it accompanies dislocation glide, it is termed dynamic (syntectonic) recrystallization. This involves the growth of strain-free grains at the expense of adjacent grains having a higher dislocation density. There is some debate concerning the mechanisms of recrystallization. In some cases there is evidence for a classic nucleation event, but two other mechanisms have recently been distinguished (Guillopé and Poirier, 1979). At lower temperatures, recrystallized grains may result from progressive subgrain rotation; when the misorientation reaches about 10°, the subgrain boundary becomes a high angle (more mobile) grain boundary, and the subgrain becomes a recrystallized grain. At higher temperatures, where the mobility of high angle boundaries is greater, recrystallized grains tend to form by boundary migration along grain boundaries, twin boundaries, or deformation bands. If dislocation creep is followed by a static anneal, then annealing recrystallization will occur, either by nucleation or by the boundary migration mechanism.

Determining slip systems

In a given deformed sample, the operative slip systems may be determined either optically or using TEM. Experiments on polished single-crystal cylinders will produce fine slip lines on the outer surface, except in a null zone perpendicular to the slip direction, and from these one can determine the slip plane and direction (e.g., Christie *et al.*, 1964). The geometry of a kink band observed in thin section also can be used to infer the slip plane and direction which caused it (e.g., Borg and Heard, 1970); however, TEM has shown that microfracturing also can produce optical kink bands (e.g., Tullis and Yund, 1977;

Marshall and McLaren, 1977a). Deformation lamellae observed in thin section are commonly assumed to result from arrays of dislocations on active slip planes, but TEM has shown that sometimes they may be the optical expression of arrays of cracks, thin zones of glass, subgrain walls, or zones of tangled dislocations marking the intersection of multiple slip systems (e.g., White, 1973). Another problem with optical determination of slip systems is that for higher temperature deformation, where recovery and/or recrystallization are significant, there may be no optical expression of the deformation mechanism itself, namely the glide.

Identification of slip systems using TEM is quite involved. Identification of the slip plane comes from observations of free dislocation loops. The anisotropy of most silicates, including feldspars, makes it difficult to determine the Burgers vector of dislocations; it is not easy to find two different diffraction vectors $\underline{g}$ producing dislocation images of low contrast corresponding to $\underline{g}.\underline{b} = 0$ and $\underline{g}\cdot\underline{b} \times u \ll 1$ (Marshall and McLaren, 1977b). Computer simulation of dislocation images may be necessary for verification (Willaime and Gandais, 1977).

Slip systems in potassic feldspars

Crystal structure considerations. The T–O bonds are the strongest ones in the feldspar structure, hence a first approximation would indicate that the easiest glide planes should be those across which there are the fewest T–O bonds per area of that plane in the unit cell. By this criterion the easiest slip planes should be $(10\bar{1})$, (010), (001), (110), (100), and $(1\bar{1}1)$, in that order.

As regards slip directions, all possible Burgers vectors in feldspar are large. In disordered monoclinic potassic feldspars ($C2/m$) seven Burgers vectors are possible for a unit (perfect) dislocation; in order of increasing length (from 7.19 to 9.25 Å) these are [001], ½[110], ½$[1\bar{1}0]$, [101], [100], ½[112], and ½$[1\bar{1}2]$ (Willaime and Gandais, 1977). A dislocation with a longer Burgers vector must dissociate into two unit dislocations from this set; for example, [010] would dissociate into ½[110] + ½$[\bar{1}10]$. Because of their long Burgers vectors, dislocations in feldspars might be expected to dissociate into partial dislocations separated by a stacking fault (Kovacs and Gandais, 1980); however, dissociation is unlikely if the stacking fault energy is high. Based on crystal structure considerations for sanidine, Kovacs and Gandais (1980) find that the only two partial dislocations which are likely to produce a low stacking fault energy are ½[100] and ½[101].

For the ordered triclinic potassic feldspars ($C\bar{1}$), the easy slip planes and the possible Burgers vectors should be the same as for sanidine. There are no obvious low energy stacking faults in the $C\bar{1}$ structure, so partial dislocations are not expected (Marshall and McLaren, 1977c). The presence of inversion twinning in these feldspars is expected to strongly inhibit slip, since most slip planes will not be continuous through both twins.

Evidence from experiments. The only experimental deformation studies on potassic feldspars are those on Westerly granite (containing microcline grains) (Tullis and Yund, 1977), and those on single crystals of sanidine (Or_{80}) (Willaime *et al.*, 1979). Both studies were done at a strain rate of 10^{-6}/sec and confining pressures of 10-15 kbar. The microcline grains (which disordered rapidly during the experiments) show deformation lamellae on (010), consistent with this being an easy slip plane. The sanidine experiments were conducted to test for slip on five possible planes: (010), (001), (110), (110), and (100). Although detailed TEM analysis has not yet been done on all the samples, results to date indicate little difference in the critical resolved shear stress for glide on the different systems. At 700°C samples oriented for (010) [100] slip were somewhat weaker than the others, but ⩾900°C all samples were about equal in strength. Optical and TEM observations bearing on the operative slip systems in these samples are summarized in Table 1, but it should be remembered that this is a preliminary and incomplete list of the slip system for sanidine.

The dislocations in the experimentally deformed sanidine crystals were observed in TEM always to trail a planar defect behind them (Willaime and Gandais, 1977; Gandais and Willaime, 1978). For the (010) dislocations this is a shear fault with displacement vector about one-tenth of the unit cell vector in the [100] direction. The weak contrast associated with these planar defects suggests that they involve configurational changes of the tetrahedra localized near the slip plane (even though the passage of dislocations normally leaves behind perfect crystals). The defects are less common at 900°C than at 700°C, presumably because the faster diffusion anneals out the atomic distortions. Similar planar defects were noted in the microcline grains of Westerly granite experimentally deformed at 300-500°C (Tullis and Yund, 1977).

Evidence of naturally deformed samples. In studies of naturally deformed potassic feldspars, dislocation glide has been inferred from optical microstructures such as kink bands, deformation bands, undulatory extinction, and deformation lamellae. However, because few of the studies involved TEM analysis, some of these features may be due instead to microcracking and/or microtwinning. Even those microstructures definitely attributable to dislocation

TABLE 1. Slip Systems in Experimentally Deformed Sanidine*

Orientation of single crystal core	Temp °C	Observed systems	Comments
High and equal resolved shear stress on (001) ½[110] and (010)[101]	700	(010) [101]	Deformation lamellae observed on (010); most dislocations of this type.
		(001) ½[110]	No deformation lamellae observed on (001); few dislocations of this type
	900	(010) [101] (001) ½[110]	Deformation lamellae observed on (010) and (001); both types of dislocations equally abundant; (010) dislocations aligned along [001]; (001) dislocations aligned along [100]; more evidence of recovery than at 700°C.
High resolved shear stress on (010)[100]; lower and equal resolved shear stress on (121)[101] and $(1\bar{1}\bar{1})$	700	$(1\bar{2}\bar{1})$ [101]	Few deformation lamellae on either plane; most dislocations are $(1\bar{2}\bar{1})$; this unexpected result may be due to dissociation on $(1\bar{2}\bar{1})$ (Willaime et al., 1979; Kovacs and Gandais, 1980).
	900	$(1\bar{2}\bar{1})$ [101] (010) [100]	More evidence of recovery and few deformation lamellae; most dislocations again are $(1\bar{2}\bar{1})$.
High and equal resolved shear stress on (010)[001] and (001)½[110].	700	(010) [001]	Deformation lamellae observed on both (010) and (001); most dislocations are (010)[001]; little evidence of climb or cross slip.
High resolved shear stress on (001)[100].	700	(110) ½$[1\bar{1}2]$ $(1\bar{1}1)$ ½[110]	No deformation lamellae observed; cracks observed at 45° to σ_1; expected slip system not observed; dislocations of both systems are straight and set in bands of high density, indicating work-hardening.

*Taken from Willaime et al.,1979, and Scandale et al., 1983; sample composition Or_{80}, pressure 15 kb, strain rate 10^{-6}/sec.

TABLE 2. Slip Systems in Naturally Deformed Potassic Feldspars

Sample	Deformation conditions	Glide plane	Burgers vector	Comments	Ref.
hoclase Or_{90} deformed anite	2 kb, 500°C	(010)		Both cells and subgrains observed	1
		(001)			
		$(1\bar{1}1)$			
		(120)			
		(130)			
		$(1\bar{2}1)$	[101]		
		(010)	[101]		
			[100]		
			[001]		
			½$[1\bar{1}2]$		
rocline Or_{93} gneiss	2 kb, 550°C then decreasing	(010)	not determined	Optically, slight undulatory extinction and grain boundary recrystallization; TEM shows higher dislocation densities and isolated subgrains near grain boundaries	2
ldspar in gen gneiss	mesozone	$(10\bar{1})$	[101]		3
ldspar in arnockite anite	catazone	(010) (130) to (120)	[001] [001]		3

1. Sacerdoti et al., 1980
2. Debat et al., 1978
3. Willaime and Gandais, 1977, Willaime, personal comm., 1982

glide seldom offer unambiguous evidence of the operative slip systems. A summary of slip systems and associated deformation microstructures reported for naturally deformed potassic feldspars is presented in Table 2.

A comparison of Tables 1 and 2 is interesting. Planar defects are associated with dislocations in both the naturally and experimentally potassic feldspars. They tend to be fewer and less clear in the natural samples, presumably due to the greater time for recovery. A comparison of the two tables also shows that [101] is a common Burgers vector and (010) is a common slip plane in all potassic feldspars (as predicted from crystal structure considerations). Many other planes and directions are also operative, but at this time there are not enough observations to say what slip systems are dominant for different conditions or deformation and for different degrees of ordering, twinning, and/or exsolution, and whether the frequency of these is predicted on the basis of crystal structure considerations. There is a need for many more TEM studies on well-characterized naturally deformed samples, before the accumulated observations will be statistically significant and will allow such generalizations.

Recovery and recyrstallization of potassic feldspars

Recovery involves cross slip and climb of dislocations. Cross slip of screw dislocations can only occur if there are several slip planes with a common Burgers vector; there are several possibilities for this in the potassic feldspars. Cross slip is greatly inhibited if the dislocations are dissociated, because the partials must recombine before cross slip can occur. However, only limited dissociation has been observed even in the disordered potassic feldspars, and evidence of cross slip has been observed in experimentally deformed sanidine crystals (Kovacs and Gandais, 1980).

For most materials, climb is the more important recovery process. For feldspars, climb should be difficult because of the large unit cell and the low diffusion coefficients (see Ch. 8), and high temperatures should therefore be necessary for significant recovery. In experimentally deformed sanidine crystals, more evidence of climb was seen in the 900°C than in the 700°C samples (Williame *et al.*, 1979), although no subgrains were reported, possibly because the samples were only taken to low strain. In experimentally deformed Westerly granite, microcline grains (which disordered rapidly during the experiment) showed some evidence of climb at 800°C, and subgrains were noted at 900°C (Tullis and Yund, 1977). In naturally deformed potassic feldspars, subgrains have been observed in augen of orthoclase (Bossiere and Vauchez, 1978; Sacerdoti *et al.*, 1980) and microcline (Vidal *et al.*, 1980; Hanmer, 1982) in gneisses deformed at 500-600°C (and thus in the disordered state). Although the subgrains indicate that dislocation climb was extensive, the free dislocations in these samples were observed to be quite straight, indicating that Peierls forces were still important.

Syntectonic (strain-induced) recrystallization should require high strains and high temperatures. In the microcline grains of experimentally deformed Westerly granite, recrystallization was observed only for sample shortenings of $\geq\sim$50% at 900°C or $\geq\sim$30% at 1000°C (Tullis and Yund, 1977). In naturally deformed rocks, strain-induced recrystallization of potassic feldspars only becomes common at amphibolite grade or higher (e.g., Voll, 1976; Ohta, 1969; Wilson, 1980). This recrystallization appears to have resulted from progressive subgrain rotation in some cases (e.g., Voll, 1976; Hanmer, 1982), and nucleation in others (e.g., Passchier, 1982). These limited observations need to be supplemented by detailed experimental studies of recovery and recrystallization, as well as further observations of naturally deformed samples.

In many cases recrystallization of potassic feldspar is not simply strain-induced, but involves changes in chemical composition; neomineralization is a term that should perhaps be used in such cases (Knopf and Ingerson, 1938). It is common to observe potassic feldspar megacrysts which are progressively reduced in size and number with increasing strain due to replacement by quartz and mica and/or albite, either along their boundaries (e.g., Potter, 1976; Allison *et al.*, 1979; Hanmer, 1982) or within fractures (e.g., Bossiere and Vauchez, 1978; Bouillier, 1980). The presence of high dislocation densities may slightly enhance the rates of neomineralization (Yund *et al.*, 1981). Even neglecting this factor, it is important to note that when potassic feldspar is not chemically stable during the conditions of deformation, neomineralization will occur at much lower temperatures than is possible for isochemical strain-induced recrystallization.

<u>Slip system in plagioclase</u>

Crystal structure considerations. Most of the general rules for slip systems in the potassic feldspars apply to the plagioclases, but there are some additional complications. The ordering relations are complex and produce four structural types which depend on the An content and the thermal history of the particular sample (see Ch. 1): $C\bar{1}$, $I\bar{1}$, $P\bar{1}$, and $I\bar{1}$*.[1] The *c* lattice parameter is doubled from $\sim$7 Å to $\sim$14 Å, and this changes the notation of some of the slip planes and directions. All of the common plagioclases are triclinic, but

---

[1] $I\bar{1}^*$ represents those feldspars with the 'e'-plagioclase superstructure.

the T-O framework is basically the same and the easiest slip planes are expected to remain the same (allowing for the difference in notation). The number of stable Burgers vectors in an "isotropic" triclinic structure is limited to seven, and Marshall and McLaren (1977b) have computed these for the $C\bar{1}$, $I\bar{1}$, and $P\bar{1}$ structures. The doubling of the c parameters in the $I\bar{1}$ and $P\bar{1}$ structures means that some of these Burgers vectors are very long, up to 19 Å.

Several limitations to slip and recovery can be predicted from crystal structure considerations. For the $C\bar{1}$ structure there are no obvious low energy stacking faults, and so dissociation into partial dislocations is not expected. However, dissociation is expected in the $I\bar{1}$, $P\bar{1}$, and $I\bar{1}*$ structures (Marshall and McLaren, 1977b), and this would hinder the recovery process of cross slip, imposing a limit on the rate of slip. The presence of a superlattice in the $I\bar{1}*$ structure of the intermediate plagioclase should inhibit glide and climb of dislocations, because they must involve antiphase boundaries (White, 1975). Thus one would expect slip and recovery to be easier in albite than in intermediate plagioclase, at least for lower temperatures where the structure is ordered.

Evidence from experiments. There have been a number of experimental studies of the deformation of single crystals and polycrystalline aggregates of plagioclase. The first question concerns the conditions necessary to produce slip. Early studies found that fracture and cataclasis were produced at lower temperatures, and that optical microstructures indicative of slip (deformation lamellae, undulatory extinction, kink bands) were only produced at ≥800°C, for a strain rate of 10^{-4}/sec and confining pressures of 5-15 kbar (Borg and Heard, 1969, 1970; Seifert, 1969; Seifert and VerPloeg, 1977). However, TEM analysis of these single crystals showed that some of the features (fine, closely spaced straight lines parallel to (010) in An_2 and An_{13}; undulatory extinction and deformation lamellae consistent with (001) [101] slip in An_{50}) were due to arrays of microcracks (Marshall and McLaren, 1977a,b). More recent optical and TEM evidence from plagioclase grains in experimentally deformed polycrystalline aggregates (An_{17} in granite, An_{71} in diabase, An_{56} in anorthosite, An_2 in albite rock) indicate that for a strain rate of 10^{-6}/sec and confining pressures of 10-15 kbar, the transition from dominantly microcracking to dominantly dislocation glide and climb occurs over the interval 600-900°C (Tullis and Yund, 1977; Kronenberg and Shelton, 1980; Tullis and Yund, 1980).

Our knowledge of what slip systems are active in plagioclase of different compositions and structural states is still quite preliminary, principally because no single crystals have been deformed at >800°C, a temperature at which slip is just starting to be important. The polycrystalline materials referred to above were deformed to higher temperatures and show clear evidence of multiple slip, but no detailed characterization of the dislocations has been performed. Table 3 summarizes the slip systems identified by Marshall and McLaren (1977b) in single crystals experimentally deformed at 800°C; this must be regarded as a preliminary and incomplete list.

It should be noted that all of the dislocations observed by Marshall and McLaren (1977b) in the experimentally deformed single crystals had planar faults trailed behind them. These faults could be due to a loss of short-range order across the slip plane, or to imperfect reconstruction of *T*-O bonds after passage of the dislocations, or to the production of very thin Pericline twin lamellae. Regardless of the detailed mechanism of their formation, they identify the active slip plane, and they seem to be associated with all dislocations in plagioclase.

Evidence from naturally deformed samples. It appears that for natural deformations ⩽~550°C, plagioclase may undergo limited, local dislocation glide but the dominant deformation mechanism is grain-scale fracture and/or distributed microcracking. At temperatures >550°C (amphibolite and granulite facies conditions) there is abundant evidence for slip accompanied by recovery or recrystallization (see next section). Unfortunately, there are not sufficient observations to allow generalizations about the effects of plagioclase composition or structural state on slip behavior, although it appears that disordering may be necessary for substantial slip and recovery. Table 4 summarizes the information available to date on slip systems observed in naturally deformed plagioclase. TEM observations are too few at present to warrant any detailed comparisons with the systems observed in experimentally deformed plagioclase (Table 3).

Recovery and recrystallization of plagioclase. Recovery is expected to be easier for plagioclase lacking a superlattice; that is, for albite and anorthite, or intermediate plagioclases deformed ⩾500-550°C (White, 1974). Phases which have undergone easy recovery should show subgrains and recrystallization by a subgrain rotation mechanism, whereas phases which have not undergone easy recovery should show no subgrains and recrystallization by a boundary migration or nucleation mechanism. For the most part, observations of recovery and recrystallization in plagioclase bear out these predictions.

For albite, subgrains and recrystallization by progressive subgrain rotation have been observed in rocks naturally deformed at greenschist facies conditions where it may or may not have been ordered (Lorimer *et al.*, 1970; Wilson,

TABLE 3. Slip Systems in Experimentally Deformed Plagioclases*

Sample	Structural state	Deformation conditions	Observed systems	Comments
An_1	$C\bar{1}$	800°C, 10 kb, 2×10^{-5}/sec	(101) ½[111]	Optical 'slip lines' parallel to (010) are due to microcracks.
An_{38}	$C\bar{1}$ and $I\bar{1}$*	"	$(\bar{1}30)$ to $(\bar{1}20)$ ½[001]	Some deformation lamellae on (001), due to walls of higher dislocation density.
An_{50}	$C\bar{1}$	800°C, 10 kb, 10^{-5}/sec	$(10\bar{1})$ ½[111] $(10\bar{1})$ ½$[1\bar{1}1]$ (001) [100]	Macroscopic fractures on (010) and (001); undulatory extinction due to arrays of microcracks.
An_{77}	$I\bar{1}$	800°C, 10 kb, 2×10^{-5}/sec	$(11\bar{2})$ ½[201] $(13\bar{2})$ ½[201] $(13\bar{2})$ ½[111] (101) ½[201] (010) ½[100] (101) ½$[1\bar{1}1]$ (101) [101]	Optical deformation lamellae due to bands of higher dislocation density.
An_{95}	$I\bar{1}$ and $P\bar{1}$	"	$(1\bar{1}0)$ [110]	Isolated dislocations, associated with cracks and voids.

*Taken from Marshall and MacLaren (1977a, 1977b); slip systems identified from TEM, and referred to a unit cell with $c \simeq 14$Å. Samples were single crystal cores (except for An_{77} which was an aggregate), oriented with core axis normal to [100] and bisecting obtuse angle between (100) and (001) for An_1, acute angle for other samples.

TABLE 4. Slip Systems in Naturally Deformed Plagioclases

Sample	Deformation conditions	Glide plane*	Burgers vector*	Comments	Ref.
An_{2-10}	upper greenschist		[100]	Recrystallized grains forming by progressive subgrain rotation.	1
An_{30}, sheared pegmatite	lower amphibolite	(001)		Recrystallization along grain boundaries and deformation bands; higher dislocation density near grain boundaries.	2
An_{25-35}	granulite	(010)	½[001] ½[110]	Dislocation density uniform within grains, varies between grains.	3
An_{40}	granulite	(010)		Deformation bands, subgrains, and recrystallized grains observed.	4
$An_?$ in mafic and ultramafic gneisses	granulite	(010)		Recrystallization along grain boundaries and kink bands.	5

* Referred to $c \sim 14$Å cell.

1. Marshall and Wilson (1976); Burgers vector identified using TEM.
2. White (1975); slip planes identified from dislocation loops using TEM.
3. Olsen and Kohlstedt (1981); slip planes identified using TEM.
4. Vernon (1975); slip plane inferred from kink band geometry.
5. Goode (1978); Slip plane inferred from kinks and highly elongated megacrysts.

1980). However, a single crystal of peristerite ($An_{4.5}$) experimentally deformed at 850°C, 10 kbar, and 10^{-5}/sec appears to have developed recrystallized grains by a nucleation mechanism (Marshall *et al.*, 1976); it may be that the very fast strain rate did not allow sufficient recovery for subgrains to form.

For the intermediate plagioclase, subgrains and recrystallization by progressive subgrain rotation are observed for samples deformed at upper amphibolite to granulite facies conditions where they were disordered (e.g., Vernon, 1975; Voll, 1976; Brown *et al.*, 1980; Hanmer, 1982). In contrast, recrystallization by a nucleation mechanism was observed in a sample deformed at lower amphibolite facies conditions where it was probably ordered (White, 1975).

Much attention recently has been focused on the fact that recrystallized plagioclase grains frequently differ in composition from their host (e.g., White, 1975; Vernon, 1975; Borges and White, 1980; Brown *et al.*, 1980). In most cases this compositional change presumably reflects the fact that recrystallization occurred at a different temperature (and thus equilibrium composition) than the original crystallization. This means that the driving force for recrystallization included not only the difference in plastic strain energy, but also a chemical free energy term. However, in cases of extreme composition changes (e.g., Allison *et al.*, 1979), plastic strain may have little to do with the recrystallization and the term neomineralization may be more appropriate.

Summary of slip in feldspars

The results presented above show certain similarities in the slip behavior of the potassic and plagioclase feldspars. More can be learned from a direct comparison of the two feldspars in the same deformed rock. Little difference in the deformation behavior of microcline and oligoclase was noted in samples of Westerly granite experimentally deformed over a wide range of temperatures and pressures (Tullis and Yund, 1977). It should be noted, however, that because of the short laboratory times, significant slip requires temperatures much higher than are characteristic of natural deformations -- temperatures which are always higher than the disordering temperature. Thus experimental studies will never be able to investigate slip in ordered feldspars; the evidence will have to come from careful observations on naturally deformed samples.

Most studies of naturally deformed gneisses and granitic rocks indicate that plagioclase remains brittle or undeformed at conditions where potassic feldspars show slip or even recrystallization (e.g., Debat *et al.*, 1978; Etheridge and Wilkie, 1981). This may be due to the lower disordering temperature for potassic feldspars. Before any comparison can be made in a given rock, however, it must be determined whether one or both of the feldspars were out of equilibrium with fluids which may have been present in the rock during deformation.

Trace amounts of water appear to have a significant effect on slip in both kinds of feldspar, similar to the hydrolytic weakening first described for quartz (e.g., Griggs, 1967). Experimental deformation studies have shown that the temperature of the transition from microcracking to dislocation glide and climb in feldspar is lowered by about 200°C if ∿0.1 wt % water is added to the sample before deformation (Tullis and Yund, 1981), and it is raised by about 400°C if ∿0.1 wt % water is removed by vacuum drying before deformation (Shelton *et al.*, 1981). Vacuum drying prior to deformation also increased the strengths of single crystals of An and An (Borg and Heard, 1970). There is some evidence that feldspars naturally deformed by slip in a hydrous environment also are weaker (e.g., Voll, 1976), and that feldspars strained "wet" at amphibolite grade have a larger recrystallized grain size than equivalent feldspars strained "dry" at granulite grade (Etheridge and Wilkie, 1981). The exact reason for these important effects of water is not known, but it is pertinent to note the effect of water on O and Al,Si diffusion in feldspars (see Ch. 8).

It is instructive to compare the slip of feldspars with that of other common silicates. Feldspars are more resistant to slip than is olivine, for deformation at the same fraction of the melting temperature. This is understandable because the crystal structure of olivine involves isolated SiO_4 tetrahedra, whereas feldspar is a framework silicate and all dislocation glide necessarily involves the breaking of *T*-O bonds. Quartz is also a framework silicate, but is observed to undergo slip, recovery, and recrystallization at lower temperatures than feldspar in both nature and experiments, despite its higher melting temperature. This may be related to the greater lengths of the Burgers vectors in feldspar (7 to 9 Å) compared to those in quartz (5 to 6 Å) as well as to the complex substructures present in most feldspars.

MECHANICAL TWINNING

Mechanical twinning is a deformation mechanism closely related to slip in many ways, but generally occurring at somewhat lower temperatures or faster strain rates (that is, at higher stresses). It appears to be a common deformation mechanism in the plagioclase, although impossible in potassic feldspars. The sections below briefly review the fundamentals of mechanical twinning, discuss the likelihood of different types of mechanical twinning in feldspars in terms of their crystal structure, and present observations from both experimental studies and naturally deformed samples as to the operative twin systems.

General concepts

All feldspar twins belong to the group of twinning by pseudomerohedry (Smith, 1974a, p. 304). The feldspar lattice has pseudosymmetry, and the twin operation results in near, although not exact, coincidence of the lattices of the twinned units. Twins of this type may be either reflection or rotation twins. For centrosymmetric crystals, reflection about the lattice plane is equivalent to rotation about the normal to that plane, and hence all feldspar twins can be thought of as rotation twins, in which the twin axis relating the adjacent individuals is parallel to a lattice row which is almost a symmetry axis of the structure. There are two types of rotation twins: normal twins have their twin axis normal to the composition plane, and parallel twins have their twin axis parallel to the composition plane. In either case the plane normal to the twin axis may be called, somewhat inexactly, the twin plane (Bloss, 1971, p. 323). The obliquity is a measure of the pseudosymmetry, or the angular misfit between the two individuals; it rarely exceeds 5° (Cahn, 1954).

Macroscopically, mechanical twinning consists of a simple shear of the lattice on the twin glide in the twin glide direction. The twin glide plane must be the twin plane (as defined above), but the twin glide direction may or may not be the same as the twin axis (depending on whether it is a normal or a parallel twin). Microscopically, successive atomic planes parallel to the twin glide plane are displaced over one another in the twin glide direction, each plane moving over those below it by a fraction of a lattice spacing. However, only in body-centered cubic materials are the atomic movements fully described by the overall shear; for all other materials atomic shuffles are necessary. Shuffles of up to about 1-2 Å seem to be common (Cahn, 1954).

Mechanical twinning requires a high resolved shear stress on the twin glide plane in the twin glide direction, but local stress concentrations are important and there may not be a simple relation to the externally applied shear stress. In fact, mechanical twins are difficult to nucleate in dislocation-free material; they commonly initiate in regions of stress concentration such as the ends of kink or slip bands or cracks. There has been some debate about whether or not there is a critical resolved shear stress criterion for twinning; certainly the necessary stress will depend on the general defect state of the material. In any event, it is almost always observed that propagation of mechanical twins is easier than their nucleation.

Dislocations are believed to be involved in the propagation of mechanical twins, because twinning occurs at stresses comparable to those for slip, namely far below the theoretical shear strength of the perfect lattice. Since a new atomic configuration is produced by twinning, the dislocations that cause it must be partial; that is, the Burgers vector is only a fraction of a lattice vector. One problem is that homogeneous shear requires either a twinning dislocation on every plane without exception, which seems unlikely, or the motion of a single dislocation from plane to plane in a regular manner. Mechanisms for the latter process have been proposed for various metals (e.g., Friedel, 1967), and such dislocations have been reported for calcite (Sauvage and Authier, 1965), but they have not been observed in any silicates to date.

Some mechanical twins disappear upon removal of the stress, if the stress is less than some critical value. These are termed elastic twins, first described by Mügge in 1888 and discussed in some detail by Cahn (1954). Elastic twins are not observed in metals, apparently because slip is so easy in these materials that the stress concentrations at the tip of a twin cause local slip which in turn "locks in" the twin. However, elastic twins are observed in materials such as calcite and feldspar, which do not undergo such easy slip. In these materials elastic twins which intersect a stress-free boundary such as a cleavage crack will become parallel-sided and be preserved after stress removal (in which case they are called residual twins).

Mechanical twinning is similar to slip in some ways, such as occurring on close-packed planes, but there are a number of important differences. Slip consists of a shear displacement of an entire block of the crystal, and the slipped portion of the grain has the same orientation as the original grain. In contrast, twinning involves a uniform shear strain, and the twinned portion is the mirror image of the original lattice. The amount of deformation by slip is unlimited; in contrast, the amount of deformation by twinning is limited to that corresponding to complete twinning. Slip can take place in either sense of the Burgers vector, the Burgers vector can be any multiple of the lattice vector, and each plane can be displaced from the one below it by any multiple of the Burgers vector. In contrast, twinning can occur in only one sense along the Burgers vector, the Burgers vector is a fraction of the lattice vector, and each plane above the twin plane is displaced by only a single Burgers vector. Both slip and twinning are inhibited by impurities, walls of tangled dislocations, and disruption of long-range order. Both slip and twinning are insensitive to pressure, since no volume change is involved. However, unlike slip, mechanical twinning is relatively insensitive to temperature and strain rate, presumably because the twin dislocations, unlike slip dislocations, undergo little or no climb (which involves diffusion). For most materials, mechanical twinning appears to require a higher stress than does slip, thus it tends to be more common at lower temperature and in lower symmetry materials with fewer slip systems.

Mechanical twinning in plagioclase

Crystal structure considerations. Mechanical twinning must be displacive rather than reconstructive. In addition, in a triclinic lattice either the twin glide plane or the twin glide direction must be rational, and Friedel (1926) postulated that mechanical twinning should be easier the closer these are to a plane or axis or symmetry, respectively (that is, the lower the obliquity). For plagioclase, deviation from monoclinic symmetry is slight; *b* and (010) are almost symmetry elements. Therefore mechanical twinning may occur in two possible ways: (1) Albite twinning, where the twin glide plane is (010) and the irrational twin glide direction is the projection of the *b* axis on (010); and (2) Pericline twinning, where the twin glide direction is the *b* axis and the irrational twin glide plane is the rhombic section, which varies markedly in orientation with composition and structural state (Smith, 1974a). The other known twin laws for plagioclase are reconstructive and therefore unlikely to be produced mechanically.

The ease of mechanical Albite and Pericline twinning depends on which of the four plagioclase structural types is involved, as well as on the degree of Al,Si order. Both Albite and Pericline twinning exchange $T_1$0 for T_1m positions, and similarly for T_2, although they do not exchange T_1 for T_2 positions (Laves, 1952a,b; 1966). As a consequence, mechanical twinning would destroy the ordering in the $C\bar{1}$ structure of low albite, and force Al to end up in other than the $T_1$0 position. Thus mechanical twinning in this ordered structure should be impossible. For high albite or analbite (also $C\bar{1}$) Al and Si are highly disordered, and so mechanical twinning is inhibited only by the need for a slight atomic shuffle (Starkey, 1963). Anorthite (structure $I\bar{1}$ or $P\bar{1}$) is well ordered at most temperatures, but because mechanical Albite and Pericline twinning do not exchange the T_1 and T_2 positions, they do not destroy the ordering and hence should be relatively easy (although again atomic shuffles are necessary). For anorthite twinned on either the Albite or Pericline law, the sheared unit is effectively offset from the host unit by a factor of $c/2$; Starkey (1963) called these pseudotwins, but they are true twins in every sense.

The intermediate plagioclases are more complex. They consist of domains similar to albite ($C\bar{1}$), which presumably cannot twin at lower temperatures where ordered, and domains similar to anorthite ($I\bar{1}$), which presumably can twin. Thus, in general, at low temperatures where there is order on the domain scale, mechanical twinning should get easier as one goes from albite toward anorthite, although at high temperatures where there is complete disorder there may not be much difference (Starkey, 1967; see Fig. 9 in Ch. 2). However, exsolution is common in the intermediate plagioclases (Ch. 10), and it is expected to hinder the propagation of twins.

In both Albite and Pericline mechanical twinning, the movement of the upper atomic layers is toward the positive end of the *c* axis when viewed along the positive end of the *b* axis. The amount of shear on both laws is the same but small; for An_{55} the angle of shear is 7°50' (twice the obliquity) and the shear is 0.137; thus the maximum possible shortening of a sample due to complete twinning is only 7 percent (Borg and Heard, 1970). In general mechanical twinning on both laws should occur simultaneously, because the two twin glide planes are close to 90° apart for all low plagioclase between An_{25} and An_{100} and for all high plagioclase. Thus if one twin system has a high resolved shear stress, so will the other (Borg and Heard, 1970).

Both Albite and Pericline twins can also form by growth, and so there has been considerable discussion about criteria for identifying mechanical twins (e.g., Spry, 1969). Evidence for mechanical twinning includes very fine-scale polysynthetic twins, twins which taper and/or curve, and twins which are restricted to small portions of grains, being more numerous at grain boundaries and internal boundaries. In contrast, evidence for growth twinning includes broader and fewer twins per grain, twins which are straight and parallel-sided, and twins which cut across the entire grain, showing no relation in position to bending and fractures.

Experimental studies. There have been a number of experimental studies of mechanical Albite and Pericline twinning in plagioclases (Borg and Handin, 1966; Borg and Heard, 1967, 1969, 1970; Seifert and VerPloeg, 1977; Marshall and McLaren, 1977c). The results for albite and anorthite confirm predictions made on the basis of crystal structure and ordering considerations, but the results for the intermediate plagioclases are less clear.

Experiments show that low albite and peristerite cannot be mechanically twinned, either at room pressure and temperature (Mügge and Heide, 1931), or at temperatures up to 800°C and pressures up to 10 kbar (Borg and Heard, 1970). However, a sample of albite disordered prior to deformation showed abundant twinning at 800°C and 10 kbar, although it did not twin at 25°C and 10 kbar (Borg and Heard, 1970).

Anorthite can be mechanically twinned relatively easily; Mügge and Heide

(1931) produced twins at room temperature and pressure. Borg and Heard (1970) observed no twins in samples deformed at 25°C and 10 kbar, but observed abundant twins at 800°C and 10 kbar. TEM observations of the latter samples showed that the boundaries of the mechanical Pericline twins involved a fault vector of ½[001] (Marshall and McLaren, 1974), as predicted by Starkey (1963).

The situation for the intermediate plagioclases is far less clear. Borg and Heard (1969, 1970) observed that compositions from An_{30} to An_{77}, which initially had a low structural state, could not be mechanically twinned at temperatures less than 800°C; however, for deformation experiments at 800°C and 8-10 kbar, abundant twinning was observed (and confirmed by the TEM observations of Marshall and McLaren, 1977c). No disordering was observed to have occurred during these experiments. A sample of An_{60} of *high* structural state showed the best-developed, most regular twin lamellae. Seifert and VerPloeg (1977) found that for samples of low transitional An_{50} deformed at pressures of 5 to 17 kbar, mechanical twinning was common at temperatures ⩾800°C, with the frequency of twinning increasing with temperature. The frequency of mechanical twins exactly correlated with that of transformation to a high structural state, which was undoubtedly promoted by the water released by their talc confining medium at ⩾800°C (see Yund and Tullis, 1980).

It is difficult to know how to interpret these results. It appears that disordering of the intermediate plagioclases aids mechanical twinning, although it is not necessary, and that high temperatures (≥800°C) are necessary for twinning of samples of low structural state (at least for the fast experimental strain rates). Such thermal activation is usually associated with diffusion-controlled processes; these may indicate that diffusion is necessary to produce twins or pseudotwins in the $C\bar{1}$ and/or $I\bar{1}$* domains (e.g., Laves, 1974).

Water also appears to be a factor. Borg and Heard (1970) observed that a sample of An_{77} disordered by heating prior to deformation was twice as strong as its more ordered equivalent and showed somewhat *less* twinning. The heating probably removed the trace of water initially in the structure, so the observations would suggest that trace amounts of water aid mechanical twinning (as they are known to aid slip; e.g., Tullis and Yund, 1980). The abundant twinning noted by Seifert and VerPloeg (1977) at ⩾800°C may in part be due directly to the water made available to the samples at those temperatures. Obviously further experiments are necessary to separately test the effects of water and disordering on mechanical twinning of intermediate plagioclases.

The experimentally produced twins appear to have originated by several different mechanisms. Although many of them are directly due to the externally imposed differential stress, others have been nucleated by the stress fields of cracks (Marshall and McLaren, 1977c). Some of the twins may be due to stresses resulting from anisotropic thermal contraction (Yund, pers. comm., 1981); the thermal expansion ellipsoid for plagioclase has two major axes which increase and one which decreases in length with increasing temperature (Willaime *et al.*, 1974). Some of the twins appear to be elastic. Laves (1952a) and Starkey and Brown (1964) produced elastic twins (which disappeared upon removal of the stress) under the microscope in both anorthite and high albite. The TEM observations of Marshall and McLaren (1977c) show that in regions adjacent to residual twins, there are often two sets of microshear bands lying on the composition planes of Albite and Pericline twins, having the same shear direction as that for twinning but a shear angle of only 4'. They believe these to be the remnants of elastic twins, leaving a faint record for much the same reason that the passage of dislocations in plagioclase leaves behind a faint fault. Marshall and McLaren (1977c) believe that the experimental twins must grow by uniform shear, because they have never observed dislocations in the twin boundaries. In addition, where twins terminate in regions of perfect crystal, they taper to a point around which strain can be seen. It should be remembered, however, that twinning dislocations in plagioclase would be difficult to observe in TEM, because the short Burgers vector (<1 Å) would produce very weak contrast. Further TEM observations are needed to determine whether dislocations are ever involved in mechanical twinning of plagioclase.

Evidence from natural samples. There have been numerous observations of Albite and Pericline twins in naturally deformed plagioclase, but the significance of these observations is limited by errors in identifying the twin law and by uncertainties in identifying the mechanical or growth origin of twins (Smith, 1974a). For example, there are some reports of a tendency for Albite twinning to dominate in sodic plagioclase and Pericline twinning to dominate in calcic plagioclase (e.g., Turner, 1951; Crawford, 1966). However, for most plagioclase compositions both laws should be about equally stressed since the twin glide planes are close to 90° apart, and Vernon (1965) did observe equal numbers of both twins in mafic gneisses, for those twins identified as being mechanical in origin. Similarly, twinning has been reported as more common in coarse grains in metamorphic rocks, and less common in fine grains (e.g., Gorai, 1951; Turner, 1951). However, this correlation may reflect a difference between deformed original grains and fine recrystallized grains (Goode, 1978; Borges and White, 1980; Brown *et al.*, 1980; Brodie, 1981).

There are a number of observations (summarized by Turner, 1951; Smith, 1974a) indicating that mechanical twinning in metamorphic rocks is more common at higher grade; this is consistent with mechanical twinning being easier in disordered sodic and intermediate plagioclases. It has also bee noted (Turner, 1951) that twins in igneous rocks are frequently polysynthetic; this may be another indication that mechanical twinning is only possible at high temperatures where the structural state is disordered (Starkey, 1967).

There have been few detailed studies to determine whether or not twinning dislocations are present in twin boundaries. Concentrations of etch pits along twin boundaries have been noted by Lundstrom (1970) and Wegner *et al.* (1978), but it is unclear whether these can be interpreted as indicating dislocations (e.g., Christie *et al.*, 1980). White (1975) used TEM to examine mechanical twins in a naturally deformed oligoclase; he observed screw dislocations lying along the Albite twin planes, and found both Albite and Pericline twins which terminated within a grain at a dislocation. This is in contrast to the observations of experimentally produced twins. Further TEM observations of natural mechanical twins are necessary, to determine the frequency and character of twinning dislocations.

Mechanical twinning in potassic feldspars

Just as for plagioclase, all twins other than Albite and Pericline twins are reconstructive and thus unlikely to be produced mechanically. Disordered potassic feldspars should show no mechanical twinning because Albite and Pericline twins cannot occur in a monoclinic structure. Microcline should also show no mechanical Albite or Pericline twinning because it is similar to low albite in having Al exclusively in the $T_1 0$ sites. Anorthoclase should show easy mechanical twinning only as long as there is complete Al,Si disorder.

There have been no experimental studies designed to investigate mechanical twinning in potassic feldspars. The only extensive experimental deformation studies on potassic feldspars were done on sanidine single crystals, for the express purpose of avoiding twinning and studying slip (Willaime *et al.*, 1979). No twins of any sort were observed optically or with TEM in these deformed samples.

The only report of mechanical twinning in a naturally deformed potassic feldspar is that of Capedri (1973), who reported polysynthetic Baveno twinning in a perthitic microcline porphyroblast of variable structural state. The twins appeared to have a composition plane of (021), but the twinned material was too fine to analyze in any detail. Mechanical Baveno twinning would seem unlikely because it is highly reconstructive.

There have been numerous suggestions in the literature (summarized by

Smith, 1974b) that shearing stress is important for the formation of microcline, and various authors (e.g., Alling, 1921) have noted an association of twinning in microcline with proximity to fault or shear zones. However, it seems more likely that most such associations reflect the positive influence of water on the rate of ordering (Yund and Tullis, 1980) and that inversion twinning accompanies this ordering.

SUMMARY OF NATURAL DEFORMATION OF FELDSPAR

The preceding sections have summarized current knowledge about the active slip and mechanical twinning systems of feldspars. It is of interest to place these in context by considering what is known about other deformation mechanisms and the "style" of deformation of feldspars over the whole range of crustal conditions.

As for other crystalline solids, there are a number of distinct grain-scale deformation mechanisms operative in feldspars, each of which has a particular flow law (relation between strain rate and stress and temperature). When stressed at a particular set of conditions all these mechanisms will tend to be activated, but usually one will produce a much faster strain rate for the imposed stress and so will be dominant. At a different set of conditions (temperature, pressure, etc.) a different mechanism will be dominant. A deformation mechanism map shows the stress-temperature conditions where the different mechanisms are dominant; the boundaries between the different fields are where two mechanisms contribute equal strain rates (Stocker and Ashby, 1973). The maps for a given mineral will vary for different fluid conditions, grain sizes, etc., and for most minerals we do not presently have the data necessary to construct them very accurately. However, the general positions of the different fields are known quite well, and a preliminary version has been attempted for feldspar (Gorman, 1980).

Microcracking

Microcracking is the dominant deformation mechanism at low temperatures and high stresses. It is an important deformation mechanism in all feldspars, in part because the excellent cleavage makes crack initiation and propagation relatively easy, and in part because thermally activated deformation mechanisms are relatively difficult. At conditions where microcracking is the dominant mechanism for both quartz and feldspar, feldspar is actually much weaker than quartz (Tullis and Yund, 1977; Dell Angelo and Tullis, 1982). However, the transition to dominantly dislocation creep occurs at a lower temperature for quartz than it does for feldspar (Tullis and Yund, 1977); thus at low to moderate metamorphic grades, quartz (deforming by dislocation creep) is weaker than feldspar (deforming by microcracking). At these conditions, if the feldspar grains in the rock form a stress-supporting framework then they will be extensively fractured and rapidly reduced in size; the fragments may be strung out in the foliation in long tails. In contrast, if the feldspar grains in the rock are effectively surrounded by a weaker matrix (e.g., quartz and mica), the rock strain will be taken up largely by the matrix and the feldspars will remain as relatively undeformed "augen" or porphyroclasts. The stresses exerted on the feldspars by the deforming matrix usually cause some cracking, local mechanical twinning, or even slip (White, 1973); the extent of this deformation obviously will be greater for higher proportions of feldspar in the rock (e.g., Debat *et al.*, 1978).

Feldspar grains in metamorphic rocks of greenschist to lower amphibolite grade often show extension and/or or shear fractures, often on cleavage planes (e.g., Debat *et al.*, 1978) although not always (Bossiere and Vauchez, 1978; Andrews, 1983). Some of the extension fractures may initiate from thermal contraction on cooling; the thermal expansion ellipsoid for feldspar is very anisotropic. For potassic feldspars contraction cracks should be approximately normal to [100], and cracks of such orientation are seen in both undeformed and deformed granitic rocks (Wilhelm and Willaime, 1976). Other cracks in the feldspars of deformed rocks may be caused by differential stress concentrations at internal flaws or boundaries, or at grain boundaries due to tractions from flow in the adjacent ductile matrix (White *et al.*, 1980) or to impingement of other feldspar grains (Debat *et al.*, 1978). These fractures do not extend into the ductile matrix, but they tend to be filled with the matrix material, or with fine-grained quartz and/or mica and/or feldspar, or with fibrous quartz (Debat *et al.*, 1978). The feldspar fragments separate as boudins, if extension fractures, or with accompanying rotation to put the largest face parallel to the foliation, if shear fractures (e.g., Watts and Williams, 1979). The grain size of the feldspar is progressively reduced with increasing strain, down to a size in equilibrium with the applied stress (Bouillier, 1980; Mitra, 1978). Often the feldspar fragments assume a distinctly avoidal shape (e.g., Wakefield, 1977). There is some evidence that potassic feldspars undergo fracturing more readily than does plagioclase in the same rock (e.g., Bossiere and Vauchez, 1978).

Mechanical twinning

For most materials, the process of mechanical twinning operates at relatively low temperatures, between those for fracture and those for slip. However, for anorthoclase and plagioclase (except anorthite) it appears that twinning is only easy when the structure is disordered, which occurs at relatively high temperatures where slip is in fact competitive (e.g., White, 1975). Although mechanical twins in feldspars are an obvious, visible sign of plastic deformation, they can result from local stress concentrations and they only accomplish a very small strain. Nonetheless, analysis of twin orientations in a deformed rock may provide a useful indicator of the compression orientation (e.g., Lawrence, 1970).

Dislocation creep

With higher temperatures of deformation, there is a transition from microcracking to dislocation glide and climb as the dominant deformation mechanism. The temperature of this transition can only be accurately determined by using TEM observations, because some optical strain features such as kink bands and undulatory extinction can result from arrays of microcracks and micro-crush zones (e.g., Marshall and McLaren, 1977c; Tullis and Yund, 1977). However, steady state ductile flow is not possible until recovery and/or recrystallization are extensive, and these processes produce unmistakable optical evidence in the form of subgrains or recrystallized grains. However, some confusion has been caused by the fact that partially recrystallized feldspar appears somewhat different from partially recrystallized quartz. Quartz shows flattened original grains at lower temperatures, flattened grains with smaller and more equant recrystallized grains along their boundaries at intermediate temperatures, and a mosaic of equant recrystallized grains at higher temperatures. In feldspars recovery is more difficult; thus at lower temperatures slip can produce only small amounts of strain before work hardening makes further strain impossible, and the high dislocation densities produce local recrystallization by a nucleation or boundary migration mechanism. At higher temperatures where recovery is easy, subgrains are produced at low strain; with increasing strain they rotate and become recrystallized grains, without the original grain ever becoming highly flattened.

The fact that feldspar recrystallizes at such low grain strains, by one of these two mechanisms, is probably responsible for this texture having been frequently attributed to brittle "granulation" or cataclasis, especially in anorthosites. The different textures produced by cataclasis and recrystallization of anorthosite can be seen by comparing Macaudiere and Brown (1982) and Kehlenbeck (1972). Evidence for recrystallization as opposed to cataclasis includes the following features: (1) the small grains usually have a narrow range of grain size; (2) they usually meet at close to 120° triple junctions; (3) the boundary between the host and the small grains is highly irregular, often curved, and convex into the host; (4) the small grains often have a crystallographic preferred orientation related to that of the host; and (5) they often have a composition slightly different from that of the host.

It appears that naturally deformed feldspars undergo easy recovery and thus steady state dislocation creep at ⩾450°-500°C; this is an important change which allows basement rocks to become significantly weaker and more homogeneously deformed (Voll, 1976). However, it should be noted that even at high temperatures, the presence of a high fluid pressure can reduce the effective pressure to near zero and thus allow at least periodic brittle deformation; this could be important during prograde metamorphism as dehydration occurs (e.g., Norris and Henley, 1976). An added complication concerning the recrystallization of feldspars is that, unlike quartz, there is the possibility of chemical change. In cases where the host and recrystallized grains have a slight difference in composition, the presence of a chemical free energy term may slightly lower the temperature necessary for recrystallization. In cases where there is a large compositional difference, the process may be neomineralization rather than syntectonic recrystallization; this may weaken the feldspar at temperatures lower than those necessary for dislocation creep. In all cases where host and recrystallized grain differ in composition, it is important to distinguish whether the rock has remained isochemical (e.g., Brodie, 1981).

There are many reports in the literature that potassic feldspars which show more evidence of dislocation creep also show more ordering, more exsolution, and/or more myrmekite. This has been attributed by some (White, 1975; Vidal *et al.*, 1980) to enhanced diffusion associated with high dislocation densities or moving dislocations. An experimental study of disordering rates of albite did show a slight enhancement due to concurrent plastic deformation over a narrow range of fast strain rates, but a much larger enhancement due to addition of trace amounts of water (Yund and Tullis, 1980). A further experimental study measured the effect of a high (static) dislocation density on the diffusion of oxygen in albite and found less than an order of magnitude enhancement (Yund *et al.*, 1981). Thus it would appear that the main factor responsible for the enhanced ordering, exsolution, etc. in feldspars of deformed rocks may be the introduction of water which accompanies the deformation.

Diffusion creep

The deformation mechanism of diffusion creep accomplishes a shape change by the solid state diffusion of atoms away from the highest compressive stress and the accompanying diffusion of vacancies toward it. If the diffusion occurs within the volume of the grains it is termed Nabarro-Herring creep; if it occurs along the grain boundaries it is termed Coble creep. Diffusion creep is more important at high temperatures and fine grain sizes. However, Nabarro-Herring creep has not been demonstrated to be an important deformation mechanism for any silicate under any set of crustal conditions, probably due to the very slow diffusion rate of Al,Si (see Chapter 8). Dry Coble creep is also very slow in silicates, but if there is a grain boundary fluid phase present (as there generally is during metamorphism) then the geometrically equivalent mechanism of pressure solution may be important.

Pressure solution involves the dissolution of a mineral across higher stress faces and precipitation on lower stress faces -- either the lower stress faces of that same mineral grain, or other low stress regions such as the "pressure shadow" of rigid insoluble grains or extension cracks. Pressure solution is an important deformation mechanism for quartz and calcite, at relatively low temperatures when there is a grain boundary fluid phase present. However, feldspars have a relatively low solubility and are only occasionally observed to undergo pressure solution (e.g., Beach, 1982).

Grain boundary sliding

A final deformation mechanism, which may be of some importance in feldspars, is grain boundary sliding. This involves the relative movement of grains (neighbor-switching) without any loss of cohesion; it requires either diffusion or dislocation motion as an accommodating process, just as dislocation glide requires climb or cross slip. This deformation mechanism has a yield strength which is inversely dependent on grain size (for dislocation creep there is no grain size dependence); it tends to be important at high temperatures for small grain sizes, and may produce a macroscopic "superplasticity" (see well-documented case for calcite studied by Schmid *et al.*, 1977). It has been postulated that a decrease in grain size due to recrystallization may allow a switch to grain boundary sliding as the dominant deformation mechanism, with a corresponding strain softening which could be important for the generation of mylonites or ductile shear zones (e.g., White *et al.*, 1980).

Feldspars are particularly susceptible to grain size reduction due to microcracking and fracturing and to syntectonic recrystallization. Furthermore, for a given stress their equilibrium recrystallized grain size is a factor of 3 to 5 smaller than that of quartz (Etheridge and Wilkie, 1981; Christie and Ord, 1980). Finally, the possibility of a chemical change accompanying recrystallization may sometimes still further reduce the size of the recrystallized grains.

All these factors would enhance the contribution of grain boundary sliding. Texturally, the operation of this mechanism is hard to prove, but it is indicated when the grain size is very fine (⩽10 μm), the grains have no crystallographic preferred orientation and no internal strain features, and the rock itself shows evidence of high strain and great ductility. Evidence for superplastic behavior of feldspar has been reported by Bouillier and Gueguin (1975) for a mylonite zone in an anorthosite, and by Allison *et al.* (1979) for a mylonite zone in a granite.

Summary

At near surface conditions feldspar is weaker than quartz due to its easier fracturing, but at low metamorphic grades (⩾300°C) quartz is weaker and shows complete syntectonic recrystallization while feldspar remains strong and brittle. Due to their great strength and low solubility, the feldspar grains in such rocks remain relatively undeformed, unless they constitute a major fraction of the rock and form a stress-supporting framework. However, rotations due to their inequant shape may provide useful indicators of the rotational strain component. At higher metamorphic grades (⩾450°-500°C) feldspars are able to undergo dislocation glide and climb more easily, and become much weaker, although still stronger than quartz. Fluids are very important here, for allowing hydrolytic weakening and promoting chemical changes. Feldspars recrystallize to a much finer grain size than does quartz, and at relatively high temperatures this may allow superplasticity by a grain boundary sliding mechanism. Although the above general trends seem clear at this time, there are many details concerning the deformation of feldspars which remain to be studied. Such studies are potentially of great value, because the structural and chemical complexity of the feldspars means that more details of the deformation history may be preserved.

ACKNOWLEDGMENTS

I would like to thank R. Yund for helpful and stimulating discussions about feldspars over many years, as well as detailed comments on this paper. I also wish to thank A. MacLaren and C. Willaime for helpful comments on an early draft of the paper, and P.H. Ribbe for his help and encouragement at all stages.

APPENDIX

GUIDES TO INDEXING FELDSPAR POWDER PATTERNS

The following pages contain a collection of powder diffraction patterns and guides to indexing them, with accompanying edited contributions by D. B. Stewart, H. Kroll and -- at press time -- A. Blasi (Instituto di Mineralogia, Petrografia e Geochimica, Milano, Italy). The additional contributions of E. Eberhard (plagioclase indexing chart), H.-U. Bambauer and W. H. Bernotat (OR→LM indexing chart), and I. Y. Borg and D. K. Smith (calculated diffraction patterns of plagioclase and alkali feldspars) are gratefully acknowledged.

Indexing plagioclase powder patterns

Borg and Smith (1968; 1969a, p. 627f.) give calculated powder patterns from five crystal structure refinements of plagioclases, as listed in the table accompanying Figures A1-A5. All possible diffraction peaks and their calculated relative intensities are listed in both of these references. E. Eberhard (in Bambauer *et al.*, 1967) prepared an excellent indexing guide (Fig. A6) which gives the variation of the peak positions within the low plagioclase series as a function of their An content (expressed as the ratio Si/Al). It was seen from Figure 1 in Chapter 4 that intermediate and high plagioclases have lattice parameters similar to those of low plagioclases with larger An content, and thus their powder patterns are similar. Therefore, Figure A6 can be used with plagioclases of any composition and structural state. The following procedure is recommended: 2θ values of the (131) and $(1\bar{3}1)$ diffraction lines are plotted in Figure A6 to identify the Si/Al value which they correspond to. At this height on the Si/Al axis the appropriate indexing can then be read off.

Indexing alkali feldspar powder patterns

Calculated and experimentally observed powder patterns of selected natural potassic feldspars and heated high sanidine are reproduced in Figures A7 - A10. Borg and Smith (1969a,b) and Wright and Stewart (1968) should be consulted and closely followed in the task of indexing powder patterns of alkali feldspars, because not only is the effect of Na,K content great, but also many unheated natural specimens contain two phases (Or- and Ab-rich) and some may contain three (monoclinic *and* triclinic K-rich feldspar, plus Na-rich feldspar); see Stewart and Wright (1974) and the partial diffraction patterns in Figure A11.

The indexing chart in Figure A12 was provided in advance of publication by Bambauer and Bernotat. It represents variation of $(t_1o - t_1m)$ for Or_{96}, ranging

Figures A1 - A5. PLAGIOCLASES

Variety	Low Albite	High Albite	Oligoclase	Bytownite	Transitional Anorthite
Composition	$Ab_{98.5}An_{0.5}Or_1$	$Ab_{97.7}An_{0.7}Or_{1.6}$	$Ab_{69}An_{29}Or_2$	$Ab_{20}An_{80}$	$Ab_{0.9}An_{99.1}$
Source	Ramona, Calif.	Amelia, Va. (inverted from low form)	Mitchell Co., N. C.	St. Louis Co., Minnesota	Miyaké, Japan:
Reference	Ribbe, Megaw and Taylor, 1969.	Ribbe, Megaw and Taylor, 1969.	Colville & Ribbe, 1968	Fleet, Chandrasekhar & Megaw, 1966	Megaw, Kempster & Radoslovich, 1962.
a	8.138	8.149	8.169	8.178	8.1815
b Å	12.789	12.880	12.851	12.870	12.8733
c	7.156	7.106	7.124	14.187	14.776
α	94.33	93.37	93.63	93.50	93.21
β deg	116.57	116.30	116.40	115.90	115.835
γ	87.65	90.28	89.46	90.63	91.137
Space Group	$C\bar{1}$	$C\bar{1}$	$C\bar{1}$	$I\bar{1}$	$I\bar{1}$ ($P\bar{1}$)

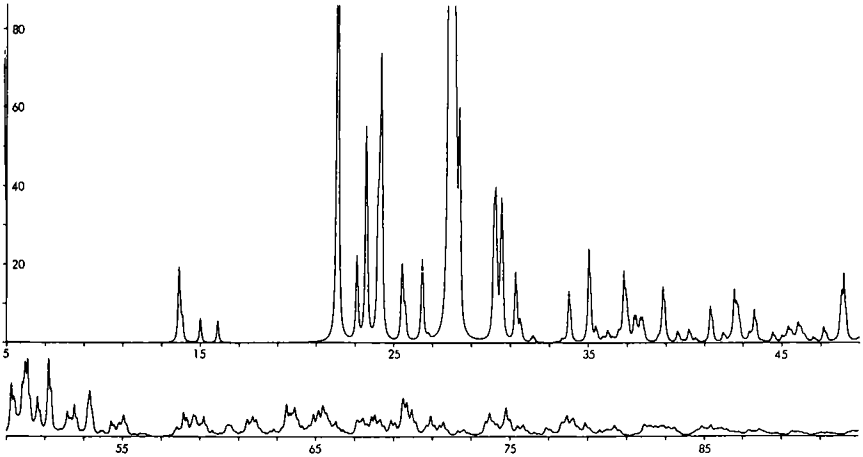

A1

Low Albite – An_0 — Ribbe, Megaw & Taylor, 1969
λ = CuKα Half width at 40°2θ: 0.11°2θ Plot scale I_{PK} (max) = 200

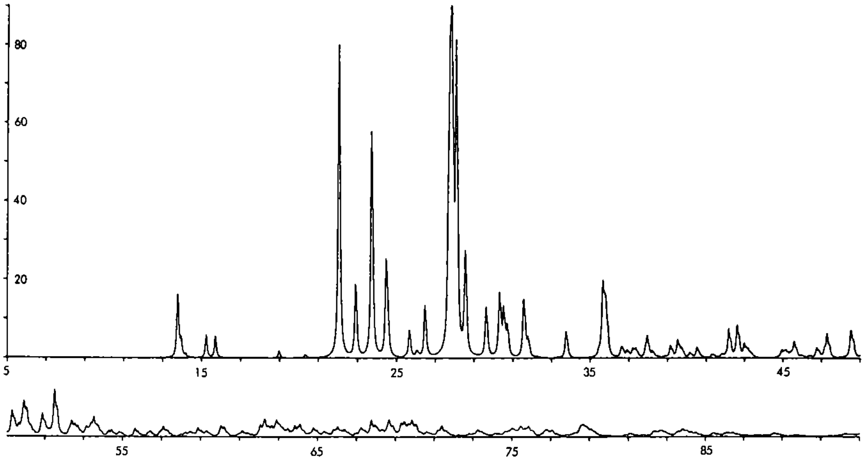

A2

High Albite – An_0 — Ribbe, Megaw, and Taylor, 1969
λ = CuKα Half width at 40°2θ: 0.11°2θ Plot scale I_{PK} (max) = 100

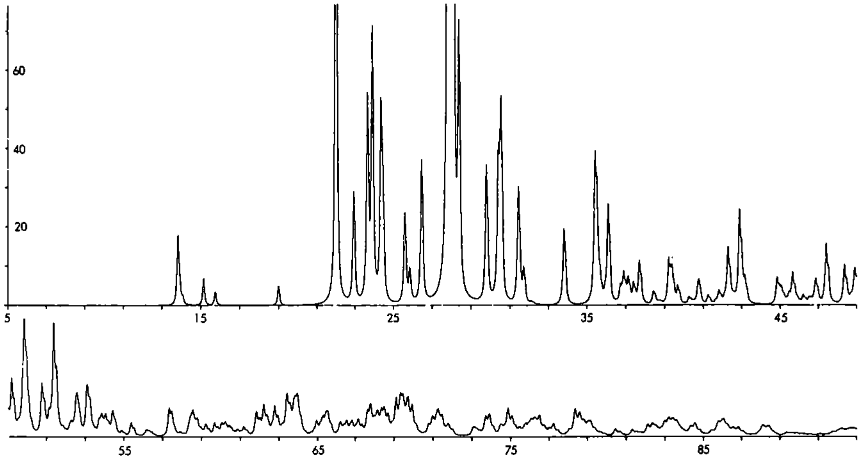

A3

Oligoclase — An_{29} — Colville and Ribbe, 1966, 1968

λ = CuKα Half width at 40°2θ: 0.11°2θ Plot scale I_{PK} (max) = 200

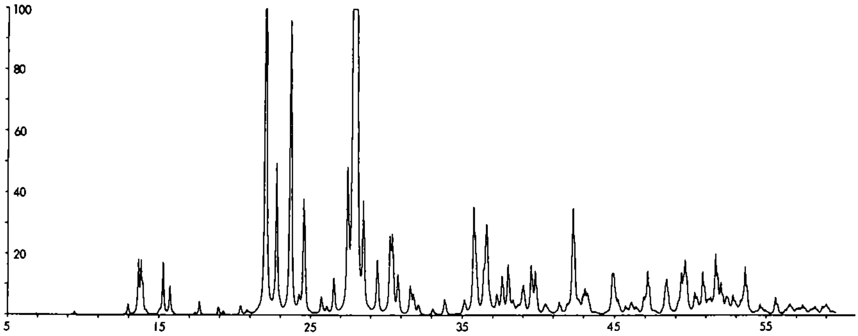

A4

Bytownite – An_{80} — Fleet, Chandrasekhar and Megaw, 1966

λ = CuKα Half width at 40°2θ: 0.11°2θ Plot scale I_{PK} (max) = 200

Figures A1 - A5 from Borg and Smith (1968).

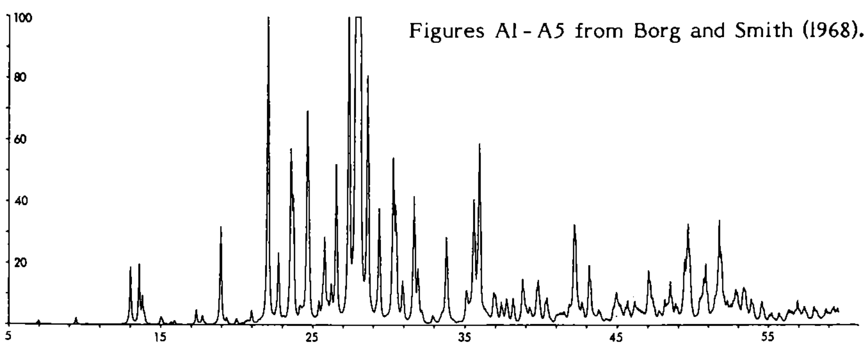

A5

Anorthite – An_{100} — Megaw, Kempster and Radoslovich, 1962

λ = CuKα Half width at 40°2θ: 0.11°2θ Plot scale I_{PK} (max) = 200

A6 2θ values (CuKα_1 radiation) of low plagioclases as a function of chemical composition (given as Si/Al ratio). Dashed lines indicate very weak powder lines in the range 13°-45° (2θ). Diagnostically important lines are drawn as heavy lines. From Bambauer, Eberhard and Viswanathan (1967). Continued on the opposite page → → →

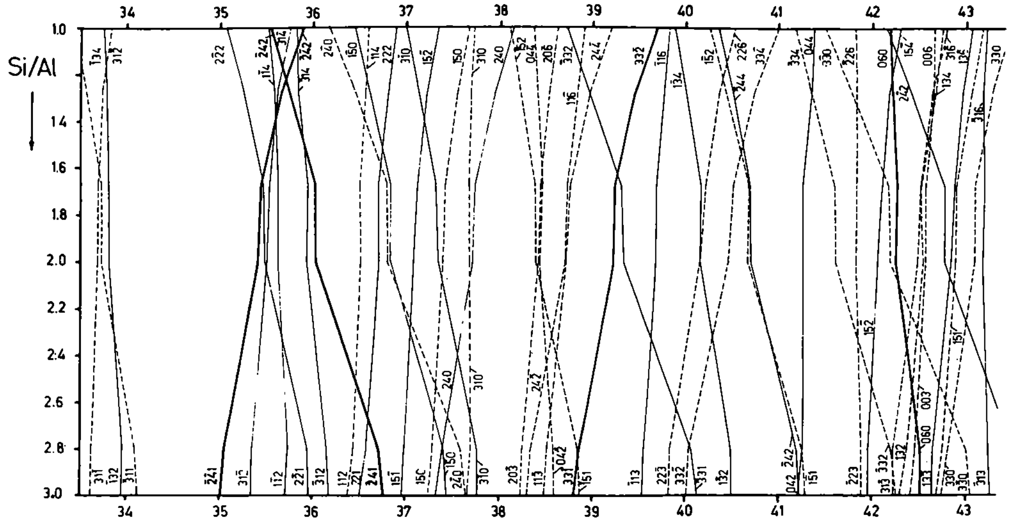

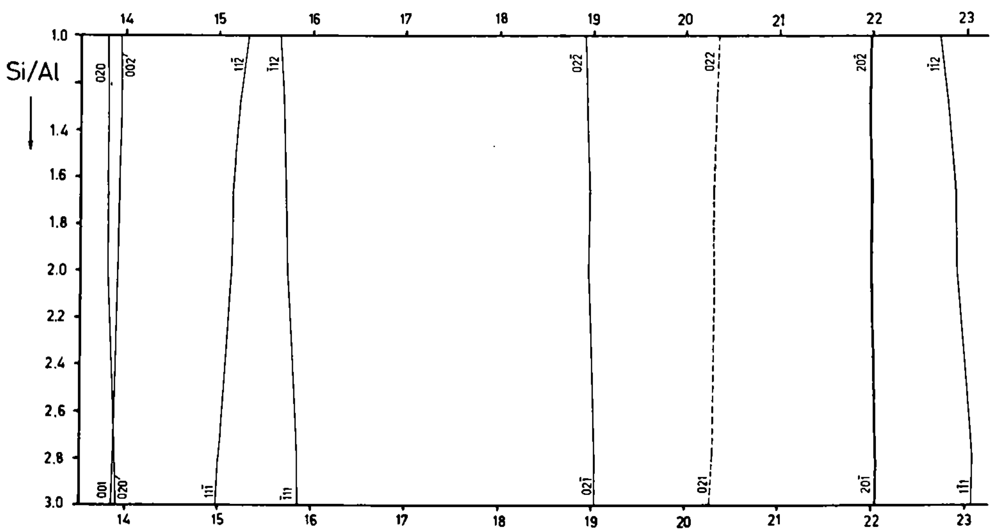

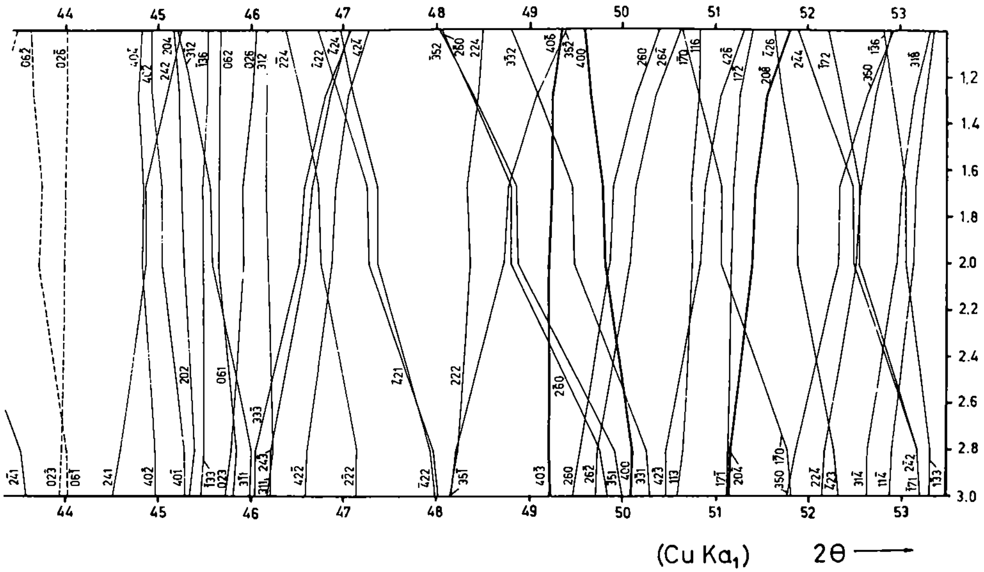
(Cu Ka1) 2θ

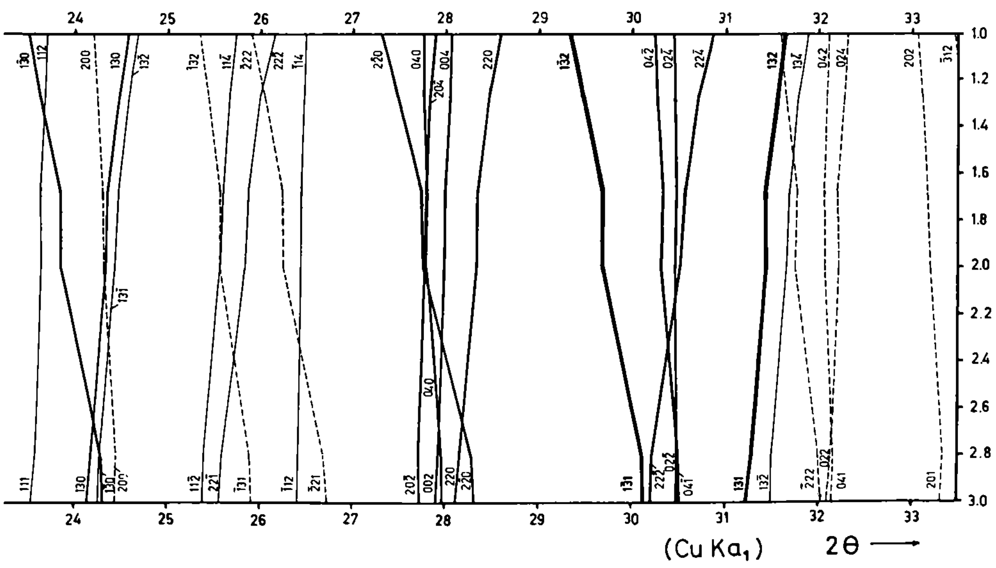
(Cu Ka1) 2θ

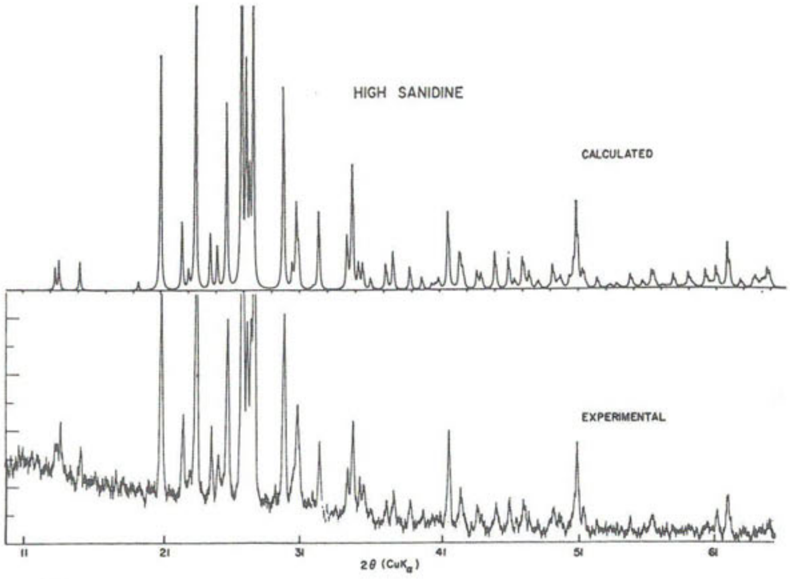

A7 Calculated and measured patterns for high sanidine, CuK_{α}. Or_{100} synthesized from glass, 800°C, 2 kbars, 1 week. $a=8.603$, $b=13.021$, $c=7.178$, $\beta=116°\ 0.6'$. Measurements and cell parameters by D. B. Stewart.

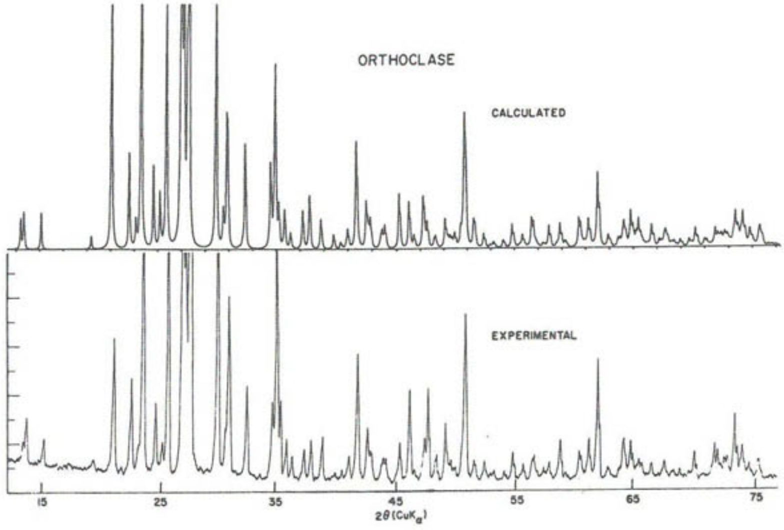

A8 Calculated and measured patterns for orthoclase, CuK_{α}. Spencer C equivalent from Bearpaw Mts., Mont. $a=8.561$, $b=12.995$, $c=7.194$, $\beta=115°\ 59.6'$ (Wright and Stewart, 1968). Measured pattern by D. B. Stewart.

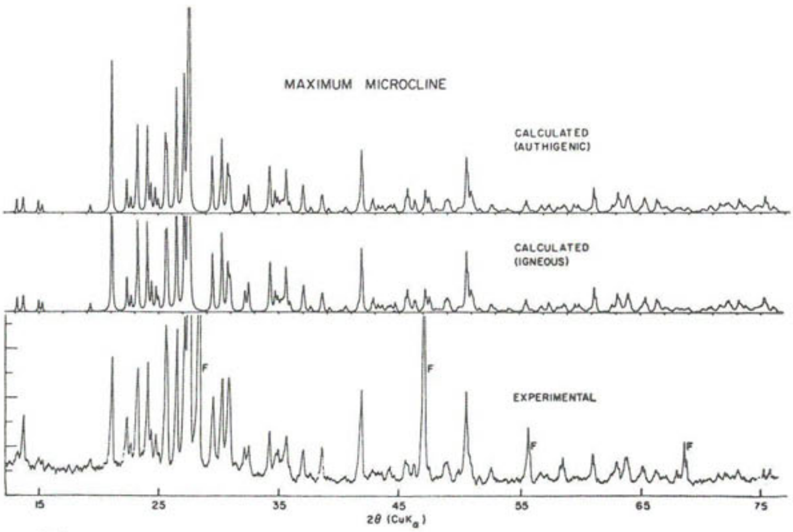

A 9 Calculated and measured patterns for maximum microcline, CuK_α. Blue Mtn., Ontario microcline, $a=8.578$, $b=12.961$, $c=7.221$, $\alpha=90°\ 39.9'$, $\beta=115°\ 58.7'$, $\gamma=87°\ 38.2'$. Measured pattern and cell parameters by D. B. Stewart. F = fluorite.

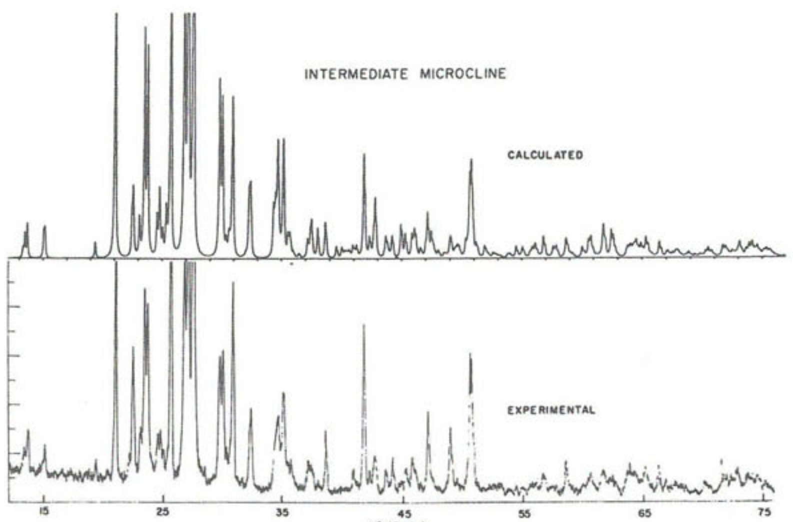

A 10 Calculated and measured patterns for intermediate microcline, CuK_α. Spencer U, $a=8.578$, $b=12.957$, $c=7.213$, $\alpha=90°\ 15.1'$, $\beta=116°\ 1.6'$, $\gamma=89°\ 13.5'$-(Wright and Stewart, 1968). Measured patterns by D. B. Stewart.

Figures A7 - A10 from Borg and Smith (1969a).

A11 Variation of line positions ($CuK\alpha_1$ radiation) in powder patterns of K-rich feldspars (Or_{96}) that range between unstrained monoclinic orthoclase ($t_1 = 0.4$) and triclinic low microcline ($t_1o = 1.0$). Only those lines have been included which are usually observed even in less well resolved powder patterns. Indexing of an unknown K-feldspar could be done by preparing a strip chart that is brought to coincidence with the indexing chart. From Bambauer and Bernotat (pers. comm., 1983). Continued on opposite page → → →

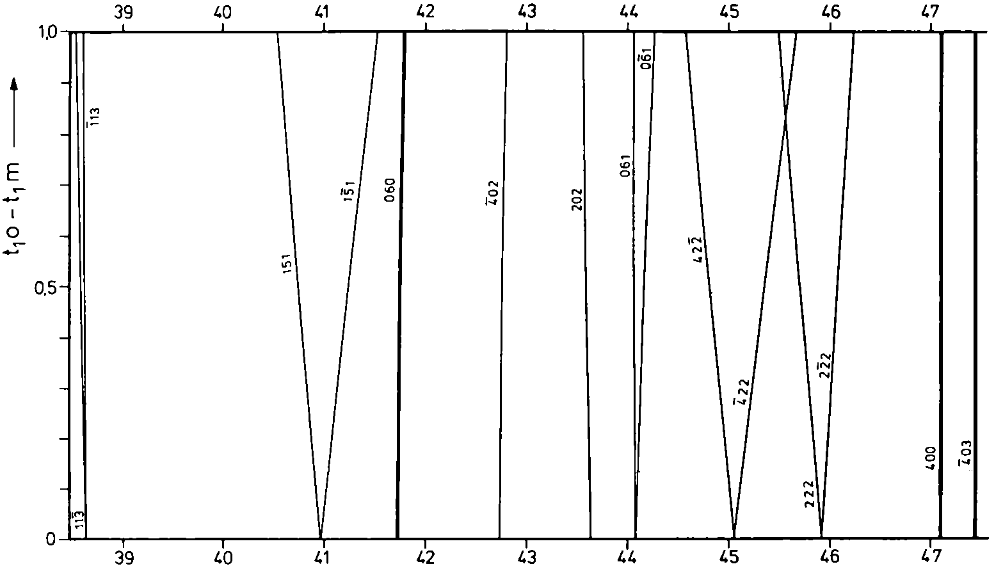

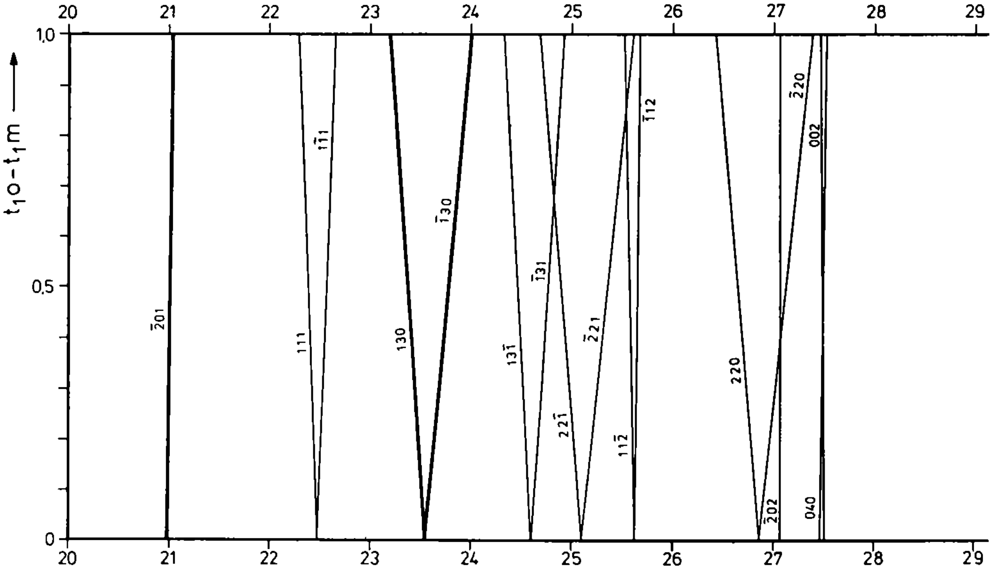

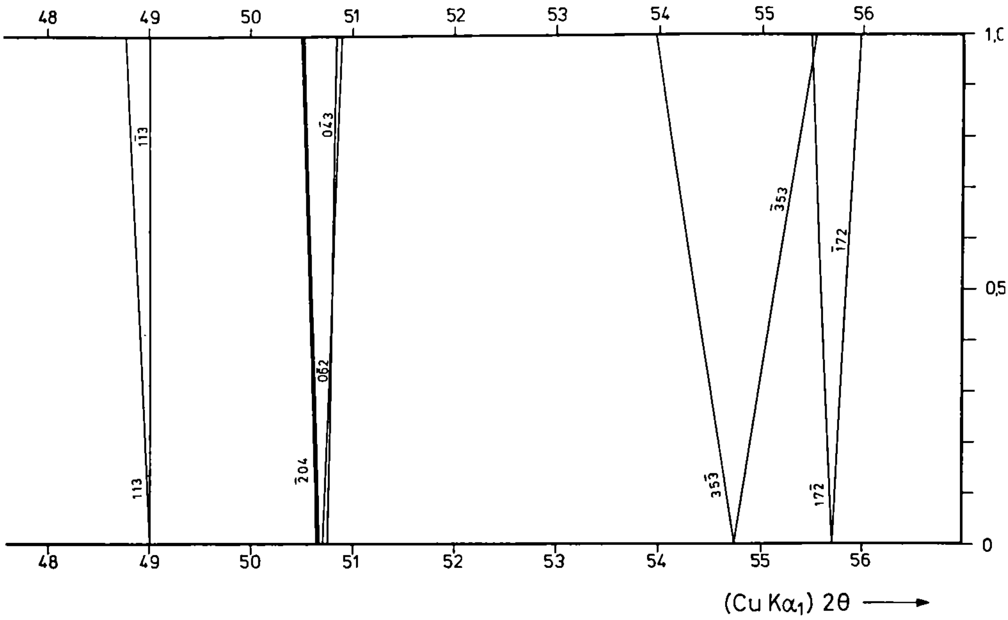

48 49 50 51 52 53 54 55 56
1,0
0,5
0
$1\bar{1}3$
113
$0\bar{4}3$
$0\bar{6}2$
$\bar{2}04$
$\bar{3}53$
$35\bar{3}$
$\bar{1}72$
$17\bar{2}$
(Cu Kα_1) 2θ

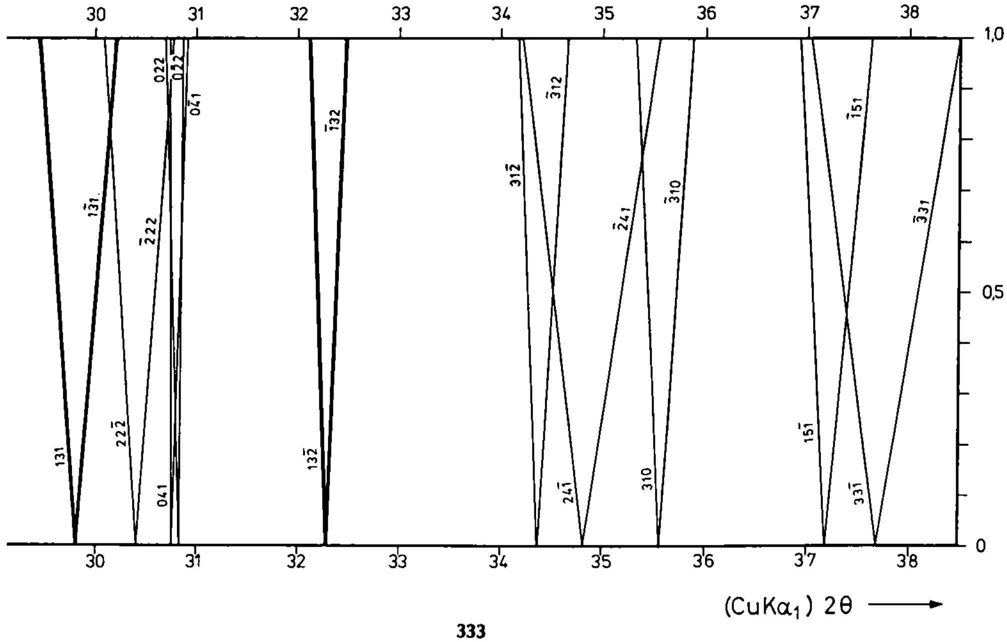

30 31 32 33 34 35 36 37 38
1,0
0,5
0
$1\bar{3}1$
131
$\bar{2}22$
$22\bar{2}$
022
$02\bar{2}$
$0\bar{4}1$
041
$\bar{1}32$
$13\bar{2}$
$31\bar{2}$
$\bar{3}12$
$\bar{2}41$
$24\bar{1}$
$\bar{3}10$
310
$\bar{1}51$
$15\bar{1}$
$\bar{3}31$
$33\bar{1}$
(Cu Kα_1) 2θ

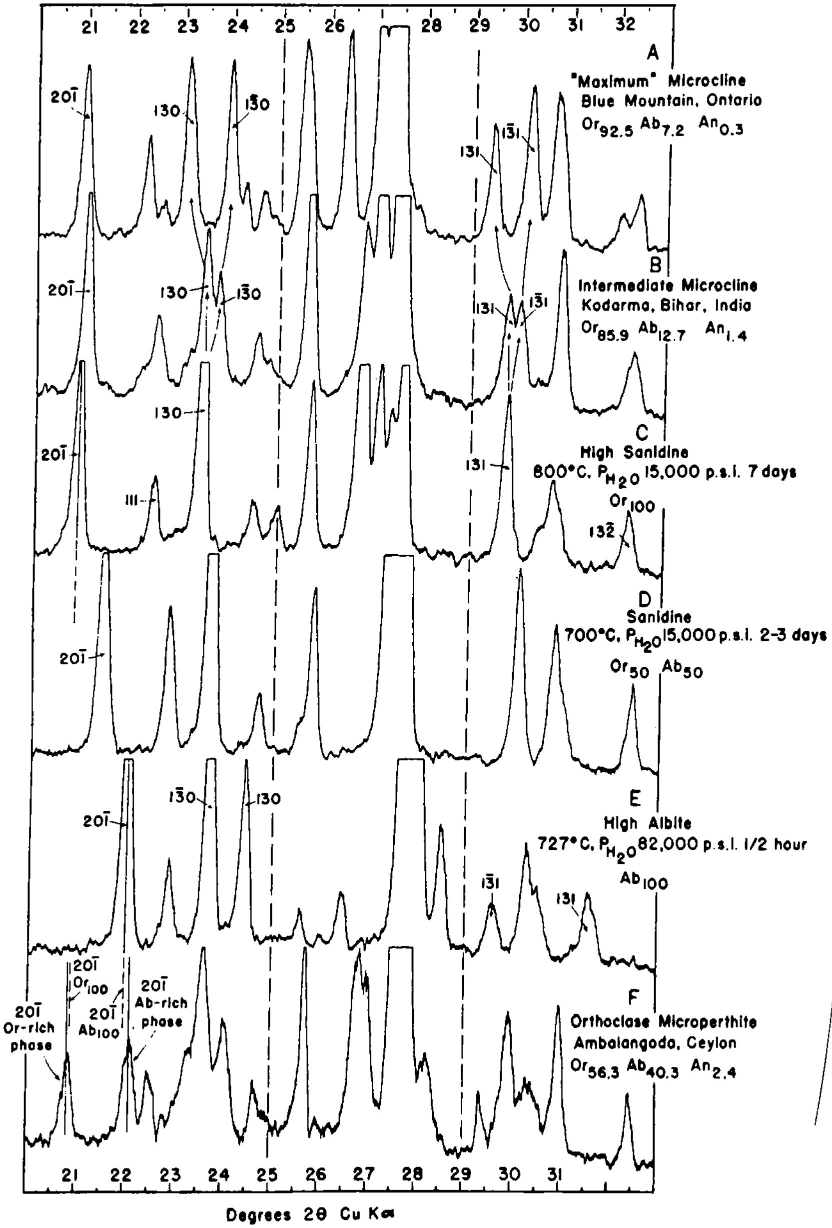

Figure A12. Powder patterns of alkali feldspars from D.B. Stewart.

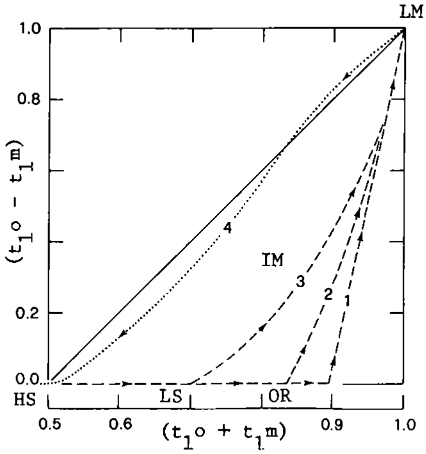

Figure A13. Several of the many possible "ordering paths" (see Ch. 3) representing the ordering of high sanidine (HS) to low microcline(LM). Paths 1, 2, and 3 are "two-step", as described in the text (and compare Fig. 1 in Ch. 2). Path 4 represents essentially "one-step" disordering as acheived by Blasi *et al.* (1983). Figure courtesy of A. Blasi.

from orthoclase with $(t_1o + t_1m) = 2t_1 = 0.8$, $(t_1o - t_1m) = 0.0$, to low microcline with $(t_1o + t_1m) = (t_1o - t_1m) = 1.0$, and is limited in application to specimens near $Or_{96\pm4}$ with Al,Si distributions in the given range.

A. Blasi kindly provided Figures A13 - A16 with a detailed text too voluminous to reproduce here, but which hopefully will be published elswhere. The editor (PHR) has abstracted his figure legends and paraphrased his manuscript as follows.

Unambiguous indexing of diffraction peaks in monoclinic and triclinic powder patterns is difficult. However, any of a number of least-squares programs for lattice parameter refinement (e.g., Burnham, 1962; Appleman and Evans, 1973) may be used with, say, 8 or 10 unambiguously indexed peaks to get "rough" cell dimensions. These programs give d-spacings for other reflections $hk\ell$, as requested, which may in turn be used to help index remaining observed peaks in the powder pattern. This should only be done with great caution, consulting such aids as the tables in Wright and Stewart (1968) and Figures A7 - A12 and A14 - A16. Numerous cell parameters of microclines reported in the literature have been incorrectly refined. This is evident from the fact that it is not uncommon to find $2\theta(131)$ calculated from those parameters to have higher values than $2\theta(1\bar{3}1)$! [See Fig. A12.]

Blasi has prepared indexing charts for K-rich feldspars that follow two of the ordering paths shown in Figure A13. Path 2 is more or less characteristic of those found in nature (see Figs. 12 and 13 in Ch. 3): it is a "two-step" path in which the K-feldspar, after initial crystallization, orders from high sanidine (HS) to low sanidine (LS), then orthoclase (OR), followed by inversion to intermediate microcline (IM) and finally to fully ordered low microcline (LM). The changes in 2θ values for numerous peaks in the powder pattern with $(t_1o + t_1m)$ are traced in Figue A14.

Figure A15 is a composite of partial diffraction patterns taken of a low microcline ($Or_{91}Ab_9$; see Blasi *et al.*, 1983 -- discussed in Ch. 3) which was dry-heated at 1050°C for various lengths of time and whose Al,Si distribution followed a nearly ideal "one-step" disordering pattern (path 4 in Fig. A13) from

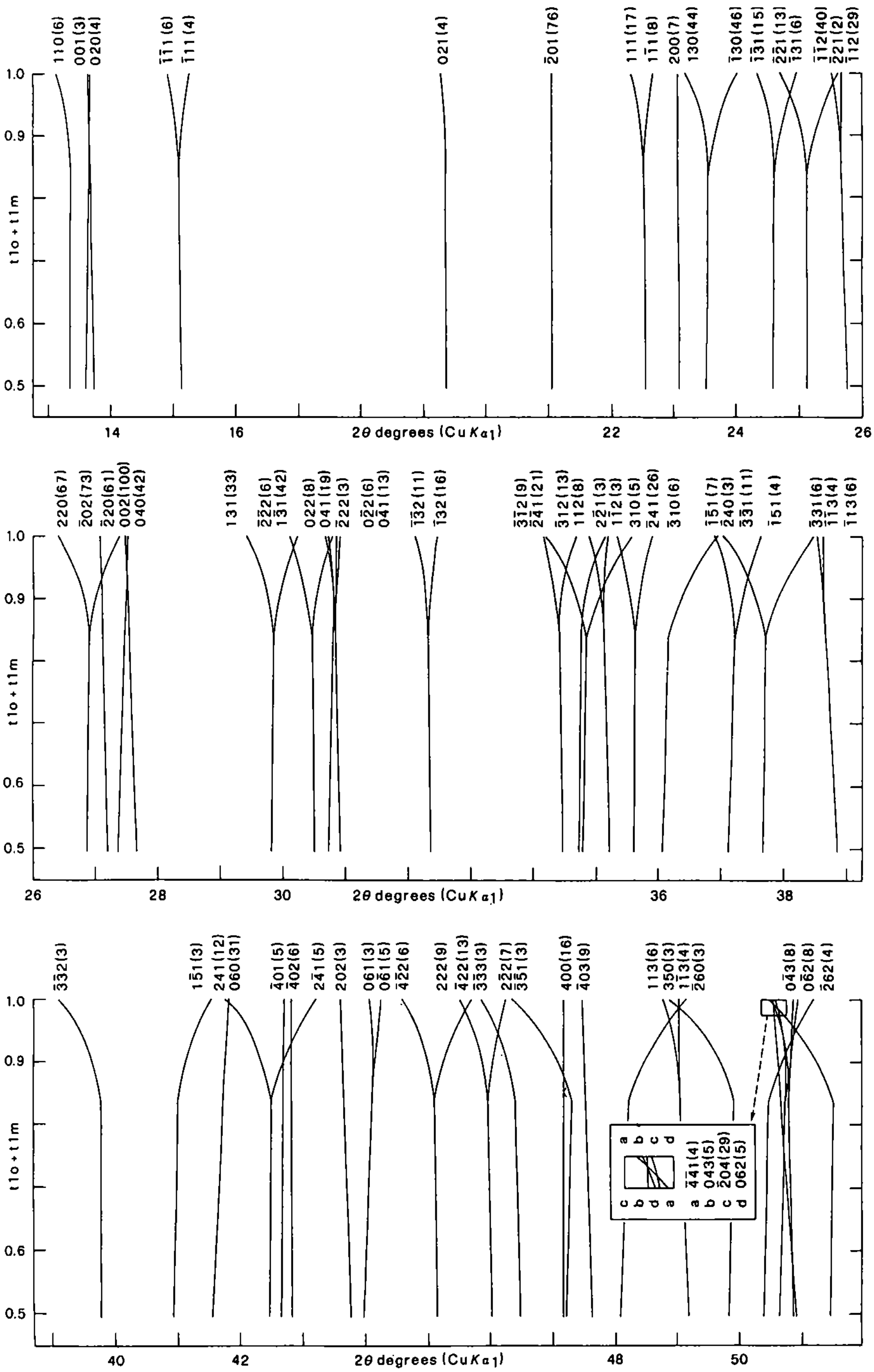

Figure A14. Blasi's indexing chart for "two-step" ordering of K-rich feldspar that follows path 2 in Figure A13.

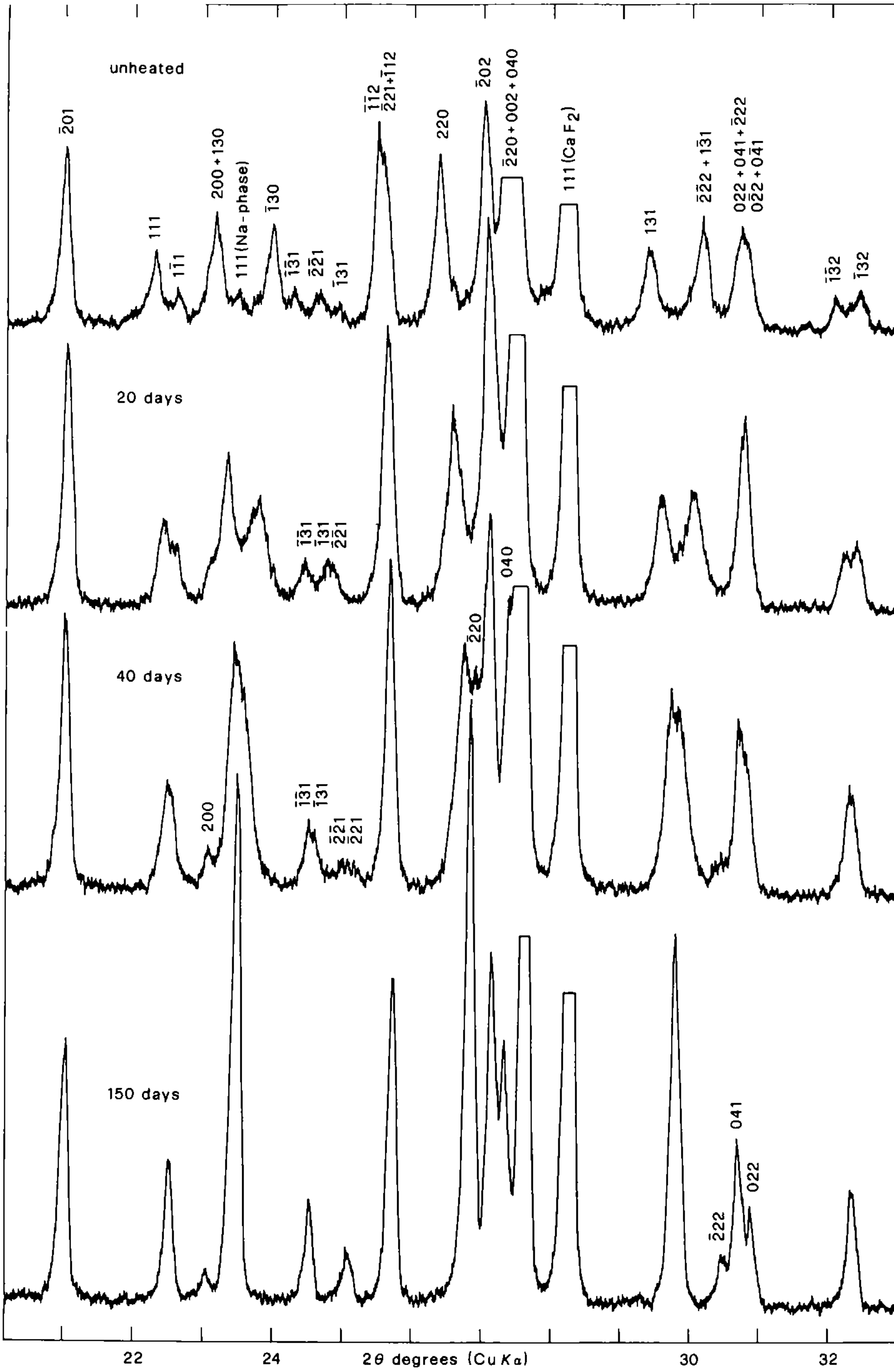

Figure A15. A composite of four partial powder diffraction patterns, starting from low microcline (top) to the intermediate microcline which is partially disordered after 20 days and 40 days and nearly completely disordered high sanidine (bottom) after 150 days. Courtesy of A. Blasi.

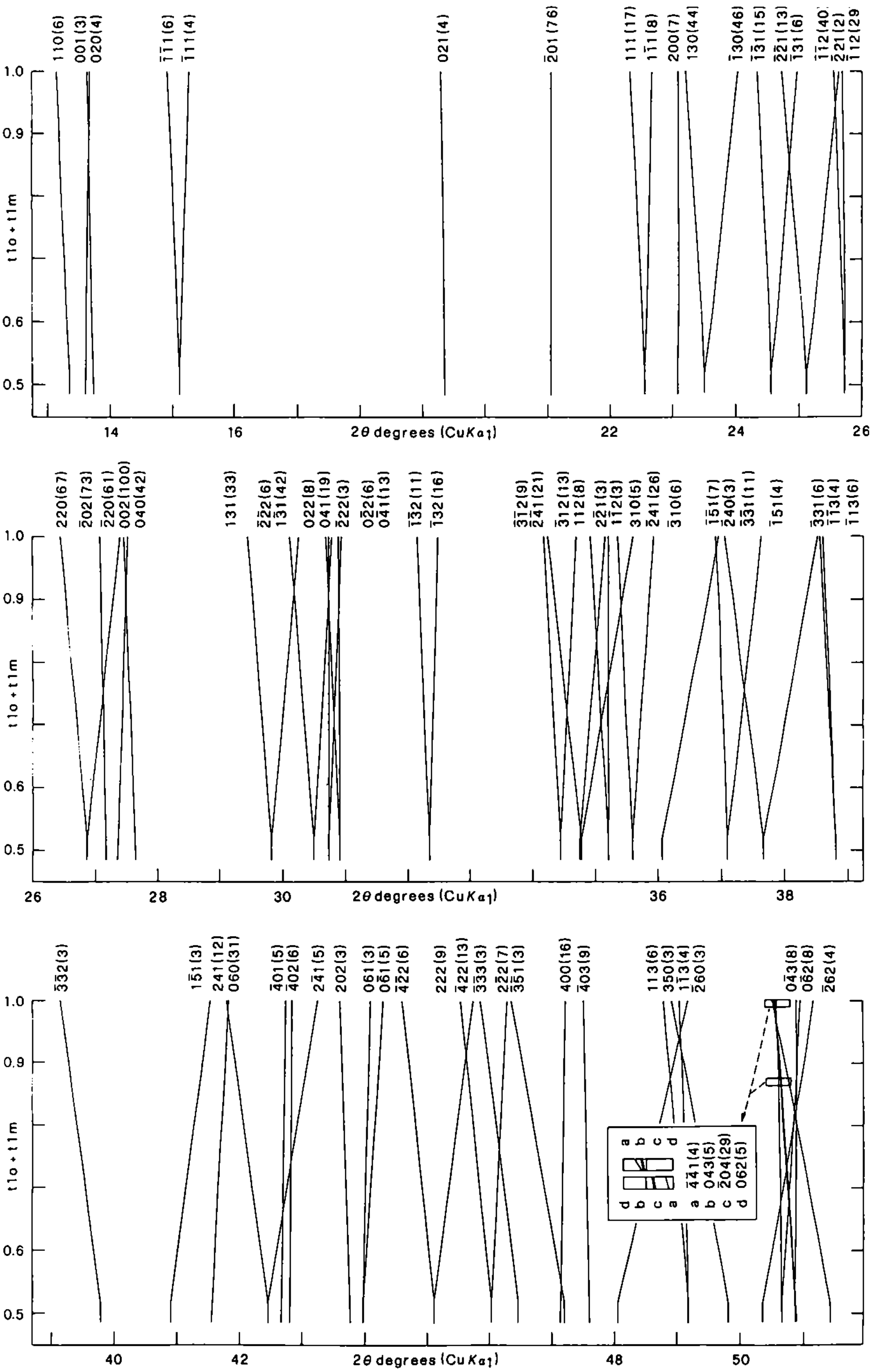

Figure A16. Indexing chart for microclines on the one-step disordering path from low microcline (top) to high sanidine (bottom), as a function of ($t_1o + t_1m$) from 1.0 to 0.5. All but the very bottom tips of the traces of the diffraction lines (in °2θ, CuKα radiation) are for triclinic K-feldspars. Prepared by A. Blasi.

LM to HS. The powder patterns of the ten heat-treated samples were used to prepare Figure A15, which represents the full range of (t_1o + t_1m) values for the triclinic K-feldspars.

Accuracy and precision of cell parameter refinements

(Table A-1 and the following text are taken from Stewart, 1975, p. St-2f.)

The cell parameters of alkali feldspars vary with composition, Al,Si order, and amount of coherence between unmixed phases. However, the total change when all of these causes are combined is only about 8 percent of the original values. It is obvious, therefore, that cell parameters must be determined accurately if meaningful results are to be obtained by comparison with standard graphs or determinative equations, and even qualitative comparisons usually require a precision of 0.1 percent or better.

The wide availability of large computers and the development of sophisticated least-squares refinement programs has made the determination of cell parameters from powder diffraction patterns for even triclinic minerals quite straightforward. Unfortunately, computer output is authoritative in appearance, even though it commonly contains many numbers lacking in significance. As a first step, the output should be rounded off at the decimal place corresponding to the first significant figure of the standard error of the refinement. The best refinements of the cell parameters of well crystallized triclinic feldspars seldom have a precision greater than one part in 10,000, though this precision can be more commonly achieved with monoclinic feldspars. It must be remembered that the standard error indicates the precision of only that specific refinement of the data. A smaller or larger set of data from the same measured powder pattern, or even an equal number but different combination of data from this pattern, will probably yield different cell parameters and different standard errors or precision (Table A-1). Another pattern measured from the same sample will most probably yield different cell parameters and associated standard errors. If an adequate number of patterns are measured and systematic errors are avoided (which is not easy to do), the probability will be increased that accurate cell parameters will be obtained by least-squares treatment of the array of individual cell refinements. If the array of individual cell parameter measurements is normally distributed about the mean, the standard error of the mean in 95 percent of cases will be twice the average standard error of the individual cell measurements. In general then, the accuracy of the measured cell parameters is twice as large as the precision of the

TABLE A-1. Successive refinements of parts of the same data set for Tiburon low albite.

Description of Lines used, all 2θ in CuKα1	a, Å	b, Å	c, Å	α, ° α*, °	β, °	γ, ° γ*, °	Vol., Å³	Standard error, °2θCuKα1
6, including $\bar{2}01$, $\bar{1}11$, $\bar{1}12$, 131, 060, $\bar{2}04$	8.131(0)	12.776(0)	7.156(0)	94.095(0) 86.455(0)	116.603 (.000)	87.930(0) 90.266(0)	662.99 (.00)	0.0000
8, 6 initial plus 2 below 16°2θ	8.133(6)	12.779(5)	7.157(2)	94.268(89) 86.389(99)	116.662 (.086)	87.675(125) 90.460(127)	662.82 (.81)	0.0175
10, 6 initial plus 4 below 26°2θ	8.133(5)	12.780(4)	7.157(2)	94.304(57) 86.355(47)	116.646 (.035)	87.664(71) 90.456(62)	662.95 (.40)	0.0138
12, 6 initial plus 6 below 34°2θ	8.133(5)	12.781(3)	7.157(1)	94.295(28) 86.359(30)	116.649 (.032)	87.677(54) 90.447(55)	663.03 (.37)	0.0131
14, 6 initial plus 8 below 36°2θ	8.134(3)	12.780(3)	7.157(1)	94.286(24) 86.354(28)	116.650 (.025)	87.704(37) 90.420(39)	663.10 (.31)	0.0124
14, all above 59°2θ	8.134(3)	12.786(3)	7.159(1)	94.286(38) 86.359(28)	116.595 (.017)	87.697(35) 90.432(26)	663.85 (.31)	0.0199
16, 6 initial, plus 10 below 36° 2θ	8.135(2)	12.781(3)	7.157(1)	94.287(22) 86.346(22)	116.644 (.017)	87.721(29) 90.401(29)	663.24 (.20)	0.0116
18, 6 initial plus 12 below 37°2θ	8.135(2)	12.781(2)	7.157(1)	94.286(18) 86.346(20)	116.644 (.015)	87.723(19) 90.400(21)	663.24 (.16)	0.0106
20, 6 initial plus 14 below 38°2θ	8.134(2)	12.784(2)	7.157(1)	94.287(23) 86.329(25)	116.647 (.019)	87.751(23) 90.366(25)	663.30 (.19)	0.0142
25, 6 initial plus 19 below 44° 2θ	8.135(2)	12.784(2)	7.157(1)	94.279(19) 86.339(19)	116.653 (.016)	87.754(16) 90.368(16)	663.34 (.15)	0.0127
30, 6 initial plus 24 below 49° 2θ	8.135(2)	12.784(2)	7.156(1)	94.261(17) 86.364(16)	116.623 (.014)	87.743(16) 90.392(15)	663.50 (.14)	0.0141
35, 6 initial plus 29 below 55° 2θ	8.135(1)	12.785(2)	7.157(1)	94.266(16) 86.364(15)	116.626 (.011)	87.732(14) 90.401(14)	663.60 (.12)	0.0138
40, 6 initial plus 34 below 60° 2θ	8.135(1)	12.785(2)	7.157(1)	94.276(14) 86.360(13)	116.614 (.010)	87.715(13) 90.415(12)	663.68 (.11)	0.0149
45, 6 initial plus 39 below 66° 2θ	8.135(1)	12.786(1)	7.158(1)	94.276(12) 86.368(11)	116.603 (.009)	87.702(12) 90.431(11)	663.79 (.10)	0.0151
50, 6 initial plus 44 below 69° 2θ	8.134(1)	12.786(1)	7.157(1)	94.270(12) 86.370(10)	116.594 (.008)	87.712(12) 90.424(10)	663.71 (.10)	0.0157
57, 6 initial plus 51 below 75° 2θ	8.134(1)	12.786(1)	7.158(1)	94.280(10) 86.362(9)	116.600 (.007)	87.703(10) 90.428(9)	663.82 (.09)	0.0163

individual refinements. In practice, however, it is the latter that is usually published, and on which most determinative curves are based.

It is necessary to be careful and not be tempted to overinterpret cell parameter data even for unusually homogeneous and well-crystallized samples. Natural samples typically consist of an array of structural states with a range of cell parameters, as well as being more or less heterogeneous in composition, and possibly may even constitute several feldspar phases that differ in coherence to one another. Although complexities may ultimately tell us much about the history of a sample when studied by appropriate methods, they may also boggle interpretation by such a simple technique as the powder diffraction method. This technique is biased toward the strongest diffraction lines and may reflect a spurious average.

REFERENCES

References from Chapter 12 are listed with trace elements in square brackets [ ].

Aaronson, H.I., G.W. Lorimer, P.E. Champness and E.T.C. Spooner (1974) On differences between phase transformations (exsolution) in metals and silicates. Chem. Geol. 14, 75-80.

Adlhart, W., F. Frey and H. Jagodzinski (1980a) X-ray and neutron investigations of the $P\bar{1}$-$I\bar{1}$ transition in pure anorthite. Acta Crystallogr. A36, 450-460.

Adlhart, W., F. Frey, and H. Jagodzinski (1980b) X-ray and neutron investigations of the $P\bar{1}$-$I\bar{1}$ transition in anorthite with low albite content. Acta Crystallogr. A36, 461-470.

Adlhart, W., F. Frey, and C. Zeyen (1981) Dynamic origin of order phenomena in feldspars (anorthite). Naturwiss. 68, 372-373.

Afonina, G.G., V.M. Makagon, B.M. Shmakin, M.P. Glebov, and A.I. Makrygin (1979) Effects of rubidium and cesium on the structural states of potash feldspars from rare-metal pegmatites. Int'l Geol. Rev. 21, 597-604. [Na K Rb Cs]

Akizuki, M. (1972) Electron microscope invesgitation of microcline twinning. Am. Mineral. 57, 797-808.

Alexandrov, K.S. (1958) Determination of the elasticity moduli of monoclinic crystals by the ultrasonic pulse method. Kristallografiya 3, 623-626 (in Russian).

Alexandrov, K.S. and T.V. Ryzhova (1962) Elastic properties of rock-forming minerals: III. Feldspars. Akademiia Nauk SSSR, Bull., Geophys. Ser., No. 7, 129-131 (pp. 186-189 in Russian).

Alling, H.L. (1921) The mineralogy of the feldspars. J. Geol. 29, 193-394.

Allison, I., R.L. Barnett and R. Kerrich (1979) Superplastic flow and changes in crystal chemistry in feldspars. Tectonophysics 53, T41-T46.

Allmann, R. (1975) Beziehungen zwischen Bindungslangen und Bindungsstrarken in Oxidstrukturen. Monatsh. Chemie 106, 779-793.

Andersen, O. (1915) On adverturine feldspar. Am. J. Sci. 40, 351-399.

Andersen, O. (1917) Adventurine labradorite from California. Am. Mineral. 2, pp. 91.

Anderson, A.T., Jr. (1966) Mineralogy of the Labrieville anorthosite, Quebec. Am. Mineral. 51, 1671-1711.

Anderson, T.F. and R.B. Kasper (1975) Oxygen self-diffusion in albite under hydrothermal conditions. Trans. Am. Geophys. Union 56, 459.

Andrews, J.R. (1983) Brittle-ductile feldspar shape fabrics in deformed quartzo-feldspathic rocks. J. Struc. Geol. (in press).

Annersten, H. (1976) New Mössbauer data on iron in potash feldspar. N. Jahrb. Mineral. Monatsh. 337-343.

Antipin, V.S., Z.I. Petrova, and M.I. Kuz'min (1975) Alkali feldspars from granitic rocks of different origin. Geochem. Int'l 12, 28-38. [Li Na K Ca Rb Sr Ba Tl Pb]

Appleman, D.E. and H.T. Evans, Jr. (1973) Job 9214: Indexing and least-squares refinement of powder diffraction data. U.S. Geol. Survey, Computer Contrib. 20, 67 pp. (NTIS Doc. PB2-16188)

Appleman, D.E., H.-U. Nissen, D.B. Stewart, J.R. Clark, E. Dowty and J.S. Huebner (1971) Studies of lunar plagioclases, tridymite, and cristobalite. Proc. 2nd Lunar Sci. Conf. 117-133.

Armbrustmacher, T.J. and N.G. Banks (1974) Clouded plagioclase in metadolerite dikes, southeastern Bighorn Mountains, Wyoming. Am. Mineral. 59, 656-665. [Li Mg Sc Ti V Cr Mn Fe Ni Co Cu Ga Rb Sr Cs Ba Zr Ag Pb]

Baadsgaard, H., J. Lipson, and R.E. Folinsbee (1961) The leakage of radiogenic argon from sanidine. Geochim. Cosmochim. Acta 25, 147-157.

Bachinski, S.W. and G. Müller (1971) Experimental determinations of the microcline-low albite solvus. J. Petrol. 12, 329-356.

Baier, E. and J. Pense (1957) Elektronenmikroskopische Untersuchungen an Labradoren. Naturwiss. 44, 110-111.

Bailey, A. (1971) Comparison of low-temperature with high-temperature diffusion of sodium in albite. Geochim. Cosmochim. Acta 35, 1073-1081.

Bailey, S.W. (1969) Refinement of an intermediate microcline structure. Am. Mineral. 54, 1540-1545.

Bambauer, H.-U. (1966) Feldspät-Familie $R_x^{I}R_{1-x}^{II}[Al_{2-x}Si_{2+x}O_8]$, $0 \geq x \geq 1$. In W.E. Troger, Optische Bestimmungen der gesteinsbildenden Minerale. Teil 2, Textband, Schweizerbart'sche Verlagsbuchhandlung: Stuttgart, pp. 645-762.

Bambauer, H.-U. and W.H. Bernotat (1982) The microcline/sanidine transformation isograd in metamorphic regions. I. Schweiz. Mineral. Petrogr. Mitt. 62, 185-230.

Bambauer, H.-U. and F. Laves (1960) Zum Adularproblem. I. Adular vom Val Casatscha: Mimetsicher Lamellenbau, Variation von Optik und Gitterkonstaten und ihre genetische Deutung. Schweiz. Mineral. Petrogr. Mitt. 40, 177-205.

Bambauer, H.-U., M. Corlett, E. Eberhard, and K. Viswanathan (1967) Diagrams for the determination of plagioclases using X-ray powder methods. (Part III of laboratory investigations on plagioclases.) Schweiz. Mineral. Petrogr. Mitt. 47, 333-350.

Bambauer, H.-U., E. Eberhard, and K. Viswanathan (1967) The lattice constants and related parameters of 'plagioclase (low).' Schwiez. Mineral. Petrogr. Mitt. 47/1, 351-364.

Bambauer, H.-U., H. Kroll, H.E. Nager, and H. Pentinghaus (1974) Feldspäte-Mischkristalle - Eine Übersicht. Bull. Soc. franc. Mineral. Cristallogr. 97, 313-345.

Bambauer, H.-U., F. Taborszky, and H.D. Trochim (1971) In, W.E. Troger, Ed., Optische Bestimmung der gesteinsbildenden Minerale (nach Teil 1. Bestimmungstabellen. 4. neu bearbeitete Auflage). Schweizerbart'sche Verlagsbuchhandlung: Stuttgart, pp. 645-762.

Bambauer, H.-U., F. Taborsky, and H.D. Trochim (1979) W.E. Troger's Optical Determination of Rock-Forming Minerals (English Edition). E. Schweizerbart'sche Verlagsbuchhandung: Stuttgart, 188 pp.

Barberi, F., G. Ferrara, R. Santacroce, M. Treuil, and M. Varet (1975) A transitional basalt-pantellerite sequence of fractional crystallization, the Boina Centre (Afar Rift, Ethiopia). J. Petrol. 16, 22-56. [Sc Cr Co Sr Rb Ba REE]

Beach, A. (1973) The mineralogy of high-temperature shear zones at Scourie, N.W. Scotland. J. Petrol. 14, 231-248.

Beach, A. (1982) Deformation mechanisms in some cover thrust sheets from the external French Alps. J. Struc. Geol. 4, 137-149.

Beaty, D.W. and A.L. Albee (1980) Silica solid solution and zoning in natural plagioclase. Am. Mineral. 65, 63-74. [Na Mg Al Si K Ca Ti Fe Ba]

Bell, P.M. and H.K. Mao (1973) Optical and chemical analysis of iron in Luna 20 plagioclase. Geochim. Cosmochim. Acta 37, 755-759.

Bell, P.M. and H.K. Mao (1973a) An analytical study of iron in plagioclase from Apollo 16 soils 64501, 64502, and 64802; Apollo 16 rock 66095; and Apollo 15 rock 15475. Carnegie Inst. Washington Year Book 72, 643-645.

Bell, P.M. and H.K. Mao (1973b) Measurements of the polarized crystal-field spectra of ferrous and ferric iron in seven terrestrial plagioclases. Carnegie Inst. Washington Year Book 72, 574-576. [Mg Ti Cr Mn Fe Ni]

Berking, B. (1976) Die Verfeinerung der Kristallstruktur eines lunaren Plagioklases An_{90}. Z. Kristallogr. 144, 189-197.

Bernotat, W.H. (1982) Ein neues Maß fur die Verzerrung der Kristallgitters in entmischten Alkalifeldspäten (Abstr.) Fortschr. Mineral. (in press).

Bernotat, W.H. and H.-U. Bambauer (1980) Die Mikroklin/Sanidin-Isograde in Aar- und Gotthard-Massiv. Eclogae Geol. Helv. 73, 559-561.

Bernotat, W.H. and H.-U. Bambauer (1982) The microcline/sanidine transformation isograd in metamorphic regions. 2. The region of Lepontine metamorphism, central Swiss Alps. Schweiz. Mineral. Petrogr. Mitt. 62, 231-244.

Bernotat, W.H. and G. Morteani (1982) The microcline/sanidine transformation isograd in metatmorphic regions: Western Tauern Window and Merano-Mules-Anterselva complex (Eastern Alps). Am. Mineral. 67, 43-53.

Bernotat, W.H., J.-P. Carron, and M. Lagache (1976) K/Rb and Rb/Cs partition between K-feldspars and biotites of Pre-Cambrian granites from Sinai. Tschermaks Mineral. Petrogr. Mitt. 23, 23-28.

Bettermann, P. and F. Liebau (1976) Lanthanum-calcium-sodium aluminosilicates $La_xCa_{8-2x}Na_x[Al_{16}Si_{16}O_{64}]$. Naturwiss. 61, 480.

Bhatty, M.S.Y., J.A. Gard, and F.P. Glasser (1970) Crystallization of anorthite from $CaO\text{-}Al_2O_3\text{-}SiO_2$ glasses. Mineral. Mag. 37, 780-789.

Bice, K.L. and S.C. Clement (1982) A study of the feldspars of the Montpelier andesine anorthosite, Hanover County, Virginia. Geol. Soc. Am. Abstracts with Programs 14, 5.

Blasi, A. (1972) "Iso-microcline" ed altre varianti strutturali del K-feldspato coexistenti in uno stesso cristallo nei graniti del Massiccio dell'Argentera. Rend. Soc. Ital. Mineral. Petrolog. 28, 375-411.

Blasi, A. (1977) Calculation of T-site occupancies in alkali feldspar from refined lattice constants. Mineral. Mag. 41, 525-526.

Blasi, A. (1978) Structural explanation for $\Delta(\alpha^*\gamma^*)$ from α^* vs. γ^* in alkali feldspars. Tschermaks Mineral. Petrogr. Mitt. 25, 47-56.

Blasi, A. (1980) Different behavior of $\Delta(bc)$ and $\Delta(b^*c^*)$ in alkali feldspar. N. Jahrb. Mineral. Abh. 138, 109-121.

Blasi, A. (1982) Appraisal of the Ferguson method and the linear model using $\Delta(bc)$, $\Delta(b^*c^*)$, $\Delta(\alpha\gamma)$, $\Delta(\alpha^*\gamma^*)$ to estimate tetrahedral Al-contents in alkali feldspars. Mineral. Mag. 46, 465-468.

Blasi, A. (1983) Inconsistencies of Jowhar's (1981) method for calculating lattice constants and T-site occupancies in alkali feldspar. Computers and Geosci. 9, in press.

Blasi, A. and C. Blasi De Pol (1977) Role and convenience of lattice elements for deriving Si,Al distribution in alkali feldspar. Rend. Soc. Ital. Mineral. Petrol. 33, 497-509.

Blasi, A. and C. Blasi De Pol (1980) Highly ordered triclinic K-feldspars from Mt. Pelago anatexites (Argentera Massif, Maritime Alps). Bull. Mineral. 103, 209-216.

Blasi, A., A. Brajkovic, C. De Pol Blasi, F. Forcella and R.F. Martin (1980) Contrasting feldspar mineralogy, textures and composition of Tertiary anorogenic and orogenic granites, Gilgit area, northwestern Pakistan. N. Jahrb. Mineral. Abh. 140, 1-16.

Blasi, A., A. Brajkovic and C. De Pol Blasi (1983) Dry-heating conversion of low microcline to high sanidine via a one-step disordering process. Abstr., N.A.T.O. Advanced Study Inst. on Feldspars and Feldspathoids, Rennes, France.

Blasi, A., C. De Pol Blasi and P.F. Zanazzi (1981) Structural study of a complex microperthite from anatexites at Mt. Caval, Argentera Massif, Maritime Alps. N. Jahrb. Mineral. Abh. 142, 71-90.

Blasi, A., A. Brajkovic, and C. De Pol Blasi (1983) Microcline overgrowth on amorouite from Pikes Peak Batholith, Colorado, USA Abstr. Proc. 3rd N.A.T.O. Advanced Study Inst. on Feldspars and Feldspathoids, Rennes, France.

Bloss, F.D. (1971) Crystallography and Crystal Chemistry. Holt, Rinehart, and Winston: New York, 543 pp.

Bloss, F.D. (1981) The Spindle Stage: Principles and Practice. Cambridge Univ. Press: Cambridge, 340 pp.

Bloss, F.D. and D. Riess (1973) Computer determination of 2V and indicatrix orientation from extinction data. Am. Mineral. 58, 1052-1061.

Bøggild, O.B. (1911) Über die Kristallform des Mikroklins. Z. Kristallogr. 48, 466-472.

Bøggild, O.B. (1924) On the labradorization of the feldspars. K. danske vidensk. selsk. Mat.-Fys. Meddel 6, 1-79.

Böhm, H. (1975) Interpretation of x-ray scattering patterns due to periodic structural fluctuations. I. The case of transverse modulation of positional parameters in primitive lattices. Acta Crystallogr. A31, 622-628.

Böhm, H. (1976) Interpretation of x-ray patterns due to modulation of positional parameters and of scattering density. Z. Kristallogr. 143, 56-66.

Bollman, W. and H.-U. Nissen (1968) A study of optimal phase boundaries: The case of exsolved alkali feldspars. Acta Crystallogr. A24, 546-557.

Bolton, H.C., L. A. Bursill, A.C. McLaren, and R.G. Turner (1966) On the origin of the colour of labradorite. Phys. Stat. Sol. 18, 221-230.

Bonin, B. and R.F. Martin (1974) Coexisting alkali feldspars in felsic members of the Cauro-Bastelica ring complex, Corsica. Lithos 7, 23-28.

Boone, G.M. (1969) Origin of clouded red feldspars: petrologic contrast in a granitic porphyry intrusion. Am. J. Sci. 267, 633-668.

Borg, I. and J. Handin (1966) Experimental deformation of crystalline rocks. Tectonophysics 3, 249-368.

Borg, I. and H.C. Heard (1967) Further studies on experimentally deformed plagioclase in rock deformation and the deformation mechanisms in torsion tests. Air Force Cambridge Res. Lab. Report, ARCRL-67-0308.

Borg, I. and H.C. Heard (1969) Mechanical twinning and slip in experimentally deformed plagioclases. Contrib. Mineral. Petrol. 23, 128-135.

Borg, I. and H.C. Heard (1970) Experimental deformation of plagioclases. In Paulitsch, Ed., Experimental and Natural Rock Deformation, Springer Verlag: New York, pp. 375-403.

Borg, I.Y. and D.K. Smith (1968) Calculated powder patterns. Part I. Five plagioclases. Am. Mineral. 53, 1709-1723.

Borg, I.Y. and D.K. Smith (1969a) Calculated X-ray powder patterns for silicate minerals. Geol. Soc. Am. Memoir 122, 896 pp.

Borg, I.Y. and D.K. Smith (1969b) Calculated powder patterns. Part II. Six potassium feldspars and barium feldspar. Am. Mineral. 54, 163-181.

Borges, F.S. and S.H. White (1980) Microstructural and chemical studies of sheared anorthosites, Roneval, South Harris. J. Struc. Geol. 2, 273-280.

Bossiere, G. and A. Vauchez (1978) Deformation naturelle par cisaillement d'un granite de Grande Kabylie occidentale (Algerie). Tectonophysics 51, 57-83.

Bouillier, A.M. (1980) A preliminary study on the behavior of brittle minerals in a ductile matrix: examples of zircons and feldspars. J. Struc. Geol. 2, 211-217.

Bouillier, A.M. and Y. Gueguen (1975) SP-mylonites: origin of some mylonites by superplastic flow. Contrib. Mineral. Petrol. 50, 93-104.

Bowen, N.L. (1913) The melting phenomena of the plagioclase feldspars. Am. J. Sci. 35, 577-599.

Bown, M.G. and P. Gay (1958) The reciprocal lattice geometry of the plagioclase feldspar structures. Z. Kristallogr. 111, 1-14.

Boyd, F.R. and J.F. Schairer (1964) The system $MgSiO_3$-$CaMgSi_2O_6$. J. Petrol. 5, 275-309.

Brady, J.B. (1975) Reference frames and diffusion coefficients. Am. J. Sci. 275, 954-983.

Brady, J.B. and R.H. McCallister (1980) Diffusion kinetics of homogenization and coarsening of pigeonite lamellae in subcalcic diopsides. Geol. Soc. Am. Abstracts with Programs 12, 391.

Brady, J.B. and R.A. Yund (1981) Interdiffusion of K and Na in alkali feldspars. Geol. Soc. Am. Abstracts with Programs 13, 415.

Braun, E. (1974) Mikrosonderuntersuchungen von Saussuriten in Abhängigkeit vom Metamorphosegrad und vom geochemischem Milieu. Contrib. Mineral. Petrol. 46, 301-327. [Mg Ti Mn Fe]

Breithaupt, A. (1847) Vollstandiges Buch der Mineralogie III. Dresden und Leipzig.

Brodie, K.H. (1979) Variation in hornblende and plagioclase composition with deformation. Tectonophysics 78, 385-402.

Brodie, K.H. (1981) Variation in amphibole and plagioclase composition with deformation. Tectonophysics 78, 389-402.

Brown, B.E. (1962) Aluminum distribution in an igneous maximum microcline and the sanidine-microcline series. Norsk Geol. Tidsskr. 42/2, 25-36.

Brown, B.E. and S.W. Bailey (1964) The structure of maximum microcline. Acta Crystallogr. 17, 1391-1400.

Brown, F.F. and A.M. Pitchard (1969) The Mössbauer spectrum of iron orthoclase. Earth Planet. Sci. Lett. 5, 259-260.

Brown, G.E., G.V. Gibbs, and P.H. Ribbe (1969) The nature and variation in length of the Si-O and Al-O bonds in framework silicates. Am. Mineral. 54, 1044-1061.

Brown, G.E., W.C. Hamilton and C.T. Prewitt (1974) Neutron diffraction study of Al/Si ordering in a sanidine: a comparison with x-ray diffraction data. In W.S. MacKenzie and J. Zussman, Eds., The Feldspars. Manchester Univ. Press: Manchester, pp. 68-80.

Brown, I.D. and K.K. Wu (1976) Empirical parameters for calculating cation-oxygen bond valences. Acta Crystallogr. B32, 1957-1959.

Brown, W.L. (1962) Peristerite unmixing in the plagioclases and metamorphic facies series. Norsk Geol. Tidsskr. 42/2, 354-382.

Brown, W.L. and I. Parsons (1981) Towards a more practical two-feldspar geothermometer. Contrib. Mineral. Petrol. 76, 369-377.

Brown, W.L. and C. Willaime (1974) An explanation of exsoltuion orientations and residual strain in cryptoperthites. In, W.S. MacKenzie and J. Zussman, Eds., The Feldspars. Manchester University Press: Manchester, pp. 440-459.

Brown, W.L., W. Hoffmann, and F. Laves (1963) Über kontinuierliche und reversible Transformationen des Anorthits ($CaAl_2Si_2O_8$) zwischen 25 und 350°C. Naturwiss. 50, 221.

Brown, W.L., C. Willaime, and C. Guillemin (1972) Exsolution selon l'association diagonale dans une cryptoperthite. Etude par microscopie electronique et diffraction des rayons X. Bull. Soc. franc. Mineral. Cristallogr. 95, 429-436.

Brown, W.L., J. Macaudiere, D. Ohnenstetter, and M. Ohnenstetter (1980) Ductile shear zones in a meta-anorthosite from Harris, Scotland: textural and compositional changes in plagioclase. J. Struc. Geol. 2, 281-287.

Bruno, E. and A. Facchinelli (1974) Correlations between the unit cell dimensions and the chemical and structural parameters in plagioclase and alkaline-earth feldspars. Bull. Soc. franc. Mineral. Cristallogr. 97, 313-345.

Bruno, E. and A. Facchinelli (1974) Experimental studies on anorthite crystallization along the join $CaAl_2Si_2O_8$-SiO_2. Bull. Soc. franc. Mineral. Cristallogr. 97, 422-432.

Bruno, E. and G. Gazzoni (1967) Richerche roentgenografiche su plagioclasi bytownitico-anortitici tra 15°C e 1300°C. Period. Mineral. (Roma) 36, 683-698.

Bruno, E. and H. Pentinghaus (1974) Substitution of cations in natural and synthetic feldspars. In, W.S. MacKenzie and J. Zussman, Eds., The Feldspars. Manchester University Press: Manchester, pp. 574-609.

Bruno, E., G. Chiari, and A. Facchinelli (1976) Anorthite quenched from 1530°C. I. Structure refinement. Acta Crystallogr. B32, 3270-3280.

Bryan, W.B. (1974) Fe,Mg relationships in sector-zoned submarine basalt plagioclase. Earth Planet. Sci. Lett. 24, 157-165. [Mg Ti Mn Fe]

Buerger, M.J. (1964) The Precession Method. John Wiley & Sons, Inc.: New York, 276 pp.

Burnham, C.W. (1962) Lattice constant refinement. Carnegie Inst. Washington Year Book 61, 132-135.

Burri, C., R.L. Parker, and E. Wenk (1967) Die optische Orientierung der Plagioklase - Unterlagen und Diagramme zur Plagioklas-bestimmung nach der Drehtische-methode. Birkhauser: Basel und Stuttgart, 334 pp.

Cahn, J.W. (1962) Coherent fluctuations and nucleation in isotropic solids. Acta Met. 10, 907-913.

Cahn, J.W. (1968) Spinodal decomposition. Trans. Metall. Soc. AIME 242, 166-180.

Cahn, R.W. (1954) Twinned crystals. Advances in Physics 3, 363-445.

Capedri, S. (1973) First evidence of secondary glide twinning in K feldspars. Tschermaks Mineral. Petrogr. Mitt. 19, 51-59.

Carmichael, I.S.E. (1967) The mineralogy and petrology of the volcanic rocks from the Leucite Hills, Wyoming. Contrib. Mineral. Petrol. 15, 24-66.

Carmichael, I.S.E., F.J. Turner, and J. Verhoogen (1974) Igneous Petrology. McGraw-Hill: New York, 739 pp.

Carpenter, M.A. (1981) A "conditional spinodal" within the peristerite miscibility gap of plagioclase feldspars. Am. Mineral. 66, 553-560.

Carron, J.-P. and M. Lagache (1972) Etude du partage des elements alcalins Na, K, Li, Rb et Cs entre les mineraux de quelques roches granitiques de France. Proc. 24th Int'l Geol. Congr. Montreal, Sect. 10, 60-66. [Li Na K Rb Cs]

Carron, J.-P. and M. Lagache (1980) Etude experimentale du fractionnement des elements Rb, Cs, Sr et Ba entre feldspaths alcalins, solutions hydrothermales et liquides silicates dans le systeme Q:Ab:Or:H_2O a 2 kbar entre 700 et 800°C. Bull. Mineral. 103, 571-578.

Carstens, H. (1967) Exsolution in ternary feldspars. I. On the formation of antipertites. II. Intergranular precipitation in alkali feldspar containing calcium in solid solution. Contrib. Mineral. Petrol. 14, 27-35 and 316-320.

Cech, F., Z. Misar, and P. Povondra (1971) A green lead-containing orthoclase. Tschermaks Mineral. Petrogr. Mitt. 15, 213-231.

Champness, P.E. and G.W. Lorimer (1971) An electron microscopic study of a lunar pyroxene. Contrib. Mineral. Petrol. 33, 171-183.

Champness, P.E. and G.W. Lorimer (1976) Exsolution in silicates. In H.-R. Wenk et al., Eds., Electron Microscopy in Mineralogy. Springer-Verlag: Berlin, pp. 173-204.

Champness, P.E. and Lorimer, G.W. (1976) Exsolution in silicates. In, H.-R. Wenk et al., Eds., Electron Microscopy in Mineralogy. Springer-Verlag: Berlin, pp. 205-208.

Chao, S.H. and W.H. Taylor (1940) Isomorphous replacement and superlattice structures in the plagioclase feldspars. Proc. Royal Soc. (London) 176A, 76-87.

Chatterjee, N.D. (1972) The upper stability limit of the assemblage paragonite + quartz and its natural occurrences. Contrib. Mineral. Petrol. 34, 288-303.

Chatterjee, N.D. and W. Johannes (1974) Thermal stability and standard thermodynamic properties of synthetic $2M_1$-muscovite, $KAl_2[AlSi_3O_{10}(OH)_2]$. Contrib. Mineral. Petrol. 48, 89-114.

Cherry, M.E. and L.T. Trembath (1978) Structural state and composition of alkali feldspars in granites of the St. George pluton, southwestern New Brunswick. Mineral. Mag. 42, 391-399.

Cherry, M.E. and L.T. Trembath (1979a) The disordering of alkali feldspars. I. Dry heating of a microcline perthite. Canadian Mineral. 17, 527-535.

Cherry, M.E. and L.T. Trembath (1979b) Order-disorder paths of alkali feldspars. Am. Mineral. 64, 66-70.

Chiari, G., M. Calleri, E. Bruno, and P.H. Ribbe (1975) The structure of partially disordered synthetic strontium feldspar. Am. Mineral. 60, 111-119.

Chiari, G., A. Facchinelli, and E. Bruno (1978) Anorthite quenched from 1530°C. II. Discussion. Acta Crystallogr. B34, 1757-1764.

Christensen, N.I. (1966) Compressional wave velocities in single crystals of alkali feldspar at pressures to 10 kilobars. J. Geophys. Res. 71, 3113-3116.

Christian, J.W. (1965) The Theory of Transformations in Metals and Alloys. Pergamon: London, 973 pp.

Christie, J.M. and A. Ord (1980) Flow stress from microstructures of mylonites: example and current assessment. J. Geophys. Res. 85, 6253-6262.

Christie, J.M., D.T. Griggs and N.L. Carter (1964) Experimental evidence of basal slip in quartz. J. Geol. 72, 734-756.

Christie, O.H.J. (1968) Spinodal precipitation in silicates. II. Short survey of theories and some additional remarks on exsolution in feldspars. Lithos 2, 285-294.

Christie, O.H.J. (1969) Spinodal precipitation in silicates. II. Short survey of theories and some additional remarks on exsolution in feldspar. Lithos 2, 285-294.

Christie, O.H.J. and A. Olsen (1974) Spindoal precipitation in minerals. Review and some new observations. Bull. Soc. franc. Mineral. Cristallogr. 97, 202-205.

Christoffersen, R. and A. Schedl (1980) Microstructure and thermal history of cryptoperthites in a dike from Big Bend, Texas. Am. Mineral. 65, 444-448.

Christoffersen, R., J. Tullis, and R.A. Yund (1981) K-Na interdiffusion in alkali feldspar: effect of crystallographic anisotropy and pressure. Trans. Am. Geophys. Union 62, 411.

Clement, S.C. and K.L. Bice (1982) Andesine anorthosite in the eastern Piedmont of Virginia. Geol. Soc. Am. Abstracts with Programs 14, 10.

Cliff, G., P.E. Champness, H.-U. Nissen, and G.W. Lorimer (1976) Analytical electron microscopy of exsolution lamellae in plagioclase feldspars. In H.-R. Wenk et al., Eds., Electron Microscopy in Mineralogy, Springer-Verlag: Berlin, pp. 257-265.

Cole, W.F., H. Sörum, and O. Kennard (1949) The crystal structures of orthoclase and sanidinized orthoclase. Acta Crystallogr. 2, 280-287.

Cole, W.F., H. Sörum and W.H. Taylor (1951) The structure of plagioclase feldspars I. Acta Crystallogr. 4, 20-29.

Collerson, K.D. (1976) Composition and structural states of alkali feldspars from high-grade metamorphic rocks, central Australia. Am. Mineral. 61, 200-211.

Colville, A.A. and P.H. Ribbe (1968) The crystal structure of an adularia and a refinement of the structure of orthoclase. Am. Mineral. 53, 25-37.

Copley, P.A. and P. Gay (1982) The heat treatment of some Norwegian aventurinized feldspars. Mineral. Mag. 45, 107-110.

Corlett, M. and P.H. Ribbe (1967) Electron probe microanalysis of minor elements in plagioclase feldspars (Part II of laboratory investigations on plagioclases). Schweiz. Mineral. Petrogr. Mitt. 47, 317-332.

Craig, J.R., S.J. Louisnathan and G.V. Gibbs (1973) Al/Si order in paracelsian. Abstr. Trans. Am. Geophys. Union 54, 497.

Crank, J. (1975) The Mathematics of Diffusion. 2nd ed., Oxford Press: Oxford, p. 347.

Crawford, M.L. (1966) Composition of plagioclase and associated minerals in some schists from Vermont, U.S.A., and South Westland, New Zealand, with inferences about the peristerite solvus. Contrib. Mineral. Petrol. 13, 269-294.

Crawford, M.L. (1972) Plagioclase and other mineral equilibria in a contact metamorphic aureole. Contrib. Mineral. Petrol. 36, 293-314.

Crosby, P. (1971) Composition and structural state of alkali feldspars from charnockitic rocks on Whiteface Mountain, New York. Am. Mineral. 56, 1788-1811.

Cruickshank, D.W.J. (1961) The role of 3d-orbitals in π bonds (a) silicon, phosphorus, sulphur, or chlorine and (b) oxygen or nitrogen. J. Chem. Soc., 5486-5504.

Cundari, A. (1979) Petrogenesis of leucite-bearing lavas in the Roman volcanic region. Italy. The Sabatini lavas. Contrib. Mineral. Petrol. 70, 9-21. [Na Mg Al Si K Ca Ti Mn Fe Sr Ba]

Curtis, D.B. and R.A. Schmitt (1979) The petrogenesis of L-6 chondrites: insight from the chemistry of minerals. Geochim. Cosmochim. Acta 43, 1091-1103. [Na Mg Al Si K Ca Sc V Mn Co Ni Zn Se Rb]

Czank, M. (1973) Strukturuntersuchungen von Anorthit im Temperaturbereich von 20°C bis 1430°C. D.Sc. Dissertation, ETH, Zürich, 75 pp.

Czank, M., F. Laves, and H. Schulz (1970) On the domains of anorthite. Naturwiss. 57, 128.

Czank, M., J. Van Landuyt, H. Schulz, F. Laves, and S. Amelinckx (1973) Electron microsocpic study of the structural changes as a function of temperature in anorthite. Z. Kristallogr. 138, 403-418.

Dal Negro, A., R. De Pieri, S. Quareni, and W.H. Taylor (1978) The crystal structures of nine K feldspars from the Adamello Massif (Northern Italy). Acta Crystallogr. B34, 2699-2707.

Day, H.W. and V.M. Brown (1980) Evolution of perthite composition and microstructure during progressive metamorphism of hypersolvus granite, Rhode Island, USA. Contrib. Mineral. Petrol. 72, 353-365.

De Pieri, R. (1979) Cell dimensions, optic axial angle and structural state in triclinic K-feldspar of the Adamello Massif, Northern Italy. Mem. Sci. Geologiche, Padova, 32, 17 p.

De Pieri, R. and S. Quareni (1973) The crystal structure of an anorthoclase: an intermediate alkali feldspar. Acta Crystallogr. B29, 1483-1487.

Debat, P., J.-C. Soula, L. Kubin, and J.-L. Vidal (1978) Optical studies of natural deformation microstructures in feldspars (gneiss and petmatites from Occitanie, southern France). Lithos 11, 133-146.

Deer, W.A., R.A. Howie, and J. Zussman (1963) Rock Forming Minerals, 4. Framework Silicates. Longmans, Green and Co.: London, 435 pp.

Delbove, F. (1978) Etude experimentale de la distribution des alcalins K,Rb,Cs et des alcalino-terreux Ca,Sr,Ba entre albite cristallisee et fondue et solution hydrothermale. Bull. Mineral. 101, 317-333.

Dell Angelo, L. and J. Tullis (1982) Textural strain softening in experimentally deformed aplite. Trans. Am. Geophys. Union 63, 438.

Demaiffe, D. and J. Hertogen (1981) Rare earth element geochemistry and strontium isotopic composition of a massif-type anorthositic-charnockitic body: the Hidra Massif (Rogaland, SW Norway). Geochim. Cosmochim. Acta 45, 1545-1561. [Sc Sr Co Rb Sr REE Hf Ta Th U]

Desborough, G.A. (1975) Authigenic albite and potassium feldspar in the Green River Formation, Colorado and Wyoming. Am. Mineral. 60, 235-239. [Li B Na K Ca]

DeVore, G.W. (1956) Al-Si positions in ordered plagioclase feldspars. Z. Kristallogr. 107, 247-264.

Dissanayake, C.B. and E.A. Vincent (1975) Mercury in rocks and minerals of the Skaergaard intrusion, East Greenland. Mineral. Mag. 40, 33-42.

Divljan, S. (1960) The results of field and laboratory studies of adventurine plagioclases from some Norwegian pegmatites. Rept. 21st Int'l Geol. Congr. Norden No. 17, 94-101.

Doman, R.C., C.G. Cinnamon, and S.W. Bailey (1965) Structural discontinuities in the plagioclase feldspar series. Am. Mineral. 50, 724-740.

Donnay, G. and J.D.H. Donnay (1952) The symmetry change in the high-temperature alkali feldspar series. Am. J. Sci. 250A, 115-132.

Donnay, J.D.H., G. Donnay, E.G. Cox, O. Kennard, and M.V. King (1963) Crystal Data. Am. Crystallogr. Assoc. Monograph 5, 1302 pp.

Dowty, E. (1980) Crystal-chemical factors affecting the mobility of ions in minerals. Am. Mineral. 65, 174-182.

Drake, M.J. (1975) The oxidation state of europium as an indicator of oxygen fugacity. Geochim. Cosmochim. Acta 39, 55-64.

Drake, M.J. and D.F. Weill (1975) Partition of Sr, Ba, Ca, Y, Eu^{2+}, Eu^{3+}, and other REE between plagioclase feldspar and magmatic liquid: An experimental study. Geochim. Cosmochim. Acta 39, 689-712.

Duchesne, J.C., I. Roelands, D. Demaiffe, J. Hertogen, R. Gijbels, and J. de Winter (1974) Rare-earth data on monzonoritic rocks related to anorthosites and their bearing on the nature of the parental magmas of the anorthositic series. Earth Planet. Sci. Lett. 24, 325-335.

Eberhard, E. (1967) Zur Synthese der Plagioklase. Schweiz. Mineral. Petrogr. Mitt. 47, 385-398.

Eby, G.N. (1975) Abundance and distribution of the rare-earth elements and yttrium in the rocks and minerals of the Oka carbonatite complex, Quebec. Geochim. Cosmochim. Acta 39, 597-620. [Y La Ce Pr Nd Sm Eu Gd Tb Dy]

Eggleton, R.A. (1979) The ordering path for igneous K-feldspar megacrysts. Am. Mineral. 64, 906-911.

Eggleton, R.A. and P.R. Buseck (1980) The orthoclase-microcline inversion: a high-resolution transmission electron microscope study and strain analysis. Contrib. Mineral. Petrol. 74, 123-133.

Emerson, R.W. and C.V. Guidotti (1974) New x-ray and chemical data on Hewlett's 1959 feldspar suite. Am. Mineral. 59, 615-617.

Emmerling, L.A. (1773) Lehrbuch der Minerologie, Griesen.

Emmons, R.C., R.M. Crump, and K.B. Ketner (1960) High- and low-temperature plagioclase. Bull. Geol. Soc. Am. 71, 1417-1420.

Emslie, R.F. (1975) Pyroxene megacrysts from anorthositic rocks: new clues to the sources and evolution of the parent magmas. Canadian Mineral. 13, 138-145.

Erd, R.C., D.E. White, J.J. Fahey, and D.E. Lee (1964) Buddingtonite, an ammonium feldspar with zeolitic water. Am. Mineral. 49, 831-850. [Na Mg Al Si K Ca H_2O NH_4]

Etheridge, M.A. and J.C. Wilkie (1981) An assessment of dynamically recrystallized grainsize as a paleopiezometer in quartz-bearing mylonite zones. Tectonophysics 78, 475-508.

Evans, H.T., Jr., D.E. Appleman, and D.S. Handwerker (1963) The least-squares refinement of crystal unit cells with powder diffraction data by an automatic computer indexing method (Abstr.). Am. Crystallogr. Assoc., Ann. Mtg. Program, 42-43.

Evenson, W.E. and Decker, D.L. (1978) Kinetic model for solid diffusion with a competing surface reaction. Phys. Rev. B, 17, 583-586.

Ewart, A., W.B. Bryan, and J.B. Gill (1973) Mineralogy and geochemistry of the younger volcanic islands of Tonga, S.W. Pacific. J. Petrol. 14, 429-465. [Mg Mn Fe Cu Zn Ga Sr Ba]

Ewart, A., V.M. Oversby, and A. Mateen (1977) Petrology and isotope geochemistry of Tertiary lavas from the northern flank of the Tweed volcano, southeastern Queensland. J. Petrol. 18, 73-113. [Rb Sr Y Zr Nb Sn Cs Ba REE Pb Th U].

Facchinelli, A., E. Bruno and G. Chiari (1979) The structure of bytownite quenched from 1723°K. Acta Crystallogr. B35, 34-42.

Faust, G.T. (1936) The fusion relations of iron orthoclase. Am. Mineral. 21, 735-763.

Faye, G.H. (1969) The optical absorption spectrum of tetrahedrally bonded Fe^{3+} in orthoclase. Canadian Mineral. 10, 112-117.

Fechtig, H., W. Gentner, and S. Kalibtzer (1961) Argonbestimmungen an Kaliummine. Geochim. Cosmochim. Acta 25, 297-311.

Fenn, P.M. and G.E. Brown (1977) Crystal structure of a synthetic, compositionally intermediate, hypersolvus alkali feldspar: evidence for Na,K site ordering. Z. Kristallogr. 145, 124-145.

Ferguson, R.B. (1980) From unit-cell parameters to Si/Al distribution in K-feldspars. Canadian Mineral. 18, 443-458.

Ferguson, R.B. (1981) Corrigendum to the above. Ibid. 19, 363-365.

Finney, J.J. and S.W. Bailey (1964) Crystal structure of an authigenic maximum microcline. Z. Kristallogr. 119, 413-436.

Fischer, W., E. Koch, and E. Hellner (1971) Zur Berechnung von Wirkungsbereichen in Strukturen anorganischer Verbindungen. N. Jahrb. Mineral. Monatsh. 5, 227-237.

FitzGerald, J.D. and A.C. McLaren (1982) The microstructure of microcline from some granitic rocks and pegmatites. Contrib. Mineral. Petrol. 80, 219-229.

Fleet, M.E. (1981) The intermediate plagioclase structure: An explanation from interface theory. Phys. Chem. Minerals 7, 64-70.

Fleet, S.G. and P.H. Ribbe (1963) An electron-microscope investigation of a moonstone. Phil. Mag. 8, 1179-1187.

Fleet, S.G. and P.H. Ribbe (1965) An electron-microscope study of peristerite plagioclases. Mineral. Mag. 35, 165-176.

Fleet, S.G., S. Chandrasekhar, and H.D. Megaw (1966) The structure of bytownite ('body-centered anorthite'). Acta Crystallogr. 21, 782-801.

Fletcher, R.C. and R.H. McCallister (1974) Spinodal decomposition as a possible mechanism in the exsolution of clinopyroxene. Carnegie Inst. Washington Year Book 73, 396-399.

Fletcher, R. and M.J.D. Powell (1963) A rapidly convergent descent method for minimization. Computer J. 6/2, 163-168.

Foit, F.F. and D.R. Peacor (1967) High temperature diffraction data on selected reflections of an andesine and anorthite. Z. Kristallogr. 125, 1-6.

Foit, F.F. and D.R. Peacor (1973) The anorthite crystal structure at 410 and 830°C. Am. Mineral. 58, 665-675.

Foland, K.A. (1974a) Alkali diffusion in orthoclase. In, A.W. Hoffman et al., Eds., Geochemical Transport and Kinetics. Carnegie Institution, Washington, pp. 77-98.

Foland, K.A. (1974b) ^{40}Ar diffusion in homogeneous orthoclase and an interpretation of Ar diffusion in K-feldspars. Geochim. Cosmochim. Acta 38, 151-166.

Foord, E.E. (1977) Famous mineral localities: the Himalaya dike system, Mesa Grande district, San Diego County, California. Mineral. Record 8, 461-474.

Foord, E.E. and R.F. Martin (1979) Amazonite from the Pikes Peak batholith. Mineral. Record 10, 373-384. [Li Be B Na Na K Mn Fe Cu Ga Rb Sr Cs Ba Pb]

Fox, P.E. and J.M. Moore, Jr. (1969) Feldspars from Adamant pluton, British Columbia. Canadian J. Earth Sci. 6, 1199-1209.

Frechen, J. and H.J. Lippolt (1965) Kalium-Argon-Daten sum alter des Laacher Vulkanismus, der Rheinterrassen und der Eiszeiteh. Eiszeitalter Gegenuart 16, 5-30.

Frey, F., H. Jagodzinski, W. Prandl, and W.B. Yelon (1977) Dynamic character of the primitive to body-centered phase transition in anorthite. Phys. Chem. Minerals 1, 227-231.

Friedel, J. (1964) Dislocations. Pergamon Press: New York. 491 pp.

Gandais, M. and C. Willaime (1978) Defauts plans dans les feldspaths alcalin. J. Physique 39, C2-C110.

Garrison, J.R., Jr. (1978) Plagioclase compositions from metabasalts, southeastern Llano Uplift: plagioclase unmixing during amphibolite-grade metamorphism. Am. Mineral. 63, 143-149.

Gay, P. (1954) The structure of the plagioclase feldspars. V. The heat treatment of lime-rich plagioclases. Mineral. Mag. 30, 428-438.

Gay, P. (1956) The structures of the plagioclase feldspars. VI. Natural intermediate plagioclases. Mineral. Mag. 31, 21-40.

Gay, P. and M.G. Bown (1956) The structures of the plagioclase feldspars. VII. The heat treatment of intermediate plagioclases. Mineral. Mag. 31, 306-313.

Gibbs, G.V., M.M. Hamil, S.J. Louisnathan, L.S. Bartell and H. Yow (1972) Correlations between Si-O bond length, Si-O-Si angle and bond overlap populations calculated using extended Huckel molecular orbital theory. Am. Mineral. 57, 1578-1613.

Gijbels, R., P. Henderson, and J. Zels (1976) Geochemistry of some trace element in mineral separates from Rhum, Inner Hebrides, with special emphasis on iridium. Econ. Geol. 71, 1364-1370. [Na Sc Cr Fe Co Rb Cs Ba REE Hf Ir Th U]

Gijbels, R.H., H.T. Millard, G.A. Desborough, and A.J. Bartel (1974) Osmium, ruthenium, iridium and uranium in silicates and chromite from the eastern Bushveld Complex, South Africa. Geochim. Cosmochim. Acta 38, 319-337. [Ru Os Ir U]

Giletti, B.J. and Nagy, K.L. (1981) Grain boundary diffusion of oxygen along lamellar boundaries in perthitic feldspar. Trans. Am. Geophys. Union 62, 428.

Giletti, B.J., M.P. Semet, and R.B. Kasper (1974) Self-diffusion of potassium in low albite using an ion microprobe. Geol. Soc. Am. Abstracts with Programs 6, 754.

Giletti, B.J., M.P. Semet, and R.A. Yund (1978) Studies in diffusion III: Oxygen in feldspars, an ion microprobe determination. Geochim. Cosmochim. Acta 42, 45-57.

Glazner, A.F. (1980) Frequency distribution of plagioclase extinction angles: precision of the Michel-Lévy technique. Am. Mineral. 65, 1050-1052.

Godinho, M.M. and J.M.P. Jaleco (1975) Feldspatos potassicos dos granitoides da regiao de Castro-Daire (Viseu Portugal). III - Parametros da celula elementar e distribuicao intra-estrutural do aluminio. - Memorias e Noticias. Publ. Mus. Lab. Mineral. Geol. Univ. Coimbra 80, 1-16.

Goldsmith, J.R. (1980) The melting and breakdown reactions of anorthite at high pressures and temperatures. Am. Mineral. 65, 272-284.

Goldsmith, J.R. (1981) The join $CaAl_2Si_2O_8$-H_2O (anorthite-water) at elevated pressures and temperatures. Am. Mineral. 66, 1183-1188.

Goldsmith, J.R. (1982a) Review of the behavior of plagioclase under metamorphic conditions. Am. Mineral. 67, 643-652.

Goldsmith, J.R. (1982b) Plagioclase stability at elevated temperatures and water pressures. Am. Mineral. 67, 653-675.

Goldsmith, J.R. and F. Laves (1954a) The microcline-sanidine stability relations. Geochim. Cosmochim. Acta 5, 1-19.

Goldsmith, J.R. and F. Laves (1954b) Potassium feldspars structurally intermediate between microcline and sanidine. Geochim. Cosmochim. Acta 6, 100-118.

Goldsmith, J.R. and F. Laves (1955) Cation order in anorthite ($CaAl_2Si_2O_8$) as revealed by gallium and germanium substitutions. Z. Kristallogr. 106, 213-226.

Goldsmith, J.R. and R.C. Newton (1974) An experimental determination of the alkali feldspar solvus. In, W.S. MacKenzie and J. Zussman, Eds., The Feldspars. Manchester University Press: Manchester, pp. 337-359.

Goode, A.D.T. (1978) High temperature, high strain rate deformation in the lower crustal Kalka Intrusion, central Australia. Contrib. Mineral. Petrol. 66, 137-148.

Gorai, M. (1951) Petrological studies of plagioclase twins. Am. Mineral. 36, 884-901.

Gorman, B.E. (1980) A model of flow and fracture in plagioclase: examples from shear zones, Fiskenaesset Complex, West Greenland. Ph.D. dissertation, Univ. Western Ontario, London, Ont. 293 pp.

Griffen, D.T. (1975) Distortions in the tetrahedral oxyanions of crystalline substances and crystal structure refinements of slawsonite and celsian. Ph.D. Thesis, Virginia Polytechnic Institute and State University, Blacksburg, Virginia, 145 pp.

Griffen, D.T., P.H. Ribbe, and G.V. Gibbs (1977) The structure of slawsonite, a strontium analog of paracelsian. Am. Mineral. 62, 31-35.

Griffin, W.L., B. Sundvoll, and H. Kristmannsdottir (1974) Trace element composition of anorthosite plagioclase. Earth Planet. Sci. Lett. 24, 213-223.

Griggs, D.T. (1967) Hydrolytic weakening of quartz and other silicates. Geophys. J. Royal Astron. Soc. 14, 39-31.

Grove, T.L. (1976) Exsolution in metamorphic bytownite. In H.-R. Wenk et al., Eds., Electron Microscopy in Mineralogy. Springer-Verlag: Berlin, pp. 266-270.

Grove, T.L. (1977a) A periodic antiphase structure model for the intermediate plagioclases (An_{33} to An_{75}). Am. Mineral. 62, 932-941.

Grove, T.L. (1977b) Structural characterization of labradorite-bytownite plagioclase from volcanic, plutonic and metamorphic environments. Contrib. Mineral. Petrol. 64, 273-302.

Grove, T.L. and Spear, F.S. (1981) Petrogenic significance of modulated structures in intermediate plagioclase. Geol. Soc. Am. Abstracts with Programs 13, 464.

Grove, T.L., J.M. Ferry, and F.S. Spear (1983) Phase transitions and decomposition relations in calcic plagioclases. Am. Mineral. 68, 41-59.

Grundy, H.D. and J. Ito (1974) The refinement of the crystal structure of a synthetic non-stoichiometric Sr-feldspar. Am. Mineral. 69, 1319-1326.

Grundy, H.D. and W.L. Brown (1967) Preliminary single-crystal study of the lattice angles of triclinic feldspars at temperatures up to 1200°C. Schweiz. Mineral. Petrogr. Mitt. 47, 21-30.

Gubser, R. and F. Laves (1967) On x-ray properties of "adularia," $(K,Na)AlSi_3O_8$. Schweiz. Mineral. Petrogr. Mitt. 47, 177-188.

Guidotti, C.V., H.H. Herd, and C.L. Tuttle (1973) Composition and structural state of K-feldspars from K-feldspar + sillimanite grade rocks in northwestern Maine. Am. Mineral. 58, 705-716.

Guillope, M. and J.P. Poirier (1979) Dynamic recrystallization during creep of single-crystalline halite: an experimental study. J. Geophys. Res. 84, 5557-5567.

Hanmer, S.K. (1982) Microstructure and geochemistry of plagioclase and microcline in naturally deformed granite. J. Struc. Geol. 4, 197-213.

Hansen, E.C., I.M. Steele, and J.V. Smith (1979) Lunar highland rocks: Element partitioning among minerals I: Electron microprobe analyses of Na, Mg, K and Fe in plagioclase; Mg partitioning with orthopyroxene. Geochim. Cosmochim. Acta Suppl. 11, 627-638. [Na Mg K Fe]

Harlow, G.E. (1982) The anorthoclase structures: the effects of temperature and composition. Am. Mineral. 67, 975-996.

Harlow, G.E. and G.E. Brown, Jr. (1980) Low albite: an x-ray and neutron diffraction study. Am. Mineral. 65, 986-995.

Harlow, G.E., G.E. Brown, and W.C. Hamilton (1973) Neutron diffraction study of Amelia low albite (Abstr.). Trans. Am. Geophys. Union 54, 497.

Harrison, T.M. and McDougall, I. (1981) Excess ^{40}Ar in metamorphic rocks from Broken Hill, New South Wales: implications for $^{40}Ar/^{39}Ar$ age spectra and the thermal history of the region. Earth Planet. Sci. Letters 55, 123-149.

Harrison, T.M. and I. McDougall (1982) The thermal significance of microcline K-Ar ages revealed by $^{40}Ar/^{39}Ar$ age spectrum results. Geochim. Cosmochim. Acta 46, 1811-1820.

Hart, S.R. (1981) Diffusion compensation in natural silicates. Geochim. Cosmochim. Acta 45, 279-291.

Hashimoto, H., H.-U. Nissen, A. Ono, A. Kumao, H. Endoh and C.F. Woensdregt (1976) High-resolution electron microscopy of labradorite feldspar. In H.-R. Wenk et al., Eds., Electron Microscopy in Mineralogy, Springer-Verlag: Berlin, pp. 332-344.

Haskin, L.A., C.-Y. Shih, B.M. Bansal, J.M. Rhodes, H. Wiesmann, and L.E. Nyquist (1974) Chemical evidence for the origin of 76535 as a cumulate. Proc. 5th Lunar Sci. Conf. 2, 1213-1225.

Hauser, J. and H.-R. Wenk (1976) Optical properties of composite crystals (submicroscopic domains, exsolution lamellae, solid solutions). Z. Kristallogr. 143, 188-219.

Hazen, R.M. and Finger, L.W. (1979) Bulk modulus-volume relationship for cation-anion polyhedra. J. Geophys. Res. 84, 6723-6728.

Hazen, R.M. and C.T. Prewitt (1977a) Effects of temperature and pressure on interatomic distances in oxygen-based minerals. Am. Mineral. 62, 309-315.

Hazen, R.M. and C.T. Prewitt (1977b) Linear compressibilities of low albite: high pressure structural implications. Am. Mineral. 62, 554-558.

Heinrich, E.W. (1965) Microscopic Identification of Minerals. McGraw-Hill: New York, p. 364.

Heinrichs, H., B. Schulz-Dobrick, and K.H. Wedepohl (1980) Terrestrial geochemistry of Cd, Bi, Tl, Pb, Zn and Rb. Geochim. Cosmochim. Acta 44, 1519-1533. [Zn Cd Tl Bi Pb]

Henderson, P., S.J. Fishlock, J.C. Laul, T.D. Cooper, R.L. Conard, W.V. Boynton, and R.A. Schmitt (1976) Rare earth element abundances in rocks and minerals from the Fiskenaesset complex, West Greenland. Earth Planet. Sci. Lett. 30, 37-49. [Na Al K Ca Sc Ti V Cr Mn Fe Co Ni Sr Ba REE Hf Ta]

Henry, N.F.M., H. Lipson and W.A. Wooster (1960) The Interpretation of X-ray Diffraction Photographs. Macmillan & Co.: London, 282 pp.

Hess, H.H. (1960) Stillwater Igneous Complex, Montana. Geol. Soc. Am. Memoir 80, 230 pp.

Heuer, A.H. and G.L. Nord, Jr. (1976) Polymorphic phase transitions in minerals. In, H.-R. Wenk et al., Eds., Applications of Electron Microscopy in Mineralogy. Springer-Verlag: Berlin, pp. 271-303.

Heuer, A.H., J.S. Lally, J.M. Christie, and S.V. Radcliffe (1972) Phase transformations and exsolution in lunar and terrestrial calcic plagioclases. Phil. Mag. 26, 465-482.

Heuer, A.H., G.L. Nord, Jr., J.S. Lally and J.M. Christie (1976) Origin of the (c) domains in anorthite. In H.-R. Wenk et al., Eds., Electron Microscopy in Mineralogy. Springer-Verlag: Berlin, 345-353.

Hewlett, C.G. (1959) Optical properties of potassic feldspars. Geol. Soc. Am. Bull. 70, 511-538.

Higgins, J.B., P.H. Ribbe and Y. Nakajima (1982) An ordering model for the commensurate antiphase structure of yoderite. Am. Mineral. 67, 76-84.

Hillard, J.E. (1970) Spinodal decomposition. In, Phase Transformations. Am. Soc. Metals: Ohio, pp. 497-560.

Hinthorne, J.R., R. Conrad, and C.A. Andersen (1975) Lead-lead age and trace element abundances in lunar troctolite, 76535. Lunar Sci. VI, 373-375.

Hintze, C. (1897) Handbuch der Mineralogie II. Verlag von Weit: Leipzig, pp. 1354-1357.

Hipple, D.L. (1971) Study of the structural state and composition of feldspars of the Bedford Augen Gneiss, New York. Geol. Soc. Amer. Bull. 82, 3213-3220.

Hirsch, P.B., A. Howie, R.B. Nicholson, D.W. Pashley, and M.J. Whelan (1965) Electron Microscopy of Thin Crystals. Butterworths: London, 549 pp.

Hofmann, A.W. (1969) Hydrothermal experiments of equilibrium partitioning and diffusion kinetics of Rb, Sr, and Na in biotite-alkali chloride solution systems. Ph.D. Dissertation, Brown University, 105 pp.

Hofmeister, A.M. and G.R. Rossman (1981) The effect of radiation on water and lead in potassium feldspar. Geol. Soc. Am. Abstracts with Programs 13, 505.

Holm, J.L. and O.J. Kleppa (1968) Thermodynamics of the disordering process in albite. Am. Mineral. 53, 123-133.

Honma, H. and Y. Itihara (1981) Distribution of ammonium in minerals of metamorphic and granitic rocks. Geochim. Cosmochim. Acta 45, 983-988. [NH_4]

Hoover, J.D. (1978) The distribution of samarium and thulium between plagioclase and liquid in the systems Au-Di and Ab-An-Di at 1300°C. Carnegie Inst. Wash. Year Book 77, 703-709.

Horst, W., T. Tagai, M. Korekawa and H. Jagodzinski (1981) Modulated structure of a plagioclase An_{52}: theory and structure determination. Z. Kristallogr. 157, 233-250.

Hovis, G.L. (1974) A solution calorimetric and x-ray investigation of Al-Si distribution in monoclinic potassium feldspars. In, W.S. MacKenzie and J. Zussman, Eds., The Feldspars. Manchester Univ. Press: Manchester, pp. 114-144.

Hovis, G.L. (1977) Unit-cell dimensions and molar volumes for a sanidine-analbite ion-exchange series. Am. Mineral. 62, 672-679.

Hovis, G.L. (1980) Angular relations of alkali feldspar series and the triclinic-monoclinic displacive transformation. Am. Mineral. 65, 770-778.

Hovis, G.L. and E. Peckins (1978) A new x-ray investigation of maximum microcline crystalline solutions. Contrib. Mineral. Petrol. 66, 345-349.

Hutcheon, I.D., I.M. Steele, J.V. Smith, and R.N. Clayton (1978) Ion microprobe, electron microprobe and cathodoluminescence data for Allende inclusions with emphasis on plagioclase chemistry. Geochim. Cosmochim. Acta Suppl. 10, 1345-1368. [Mg]

Huttenlocher, H. (1942) Beitrage zur Petrographie des Gesteinzuges Ivrea Verbans I. Allgemeines. Die Gabbroiden Gesteine von Anzola. Schweiz. Mineral. Petrogr. Mitt. 22, 326-366.

Iball, D.R. and F.H. Hubbard (1982) Lattice structural variation in K-feldspar megacrysts of associated charnockite and alkali granite. Mineral. Mag. 46, 247-251.

Iiyama, J.T. (1972) Fixation des elements alcalinoterreux, B, Sr et Ca dans les feldspaths - etude experimentale. Proc. 24th Int'l Geol. Congr., Sec. 10, 122-130.

Iiyama, J.T. (1974a) Behaviour of trace elements in feldspars under hydrothermal conditions. In, W.S. MacKenzie and J. Zussman, Eds., The Feldspars. Manchester Univ. Press: Manchester, pp. 552-573.

Iiyama, J.T. (1974b) Substitution, deformation locale de la maille et equilibre de distribution des elements en traces entre silicates et solution hydrothermale. Bull. Soc. franc. Mineral. Cristallogr. 97, 143-151.

Isshiki, N. (1958) Red coloration of anorthite from Hachijo-jima. J. Geol. Soc. Japan 64, 644-646.

Iwasaki, B. and N. Kimizuka (1978) Synthesis, X-ray crystallography and infrared absorption spectroscopy of $EuAl_2Si_2O_8$. Geochem. J. 12, 1-6.

Jagodzinski, H. and M. Korekawa (1978) Satellite reflections of labradorite. Phys. Chem. Minerals 3, 69-72.

Jahns, R.H. and L.A. Wright (1951) Gem and lithium bearing pegmatites of the Pala district, San Diego County, California. Calif. Div. Mines, Special Rep. 7-A, 72 pp.

Jenkins, J.E. (1980) Albitization of Ca-Plagioclase: An Experimental Study. M.S. Thesis, University of North Carolina, Chapel Hill.

Jensen, M.L. (1952) Solid diffusion of radioactive sodium in perthite. Am. J. Sci. 250, 808-821.

Jiránek, J. (1982) A rapid x-ray method of assessing the structural state of monoclinic K-feldspars. Lithos 15, 85-87.

Johannes, W. (1979) Ternary feldspars: Kinetics and possible equilibria at 800°C. Contrib. Mineral. Petrol. 68, 221-230.

Jones, J.B. (1968) Al-O and Si-O tetrahedral distances in alumosilicate framework structures. Acta Crystallogr. B24, 355-358.

Joswig, W., M. Korekawa, and S. Wilson (1977) Neutron and X-ray diffraction study on the superstructure of a sodium-rich low plagioclase $An_{16.5}$. N. Jahrb. Mineral. Monatsh. 132-135.

Joswig, W., T. Tagai, M. Korekawa and H.-R. Wenk (1976) Verfeinerung der gemittelten Struktur eines Plagioklases An_{66} von der Insel Surtsey, Island, mittels Neutronenbeugung (Abstr.). Z. Kristallogr. 144, 433.

Jovanovic, S. and G.W. Reed, Jr. (1979) Cl and P_2O_5 in mineral separates from a lunar basalt. Lunar Planet. Sci. X, 633-635. [P Cl Br U]

Jowhar, T.N. (1981) AFEL, a Fotran IV computer program for calculating lattice parameters and distribution of aluminium in tetrahedral sites of alkali feldspars. Computers and Geosci. 7, 407-413.

Kroll, H. (1971) Determination of Al,Si distribution in alkali feldspars from X-ray powder data. N. Jahrb. Mineral. Monatsh. 91-94.

Kroll, H. (1971) Feldspäte im System $K[AlSi_3O_8]$-$Na[AlSi_3O_8]$-$Ca[Al_2Si_2O_8]$: Al,Si-Verteilung und Gitterparameter, Phasen-Transformationen und Chemismus. Inaug.-Diss. Westf. Wilhelms-Univ., Münster, 119 pp.

Kroll, H. (1973) Estimation of the Al,Si distribution of feldspars from the lattice translations Tr[110] and Tr[1$\bar{1}$0]. I. Alkali feldspars. Contrib. Mineral. Petrol. 39, 141-156.

Kroll, H. (1978) The structure of heat-treated plagioclases An28, An52, An69 and the estimation of Al,Si order from lattice parameters (Abstr.). Phys. Chem. Minerals 3, 76-77.

Kroll, H. (1980) Struktur und Metrik der Feldspäte. Habilitations-schrift, Westf. Wilhelms-Univ., Münster.

Kroll, H. and H.U. Bambauer (1971) The displacive transformation of (K,Na,Ca)-feldspars. N. Jahrb. Mineral. Monatsh., pp. 413-416.

Kroll, H. and H.-U. Bambauer (1981) Diffusive and displacive transformation in plagioclase and ternary feldspar series. Am. Mineral. 66, 763-769.

Kroll, H. and W.F. Müller (1980) X-ray and electron-optical investigation of synthetic high-temperature plagioclases. Phys. Chem. Minerals 5, 255-277.

Kroll, H. and P.H. Ribbe (1980) Determinative diagrams for Al,Si order in plagioclases. Am. Mineral. 65, 449-457.

Kroll, H. and D. Stöckelmann (1979) Harmonische Least-Squares Datenanalyse. Fortschr. Mineral. 57/1, 74-75.

Kroll, H., H.-U. Bambauer, and U. Schirmer (1980) The high albite-monalbite and analbite-monalbite transitions. Am. Mineral. 65, 1192-1211.

Kronenberg, A.K. and G.L. Shelton (1980) Deformation microstructures in experimentally deformed Maryland diabase. J. Struc. Geol. 2, 341-353.

Kudo, A.M. and D.F. Weill (1970) An igneous plagioclase thermometer. Contrib. Mineral. Petrol. 25, 52-65.

Kumao, A., H. Hashimoto, H.-U. Nissen, and H. Endoh (1981) Ca and Na positions in labradorite feldspar as derived from high-resolution electron microscopy and optical diffraction. Acta Crystallogr. A37, 229-238.

Kyle, P.R. and P.C. Rankin (1976) Rare earth geochemistry of Late Cenozoic alkaline lavas of the McMurdo Volcanic Group, Antarctica. Geochim. Cosmochim. Acta 40, 1497-1507. [Na Mg Al Si K Ca Ti Mn Fe Cu Zn Rb Sr Ba REE]

Lambert, R.S.J. and J.G. Holland (1974) Yttrium geochemistry applied to petrogenesis utilizing calcium-yttrium relationships in minerals and rocks. Geochim. Cosmochim. Acta 38, 1393-1414.

Langer, J.S. (1971) Theory of spinodal decomposition in alloys. Ann. Physics (N.Y.) 65, 53-86.

Langer, J.S. (1973) Statistical methods in the theory of spinodal decomposition. Acta Met. 21, 1649-1659.

Laves, F. (1952a) Phase relations of the alkali feldspars. I. Introductory remarks. II. The stable and pseudostable phase relations in the alkali feldspar system. J. Geol. 60, 436-450, 549-574.

Laves, F. (1952b) Mechanische Zwillingsbildung in Feldspäten in Abhangigkeit von Ordnung-Unordnung der Si/Al - Verteilung innerhalb des $(Si,Al)_4O_8$-Gerustes. Naturwiss. 39, 546-547.

Kasper, R.B. (1974) Cation diffusion in low albite (Abstr.). Geol. Soc. Am. Abstracts with Programs 6, 815.

Kastner, M. (1971) Authigenic feldspars in carbonate rocks. Am. Mineral. 56, 1403-1442.

Kay, S.M. (1977) The origin of antiperthites in anorthites. Am. Mineral. 62, 905-912.

Kay, S.M. (1978) Exsolution in potassium-calcium feldspars: experimental evidence and relationship to antiperthites and Bøggild lamellae. Am. Mineral. 63, 136-142.

Keefer, K.D. and G.E. Brown (1978) Crystal structures and compositions of sanidine and high albite in cryptoperthitic intergrowth. Am. Mineral. 63, 1264-1273.

Kehlenbeck, M.M. (1972) Deformation textures in the lac Rouvray Anorthosite Mass. Canadian J. Earth Sci. 9, 1087-1098.

Kim, K. and B.J. Burley (1971) Phase equilibria in the system $NaAlSi_3O_8$-$NaAlSiO_4$-H_2O with special emphasis on the stability of analcite. Canadian J. Earth Sci. 8, 311-337.

Kitamura, M. and N. Morimoto (1975) The superstructure of intermediate plagioclase. Proc. Japan Acad. 51, 419-424.

Kitamura, M. and N. Morimoto (1977) The superstructure of plagioclase feldspars. Phys. Chem. Minerals 1, 199-212.

Klein, S. and M. Korekawa (1976) Die gemittelte Struktur des Labradorite. N. Jahrb. Mineral. Monatsh. 66-68.

Knopf, E.B. and E. Ingerson (1938) Structural Petrology. Geol. Soc. Am. Memoir 6, 270 p.

Korekawa, M. (1967) Theorie der Satellitenreflexe. Habilitatiions-schrift Ludwigs-Maximilians Univ., München. 140 pp.

Korekawa, M. and H. Jagodzinski (1967) Die Satellitenreflexe des Labradorits. Schweiz. Mineral. Petrogr. Mitt. 47, 269-278.

Korekawa, M. and D. Philipp (1971) Über zwei verschiedene Arten von Sattellitenreflexen beobachtet an einem Tieftemperature-Plagioklas $An_{16.5}$. Z. Kristallogr. 134, 145-147.

Korekawa, M., H.-U. Nissen, and D. Philipp (1970) X-ray and electron-microscopic studies of a sodium-rich low plagioclase. Z. Kristallogr. 131, 418-436.

Kosals, Ya.A., P.G. Nedashkovskiy, L.L. Petrov, and V.I. Serykh (1973) Beryllium distribution in granitoid plagioclase. Geochem. Int'l 10, 753-767. Trans. from Geokhimiya, pp. 998-1013.

Kotelnikov, A.R., A.M. Bychkov, and N.I. Chernavina (1981) Experimental study of calcium distribution between plagioclase and water-salt fluid at 700°C and Pfl = 1000 atm. Geokhimiya, 707-721 (in Russian).

Kovacs, M.P. and M. Gandais (1980) Transmission electron microscope study of experimentally deformed K feldspar single crystals. Phys. Chem. Minerals 6, 61-76.

Kraeft, U. and H. Saalfeld (1967) Über die Adverturin-Oligoklase von Tvedestrand und Bjordan (Norweigen). Schweiz. Mineral. Petrogr. Mitt. 47, 247-256.

Krahl, M. (1976) Verfeinerung der gemittelten Struktur des Labradorits An_{52} und ein Beitrag zur Messung von Satellitenreflexen. Diplomarbeit, Frankfurt/Main, Germany.

Kravchuk, I.F. (1981) Energetics, thermodynamics and stability of solid solution of feldspars. Geokhimiya, 1305-1317 (in Russian). Translation expected in Geochemistry Int'l.

Kravchuk, I.K., I.V. Chernysheva, and V.S. Urusov (1980) Element distribution between plagioclase phenocrysts and groundmass as an indicator for crystallization conditions of the basalts in the southern vent of Tolbachik. Geochem. Int'l 17, 18-24.

Laves, F. (1960) The feldspars, their polysynthetic twinning and their phase relations. Rend. Soc. Mineral. Ital. 16, 37-100.
Laves, F. (1966) What is a twin and what is a "twin"? Acta Met. 14, 58.
Laves, F. (1974) Domain and deformation textures in plagioclases and their investigation by photo-emission-electron-microscopy (FEEM) and by transmission electron microscopy. In, W.S. MacKenzie and J. Zussman, Eds., The Feldspars. Manchester Univ. Press: Manchester, pp. 536-550.
Laves, F. and U. Chaisson (1950) An x-ray investigation of the "high"-"low" albite relations. J. Geol. 58, 584-592.
Laves, F. and J.R. Goldsmith (1954) Long-range-short-range order in calcic plagioclases as a continuous and reversible function of temperature. Acta Crystallogr. 7, 465-472.
Laves, F. and J.R. Goldsmith (1961) Polymorphism, order, disorder, diffusion and confusion in the feldspars. Curs. y Conf. del Inst. "Lucas Mallada" 8, 71-80.
Laves, F. and K. Soldatos (1963) Die Albit/Mikroklin-Orienteirungs-beziehungen in Mikroklinperthiten und deren genetische Deutung. Z. Kristallogr. 118, 69-102.
Laves, F. and K. Viswanathan (1967) Relations between optic axial angle and triclinicity of potash feldspars, and their significance for the definition of "stable" and "unstable" states of alkali feldspars. Schweiz. Mineral. Petrogr. Mitt. 47, 147-162.
Laves, F., H.-U. Nissen and W. Bollmann (1965) On schiller and submicroscopic lamellae of labradorite $(Na,Ca)(Si,Al)_4O_8$. Naturwiss. 52, 427-428.
Laves, F., M. Czank, and H. Schulz (1970) The temperature dependence of the reflection intensities of anorthite ($CaAl_2Si_2O_8$) and the corresponding formation of domains. Schweiz. Mineral. Petrogr. Mitt. 50, 519-525.
Lawrence, R.D. (1970) Stress analysis based on albite twinning of plagioclase feldspars. Geol. Soc. Am. Bull. 81, 2507-2512.
Lazarus, D. and N.H. Nachtrieb (1963) Effect of high pressure on diffusion. In, W. Paul and D.M. Warschauer, Eds., Solids Under Pressure. McGraw-Hill: New York, pp. 43-69.
Leeman, W.P. and D.W. Phelps (1981) Partitioning of rare earths and other trace elements between sanidine and coexisting volcanic glass. J. Geophys. Res. 86, 10193-10199. [Na K Ca Sc Fe Rb Zr Hf Ta REE Cs Ba Th]
Leeman, W.P. (1979) Partitioning of Pb between volcanic glass and coexisting sanidine and plagioclase feldspars. Geochim. Cosmochim. Acta 43, 171-175. [Pb]
Lesnov, F.P., M.Ya. Shcherbakova, and V.E. Istomin (1980) The e.p.r. spectra of Fe^{3+} in basic plagioclases, their classification and petrogenetic significance. Geol. Geofiz. 139-146 (in Russian).
Liebermann, R.C. and A.E. Ringwood (1976) Elastic properties of anorthite and the nature of the lunar crust. Earth Planet. Sci. Letters 31, 69-74.
Lifshitz, I.M. and V.V. Slyozov (1961) The kinetics of precipitation from supersaturated solid solutions. J. Phys. Chem. Solids 19, 32-50.
Lin, F.-H. and R.A. Yund (1972) Potassium and sodium self-diffusion in alkali feldspar. Contrib. Mineral. Petrol. 34, 177-184.
Lindsley, D.H. (1968) Melting relations of plagioclase at high pressures. New York State Museum Sci. Service Memoir 18, 39-46.
Liotard, J.V., J. Vernieres, and C. Dupuy (1979) Variabilite des valeurs de coefficient de pastage--influence de la structure des liquides magmatiques. Chem. Geol. 26, 237-247.
Lipman, P.W., B.R. Doe, C.E. Hedge, and T.A. Steven (1978) Petrologic evolution of the San Juan volcanic field, southwestern Colorado: Pb and Sr isotopic evidence. Geol. Soc. Am. Bull. 89, 59-82. [Rb Sr Pb Th U]
Loewenstein, W. (1954) The distribution of aluminum in the tetrahedra of silicates and aluminates. Am. Mineral. 39, 92-96.
Long, P.E. (1978) Experimental determination of partition coefficients for rubidium, strontium, and barium between alkali feldspar and silicate liquid. Geochim. Cosmochim. Acta 42, 833-846.
Longhi, J., D. Walker, and J.F. Hays (1976) Fe and Mg in plagioclase. Geochim. Cosmochim. Acta Suppl. 7, 1281-1300.
Longhi, J. and J.F. Hays (1979) Phase equilibria and solid solution along the join $CaAl_2Si_2O_8$-SiO_2. Am. J. Sci. 279, 876-890.
Lorimer, G.W. and P.E. Champness (1973) The origin of the phase distribution in two perthitic alkali feldspars. Phil. Mag. 28, 1391-1403.
Lorimer, G.W., H.-U. Nissen, and P.E. Champness (1974) High voltage electron microscopy of a deformed plagioclase from an Alpine gneiss. Schweiz. Mineral. Petrogr. Mitt. 54, 707-715.
Ludwig, K.R. and L.T. Silver (1977) Lead-isotope inhomogeneity in Pre-cambrian igneous K-feldspars. Geochim. Cosmochim. Acta 41, 1457-1471. [Pb Th U]
Luecke, W. (1981) Lithium pegmatites in the Leinster granite (southeast Ireland). Chem. Geol. 34, 195-233. [Li Be Na Mg Al Si P K Ca Ti Mn Fe Rb Sr Cs Ba]
Luhr, J.F. and I.S.E. Carmichael (1980) The Colima volcanic complex, Mexico. Contrib. Mineral. Petrol. 71, 343-372. [Na Al Si K Ca Sc Ti V Cr Mn Fe Ni Zn Sr Cs Ba REE Hf Th]
Lundstrom, I. (1970) Etch pattern and albite twinning in two plagioclases. Arkiv Mineral. Geol. 5, 63-91.
Luth, W.C. (1974) Analysis of experimental data on alkali feldspars; unit cell parameters and solvi. In, W.S. MacKenzie and J. Zussman, Eds., The Feldspars. Manchester Univ. Press: Manchester, pp. 249-296.
Luth, W.C. and P.M. Fenn (1973) Calculation of binary solvi with special reference to the sanidine-high albite solvus. Am. Mineral. 58, 1009-1015.
Luth, W.C. and F. Querol-Suné (1970) An alkali feldspar series. Contrib. Mineral. Petrol. 25, 25-40.
Luth, W.C. and O.F. Tuttle (1966) The alkali feldspar solvus in the system Na_2O-K_2O-Al_2O_3-SiO_2-H_2O. Am. Mineral. 51, 1359-1373.
Luth, W.C., R.F. Martin, and P.M. Fenn (1974) Peralkaline alkali feldspar solvi. In, W.S. MacKenzie and J. Zussman, Eds., The Feldspars. Manchester Univ. Press: Manchester, pp. 297-312.
Macandiere, J. and W.L. Brown (1982) Transcrystalline shear fracturing and pseudotachylite generation in a meta-anorthosite (Harris, Scotland). J. Struc. Geol. 4, 399-406.
Macek, J.J. (1975) Concerning the construction of the optical orientation diagram of acid and intermediate plagioclases by A.S. Marfunin. Canadian Mineral. 13, 105-109.
Machatschki, F. (1928) The structure and constitution of feldspars. Centr. Mineral. Abt. A, 97-104.
MacKenzie, W.S. (1957) The crystalline modifications of $NaAlSi_3O_8$. Am. J. Sci. 255, 481-516.
MacKenzie, W.S. and J.V. Smith (1955) The alkali feldspars: I. Orthoclase-microperthites. Am. Mineral. 40, 707-732.

MacKenzie, W.S. and J.V. Smith (1956) The alkali feldspars. III. An optical and x-ray study of high-temperature feldspars. Am. Mineral. 41, 405-427.

MacKenzie, W.S. and J.V. Smith (1962) Single crystal x-ray studies of crypto- and microperthites. Norsk Geol. Tidsskr. 42/2, 72-103.

Manning, J.R. (1968) Diffusion Kinetics for Atoms in Crystals. Van Nostrand: New York.

Mardon, D. and R.A. Yund (1981) The effect of anorthite on exsolution rates and the coherent solvus for sanidine-high albite (Abstr.). Trans. Am. Geophys. Union 62, 411.

Marfunin, A.S. (1966) The feldspars: phase relations, optical properties, and geological distribution. (Transl. from the Russian edition, 1962). Israel Prog. Sci. Translations: Jerusalem, 317 pp.

Marfunin, A.S. and L.V. Bershov (1970) Paramagnetic center in feldspar and their possible crystallo-chemical and petrological significance. Dokl. Akad. Nauk. Trans. 193, 129-130.

Marshall, D.B. and A.C. McLaren (1974) The structure of albite and pericline twin boundaries in anorthite. 8th Congr. Electron Micros., Canberra, 1, 490-491.

Marshall, D.B. and A.C. McLaren (1977a) Deformation mechanisms in experimentally deformed plagioclase feldspars. Phys. Chem. Minerals 1, 351-370.

Marshall, D.B. and A.C. McLaren (1977b) The direct observation and analysis of dislocations in experimentally deformed plagioclase feldspars. J. Mater. Sci. 12, 893-903.

Marshall, D.B. and A.C. McLaren (1977c) Elastic twinning in experimentally deformed plagioclase feldspars. Phys. Status Solidi 41, 231-240.

Marshall, D.B., R.H. Vernon and B.E. Hobbs (1976) Experimental deformation and recrystallization of a peristerite. Contrib. Mineral. Petrol. 57, 49-54.

Martin, R.F. (1969) The hydrothermal synthesis of low albite. Contrib. Mineral. Petrol. 23, 323-339.

Martin, R.F. (1970) Cell parameters and infra-red absorption of synthetic high to low albites. Contrib. Mineral. Petrol. 26, 62-74.

Martin, R.F. (1974a) Controls of ordering and subsolidus phase relations in the alkali feldspars. In, W.S. MacKenzie and J. Zussman, Eds., The Feldspars. Manchester Univ. Press: Manchester, pp. 313-336.

Martin, R.F. (1974b) The alkali feldspar solvus: The case for a first-order break on the K-limb. Bull. Soc. franc. Mineral. Cristallogr. 97, 346-355.

Martin, R.F. (1977) The association hypersolvus granite - subsolvus granite - "solvsbergite" at Andrew's Point, Cape Ann, Massachusetts: a case of localized fenitization. Am. J. Sci. 277, 273-287.

Maruyama, S., J.G. Liou, and K. Suzuki (1981) Peristerite from low-grade metamorphic rocks (Abstr.). Trans. Am. Geophys. Union, EOS 62, 1060.

Mason, B. and A.L. Graham (1970) Minor and trace elements in meteoritic minerals. Smithsonian Contrib. Earth Sciences no. 3, 1-17. [B Sc Ti V Cr Mn Co Ni Cu Zn Ga Rb Sr Y Zr Cs Ba REE]

Mason, R.A. (1982) Trace element distributions between the perthite phases of alkali feldspars from pegmatites. Mineral. Mag. 45, 101-106. [Li Na Mg P K Ca Fe Rb Sr Cs Ba Pb]

Mason, R.A., J.V. Smith, J.B. Dawson, and S.B. Treves (1982) A reconnaissance of trace elements in anorthoclase megacrysts. Mineral. Mag. 46, 7-11. [Li B Na Mg P K Ca Ti Fe Rb Sr Cs Ba]

Mathez, E.A. (1973) Refinement of the Kudo-Weill plagioclase thermometer and its application to basaltic rocks. Contrib. Mineral. Petrol. 41, 61-72.

Maury, R. (1968) Conductibilite electrique des tectosilicates II. Discussion des resultats. Bull. Soc. franc. Mineral. Cristallogr. 91, 355-366.

McCallister, R.H. (1978) The coarsening kinetics associated with exsolution in an iron-free clinopyroxene. Contrib. Mineral. Petrol. 65, 327-331.

McConnell, J.D.C. (1965) Electron optical study of effects associated with partial inversion in a silicate phase. Phil. Mag. 11, 1289-1301.

McConnell, J.D.C. (1971) Electron-optical study of phase transformation. Mineral. Mag. 38, 1-20.

McConnell, J.D.C. (1972a) Analysis of the time-temperature-transformation behaviour of the plagioclase feldspars. Abstr. 5.1 in program for N.A.T.O. Advanced Study Institute on Feldspars, July 1972, Manchester, England.

McConnell, J.D.C. (1972b) Electron-optical study of the fine structure of a schiller labradorite. Abstr. 4.4 in program for Advanced Study Institute on Feldspars, July 1972, Manchester, England.

McConnell, J.D.C. (1974a) Analysis of the time-temperature-transformation behaviour of the plagioclase feldspars. In, W.S. MacKenzie and J. Zussman, Eds., The Feldspars. Manchester Univ. Press: Manchester, pp. 460-477.

McConnell, J.D.C. (1974b) Electron-optical study of the fine structure of a schiller labradorite. In, W.S. MacKenzie and J. Zussman, Eds., The Feldspars. Manchester Univ. Press: Manchester, pp. 478-490.

McConnell, J.D.C. (1975) Microstructures of minerals as petrogenic indicators. In, F. Donath, Ed., Annual Rev. Earth Planet. Sci. 3, Annual Reviews Inc.: Palo Alto, California, pp. 129-136.

McConnell, J.D.C. (1978) The intermediate plagioclase feldspars: an example of a structural resonance. Z. Kristallogr. 147, 45-62.

McConnell, J.D.C. (1983) A review of structural resonance and the nature of long-range interactions in modulated mineral structures. Am. Mineral. 68, 1-10.

McConnell, J.D.C. and S.G. Fleet (1963) Direct electron-optical resolution of anti-phase domains in a silicate. Nature 199, 586.

McConnell, J.D.C. and D. McKie (1960) The kinetics of the ordering process in triclinic $NaAlSi_3O_8$. Mineral. Mag. 32, 436-454.

McKie, D. and J.D.C. McConnell (1963) The kinetics of the low → high transformation in albite under dry conditions. Mineral. Mag. 33, 581-588.

McLaren, A.C. (1972) Transmission electron microscopy of the feldspars. Abstr. 4.1 in program for N.A.T.O. Advanced Study Institute on Feldspars, July 1972, Manchester, England.

McLaren, A.C. (1974) Transmission electron microscopy of the feldspars. In, W.S. MacKenzie and J. Zussman, Eds., The Feldspars. Manchester Univ. Press: Manchester, pp. 378-423.

McLaren, A.C. (1978) Defects and microstructures in feldspars. Chemical physics of solids and their surfaces. Chemical Soc. 7, 1-30.

McLaren, A.C. (1983) The microstructure of microclines. Abstr. N.A.T.O. Advanced Study Inst. on Feldspars and Feldspathoids, Rennes, France.

McLaren, A.C. and D.E. Marshall (1974) Transmission electron microscope study of the domain structures associated with the b-, c-, d-, e- and f-reflections in plagioclase feldspars. Contrib. Mineral. Petrol. 44, 237-249.

Megaw, H.D. (1956) Notation for felspar structures. Acta Crystallogr. 9, 56-60.

Megaw, H.D. (1960) Order and disorder. I. Theory of stacking faults and diffraction maxima. II. Theory of diffraction effects in the intermediate plagioclase felspars. III. The structure of the intermediate plagioclase felspars. Proc. Roy. Soc. (London) 259 A, 59-78, 159-183, 184-202.

Megaw, H.D. (1960) Order and disorder. I. Theory of stacking faults and diffraction maxima. II. Theory of diffraction effects in the intermediate plagioclase feldspars. III. The structure of the intermediate plagioclase feldspars. Proc. Roy. Soc. (Lond.), Ser. A259, 59-78, 159-183, 184-202.

Megaw, H.D. (1962) Order and disorder in felspars. Norsk Geol. Tidsskr. 42/2, 104-137.

Megaw, H.D. (1970) Structural relationship between coesite and felspar. Acta Crystallogr. B26, 261-265.

Megaw, H.D. (1973) Crystal Structures: A Working Approach. W.B. Saunders Co.: London, pp. 269-275.

Megaw, H.D. (1974a) The architecture of the feldspars. In, W.S. MacKenzie and J. Zussman, Eds., The Feldspars. Manchester Univ. Press: Manchester, pp. 2-24.

Megaw, H.D. (1974b) Tilts and tetrahedra in feldspars. In, W.S. MacKenzie and J. Zussman, Eds., The Feldspars. Manchester Univ. Press: Manchester, pp. 87-113.

Mehnert, K.R. and W. Busch (1981) The Ba content of K-feldspar megacrysts in granites. N. Jahrb. Mineral. Abh. 140, 221-252. [Ba]

Mérigoux, H. (1968) Etude de la mobilite de l'oxygene dans les feldspaths alcalins. Bull. Soc. franc. Mineral. Cristallogr. 91, 51-64.

Meyer, C., Jr., D.H. Anderson, and J.G. Bradley (1974) Ion microprobe mass analysis of plagioclase from "non-mare" lunar samples. Proc. Fifth Lunar Sci. Conf. 1, 685-706. [Li Na Mg K Ti Sr Ba]

Michel-Lévy, A. (1877) De l'emploi du microscope polarisant a lumiere parallele.

Michel-Lévy, A. (1894) Etude sur la determination des feldspathes. Lib. Polytech., Paris.

Misra, N.K. and V.S. Venkatasubramanian (1977) Strontium diffusion in feldspars - a laboratory study. Geochim. Cosmochim. Acta 41, 837-838.

Mitchell, W.S. and F. Aumento (1977) Uranium in oceanic rocks: DSDP Leg 37. Canadian J. Earth Sci. 14, 794-808. [U]

Mitra, G. (1978) Ductile deformation zones and mylonites: The mechanical processes involved in the deformation of crystalline basement rocks. Am. J. Sci. 278, 1057-1084.

Miúra, Y. (1976) Micro- and fine-structures of plagioclase feldspars. Japan. Assoc. Mineral. Petrol. Econ. Geol. Spec. Ed. 1, 73-91.

Miúra, Y. (1977) Microstructure of polymetamorphic plagioclase feldspars. 5th Int'l. Conf. on High Voltage Electron Microscopy, Kyoto, Japan.

Miúra, Y. (1978) Color zoning in labradorescence. Mineral. J. (Japan) 9, 91-105.

Miúra, Y. (1979) Modulated microstructure of plagioclase feldspars from Hida, Hidaka and Abukuma metamorphic rocks of Japan. In J.M. Cowley et al., Eds., Modulated Structures - 1979. Am. Inst. Phys. Conf. Proc. 53, 314-316.

Miúra, Y. and J.C. Rucklidge (1979) Ion microprobe analyses of exsolution lamellae in peristerites and cryptoperthites. Am. Mineral. 64, 1272-1279.

Miúra, Y. and T. Tomisaka (1978) Ion microprobe mass analysis of exsolution lamellae in labradorite feldspar. Am. Mineral. 63, 584-590.

Miúra, Y., T. Tomisaka, and T. Kato (1974) Experimental and theoretical approaches to iridescent labradorite. Geol. Soc. Japan, Memoir 11, 145-165.

Miúra, Y., T. Tomisaka, and T. Kato (1975) Labradorescence and the ideal behavior of thicknesses of alternate lamellae in the Boggild intergrowth. Mineral. J. (Japan) 7, 526-541.

Morimoto, N., M. Kitamura, and Y. Nakajima (1975a) Antiphase relations in superstructures of the e-plagioclases. Proc. Japan Acad. 51, 729-732.

Morimoto, N., Y. Nakajima, and M. Kitamura (1975b) Direct observation of the superstructure of labradorite by electron microscopy. Proc. Japan Acad. 51, 725-728.

Morris, R.V. (1975) Electron paramagnetic resonance study of the site preferences of Gd^{3+} and Eu^{2+} in polycrystalline silicate and aluminate minerals. Geochim. Cosmochim. Acta 39, 621-634.

Morris, R.V., L.A. Haskin, G.M. Biggar, and M.J. O'Hara (1974) Measurement of the effects of temperature and partial pressure of oxygen on the oxidation states of europium in silicate glasses. Geochim. Cosmochim. Acta 38, 1447-1459.

Morse, S.A. (1968) Revised dispersion method for low plagioclase. Am. Mineral. 53, 105-115.

Morse, S.A. (1969) Feldspars. Carnegie Inst. Washington Year Book 67, 120-126.

Morse, S.A. (1970) Alkali feldspars with water at 5 kb pressure. J. Petrol. 11, 221-253.

Morse, S.A. (1975) Plagioclase lamellae in hypersthene, Tikkoatokhakh Bay, Labrador. Earth Planet. Sci. Lett. 26, 331-336.

Morse, S.A. (1978) Test of plagioclase dispersion method and rapid probe analysis. Am. Mineral. 63, 768-770.

Morse, S.A. (1981) Kiglapait geochemistry III: Potassium and rubidium. Geochim. Cosmochim. Acta 45, 163-180. [K Rb]

Morteani, G. and P. Raase (1974) Metamorphic plagioclase crystallization and zones of equal anorthite content in epidote-bearing, amphibole-free rocks of the western Tavernfenster, eastern Alps. Lithos 7, 101-111.

Muehlenbachs, K. and I. Kushiro (1974) Oxygen isotope exchange and equilibrium of silicates with CO_2 or O_2. Carnegie Inst. Washington Year Book 73, 232-236.

Mügge, O. (1898) Uber Translationen und verwandte Erscheinungen in Kristallen. N. Jahrb. Mineral. Geol. Paleontol. 1, 71-159.

Mügge, O. (1888) N. Jahrb. Mineral. 1, 131f.

Mügge, O. and F. Heide (1931) Einfache Schiebung am Anorthite. N. Jahrb. Mineral. 64, 103-169.

Muir, I.D. and J.V. Smith (1956) Crystallization of feldspars in larvikites. Z. Kristallogr. 107, 182-195.

Müller, G. (1969) Die Abhangigkeit der Gitterkonstanten und der Misch Kristallbildung der Na- und K-Feldspate vom Orgnungszustand. Ph.D. Dissertation, Technische Univ., Karlsruhe.

Müller, G. (1970) Der Ordnungs-Unordnungsubergang in getemperten Mikroklinen und Albiten. Z. Kristallogr. 132, 212-227.

Müller, W.F. (1976) On polymorphism of $BaAl_2Si_2O_8$. In, H.-R. Wenk et al., Eds., Electron Microscopy in Mineralogy, Springer-Verlag: Berlin, pp. 353-360.

Müller, W.F. and H.-R. Wenk (1973) Changes in the domain structure of anorthites induced by heating. N. Jahrb. Mineral. Monatsh., 17-26.

Müller, W.F., H.-R. Wenk, W.L. Bell, and G. Thomas (1973) Analysis of displacement vectors of antiphase domain boundaries in anorthites ($CaAl_2Si_2O_8$). Contrib. Mineral. Petrol. 40, 63-72.

Nagasawa, H., D.P. Blanchard, J.W. Jacobs, J.C. Brannon, J.A. Philpotts, and N. Onuma (1977) Trace element distribution in mineral separates of the Allende inclusions and their genetic significance. Geochim. Cosmochim. Acta 41, 1587-1600.

Nagy, K.L. (1981) Experimental determination of grain boundary transport for oxygen along lamellar boundaries in a perthitic feldspar. M.Sc. Thesis, Brown Univ.: Providence, R.I., 139 pp.

Nagy, K.L. and B.J. Giletti (1980) Grain boundary transport of oxygen in perthites. Geol. Soc. Am. Abstracts with Programs 12, 490.

Nagy, K.L. and E.M. Parmentier (1981) Diffusive transport of oxygen near an intrusive contact (Abstr.). Trans. Am. Geophys. Union 62, 428.

Nakajima, Y. and P.H. Ribbe (1981) Twinning and superstructure of Al-rich mullite. Am. Mineral. 66, 142-147.

Nakajima, Y., N. Morimoto, and M. Kitamura (1977) The superstructure of plagioclase feldspars. Phys. Chem. Minerals 1, 213-225.

Neiva, A.M.R. (1972) Sobre a microclina des alguns aplitose pegmatitos de Alijo-Sanfins (Vila-Real), Norte de Portugal. Memorias et Noticias, Coimbra, No. 74, 5-10. [Li Be Na K Ca Cr Ni Ga Rb Sr Zr Cs Ba Pb]

Neiva, A.M.R. (1973) Geochemistry of the granites and their minerals from the central area of northern Portugal. Memorias et Noticias, Coimbra, No. 76, 1-43. [Li Be Na K Ca Ni Ga Rb Sr Zr Cs Ba Pb]

Neiva, A.M.R. (1974) Greisenization of a muscovite-biotite albite granite of northern Portugal. Chem. Geol. 13, 295-308. [Li Be Na K Ca Cr V Ni Ga Rb Sr Zr Cs Ba Pb]

Neiva, A.M.R. (1974) Geochemistry of the aplites and their minerals of Central Northern Portugal. Services Geol. Portugal Comm. 58, 213-237. [Li Be Na K Ca Cr V Ni Ga Rb Sr Zr Cs Ba Pb]

Neiva, A.M.R. (1975) Geochemistry of coexisting aplites and pegmatites and of their minerals from central northern Portugal. Chem. Geol. 16, 153-177. [Li Be Na K Ca V Gu Rb Sr Cs Ba Pb]

Neiva, A.M.R. (1977a) Distribution of some elements between coexisting minerals from granites, aplites and pegmatites from central northern Portugal. Chem. Geol. 20, 223-233.

Neiva, A.M.R. (1977b) Geochemistry of the pegmatites and their minerals from central northern Portugal. Anais Faculdade Ciecias de Porto 60, 3-28. [Li Be Na K Ca V Ni Ga Rb Sr Zr Cs Ba Pb]

Neiva, A.M.R. (1980) Geochemistry and petrology of a hybrid granitoid rock from the near west and southwest of Senhora de Cunha (Alijo, Portugal. VI Reuniao Geologica Oeste Peninsular, Univ. Oporto, Portugal, 41, 91-100. [Li Be Na K Ca V Ni Ga Rb Sr Zr Cs Ba Pb]

Neumann, H. and O.H.J. Christie (1962) Observations on plagioclase adverturines from Southern Norway. Norsk Geol. Tidsskr. 42/2, 389-393.

Newland, B.T. (1963) On the diffusion of radiogenic argon from potassium feldspars. M.Sc. Thesis, University of Alberta: Edmonton, 119 pp.

Nicolas, A. and J.P. Poirier (1976) Crystalline Plasticity and Solid State Flow in Metamorphic Rocks. John Wiley and Sons: New York. 444 pp.

Niggli, A. (1967) Die Ordnungsmöglichkeiten der Si-Al-Verteilung in Plagioklasen. Schweiz. Mineral. Petrogr. Mitt. 47, 279-287.

Nissen, H.-U. (1968) A study of bytownites in amphibolites of the Ivrea zone (Italian Alps) and in anorthosites: a new unmixing gap in the low plagioclases. Schweiz. Mineral. Petrogr. Mitt. 48, 53-55.

Nissen, H.-U. (1969) Lattice changes in the low plagioclase series. Schweiz. Mineral. Petrogr. Mitt. 49, 491-508.

Nissen, H.-U. (1971) End member compositions of the labradorite exsolution. Naturwiss. 58, 454.

Nissen, H.-U. (1974) Exsolution phenomena in bytownite plagioclases. In, W.S. MacKenzie and J. Zussman, Eds., The Feldspars. Manchester Univ. Press: Manchester, pp. 491-521.

Nissen, H.-U. and W. Bollmann (1968) Doubled Kikuchi lines as a means of distinguishing quasi-identical phases. IVth Europ. Reg. Conf. Electron Microscopy, Rome.

Nissen, H.-U., H. Eggmann, and F. Laves (1967) Schiller and submicroscopic lamellae of labradorite. A preliminary report. Schweiz. Mineral. Petrogr. Mitt. 47, 289-302.

Nissen, H.-U., P.E. Champness, G. Cliff, and G.W. Lorimer (1973) Chemical evidence for exsolution in a labradorite. Nature Phys. Sci. 245, 135-137.

Nord, G.L., A.H. Heuer, and J.S. Lally (1974) Transmission electron microscopy of substructures in Stillwater bytownites. In, W.S. Mackenzie and J. Zussman, Eds., The Feldspars. Manchester Univ. Press: Manchester, pp. 522-535.

Nord, G.L., Jr., J. Hammarstrom, and E. Zen (1978) Zoned plagioclase and peristerite formation in phyllites from southwestern Massachusetts. Am. Mineral. 63, 947-955.

Nord, G.L., A.H. Heuer, J.S. Lally, and J.M. Christie (1975) Substructures in lunar clinopyroxenes as petrologic indicators. Lunar Sci. VI, 601-603.

Norris, R.J. and R.W. Henley (1976) Dewatering of a metamorphic pile. Geology 4, 333-336.

Nunes, J.L. (1979) Amazonites de Mocambique. Communic. Serv. Geol. Portugal LXIV, 71-79.

Nye, J.F. (1957) The Physical Properties of Crystals. Oxford Press: London, 322 pp.

O'Neil, J.R. and H.P. Taylor (1967) The oxygen isotope and cation exchange chemistry of feldspars. Am. Mineral. 52, 1414-1437.

Oftedal, I. (1957) Heating experiments on amazonite. Mineral. Mag. 31, 417-419.

Ohashi, Y. and L.W. Finger (1973) Lattice deformation in feldspars. Carnegie Inst. Washington Year Book 72, 569-573.

Ohashi, Y. and L.W. Finger (1975) An effect of temperature on feldspar structure: crystal structure of sanidine at 800°C. Carnegie Inst. Washington Year Book 74, 569-572.

Ohashi, Y., and L.W. Finger (1974) Refinement of the crystal structure of sanidine at 25° and 400° Carnegie Inst. Washington Year Book 73, 539-544.

Ohta, Y. (1969) On the formation of augen structures. Lithos 2, 109-132.

Okamura, F.P. and S. Ghose (1975) Analbite → monalbite transition in a heat treated twinned Amelia albite. Contrib. Mineral. Petrol. 50, 211-216.

Olsen, A. (1974) Schiller effects and exsolution in sodium-rich plagioclases. Contrib. Mineral. Petrol. 47, 141-152.

Olsen, A. (1975) Study of peristerites using transmission electron microscopy and energy dispersive X-ray analysis. Contrib. Mineral. Petrol. 51, 297-302.

Olsen, A. (1977) Lattice parameter determination of exsolution structures in labradorite feldspars. Acta Crystallogr. A33, 706-712.

Olsen, A. (1979) Coherent elastic energies of exsolution boundaries in peristerite and Boggild intergrowths. Phys. Chem. Minerals 4, 115-127.

Olsen, T.S. and D.L. Kohlstedt (1981) Dislocations in some naturally deformed plagioclase feldspars. Trans. Am. Geophys. Union 62, 395.

Orville, P.M. (1963) Alkali ion exchange between vapor and feldspar phases. Am. J. Sci. 261, 201-237.

Orville, P.M. (1967) Unit-cell parameters of the microcline-low albite and the sanidine-high albite solid solution series. Am. Mineral. 52, 55-86.

Orville, P.M. (1972) Plagioclase cation exchange equilibria with aqueous chloride solution: results at 700°C and 2000 bars in the presence of quartz. Am. J. Sci. 272, 234-272.

Orville, P.M. (1974) The "peristerite" gap as an equilibrium between ordered albite and disordered plagioclase solid solution. Bull. Soc. franc. Mineral. Cristallogr. 97, 386-392.

Oversby, V.M. (1975) Lead isotope systematics and ages of Archaean acid intrusives in the Kalgoorlie-Norseman area, Western Australia. Geochim. Cosmochim. Acta 39, 1107-1125.

Owen, D.C. and J.D.C. McConnell (1974) Spinodal unmixing in an alkali feldspar. In, W.S. MacKenzie and J. Zussman, Eds., The Feldspars. Manchester Univ. Press: Manchester, pp. 424-439.

Pallister, J.S. and R.J. Knight (1981) Rare-earth element geochemistry of the Samail ophiolite near Ibra, Oman. J. Geophys. Res. 86, 2673-2697. [La Ce Nd Sm Eu Gd Tb Dy Tm Yb Lu]

Park, M., T.E. Mitchell, and A.H. Heuer (1976) Coarsening in a spinodally decomposing system: TiO_2-SnO_2. In, H.-R. Wenk et al., Eds., Electron Microscopy in Mineralogy. Springer-Verlag: Berlin, pp. 205-208.

Parmentier, E.M. (1981) Numerical experiments on ^{18}O depletion in igneous intrusions cooling by groundwater convection. J. Geophys. Res. 86, 7131-7144.

Parsons, I. (1968) An experimental study of ordering in sodium-rich alkali feldspars. Mineral. Mag. 36, 1061-1077.

Parsons, J. (1978) Feldspars and fluids in cooling plutons. Mineral. Mag. 42, 1-18.

Passchier, C.W. (1982) Mylonitic deformation in the Saint-Barthelemy Massif, French Pyrenees, with emphasis on the genetic relationship between ultramylonite and pseudotachylite. GUA Papers of Geology, Ser. 1, No. 16, Amsterdam, 173 p.

Paster, T.P., D.S. Schauwecker, and L.A. Haskin (1974) The behavior of some trace elements during solidification of the Skaergaard layered series. Geochim. Cosmochim. Acta 38, 1549-1577. [Sc Cr Mn Co Ni Cu Zn Ga As Ag Ba La Ce Nd Sm Eu Gd Tb Ho Yb]

Patchett, P.J., O. van Breemen, and R.F. Martin (1979) Sr isotopes and the structural state of feldspars as indicators of post-magmatic hydrothermal activity in continental dolerites. Contrib. Mineral. Petrol. 69, 65-73.

Pauling, L. (1929) The principles determining the structure of complex ionic crystals. J. Am. Chem. Soc. 51, 1010-1026.

Pazyuk, L.I. (1957) Iridescence of andesine-labradorites. Partsi Odes'k. Univ. 147, Ser. Geol., Geograf. Nauk, 149-158 [in Russian].

Pentinghaus, H. (1975) Hexacelsiane. Fortschr. Mineral. 53, 65.

Pentinghaus, H. (in preparation) Polymorphie in den Feldspätbildenden Systemen $A^+[T^{3+}T^{4+}{}_3O_8]$ und $A^{2+}[T^{3+}{}_2T^{4+}{}_2O_8]$. Alkali- und Erdalkali-, Bor-, Aluminum-, Gallium-, Eisen-Silikate und -Germanate. Habilitationsschrift in Fachbereich Chemie, Westf. Wilhelms-Univ., Münster.

Peterson, N.V. (1972) Oregon "sunstones." The Ore Bin, State of Oregon, Dept. Geol. Min. Industr. 34, 197-215.

Petrović, R. (1972) Alkali ion diffusion in alkali feldspars. Ph.D. Dissertation, Yale University, New Haven, Connecticut, 131 pp.

Petrović, R. (1974) Diffusion of alkali ions in alkali feldspars. In, W.S. MacKenzie and J. Zussman, Eds., The Feldspars. Manchester University Press, Manchester, pp. 174-182.

Phillips, E.R., B.E. Chenhall, I.J. Stone, and J.W. Perberton (1977) An intergrowth of calcic labradorite in a plagioclase-quartz-biotite gneiss from Broken Hill, New South Wales. Mineral. Mag. 41, 469-471.

Phillips, M.W. and P.H. Ribbe (1973a) The variation of tetrahedral bond lengths in sodic plagioclase feldspars. Contrib. Mineral. Petrol. 39, 327-339.

Phillips, M.W. and P.H. Ribbe (1973b) The structures of monoclinic potassium-rich feldspars. Am. Mineral. 58, 263-270.

Phillips, M.W., A.A. Colville, and P.H. Ribbe (1971) The crystal structures of two oligoclases: a comparison with low and high albite. Z. Kristallogr. 133, 43-65.

Phillips, M.W., G.V. Gibbs, and P.H. Ribbe (1974) The crystal structure of danburite: a comparison with anorthite, albite and reedmergnerite. Am. Mineral. 59, 79-85.

Phillips, M.W., P.H. Ribbe, and G.V. Gibbs (1973) Tetrahedral bond length variations in anorthite. Am. Mineral. 58, 495-499.

Phillips, W.R. and D.T. Griffen (1981) Optical Mineralogy: The Nonopaque Minerals. Freeman and Company: San Francisco, pp. 331-363.

Philpotts, A.R. (1966) Origin of the anorthosite-mangerite rocks in Southern Quebec. J. Petrol. 7, 1-64.

Plimer, I.R. (1976) A plumbian feldspar pegmatite associated with the Broken Hill ore bodies, Australia. N. Jahrb. Mineral. Monatsh. 272-288. [Na Mg Al Si P K Ca Ti V Cr Mn Fe Ni Cu Zn Ga Rb Sr Y Zr Pb Th U H_2O]

Plyusnin, G.S. (1969) On the coloration of amazonite. Zap. Vses. Mineral. Obstchest. 98, 3-17 [in Russian].

Potter, C.J. (1976) Alkali feldspar deformation in shear zones in the Kinsman quartz-monzonite. Trans. Am. Geophys. Union 57, 322.

Prewitt, C.T., S. Sueno, and J.J. Papike (1974) Models for albite in different structural states. Trans. Am. Geophys. Union 55, 464.

Prewitt, C.T., S. Sueno, and J.J. Papike (1976) The crystal structures of high albite and monalbite at high temperatures. Am. Mineral. 61, 1213-1225.

Priess, U. (1981) Untersuchungen zur Tief-Hoch-Umwandlung von Fe-hältigen Orthoklas-Kristallen aus Madagascar. N. Jahrb. Mineral. Abh. 141, 17-29.

Prince, E., G. Donnay, and R.F. Martin (1973) Neutron diffraction refinement of an ordered orthoclase structure. Am. Mineral. 58, 500-507.

Przibram, K. (1956) Irradiation Colors and Luminescence. Permagon Press: London.

Putnis, A. and J.D.C. McConnell (1980) Principles of Mineral Behaviour. Elsevier: New York, 257 pp.

Raase, P. (1971) Zur Synthese und Stabilität der Albit-Modifikationen. Tschermaks Mineral. Petrogr. Mitt. 16, 136-155.

Raase, P. (1978) Extinction angles of synthetic intermediate albites. Am. Mineral. 63, 466-469.

Raase, P. and H. Kern (1969) Über die Synthese von Albiten bei Temperaturen von 250 bis 700°C. Contrib. Mineral. Petrol. 21, 225-237.

Raase, P. and G. Morteani (1976) The potassic feldspar in metamorphic rocks from the western Hohe Tauern area, eastern Alps. Geol. Rundschau 65, 422-436.

Raith, M. (1969) Peristerite aus alpidischmetamorphen Gneisen der Zillertaler Alpen (Tirol, Osterreich). Contrib. Mineral. Petrol. 21, 357-364.

Rankin, D.W. (1967) Axial angle determinations in Orville's microcline-low albite solid solution series. Am. Mineral. 52, 414-417.

Rayleigh, Lord (1923) Studies of iridescent colour, and the structure producing it. III. The colours of labrador felspar. Proc. Roy. Soc. (London) 103A, 34-45.

Reddy, K.P.R., S.M. Oh, L.D. Major, and A.R. Cooper (1980) Oxygen diffusion in forsterite. J. Geophys. Res. 85, 323-326.

Ribbe, P.H. (1960) An x-ray and optical investigation of peristerite plagioclases. Am. Mineral. 45, 626-644.

Ribbe, P.H. (1962) Observations on the nature of unmixing in peristerite plagioclases. Norsk Geol. Tidsskr. 42/2, 138-151.

Ribbe, P.H. (1963) Structural Studies of Plagioclase Felspars. Ph.D. Dissertation, Univ. of Cambridge: Cambridge, England, 279 pp.

Ribbe, P.H. (1972a) One-parameter characterization of the average Al/Si distribution in plagioclase feldspars. J. Geophys. Res. 77, 5790-5797.

Ribbe, P.H. (1972b) Interference colors in oil slicks and feldspars. Mineral. Record 3, 18-22.

Ribbe, P.H. (1975) The chemistry, structure and nomenclature of feldspars. Optical properties and lattice parameters of plagioclase feldspars. In, P.H. Ribbe, Ed., Feldspar Mineralogy, Mineral. Soc. Am., Short Course Notes, Vol. 2, First Ed.

Ribbe, P.H. (1979) The structure of a strained intermediate microcline in cryptoperthitic association with twinned plagioclase. Am. Mineral. 64, 402-408.

Ribbe, P.H. and A.A. Colville (1968) Orientation of the boundaries of out-of-step domains in anorthite. Mineral. Mag. 36, 814-819.

Ribbe, P.H. and G.V. Gibbs (1969) Statistical analysis and discussion of mean Al/Si-O bond distances and the aluminum content of tetrahedra in feldspars. Am. Mineral. 54, 85-94.

Ribbe, P.H. and J.V. Smith (1966) X-ray emission microanalysis of rock-forming minerals. IV. Plagioclase feldspars. J. Geol. 74, 217-233.

Ribbe, P.H. H.D. Megaw, and W.H. Taylor (1969) The albite structures. Acta Crystallogr. B25, 1503-1518.

Ribbe, P.H., M.W. Phillips, and G.V. Gibbs (1974) Tetrahedral bond length variations in feldspars. In, W.S. MacKenzie and J. Zussman, Eds., The Feldspars. Manchester Univ. Press: Manchester, pp. 25-48.

Ried, H. and M. Korekawa (1978) Twinning and exsolution in an antiperthite. Phys. Chem. Minerals 3, 263-270.

Rimsaite, J. (1967) Optical heterogeneity of feldspars observed in diverse Canadian rocks. Schweiz. Mineral. Petrogr. 47, 61-76.

Robin, P.-Y.F. (1974a) Thermodynamic equilibrium across a coherent interface in a stressed crystal. Am. Mineral. 59, 1299-1318.

Robin, P.-Y.F. (1974b) Stress and strain in cryptoperthite lamellae and the coherent solvus of alkali feldspars. Am. Mineral. 59, 1299-1318.

Robinson, K., G.V. Gibbs, and P.H. Ribbe (1971) Quadratic elongation: A quantitative measure of distortion in coodination polyhedra. Science 172, 567-570.

Rosenquist, I.T. (1949) Some investigations in the crystal chemistry of silicates I. Diffusion of Pb and Ra in feldspars. Acta Chem. Scandinavica 3, 569-583.

Rudenko, S.A. and A.Ya. Vokhmentsev (1969) Plagioclase-amazonite. Dokl. Akad. Nauk. Trans. 184, 113-115.

Ryzhova, T.V. (1964) Elastic properties of plagioclase. Akad. Nauk SSSR, Bull. Geophys. Ser. No. 7, 633-635 (pp. 1049-1051 in Russian).

Ryzhova, T.V. and K.S. Alexsandrov (1965) The elastic properties of potassium-sodium feldspars. Akad. Nauk SSSR, Bull. Geophys. Ser. No. 1, 53-56 (pp. 98-102 in Russian).

Sacerdoti, M., H. Labernadiere and M. Gandais (1980) Transmission electron microscope (TEM) study of geologically deformed potassic feldspars. Bull. Mineral. 103, 148-155.

Sanders, J.V. and P.J. Darragh (1971) The microstructure of precious opal. Mineral. Record 2, 261-268.

Sauvage, M. and A. Authier (1965) Etude des bandes de croissance et des dislocations de macle dans la calcite. Bull. Mineral. 88, 379-385.

Scandale, E., M. Gandais and C. Willaime (1983) Transmission electron microscopic study of experimentally deformed K-feldspar single crystals. The (010)[001], (001)1/2[110], (110)1/2[112] and (111)1/2[110] slip systems. Phys. Chem. Minerals 9, 182-187.

Schairer, J.F., J.R. Smith, and F. Chayes (1956) Refractive indices of plagioclase glasses. Carnegie Inst. Washington Year Book 55, 195-197.

Schmid, S.M., J.M. Boland and M.S. Paterson (1977) Superplastic flow in finegrained limestone. Tectonophysics 43, 257-291.

Schurmann, K. and S.S. Hafner (1972) On the amount of ferric iron in plagioclases and from lunar rocks. Proc. 3rd Lunar Planet. Sci. Conf. I, 615-621.

Sclar, C.B. and A.I. Benimoff (1980) Magnesium in anorthite: synthesis and petrological significance of $CaMgSi_3O_8$ (Abstr.). Trans. Am. Geophys. Union, EOS 61, 392.

Sclar, C.B. and R.L. Kastelic (1979) Iron in anorthite: synthesis and characterization of the $CaAl_2Si_2O_8$-$CaFeSi_3O_8$ series (Abstr.). Trans. Am. Geophys. Union, EOS 60, 421.

Scotford, D.M. (1969) Metasomatic augen gneiss in greenschist facies, western Turkey. Geol. Soc. Amer. Bull. 80, 1079-1094.

Scott, E.R.D. and R.W. Bild (1974) Structure and formation of the San Cristobal meteorite, other IB irons and group III CD. Geochim. Cosmochim. Acta 38, 1379-1391.

Scott, R.B., S.W. Bachinski, R.W. Nesbitt, and M. Scott (1971) Rate of Al-Si ordering in sanidines from an ignimbrite cooling unit. Am. Mineral. 56, 1208-1221.

Seck, H.A. (1971) Koexistierend Alkali-feldspäte und Plagioklase im System $NaAlSi_3O_8$-$KAlSi_3O_8$-$CaAl_2Si_2O_8$-H_2O bei temperaturen von 650°C bis 900°C. N. Jahrb. Mineral. Abh. 115, 315, 395.

Seck, H.A. (1972) The influence of pressure on the alkali feldspar solvus from peraluminous and persilicic materials. Fortschr. Mineral. 49, 31-49.

Seifert, K.E. (1969) Strength of Adirondack anorthosite at elevated temperatures and pressures. Geol. Soc. Am. Bull. 80, 2053-2060.

Seifert, K.E. and A.J. VerPloeg (1977) Deformation charateristics of experimentally deformed Adirondack anorthosite. Canadian J. Earth Sci. 14, 2706-2717.

Senderov, E.E. (1980) On the theory of Al,Si ordering in albite. Phys. Chem. Minerals 6, 251-268.

Senderov, E.E. and T.I. Shchekina (1976) Natural production conditions and stability of structural forms of albite. Geochemistry Int'l 13, 99-112. Trans. from Geokhimiya, 159-175.

Shelton, G.L., J. Tullis and T.E. Tullis (1980) Experimental faults at high temperature and pressure. Geophys. Res. Letters 8, 55-58.

Shimizu, N. (1978) Analysis of the zoned plagioclase of different magmatic environments: a preliminary ion-microprobe study. Earth Planet. Sci. Lett. 39, 398-406. [Na Mg Al Si K Ca Fe Sr]

Shmakin, B.M. (1968) Enigma of the amazonstone. Priroda No. 8, 52-57, [in Russian].

Shmakin, B.M. (1979) Composition and structural state of K-feldspars from some U.S. pegmatites. Am. Mineral. 64, 49-56. [Rb Sr Cs Ba]

Siemiatkowska, K.M. and R.F. Martin (1975) Fenitization of Mississagi quartzite, Sudbury area, Ontario. Geol. Soc. Amer. Bull. 86, 1109-1122.

Simmons, G. (1964) Velocity of compressional waves in various minerals at pressures to 10 kilobars. J. Geophys. Res. 69, 1117-1121.

Simpson, D.R. (1977) Aluminum phosphate variants of feldspar. Am. Mineral. 62, 351-355.

Sinkankis, J. (1976) Gemstones of North America II. Von Nostrand and Reinhold: New York.

Sipling, P.J. (1975) Coherent Exsolution in the Sanidine-Analbite Series. Ph.D. Dissertation, Brown University, Providence, R.I.

Sipling, P.J. and R.A. Yund (1974) The coherent solvus for the sanidine-analbite series. Geol. Soc. Am. Abstracts with Programs 6, 958.

Sipling, P.J. and R.A. Yund (1976) Experimental determination of the coherent solvus for sanidine-high albite. Am. Mineral. 61, 897-906.

Sippel, R.F. (1963) Sodium self-diffusion in natural minerals. Geochim. Cosmochim. Acta 27, 107-120.

Slimming, E.H. (1976) An electron diffraction study of some intermediate plagioclases. Am. Mineral. 61, 54-59.

Smith, J.R. (1960) Optical properties of low-temperature plagioclase. In, H.H. Hess, Ed., Stillwater Igneous Complex, Montana. Geol. Soc. Am. Memoir 80.

Smith, J.R. and H.S. Yoder, Jr. (1956) Variations in X-ray powder diffraction patterns of plagioclase feldspars. Am. Mineral. 41, 632-647.

Smith, J.V. (1954) A review of the Al-O and Si-O distances. Acta Crystallogr. 7, 479-483.

Smith, J.V. (1956) The powder patterns and lattice parameters of plagioclase feldspars. I. The soda-rich plagioclases. Mineral. Mag. 31, 47-68.

Smith, J.V. (1961) Explanation of strain and orientation effects in perthites. Am. Mineral. 46, 1489-1493.

Smith, J.V. (1962) Genetic aspects of twinning in feldspars. Norsk Geol. Tidsskr. 42/2, 244-263.

Smith, J.V. (1968) Cell dimensions b^*, c^*, α^*, γ^* of alkali feldspars permit qualitative estimates of Si,Al ordering: albite ordering process. Abstr. Geol. Soc. Am. Spec. Paper 121, 283.

Smith, J.V. (1983) Phase relations of plagioclase feldspars. Abstr. N.A.T.O. Advanced Study Inst. on Feldspars and Feldspathoids, Rennes, France.

Smith, J.V. and H.-R. Wenk (1983) Reinterpretation of a Verzasca plagioclase. A correction. Am. Minerral. 68 (in press).

Smith, J.V. (1970) Physical properties of order-disorder structures with special reference to feldspar minerals. Lithos 3, 145-160.

Smith, J.V. (1972) Critical review of synthesis and occurrence of plagioclase feldspars and a possible phase diagram. J. Geol. 80, 505-525.

Smith, J.V. (1974a) Feldspar Minerals. I. Crystal Structure and Physical Properties. Springer-Verlag: Heidelberg, 627 pp.

Smith, J.V. (1974b) Feldspar Minerals. II. Chemical and Textural Properties. Springer-Verlag: Heidelberg, 690 pp.

Smith, J.V. and S.W. Bailey (1963) Second review of Al-O and Si-O tetrahedral distances. Acta Crystallogr. 16, 801-811.

Smith, J.V. and P. Gay (1958) The powder patterns and lattice parameters of plagioclase felspars. II. Mineral. Mag. 31, 744-762.

Smith, J.V. and W.S. MacKenzie (1958) The alkali feldspars: IV. The cooling history of high-temprature sodium-rich feldspars. Am. Mineral. 43, 872-889.

Smith, J.V. and I.D. Muir (1958) The reaction sequence in larvikite feldspars. Z. Kristallogr. 110, 11-20.

Smith, J.V. and P.H. Ribbe (1966) X-ray-emission microanalysis of rock-forming minerals. III. Alkali feldspars. J. Geol. 76, 197-216.

Smith, J.V. and P.H. Ribbe (1969) Atomic movements in plagioclase feldspars: kinetic interpretation. Contrib. Mineral. Petrol. 21, 157-202.

Smith, J.V. and F. Rinaldi (1962) Framework structures formed from parallel four- and eight-member rings. Mineral. Mag. 33, 202-212.

Smith, J.V. and I.M. Steele (1974) Intergrowths in lunar and terrestrial anorthosites with implications for lunar differentiation. Am. Mineral. 59, 673-680.

Smith, J.V. and H.-R. Wenk (1983) Reinterpretation of a Verzasca plagioclase. A correction. Am. Mineral. 68 (in press).

Smith, J.V., I.M. Steele, and B.E. Leake (1973) Plagioclase compositions in the Connemara migmatites of the Cashel district, Connemara, Ireland. J. Geol. 81, 648-650.

Smith, P. (1978) The effect of anorthite on the alkali feldspar solvus at P(water) = 1 kb. Progr. Experimental Petrol., Natural Environ. Res. Council, D. 247-248.

Smith, P. and I. Parsons (1974) The alkali-feldspar solvus at 1 kilobar water-vapour pressure. Mineral. Mag. 39, 747-767.

Spear, F.S. (1977) Evidence of a miscibility gap in plagioclase feldspar in the composition range An_3?-An_{88}. Carnegie Inst. Washington Year Book 76, 619-621.

Spear, F.S. (1980) NaSi → CaAl exchange equilibria between plagioclase and amphibole. Contrib. Mineral. Petrol. 72, 33-41.

Speer, J.A. and P.H. Ribbe (1973) The feldspars of the Kiglapait intrusion, Labrador. Am. J. Sci. 273-A, 468-478.

Speit, B. and G. Lehmann (1976) Hole centers in the feldspar sanidine. Phys. Stat. Sol. A36, 471-481.

Spencer, E. (1930) A contribution to the study of moonstone from Ceylon and other areas and of the stability releation of the alkali-feldspars. Mineral. Mag. 22, 291-367.

Spencer, E. (1937) The potash-soda feldspars I. Thermal stability. Mineral. Mag. 24, 453-494.

Staehli, J.L. and D. Brinkmann (1974) A nuclear magnetic resonance study of the phase transiion in anorthite, $CaAl_2Si_2O_8$. Z. Kristallogr. 140, 360-373; 374-392.

Starkey, J. (1963) Glide twinning in the plagioclase feldspars. In, R.E. Reed-Hill et al., Eds., Deformation Twinning, Metallurgical Soc. Conf. 25, 177-191.

Starkey, J. (1967) On the relationship of Pericline and Albite twinning to the composition and structural state of plagioclase feldspars. Schweiz. Mineral. Petrogr. Mitt. 47, 257-268.

Starkey, J. and W.L. Brown (1964) Kunstliche Erzeugung mechanischer Zwillinge in Anorthit. Z. Kristallogr. 120, 388-392.

Steele, I.M. and J.V. Smith (1982a) Trace elements in plagioclase from banded zone of Stillwater: variation with stratigraphy and Na content of plagioclase. Lunar Planet. Sci. XIII, in press.

Steele, I.M. and J.V. Smith (1982b) Ion probe analysis of plagioclase in three howardites and three eucrites. Geochim. Cosmochim. Acta, Suppl. in press.

Steele, I.M., I.D. Hutcheon, and J.V. Smith (1980a) Ion microprobe analysis of plagioclase feldspar ($Ca_{1-x}Na_xAl_{2-x}Si_{2+x}O_8$) for major, minor and trace elements. Eighth Int'l Congr. X-Ray Optics Microanalysis, pp. 515-525. Pendell Publishing Co.: Midland, Michigan. [Li Be B F Mg P K Ti V Mn Fe Sr Ba]

Steele, I.M., I.D. Hutcheon, and J.V. Smith (1980b) Ion microprobe analysis and petrogenetic interpretations of Li, Mg, Ti, K, Sr, Ba in lunar plagioclase. Geochim. Cosmochim. Acta Suppl. 14, 571-590. [Li Mg K Ti Sr Ba]

Steele, I.M., J.V. Smith, L.D. Raedeke, and I.S. McCallum (1981) Ion probe analysis of Stillwater plagioclase and comparison with lunar analyses. Lunar Planet. Sci. XII, 1034-1036.

Stewart, D.B. (1974) Optic axial angle and extinction angles of alkali feldspars related by cell parameters to Al/Si order and composition. In, W.S. MacKenzie and J. Zussman, Eds., The Feldspars. Manchester Univ. Press: Manchester, pp. 145-161.

Stewart, D.B. (1975) Lattice parameters, composition and Al/Si order in alkali feldspars. In, P.H. Ribbe, Ed., Feldspar Mineralogy, Mineral. Soc. Am., Short Course Notes, Vol. 2, First Ed.

Stewart, D.B. and D. von Limbach (1967) Thermal expansion of low and high albite. Am. Mineral. 52, 389-413.

Stewart, D.B. and P.H. Ribbe (1969) Structural explanation for variations in cell parameters of alkali feldspar with Al/Si ordering. Am. J. Sci. 267-A, 144-462.

Stewart, D.B. and T.L. Wright (1974) Al/Si order and symmetry of natural alkali feldspars, and the relationship of strained cell parameters to bulk composition. Bull. Soc. franc. Mineral. Cristallogr. 97, 356-377.

Stewart, D.B., G.W. Walker, T.L. Wright, and J.J. Fahey (1966) Physical properties of calcic labradorite from Lake County, Oregon. Am. Mineral. 51, 177-197.

Stocker, R.L. and M.F. Ashby (1973) On the rheology of the upper mantle. Rev. Geophys. 11, 391-426.

Stookey, S.D., G.H. Beall, and J.E. Pierson (1978) Full-color photosensitive glass. J. Appl. Phys. 40, 5114-5123.

Streckeisen, A., E. Wenk, and M. Frey (1974) On steep isogradic surfaces in the Simplon area. Contrib. Mineral. Petrol. 47, 81-95.

Strob, W. (1983) Strukturverfeinerung eines Tief-Mikroklins, Zusammenhange zwischen <T-O> Abstanden und Al,Si-Ordnungsgrad und metrische Variation in einer Tief-Albit/Tief-Mikroklin-Mischkristallreihe. Diplomarbeit, Inst. Mineralogie, Westf. Wilhelms-Univ., Münster.

Su, S.-C. and D. Ye (1981) X-ray powder method for simultaneous determination of composition and structural state of plagioclases. Scientia Sinica 24/5, 670-677.

Su, S.-C., F.D. Bloss, P.H. Ribbe and D.B. Stewart (1983) Rapid and precise optical determination of Al,Si ordering in potassic feldspars. Abstr. N.A.T.O. Advanced Study Inst. on Feldspars and Feldspathoids, Rennes, France.

Sun, C.-O. and R.J. Williams (1973) Experimentally determined distribution coefficients of Eu and Sr for plagioclase-liquid and clinopyroxene-liquid equilibria in an oceanic ridge basalt. Geol. Soc. Am. Abstracts with Programs 5, 830.

Sun, C.-O., R.J. Williams, and S.-S. Sun (1974) Distribution coefficients of Eu and Sr for plagioclase-liquid and clinopyroxene-liquid equilibria in oceanic ridge basalt: an experimental study. Geochim. Cosmochim. Acta 38, 1415-1433.

Sun, S. and G.N. Hanson (1976) Rare earth element evidence for differentiation of McMurdo volcanics, Ross Island, Antarctica. Contrib. Mineral. Petrol. 54, 139-155. [Rb Sr Ba REE]

Tagai, T. and M. Korekawa (1981) Crystallographic investigation of the Huttenlocher exsolution at high temperature. Phys. Chem. Minerals 7, 77-81.

Tagai, T., W. Joswig, M. Korekawa and H.-R. Wenk (1978) Determination of Al/Si distribution in a plagioclase An_{66} using neutron diffraction data. Abstr. 11th Congr. Int'l Union Crystallogr., Warsaw, 183.

Takéuchi, Y. and N. Haga (1973) The crystal structure of monoclinic $CaAl_2Si_2O_8$: a case of monoclinic structure closely simulating orthorhombic symmetry. Z. Kristallogr. 137, 380-398.

Tatekawa, M. (1975) On the perthitic structure of moonstone. (III) A moonstone having sodium phase twinned according to pericline law. Mineral. J. (Japan) 7, 562-574.

Taylor, H.P., Jr. (1974) The application of oxygen and hydrogen isotope studies to problems of hydrothermal alteration and ore deposition. Econ. Geol. 69, 843-883.

Taylor, H.P., Jr. (1977) Water-rock interactions and the origin of H_2O in granitic batholiths. J. Geol. Soc. London 133, 509-558.

Taylor, S.R., K.S. Heier, and T.L. Sverdrup (1960) Trace element variations in three generations of feldspar from the Landsverk I pegmatite, Evje, Southern Norway. Norsk Geol. Tidsskr. 40, 133-156.

Taylor, W.H. (1933) The structure of sanidine and other felspars. Z. Kristallogr. 85, 425-442.

Thomas, G. (1962) Transmission Electron Microscopy of Metals. John Wiley & Sons: New York, 299 pp.

Thompson, J.B., Jr. (1967) Thermodynamic properties of simple solution. In, P.H. Abelson, Ed., Researches in Geochemistry, Vol. II. John Wiley & Sons: New York, pp. 340-361.

Thompson, J.B., Jr. and G.L. Hovis (1978) Triclinic feldspars: angular relations and the representation of feldspar series. Am. Mineral. 63, 981-990.

Thompson, J.B., Jr. and D.R. Waldbaum (1969a) Analysis of the two-phase region halite-sylvite in the system NaCl-KCl. Geochim. Cosmochim. Acta 33, 671-690.

Thompson, J.B., Jr. and D.R. Waldbaum (1969b) Mixing properties of sanidine crystalline solutions. III. Calculations based on two-phase data. Am. Mineral. 54, 811-838.

Thompson, J.B., Jr., D.R. Waldbaum, and G.L. Hovis (1974) Thermodynamic properties related to ordering in end-member alkali feldspars. In, W.S. MacKenzie and J. Zussman, Eds., The Feldspars. Manchester Univ. Press: Manchester, pp. 218-248.

Thompson, P.H. (1973) Mineral zones and isograds in "impure" calcareous rocks, an alternative means of evaluating metamorphic grade. Contrib. Mineral. Petrol. 42, 63-80.

Tilling, R.I. (1968) Zonal distribution of variations in structural state of alkali feldspar within the Radar Creek pluton, Boulder batholith, Montana. J. Petrol. 9, 331-357.

Toman, K. and A.J. Frueh (1971) On the origin of plagioclase satellite reflections. Acta Crystallogr. B27, 2182-2186.

Toman, K. and A.J. Frueh (1972) Intensity averages of plagioclase satellites: distribution in reciprocal space. Acta Crystallogr. B28, 1657-1662.

Toman, K. and A.J. Frueh (1973a) The intensities and Fourier transforms of difference reflections. Acta Crystallogr. A29, 121-127.

Toman, K. and A.J. Frueh (1973b) Patterson function of plagioclase satellites. Acta Crystallogr. A29, 127-133.

Tsuboi, S. (1934) A straight-line diagram for determining plagioclases by the dispersion method. Japan Geol. Geogr. 11, 325-326.

Tsuboi, S., S. Mizutani, K. Suwa, and Y. Tsuzuki (1977) Charts of plagioclase optics, Iwanami Shoten: Tokyo, 177 pp.

Tullis, J. (1975) Elastic strain effects in coherent perthitic feldspars. Contrib. Mineral. Petrol. 49, 83-91.

Tullis, J. and R.A. Yund (1977) Experimental deformation of dry Westerly granite. J. Geophys. Res. 82, 5707-5718.

Tullis, J. and R.A. Yund (1979) Calculation of coherent solvi for alkali feldspars, iron-free clinopyroxene, nepheline-kalsilite, and hematite-ilmenite. Am. Mineral. 64, 1063-1074.

Tullis, J. and R.A. Yund (1980) Hydrolytic weakening of experimentally deformed Westerly granite and Hale albite rock. J. Struc. Geol. 2, 439-451.

Turner, F.J. (1951) Observations on twinning of plagioclase in metamorphic rocks. Am. Mineral. 36, 581-589.

Tuttle, O.F. (1952) Optical studies on alkali feldspars. Am. J. Sci., Bowen Vol., 553-568.

Tuttle, O.F. and N.L. Bowen (1950) High-temperature albite and contiguous feldspars. J. Geol. 58, 572-583.

Tuttle, O.F. and N.L. Bowen (1958) Origin of granite in light of experimental studies in the system $NaAlSi_3O_8$-$KAlSi_3O_8$-SiO_2-H_2O. Geol. Soc. Am. Memoir 74, 153 pp.

Van der Biest, O. and G. Thomas (1976) Fundamentals of electron microscopy. In H.-R. Wenk et al., Eds., Electron Microscopy in Mineralogy, Springer-Verlag: Berlin, pp. 15-51.

Van der Plase, L. (1966) The Identification of Detrital Feldspars. Elsevier: Amsterdam, 305 pp.

Van Schmus, W.R. and P.H. Ribbe (1968) The composition and structural state of feldspar from chondritic meteorites. Geochim. Cosmochim. Acta 32, 1327-1342.

Veremeichik, T.F., B.N. Grechusnikov, T.M. Varina, D.T. Sviridov and I.N. Kalinkina (1975) Absorption spectra and calculation of energy-level diagram of Fe^{3+} and Mn^{2+} ions in single crystals of yttrium aluminum garnet, orthoclase, and manganese silicate. Kristallografiya 19, 1194-1199. (Trans: Sov. Phys. Crystallogr. 19, 742-744).

Vernieres, J., J.L. Joron, M. Trenil, C. Coulon, and C. Dupuy (1977) Coefficient de partage de quelques elements en trace entre plagioclase et verre dans les ignimbrites--implications petrogenetiques. Chem. Geol. 19, 309-325.

Vernon, R.H. (1965) Plagioclase twins in some mafic gneisses from Broken Hill, Australia. Mineral. Mag. 35, 440-507.

Vernon, R.H. (1975) Deformation and recrystallization of a plagioclase grain. Am. Mineral. 60, 884-888.

Vidal, J.-L., L. Kubin, P. Debat and J.-C. Soula (1980) Deformation and dynamic recrystallization of K feldspar augen in orthogneiss from Montagne Noire, Occitania, southern France. Lithos 13, 247-255.

Vincent, E.A. and J.H. Crockett (1960) Studies in the geochemistry of gold - I. The distribution of gold in rocks and minerals of the Skaergaard intrusion, East Greenland. Geochim. Cosmochim. Acta 18, 130-142.

Vincent, E.A. and G. Nightingale (1974) Gallium in rocks and minerals of the Skaergaard intrusion. Chem. Geol. 14, 63-74.

Viswanathan, K. (1971) A new X-ray method to determine the anorthite content and structural state of plagioclases. Contrib. Mineral. Petrol. 30, 332-335.

Viswanathan, K. (1972) Kationenaustausch an Plagiokasen. Contrib. Mineral. Petrol. 37, 277-290.

Viswanathan, K. (1973) Kation enaustausch von Peristeriten mit Beobachtungen an Pulver-und Einkristallenaufnahmen. Contrib. Mineral. Petrol. 41, 145-150.

Viswanathan, K. and E. Eberhard (1968) The peristerite problem. Schweiz. Mineral. Petrol. Mitt. 48, 803-814.

Vogel, T.A., R. Ehrlich, and W.C. Luth (1973) Non-linear variation of cell parameters with composition in alkali feldspar series. Am. Mineral. 58, 905-908.

Volfinger, M. (1976) Effet de la temperature sur les distributions de Na, Rb et Cs entre la sanidine, la muscovite, la phlogopite et une solution hydrothermale sous une pression de 1 kbar. Geochim. Cosmochim. Acta 40, 267- 282.

Voll, B. (1971) Entmischung von Plagioklasen mit An_{50-55} zu An_{18} + An_{93}. Fortschr. Mineral. 49, 61-63.

Voll, G. (1976) Recrystallization of quartz, biotite, and feldspars from Erstfeld to the leventina Nappe, Swiss Alps, and its geological significance. Schweiz. Mineral. Petrogr. Mitt. 56, 641-647.

Wager, L.R., J. van R. Smit, and H. Irving (1958) Indium content of rocks and minerals from the Skaergaard intrusion, East Greenland. Geochim. Cosmochim. Acta 13, 81-86.

Wagner, C. (1961) Theorie der Alterung von Niederschlagen durch Umlösen. Z. Elektrochemie 65, 581-591.

Wagner, C. (1969) The evaluation of data obtained with diffusion couples of binary single-phase and multiphase systems. Acta Met. 17, 99-107.

Wainwright, J.E. (1969) A refined structure for bytownite. Progr. 8th Int'l Congr. Crystallogr., Abstr. XII-48.

Wainwright, J.E. and J. Starkey (1968) Crystal structure of a metamorphic low albite. Progr. Geol. Soc. Annual Mtg., Mexico City, p. 310.

Wainwright, J.E. and J. Starkey (1971) A refinement of the structure of anorthite. Z. Kristallogr. 133, 75-84.

Wakefield, J. (1977) Mylonitization in the Lethakane shear zone, eastern Botswana. J. Geol. Soc. London 133, 203-276.

Waldbaum, D.R. and R.A. Robie (1971) Calorimetric investigation of Na-K mixing and polymorphism in the alkali feldspars. Z. Kristallogr. 134, 381-420.

Waldbaum, D.R. and J.B. Thompson, Jr. (1969) Mixing properties of sanidine crystalline solutions: IV. Phase diagrams from equation of state. Am. Mineral. 54, 1274-1298.

Watts, M.J. and G.D. Williams (1979) Fault rocks as indicators of progressive shear deformation in the Guingamp region, Brittany. J. Struc. Geol. 1, 323-332.

Weber, L. (1972) Das Entmischungsverhalten der Peristerite. Schweiz. Mineral. Petrogr. Mitt. 52, 349-372.

Wegner, M.W., R.E. Jones and J.M. Christie (1978) Exsolution in terrestrial and lunar plagioclases revealed by chemical etching. Contrib. Mineral. Petrol. 65, 283-291.

Weitz, G. (1972) Die Struktur des Sanidins bei verschiedenen Ordnungsgraden. Z. Kristallogr. 136, 418-426.

Wenk, E. and H.-R. Wenk (1977) An-variaticn and intergrowths of plagioclases in banded metamorphic rocks from Val Carecchio (Central Alps). Schweiz. Mineral. Petrogr. Mitt. 57, 41-57.

Wenk, E., H.-R. Wenk, A. Glauser, and H. Schwander (1975) Intergrowth of andesine and labradorite in marbles of the central Alps. Contrib. Mineral. Petrol. 53, 311-326.

Wenk, H.-R. (1978) Ordering of the intermediate plagioclase structure during heating. Am. Mineral. 63, 132-135.

Wenk, H.-R. (1979) Superstructure variation in metamorphic intermediate plagioclase. Am. Mineral. 64, 71-76.

Wenk, H.-R. and Y. Nakajima (1981) Structure, formation, and decomposition of APB's in calcic plagioclase. Phys. Chem. Minerals 6, 169-186.

Wenk, H.-R. and W.R. Wilde (1973) Chemical anomalies of lunar plagioclase, described by substitution vectors and their relation to optical and structural properties. Contrib. Mineral. Petrol. 41, 89-104.

Wenk, H.-R., W.F. Müller and G. Thomas (1973) Antiphase domains in lunar plagioclase. Proc. 4th Lunar Sci. Conf., Geochim. Cosmochim. Acta, Suppl. 4, 1, 909-923.

Wenk, H.-R., W. Joswig, T. Tagai, M. Korekawa, and B.K. Smith (1980) The average structure of An_{62-66} labradorite. Am. Mineral. 65, 81-95.

White, S. (1973) The dislocation structures responsible for the optical effects in some naturally deformed quartzes. J. Mater. Sci. 9, 490-499.

White, S. (1975) Tectonic deformation and recrystallization of oligoclase. Contrib. Mineral. Petrol. 50, 287-304.

White, S.H., S.E. Burrows, J. Carreras, N.W. Shaw and F.J. Humphreys (1980) On mylonites in ductile shear zones. J. Struc. Geol. 2, 175-188.

Wilhelm, S. and C. Willaime (1976) A propos des fentes dites d'extension dans les phenocristaux feldspathiques des granites et des gneiss: role de la contraction thermique. Comptes Rendus de Acad. Sci. Paris 282, 255-258.

Willaime, C. and W.L. Brown (1974) A coherent elastic model for the determination of the orientation of exsolution boundaries: Application to the feldspars. Acta Crystallogr. A30, 316-331.

Willaime, C. and M. Gandais (1972) Study of exsolution in alkali feldspars. Calculation of elastic stresses inducing periodic twins. Phys. Stat. Sol. (a) 9, 529-539.

Willaime, C. and M. Gandais (1977) Electron microscope study of plastic defects in experimentally deformed alkali feldspars. Bull. Soc. franc. Mineral. Cristallogr. 100, 263-271.

Willaime, C., W.L. Brown, and M. Gandais (1973) An electron-microscopic and x-ray exsolution textures in a cryptoperthitic alkali feldspar. J. Mater. Sci. 8, 461-466.

Willaime, C., W.L. Brown, and M. Gandais (1976) Physical aspects of exsolution in natural alkali feldaprs. In, H.-R. Wenk et al., Eds., Electron Microscopy in Mineralogy. Springer-Verlag: Berlin, pp. 248-257.

Willaime, C., W.L. Brown, and M.C. Perucaud (1974) On the orientation of the thermal and compositional strain ellipsoids. Am. Mineral. 59, 457-464.

Willaime, C., J.M. Christie and M.-P. Kovacs (1979) Experimental deformation of K feldspar single crystals. Bull. Mineral. 102, 168-177.

Wilson, C.J.L. (1980) Shear zones in a pegmatite: a study of albite-mica-quartz deformation. J. Struc. Geol. 2, 203-209.

Winchell, A.N. and H. Winchell (1951) Elements of Optical Mineralogy. An Introduction to Microscopic Petrography. Part II. Descriptions of Minerals. 4th Ed., John Wiley & Sons: New York, 551 pp.

Winter, J.K., S. Ghose, and F.P. Okamura (1977) A high-temperature study of the thermal expansion and the anisotropy of the sodium atom in low albite. Am. Mineral. 62, 921-931.

Winter, J.K., F.P. Okamura, and S. Ghose (1979) A high temperature structural study of high albite, monalbite, and the analbite-monalbite phase transition. Am. Mineral. 64, 409-423.

Wolfe, H.E. (1976) Optical and X-ray Study of Low Plagioclases. M.S. Thesis, Virginia Polytechnic Institute and State University: Blacksburg, Va. 86 pp.

Wones, D.R., D.B. Tatlock, and D. von Limbach (1967) Coexisting orthoclase and microcline in altered volcanic rocks, West Humboldt Range, Pershing County, Nevada. Schweiz. Mineral. Petrogr. Mitt. 47, 169-176.

Wright, T.L. (1964) The alkali feldspars of the Tatoosh pluton in Mount Rainier National Park. Am. Mineral. 49, 715-735.

Wright, T.L. (1968) X-ray and optical study of alkali feldspar II. An x-ray method of determining the composition and structural state from measurement of 2θ values for three reflections. Am. Mineral. 53, 88-104.

Wright, T.L. and D.B. Stewart (1968) X-ray and optical study of alkali feldspar: I. Determination of composition and structural state from refined unit-cell parameters and 2V. Am. Mineral. 53, 38-87.

Yoder, H.S., Jr., D.B. Stewart, and J.R. Smith (1956) Ternary feldspars. Carnegie Inst. Washington Year Book 55, 190-194.

Yund, R.A. (1974) Coherent exsolution in the alkali feldspars. In, A.W. Hofmann et al., Eds., Geochemical Transport and Kinetics. Carnegie Inst. Washington and Academic Press: New York, pp. 173-183.

Yund, R.A. and D. Ackermand (1979) Development of perthite and microstructures in the Storm King Granite, N.Y. Contrib. Mineral. Petrol. 70, 273-280.

Yund, R.A. and T.F. Anderson (1974) Oxygen isotope exchange between potassium feldspar and KCl solution. In, A.W. Hofmann et al., Eds., Geochemical Transport and Kinetics, Carnegie Inst. Washington and Academic Press: New York, pp. 99-105.

Yund, R.A. and T.F. Anderson (1978) Oxygen isotope exchange between feldspar and fluid as a function of fluid pressure. Geochim. Cosmochim. Acta 42, 235-239.

Yund, R.A. and W.M. Chapple (1980) Thermal histories of two lava flows estimated from cryptoperthite lamellar spacings. Am. Mineral. 65, 438-443.

Yund, R.A. and P. Davidson (1978) Kinetics of lamellar coarsening in cryptoperthites. Am. Mineral. 63, 470-477.

Yund, R.A. and R.H. McCallister (1970) Kinetics and mechanisms of exsolution. Chem. Geol. 6, 5-30.

Yund, R.A. and J. Tullis (1980) The effect of water, pressure and strain on Al/Si order-disorder kinetics in feldspar. Contrib. Mineral. Petrol. 72, 297-302.

Yund, R.A. and J. Tullis (1983) Strained cell parameters for coherent lamellae in alkali feldspars and iron-free pyroxenes. N. Jahrb. Mineral. Monatsh., 22-34.

Yund, R.A., D. Ackermand, and F. Seifert (1980) Microstructures in the alkali feldspars from the granulite complex of Finnish Lapland. N. Jahrb. Mineral. Monatsh., 109-117.

Yund, R.A., A.C. McLaren, and B.E. Hobbs (1974) Coarsening kinetics of the exsolution microstructure in alkali feldspar. Contrib. Mineral. Petrol. 48, 45-55.

Yund, R.A., B.M. Smith, and J. Tullis (1981) Dislocation-assisted diffusion of oxygen in albite. Phys. Chem. Minerals 7, 185-189.

Zeipert, C. and H. Wondratschek (1981) Ein ungewöhnliches Temperverhalten bei Sanidin von Volkesfeld/Eiffel. N. Jahrb. Mineral. Monatsh. 407-415.

Zhirov, K.K. and S.N. Stishov (1965) Geochemistry of amazonitization. Geochem. Int'l 2, 16-24.

Zoltai, T. (1960) Classification of silicates and other minerals with tetrahedral structures. Am. Mineral. 45, 960-973.